UNIVERSITAT DE BARCELONA

Nuevas estrategias para la mejora de la sensibilidad y la selectividad en el análisis de biomarcadores proteómicos y miRNómicos en fluidos biológicos mediante CE-MS

Roger Peró Gascón

Roger Peró Gascón

Tesis Doctoral

2020

Nuevas estrategias para la mejora de la sensibilidad y la selectividad en el análisis de biomarcadores proteómicos y miRNómicos en fluidos biológicos mediante CE-MS

Roger Peró Gascón

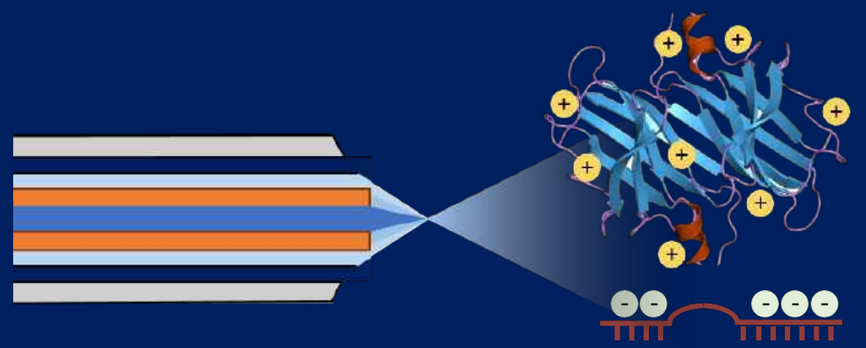

UNIVERSITAT DE BARCELONA

Nuevas estrategias para la mejora de la sensibilidad y la selectividad en el análisis de biomarcadores proteómicos y miRNómicos en fluidos biológicos mediante CE-MS

Roger Peró Gascón

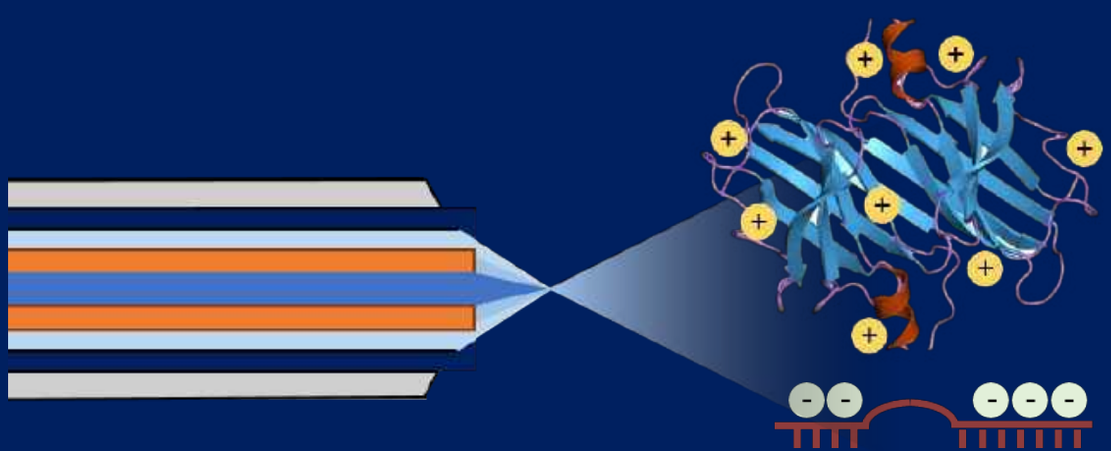

UNIVERSITAT DE BARCELONA

FACULTAD DE QUÍMICA

DEPARTAMENTO DE INGENIERÍA QUÍMICA Y QUÍMICA ANALÍTICA

Programa de Doctorado:

Química Analítica i Medi Ambient

Nuevas estrategias para la mejora de la sensibilidad y la selectividad en el análisis de biomarcadores proteómicos y miRNómicos en fluidos biológicos mediante CE-MS

Memoria presentada por

Roger Peró Gascón

para optar al grado de Doctor por la Universidad de Barcelona

Bajo la dirección de

Dra. M. Victòria Sanz Nebot

Dr. Fernando J. Benavente Moreno

del Departamento de Ingeniería Química y Química Analítica de la Universidad de Barcelona

La Dra. M. Victòria Sanz Nebot, profesora titular del Departamento de Ingeniería Química y Química Analítica de la Universidad de Barcelona, y el Dr. Fernando J. Benavente Moreno, profesor agregado del mismo Departamento,

HACEN CONSTAR,

Que la presente memoria titulada: "**Nuevas estrategias para la mejora de la sensibilidad y la selectividad en el análisis de biomarcadores proteómicos y miRNómicos en fluidos biológicos mediante CE-MS**", ha sido realizada bajo nuestra dirección por el Sr. **Roger Peró Gascón** y que todos los resultados presentados son fruto de las experiencias realizadas por el citado doctorando.

Y para que así conste, expedimos el presente certificado.

Barcelona, septiembre de 2020

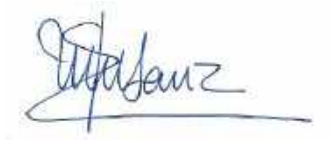

Dra. M. Victòria Sanz Nebot

Dr. Fernando J. Benavente Moreno

“*El esqueleto de la ciencia son los hechos, pero los músculos y los nervios son el significado que se les confiere, y el alma de la ciencia son las ideas.*”

Ruy Pérez Tamayo

Agraïments

Aquesta tesi doctoral no hagués estat possible sense totes aquelles persones que al llarg d'aquests anys m'han ajudat a fer front i a superar aquest repte. A tots vosaltres us vull dedicar aquest treball.

En primer lloc, vull agrair als meus directors de tesi, la Dra. Victòria Sanz i el Dr. Fernando Benavente, el seu entusiasme per la ciència, la seva orientació i haver-me proposat projectes que han estat un repte però, alhora, interessants i engrescadors. Vicki, gràcies pels teus ànims, les teves aportacions i per la teva disposició a buscar la millor solució a cada situació. Fernando, gràcies per la teva dedicació, tenacitat i constància, per proposar una infinitat de noves idees i potenciar que els treballs sempre acabessin sent el millor possible.

Al Dr. José Barbosa vull agrair haver-me donat l'oportunitat d'incorporar-me al grup de recerca Bioanàlisi, així com els seus consells i orientació.

A la Dra. Estela Giménez agrair-li els seus consells i la seva ajuda quan m'han sorgit dubtes.

Als companys i companyes de laboratori amb els que he compartit tantes hores i experiències. Per ordre d'antiguitat al laboratori, gràcies Dr. Albert Barroso per sempre estar disposat a ajudar en tot el que fos necessari. Dra. Laura Pont, gràcies per guiar-me en els meus inicis en el laboratori, per la teva ajuda i per tots els estudis que hem pogut tirar endavant junts, "que ja és molt!". Amb la Montse Mancera he compartit moltes hores de treball al laboratori i també moltes vivències. Finalitzem ara la nostra etapa de doctorat i d'aquí a poques setmanes defensarem les nostres respectives tesis doctorals. Montse, vull donar-te les gràcies pel teu suport, la teva alegria, cançons i àudios. Ets una gran companya de laboratori i de viatges! Irena, gràcies per la teva dedicació i per sempre estar disposada a fer del laboratori un lloc més confortable. Lorena, moltes gràcies per ser un exemple d'esforç i constància. I would also like to thank Mulugeta for sharing with us his experience and being an ambassador of his interesting country. També voldria destacar la companyonia i bon ambient que han creat totes les persones que durant aquests anys han format part del grup de recerca: Oumaima, Abel, Aysenur, Víctor, María, Cristina, Karen, Leo, Kader,... i els MSc.: Hiba, Rocío, Karina, Laura, Gemma, Marina, Nejsi, Berta, Ana, Lídia, Sergio i Aleix.

Vull donar les gràcies als doctorands del departament per tots els bons moment viscuts, especialment, els migdies compartits, els riures i les converses de temàtica diversa: Alejandro, Alex, Ane, Clara, Guillem, Juanfra, Mariale, Nerea, Noe i Sara.

Als Drs. Javier Santos, Àngels Sahuquillo, Fermín López i Sergio Carneado vull agrair el seu suport i haver despertat en mi l'interès per la Química Analítica. També vull agrair els seus consells a la Dra. Irene Fernández del Laboratori d'Espectrometria de Masses del CCiT. Vull donar les gràcies a la Dra. Cristina Ariño, coordinadora del programa de doctorat "Química Analítica i Medi Ambient", per resoldre els meus dubtes amb celeritat i eficàcia. També ha estat inestimable l'ajuda del Personal d'Administració i Serveis per tal que les tramitacions fossin senzilles. Voldria destacar la facilitat per tramitar les comandes amb el Sr. Íñigo Aura i les petites compres amb el Sr. Andreu Márquez, la gestió de les activitats del doctorat de les Sres. Carmen Muñoz i Marta Valls i del material de les Sres. Nuria Sánchez, Ana Salamià i Cristina Núñez.

I would also like to thank Dr. Christian Neusüß for giving me the opportunity of working in his laboratory and his support during my stay in Aalen. *Vielen Dank* to Cristina, Oli, Johannes, Jenni, Alex and Lukas for the hospitality and for making my stay enjoyable. *Danke schön*!

A la Mercè Talló, professora de Batxillerat a l'escola IPSI, donar-li les gràcies per potenciar el meu interès per la Química i que jo decidís fer els meus estudis universitaris en aquesta branca tan apassionant de la ciència.

Als meus pares, família i amics, en particular els d'IPSI i els del Grau de Química, gràcies pel vostre suport continu, especialment necessari en els moments de dubte i desànim.

Finalment vull agrair el suport econòmic del Ministerio de Educación, Cultura y Deporte a través d'una beca FPU, de l'Institut de Recerca en Nutrició i Seguretat Alimentària (INSA·UB) i del Ministerio de Economia y Competitividad pel finançament dels projectes CTQ2014-56777-R i RTI2018-097411-B-I00.

Moltes gràcies a tots!

Abbreviations and acronyms

A

%A	Relative abundance (%)
AA	Aptamer affinity
AA-SPE-CE	On-line aptamer affinity solid-phase extraction capillary electrophoresis
AA-SPE-CE-MS	On-line aptamer affinity solid-phase extraction capillary electrophoresis-mass spectrometry
Ab	Antibody
Aβ	Amyloid beta
ACN	Acetonitrile
AD	Alzheimer's disease
$\alpha_{i,j}$	Selectivity between a pair of compounds (classic definition)
α-CSN	α-casein
α-CSN1	α-S1-casein
α-CSN2	α-S2-casein
α-syn	α-synuclein
Amino acids	

Amino acid	Code (3 letters)	Code (1 letter)
Aspartic acid	Asp	D
Glutamic acid	Glu	E
Alanine	Ala	A
Arginine	Arg	R
Asparagine	Asn	N
Cysteine	Cys	C
Phenylalanine	Phe	F
Glycine	Gly	G
Glutamine	Gln	Q
Histidine	His	H
Isoleucine	Ile	I
Leucine	Leu	L
Lysine	Lys	K
Methionine	Met	M
Proline	Pro	P
Serine	Ser	S
Tyrosine	Tyr	Y
Threonine	Thr	T
Tryptophan	Trp	W
Valine	Val	V

A_p	Peak area

B

β-CSN	β-casein

BGE	Background electrolyte
β-LG	β-lactoglobulin
BS3	Bissulfosuccinimidyl suberate

C

C	Constant domain
CE	Capillary electrophoresis
CEC	Capillary electrochromatography
CE-MS	Capillary electrophoresis-mass spectrometry
CE-MS/MS	Capillary electrophoresis-tandem mass spectrometry
CE-UV	Capillary electrophoresis with ultraviolet spectrophotometry detection
CGE	Capillary gel electrophoresis
CIEF	Capillary isoelectric focusing
CLL	B-cell chronic lymphocytic leukemia
CSF	Cerebrospinal fluid
CZE	Capillary zone electrophoresis

D

DI	Dimer
DMSO	Dimethyl sulfoxide
DNA	Deoxyribonucleic acid
Dyn A	Dynorphin A (1-7)
DyPA	Dynabeads® Protein A

E

E. coli	*Escherichia coli*
EIE	Extracted ion electropherogram
End 1	Endomorphin 1
EOF	Electroosmotic flow
E_r	Mass error
ESI	Electrospray ionization
ESI-	Electrospray negative ionization mode
ESI+	Electrospray positive ionization mode

F

Fab’	Fragment antigen-binding

FAP	Familial amyloidotic polyneuropathy
FAP-I	Familial amyloidotic polyneuropathy type I
FASS	Field-amplified sample stacking
Fc	Fragment crystallizable region
FDA	Food and Drug Administration of the United States of America
FT-ICR	Fourier transform ion cyclotron resonance

G

γ	Activity coefficient
GnRH	Gonadotropin-releasing hormone

H

H	Heavy chain
HAc	Acetic acid
η	Viscosity
HFor	Formic acid
His-peptide	Histidine containing peptide
His-tag	Polyhistidine-tag
HPC	Hydroxypropyl cellulose

I

I	Ionic strength
IA	Immunoaffinity
IA-MBs	Immunoaffinity magnetic beads
IA-SPE	Immunoaffinity solid-phase extraction
IA-SPE-CE	On-line immunoaffinity solid-phase extraction capillary electrophoresis
IA-SPE-CE-MS	On-line immunoaffinity solid-phase extraction capillary electrophoresis-mass spectrometry
i.d.	Inner diameter
IDA	Iminodiacetic acid
Ig	Immunoglobulin
IgG	Immunoglobulin G
IMA	Immobilized metal affinity
IMA-SPE-CE	On-line immobilized metal affinity solid-phase extraction capillary electrophoresis
IMA-SPE-CE-MS	On-line immobilized metal affinity solid-phase extraction capillary electrophoresis-mass spectrometry

IMA-SPE-CE-UV	On-line immobilized metal affinity solid-phase extraction capillary electrophoresis with ultraviolet spectrophotometry detection
IMER	Immobilized enzyme microreactor
IMER-CE	On-line immobilized enzyme microreactor capillary electrophoresis
IMER-CE-MS	On-line immobilized enzyme microreactor capillary electrophoresis-mass spectrometry
IP	Immunoprecipitation
iso-miR-16	Hsa-iso-miR16-5p
IT	Ion trap mass analyzer
ITP	Isotachophoresis

K

K_a	Acid dissociation constant
k	Retention factor
κ-CSN	κ-casein

L

L	Light chain
LC	Liquid chromatography
LC-MS	Liquid chromatography-mass spectrometry
LC-MS/MS	Liquid chromatography-tandem mass spectrometry
L_D	Effective capillary length
let-7g	Hsa-let-7g-5p
LIF	Laser induced fluorescence
LOD	Limit of detection
L_T	Total capillary length

M

MALDI-MS	Matrix assisted laser desorption ionization-mass spectrometry
m_{app}	Apparent mobility
m_{avg}	Mean value of the electrophoretic mobility of a pair of compounds
MBs	Magnetic particles/beads
m_e	Electrophoretic mobility
MEKC	Micellar electrokinetic chromatography
m_{EOF}	Mobility of the electroosmotic flow
MeOH	Methanol
Met	Met-enkephalin
miRNA	MicroRNA

miR-21	Hsa-miR-21-5p
MO	Monomer
M_r	Relative molecular mass
mRNA	Messenger ribonucleic acid
MS	Mass spectrometry
MS/MS	Tandem mass spectrometry
m/z	Mass-to-charge ratio

N

n	Number of replicates
n.d.	Not detected
NGS	Next-generation sequencing
NH_4Ac	Ammonium acetate
NIH	National Institutes of Health of the United States of America
NMR	Nuclear magnetic resonance
non-His-peptide	Non-histidine containing peptide
NTA	Nitrilotriacetic acid
nvSPE-CE	On-line solid-phase extraction capillary electrophoresis with a nanoliter valve
nvSPE-CE-MS	On-line solid-phase extraction capillary electrophoresis-mass spectrometry with a nanoliter valve

O

oa	Orthogonal acceleration
o.d.	Outer diameter

P

PBS	Phosphate-buffered saline
PCA	Phenol-chloroform-isoamyl alcohol mixture
PCR	Polymerase chain reaction
PD	Parkinson's disease
PEEK	Polyetheretherketone
pK_a	Minus logarithm of the acid dissociation constant
pK_a'	Apparent pK_a
$pK_a(A)$	pK_a of the free amino acid

$pK_a(R)$	Average pK_as for amino acids reported by Rickard et al. [1]
ppm	Parts-per-million
ProA	Protein A
PTM	Post-translational modification
PVA	Poly(vinyl alcohol)

Q

q	Total ion charge
Q	Quadrupole mass analyzer
q/M_r	Charge-to-molecular mass ratio
QqQ	Triple quadrupole mass analyzer
Q-TOF	Hybrid quadrupole time-of-flight mass analyzer

R

r	Solvated ion radius
RISC	RNA-induced silencing complex
RNA	Ribonucleic acid
%RSD	Relative standard deviation (%)
RT-qPCR	Reverse transcription–quantitative polymerase chain reaction

S

SiC	Silicon carbide
SiC-SPE-CE-MS	On-line silicon carbide solid-phase extraction capillary electrophoresis-mass spectrometry
$S_{i,j}$	Selectivity between a pair of compounds (definition by Jorgenson and Lukacs) [2]
$S_{crítica}$	Minimum value of $S_{i,j}$
SiOH	Silanol groups
SiPA	SiMAG-Protein A
SELEX	Systematic evolution of ligands by exponential enrichment
SL	Sheath liquid
SPE	Solid-phase extraction
SPE-CE	On-line solid-phase extraction capillary electrophoresis

[1] E.C. Rickard, M.M. Strohl, R.G. Nielsen, Correlation of electrophoretic mobilities from capillary electrophoresis with physicochemical properties of proteins and peptides, Anal. Biochem. 197 (1991) 197–207. https://doi.org/10.1016/0003-2697(91)90379-8.

[2] J.W. Jorgenson, K.D. Lukacs, Zone electrophoresis in open-tubular glass capillaries, Anal. Chem. 53 (1981) 1298–1302. https://doi.org/10.1002/jhrc.1240040507.

SPE-CE-MS	On-line solid-phase extraction capillary electrophoresis-mass spectrometry

T

TE	Thermo-enriched
t_{EOF}	Migration time of a neutral marker
TIE	Total ion electropherogram
t_{inj}	Time of hydrodynamic injection
t_m	Migration time
TOF	Time-of-flight mass analyzer
TTR	Transthyretin
TTR(Met30)	Transthyretin with Met30 mutation

U

UAAF	AffiAmino ultrarapid agarose
UAPA	Protein A ultrarapid agarose
UV	Ultraviolet

V

V	Variable region
v/v	Volume percent

X

χ	Molar fraction

Z

z	Maximum positive net charge

Index

ABSTRACT 1

AIMS 9

CHAPTER 1. INTRODUCTION 13

1.1. Omics sciences 15

1.1.1. Proteomics 16

1.1.2. MiRNomics 20

1.2. Biomarker discovery 22

1.2.1. Neurodegenerative diseases 22

1.2.2. Cancer. B-cell chronic lymphocytic leukemia 27

1.3. Analytical techniques 28

1.3.1. Capillary electrophoresis (CE) 28

1.3.1.1. Separation principles in CE 29

1.3.1.2. Determination of electrophoretic mobility and acid dissociation constants by CE 31

1.3.1.3. Prediction of electrophoretic migration with the classical semiempirical models 33

1.3.1.4. Criteria to optimize separation in CE 35

1.3.2. Mass spectrometry (MS) 36

1.3.2.1. Ionization techniques. Electrospray ionization (ESI) 37

1.3.2.2. Mass analyzers 41

1.4. On-line preconcentration by solid-phase extraction capillary electrophoresis (SPE-CE) 43

1.4.1. SPE-CE designs and configurations 46

1.4.1.1. Unidirectional SPE-CE 49

1.4.1.2. SPE-CE with a nanoliter valve (nvSPE-CE) 50

1.4.2. SPE-CE sorbents 51

1.4.2.1. Conventional chromatographic sorbents. Reversed-phase SPE 52

1.4.2.2. Affinity sorbents 53

Immunoaffinity (IA-SPE-CE) 53

Aptamer affinity (AA-SPE-CE) 56

Immobilized metal affinity (IMA-SPE-CE) 58

Silicon carbide (SiC) 59

1.5. On-line immobilized enzyme microreactor capillary electrophoresis-mass spectrometry (IMER-CE-MS) 61

CHAPTER 2. NOVEL DEVELOPMENTS FOR PREDICTION AND OPTIMIZATION OF SEPARATIONS IN CAPILLARY ELECTROPHORESIS 63

Publication 2.1. Determination of acidity constants and prediction of electrophoretic separation of amyloid beta peptides 67

Publication 2.2. Improving separation optimization in capillary electrophoresis by using a general quality criterion 77

CHAPTER 3. IMPROVING THE SENSITIVITY AND THE SELECTIVITY IN CAPILLARY ELECTROPHORESIS BY UNIDIRECTIONAL ON-LINE SOLID-PHASE EXTRACTION CAPILLARY ELECTROPHORESIS 85

Publication 3.1. A critical retrospective and prospective review of designs and materials in in-line solid-phase extraction capillary electrophoresis 89

Publication 3.2. Analysis of serum transthyretin by on-line immunoaffinity solid-phase extraction capillary electrophoresis mass spectrometry using magnetic beads 109

Publication 3.3. On-line aptamer affinity solid-phase extraction capillary electrophoresis-mass spectrometry for the analysis of blood α-synuclein 121

Publication 3.4. Enrichment of histidine containing peptides by on-line immobilised metal affinity solid-phase extraction capillary electrophoresis-mass spectrometry 141

Publication 3.5. Analysis of circulating microRNAs and their post-transcriptional modifications in cancer serum by on-line solid-phase extraction−capillary electrophoresis−mass spectrometry 151

CHAPTER 4. IMPROVING THE SENSITIVITY AND THE SELECTIVITY IN CAPILLARY ELECTROPHORESIS BY ON-LINE SOLID-PHASE EXTRACTION CAPILLARY ELECTROPHORESIS WITH A NANOLITER VALVE 165

Publication 4.1. Evaluation of on-line solid-phase extraction capillary electrophoresis–mass spectrometry with a nanoliter valve for the analysis of peptide biomarkers 169

CHAPTER 5. HIGH-THROUGHPUT BOTTOM-UP ANALYSIS OF PROTEINS. ON-LINE IMMOBILIZED ENZYME MICROREACTOR CAPILLARY ELECTROPHORESIS-MASS SPECTROMETRY **191**

Publication 5.1. On-line protein digestion by immobilized enzyme microreactor capillary electrophoresis-mass spectrometry 195

CAPÍTULO 6. RESULTADOS Y DISCUSIÓN **209**

6.1. Nuevos desarrollos para la predicción y optimización de las separaciones en CE **211**

6.1.1. Determinación del comportamiento electroforético y las constantes de acidez de los fragmentos de los péptidos Aβ. Estimación de los valores de pKa de los péptidos Aβ 1-40 y 1-42 212

6.1.2. Predicción de la migración electroforética de los fragmentos de los péptidos Aβ mediante los modelos semiempíricos clásicos 220

6.1.3. Optimización de la separación de los fragmentos de los péptidos Aβ 222

6.1.4. Predicción de la migración electroforética de los péptidos Aβ y optimización de su separación 228

6.2. SPE-CE-MS unidireccional para la mejora de la sensibilidad y la selectividad **233**

6.2.1. Análisis dirigido de biomarcadores proteicos mediante IA-SPE-CE-MS. La transtiretina en la polineuropatía amiloidótica familiar tipo I 236

6.2.1.1. Análisis de TTR en muestras de suero humano mediante inmuno-precipitación con partículas magnéticas y CE-MS 238

6.2.1.2. Análisis de patrones de TTR por IA-SPE-CE-MS 244

6.2.1.3. Análisis de TTR en muestras de suero humano por IA-SPE-CE-MS 249

6.2.2. Análisis dirigido de biomarcadores proteicos mediante AA-SPE-CE-MS. La α-sinucleína en la enfermedad de Parkinson 252

6.2.2.1. Análisis de patrones de α-syn por CE-MS 252

6.2.2.2. Análisis de patrones de α-syn por AA-SPE-CE-MS 254

6.2.2.3. Análisis de α-syn en muestras de sangre por AA-SPE-CE-MS 257

6.2.3. Análisis de un subproteoma. Enriquecimiento de His-peptides mediante IMA-SPE-CE-MS 264

6.2.3.1. Análisis de la α-CSN 265

6.2.3.2. Análisis de la β-CSN y la κ-CSN 272

6.2.3.3. Análisis de un lisado celular de E. coli 274

6.2.4. Análisis de biomarcadores miRNómicos. MicroRNAs en cáncer 277

6.2.4.1. Análisis de patrones de miRNAs por CE-MS y sample stacking CE-MS 278

6.2.4.2. Análisis de patrones de miRNAs por SiC-SPE-CE-MS 282

6.2.4.3. Análisis de miRNAs en suero humano por SiC-SPE-CE-MS 285

6.2.5. Comparativa de las metodologías de SPE-CE-MS unidireccional 288

6.3. SPE-CE-MS con una válvula para la mejora de la sensibilidad y la selectividad 292

6.3.1. Análisis de patrones de péptidos opioides y Aβ por CE-MS 293

6.3.2. Análisis de péptidos opioides por SPE-CE-MS unidireccional 297

6.3.3. Análisis de péptidos opioides y Aβ por nvSPE-CE-MS 299

6.4. Análisis bottom-up de proteínas por IMER-CE-MS 305

6.4.1. Análisis de β-LG por digestión off-line en disolución y CE-MS 306

6.4.2. Análisis de β-LG por digestión off-line con tripsina inmovilizada y CE-MS 309

6.4.3. Análisis de β-LG por IMER-CE-MS 311

6.4.4. Análisis de α-CSN, β-CSN y κ-CSN por IMER-CE-MS 313

6.4.5. Análisis de un lisado de E. coli 320

CONCLUSIONS 323

REFERENCES 331

APPENDIX 367

Abstract

In recent years, an increased emphasis has been placed on the analysis of biomarker compounds in biological samples for the diagnosis, follow-up and prognosis of numerous diseases. The leading difficulties in many of these analyses are the low concentration of the biomarkers, their structural complexity, the sample matrix effects and the limited availability of sample.

In this doctoral thesis, we present novel strategies based on capillary electrophoresis-mass spectrometry (CE-MS) for the separation, detection, characterization and quantification of peptide, protein and microRNA (miRNA) biomarkers in biological fluids.

MS is a powerful technique for the unequivocal identification of biomolecules due to its potential with regard to the detailed structural characterization of unknown compounds. However, due to the complexity of most biological fluids, the hyphenation of high-performance separation techniques is essential prior to MS analysis. In this regard, CE is a microscale technique that is very suitable for the separation of charged biomolecules. Nevertheless, electrophoretic separation methods must be properly optimized to achieve rapid, efficient, sensitive and high-resolution separations.

In this thesis, we have investigated novel strategies to predict and optimize the separation of complex mixtures in CE. To assess these strategies, amyloid beta (Aβ) peptides, which are biomarkers of Alzheimer's disease, were studied, namely Aβ 1-40 and 1-42 and five of their fragments (Aβ 1-15, 10-20, 20-29, 25-35 and 33-42). The electrophoretic behavior of the Aβ peptide fragments as a function of pH was studied to determine the acidity constants of their ionizable groups (K_a or pK_a, their negative logarithm) and, simultaneously, select the optimum pH for their separation. Since the determination of the pK_as of polyprotic compounds with many ionizable groups is very difficult, we demonstrated that the pK_as of Aβ 1-40 and 1-42 can be estimated from the pK_a values determined for their building peptide fragments. In addition, the electrophoretic migration of the Aβ peptides was predicted with the classical semiempirical models relating the electrophoretic mobility (m_e) to the charge-to-molecular mass ratio ($q/M_r^{1/2}$, for the classical polymer model), which can be easily calculated if adequate pK_a values are

available. The optimum pH for the separation of the mixture of Aβ peptides was successfully selected with the quality criteria $S_{i,j}$ and T' and it was demonstrated that it is possible to use as a pH optimization variable both the m_e of the Aβ peptides or their $q/M_r^{1/2}$.

A major limitation of CE is the relatively poor concentration sensitivity for most analytes due to the small sample volume that can be injected in the separation capillary. In this thesis, we have developed different on-line solid-phase extraction capillary electrophoresis-mass spectrometry (SPE-CE-MS) methodologies to improve the selectivity and the sensitivity for the analysis of several biomarkers of interest, in their intact or enzymatically digested forms. In SPE-CE, analytes from a large volume of sample (~25-200 µL) are retained on a sorbent contained in a microcartridge. In unidirectional SPE-CE, the most typical configuration, the microcartridge is mounted in series to the separation capillary, inserted near the capillary inlet. After sample loading, the microcartridge is washed to remove non-selectively retained molecules. Then, the retained analytes are desorbed in a small volume of eluent (~50-100 nL), resulting in sample clean-up and concentration enhancement before electrophoretic separation and detection. Nowadays, conventional chromatographic (e.g. C_8, C_{18}, polymeric with hydrophilic-lipophilic balance, etc.) particle sorbents, are the most widely applied sorbents in SPE-CE. However, their major drawback is their limited selectivity. In the present thesis, sorbents with improved selectivity, such as immunoaffinity (IA), aptamer affinity (AA), immobilized metal affinity (IMA) and silicon carbide (SiC) sorbents have been explored in unidirectional SPE-CE-MS for the analysis of protein and miRNA biomarkers in biological fluids.

IA-SPE-CE-MS has been investigated for the analysis of human serum transthyretin (TTR), an oligomeric protein related to different types of amyloidosis. The most common hereditary systemic amyloidosis is familial amyloidotic polyneuropathy type I (FAP-I), which is associated with a TTR variant that presents a single amino acid substitution of valine for methionine at position 30 (Met30). First, we developed a method for the analysis of serum TTR based on off-line immunoprecipitation with different immunoaffinity magnetic particles (IA-MBs) and CE-MS. Compared to the off-line method, IA-SPE-CE-MS allowed increasing the

throughput and reducing the consumption of IA-MBs. Under the optimized conditions with TTR standards, repeatability for migration time (t_m) and peak area (A_p) was acceptable (the percent relative standard deviation (%RSD) (n = 3) was 2.9 and 4.3%, respectively), microcartridge lifetime was good (>20 analyses in the same day), the method was linear between 5 and 25 µg/mL and LOD was around 1 µg/mL (25 times lower than by CE-MS, 25 µg/mL). For the analysis of serum samples by IA-SPE-CE-MS, a simple off-line sample pretreatment based on precipitation of the most abundant proteins with 5% (v/v) of phenol was necessary to clean-up the samples. Using this sample pretreatment, t_m increased compared to the analysis of TTR standards due to irreversible adsorption of matrix components in the inner wall of the separation capillary. Nevertheless, results were repeatable in terms of t_m and A_p (%RSD (n = 3) was 4.7 and 3.2%) and microcartridge lifetime was >10 analyses during the same day. In serum samples from healthy controls, the five most abundant proteoforms of normal TTR were detected. In FAP-I patients samples, the main mutant TTR(Met30) proteoform (TTR(Met30)-Cys) was unequivocally detected, demonstrating the potential of the IA-SPE-CE-MS method to screen serum samples for FAP-I.

AA-SPE-CE-MS has been demonstrated for the first time and applied for the analysis of blood α-synuclein, which is a potential biomarker of Parkinson's disease. For α-syn standards the only detected proteoform was free α-syn, repeatability for t_m and A_p was acceptable (%RSD (n = 3) was 2.1 and 5.4%), microcartridge lifetime was good (around 20 analyses in the same day), the method was linear between 0.5 and 10 µg/mL and LOD was 0.2 µg/mL (100 times lower than by CE-MS, 20 µg/mL). The method was subsequently applied to the analysis of endogenous α-syn in erythrocyte lysate samples, requiring an off-line thermal pretreatment in order to remove the most abundant proteins. Similar to the analysis of serum samples by IA-SPE-CE-MS, the inner wall of the separation capillary was modified due to irreversible adsorption of sample matrix components. Compared to the analysis of α-syn standards, repeatability was slightly poorer (%RSD (n = 3) was 6.7 and 10.8% for t_m and A_p), microcartridge lifetime was shorter (around 10 analyses in the same day) and non-specific adsorption in the AA sorbent of mainly ubiquitin was observed. N-acetylated α-syn was detected to be the main proteoform in healthy controls and

stage III-IV Parkinson's disease patient samples, and no other minor proteoforms were detected. Therefore, no apparent alteration of blood α-syn proteoforms at the level of a few hundreds of ng/mL seems to occur during Parkinson's disease.

IMA-SPE-CE-MS with a Ni(II) sorbent has been investigated for the selective enrichment of histidine containing peptides (His-peptides) in order to reduce the complexity of the protein digests generated in bottom-up proteomic studies. The method was optimized and validated with tryptic digests of α-casein (α-CSN). Under the optimized conditions, repeatability for t_m and A_p was good (%RSD (n = 3) were <3.0 and <11%) but microcartridge lifetime was short (10 analyses). Preconcentration factors for the detected His-peptides ranged from 25 to 98. The IMA sorbent showed selectivity towards short His-peptides, which was confirmed analyzing β-casein (β-CSN) and κ-casein (κ-CSN) after digestion with trypsin and trypsin:chymotrypsin mixture. The IMA-SPE-CE-MS method was evaluated for the analysis of complex biological samples with a tryptic digest of a cell lysate of *Escherichia coli* that expresses human α-lactalbumin with a polyhistidine-tag (His-tag). Short His-peptides, mainly between 2 and 4 amino acids long, and the α-lactalbumin His-tagged peptide were identified, indicating the potential of the methodology to specifically map certain regions of the proteomes and analyze His-tagged compounds.

SiC-SPE-CE-MS has been investigated for the analysis of miRNAs and their post-transcriptional modifications in serum. MiRNAs are single-stranded, 19–23 nucleotides long, non-protein-coding RNAs, that regulate messenger RNA. Alterations in the sequences and concentrations of miRNAs has been associated with different diseases, especially cancer, such as B-cell chronic lymphocytic leukemia (CLL). The SiC-SPE-CE-MS method was optimized with hsa-miR-21-5p and hsa-let-7g-5p standards. Under the optimized conditions, repeatability for the t_m and A_p (%RSD (n = 3) was 2.8 and <6.5%) and the microcartridge lifetime (>25 analyses) were good. The method was linear between 25 and 100 nM and LOD was around 10 nM (50 times lower than by CE-MS, 500 nM). To analyze serum samples, an off-line sample pretreatment based on phenol-chloroform-isoamyl alcohol extraction was necessary prior to SiC-SPE-CE-MS. The potential of the method to screen for CLL was demonstrated by the analysis of serum samples from healthy controls and patients. MiRNAs, specifically hsa-miR-21-5p and a 23 nucleotide long

5’-phosphorylated miRNA with 3’-uridylation (hsa-iso-miR-16-5p), were only detected in the CLL patient samples.

Unidirectional SPE-CE-MS is straightforward to implement. However, this simple setup has some inherent limitations. On the one hand, the sample volumes introduced using pressure depend on the dimensions of the separation capillary. On the other hand, sample loading is conducted in the same direction as the subsequent separation. Therefore, some of the matrix components could be irreversibly adsorbed in the inner wall of the separation capillary. Furthermore, in many cases, the requirements of on-line preconcentration are incompatible with the BGE necessary for an efficient separation or sensitive MS detection. In order to overcome these drawbacks, we have investigated SPE-CE-MS with a nanoliter valve (nvSPE-CE-MS), a novel setup that uses an electrically isolated 4-port valve with an internal nanoliter loop. NvSPE-CE-MS is operated with a single CE instrument and two capillaries for independent and orthogonal SPE clean-up, preconcentration and electrophoretic separation.

First, the analysis of a set of opioid peptides and Aβ peptide fragments by CE-MS was evaluated. Then, a unidirectional SPE-CE-MS method with a C18 sorbent for the analysis of opioid peptides previously developed by our research group was adapted to the new instrumentation. Finally, a nvSPE-CE-MS method was developed and compared to the unidirectional SPE-CE-MS for the analysis of opioid peptides and Aβ peptide fragments in standards and plasma samples. NvSPE-CE-MS allowed using different capillary dimensions for loading and separation, without flushing the sample through the separation capillary. With regard to CE-MS, nvSPE-CE-MS allowed decreasing the LODs 200 times. Compared to unidirectional SPE-CE-MS, peak efficiencies were better and repeatabilities similar, but total analysis times were longer and LODs were 5 times higher for opioid peptides standards due to the heart-cut operation and the limited volume of the valve loop (20 nL). Nevertheless, the LODs of both methodologies for the analysis plasma samples were similar, indicating a lower effect of the plasma sample matrix in the analysis by nvSPE-CE-MS.

Abstract

New strategies for high-throughput bottom-up analysis of proteins have also been investigated. Tryptic digestion has been traditionally conducted in solution and requires long digestion times. In contrast, immobilized enzymes allow decreasing the sample volume and the total digestion times, minimize the sample handling, improve the digestion yields, as well as to stabilize the enzyme, avoid its autoproteolysis and simplify its recovery making it reusable. In this thesis, we have investigated on-line immobilized enzyme microreactor capillary electrophoresis-mass spectrometry (IMER-CE-MS) using microreactors packed with immobilized trypsin particles. First, the off-line digestion of β-lactoglobulin (β-LG) with trypsin in solution and immobilized trypsin, both followed by CE-MS analysis, were optimized. Then, the IMER-CE-MS methodology was also optimized with β-LG. Under the optimized conditions, the LOD for complete sequence coverage of β-LG was around 10 μg/mL, the repeatability was comparable to the off-line digestion methods (%RSD (n = 3) was ≤7.6% for t_m and ≤15% for A_p) and the microreactor could be reused until 30 times. The developed method was validated with α-CSN, β-CSN, κ-CSN and a cell lysate of *Escherichia coli*, and sequence coverages were comparable to the off-line digestion methods.

Aims

This doctoral thesis is focused on the development of analytical methodologies based on capillary electrophoresis-mass spectrometry (CE-MS) for the separation, detection, characterization and quantification of peptide, protein and microRNA biomarkers in biological samples. Specifically, it adresses the analysis of amyloid beta (Aβ) peptides, which form plaques in Alzheimer's disease, transthyretin (TTR), an oligomeric protein related to familial amyloidotic polyneuropathy type-I (FAP-I), α-synuclein (α-syn), which is a major component of the protein deposits found in Parkinson's disease, and microRNAs, which have been associated with cancer.

Different strategies to predict and optimize the separation of complex mixtures of ionizable peptide biomarkers in CE are presented. In addition, on-line solid-phase extraction capillary electrophoresis-mass spectrometry (SPE-CE-MS) methodologies are developed in order to improve the selectivity and the sensitivity for the analysis of the biomarkers of interest in their intact or enzymatically digested forms. Finally, on-line immobilized enzyme microreactor capillary electrophoresis-mass spectrometry (IMER-CE-MS) is investigated for the high-throughput bottom-up analysis of proteins.

In order to achieve these main objectives, the work plan has been the following:

- Novel developments for prediction and optimization of separations in CE:
    - Determination of the electrophoretic behavior and the acidity constants of five Aβ peptide fragments by CE with ultraviolet spectrophotometry detection. Estimation of the acidity constants of Aβ 1-40 and 1-42 from the pK_a values previously determined for their fragments.
    - Prediction of the electrophoretic migration of the Aβ peptides with the classical semiempirical models and selection of the optimum pH for their separation with the quality criteria $S_{i,j}$ and T'.

- Improving the sensitivity and the selectivity by SPE-CE-MS:
  - Development of an on-line immunoaffinity-SPE-CE-MS method for the analysis of human serum TTR. Characterization of TTR proteoforms in order to distinguish between healthy controls and FAP-I patients.
  - Development of an aptamer affinity-SPE-CE-MS method for the analysis of α-syn in blood samples from healthy controls and Parkinson's disease patients. Characterization of blood α-syn and evaluation of its suitablity as a biomarker.
  - Investigation of immobilized metal affinity-SPE-CE-MS with a Ni(II) sorbent for the selective enrichment of histidine containing peptides. Optimization with model proteins and application for the analysis of complex protein digests.
  - Development of a SPE-CE-MS method with a silicon carbide sorbent for the analysis of microRNAs and their post-transcriptional modifications in serum samples from healthy controls and patients with B-cell chronic lymphocytic leukemia. Investigation of miRNA expression signatures to screen for this cancer type.
  - Investigation of SPE-CE-MS with a nanoliter valve. Application to the analysis of opioid peptides and Aβ peptide fragments in human plasma samples using a C18 sorbent. Evaluation of advantages and disadvantages compared to unidirectional SPE-CE-MS.

- High-throughput bottom-up analysis of proteins by IMER-CE-MS:
  - Development of an IMER-CE-MS method for the straightforward, rapid and efficient bottom-up analysis of proteins. Application for the analysis of complex protein mixtures.

Chapter 1. Introduction

1.1. Omics sciences

The term omics refers to any field of study addressed to identify, characterize and quantify biological molecules, as well as to explore their roles, relationships and action in a biological system. Conventional omics sciences are primarily aimed at the universal detection of genes (genomics), messenger ribonucleic acid (mRNA; transcriptomics), proteins (proteomics) and metabolites (metabolomics) (**Figure 1.1**) [1,2]. Nevertheless, new fields are constantly being added, such as the study of lipids (lipidomics), glycans (glycomics) and microRNAs (miRNomics) [3–5]. The different omics sciences provide information that complements each other. Furthermore, they can be applied not only for the greater knowledge of normal physiological processes, but also for screening, diagnosis and prognosis of diseases as well as for the understanding of the causes.

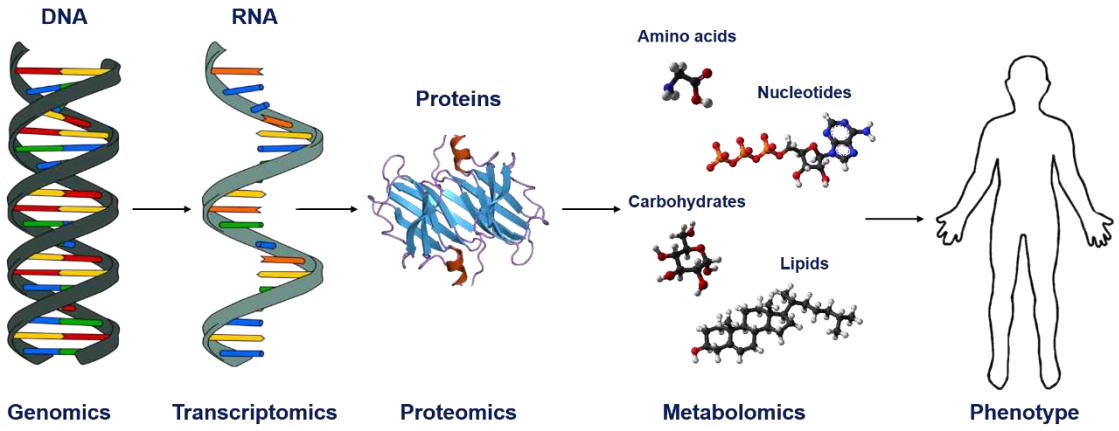

Figure 1.1. Conventional omics sciences and their interaction.

The first omic science developed was genomics. Genomics studies the structure, function, evolution and mapping of the complete set of deoxyribonucleic acid (DNA) (i.e. genome) in an organism and aims at the characterization and quantification of genes. With the advent of massive parallel sequencing technology, also known as next-generation sequencing (NGS), the acquisition of genome-scale data has never been easier, expanding the ability to analyze and understand whole genomes [6]. For its part, transcriptomics deals with the study of the complete set of RNA

transcripts produced by the genome (i.e. transcriptome), which direct the production of proteins. Amongst proteins, are found the enzymes that catalyze the reactions of the metabolic pathways involving the low molecular mass molecule set known as metabolome.

1.1.1. Proteomics

Proteomics is the study of all sets of proteins in a biological system (i.e. proteome), including their identification, characterization, quantification and functional roles [2]. Proteins suffer continuous modifications due to interactions with other molecules through complex biochemical networks. Furthermore, protein expression is affected by cellular response to environmental factors and health. Therefore, changes in protein abundances and function can be attributed not only to altered gene expression but also to multiple co-translational and post-translational mechanisms [7,8]. A proteoform consists of a specific molecular form of a protein produced from a specific gene. The study of proteoforms includes isoforms, post-translational modifications (PTMs) and multiproteoform complexes (**Figure 1.2**) [9,10].

		Definition	Example
Proteoforms	**Isoform**	A specific molecular form with a unique primary amino acid sequence	Albumin (P02768) 
	Post-translational modification (PTM) [a]	A specific isoform including chemical modifications after protein synthesis (e.g. N-terminal acetylation)	N-acetylated α-syn (P37840) 
	Multiproteoform complex	A protein complex formed by the association of several proteoforms	Pyruvate kinase (P14618) 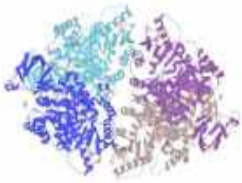

[a] Molecular forms generated by co-translational modification are in general included in this category.

Figure 1.2. Nomenclature in proteomics.

In particular, PTMs greatly contribute to the much larger diversity of proteins than genes. PTMs increase the functional diversity of the proteome by modifying proteins through the covalent addition of functional groups (e.g. acetylation, phosphorylation and glycosylation) or other proteins and peptides (e.g. SUMOylation and ubiquitination), redox reactions (e.g. formation of disulphide bonds), or proteolytic cleavage (e.g. specific cleavage of precursor proteins) [11]. These modifications influence almost all aspects of normal cell biology including protein activation, transport, degradation and pathogenesis [11]. Therefore, identifying and characterizing protein proteoforms with high throughput and on a large scale is critical in the study of cell biology and disease treatment and prevention. In this regard, the core of modern proteomics is mass spectrometry (MS) and hyphenated separation techniques (i.e. liquid chromatography-tandem mass spectrometry (LC-MS/MS) and capillary electrophoresis-tandem mass spectrometry (CE-MS/MS)) [12–14]. The reasons for MS success in proteomics include its inherent specificity of identification, the generic nature of the proteomics workflow and its potential for extreme sensitivity and detailed characterization [12]. However, the goal of profiling proteins represents an analytical challenge, mainly due to the structural protein complexity, the heterogeneity of biological samples and the wide range of relative abundances of the different proteins (i.e. dynamic range) [15].

MS-based proteomics methods fall into two main complementary approaches (**Figure 1.3**). The most common approach is bottom-up proteomics that provides an indirect analysis of the proteins through peptides derived from proteolytic digestion [16]. Typically, bottom-up proteomics methods use individual proteases or protease mixtures to cleave proteins selectively at multiple amino acid sites to produce a mixture of small peptides. Optimum peptide length for bottom-up MS-proteomics is considered to be 6–25 amino acid residues (relative molecular mass (M_r) < 3,000) for effective computational analysis. Therefore, the most typically used proteolytic enzyme is trypsin, which cleaves proteins at the carboxyl-terminal side of lysine and arginine residues, resulting in peptides with an average length of 14 amino acids [16,17]. The bottom-up approach offers multiple advantages including increased separation efficiency and limited number of charges on each peptide, which are all beneficial for MS detection. However, it has also some

limitations. Since proteins often contain homologous sequence regions, a number of the identified peptides can reasonably emanate from more than one protein. In addition, large regions of the protein may not be identified, which can leave behind important information regarding isoforms and PTMs.

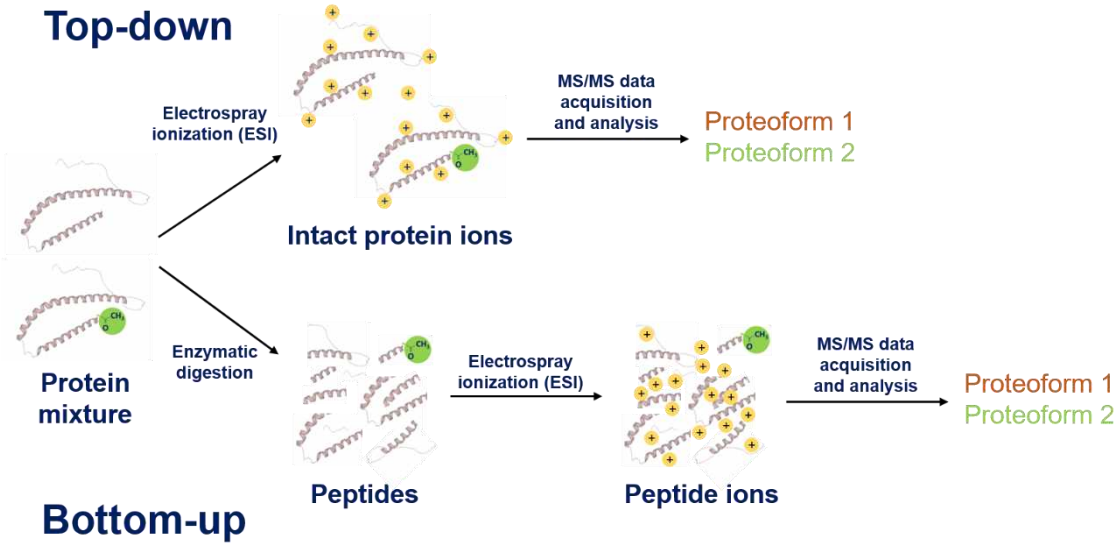

Figure 1.3. Top-down (intact proteins) and bottom-up (peptides) proteomics based on MS/MS analysis.

Top-down proteomics seeks to overcome these major drawbacks by analyzing the intact proteins and its fragment ions by MS/MS. This approach potentially allows the complete sequence coverage and the direct detection of PTMs, providing a more in-depth understanding of the action of specific proteoforms in vivo [10,18]. However, it is subject to many analytical challenges owing to the low abundance of many proteoforms and the difficulty in ionizing and measuring the mass of large molecules. Anyway, top-down proteomics is regarded as a powerful alternative that complements the digestion-based approaches. Recent advances in high performance separation techniques and the advent of high-sensitivity, high-resolution and high-accuracy mass spectrometers has paved the way for high-throughput top-down MS proteomics [18–20].

Despite all these technological advances, top-down MS proteomics is extremely challenging. For this reason, in recent years, a hybrid of bottom-up and top-down approaches has been introduced as middle-down proteomics [21,22]. This approach analyzes larger peptide

fragments (usually M_r >7,000) than bottom-up proteomics, minimizing peptide redundancy between proteins. Additionally, larger peptide fragments yield similar advantages as top-down proteomics, such as gaining further insight into PTMs, without the analytical challenges of analyzing intact proteins [22].

Bottom-up, middle-down and top-down proteomics approaches can be addressed using targeted or untargeted analysis [23] . Targeted proteomics provides information for a predefined list of proteins and the selected analytical method can be established using commercially available standards or chemically synthesized compounds. Targeted strategies offer higher sensitivity, accuracy and reproducibility than untargeted approaches [23,24]. In this regard, targeted strategies are especially preferable for the analysis of proteins found at low concentrations, which often play important roles in biological systems [23,24].

Untargeted proteomics or global profiling aims at identifying and/or quantifying of as many proteins as possible in order to obtain a comprehensive profile or fingerprint of a biological sample. Untargeted proteomics can implicate previously unrecognized proteins and, therefore, it is a powerful strategy to elucidate novel biomarkers and gain insight into disease pathogenesis [23,25]. However, the most difficult tasks in untargeted approaches are the simultaneous analysis of a broad range of proteins with different properties and concentrations, as well as the identification of unknowns. Furthermore, it is practically impossible to detect all the proteins present in a biological sample with a single analysis [26].

The current magnitude of the proteomic data obtained by the research community can be assessed in several databases, including UniProt (https://www.uniprot.org), a freely accessible database of protein sequence and functional information derived from the research literature. UniProtKB/Swiss-Prot release “2020_01” (26 February 2020) contains 561,911 sequence entries, of which 102,492 there are evidences of existence at protein level.

1.1.2. MiRNomics

In recent years, microRNAs (miRNAs), a class of single-stranded, 19-23 nucleotides long, non-protein-coding RNA molecules, have received great notoriety. MiRNAs were discovered in 1993 by joint efforts of Ambros and Ruvkun groups [27,28]. Since then, thousands of miRNAs have been identified. In miRBase (release 22.1, October 2018), which is a comprehensive database of miRNA sequences and expression, are listed more than 30,000 mature miRNA sequences, and about 2,600 are human (http://www.mirbase.org) [29].

MiRNAs play a major role in controlling post-transcriptional regulation by targeting the 3′ untranslated region of specific mRNAs for degradation or inhibition of translation initiation (**Figure 1.4**) [30,31]. Mature miRNA is incorporated into the ribonucleoprotein RNA-induced silencing complex (RISC) to bind the target mRNAs, causing mRNA degradation or a block in translation depending on the level of complementarity. Therefore, miRNAs are very powerful regulators involved in a wide range of normal cellular processes, including cell proliferation, development and apoptosis [30].

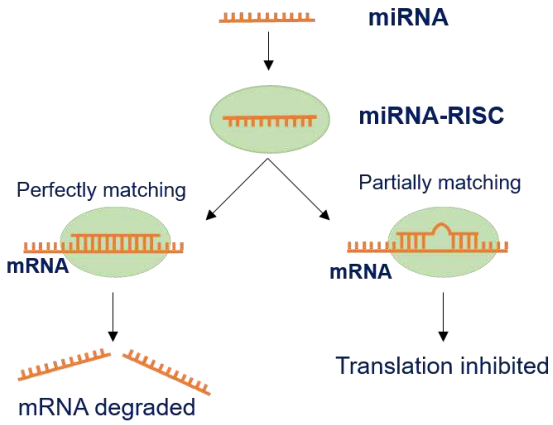

Figure 1.4. MicroRNA biological function.

MiRNAs can undergo several post-transcriptional modifications, including the covalent addition of functional groups (e.g. 5'-end phosphorylation [32] and adenosine methylation [33]) and the generation of variant miRNA sequences, known as isomiRs, due to 5'-trimming and 3'-nucleotide addition [32]. These modifications have been reported to affect the stability of

miRNAs and to be a mechanism for the regulation of miRNA activity [34,35]. Alterations in the sequences, post-transcriptional modifications and concentrations of miRNAs can perturb a great number of cell signaling pathways and has been associated with different diseases, such as cardiovascular diseases [36], diabetes [37], aberrant immune function and especially cancer [30,31]. It has been established that some miRNAs are overexpressed or downregulated exclusively or preferentially in certain cancer types [38,39].

MiRNAs have been found in the extracellular environment, including in various biological fluids, such as serum [40,41], saliva [42] and urine [43]. The circulating miRNAs are packaged in exosomes [42,44] or associated with RNA-binding proteins [45], leading to high stability and resistance to endogenous RNase activity, extreme temperature and pH [41]. The presence and stability of miRNAs in accessible biofluids, their specificity and the relatively low number of candidate sequences due to their small size, make miRNAs useful biomarkers for diagnostic, follow-up and prognostic purposes with robustness and reproducibility. However, the concentration of circulating miRNAs is extremely low and hence amplification of the starting material and/or highly sensitive techniques are necessary. The entire RNA sequencing by NGS [46] is a high-throughput untargeted assay but it is expensive and may produce sequence-specific biases owing to adaptor ligation steps in RNA library preparation [47]. As an alternative to NGS, the current routine methods for miRNAs analysis include northern blotting [48], microarrays [49] and reverse transcription–quantitative polymerase chain reaction (RT-qPCR) [50], which is the gold standard. These methods only allow indirect identification of the targeted miRNA sequences [51,52] and each of them have their own specific limitations. Northern blotting is relatively time consuming and requires a high amount of sample [52] and microarrays are expensive and relatively limited in terms of sensitivity and specificity [53]. RT-qPCR is very sensitive but it does not provide information related to post-transcriptional modifications of miRNAs [32]. Due to these limitations, the development of more efficient and low-cost direct, label-free and multiplex methods for the analysis of miRNAs is of great interest.

1.2. Biomarker discovery

The Food and Drug administration (FDA) and the National Institutes of Health (NIH) of the United States of America have defined a biological marker (biomarker) as "a defined characteristic that is measured as an indicator of normal biological processes, pathogenic processes, or responses to an exposure or intervention, including therapeutic treatments" [54]. Biomarkers are of great interest in early detection and diagnosis of several diseases as well as a prognosis, prediction and monitoring tool. Over the past decades, there has been a growing interest in applying proteomics strategies to search for novel biomarkers related to neurodegenerative diseases [55,56]. In the case of miRNAs, their recent discovery has captured increased attention of researchers as cancer biomarkers [57,58]. The goal of current research is to identify a biomarker or a panel of biomarkers that could allow a non-invasive and cost-effective diagnosis, follow-up and prognosis, as well as monitoring and developing treatments. The measurement of biomarkers in biological fluids is usually preferred because of the homogeneity of the sample and the easy accessibility in the case of blood, serum, plasma, urine, saliva or tears [54,56–58]. This thesis in particular will present novel targeted strategies for the analysis of protein biomarkers related to neurodegenerative diseases and miRNA biomarkers related to cancer in biological fluids.

1.2.1. Neurodegenerative diseases

Neurodegenerative diseases are disorders characterized by the deterioration of nerve cells [59,60]. These diseases primarily occur in the later stages of life and have a chronic and progressive nature [59]. There are no specific cures because the neurons and the synaptic connections cannot regenerate after damage. Several neurodegenerative diseases, such as Alzheimer's disease (AD), Parkinson's disease (PD), amyotrophic lateral sclerosis, Huntington's disease and familial amyloidotic polyneuropathy (FAP), are associated with protein misfolding, oligomerization, aggregation, deposition and accumulation in the brain [59,60]. Nowadays, diagnosis of these proteopathies is primarily made on clinical grounds including

neuropsychological testing and brain imaging, which often lead to misdiagnosis or late diagnosis. Therefore, there is an urgent need to develop a more reliable approach based on the detailed analysis of the involved protein biomarkers.

Although the protein biomarkers associated to these neurodegenerative diseases do not exhibit obvious similarities in terms of sequence, size, structure, expression level, or function, the process of protein misfolding and aggregation is remarkably similar. All these proteins undergo misfolding, which can be promoted by amino acid substitutions, PTMs, sequence expansions or truncations and environmental changes such as temperature and pH. They transit from their native states to form highly ordered aggregates known as amyloids [61]. The mechanism of aggregation of misfolded proteins to form amyloid fibrils is thought to be best described by the seeding–nucleation model (**Figure 1.5**) [61,62]. During this process, misfolded protein form aggregation-prone structures that oligomerize and grow by an autocatalytic mechanism. Once the amyloid fibrils are formed, they can fragment in a not well-understood process to generate more seeds to propagate the reaction, hence the growth of the amyloid aggregate.

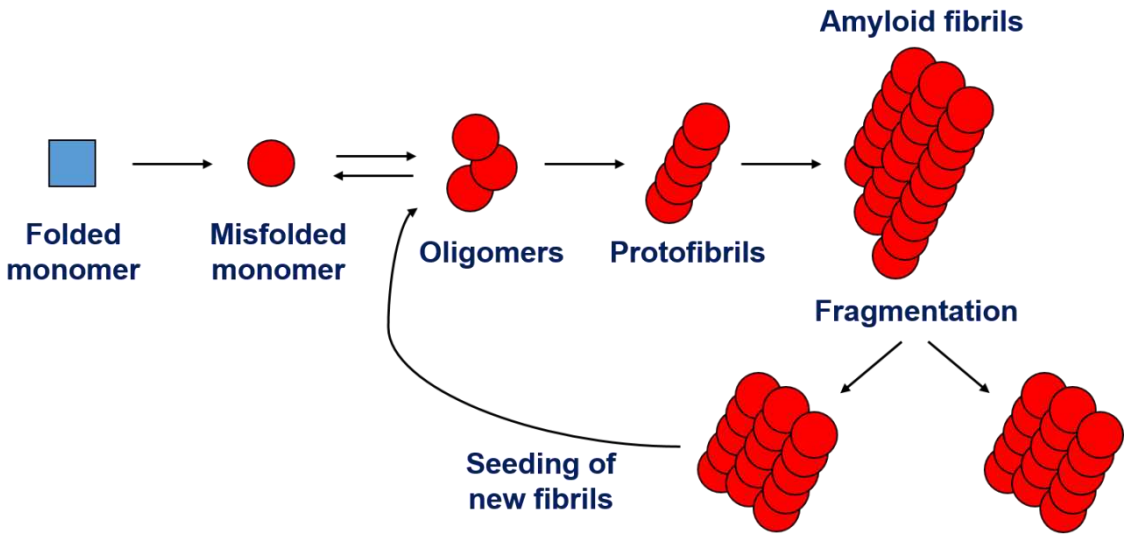

Figure 1.5. Seeding–nucleation model for the aggregation of misfolded proteins in amyloid neurodegenerative diseases.

The protein biomarkers forming amyloid deposits in some relevant amyloid neurodegenerative diseases are shown in **Table 1.1**.

Table 1.1. Protein biomarkers deposited in some relevant amyloid neurodegenerative diseases.

Protein/peptide	Characteristic aggregates	Predominant location	Type	Disease	Reference
Amyloid beta (Aβ) 1-40/1-42	Amyloid plaques	Brain extracellular space	Acquired	Sporadic Alzheimer's disease	[63]
		Cerebral blood vessel walls	Hereditary	Hereditary cerebral amyloid angiopathy	[64]
Tau	Neurofibrillary tangles	Neurons	Acquired	Sporadic Alzheimer's disease	[63]
			Acquired	Pick's disease	[65]
α-synuclein (α-syn)	Lewy bodies and neurites	Neurons	Acquired	Parkinson's disease	[66]
		Glial cells	Acquired	Multiple system atrophy	[67]
Prion protein	Spongiform change and amyloid plaques	Brain extracellular space	Acquired	Sporadic Creutzfeldt–Jakob disease	[68]
			Hereditary	Familial Creutzfeldt–Jakob disease	[68]
Superoxide dismutase I	Inclusion bodies	Neurons	Acquired	Amyotrophic lateral sclerosis	[69]
Huntingtin	Inclusion bodies	Neurons	Hereditary	Huntington's disease	[70]
Transthyretin (TTR)	Amyloid plaques	Systemic	Hereditary	Familial amyloidotic polyneuropathy	[71]
		Systemic	Acquired	Senile systemic amyloidosis	[71]

Amyloid beta (Aβ) peptide fibrils are the major component of the amyloid plaques found in the brain extracellular space of patients with AD [63]. AD, first reported by Alois Alzheimer in 1906 [72], is nowadays the most common neurodegenerative disease, affecting the 10% of people at age 65 and older, and the cause of 60 to 80% of cases of dementia [73]. In the USA, the costs of health care and long-term care for individuals with dementia were estimated $290 billion in 2019 [73]. AD is a slowly progressive brain disease that begins many years before symptoms emerge. It causes symptoms of dementia such as memory loss, difficulty performing daily activities and changes in judgement, reasoning, behavior and emotions [74]. Therefore, there is a considerable interest about molecular biomarkers related to AD, including Aβ peptides.

Aβ peptides are generated by proteolysis of the much larger amyloid precursor protein, which is cleaved by different secretase enzymes to yield different peptides such as Aβ 1-42 and carboxyl-terminal truncated fragments down to Aβ 1-13 [75]. Aβ 1-40 and 1-42 (M_r~4,000) are the most common Aβ peptides, being the longer form with two additional hydrophobic amino acids the most fibrillogenic [76,77]. Nowadays, Aβ 1-40 and 1-42 in cerebrospinal fluid (CSF) and plasma are established biomarkers for AD [75,78,79]. However, the relevance of the Aβ fragments for the pathogenesis of AD remains largely understudied. Current bioanalytical immunoassay methods provide adequate analytical sensitivity, but they are not able to reliably distinguish Aβ 1-40 and 1-42 peptides from their fragments, which may present different solubility and fibrillogenic properties [80,81]. Therefore, it is critical to develop new methods for the characterization and the unequivocal detection of the Aβ peptides and their fragments in biological fluids.

α-synuclein (α-syn) is a protein composed of 140 amino acids (M_r~14,500), present at high levels in the brain, where it is mainly localized in presynaptic terminals of nerve cells [82]. Recent research supports the physiological existence of α-syn multimers, especially tetramers, in addition to the widely accepted monomers, but these results have generated some controversy [83]. α-syn is a major component of Lewy bodies, the intracellular protein aggregates in neurons that represent the morphological hallmark of PD and other synucleinopathies [66,84]. PD, first

medically described by James Parkinson in 1817 [85], is one the most common progressive neurodegenerative motor disorders, with a prevalence of ~2% in people over 65 years of age [86]. PD is characterized by tremor, slowness or rigidity and may evolve to various degrees of dementia during the disease course [87].

The potential of certain α-syn proteoforms as biomarkers for PD is continuously investigated. In this regard, α-syn presents numerous PTMs as phosphorylation, ubiquitination, nitration and acetylation [66,84,88]. Phosphorylated α-syn at Ser-129 is the major component (~90% of α-syn) in the Lewy bodies [66]. In contrast, this proteoform involves only about 4% of normal α-syn in normal brain cytosol [66]. Full length N-terminal acetylated α-syn is the main proteoform of normal α-syn [84]. α-Syn has been frequently analyzed in brain tissue or CSF [82,84]. However, more accessible biofluids, such as blood, are also being investigated [82,89], where it is still necessary to broaden the knowledge about the different proteoforms using sensitive and selective analytical methods.

Native transthyretin (TTR) is a homotetrameric protein composed of four identical, non-covalently associated subunits. Each monomer consists of 127 amino acid residues (M_r~13,800). TTR is predominantly expressed in the liver and in the choroid plexus of the brain and it is highly abundant in serum (200-400 µg/mL) [90]. Some of the many point mutations that are currently known in the TTR-gene are related to different types of hereditary TTR amyloidosis, characterized by amyloid deposition mainly in the peripheral nervous system and the heart [71]. The most common hereditary systemic amyloidosis is familial amyloidotic polyneuropathy type I (FAP-I), which was first identified by Corino Andrade in 1952 [91]. FAP-I is associated with a TTR variant that presents a single amino acid substitution of valine for methionine at position 30 (Met30) [71]. FAP-I is a fatal disease and liver transplantation is the most promising therapy today [71].

In addition to the existence of isoforms, this protein presents numerous PTMs, many of them related to a cysteine residue at position 10 (Cys10) of the monomer. The most common PTMs related to Cys10 are S-cysteinylation (TTR-Cys), S-sulfonation (TTR-Sulfonated), S-

glycinylcysteinylation (TTR-CysGly), S-glutamylcysteinylation (TTR-CysGlu), S-glutathionylation (TTR-Glutathione) and oxidation to glycine ((10) C-G) or cysteine sulfinic acid (TTR-Sulfinic) [92]. Other PTMs are phosphorylation (TTR-Phosphorylated) and dehydroxylation (TTR-Dehydroxylated).

Nowadays, diagnosis of FAP-I is based on clinical genetic testing [71]. In the last years, a special effort has been placed on the analysis of TTR as a biomarker for FAP-I in biological fluids to confirm diagnosis, but specially to clarify the aggregation mechanism, which may have implications in predicting the onset and developing new treatments [71,93].

The present thesis will describe new strategies based on CE and MS for the separation and characterization of Aβ peptides, α-syn and TTR in blood-derived samples (i.e. plasma, erythrocytes and serum, respectively).

1.2.2. Cancer. B-cell chronic lymphocytic leukemia

Cancer comprise a group of diseases characterized by abnormal cell growth with the potential to invade or spread to other parts of the body [94]. Their development and progress are believed to be due to genetic alterations that disrupt normal cellular processes such as cell cycle, DNA damage response, survival and migration [95]. Cancer is a leading cause of death, with estimations of mortality around 10 million worldwide in 2018 [96].

There are evidences that miRNA expression is dysregulated in cancer [31]. The earliest indication of miRNA involvement in human cancer was reported in studies attempting to identify tumor suppressors in B-cell chronic lymphocytic leukemia (CLL). CLL is characterized by the accumulation of a clonal population of small mature B-lymphocytes in blood, bone marrow and lymphoid organs and is the most common hematological malignancy in Western countries [97]. Calin et al. found frequent deletion and down-regulation of two miRNA genes, miR-15 and miR-16, in CLL patients [98], and distinctive miRNA expression signatures were also found in other malignant tissues from cancer patients [38,39]. In these studies, genome-wide profiling demonstrated that miRNA expression signatures can be used to discriminate different types of

cancer with high accuracy and that selective groups of miRNAs are commonly down-regulated or up-regulated in different types of human cancers.

Aberrant expression of miRNAs in plasma and serum has emerged as diagnostic biomarker in patients with CLL. This thesis will describe new strategies based on CE and MS for the untargeted analysis of miRNAs and their post-transcriptional modifications in serum from CLL patients.

1.3. Analytical techniques

Novel sensitive and selective methods are required for the reliable analysis of biomarkers in biological samples. In this regard, MS is a powerful technique for the unequivocal identification of biomolecules due to its selectivity and potential with respect to the detailed structural characterization of unknown compounds. However, due to the complexity of most biological samples, the hyphenation of high-performance separation techniques is essential prior to MS analysis. Furthermore, separation prevents ion suppression, which combined with analyte detection as highly efficient peaks, allow enhanced sensitivity. In this respect, CE, and other microscale separation techniques such as capillary LC, nano LC and microchips, are proficient high-performance separation techniques when limited sample volumes are available [99,100]. In particular, CE-MS is regarded nowadays as a very suitable technique for the highly efficient separation and characterization of polar and charged biomolecules.

1.3.1. Capillary electrophoresis (CE)

Since the first introduction of CE in 1981 by Jorgenson and Lukacs [101], the technique has evolved into a versatile and powerful separation tool. Current CE applications range from determination of small inorganic ions to characterization of large biomolecules, particles or intact cells [99,102,103]. With the strong advent of biopharmaceuticals, CE has shown to be particularly useful for routine quality control of therapeutic proteins, such as peptide hormones and

monoclonal antibodies [104,105]. Another current niche in the pharmaceutical industry is chiral analysis [106].

CE has many desirable characteristics such as high separation efficiency, low consumption of sample and reagents, short analysis time, instrumental simplicity and full automation [99,103]. CE is also very versatile due to the several operation modes. The most common are capillary zone electrophoresis (CZE, in general referred to as CE), capillary gel electrophoresis (CGE), micellar electrokinetic chromatography (MEKC), capillary electrochromatography (CEC), capillary isoelectric focusing (CIEF) and isotachophoresis (ITP) [107]. This thesis will present methods based on CZE (from now on it will be referred to as simply CE) for the analysis of peptide, intact and digested protein and microRNA biomarkers.

1.3.1.1. Separation principles in CE

First described by Tiselius in the 1930s [108], electrophoresis is defined as the migration of charged species (ions) within an electrolyte solution under the influence of an electric field [109]. However, separation efficiency in free solution is limited by thermal diffusion and convection. In this regard, narrow capillaries have a large surface area-to-volume ratio enabling the efficient dissipation of the heat generated when very high electrical fields are applied [101].

CE is a microscale analytical technique where electrophoretic separation is performed in a fused silica capillary of small inner diameter (i.d.) (in general, between 50-75 μm i.d.) filled with an appropriate background electrolyte (BGE). CE instrumentation is relatively simple (**Figure 1.6**), roughly a high-voltage power source, two electrodes, a fused silica capillary and a detector.

In a typical CE experiment, sample solution (typically between 1 and 20 nL) is injected into the inlet end of the capillary filled with BGE, on the opposite side to the detector. Then, a high voltage is applied (typically between 10 and 30 kV) causing migration and separation of the ionic species along the capillary. The electrophoretic mobility (m_e) of a target solute ion is governed by its charge and size, as deduced from the following equation [107]:

$$m_e = \frac{q}{6\pi\eta r} \qquad \textbf{Eq. 1}$$

where q is the total ion charge, η is the viscosity of the BGE and r is the solvated ion radius, which is related to the size.

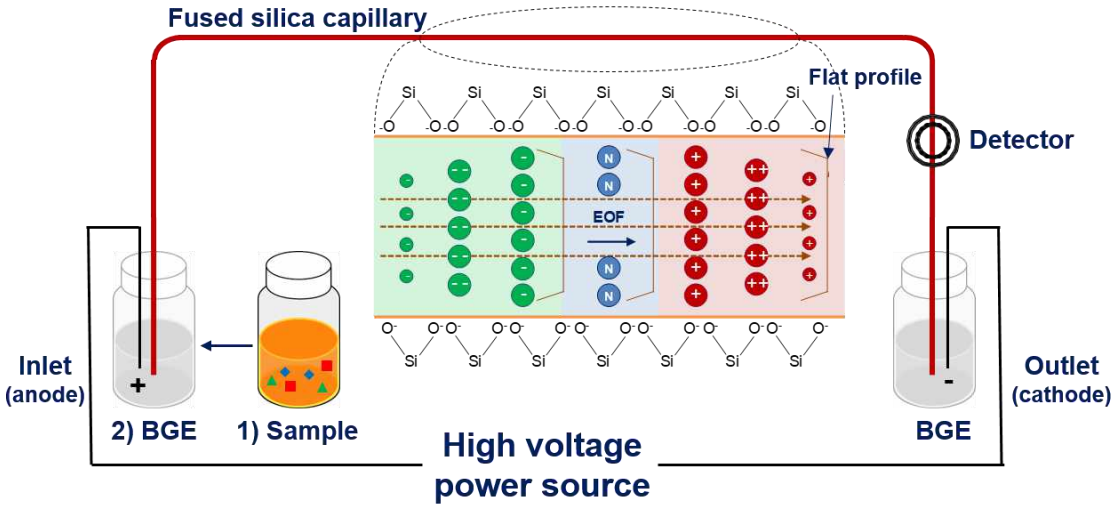

Figure 1.6. Basic components of CE instrumentation. The inset shows a schematic representation of the migration behavior of cations (positive charge), neutrals and anions (negative charge) in the fused silica capillary under the influence of the electric field (normal polarity, cathode at the outlet end). Small, highly charged species have higher mobilities than large, minimally charged species (see **Equation 1**).

In addition to the electrophoretic migration of charged species, another constituent of CE operation is the electroosmotic flow (EOF) (**Figure 1.6**). EOF is the bulkflow of liquid in the capillary as a consequence of the surface charge on the inner wall of the uncoated fused silica capillary. The inner wall of the capillary contain silanol groups (SiOH) that ionize at pH above 2. Therefore, using a BGE at a specific pH value, the inner wall present a certain amount of negative charges that favor the formation of a diffuse double-layer near the surface where counterions (cations) build up to maintain the charge balance. When voltage is applied, the counterions and their associated solvating water molecules migrate towards the cathode, at the capillary end where is placed the detector.

The generation of the EOF provides several advantages. Since the electro-driven force of the flow is uniformly distributed along the capillary, the velocity is nearly uniform. This flat flow velocity profile is beneficial since it does not contribute to the broadening of analyte zones. This contrasts with the flow velocity profile generated in pressure-driven systems, such as LC, where

frictional forces at the liquid–solid interface result in substantial pressure drops, generating a laminar flow with a parabolic flow velocity profile. Another benefit of the EOF is that it causes movement of all the species in the same direction (towards the cathode in a fused silica capillary). Therefore, cations, neutrals and many large anions can be analyzed in a single run since they all migrate to the detector (see inset in **Figure 1.6**). Cations migrate the fastest since their m_e towards the cathode and the EOF mobility (m_{EOF}) are in the same direction, neutrals migrate with the EOF and anions migrate after the EOF, if the m_{EOF} is higher than their own m_e towards the anode.

1.3.1.2. Determination of electrophoretic mobility and acid dissociation constants by CE

The m_e of a solute ion can be measured by CE as the difference between the apparent mobility (m_{app}, the sum of electrophoretic and electroosmotic contributions) and the m_{EOF}, measured using an appropriate neutral marker (e.g. acetone or dimethyl sulfoxide (DMSO) with ultraviolet (UV) detection) [110,111]:

$$m_e = m_{app} - m_{EOF} = \frac{L_T L_D}{V}\left(\frac{1}{t_m} - \frac{1}{t_{EOF}}\right) \qquad \textbf{Eq. 2}$$

where L_T is the total capillary length, L_D is the distance from the injection point to the detector and t_m and t_{EOF} are the migration time of the solute ion and the neutral marker, respectively.

The acid dissociation constant (K_a, or pK_a in minus logarithm scale) is a fundamental physicochemical characteristic of weak electrolytes (i.e. weak acids, bases and ampholytes) [110,111]. CE has been widely used for accurate determination of pK_a of a great variety of polyprotic compounds [110–115] and it is an excellent alternative to potentiometric [116], UV spectrophotometric [117] and nuclear magnetic resonance (NMR) determination [118]. CE is not limited by sample volume, purity or number of analytes, it can be fully automated and it allows a great versatility in the selection of the separation conditions. The CE determination of pK_as is usually performed measuring the m_e of the target solute ions as a function of pH within an

appropriate pH range using fused silica capillaries and, typically, with UV detection [112,119]. For this purpose, it is also necessary to establish relationships between pH, apparent pK_a (pK'_a) and m_e, as described below. The i[th] dissociation equilibrium for a generic polyprotic compound H_nX^z (n = total number of ionogenic groups and z = maximum positive net charge) can be represented as:

$$H_{n-(i-1)}X^{z-(i-1)} \leftrightarrow H_{n-i}X^{z-i} + H^+ \qquad K_i = \frac{[H_{n-i}X^{z-i}]\gamma^{z-i}a_{H^+}}{[H_{n-(i-1)}X^{z-(i-1)}]\gamma^{z-(i-1)}} \qquad \textbf{Eq. 3}$$

where K_i is the dissociation equilibrium constant of the i[th] dissociation step, γ are the activity coefficients of the solutes and a_{H+} is the activity of protons. Before obtaining the final expression for the m_e, the apparent dissociation constant at the i[th] dissociation step (K'_i) can be defined as:

$$K'_i = \frac{\gamma^{z-(i-1)}}{\gamma^{z-i}} \cdot K_i \qquad \textbf{Eq. 4}$$

The m_e is a function of the mobility and the molar fraction (χ) of the individual ion species:

$$m_e = \sum_{i=0}^{n} \chi_{H_{n-i}X^{z-i}} m_{H_{n-i}X^{z-i}} \qquad \textbf{Eq. 5}$$

The general equation relating m_e to pH of the BGE can be obtained replacing the χ by its concentration expression and taking into account K'_i definition (**Equation 4**), as well as considering $a^n_{H^+} = 10^{-npH}$ and $K'_i = 10^{-pK'_i}$ [112]:

$$m_e = \frac{\sum_{i=0}^{r-1} 10^{\left[-(r-i)pH + \sum_{j=i+1}^{r} pK'_j\right]} m_{H_{n-i}X^{z-i}} + m_{H_{n-r}X^{z-r}} + \sum_{i=r+1}^{n} 10^{\left[(i-r)pH - \sum_{j=r+1}^{i} pK'_j\right]} m_{H_{n-i}X^{z-i}}}{\sum_{i=0}^{r-1} 10^{\left[-(r-i)pH + \sum_{j=i+1}^{r} pK'_j\right]} + 1 + \sum_{i=r+1}^{n} 10^{\left[(i-r)pH - \sum_{j=r+1}^{i} pK'_j\right]}} \qquad \textbf{Eq. 6}$$

where *r* can take any value higher than zero and less or equal to the maximum positive net charge *z*. However, when the zwitterionic form is present in the pH range considered, it is advantageous to take r = z because the resulting zwitterionic species $H_{n-z}X$, has no net charge and hence its mobility is assumed to be nil ($m_{HX} = 0$). In this way, further simplifications regarding **Equations**

5 and **6** can be made. Using the expression of **Equation 6** for the analyte of interest, pK_a' values can be determined by nonlinear regression analysis of data pairs of m_e–pH. The thermodynamic pK_a values can be calculated from the determined pK_a' values using a derived expression from **Equation 4**:

$$pK_i = pK_i' + log\frac{\gamma^{z-(i-1)}}{\gamma^{z-i}} \quad \textbf{Eq. 7}$$

The γ can be calculated from the Güntelberg approximation of the extended law of Debye-Hückel (valid for ionic strength (I) < 0.1 M):

$$\log\gamma = \frac{-z^2 A\sqrt{I}}{1+\sqrt{I}} \quad \textbf{Eq. 8}$$

where A is a temperature and solvent dielectric dependent constant with value of 0.509 in water at 25 °C. γ of neutral species (γ_0) are assumed to be unity.

Accurate quantitative relationships between the m_e of ionizable compounds and the pH of the BGE have proved to be very useful to simultaneously determine their pK_a values, predict their m_e as a function of pH and select the optimum pH for their separation in a complex mixture [112]. However, these relationships are complex for polyprotic compounds with many ionizable groups. This is the case of proteins and polypeptides, which may have dozens of pK_as [114]. An interesting approach to estimate the pK_as of polypeptides may be the study of several fragment peptides with a smaller number of ionizable groups to cover the complete parent sequence. In this thesis, it will be demonstrated that pK_a values from Aβ peptide fragments can be used to model the migration behavior of more complex Aβ 1-40 and 1-42.

1.3.1.3. Prediction of electrophoretic migration with the classical semiempirical models

As an alternative to m_e-pH relationships, several semiempirical models relating the m_e of the analytes to their structure (charge, M_r or number of amino acid residues) have been also proposed to easily predict the electrophoretic migration behavior of ionic solutes.

As explained before, the m_e of a solute ion is proportional to its charge and inversely proportional to its solvated ion radius (**Equation 1**). The solvated ion radius is generally expressed in terms of M_r, because the volume of a molecule is proportional to its mass if the density is constant. The classical equations describing semiempirical models are deduced from assumptions concerning the solute shape and the forces that they undergo during electrophoretic motion. The general form of the equation relating m_e, M_r and q is as follows:

$$m_e = B \frac{q}{M_r^{\alpha}} \qquad \textbf{Eq. 9}$$

where B is a constant and the parameter α takes different values depending on the assumptions made on deduction of the semiempirical model (α = 1/2, 1/3 and 2/3 for the classical polymer model, the Stoke's law and the Offord's surface law, respectively). Specifically, in the classical polymer model the solutes are modelled as polymers with lower charge densities, whereas they are modelled as spherical particles in the Stoke's law and as larger molecules with more rigid structures, which experience frictional forces that are proportional to their surface area, in the Offord's surface law [120,121].

If accurate pK_a values are known, q can be calculated at each separation pH using Sillero and Ribeiro expression [122], which is based on the Henderson–Hasselbalch equation:

$$q = \sum_{n=1-4} \frac{P_n}{1+10^{pH-pK(P_n)}} - \sum_{n=1-5} \frac{N_n}{1+10^{pK(N_n)-pH}} \qquad \textbf{Eq. 10}$$

where P_n and N_n are the number of cationic (i.e. P_1 = terminal NH_2, P_2 = His, P_3 = Lys and P_4 = Arg) and anionic (i.e. N_1 = terminal COOH, N_2 = Asp, N_3 = Glu, N_4 = Cys and N_5 = Tyr) ionizable groups found in the amino acids and $pK_a(P_n)$ and $pK_a(N_n)$ are the pK_a values of these groups.

Once the linearity between m_e and q/M_r^{α} is demonstrated (**Equation 9**), q/M_r^{α} of the analytes as a function of pH of the BGE can be used for a straightforward and experimental-free separation prediction and optimization [114,115,123].

1.3.1.4. Criteria to optimize separation in CE

Optimization of CE separations has been traditionally developed as a branch of the chromatographic optimization methods [101,107]. In CE, quality criteria based on m_e, which solely consider ratios or differences on the separation between pairs of compounds, have been preferred for separation optimization [101,124]. Nowadays, selectivity between a pair of compounds ($\alpha_{i,j}$) in CE is widely accepted to be defined as the ratio between their m_e [124]:

$$\alpha_{i,j} = \frac{m_{e,i}}{m_{e,j}} \qquad (m_{e,i} > m_{e,j}) \qquad \textbf{Eq. 11}$$

This definition is algebraically analogous to the one used in chromatography, where $\alpha_{i,j}$ is defined as the ratio of the retention factors ($k_{i,j}$) [125]. Nevertheless, in CE m_e values can range from certain discrete positive numbers (i.e. the m_e of the hydrogen ion) to other discrete negative numbers (i.e. the m_e of the hydroxyl ion). Furthermore, many analytes can be uncharged at some pH values (e.g. zwitterionic compounds at the isoelectric points). In this regard, **Equation 11** presents issues of mathematical optimization by maximization because $\alpha_{i,j}$ approaches to infinite when $m_{e,j}$ in the denominator approaches to zero. This problem was identified by Jorgenson and Lukacs, which proposed a definition of selectivity ($S_{i,j}$) based on the difference between the pair of compounds and included the EOF in the denominator [101]:

$$S_{i,j}(m_e) = \frac{m_{e,i} - m_{e,j}}{m_{avg} + m_{EOF}} \qquad (m_{e,i} > m_{e,j}) \qquad \textbf{Eq. 12}$$

where m_{avg} is the mean value of m_e of the pair of compounds. However, $S_{i,j}$ still presents certain drawbacks related to changes in migration order and the denominator of $S_{i,j}$ can still become zero.

Recently, the theoretical parameter $t'_{i,j}$ has been proposed as an improved elementary criterion to qualify and optimize separations in CE [126]:

$$t'_{i,j}(m_e) = \left[m_{e,i} m_{e,j} \left(m_{e,i} - m_{e,j}\right)\right]^2 \qquad \textbf{Eq. 13}$$

The parameter $t'_{i,j}$ takes into account the separation between the pair of compounds and the multiplication qualifies the separation of each of them from the EOF. In addition, squaring the

expression results always in positive values, solving the inconvenient related to changes on migration order or direction, hence $t'_{i,j}$ is continuous in its domain. Furthermore, $t'_{i,j}$ can be extended for complex mixtures of n-compounds to compose a global optimization function T':

$$T'(m_e)=\left[\left(\prod_i^n m_{e,i}\right)\left(\prod_{(i,j)(j<i)}^{n,(n-1)} \Delta m_{e(i,j)}\right)\right]^2 \qquad \textbf{Eq. 14}$$

for a rapid, simple and reliable selection of optimized separation conditions by mathematical maximization. In this thesis, the versatility of T' will be demonstrated extending **Equation 14** to use $q/M_r^{1/2}$ instead of m_e, for a straightforward and experimental-free separation optimization in CE.

1.3.2. Mass spectrometry (MS)

CE-MS has become very popular in a wide range of applications [102,103] and, in particular, for the detection and characterization of biomolecules, such as peptides, proteins and miRNAs [14,20,127]. MS is an analytical technique that measures the mass-to-charge ratio (m/z) of ions in the gas phase. MS provides information on the analyte M_r and, therefore, it enables the identification of the separated substances by CE. Additionally, structural elucidation and identity confirmation can be carried out by interpreting the fragmentation patterns obtained by MS/MS [128,129].

Even though different mass spectrometers are available with different capabilities, in general they are all composed of the same major components, being the most important ones the ionization source, the mass analyzer and the detector [130]. Briefly, the ionization source allows molecules in the liquid phase to be transferred directly into ions in the gas phase. Then, in the mass analyzer, ions are separated on the basis of their m/z value. The mechanism behind ion separation depends on the type of analyzer, which could also affect the sensitivity, accuracy and resolution of the mass spectrum. Finally, the detector records either the charge induced or the current produced when an ion passes by or hits a surface.

1.3.2.1. Ionization techniques. Electrospray ionization (ESI)

The use of electrospray ionization (ESI) with MS was first reported by Malcom Dole in 1968 [131] and was further developed by John Fenn in the late 1980s [132]. ESI is the most common ionization technique for CE-MS because it enables at atmospheric pressure the efficient transfer of charged molecules from the CE effluent solution into the gas-phase for MS analysis [107,133]. ESI is a soft ionization technique because relatively little energy is imparted to the target molecules; hence molecular ions are in general detected because in-source fragmentation of labile ions during the ionization process is prevented. ESI is a suitable ionization technique for both small and large molecules because it produces multiply-charged ions. As a result, ions with m/z values of typically 100–3,000 are in general obtained hence can be easily measured by a mass analyzer with a limited m/z scanning range. Later, M_r can be determined taking into account the m/z values of the detected molecular ions by direct calculation or deconvolution of the mass spectrum with appropriate mathematical algorithms.

Several parameters can affect ESI efficiency and, consequently, alter the sensitivity and reproducibility of the method, being the composition and pH of the solutions (e.g. sheath liquid and BGE), the molecular size and number of ionizable groups of the target analyte the most important ones. In CE-MS, a volatile BGE of relatively low conductivity is required to maintain CE currents below 50 μA. In this way, a stable electrospray can be obtained and arcing between the interface and the mass spectrometer is avoided. In general, BGEs composed of formic acid, acetic acid or their ammonium salts are employed. CE-MS requires closure of both the CE and ESI electrical circuit. Furthermore, as flow rates of the CE effluent are EOF dependent and very low (nL/min), direct coupling with conventional ESI sources designed to work with flow rates in the μL/min range is not possible. In order to facilitate CE-MS, a dedicated interface is required to achieve proper voltages and flow rate handling. Three main types of interfaces for the on-line coupling of CE with ESI-MS have been developed: sheath flow, liquid-junction and sheathless interfaces (**Figure 1.7**) [134–136].

Both sheath flow and liquid-junction interfaces use an additional flow of liquid known as sheath liquid in the μL/min range, which mixes with the CE effluent as it exits from the outlet

A) Sheath flow CE-MS interface

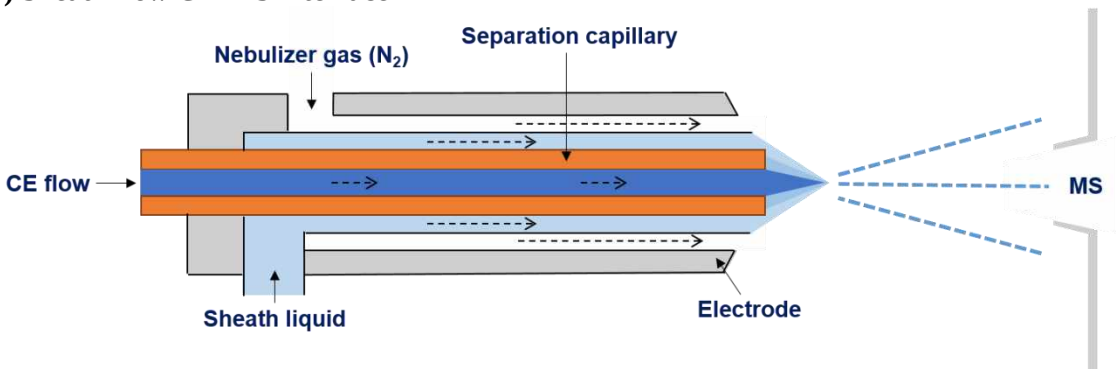

B) Liquid-junction interface

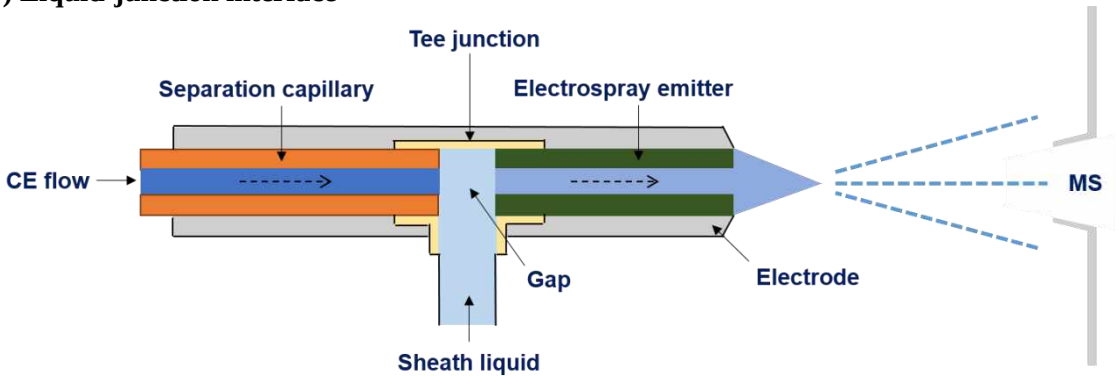

C) Sheathless CE-MS interface

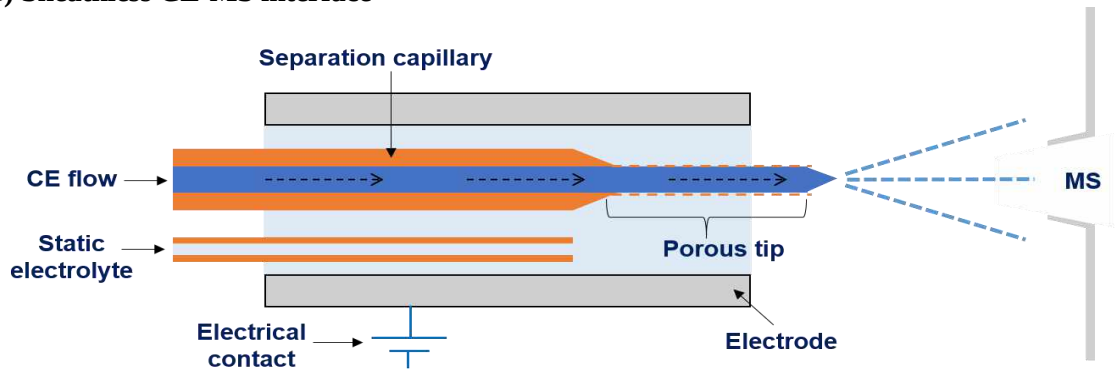

Figure 1.7. Typical ESI interfaces for CE-MS: (A) sheath flow, (B) liquid-junction and (C) sheathless.

of the separation capillary. The sheath liquid allows establishing electrical contact between an electrode and the BGE inside the separation capillary in order to drive the CE separation, while increasing the flow rate for an appropriate ESI process. Furthermore, the addition of the sheath liquid after the CE separation enables to modify the composition of the BGE of the CE effluent to make it more compatible with ESI-MS. In this regard, the sheath liquid composition affects

the signal intensity of the analyte molecular ions as well as their charge state distribution. Typically, sheath liquid is a hydroorganic solution. For electrospray positive ionization mode (ESI+), a volatile acid is added (e.g. formic acid or acetic acid).

Sheath flow interface was first developed by Smith et al. [137]. The typical configuration is the coaxial sheath flow interface using a triple tube system (**Figure 1.7-A**). In this design, the separation capillary is concentrically inserted inside a stainless steel tube, with the capillary end slightly protruding beyond the tube. With this design, the mixture between the sheath liquid and the CE effluent is gentler than in the liquid-junction interface (**Figure 1.7-B**) and excessive void volumes that would deteriorate separation are avoided. The sheath liquid is pumped through the tube and merges with the CE effluent at the capillary outlet, while the nebulizer gas is supplied through a second coaxial stainless steel tube to assist the spray formation. The nebulizer gas produces a small suction of the CE effluent, which affects separation resolution. Furthermore, some authors suggest that the generated parabolic flow profile could cause band broadening and lower separation efficiency [134,138].

The main drawback of the sheath liquid is the dilution of the CE effluent, which would impair sensitivity. With the aim to improve sensitivity by allowing nanoESI instead of microESI, sheathless interfaces have gained popularity in recent years. In the sheathless interfaces, the CE electrical circuit is closed directly using the BGE just before or after it leaves the separation capillary, eliminating the need for sheath liquid. This can be achieved by different strategies. Some interface designs coat the end of the capillary spraying tip with metal [139], while others attach a metal-coated sprayer tip [140] or insert a microelectrode [141] into the end of the separation capillary. However, most of these designs are lab-made and not commercially available. Since recently, AB Sciex LLC (Framingham, MA, USA) commercializes the porous tip nanospray sheathless interface (CESI 8000), which is based on the design of Moini [142]. In this design (**Figure 1.7-C**), the outlet end of the separation capillary is etched with hydrofluoric acid producing a porous wall that is conductive when in contact with a conductive solution. The porous capillary outlet protrudes from a stainless steel electrode filled with a static electrolyte, hence allowing electrical contact for the separation and electrospray formation at the capillary

tip. To obtain the porous tip by HF etching, a capillary with a thin wall is required. In this regard, this interface is limited to use the fused-silica capillaries (30 µm i.d. x 150 µm outer diameter (o.d.)) provided by the manufacturer. Other drawbacks of this sheathless interface are the limited robustness due to the delicate setup, the spray instability due to the very low flow rates produced in some separation conditions and the limited choices of BGE, which in many cases require to be hydroorganic, due to lack of post column chemistry.

A) Triple tube coaxial sheath flow interface (G1607A, Agilent Technologies, Inc.)

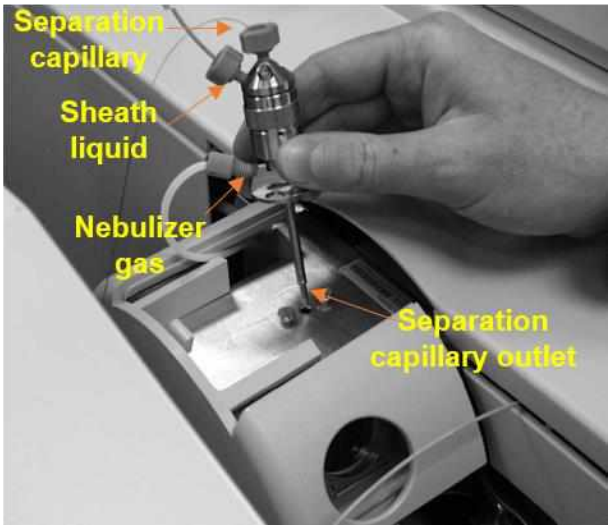

B)

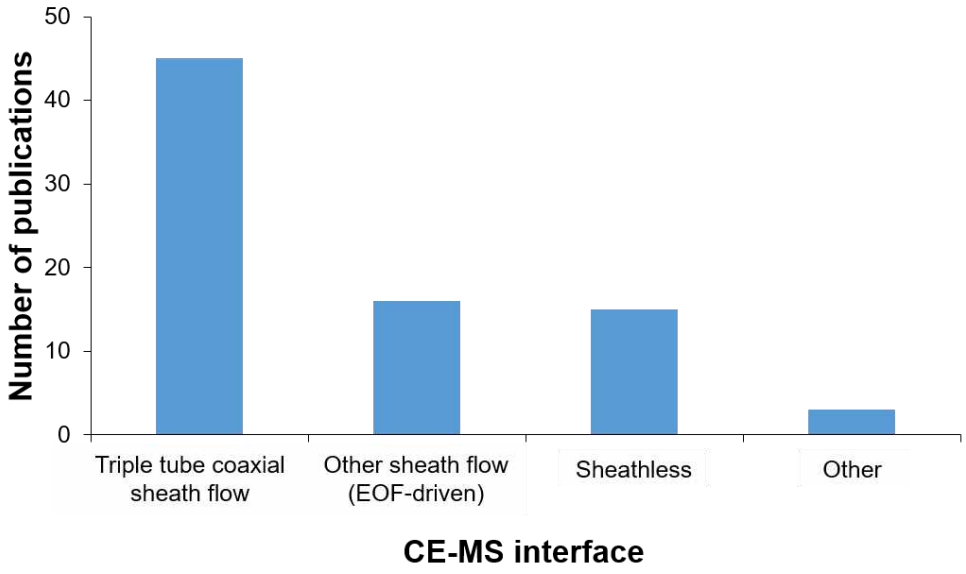

Figure 1.8. Most widely used CE-MS interfaces for the analysis of peptides and proteins: (A) Triple tube coaxial sheath flow (G1607A, Agilent Technologies, Inc.) and (B) publications on CE-MS in the period 2016-2018 classified according to the CE-MS interface (adapted from [136]).

Nowadays, the triple tube coaxial sheath flow interface with nebulizer gas (N_2) assistance commercialized since 1995 by Agilent Technologies, Inc. (Waldbronn, Germany) (G1607A sprayer) (**Figures 1.7-A** and **1.8-A**) continues to be the most widely used CE-MS interface (**Figure 1.8-B**). This is mainly due to its robustness, reliability, easy operation, appropriate sensitivity and versatility regarding capillary dimensions, sheath liquid and BGE selection [133,136,143]. This interface has been used in all the CE-MS studies of this thesis.

1.3.2.2. Mass analyzers

The mass analyzer is the part of the mass spectrometer in which gas-phase ions are separated based on their m/z values. Nowadays, five analyzers are mainly used, namely, quadrupole (Q), ion trap (IT), time-of-flight (TOF), orbitrap and Fourier transform ion cyclotron resonance (FT-ICR). These analyzers vary in terms of size, price, resolving power, accuracy, scanning range, scanning speed, dynamic range and the ability to perform MS/MS experiments. Several high-end instruments combine two or more analyzers to form complex hybrid instruments with enhanced performance and increased MS/MS capabilities (e.g. Q-TOF or triple quadrupole (QqQ)). In this regard, CE-MS/MS is frequently used in top-down and bottom-up approaches because it allows intact protein and peptide characterization, respectively [136,144].

TOF mass analyzers are widely used in the CE-MS analysis of intact proteins, peptides, oligonucleotides and other small molecules because of their ease of operation, simplicity, affordability, high mass accuracy, high mass resolution, good scanning speed and wide dynamic and scanning ranges (**Figure 1.9**) [136,143–147]. FT-ICR and orbitrap mass analyzers have also been used providing extremely high resolutions, however, at expense of a higher price, less robust CE-MS couplings and longer duty cycles, which may compromise the sensitivity of the analysis and may not allow adequate sampling of narrow CE peaks [146]. In this thesis, TOF mass analyzers have been preferentially used for the analysis of peptides, proteins and miRNAs.

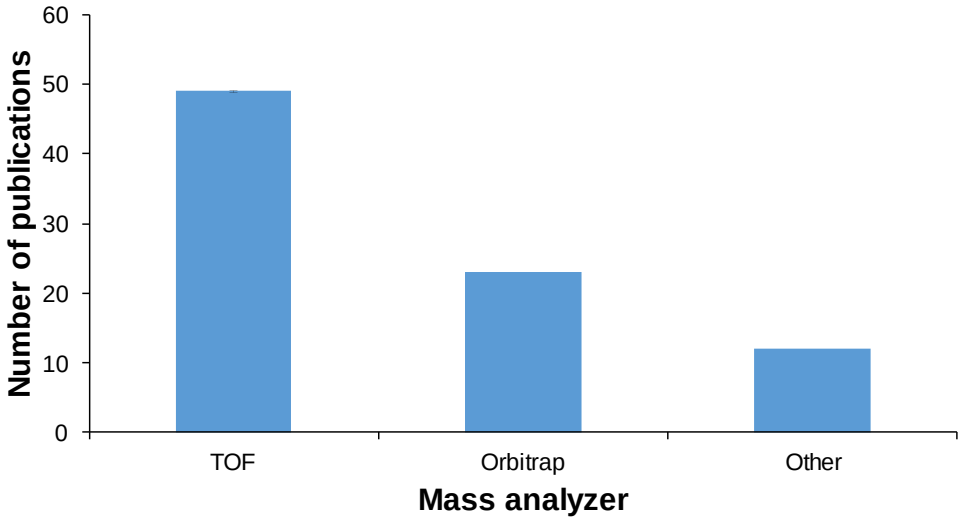

Figure 1.9. Publications on CE-MS for the analysis of peptides and proteins classified according to the mass analyzer (period 2016-2018; adapted from [136]).

The essential principle of TOF mass analyzers is that a population of ions moving in the same direction and having a distribution of masses but a constant kinetic energy will have a corresponding distribution of velocities inversely proportional to the square root of their m/z values. By measuring the time that an ion requires to travel a specific distance within the flight tube (usually 1-2 m length) before reaching the detector, the m/z value can be deduced according to the following equation [148]:

$$m/z = \frac{2V_i}{L_F^2} t_F^2 \qquad \textbf{Eq. 15}$$

where V_i is the initial accelerating voltage, L_F is the length of the flight path and t_F is the time that the ion takes to reach the detector. As can be deduced from **Equation 15**, ions with lower mass and higher charge will cross the tube before those with higher mass and lower charge. As the initial accelerating voltage is pulsed, the output of the detector as a function of time can be conveniently converted into a mass spectrum [149].

The most important advancement in TOF technology was the development of the orthogonal acceleration (oa-TOF) (**Figure 1.10**) [150]. The main difference is the use of a distinct direction for the separation of ions, orthogonal to the continuous ion-beam of the ion source. This configuration provides several advantages, including better efficiency in gating ions from an

external continuous source (e.g. ESI), reduction of velocity and spatial dispersion and, consequently, improved mass accuracy and resolving power.

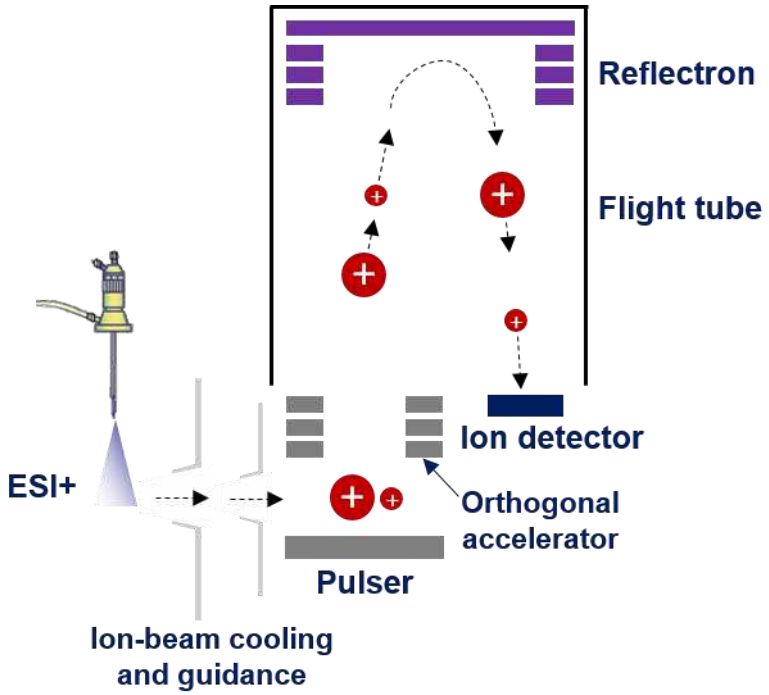

Figure 1.10. Schematic representation of an orthogonal acceleration-time-of-flight mass spectrometer (oa-TOF).

1.4. On-line preconcentration by solid-phase extraction capillary electrophoresis (SPE-CE)

A major limitation of CE is the relatively poor concentration sensitivity for most analytes due to the small sample volumes that can be injected in the separation capillaries (i.e. nL). In this regard, in addition to the use of more selective and sensitive detectors, the concentration sensitivity of CE can be enhanced by the traditional off-line sample clean-up and preconcentration techniques [151,152] or by improving the loadability through on-line electrophoretic [153–155] or chromatographic [156–160] preconcentration techniques. The advantages of these on-line preconcentration approaches are the minimization of sample handling and the increase in analysis throughput.

Electrophoretic preconcentration techniques rely on changes in electrophoretic velocity. The main types of electrophoretic preconcentration techniques include stacking [161], isotachophoresis [162], dynamic pH junction [163] and sweeping [164]. Field-amplified sample stacking (FASS) is perhaps the oldest and most well-known on-line sample preconcentration technique for CE [155,161]. In FASS, the sample in a low conductivity matrix is injected hydrodynamically into the separation capillary filled with a higher conductivity BGE. When the separation voltage is applied, the electric field strength becomes higher in the sample region than in the BGE. Consequently, the ions in the sample zone migrate rapidly until they reach the sample/BGE interface, where their velocities are slowed down abruptly and the ions are stacked and focused, hence preconcentrated. The conductivity ratio between the sample matrix and the BGE determines the preconcentration factor that can be obtained by FASS. However, although considerable concentration sensitivity enhancement can be obtained with such electrophoretic preconcentration techniques, their dependence on the analyte and sample matrix physicochemical properties hinders their performance in many applications. Furthermore, in many cases, the maximum loaded sample volume is limited to the total capillary volume.

Chromatographic preconcentration techniques employing on-line solid-phase extraction capillary electrophoresis (SPE-CE) show a more general applicability and versatility. These techniques enable improved loadability and, consequently, higher preconcentration factors and lower limits of detection (LODs) [155–160]. Moreover, they can be used for effective sample clean-up and purification. In SPE-CE (**Figure 1.11**), analytes from a large volume of sample (~25-200 µL) are retained on a sorbent contained in a microcartridge (or analyte concentrator). After sample loading, the microcartridge is washed to remove non-selectively retained molecules. Then, the retained analytes are desorbed in a small volume of eluent (~50-100 nL), resulting in sample clean-up and concentration enhancement before electrophoretic separation and detection [165].

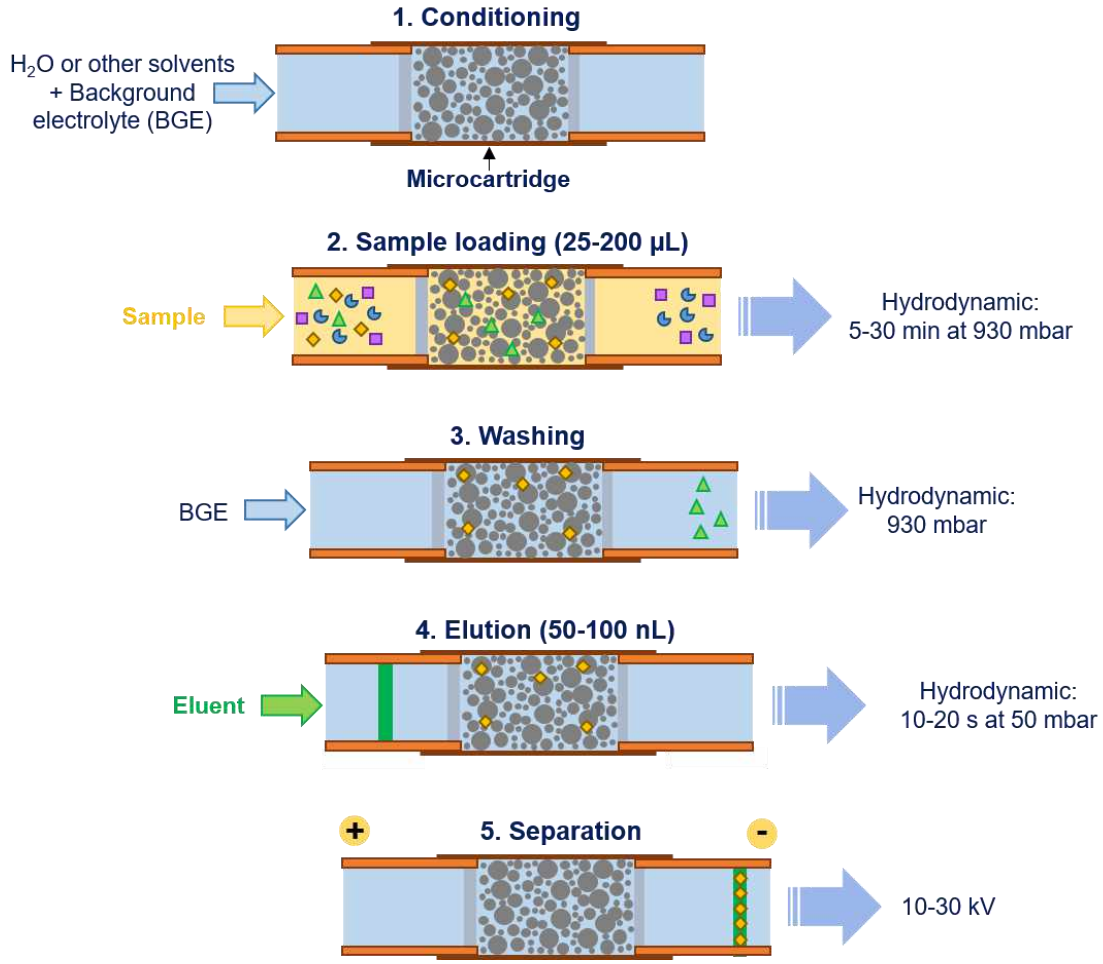

Figure 1.11. Methodology of SPE-CE: (1) conditioning, (2) sample loading, (3) washing, (4) elution and (5) separation. Volumes are estimated using **Equation 16**, considering a 72 cm L_T x 75 µm i.d. x 365 µm o.d. separation capillary.

In general, sample loading is performed hydrodynamically as in a conventional CE injection, applying a difference in pressure (ΔP) across the capillary by pressurizing the sample vial. The loaded sample volume is dependent on the ΔP, the time of pressure application (t_{inj}) and the capillary dimensions (i.d. and L_T) and can be estimated for an empty capillary using the Hagen–Poiseuille equation [107]:

$$V_{inj} = \frac{\Delta P\, t_{inj}\, id^4\, \pi}{128\, \eta\, L_T} \qquad \textbf{Eq. 16}$$

The higher the volume of sample loaded while the analyte is retained without exceeding the breakthrough volume (i.e. the maximum loadable sample volume without eluting the analytes

while loading [166]), the higher the preconcentration factors obtained for a certain elution volume. The breakthrough volume is specific for each analyte and sorbent and also depends on the concentration of the analytes in the loaded sample, the temperature and the flow rate [157,166]. In SPE-CE, the breakthrough volume can be studied with the breakthrough curve, plotting the amount of detected analyte after the elution against the loaded sample volume.

In some cases, especially when analyzing complex samples (e.g. biological fluids), the sample must be minimally pretreated to prevent the saturation of the on-line SPE microcartridge [165,167], even with highly selective sorbents (e.g. immunoaffinity sorbents).

Nowadays, the main disadvantage to expand SPE-CE applicability is the lack of commercially available capillary columns modified with microcartridges, which must be fabricated by the interested users. However, the description of a wide variety of microcartridge designs and construction procedures, as well as the availability of appropriate commercial sorbents or activated supports to prepare sorbents with novel affinity ligands, have continuously broadened the applicability of SPE-CE [156–160,165]. Several of the SPE-CE-MS contributions in this thesis are focused on the development of important biomedical applications with innovative sorbents.

1.4.1. SPE-CE designs and configurations

Since the first report of SPE-CE by N.A. Guzman et al. in 1991 [168], several microcartridge designs for SPE-CE have been described. In many cases, the microcartridge body connected to the fused silica separation capillary consists in another small piece of fused silica capillary with a wide i.d. to ensure the maximum amount of sorbent inside [165]. Microcartridges packed with sorbent particles are the most common and can be divided into two main groups: with frits and fritless.

Microcartridges with frits (**Figure 1.12**) use frits to avoid particle leaking during the analyses. Frits form a porous wall or net structure (<100 μm thickness) that allow the passage of solution and analytes, without restricting the flow or the electrical current circulation.

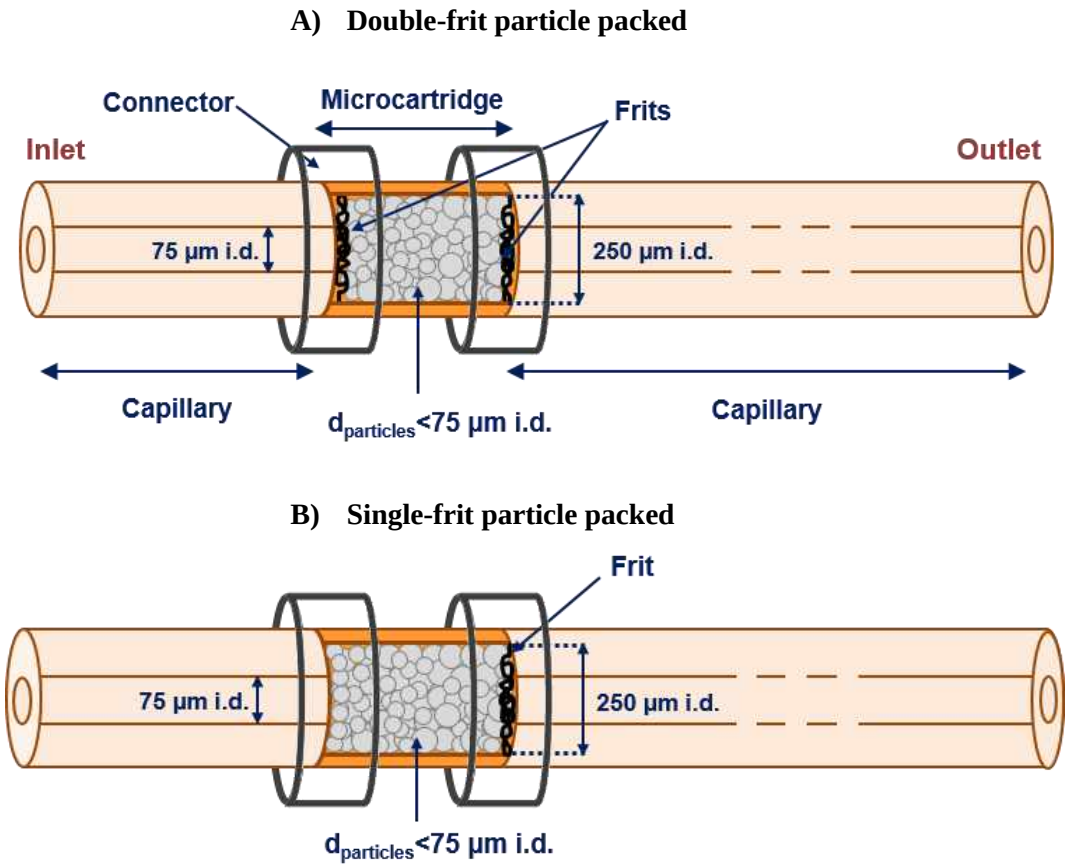

Figure 1.12. Microcartridge designs with frits for SPE-CE: (A) double-frit particle packed and (B) single-frit particle packed.

In general, double-frit microcartridges (**Figure 1.12-A**) are preferred because sorbent leaking is totally prevented [165]. However, packed microcartridges with a single frit in the outlet (**Figure 1.12-B**) can be necessary with certain sorbents and frit materials to avoid an excessive backpressure with two frits [169]. These microcartridges perform well when no sorbent leaking through the inlet or poor packing is observed.

In fritless microcartridges no frit is used (**Figure 1.13**). Fritless particle-packed microcartridges can be prepared using sorbent particles with a slightly larger size than the separation capillary i.d. (**Figure 1.13-A**) [170]. Other fritless designs for SPE-CE include open tubular microcartridges [171,172], monolithic microcartridges [173,174] and the use of fibers [175], sorbent membranes [176] and magnetic particles (i.e. beads, MBs) [177,178]. In recent years, MBs have become commercially available at a reasonable price and they are very suitable

to prepare fritless microcartridges because MBs can be held in position by an external magnet or electromagnet (**Figure 1.13-B**).

A) Sorbent particles with a larger size than the inner diameter of the separation capillary

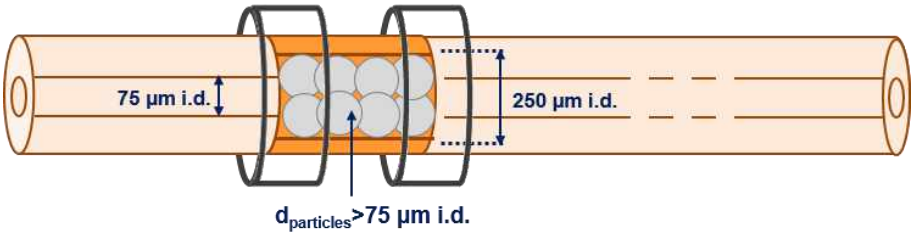

B) With magnetic particles

i)

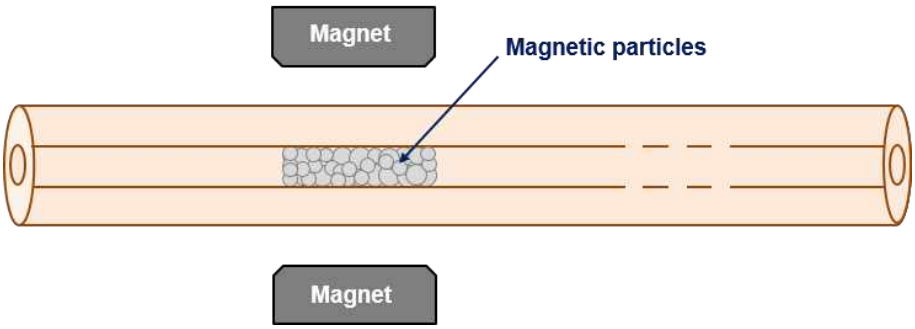

ii)

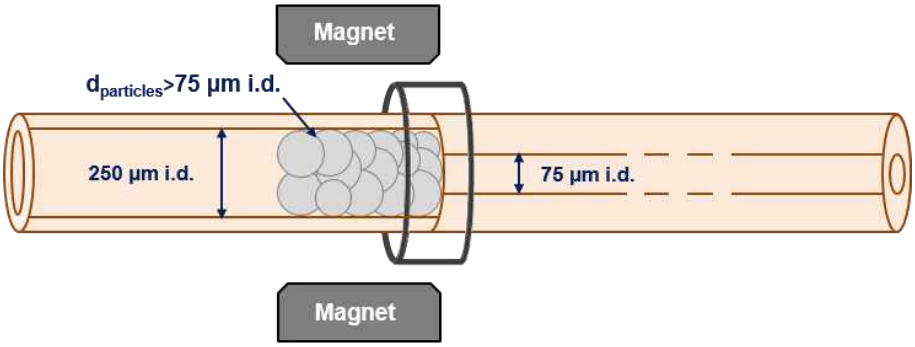

Figure 1.13. Fritless microcartridge designs for SPE-CE: packed with (A) sorbent particles with a larger size than the inner diameter of the separation capillary and (B) magnetic particles (i-ii).

Several configurations have been described for integrating the microcartridge in the analytical system [156,157,160]. Unidirectional SPE-CE is the most typical design due to its simplicity and low cost [165]. This configuration is used in most of the SPE-CE-MS studies in this thesis. In addition, a novel orthogonal SPE-CE setup with a nanoliter valve will also be presented.

1.4.1.1. Unidirectional SPE-CE

In unidirectional SPE-CE, the microcartridge is mounted in series to the separation capillary, inserted near the capillary inlet (**Figure 1.14**). Sample loading is conducted from the inlet to the outlet, in the same direction as the subsequent separation. As the microcartridge is integrated in the separation capillary and the extraction happens immediately before the separation, the coupling has been referred as "on-line" by many authors since the late 80s [179–182]. This nomenclature coexists in the literature with the term "in-line" that was introduced in the late 90s by U. A. Th. Brinkman and coworkers [183]. The term in-line SPE-CE has been preferred in the last years by several authors because is more specific, as it allows differentiation from on-line devices using valves or more complex instrumental setups [156,160].

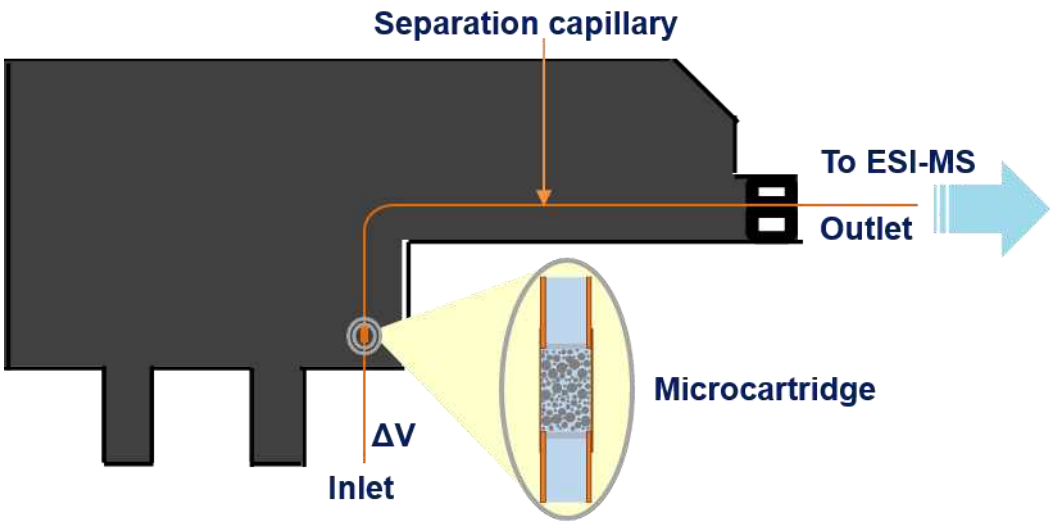

Figure 1.14. Unidirectional SPE-CE setup used in this thesis.

The simplicity, low cost and valve-free operation are the main advantages of unidirectional SPE-CE. However, it also has several drawbacks. First, the loading time to introduce a certain sample volume by pressure depends on the i.d. and L_T of the separation capillary (**Equation 16**). Second, some of the matrix components could be irreversibly adsorbed in the inner wall of the separation capillary. Third, in many cases, the requirements of on-line preconcentration are incompatible with the BGE necessary to fill the capillary for an efficient separation or sensitive MS detection.

1.4.1.2. SPE-CE with a nanoliter valve (nvSPE-CE)

In order to overcome the drawbacks of unidirectional SPE-CE, some new configurations where the sample is introduced in an orthogonal direction to the separation have been proposed [157,160]. These orthogonal configurations require the use of valves. Debets et al. [184] described in 1992 a pioneering SPE-CE-UV system using a rotary-type valve containing a SPE column, where the sample is introduced using a LC pump. After switching the valve position, the analytes are eluted and separated in the CE capillary. Much later, Tempels et al. [185] demonstrated SPE-CE-MS via a valve interface. However, the described system implies certain complexity because a LC pump and three valves are required. N.A. Guzman has proposed new cruciform and staggered (i.e. zigzag or z-shaped) microcartridge designs in microchannelled devices with valves [182,186,187], where the sample is introduced through a transport or passage tube (usually made of a polymeric material such as polyetheretherketone (PEEK) tubing), whereas elution and separation are performed in the orthogonal direction. However, overall, in the last years, the contributions about SPE-CE using capillaries and valves have been scarce due to the complexity of the instrumental setups and poor performance of the available valves.

SPE-CE with a nanoliter valve (nvSPE-CE) is a novel SPE-CE setup that uses an electrically isolated 4-port valve with an internal nanoliter loop. This nanoliter valve has been introduced by Neusüβ's group in 2016 for the direct coupling of two capillaries in two-dimensional CE [188]. NvSPE-CE (**Figure 1.15**) is operated with a single CE instrument and two capillaries for independent and orthogonal SPE clean-up and preconcentration (loading capillary) and electrophoretic separation (separation capillary). As can be observed in **Figure 1.15**, the valve can be switched between two positions using an actuator controlled via two buttons. In loading position (**Figure 1.15-i**), the sample is loaded hydrodynamically in the loading capillary and the analytes are retained in the microcartridge. Then, the loading capillary is washed to eliminate the non-selectively retained compounds. Finally, the eluent is injected, mobilized by pressure by pushing with an appropriate solution and transferred to the separation capillary by switching the valve. In separation position (**Figure 1.15-ii**), the voltage is applied and the eluted analytes are separated, detected and characterized by CE-MS. In this thesis, the potential of nvSPE-CE-MS is

investigated as an alternative to unidirectional SPE-CE-MS for the analysis of peptide biomarkers.

i) Loading position

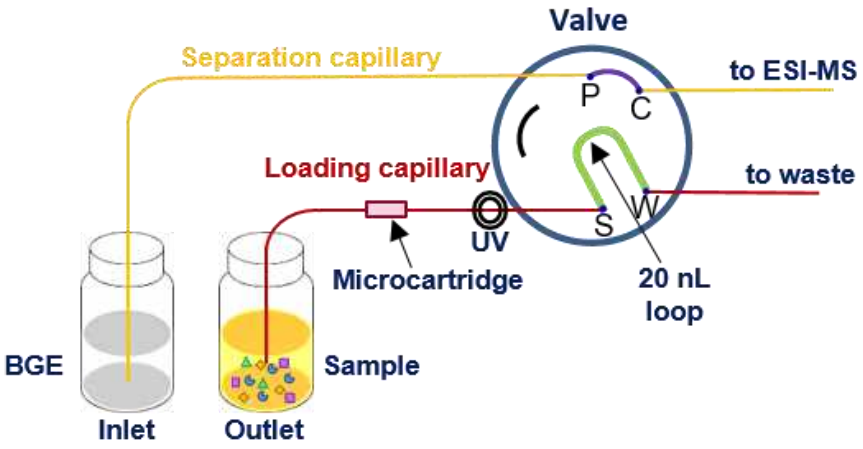

ii) Separation position

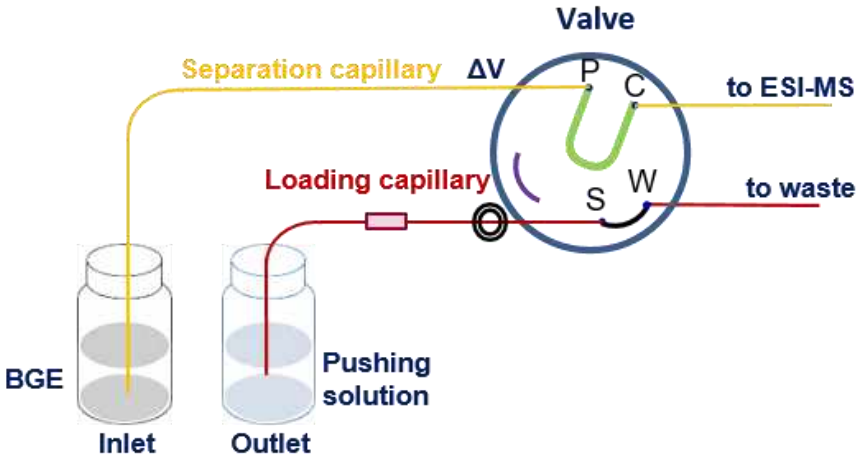

Figure 1.15. NvSPE-CE-MS setup. (i) Loading and (ii) separation positions.

1.4.2. SPE-CE sorbents

Many different sorbents have been described to analyze by SPE-CE a great variety of compounds, in a wide range of applications [156–160,165]. The sorbent must fulfill the requirements of SPE-CE, i.e. the reduced dimensions of the microcartridges and the fact that the extraction is undertaken on-line with a voltage-driven separation. It must allow operation without promoting flow restriction and backpressure, which may disturb the EOF and produce current instability or power failures. Furthermore, sorbent stability and reproducibility, high recovery,

rapid elution, low non-specific retention and extended lifetime are required for adequate SPE-CE performance. Recovery is mainly governed by the compromise between the eluotropic strength and the volume of the eluent and the sorbent capacity. Sorbent capacity depends on the affinity strength and selectivity of the target analyte to the sorbent and the number of active sites available for the extraction [189].

Particle sorbents have been the most widely applied in SPE-CE, from the low-selective conventional chromatographic sorbents [190] until more selective sorbents with metals [191], molecular imprinted polymers [192], lectins [193], antibodies [182], aptamers [174], etc.

1.4.2.1. Conventional chromatographic sorbents. Reversed-phase SPE

Nowadays, conventional chromatographic particle sorbents, especially reversed-phase, polymeric with hydrophilic-lipophilic balance and ionic exchange sorbents, are the most applied sorbents in SPE-CE, as they fulfill most of the requirements for optimum performance. On the one hand, they provide a large active surface area, without interfering with the on-line electrophoretic separation and detection. On the other hand, they are commercially available, have been optimized and widely used for the analysis of a great variety of compounds and can be purchased at a reasonable price. In particular, silica-based sorbents are widely recognized for their good extraction capacities and compatibility with a wide range of conditions (e.g. acidic BGEs and hydroorganic eluents), being C_{18} one of the most common chromatographic sorbent used for SPE-CE applications [160,165,190]. However, the major drawback of these conventional chromatographic sorbents is their limited selectivity, which precludes the direct analysis of complex samples such as biological fluids. In such cases, a previous clean-up pretreatment is required to purify and enrich the target analytes in order to prevent microcartridge saturation [194]. However, these pretreatments or the use of MS detection are not enough for the interference-free analysis of certain compounds.

In this thesis, a C_{18} sorbent will be used for the analysis of peptide biomarkers in human plasma samples by nvSPE-CE-MS.

1.4.2.2. Affinity sorbents

Affinity sorbents are a powerful tool to enhance SPE-CE-MS performance due to their high selectivity, which is advantageous in order to purify and preconcentrate the target analytes from complex matrices. In this thesis, immunoaffinity (IA), aptamer affinity (AA), immobilized metal affinity (IMA) and silicon carbide (SiC) sorbents are explored in SPE-CE-MS.

Immunoaffinity (IA-SPE-CE)

Immunoaffinity SPE-CE (IA-SPE-CE) is based on the reversible non-covalent interaction between the target analyte, or antigen, and an antibody (Ab), or immunoglobulin (Ig), which is immobilized on a solid support. IgG (**Figure 1.16**) is the most common Ab in mammals. IgG is roughly a Y-shaped structure consisting of four polypeptide chains: two identical heavy (H) chains (M_r~50,000) and two identical light (L) chains (M_r~25,000) joined by disulfide bonds and non-covalent interactions. Each chain has a variable (V) region located in the amino terminal portion and a constant (C) domain in the carboxyl terminal portion of the antibody [195]. Antigens bind to the fragment antigen binding (Fab') region, the variable region of the antibody, while the constant stem region, the fragment crystallizable (Fc) region, interacts with receptors and molecules on cells.

Abs bind to a specific region of the antigen known as antigenic determinant or epitope. Depending on how the Abs have been generated, they can be divided in two types, monoclonal or polyclonal. Monoclonal Abs are produced by a single line of clones of the same B cell and only recognize one epitope on an antigen [196]. In contrast, as in nature, polyclonal Abs are generated by multiple clones of different B cells and recognize various epitopes on an antigen. The decision regarding whether to use a polyclonal or monoclonal Abs in SPE-CE-MS depends on the intended use and the availability. Polyclonal Abs can be generated much more rapidly, are less expensive and require less technical skills, but require the use of animals. In contrast, monoclonal antibodies are prepared in cells and can be more selective, a useful characteristic when working with complex samples. However, this high selectivity may represent a drawback in some cases, e.g.

when the analytical method is focused on the analysis of a family of structurally related compounds. For instance, some changes in the structure of the targeted compounds, may lead to poor or no recognition by the antibody. Conversely, these small changes do not affect polyclonal antibodies, since they are heterogeneous and recognize a set of antigenic epitopes [197,198]. Furthermore, it should not be underestimated the very often higher affinity of polyclonal Abs compared to monoclonal Abs [199].

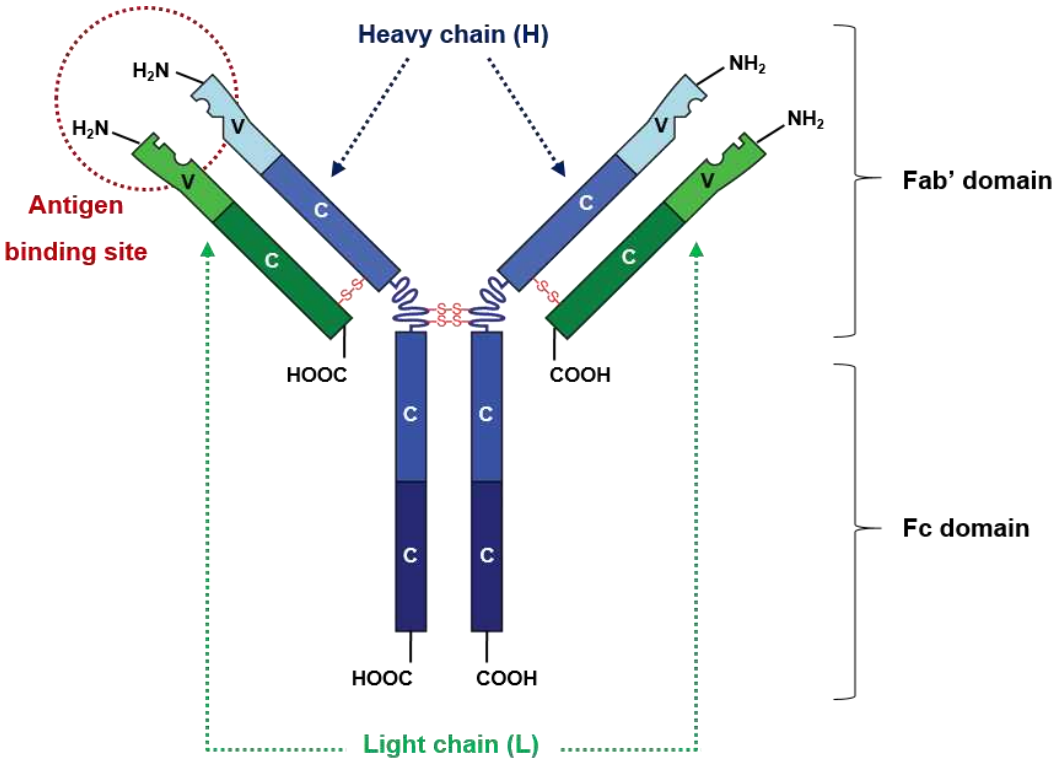

Figure 1.16. Structure of an immunoglobulin G (IgG).

IA-SPE-CE was introduced by Guzman and coworkers in the early 1990s [168], being primarily described with laser-induced-fluorescence detection (LIF) for preconcentration of small molecules, mostly peptides, from biological samples [180,182,186,187]. IA-SPE-CE-MS was first reported in 2000 [181] and has been demonstrated to a much lesser extent due to the difficulties of making compatible the requirements of IA-SPE-CE with on-line MS detection [200–202]. In general, IA sorbents are prone to degradation due to Ab denaturation when exposed to extreme pH values or organic solvents for extended time periods. Another important issue in

IA-SPE-CE is the limited commercial availability of compatible IA sorbents. Generally, researchers develop their own IA sorbents with the most suitable features for IA-SPE-CE. There is a wide variety of methods for preparing IA sorbents, based on the immobilization onto different supports of intact Abs or their active fragments (obtained after enzymatic digestion). In particular, many different MBs are commercially available with a wide range of surface chemistries ready to immobilize the affinity ligands [203,204]. As with other supports, orientation of the Abs on the MBs is of great concern because the molecular recognition depends on the availability of the binding sites for the antigen-antibody interaction. Specifically, MBs with Protein A or Protein G attached on the surface allow an optimum orientation of the Ab through its carboxyl-terminal Fc region, making them highly adequate for off-line immunoprecipitation (IP) [205]. However, the interaction between Protein A or Protein G and the Ab is non-covalent and the Ab-target analyte complex is desorbed during the elution. IA-MBs prepared by covalent immobilization of the Ab are more suitable for IA-SPE-CE because of the improved stability of the IA sorbent, which avoids the need for separation of the Ab from the target analyte and makes the microcartridge reusable [178] (**Figure 1.17**).

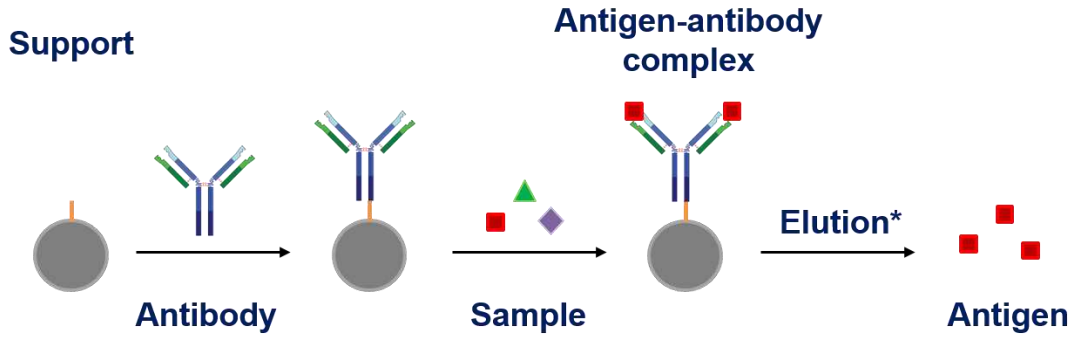

*If the antibody is not covalently coupled to the support, it will be eluted with the antigen.

Figure 1.17. Schematic representation of IA-SPE extraction (Ab is immobilized through the Fc region).

In this thesis, the potential of IA-SPE-CE-MS using MBs, taking advantage of their magnetic properties or their size to prepare fritless microcartridges, is investigated to purify, preconcentrate and characterize TTR from human serum samples.

Aptamer affinity (AA-SPE-CE)

Aptamers are polymeric biomolecules, typically single-stranded oligonucleotides with less than 100 bases, that fold into specific three-dimensional structures and hence can interact with the target molecule with high selectivity and affinity [206,207]. In nature, they exist as riboswitches, segments of non-coding mRNA that serve as specific receptors [208].

In 1990, three research groups independently reported the isolation in vitro of small nucleic acids with predefined functions and developed the technique generally used nowadays for isolation of aptamers [209–211], which is called systematic evolution of ligands by exponential enrichment (SELEX). SELEX is an iterative cycle of selection and amplification steps that enriches high-affinity and selective aptamers from a large combinatorial library [212,213]. The procedure (**Figure 1.18**) involves repeated cycles of incubation of the high complexity library with the targets (binding), washing of non-retained sequences, elution of the retained oligonucleotides and amplification by polymerase chain reaction (PCR; for DNA library) or reverse transcription–PCR and again transcription (for RNA library). By means of SELEX, aptamers have been generated for a wide variety of targets, ranging from small molecules to proteins and whole cells [214–216].

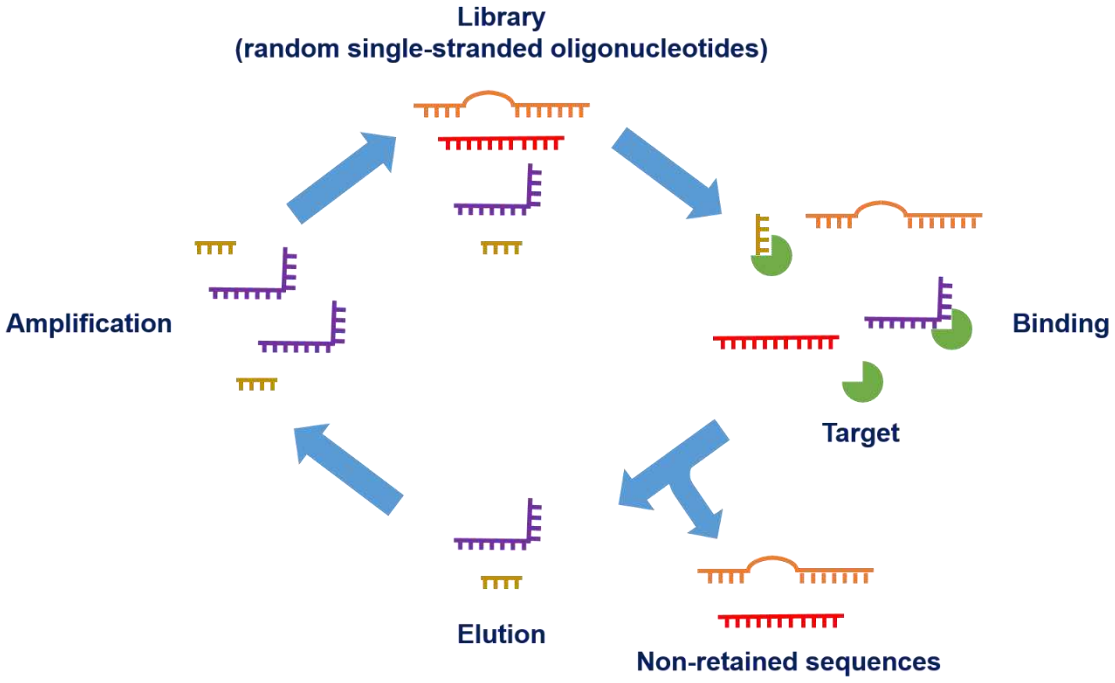

Figure 1.18. Schematic representation of aptamer generation by SELEX.

As aptamers can be used to recognize extracellular and intracellular targets [207], they are regarded as a promising approach in therapeutics. In 2004, pegaptanib was the first therapeutic aptamer approved by the FDA. This RNA aptamer against vascular endothelial growth factor is useful for the treatment of age-related macular degeneration [217]. Currently, several other aptamers are in different phases of clinical trials, especially for thrombotic events [218] and cancer [219].

Aptamers have low blood residence times compared to Abs and do not seem to be immunogenic [220,221]. Therefore, they have also been demonstrated for drug delivery [222]. In particular, aptamers with specificity for cell surface receptors that are internalized can provide a means of intracellular delivery of drugs that are themselves not permeable to cells [223]. Aptamers have also been applied in diagnostics, imaging and biosensing [224–226].

Affinity of aptamers for their targets is comparable or even higher than their Ab counterparts, with a dissociation constant values in the picomolar range [227,228]. Once selected by SELEX, in contrast to Abs, aptamers are chemically synthesized, which eliminates the requirement of animals or cells and the possible batch-to-batch variations, and are significantly faster and much cheaper to produce [212]. In addition, aptamers can be selected against non-immunogenic and toxic substances [229]. Other interesting advantages of aptamers are their smaller size, high robustness, thermal stability and tolerance to wide pH ranges and salt concentration [207,221].

Aptamer affinity SPE-CE (AA-SPE-CE) is a promising tool that combines the high selectivity of aptamers with the high separation efficiency of CE. As with IA-SPE-CE, appropriate orientation and covalent immobilization of the aptamer on the support are crucial for adequate AA-SPE-CE performance and microcartridge reusability. In this sense, aptamers can be chemically modified at either 3’ or 5’-terminus to incorporate various functional groups and spacer arms to facilitate the covalent immobilization with an appropriate orientation and minimal steric hindrance on a solid support [230,231]. Aptamer sorbents have been prepared for the selective extraction of different target analytes [230–234]. However, the elevated cost of SELEX and the lack of a comprehensive database of aptamer sequences hinders a more widespread

application. Efforts are currently being made, such as Apta-Index (https://www.aptagen.com/apta-index/), a database with more than 500 aptamer sequences from the literature [235].

At the time of this thesis, there was only a publication demonstrating AA-SPE-CE. In that report, Marechal et al. described the use of a monolithic microcartridge for the analysis of ochratoxin A in standards, beer and wine by AA-SPE-CE with LIF detection [174]. Here, AA-SPE-CE-MS is demonstrated for the first time and it is applied to investigate, purify, preconcentrate and characterize α-syn in human blood samples.

Immobilized metal affinity (IMA-SPE-CE)

Immobilized metal affinity (IMA) is based on the affinity for metal ions of certain exposed electron-donating groups present in the target compounds, in general, peptides, proteins and nucleic acids [236–239]. This affinity is derived from the reversible formation of coordination bonds with the metal ions that are immobilized by chelation with a ligand covalently attached to an appropriate solid support, usually agarose, polymeric or silica-based particles. Nowadays, several IMA sorbents containing different transition metals are commercially available. The most popular metal ions for IMA are the borderline transition metals, including Fe(III), Co(II), Ni(II), Cu(II) and Zn(II) [239]. The most widely used chelating agents are iminodiacetic acid (IDA) and nitrilotriacetic acid (NTA), which are tridentate and tetradentate ligands, respectively [238,240]. In general, it is widely accepted that IMA-NTA sorbents are more stable due to the higher chelation with the solid support, resulting in reduced ion leaching [240,241].

Since the pioneering work of Porath and coworkers [238], many authors have contributed to the development of IMA into a widespread protein purification approach [240,242]. In peptides and proteins, the electron-donating groups are predominantly located in cysteine, tryptophan or, especially, histidine side-chains (**Figure 1.19**) [239,242]. Nowadays, IMA chromatography is the most common method used for the purification of recombinant proteins with a polyhistidine-tag (His-tag), which contains six or more consecutive histidine residues. After this purification, the His-tag can then be removed either chemically or enzymatically to generate the protein with the

final desired amino acid sequence. His-tags are widely used in preparation of recombinant proteins due to their small size and neutral charge at physiological pH and, therefore, usually do not affect protein folding, structure and function [243].

IMA sorbents have also often been used in off-line SPE for the selective enrichment of histidine containing peptides (His-peptides) before LC-MS analysis [241,244,245]. However, the use of IMA before CE has been little explored. Although a few authors have evaluated the influence of IMA in affinity CE separations [246,247], most interest has been focused on IMA-SPE-CE-UV [248–250], while IMA-SPE-CE-MS has been explored to a lesser extent and for synthetic peptides [191] or phosphopeptides [251]. In this thesis, the potential of IMA-SPE-CE-MS with a Ni(II)-NTA sorbent is investigated to selectively enrich His-peptides from complex protein digests.

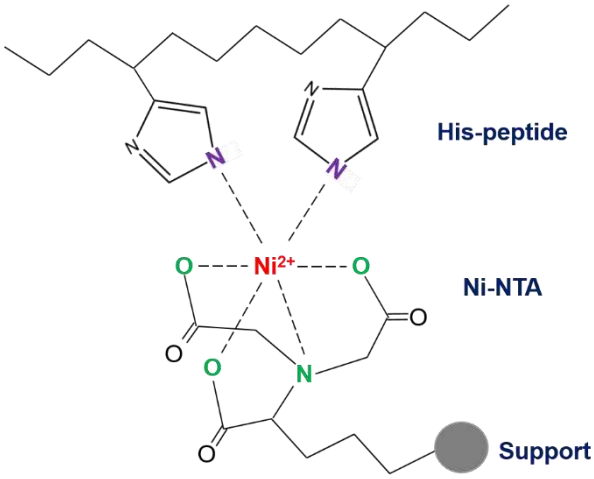

Figure 1.19. Schematic representation of the interaction between the histidine residues of a His-peptide and the Ni(II)-NTA sorbent.

Silicon carbide (SiC)

From the late-1980s, the gold standard method for RNA isolation was based on phenol-chloroform-isoamyl alcohol [252] or guanidinium thiocyanate-phenol-chloroform [253] extraction. However, these phenol-based extraction procedures use very toxic, corrosive and carcinogenic reagents and phenol-free methods have been proposed. Nowadays, an excellent alternative for RNA isolation are the commercially available SPE spin-column kits [254] which

allow a quick and efficient purification, with comparable recoveries to the traditional methods. Furthermore, many of the issues that are associated with liquid-liquid extraction such as incomplete phase separation are prevented. The principle of RNA purification by these SPE methods is the high affinity of RNAs towards sorbents made of silica, SiC, glass or diatomaceous earth [255–258]. Sodium ions act as a cation bridge between the negatively charged phosphate RNA backbone and the negatively charged silanol groups on the sorbent surface (**Figure 1.20**) [256]. The retained RNAs can be eluted using a low ionic strength aqueous or hydroorganic solution [256]. Silica sorbents favor the retention of large RNA molecules and are not capable to isolate RNA <200 nucleotides [258]. In contrast, SiC sorbents do not exhibit size-bias [258].

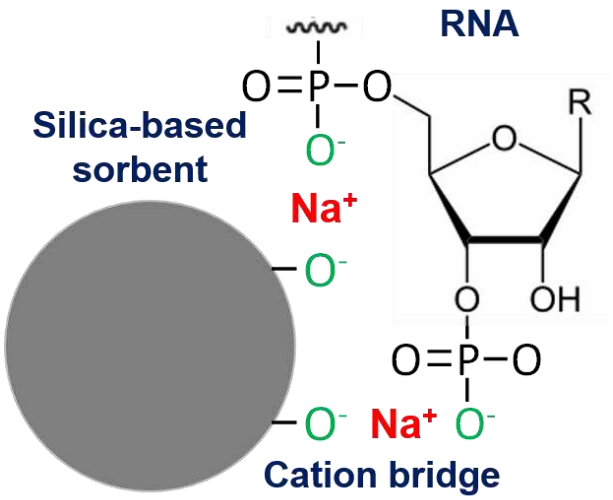

Figure 1.20. Schematic representation of the interaction between the phosphate backbone of RNAs and the silica-based sorbents. Sodium ions act as a cation bridge.

At present, there is a variety of commercially available SPE spin-column kits for the selective enrichment of small RNAs, including miRNAs [259]. In this thesis, the potential of SPE-CE-MS for the analysis of miRNAs is investigated for the first time, using as a sorbent a commercially available SiC sorbent from one of these spin-column kits.

1.5. On-line immobilized enzyme microreactor capillary electrophoresis-mass spectrometry (IMER-CE-MS)

Bottom-up approaches in MS-based proteomics show, as previously mentioned, multiple advantages including increased separation efficiency and limited number of charges on small peptides, which are all beneficial for the enhanced concentration sensitivity with MS detection compared to top-down approaches [16].

The enzymatic digestion with trypsin is typically performed in a homogeneous solution after mixing the free enzyme and the protein solutions. The enzyme-to-protein ratio, the pH, the temperature and the reaction time can be optimized to obtain the maximum digestion yield. However, in general, very long times (e.g. 18 h) are recommended for an appropriate digestion [260]. Immobilized enzymes have been alternatively explored to decrease the sample volume and the total digestion times, improve the digestion yields and make the enzyme reusable [261]. Specifically, on-line immobilized enzyme microreactor capillary electrophoresis-mass spectrometry (IMER-CE-MS) allows to increase the analysis throughput while further reducing the sample handling and the required sample volumes [262,263]. IMER-CE microreactors can be regarded as an analogue of SPE-CE microcartridges. However, instead of an affinity ligand to retain the target analytes, a proteolytic enzyme is immobilized on the support.

In the last three decades, the number of scientific articles about IMER-CE has been scarce, probably due to the instrumental and methodological difficulties of the on-line coupling and the limited applicability of the methods without on-line MS detection [263]. Since the pioneering work of Amankwa et al. [264], most IMER-CE designs described are based on open tubular microreactors with immobilized trypsin on the inner capillary surface (**Figure 1.21**) [265–267].

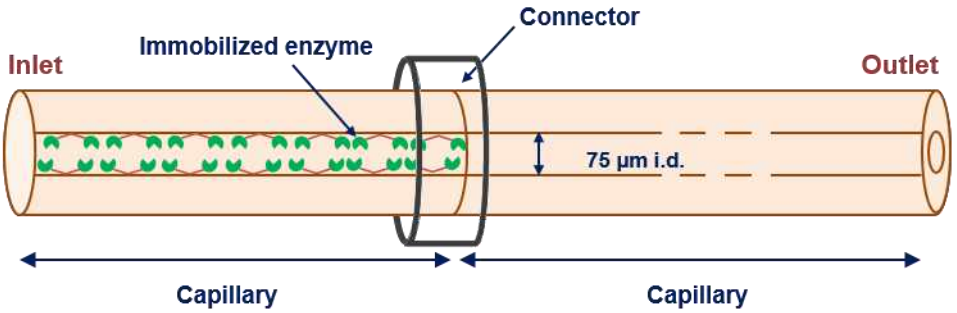

Figure 1.21. Open tubular immobilized enzyme microreactor capillary electrophoresis (IMER-CE).

Nevertheless, it is widely accepted that digestion yields with these microreactors are in general low due to the limited interaction between the protein and the immobilized trypsin during the very short time of the on-line digestion [262,263]. Monolithic [268], sol-gel [269] and particle packed (**Figure 1.12**) [262] supports with immobilized trypsin were developed to increment the digestion yield owing to the extended active surface areas and the reduced distances between the protein and the immobilized enzyme. Nowadays, preparation of monoliths with immobilized trypsin is promising but requires rather challenging, long and tedious synthesis procedures to obtain reproducible results [263]. Conversely, activated particle supports ready to immobilize trypsin or with immobilized trypsin are commercially available. However, at the time of this thesis, the number of studies describing completely on-line IMER-CE-MS were rather scarce and all of them were using open tubular IMERs [265,266]. Here, the potential of IMER-CE-MS using commercial cellulose resin particles with immobilized trypsin will be evaluated for the rapid and efficient bottom-up analysis of proteins and complex protein mixtures.

Chapter 2. Novel developments for prediction and optimization of separations in capillary electrophoresis

In recent years, an increased emphasis has been placed on the detection, characterization and quantification of biomarker compounds in biological fluids for non-invasive and cost-effective diagnosis, follow-up and prognosis of numerous diseases. In this regard, MS is a powerful technique for the unequivocal identification of biomolecules due to its selectivity and potential with respect to the detailed structural characterization of unknown compounds. However, due to the complexity of most biological samples, the hyphenation of high-performance separation techniques is essential prior to MS analysis. Separation prevents ion suppression, which combined with analyte detection as highly efficient peaks allow enhanced sensitivity. In this respect, CE is a microscale technique whose separation mechanism is based on m_e, which is related in the simplest mode to the ion charge-to-radius ratio of the solutes and, therefore, it is very suitable for the separation of charged biomolecules. Nevertheless, electrophoretic separation methods must be properly optimized to achieve rapid, efficient, sensitive and high-resolution separations.

The present chapter is focused on the development of novel strategies for prediction and optimization of separations in CE. To assess these strategies, Aβ peptides, which are biomarkers of Alzheimer's disease, are studied, namely Aβ 1-40 and 1-42 and five of their fragments (Aβ 1-15, 10-20, 20-29, 25-35 and 33-42) covering their entire amino acid sequence.

The electrophoretic behavior of the Aβ peptide fragments has been studied as a function of pH to determine the acidity constants of their ionizable groups and, simultaneously, select the optimum pH for their separation. Since the determination of the pK_as of polyprotic compounds with many ionizable groups is very difficult, an interesting approach proposed in this study has been to estimate the pK_as of Aβ 1-40 and 1-42 from the pK_a values determined for their fragments. In addition, the electrophoretic migration of the Aβ peptides has been predicted with the classical semiempirical models relating the m_e of the analytes to their structure, specifically to the charge-to-molecular mass ratio ($q/M_r^{1/2}$, for the classical polymer model), which can be easily calculated if adequate pK_a values are available. To select the optimum pH for the separation of the mixture of Aβ peptides, quality criteria $S_{i,j}$ and T' have been evaluated, demonstrating that it is possible to use as a pH optimization variable both the m_e of the Aβ peptide fragments or their $q/M_r^{1/2}$.

This chapter includes the following publications:

- **Publication 2.1.** R. Pero-Gascon, F. Benavente, J. Barbosa, V. Sanz-Nebot, Determination of acidity constants and prediction of electrophoretic separation of amyloid beta peptides, J. Chromatogr. A. 1508 (2017) 148–157. https://doi.org/10.1016/j.chroma.2017.05.069.

- **Publication 2.2.** R. Pero-Gascon, M. Tascon, V. Sanz-Nebot, L.G. Gagliardi, F. Benavente, Improving separation optimization in capillary electrophoresis by using a general quality criterion, Talanta. 208 (2020) 120399. https://doi.org/10.1016/j.talanta.2019.120399.

Journal of Chromatography A, 1508 (2017) 148–157

Contents lists available at ScienceDirect

Journal of Chromatography A

journal homepage: www.elsevier.com/locate/chroma

Determination of acidity constants and prediction of electrophoretic separation of amyloid beta peptides

Roger Peró-Gascón, Fernando Benavente, José Barbosa, Victoria Sanz-Nebot*

Department of Chemical Engineering and Analytical Chemistry, University of Barcelona, c/ Martí i Franquès 1-11, 3rd floor, 08028 Barcelona, Spain

ARTICLE INFO

Article history:
Received 15 March 2017
Received in revised form 16 May 2017
Accepted 31 May 2017
Available online 3 June 2017

Keywords:
Acid dissociation constant
Amyloid beta
Capillary electrophoresis
Peptides
pKa
Prediction

ABSTRACT

In this paper we describe a strategy to estimate by CE the acidity constants (pK_a) of complex polyprotic peptides from their building peptide fragments. CE has been used for the determination of the pK_as of five short polyprotic peptides that cover all the sequence of amyloid beta (Aβ) peptides 1–40 and 1–42 (Aβ fragments 1–15, 10–20, 20-29, 25–35 and 33–42). First, the electrophoretic mobility (m_e) was measured as a function of pH of the background electrolyte (BGE) in the pH range 2–12 (bare fused silica capillary, I = 25 mM and T = 25 °C). Second, the m_es were fitted to equations modelling the ionisable behaviour of the different fragments as a function of pH to determine their pK_as. The accuracy of the pK_as was demonstrated predicting the electrophoretic behaviour of the studied fragments using the classical semiempirical relationships between m_e and peptide charge-to-mass ratio (m_e vs. $q/M_r^{1/2}$, classical polymer model, q = charge and M_r = relative molecular mass). Separation selectivity in a mixture of the fragments as a function of pH was evaluated, taking into account the influence of the electroosmotic flow (EOF) at each pH value, and a method for the simple and rapid simulation of the electropherograms at the optimum separation pH was described. Finally, the pK_as of the fragments were used to estimate the pK_as of the Aβ peptides 1–40 and 1–42 (^{1}C and D 3.1, E 4.6 and Y 10.8 for acidic amino acids and ^{1}N-D 8.6, H 6.0, K 10.6 and R 12.5 for basic amino acids), which were used to predict their behaviour and simulate their electropherograms with excellent results. However, as expected due to the very small differences on $q/M_r^{1/2}$ values, separation resolution of their mixtures was poor over the whole pH range. The use of poly(vinyl alcohol) (PVA) coated capillaries allowed reducing the EOF and a slight improvement of resolution.

1. Introduction

The acid dissociation constant (K_a, or pK_a in minus logarithm scale) is a fundamental parameter for physicochemical characterization of biologically and pharmacologically relevant compounds [1,2]. Capillary electrophoresis (CE) has been widely used for accurate determination of pK_a of a great variety of polyprotic compounds [1–4]. It is an excellent alternative to potentiometric [2,5], ultraviolet-visible (UV/Vis) spectrophotometric [2,6] and NMR [2,7] determination because it is not limited by sample volume or purity, it can be fully automated and it allows a great versatility in the selection of the separation conditions. The CE determination of pK_a is usually performed measuring the electrophoretic mobility (m_e) of the target compounds as a function of pH within an appropriate pH range in aqueous solutions [4], mixed hydro-organic [8] or non-aqueous media [9] using fused silica capillaries with UV detection [4,8,9]. During the last decade, different interesting alternatives have been proposed to increase the reproducibility and throughput of these typical procedures, such as application of multiplexed [10] and miniaturized instrumentation [11], coated capillaries [12,13], mass spectrometry detection [14,15] or internal standard-based methods [16]. However, most of the applications have been described for small molecules with only a few ionisable groups (less than 4). The determination of pK_as is troublesome for polyprotic compounds with many ionisable groups, especially when expected pK_as are extreme or correspond to the same or similar ionisable groups. This is the case of proteins and polypeptides, which may have dozens of pK_as. An interesting approach to estimate the pK_as of polypeptides may be the study of several fragment peptides with a smaller number of ionisable groups to cover the complete parent sequence. Following a similar strategy, Rickard et al. reported an excellent general set of average pK_a values for amino acids in polypeptides using biosynthetic human insulin (BHI)

* Corresponding author.
E-mail address: vsanz@ub.edu (V. Sanz-Nebot).

http://dx.doi.org/10.1016/j.chroma.2017.05.069
0021-9673/

and human growth hormone (hGH) short fragments with a few ionisable groups [17].

The development of rapid, efficient and high-resolution separations in CE requires a previous optimisation. This optimisation can be assisted by modelling the electrophoretic behaviour of the target compounds to avoid excessive experimental work [15,18–21]. Accurate quantitative relationships between the m_e of ionisable compounds and the pH of the background electrolyte (BGE) have proved to be very useful to simultaneously determine their pK_as and the optimum pH for their separation in a complex mixture [15,18]. Moreover, several semiempirical relationships relating the m_e of the analytes to their structure (charge, molecular mass or number of amino acid residues) have been proposed [15,18–21]. In previous works, these classical semiempirical relationships yielded excellent correlations for several peptide hormones [15], neuropeptides [18], apothioneins [19], peptides and glycopeptides from tryptic digests of glycoproteins [20] and quinolones [21] when good estimates of pK_a values were available for charge calculations.

In this work, a general equation relating the m_e with pH, pK_as and activity coefficients is used to model the migration behaviour and determine the pK_as of five amyloid beta (Aβ) peptide fragments (1–15, 10–20, 20–29, 25–35 and 33–42) that cover all the sequence of Aβ peptides 1–40 and 1–42. Aβ 1–40 and 1–42 are clinical biomarkers used for Alzheimer's disease diagnosis, which is nowadays one of the most common age-related neurodegenerative disorders [22,23]. Aβ peptides are produced during normal cellular metabolism and are constituents of biological fluids but under pathological conditions they aggregate and form amyloidotic fibrils which are deposited and accumulated in the brain as plaques. As protein aggregation depends on pH [24,25], characterization of the physicochemical parameters of these peptides is important. Once the pK_as of the Aβ peptide fragments were determined by CE, the classical polymer model (m_e vs. $q/M_r^{1/2}$, q = charge and M_r = relative molecular mass) was used to predict the separation of a mixture of the fragments and confirm the accuracy of the pK_as. Finally, we demonstrated that the pK_as of the fragments were good estimates for the ionisable groups of Aβ peptides 1–40 and 1–42 by predicting separations in bare fused silica and poly(vinyl alcohol) (PVA) capillaries.

2. Materials and methods

2.1. Chemicals and reagents

All the chemicals used in the preparation of BGEs and solutions were of analytical reagent grade or better. Acetone, ammonia (25%), boric acid, diethylmalonic acid, hydrochloric acid (25%), methanol, phosphoric acid (85%), sodium acetate, potassium hydroxide, sodium dihydrogen phosphate, sodium formate and sodium hydroxide were supplied by Merck (Darmstadt, Germany). Tris(hydroxymethyl)aminomethane (Tris) was purchased from J.T. Baker (Deventer, Netherlands). Glutaraldehyde (50%) and PVA (hydrolysis grade 99%, average M_r 90,000) were purchased from Sigma-Aldrich (Steinheim, Germany). Water with conductivity lower than 0.05 S cm^{-1} was obtained using a Milli-Q water purification system (Millipore, Molsheim, France). The fragments of Aβ peptides 1–15, 10–20, 20–29, 25–35 and 33–42 and Aβ peptides 1–40 and 1–42 were provided by Bachem (Bubendorf, Switzerland). Their sequences, ionisable groups and M_r are shown in Table 1.

2.2. Electrolyte solutions and samples solutions

The BGEs for the determination of m_e covered the pH range 2–12. They were prepared at the following concentrations (pH was adjusted with 1.0 M HCl or 1.0 M NaOH and the I was calculated to be 25 mM): 15 mM NaH_2PO_4 (pH 2.0), 25 mM NaH_2PO_4 (pH 2.5–3.0), 25 mM sodium formate (pH 3.5–4.0), 25 mM sodium acetate (pH 4.5–5.0), 20 mM diethylmalonic acid (pH 5.5–6.5), 25 mM Tris (pH 7.0–9.0), 30 mM H_3BO_3 (pH 9.5–10.5) and 5 mM H_3PO_4 (pH 11.0–12.0). BGEs were passed through a 0.22 μm nylon filter (Panreac Applichem, Barcelona, Spain).

Individual stock solutions (1000 mg L^{-1}) of Aβ 1–15, 10–20, 20–29, 25–35 were prepared in water and Aβ 33–42 in 5% (v/v) DMSO because it was less soluble in water. The working solutions (200 mg L^{-1}) contained 3% (v/v) acetone or 5% (v/v) DMSO (Aβ 33–42) as electroosmotic flow (EOF) marker. A mixture of the five peptides (200 mg L^{-1}) was also prepared in water. Solvent and storage conditions were especially critical for Aβ 1–40 and 1–42, which were prone to aggregation. Aβ 1–40 and 1–42 were dissolved (1000 mg L^{-1}) in 50 mM and 100 mM ammonium hydroxide aqueous solutions, respectively, following the manufacturer's recommendation. A mixture of the two Aβ peptides (200 mg L^{-1}) was prepared in 100 mM ammonium hydroxide aqueous solution. All the stock solutions were divided into several aliquots and individually stored at −20 °C. Each aliquot was thawed only once, preserved in the refrigerator between injections and immediately discarded after the analyses.

2.3. Instrumental parameters

All CE-UV experiments were performed in an Agilent HP 3DCE system (Agilent Technologies, Waldbronn, Germany). Unless otherwise indicated, separations were performed at 25 °C in a 57 cm total length (L_T) × 75 μm internal diameter (i.d.) × 365 μm outer diameter (o.d.) bare fused silica capillary (Polymicro Technologies, Phoenix, AZ, USA). All capillary rinses were performed at high pressure (930 mbar). New capillaries were flushed with 1 M NaOH (15 min), water (15 min) and BGE (30 min). The system was finally equilibrated by applying 25 kV of separation voltage for 20 min (normal polarity, cathode in the outlet). Samples were injected at 50 mbar for 3 s. Between runs, capillaries were conditioned by rinsing with 1 M NaOH (1 min), water (1 min) and BGE (1 min). Between workdays or after a change of BGE, the capillary was conditioned by rising with 1 M NaOH (5 min), water (5 min) and BGE (10 min). The system was finally equilibrated by applying 25 kV of separation voltage for 20 min. Capillaries were stored overnight filled with water. For experiments with PVA capillaries, bare fused silica capillaries were coated with PVA following a procedure described elsewhere and cut to a L_T of 57 cm [26,27]. The conditioning, rinsing and separation methods were the same as in bare fused silica capillaries, but without using NaOH to prevent coating damage.

pH measurements were made with a Crison 2002 potentiometer and a Crison electrode 52-03 (Crison Instruments, Barcelona, Spain).

2.4. Determination of electrophoretic mobility and acidity constants

The m_e of each Aβ fragment was measured by CE-UV as the difference between the apparent mobility of each peptide, m_{app}, and the mobility of the neutral marker, m_{EOF} [15,18–21]:

$$m_e = m_{app} - m_{EOF} = \frac{L_C L_D}{V}\left(\frac{1}{t_{app}} - \frac{1}{t_{EOF}}\right) \quad (1)$$

Where L_C is the capillary length, L_D is the distance from the injection point to the detector and t_{app} and t_{EOF} are the migration time of the peptide and the neutral marker, respectively. Individual solutions of each peptide were injected at each pH and m_e was obtained as the average of five replicates. BGEs indicated in Section 2.2 were run in sequence from low to high pH.

Table 1
Amino acid sequence, relative monoisotopic molecular mass (M_r) and ionisable groups for the studied Aβ peptides.

Aβ peptide sequence	M_r	Ionisable amino acids		Formula	
		Acidic [a]	Basic [b]	$H_nABH_z^z$	H_nX^z
1–15 **DAEFRHDSGYEVHHQ**	1826.9	1 ^{t}C-Q [c1] 2 D [c1] 2 E [c2] 1 Y	1 ^{t}N-D 3 H [c3] 1 R [d]	$\boldsymbol{H_6ABH_5^{5+}}$	$H_{11}X^{5+}$
10–20 **YEVHHQKLVFF**	1446.7	1 ^{t}C-F 1 E 1 Y [e2]	1 ^{t}N-Y 2 H [e1] 1 K [e2]	$\boldsymbol{H_3ABH_4^{4+}}$	H_7X^{4+}
20–29 **FAEDVGSNKG**	1023.1	1 ^{t}C-G [f] 1 D [f] 1 E	1 ^{t}N-F 1 K	$\boldsymbol{H_3ABH_2^{2+}}$	H_5X^{2+}
25–35 **GSNKGAIIGLM**	1060.3	1 ^{t}C-M	1 ^{t}N-G 1 K	$\boldsymbol{HABH_2^{2+}}$	H_3X^{2+}
33–42 **GLMVGGVVIA**	915.2	1 ^{t}C-A	1 ^{t}N-G	$\boldsymbol{HABH^{+}}$	H_2X^{+}
1–40 **DAEFRHDSGYEVHHQKLVFFAEDVGSNKGAIIGLMVGGVV**	4329.9	1 ^{t}C-V 3 D 3 E 1 Y	1 ^{t}N-D 3H 2 K 1 R	$\boldsymbol{H_6ABH_7^{7+}}$	$H_{15}X^{7+}$
1–42 **DAEFRHDSGYEVHHQKLVFFAEDVGSNKGAIIGLMVGGVVIA**	4514.1	1 ^{t}C-A 3 D 3 E 1 Y	1 ^{t}N-D 3H 2 K 1 R	$\boldsymbol{H_6ABH_7^{7+}}$	$H_{15}X^{7+}$

[a] In this column ^{t}C-: Terminal COOH.
[b] In this column ^{t}N-: Terminal NH_2. The following ionisable groups were combined for the calculations:
[c1] 1 ^{t}C-Q and 2 D.
[c2] 2 E.
[c3] 3 H.
[d] R was not considered for the calculations because the expected pK_a was outside the studied pH range (2–12).
[e1] 2 H.
[e2] 1 Y and 1 K.
[f] 1 ^{t}C-G and 1 D.

Table 2
Electrophoretic models for the studied Aβ fragments in the pH range 2–12.

Aβ fragment	H_nX^z	Electrophoretic model
1–15 [a,b]	$H_{11}X^{5+}$	$m_e = \frac{10^{(3pK_1' + 2pK_2' - 5pH)} m_{H_{11}X^{5+}} + 10^{(2pK_2' - 2pH)} m_{H_8X^{2+}} + 10^{(3pH - 3pK_3')} m_{H_5X^{3-}} + 10^{(4pH - 3pK_3' - pK_4')} m_{H_2X^{4-}} + 10^{(5pH - 3pK_3' - pK_4' - pK_5')} m_{HX^{5-}}}{10^{(3pK_1' + 2pK_2' - 5pH)} + 10^{(2pK_2' - 2pH)} + 1 + 10^{(3pH - 3pK_3')} + 10^{(4pH - 3pK_3' - pK_4')} + 10^{(5pH - 3pK_3' - pK_4' - pK_5')}}$
10–20 [c]	H_7X^{4+}	$m_e = \frac{10^{(pK_1' + pK_2' + 2pK_3' - 4pH)} m_{H_2X^{4+}} + 10^{(pK_2' + 2pK_3' - 3pH)} m_{H_6X^{3+}} + 10^{(2pK_3' - 2pH)} m_{H_5X^{2+}} + 10^{(2pH - pK_4')} m_{H_2X^{-}} + 10^{(3pH - pK_4' - 2pK_5')} m_{X^{3-}}}{10^{(pK_1' + pK_2' + 2pK_3' - 4pH)} + 10^{(pK_2' + 2pK_3' - 3pH)} - 10^{(2pK_3' - 2pH)} + 1 + 10^{(pH - pK_4')} + 10^{(3pH - pK_4' - 2pK_5')}}$
20–29 [d]	H_5X^{2+}	$m_e = \frac{10^{(2pK_1' - 2pH)} m_{H_2X^{2+}} + 10^{(pH - pK_2')} m_{H_2X^{-}} + 10^{(2pH - pK_2' - pK_3')} m_{HX^{2-}} + 10^{(3pH - pK_2' - pK_3' - pK_4')} m_{X^{3-}}}{10^{(2pK_1' - 2pH)} + 1 + 10^{(pH - pK_2')} + 10^{(2pH - pK_2' - pK_3')} + 10^{(3pH - pK_2' - pK_3' - pK_4')}}$
25–35	H_3X^{2+}	$m_e = \frac{10^{(pK_1' + pK_2' - 2pH)} m_{H_3X^{2+}} + 10^{(pK_2' - pH)} m_{H_2X^{+}} + 10^{(pH - pK_3')} m_{X^{-}}}{10^{(pK_1' + pK_2' - 2pH)} + 10^{(pK_2' - pH)} + 1 + 10^{(pH - pK_3')}}$
33–42	H_2X^{+}	$m_e = \frac{10^{(pK_1' - pH)} m_{H_2X^{+}} + 10^{(pH - pK_2')} m_{X^{-}}}{10^{(pK_1' - pH)} + 1 + 10^{(pH - pK_2')}}$

[a] R (Arg) was not considered for the calculations because the expected pK_a was outside the studied pH range (2–12). The ionisable groups of the following amino acids were combined for the calculations because the pK_a values were expected to be very similar:
[b] 1 ^{t}C-Q and 2 D (pK_1'), 2 E (pK_2'), 3 H (pK_3').
[c] 2 H (pK_3'), 1 Y and 1 K (pK_5').
[d] 1 ^{t}C-G and 1 D (pK_1').

In previous studies [15,18–21] we established a general equation relating the m_e of a polyprotic substance H_nX^z (n = number of ionogenic groups and z = maximum net charge), to the pH of the BGE, taking into account the apparent pK_a values (pK_a') over the selected pH range. Table 2 shows the equation derived for each Aβ fragment. It is worth mentioning that Aβ 1–15, 10–20 and 20–29 contained ionisable groups with equal or very similar pK_a' values, which were not possible to be separately determined by CE-UV (pK_a difference with Rickard et al. values [17] was less than 0.5 units, Table 3). Therefore, they were considered as a single group for ease of calculation (e.g. ^{t}C-Q and 2 D amino acids were combined in Aβ 1–15, Tables 1–3). Also note that acid-base equilibrium for the guanidine group in the R residue (Arg pK_a 12.5 [17]) fell outside

Table 3
CE-UV apparent pK_as (pK_a'), thermodynamic pK_as, pK_as of Rickard et al. [17] and pK_as of the free amino acid [35].

Aβ fragment	pK_a'	pK_i'	γ_i/γ_j	pK_a	pK_a Rickard et al.	pK_a free amino acid	Amino acid [a]
1–15	3.5±0.3 [b1]	1	γ_{5+}/γ_{4+}	2.9	3.2	2.2	[c]C-Q
			γ_{4+}/γ_{3+}	3.0	3.5	3.7	D
			γ_{3+}/γ_{2+}	3.1	3.5	3.7	D
	4.7±0.7 [b2]	2	γ_{2+}/γ_{+}	4.5	4.5	4.3	E
			γ_{+}/γ_{0}	4.6	4.5	4.3	E
	6.0±0.1 [b3]	3	γ_{0}/γ_{-}	6.0	6.2	6.0	H
			γ_{-}/γ_{2-}	6.2	6.2	6.0	H
			γ_{2-}/γ_{3-}	6.3	6.2	6.0	H
	8.1±0.4	4	γ_{3-}/γ_{4-}	8.6	8.6	9.6	[c]N-D
	10.4±0.7	5	γ_{4-}/γ_{5-}	11.1	10.3	10.1	Y
	- [c]	-	γ_{5-}/γ_{6-}	-	12.5	12.5	R
10–20	3.8±0.2	1	γ_{4+}/γ_{3+}	3.3	3.2	1.8	[c]C-F
	4.9±0.6	2	γ_{3+}/γ_{2+}	4.5	4.5	4.3	E
	6.0±0.2 [d1]	3	γ_{2+}/γ_{+}	5.7	6.2	6.0	H
			γ_{+}/γ_{0}	5.9	6.2	6.0	H
	8.0±0.1	4	γ_{0}/γ_{-}	8.0	7.7	9.1	[c]N-Y
	10.2±0.1 [d2]	5	γ_{-}/γ_{2-}	10.4	10.3	10.1	Y
			γ_{2-}/γ_{3-}	10.6	10.3	10.5	K
20–29	3.2±0.1 [e]	1	γ_{2+}/γ_{+}	2.9	3.2	2.3	[c]C-G
			γ_{+}/γ_{0}	3.1	3.5	3.7	D
	4.6±0.1	2	γ_{0}/γ_{-}	4.7	4.5	4.3	E
	7.8±0.2	3	γ_{-}/γ_{2-}	8.1	7.7	9.1	[c]N-F
	10.5±0.2	4	γ_{2-}/γ_{3-}	10.8	10.3	10.5	K
25–35	3.3±0.1	1	γ_{2+}/γ_{+}	3.1	3.2	2.3	[c]C-M
	8.3±0.1	2	γ_{+}/γ_{0}	8.2	8.2	9.6	[c]N-G
	10.5±0.1	3	γ_{0}/γ_{-}	10.5	10.3	10.5	K
33–42	3.2±0.1	1	γ_{+}/γ_{0}	3.1	3.2	2.3	[c]C-A
	8.3±0.1	2	γ_{0}/γ_{-}	8.3	8.2	9.6	[c]N-G

[a] C-: Terminal COOH; [c]N-: Terminal NH_2.
[c] R (Arg) was not considered for the calculations because the expected pK_a was outside the studied pH range (2–12).
[b1, b2, b3, d1, d2 and e] The ionisable groups were combined for the calculations (See Table 1).

the studied pH range and was not considered for the calculations (Tables 1–3).

The pK_a' values were determined from nonlinear regression analysis of data pairs of m_e–pH (SciDAVis free software, 1.D009, Russell Standish, Sydney, Australia).

The effect of ionic strength (I) upon pK_a' was taken into account, considering the activity coefficients of the solutes (γ), obtained from the Guntelberg approximation of the extended law of Debye-Hückel (valid for I < 0.2 M):

$$\log \gamma = \frac{-z^2 A\sqrt{I}}{1+\sqrt{I}} \quad (2)$$

Where A is a temperature and solvent dielectric dependent constant with value of 0.509 in water at 25 °C. γ of neutral species (γ_0) were assumed to be unity. Then, the thermodynamic pK_a values were easily calculated from the expression:

$$pK_{ai} = pK_{ai}' + log\frac{\gamma^{z-(i-1)}}{\gamma^{z-i}} \quad (3)$$

The pK_as for Aβ peptides 1–40 and 1–42 were estimated taking into account the thermodynamic pK_as obtained by CE-UV for the Aβ fragments (Table 4).

2.5. Prediction of migration with the classical semiempirical models

In general, the m_e of a peptide is proportional to its q and inversely proportional to its Stoke's radius (r). The r is generally expressed in terms of M_r, because the volume of a molecule is proportional to its mass if the density is constant [28,29]. The classical equations describing semiempirical models are deduced from assumptions concerning the peptide shapes and the forces that they undergo during electrophoretic motion. The general form of the equation relating m_e, M_r and q is as follows:

$$m_e = B\frac{q}{M_r^{\alpha}} \quad (4)$$

where B is a constant and the parameter α takes different values depending on the assumptions made on deduction of the semiempirical model (α = 1/2, 1/3 and 2/3 for the classical polymer model, the Stoke's law and the Offord's surface law, respectively) [28,29].

In order to obtain q/M_r^{α} values for the studied peptides, M_r was calculated from the amino acid sequences (Table 1) and q was calculated at each separation pH using the experimental CE-UV pK_as (Table 3) and Sillero and Ribeiro expression [30], which is based on the Henderson–Hasselbalch equation:

$$q = \sum_n \frac{P_n}{1+10^{pH-pK(P_n)}} - \sum_j \frac{N_j}{1+10^{pK(N_j)-pH}} \quad (5)$$

Where P_n and N_n are the cationic (i.e. P_1 = terminal NH_2, P_2 = H, P_3 = K and P_4 = R) and anionic (i.e. N_1 = terminal COOH, N_2 = D, N_3 = E and N_4 = Y) ionisable groups found in the amino acids, and pK_a (P_n) and pK_a (N_n) are the pK_as of these groups. The accuracy of the q calculated in this way depends on the proposed sequence and the reliability of the pK_a considered for the ionisable groups [15]. Only for Aβ 1–15 (or later for Aβ 1–40 and 1–42), the average pK_a given by Rickard et al. [17] was used for the guanidine group in the R residue (12.5) because this pK_a could not be obtained by CE-UV (Tables 1–3).

Once linearity between m_e and q/M_r^{α} was demonstrated for all the peptides at the different pH values, q/M_r^{α} could be obtained at a certain pH to predict separation resolution or selectivity, as well as to simulate the electropherogram of a mixture, showing a pure Gaussian peak for each peptide [31]. As q/M_r^{α} was inversely proportional to migration time, M_r^{α}/q was considered for the graphic representations to show a correct migration order in the simulated electropherograms. In contrast to our previous works [18–21], now

Table 4
Thermodynamic pK_as for Aβ fragments obtained by CE (from Table 3) and average pK_as calculated as an estimate of the pK_as of Aβ peptides 1–40 and 1–42.

Ionisableamino acid [a]	Aβ fragment	pK_a [b]	Average pK_a	Standard deviation	Number of residues in the sequence of the Aβ peptide	
					1–40	1–42
[t]C	1-15	**2.9 (Q)**	3.1	**0.2**	1 (V)	**1 (A)**
	10-20	**3.3 (F)**				
	20-29	**2.9 (G)**				
	25-35	**3.1 (M)**				
	33-42	**3.1 (A)**				
D	1-15	**3.0**	3.1	**0.1**	3	**3**
		3.1				
	10-20	**3.1**				
E	1-15	**4.5**	4.6	**0.1**	3	**3**
		4.6 [c]				
	10-20	**4.5** [c]				
	20-29	**4.7**				
H	1-15	**6.0**	6.0	**0.1**	3	**3**
		6.2 [d1]				
		6.3 [d2]				
	10-20	**5.7** [d1]				
		5.9 [d2]				
[t]N	1-15	**8.6 (D)**	8.6	-	1 (D)	**1 (D)**
K	10-20	**10.6**	10.6	**0.2**	2	**2**
	20-29	**10.8** [e]				
	25-35	**10.5** [e]				
Y	1-15	**11.1**	10.8	**0.5**	1	**1**
	10-20	**10.4**				
R	1-15	- [f]	12.5 [g]	-	1	**1**

[a] [t]C: Terminal COOH; [t]N: Terminal NH_2. The terminal amino acids are indicated between parentheses.
[b] Experimental CE-UV thermodynamic pK_as for Aβ fragments (See Table 3).
[c, d1, d2 and e] The same position of the amino acid sequence is repeated in both Aβ fragments.
[f] pK_a of R (Arg) was not determined by CE-UV because the expected pK_a was outside the studied pH range (2–12).
[g] pK_a of R (Arg) of Rickard et al. [17].

the influence of the EOF on migration time was also considered in the simulations:

$$h(x) = h_0 e^{-\frac{1}{2}\left[\frac{x-x_i}{\sigma}\right]^2} \quad (6)$$

Where x corresponds to M_r^{α}/q and defined the x-scale, h_0 defined the peak height, σ was the standard deviation of the Gaussian peak ($w_{1/2}$ (width at half height) = 2.354*σ) and x_i was related to the target peptide and the EOF at the studied pH value ($M_r^{\alpha}/q_i + 1/(C^*E)$) and it was the function value at the peak maximum for each peptide. The EOF influence at each pH value was taken into account adding the term $1/(C^*E)$ in x_i, since the EOF was inversely related to migration time [32,33]. C ranged between 0 and 1 and was the relative change of the EOF in a bare fused silica capillary at the studied pH values. It was calculated as the ratio between the EOF mobility (m_{EOF}) at the studied pH value and the maximum m_{EOF}, which corresponded in bare fused silica to pH 12. The curves of m_{EOF} variation as a function of pH were obtained from the literature [33]. E was a constant to normalize the 1/C values, in order to prevent the magnitude differences between 1/C and M_r^{α}/q_i. E was arbitrarily selected as 1.1 times the most negative value of the M_r^{α}/q_i calculated for the peptides at the different pH values, in order to ensure simulation of all the negative ions because they migrated to the detector.

For PVA capillaries, the same reasoning was applied and the curves of m_{EOF} variation as a function of pH were also obtained from the literature [34]. An average $w_{1/2}$ value of 0.2 to calculate σ was fixed taking into account measurements of $w_{1/2}$ in the experimental electropherograms. A value of 50 and 90 was arbitrarily selected as h_0 for all the peptide peaks and for the EOF marker peak, respectively. In order to simplify the simulation procedure no other assumptions were made regarding peak shape or the influence of BGE composition on migration time and resolution. Microsoft Office Excel 2010 for Windows was used for all the calculations and simulations.

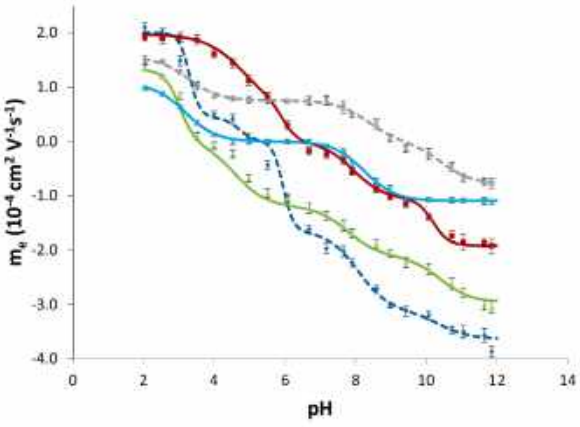

Fig. 1. Experimental (symbols) and predicted (lines) m_e vs. pH of the BGEs for Aβ fragments 1–15 (♦), 10–20 (■), 20–29 (▲), 25–35 (X) and 33–42 (✻). The error bars show standard deviations (n=5).

3. Results and discussion

3.1. Electrophoretic behaviour and determination of pK_a by CE-UV

The study of the electrophoretic behaviour of polyprotic compounds (e.g. peptides) as a function of pH can be simultaneously used for the accurate determination of their pK_as and for selection of the optimum pH for separation of mixtures of the modelled compounds [15,18]. Fig. 1 shows a plot of the experimental m_e for the studied Aβ fragments (symbols) against the pH of the BGE. Good correlations were observed when these experimental m_e–pH data pairs were fitted to the corresponding equations of Table 2 using

nonlinear regression analysis (predicted m_es are shown as solid curve lines, $R^2 > 0.995$). Therefore, the proposed equations, which were deduced combining acid-base groups for some of the fragments (i.e. Aβ 1–15, 10–20 and 20–29), performed well despite the complexity of the polyprotic peptides and the approximations made to derive the equations for the different fragments (Tables 1 and 2). It is worth mentioning that when the electrophoretic models were modified in Aβ 1–15, 10–20 and 20–29 to consider all the non-equivalent ionisable groups separately (e.g. ^{1}C-Q and 2 D amino acids in Aβ 1–15, Tables 1–3), the calculation did not converge or the obtained pK_a values did not make chemical sense.

The thermodynamic pK_a of the peptides were calculated using the apparent pK_a' obtained from the best-fit parameters of each nonlinear regression model and are summarized in Table 3, together with the corresponding average pK_as given by Rickard et al. [17] and the pK_as of the free amino acids [35]. The average pK_as given by Rickard et al. were established for amino acids using the information collected for a large set of biosynthetic human insulin (BHI) and human growth hormone (hGH) short fragments with a few ionisable groups and are broadly used for proteins, polypeptides and small peptides studies. As can be seen, in general, the experimental pK_as obtained by CE-UV for the Aβ fragments were very similar to the average pK_as given by Rickard et al., especially for the Aβ 25–35 and 33–42, which presented a lower number of ionisable groups. For the longer fragments, the most important shifts were found in the terminal ionisable carboxylic acid and amino groups, but not in the ionisable groups of the side chains. This effect was already observed by Rickard et al. when they compared their average pK_a values with the pK_a values for the free amino acids (Table 3) [17]. The acidity of these terminal groups becomes weaker because the formation of the peptide bond induces an electrostatic change in the charge on the neighboring amino and carboxy groups. As the difference between our CE-UV pK_as and the average pK_as of Rickard et al. is very small, we recommend the use of these average pK_as for the amino acids when accurate pK_as for proteins and peptides are not available, for example, for electrophoretic separation prediction. These values are a far better approximation to the real pK_as than the pK_as of the free amino acids [15,18–20].

3.2. Classical semiempirical models for migration prediction

The usefulness of equations in Table 2 for prediction of the electrophoretic behaviour of the studied peptides as a function of pH is limited because the number of experimental m_e-pH data pairs necessary for an accurate migration prediction is relatively large and increases with the number of ionisable groups. If accurate pK_a values are known (e.g. CE-UV pK_as) or an appropriate estimation is available (e.g. Rickard et al. pK_as [17]), a better option to estimate a suitable pH for separation of the mixture is the approach based on the classic semiempirical relationships between m_e and q/M_r^{α} [15,18–21]. Fig. 2 shows for all the studied peptides in the pH range 2–12 the plot of m_e against q/M_r^{α} for the classical polymer model ($\alpha = 1/2$), the Stoke's law ($\alpha = 1/3$) and the Offord's surface law ($\alpha = 2/3$). In all cases, good linear correlations were observed ($r^2 > 0.97$), confirming the validity of the classical semiempirical models in the whole pH range and the accuracy of the CE-UV pK_as used for charge calculation. The classical polymer model ($r^2 \geq 0.978$) was considered for prediction of the separation of a mixture of the Aβ fragments. This model was also the preferred model in our previous works to explain the migration behaviour of peptide hormones [15], neuropeptides [18], apothioneins [19] and glycopeptides from tryptic digests of recombinant human erythropoietin [20].

Once the validity of the relationship between m_e and $q/M_r^{1/2}$ is verified, a suitable pH for separation of the mixture can be estimated by selecting the appropriate pH to obtain the greatest differences between the curves of $q/M_r^{1/2}$ vs pH for the Aβ fragments. However, it is preferable to predict other parameters that quantitatively describe the extent of separation and the influence of the EOF. Predicting resolution (R_s) between critically adjacent peaks is the best way to evaluate separation because efficiency and selectivity are simultaneously taken into account. In electrophoretic separations, R_s is usually calculated from the expression [32]:

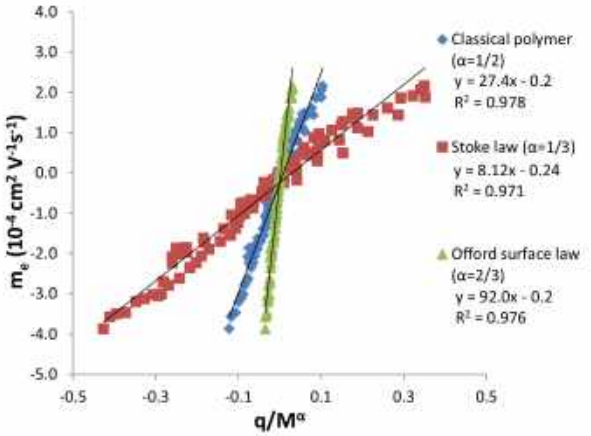

Fig. 2. Correlation between m_e and q/M_r^{α} for the Aβ fragments in the pH range 2–12. α = 1/2, 1/3 and 2/3 for the classical polymer model, the Stoke's law and the Offord's surface law, respectively. (q/M_r^{α} values were calculated with the experimental CE-UV pK_as, excepting for the guanidine group in the R residue in Aβ 1–15 [17] (Table 3)).

$$R_s = \frac{\sqrt{N}}{4} \cdot \frac{(m_i - m_{i+1})}{(m_{avg} + m_{EOF})} \qquad (7)$$

Efficiency Selectivity.

Where N is the number of theoretical plates, m_i is the m_e of the peptides, m_{avg} is the average of m_i values and m_{EOF} is the EOF mobility. Resolution has been widely studied to optimise separations as a function of pH in CE with fused silica and coated capillaries [32,36]. If we suppose similar N values for all the peptides of the mixture, efficiency is considered as constant and only accounts for resolution the selectivity term. Furthermore, Eq. (7) can be adapted to predict a parameter related to separation selectivity (S) from the predicted $q/M_r^{1/2}$, taking into account the linear relationship between m_e and $q/M_r^{1/2}$:

$$S = \frac{\left(q/M_{ri}^{1/2} - q/M_{ri+1}^{1/2}\right)}{\left(q/M_{ravg}^{1/2} + C * E\right)} \qquad (8)$$

Where $q/M_{ri}^{1/2}$ is the predicted $q/M_r^{1/2}$ of the peptide i, $q/M_{ravg}^{1/2}$ is the average of $q/M_{ri}^{1/2}$ values and C*E is the term taking into account the influence of the EOF at each pH value, as explained for Eq. (6) in Section 2.5.

Eq. (8) was used to predict S between adjacent peak pairs, considering the changes in migration orders that can be observed in Fig. 1 and including the neutral marker peak, which migrates with the EOF ($q/M_r^{1/2} = 0$). A plot of the predicted S between the worst-separated peak pair over the studied pH range permitted selection of the optimum pH for the separation of the five Aβ fragments (Fig. 3A). As observed in Fig. 3A, the best separations were expected to be obtained at pH 3.0 and 10.5 because S was the highest. Separations were the worst in the pH range 5–9 because of the slight differences between $q/M_r^{1/2}$ of the peptides or because they co-migrated with the EOF (their pIs were within that pH range, see

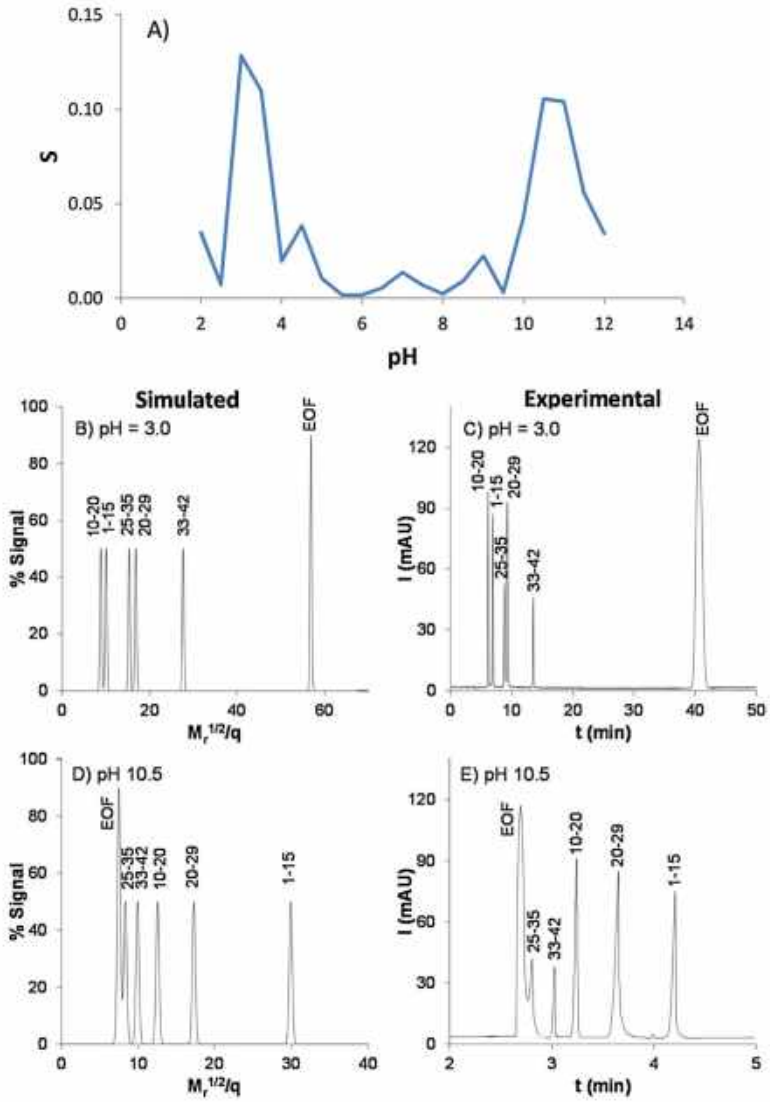

Fig. 3. A) Selectivity (S) of the worst-separated peak pair in a mixture of the five Aβ fragments in the pH range 2–12. Simulated and experimental electropherograms of a mixture of the five Aβ fragments at pH 3.0 (B and C) and 10.5 (D and E).

Fig. 1). In terms of selecting the optimum pH for the separation, this approach dramatically cuts down total optimisation time. Similar conclusions were drawn with an alternative quality criterion to optimise separations that Tascon et al. recently described [36], adapting t' to use $q/M_r^{1/2}$ and considering the influence of the EOF.

$$t' = \frac{\left[q/M_{ri}^{1/2} * q/M_{ri+1}^{1/2}\left(q/M_{ri}^{1/2} - q/M_{ri+1}^{1/2}\right)\right]^2}{C * E} \quad (9)$$

In this case, there was no need to consider the EOF peak to predict the separation from the neutrals but, as in S parameter, we introduced the term C*E in the denominator to take into account that separation decreases when EOF increases [32,33].

In order to further confirm the pH selection, the electropherograms for the separation of the mixture were simulated at pH 3.0 and 10.5 (Fig. 3B and D). As can be observed, despite the simplicity of the approach, the agreement with the experimental electropherograms was good (Fig. 3C and E). The mixture of the five Aβ fragments was better resolved at acidic pH than at basic pH, where one of the peptides slightly comigrated with the EOF. However, at pH 10.5 the total separation times were the lowest because the EOF in the fused silica capillary was much higher than at pH 3.0.

With regard to the Aβ peptides 1–40 and 1–42, both contain a total of 15 ionisable groups corresponding to 8 different ionisable amino acids (Table 1). Once the accuracy of the experimental CE-UV pK_as of the Aβ fragments was demonstrated predicting the electrophoretic behaviour and the selectivity of the separations, as well as simulating the electropherograms, these pK_as were used to estimate the pK_as of the 8 ionisable amino acids of the Aβ peptides 1–40 and 1–42. An estimate of these pK_as was calculated as an average of the thermodynamic pK_as obtained by CE-UV for the Aβ fragments (Table 4). As can be observed in Table 4, in most cases, the standard deviation of the pK_as of the Aβ fragments used for the estimation was less than 0.2, hence justifying the validity of the approximation. Note in Table 4 that the average pK_a given by Rickard et al. [17] was used as an estimate for the guanidine group in the R residue (12.5) of the Aβ peptides 1–40 and 1–42 because this pK_a could

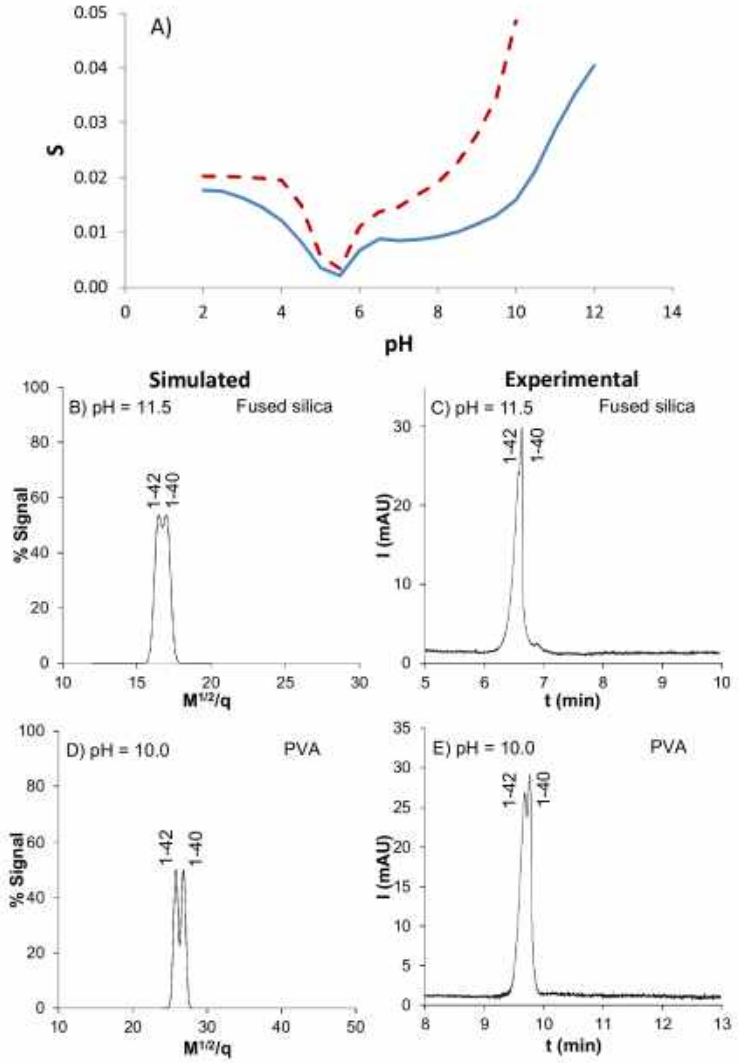

Fig. 4. A) Selectivity (S) between the Aβ 1–40 and 1–42 peptides in the pH range 2–12 in a bare fused silica capillary (solid line) and in the pH range 2–10 in a PVA coated capillary (dash line). (q/M, $^{1/2}$ values were calculated with the estimated pK_as of the Aβ peptides 1–40 and 1–42, excepting for the guanidine group in the R residue [17] (Table 4)). Simulated and experimental electropherograms of a mixture of Aβ 1–40 and 1–42 peptides at pH 11.5 (bare fused silica capillary) (B and C) and 10.0 (PVA coated capillary) (D and E).

not be obtained by CE-UV for the fragments. The estimated pK_as of Table 4 are used to evaluate separations of Aβ peptides 1–40 and 1–42. The plot of S between the Aβ peptides over the pH range 2–12 allowed again a rapid selection of an appropriate pH for the separation (Fig. 4A). As can be observed, the S values between the Aβ 1–40 and 1–42 were much smaller than before between the Aβ fragments (compare the y-axis scale of Figs. 3 A and 4 A). The best separation was predicted in the pH range 11.5-12. However, even at those conditions, S was very low, due to the very small structural differences between both peptides, which differ only in two amino acids that do not contain ionisable groups (Table 1). Fig. 4B and C shows the simulated and experimental electropherograms of the mixture at pH 11.5 in a fused silica capillary (fused silica is not very stable at pH 12.0). The simulation was in good agreement with the experimental results and, as expected, separation resolution was poor. The separation was also tested using 50 μm and 30 μm i.d bare fused silica capillaries, but resolution did not improve. Another interesting approach is the use of coated capillaries to control the EOF and to suppress analyte-wall interactions. Hydrophilic non-ionic coatings significantly reduce the EOF, suppress the adsorption of basic compounds to the capillary wall and, in some cases, could act as a pseudo-stationary phase. Among these, permanently coated hydroxypropyl cellulose (HPC) and PVA capillaries have proven to exhibit a particularly good performance in terms of stability and reproducibility [26,27,37,38]. In our case, only PVA capillaries gave remarkable results with regard to separations of Aβ 1–40 and 1–42 peptides. In order to ensure the stability of the coating, separation was done at pH 10.0 instead of pH 11.5 (Fig. 4A). Fig. 4D and E shows that again concordance between the simulated and experimental electropherograms is good, because the EOF magnitude is taken into account for the simulations [34]. Furthermore, the EOF reduction at pH 10.0 in PVA capillaries, with regard to a fused silica capillary at pH 11.5 (more than 40% in our case), allowed a slight improvement of the resolution between both peptides, at the expense of a slight increase in total separation time. In order to further improve this separation, it would be necessary to

explore complementary mechanisms based on interactions with a pseudo-stationary phase, a complexing agent or to use on-line MS detection.

4. Concluding remarks

In this study, we have estimated by CE-UV the pK_as of Aβ peptides 1–40 and 1–42 from five Aβ peptide fragments covering all their complete amino acid sequence. First, the experimental m_es of the five fragments in the studied pH range were fitted to equations modelling their ionisable behaviour as a function of pH. The accuracy of the pK_as was demonstrated predicting the electrophoretic behaviour of the studied fragments and separation selectivity of their mixture using the classical polymer model. Bearing in mind the excellent results and the simplicity of the approach, if accurate pK_a values are available for the target compounds, this is a remarkable strategy for making a rapid and "dry" selection of the optimum pH for the separation of their mixtures. The pK_as of the fragments were also valuable estimates for the Aβ 1–40 and 1–42 (^{1}C and D 3.1, E 4.6 and Y 10.8 for acidic amino acids and ^{t}N-D 8.6, H 6.0, K 10.6 and R 12.5 for basic amino acids). Therefore, the estimation of pK_as of complex polyprotic peptides from their building peptide fragments can be regarded as a straightforward and reliable method to acquire information that could not be readily acquired by other means.

Acknowledgements

This study was supported by a grant from the Spanish Ministry of Economy and Competitiveness (CTQ2014-56777-R). Roger Peró-Gascón acknowledges the Generalitat de Catalunya for a FI-DGR fellowship. We also thank Lleonart Quiles for his collaboration in part of this study.

References

[1] S.K. Poole, S. Patel, K. Dehring, H. Workman, C.F. Poole, Determination of acid dissociation constants by capillary electrophoresis, J. Chromatogr. A 1037 (2004) 445–454, http://dx.doi.org/10.1016/j.chroma.2004.02.087.
[2] S. Babič, A.J.M. Horvat, D. Mutavdžič Pavlovič, M. Kaštelan-Macan, Determination of pKa values of active pharmaceutical ingredients, TrAC Trends Anal. Chem. 26 (2007) 1043–1061, http://dx.doi.org/10.1016/j.trac.2007.09.004.
[3] P. Nowak, M. Wozniakiewicz, P. Koscielniak, Application of capillary electrophoresis in determination of acid dissociation constant values, J. Chromatogr. A 1377 (2015) 1–12, http://dx.doi.org/10.1016/j.chroma.2014.12.032.
[4] R. Konášová, J.J. Dytrtová, V. Kašička, Determination of acid dissociation constants of triazole fungicides by pressure assisted capillary electrophoresis, J. Chromatogr. A 1408 (2015) 243–249, http://dx.doi.org/10.1016/j.chroma.2015.07.005.
[5] Z. Qiang, C. Adams, Potentiometric determination of acid dissociation constants (pKa) for human and veterinary antibiotics, Water Res. 38 (2004) 2874–2890, http://dx.doi.org/10.1016/j.watres.2004.03.017.
[6] R.I. Allen, K.J. Box, J.E.A. Comer, C. Peake, K.Y. Tam, Multiwavelength spectrophotometric determination of acid dissociation constants of ionizable drugs, J. Pharm. Biomed. Anal. 17 (1998) 699–712, http://dx.doi.org/10.1016/S0731-7085(98)00010-7.
[7] J. Bezençon, M.B. Wittwer, B. Cutting, M. Smieško, B. Wagner, M. Kansy, B. Ernst, pKa determination by 1H NMR spectroscopy – An old methodology revisited, J. Pharm. Biomed. Anal. 93 (2014) 147–155, http://dx.doi.org/10.1016/j.jpba.2013.12.014.
[8] J. Barbosa, D. Barrón, E. Jiménez-Lozano, V. Sanz-Nebot, Comparison between capillary electrophoresis, liquid chromatography, potentiometric and spectrophotometric techniques for evaluation of pKa values of zwitterionic drugs in acetonitrile-water mixtures, Anal. Chim. Acta 437 (2001) 309–321, http://dx.doi.org/10.1016/S0003-2670(01)00997-7.
[9] S. Ehala, J. Míšek, I.G. Stará, I. Starý, V. Kašička, Determination of acid-base dissociation constants of azahelicenes by capillary zone electrophoresis, J. Sep. Sci. 31 (2008) 2686–2693, http://dx.doi.org/10.1002/jssc.200800227.
[10] M. Shalaeva, J. Kenseth, F. Lombardo, A. Bastin, Measurement of dissociation constants (pKa values) of organic compounds by multiplexed capillary electrophoresis using aqueous and cosolvent buffers, J. Pharm. Sci. 97 (2008) 2581–2606, http://dx.doi.org/10.1002/jps.21287.
[11] C.A. Currie, W.R. Heineman, H.B. Halsall, C.J. Seliskar, P.A. Limbach, F. Arias, K.R. Wehmeyer, Estimation of pKa values using microchip capillary electrophoresis and indirect fluorescence detection, J. Chromatogr. B Anal. Technol. Biomed. Life Sci. 824 (2005) 201–205, http://dx.doi.org/10.1016/j.jchromb.2005.07.035.
[12] X. Fu, Y. Liu, W. Li, Y. Bai, Y. Liao, H. Liu, Determination of dissociation constants of aristolochic acid I and II by capillary electrophoresis with carboxymethyl chitosan-coated capillary, Talanta 85 (2011) 813–815, http://dx.doi.org/10.1016/j.talanta.2011.03.088.
[13] G. Aptisa, F. Benavente, V. Sanz-Nebot, E. Chirila, J. Barbosa, Evaluation of migration behaviour of therapeutic peptide hormones in capillary electrophoresis using polybrene-coated capillaries, Anal. Bioanal. Chem. 396 (2010) 1571–1579, http://dx.doi.org/10.1007/s00216-009-3344-1.
[14] H. Wan, A.G. Holmén, Y. Wang, W. Lindberg, M. Englund, M.B. Nàgård, R.A. Thompson, High-throughput screening of pKa values of pharmaceuticals by pressure-assisted capillary electrophoresis and mass spectrometry, Rapid Commun. Mass Spectrom. 17 (2003) 2639–2648, http://dx.doi.org/10.1002/rcm.1229.
[15] F. Benavente, E. Balaguer, J. Barbosa, V. Sanz-Nebot, Modelling migration behavior of peptide hormones in capillary electrophoresis-electrospray mass spectrometry, J. Chromatogr. A 1117 (2006) 94–102, http://dx.doi.org/10.1016/j.chroma.2006.03.049.
[16] J.M. Cabot, E. Fuguet, M. Rosés, P. Smejkal, M.C. Breadmore, Novel instrument for automated pKa determination by internal standard capillary electrophoresis, Anal. Chem. 87 (2015) 6165–6172, http://dx.doi.org/10.1021/acs.analchem.5b00845.
[17] E.C. Rickard, M.M. Strohl, R.G. Nielsen, Correlation of electrophoretic mobilities from capillary electrophoresis with physicochemical properties of proteins and peptides, Anal. Biochem. 197 (1991) 197–207, http://dx.doi.org/10.1016/0003-2697(91)90379-8.
[18] V. Sanz-Nebot, F. Benavente, E. Hernández, J. Barbosa, Evaluation of the electrophoretic behaviour of opioid peptides. Separation by capillary electrophoresis-electrospray ionization mass spectrometry, Anal. Chim. Acta 577 (2006) 68–76, http://dx.doi.org/10.1016/j.aca.2006.06.035.
[19] F. Benavente, B. Andón, E. Giménez, J. Barbosa, V. Sanz-Nebot, Modeling the migration behavior of rabbit liver apothioneins in capillary electrophoresis, Electrophoresis 29 (2008) 2790–2800, http://dx.doi.org/10.1002/elps.200700852.
[20] A. Barroso, E. Gimenez, F. Benavente, J. Barbosa, V. Sanz-Nebot, Modelling the electrophoretic migration behaviour of peptides and glycopeptides from glycoprotein digests in capillary electrophoresis-mass spectrometry, Anal. Chim. Acta 854 (2015) 169–177, http://dx.doi.org/10.1016/j.aca.2014.10.038.
[21] F. Benavente, E. Giménez, D. Barrón, J. Barbosa, V. Sanz-Nebot, Modeling the electrophoretic behavior of quinolones in aqueous and hydroorganic media, Electrophoresis 31 (2010) 965–972, http://dx.doi.org/10.1002/elps.200900344.
[22] S. Sabella, M. Quaglia, C. Lanni, M. Racchi, S. Govoni, G. Caccialanza, A. Calligaro, V. Bellotti, E. De Lorenzi, Capillary electrophoresis studies on the aggregation process of beta-amyloid 1–42 and 1–40 peptides, Electrophoresis 25 (2004) 3186–3194, http://dx.doi.org/10.1002/elps.200406062.
[23] N.E. Pryor, M.A. Moss, C.N. Hestekin, Capillary electrophoresis for the analysis of the effect of sample preparation on early stages of Aβ(1–40) aggregation, Electrophoresis 35 (2014) 1814–1820, http://dx.doi.org/10.1002/elps.201400012.
[24] D. Bhowmik, C.M. MacLaughlin, M. Chandrakesan, P. Ramesh, R. Venkatramani, G.C. Walker, S. Maiti, pH changes the aggregation propensity of amyloid-β without altering the monomer conformation, Phys. Chem. Chem. Phys. 16 (2014) 885–889, http://dx.doi.org/10.1039/c3cp54151g.
[25] S. Kobayashi, Y. Tanaka, M. Kiyono, M. Chino, T. Chikuma, K. Hoshi, H. Ikeshima, Dependence pH and proposed mechanism for aggregation of Alzheimer's disease-related amyloid-B (1–42) protein, J. Mol. Struct. 1094 (2015) 109–117, http://dx.doi.org/10.1016/j.molstruc.2015.03.023.
[26] M. Gilges, M.H. Kleemiss, G. Schomburg, Capillary zone electrophoresis separations of basic and acidic proteins using poly(vinyl alcohol) coatings in fused silica capillaries, Anal. Chem. 66 (1994) 2038–2046, http://dx.doi.org/10.1021/ac00085a019.
[27] Y. Shen, R.D. Smith, High-resolution capillary isoelectric focusing of proteins using highly hydrophilic-substituted cellulose-coated capillaries, J. Microcolumn Sep. 12 (3) (2000) 135–141, 10.1002/(SICI)1520-667X(2000)12<135:AID-MCS2>3.0.CO;2-5.
[28] N.J. Adamson, E.C. Reynolds, Rules relating electrophoretic mobility, charge and molecular size of peptides and proteins, J. Chromatogr. B Biomed. Appl. 699 (1997) 133–147, http://dx.doi.org/10.1016/S0378-4347(97)00202-8.
[29] A. Cifuentes, H. Poppe, Behavior of peptides in capillary electrophoresis: effect of peptide charge, mass and structure, Electrophoresis 18 (1997) 2362–2376, http://dx.doi.org/10.1002/elps.1150181227.
[30] A. Sillero, J.M. Ribeiro, Isoelectric points of proteins: theoretical determination, Anal. Biochem. 179 (1989) 319–325, http://dx.doi.org/10.1016/0003-2697(89)90136-X.
[31] J.R. Torres-Lapasió, J.J. Baeza-Baeza, M.C. García-Alvarez-Coque, A model for the description, simulation, and deconvolution of skewed chromatographic peaks, Anal. Chem. 69 (1997) 3822–3831, http://dx.doi.org/10.1021/ac970223g.
[32] J.W. Jorgenson, K.D. Lukacs, Zone electrophoresis in open-tubular glass capillaries, Anal. Chem. 53 (1981) 1298–1302, http://dx.doi.org/10.1002/jhrc.1240040507.

[33] K.D. Lukacs, J.W. Jorgenson, Capillary zone electrophoresis: effect of physical parameters on separation efficiency and quantitation, J. High Resol. Chromatogr. 8 (1985) 407–411, http://dx.doi.org/10.1002/jhrc.1240080810.
[34] M. Poitevin, A. Morin, J.M. Busnel, S. Descroix, M.C. Hennion, G. Peltre, Comparison of different capillary isoelectric focusing methods-use of narrow pH cuts of carrier ampholytes as original tools to improve resolution, J. Chromatogr. A 1115 (2007) 230–236, http://dx.doi.org/10.1016/j.chroma.2007.02.013.
[35] D.L. Nelson, M.M. Cox, Lehninger Principles of Biochemistry, 5th ed., W.H Freeman, New York, 2008.
[36] M. Tascon, F. Benavente, C.B. Castells, L.G. Gagliardi, Quality criterion to optimize separations in capillary electrophoresis: application to the analysis of harmala alkaloids, J. Chromatogr. A. 1460 (2016) 190–196, http://dx.doi.org/10.1016/j.chroma.2016.07.032.
[37] D. Belder, A. Deege, H. Husmann, F. Kohler, M. Ludwig, Cross-linked poly(vinyl alcohol) as permanent hydrophilic column coating for capillary electrophoresis, Electrophoresis 22 (2001) 3813–3818, http://dx.doi.org/10.1002/1522-2683(200109)22:17<3813:AID-ELPS3813>3.0.CO;2-D.
[38] G.G. Wolken, E.A. Arriaga, Simultaneous measurement of individual mitochondrial membrane potential and electrophoretic mobility by capillary electrophoresis, Anal. Chem. 86 (2014) 4217–4226, http://dx.doi.org/10.1021/ac403849x.

Talanta 208 (2020) 120399

Contents lists available at ScienceDirect

Talanta

journal homepage: www.elsevier.com/locate/talanta

Improving separation optimization in capillary electrophoresis by using a general quality criterion

Roger Pero-Gascon[a], Marcos Tascon[b], Victoria Sanz-Nebot[a], Leonardo G. Gagliardi[c], Fernando Benavente[a,*]

[a] Department of Chemical Engineering and Analytical Chemistry, Institute for Research on Nutrition and Food Safety (INSA•UB), University of Barcelona, Martí i Franquès 1-11, 08028, Barcelona, Spain
[b] Instituto de Investigación e Ingeniería Ambiental (IIIA-CONICET-UNSAM), Universidad Nacional de San Martín, 25 de Mayo y Francia, B1650, San Martín, Argentina
[c] Laboratorio de Investigación y Desarrollo de Métodos Analíticos, LIDMA, Facultad de Ciencias Exactas, Universidad Nacional de La Plata, CIC-PBA CONICET, Calle 47 Esq. 115, B1900AJI. La Plata, Argentina

ARTICLE INFO

Keywords:
Capillary electrophoresis
Optimization
pH
Prediction
Quality criterion
Separation

ABSTRACT

In this paper we extend the use of the quality criterion t' to optimize separations in capillary electrophoresis (CE). The theoretical parameter t' takes into account not only the relative separation between a given pair of compounds but also their separation from the neutral species migrating with the electroosmotic flow (EOF). Furthermore, it can be composed for complex mixtures as a global multicriterium optimization function T', for a rapid, simple and reliable selection of optimized separation conditions by mathematical maximization. Here, we demonstrate the applicability of T' using as a variable the electrophoretic mobility (m_e) for the optimization of pH in the separation of a mixture of amyloid beta (Aβ) peptide fragments. In addition, it is shown the versatility of T' using other variables related to m_e, which do not require experimental measurements. This is the case with ionizable compounds as the Aβ peptide fragments, whose charge-to-mass ratios can be calculated if accurate pK_a values are available in the literature. The excellent performance of T' for Aβ peptide fragments is further validated optimizing the pH for the separation of mixtures of harmala alkaloids (HAlks) and quinolone antibiotics.

1. Introduction

The optimization of experimental conditions in CE is critical for the development of rapid, efficient, sensitive and high-resolution separations [1–3]. When dealing with complex mixtures, separation between the different compounds is one of the most critical aspects to optimize [2,3]. Separation optimization requires a number of exploratory experiments [3], which can be minimized if the parameter or criterion used to qualify the separations can be accurately predicted. In contrast to liquid chromatography (LC) [4,5], resolution (R_s) is a difficult parameter to predict in CE, because many phenomena affect peak widths and shapes [1,2,6]. Therefore, quality criteria based on migration velocities or electrophoretic mobilities (m_e), which solely consider ratios or differences on the separation between pairs of compounds, have been traditionally preferred [2,7–10]. Nowadays, selectivity between a pair of compounds (α_{ij}) in CE is widely accepted to be defined as the ratio of their m_e (Equation (1)).

$$\alpha_{ij} = \frac{m_{e,i}}{m_{e,j}} \qquad (m_{e,i} > m_{e,j}) \tag{1}$$

However, a parameter based on the difference between m_e of the analytes being considered (d_{ij}, Equation (2)) is more robust, because it overcomes the issue of mathematical optimization by maximization when $m_{e,j}$ in the denominator approaches to zero (i.e. $\alpha_{i,j}$ approaches to infinite, see Equation (1)) [2].

$$d_{i,j} = m_{e,i} - m_{e,j} = \Delta m_{i,j} \qquad (m_{e,i} > m_{e,j}) \tag{2}$$

However, d_{ij} still presents certain drawbacks related to changes in migration order and the separation from the neutral compounds migrating with the EOF.

In a previous work, we proposed $t'_{i,j}$ as an improved elementary criterion to qualify and optimize separations in CE [11]:

$$t'_{i,j} = [m_{e,i} m_{e,j} (m_{e,i} - m_{e,j})]^2 \tag{3}$$

The parameter $t'_{i,j}$ takes into account the separation between both compounds ($d_{i,j}$). In addition, the multiplication of m_e qualifies the

* Corresponding author.
E-mail address: fbenavente@ub.edu (F. Benavente).

https://doi.org/10.1016/j.talanta.2019.120399
Received 3 June 2019; Received in revised form 26 September 2019; Accepted 27 September 2019
Available online 27 September 2019

separation of each of them from the EOF, and squaring the expression results always in positive values, solving the inconvenient related to changes on migration order or direction (i.e. net charge changes). $t'_{i,j}$ is continuous in its domain and mathematical optimization by maximization does not require to impose arbitrary restrictions. The definition of $t'_{i,j}$ can be extended for complex mixtures of n-compounds to compose a global multicriterium optimization function (MCOF) called T':

$$T' = \left[\left(\prod_{i}^{n} m_{e,i}\right)\left(\prod_{(i,j)(j<i)}^{n.(n-1)} \Delta m_{e(i,j)}\right)\right]^2 \quad (4)$$

So far, the success in the use of $t'_{i,j}$ and T' has been demonstrated for the separation optimization of complex mixtures of harmala alkaloids (HAlks, i.e. harmine, harmaline, harmol, harmalol, harmane and norharmane) as a function of pH of the BGE [11] and of racemic mixtures of chiral pharmaceutical drugs (i.e. oxprenolol, pindolol, propranolol and homatropine methylbromide) as a function of the chiral ligand or selector concentration ([L], i.e. L = 2-hydroxypropyl-β-cyclodextrin) in the BGE [12]. In both cases, it has been demonstrated that prediction of mobilities considering their behavior as a function of the optimization variables can be a very useful tool to reduce the number of experiments required for the optimization. However, establishing accurate quantitative relationships between the m_e of ionizable compounds as the HAlks and pH or between the apparent mobility (m_{app}) of chiral compounds and pL (-log[L], where [L] is the ligand concentration), still require a number of experimental measurements [11,12]. In this paper, it is presented as an alternative that other variables related to mobilities can be used to compose $t'_{i,j}$ and T' without the need of experimental measurements. This is the case of variables based on charge-to-mass ratios when dealing with complex mixtures of ionizable compounds. In this context, several semiempirical relationships relating the m_e of ionizable compounds to their structure (charge (q), relative molecular mass (M_r) or, for peptides, number of amino acid residues) have been proposed [13–18], as well as modifications based on those models [14,19]. In previous works, we demonstrated that the classical semiempirical models give excellent correlations for several peptide hormones [17], neuropeptides [18], amyloid beta (Aβ) peptide fragments [10], apothioneins [20], peptides and glycopeptides from tryptic digests of glycoproteins [21] and quinolones [22] when good pK_a values are available in the literature for charge calculations. For instance, the migration behavior of Aβ peptide fragments was accurately modelled using the classical polymer model (m_e vs. $q/M_r^{1/2}$) [10]. This is considered herein to demonstrate that $q/M_r^{1/2}$ values of Aβ peptide fragments as a function of pH can be directly used to compose T' as an alternative to m_e for a straightforward and experimental-free separation optimization. The excellent performance of T' using charge-to-mass ratios for Aβ peptide fragments is also proved for mixtures of other ionizable compounds, namely HAlks and quinolone antibiotics.

2. Materials and methods

2.1. Chemicals and reagents

All the chemicals used in the preparation of BGEs and solutions were of analytical reagent grade or better. Acetone, ammonium hydroxide (25%), boric acid, diethylmalonic acid, hydrochloric acid (25%), methanol, phosphoric acid (85%), sodium acetate, potassium hydroxide, sodium hydrogen phosphate, sodium formate and sodium hydroxide were supplied by Merck (Darmstadt, Germany). Tris(hydroxymethyl)aminomethane (Tris) was purchased from J.T. Baker (Deventer, Netherlands). Water with conductivity lower than 0.05 S cm^{-1} was obtained using a Milli-Q water purification system (Millipore, Molsheim, France). The Aβ peptide fragments 1–15, 10–20, 20–29, 25–35 and 33–42 were provided by Bachem (Bubendorf, Switzerland). Their sequences, ionizable groups, M_r and pK_a values are shown in Table 1.

Table 1
Amino acid sequence, relative molecular mass (M_r), ionizable groups and pKa values for the studied Aβ peptide fragments.

Aβ peptide sequence	M_r (average)	Ionizable amino acids[a]	pK_a	
			CE-UV[b]	Rickard et al.[c]
1–15	1826.9	^{t}C-Q	2.9	3.2
DAEFRHDSGYEVHHQ		D	3.0	3.5
		D	3.1	3.5
		E	4.5	4.5
		E	4.6	4.5
		H	6.0	6.2
		H	6.2	6.2
		H	6.3	6.2
		^{t}N-D	8.6	8.6
		Y	11.1	10.3
		R	–	12.5
10–20	1446.7	^{t}C-F	3.3	3.2
YEVHHQKLVFF		E	4.5	4.5
		H	5.7	6.2
		H	5.9	6.2
		^{t}N-Y	8.0	7.7
		Y	10.4	10.3
		K	10.6	10.3
20–29	1023.1	^{t}C-G	2.9	3.2
FAEDVGSNKG		D	3.1	3.5
		E	4.7	4.5
		^{t}N-F	8.1	7.7
		K	10.8	10.3
25–35	1060.3	^{t}C-M	3.1	3.2
GSNKGAIIGLM		^{t}N-G	8.2	8.2
		K	10.5	10.3
33–42	915.2	^{t}C-A	3.1	3.2
GLMVGGVVIA		^{t}N-G	8.3	8.2

[a] In this column tC-: terminal COOH and tN-: terminal NH_2.
[b] pK_a of R could not be determined by CE-UV [10].
[c] These average pK_a values for amino acids in polypeptides were determined using a large set of short fragments from biosynthetic human insulin (BHI) and human growth hormone (hGH) with a few ionizable groups [23].

2.2. Electrolyte solutions and samples solutions

The BGEs for the determination of m_e covered the pH range within 2–12. They were prepared at the following concentrations (pH was adjusted with 1.0 M HCl or 1.0 M NaOH and ionic strength (I) was calculated to be around 25 mM): 50 mM H_3PO_4 (pH 2.0), 30 mM H_3PO_4 (pH 2.5 and 3.0), 25 mM sodium formate (pH 3.5 and 4.0), 25 mM sodium acetate (pH 4.5 and 5.0), 20 mM diethylmalonic acid (pH 5.5, 6.0 and 6.5), 25 mM Tris (pH 7.0, 7.5, 8.0, 8.5 and 9.0), 30 mM H_3BO_3 (pH 9.5, 10.0 and 10.5), and 5 mM Na_2HPO_4 (pH 11.0, 11.5 and 12.0). BGEs were passed through a 0.22 μm nylon filter (Panreac Applichem, Barcelona, Spain).

Individual stock solutions (1000 mg L^{-1}) of Aβ 1–15, 10–20, 20–29, 25–35 were prepared in water. Aβ 33–42 was prepared in 5% (v/v) DMSO because it was poorly soluble in water. The working solutions (200 mg L^{-1}) contained 3% (v/v) acetone or 5% (v/v) DMSO (Aβ 33–42) as electroosmotic flow (EOF) marker. The mixture of five peptides (200 mg L^{-1}) was prepared with 5% (v/v) DMSO. All the stock solutions were divided into several aliquots and individually stored at −20 °C. Each aliquot was thawed only once, preserved in the refrigerator between injections and immediately discarded after the analyses.

2.3. Instrumental parameters

All CE-UV experiments were performed in an Agilent HP 3DCE system (Agilent Technologies, Waldbronn, Germany). Separations were performed at 25 °C in a 57 cm total length (L_T) × 75 μm internal diameter (i.d.) × 365 μm outer diameter (o.d.) bare fused silica capillary (Polymicro Technologies, Phoenix, AZ, USA). All capillary rinses were

performed at high pressure (930 mbar). New capillaries were flushed with 1 M NaOH (15 min), water (15 min) and BGE (30 min). The system was finally equilibrated by applying 25 kV of separation voltage for 20 min (normal polarity, cathode in the outlet). Samples were hydrodynamically injected at 50 mbar for 3 s. Between runs, capillaries were conditioned by rinsing with 1 M NaOH (1 min), water (1 min) and BGE (1 min). Between workdays or after a change of BGE, the capillary was conditioned by rising with 1 M NaOH (5 min), water (5 min) and BGE (10 min). The system was finally equilibrated by applying 25 kV of separation voltage for 20 min (the Ohm's law was fulfilled under all the working conditions). The UV window was placed at 48.5 cm from the inlet of the capillary (L_D, effective capillary length) and detection was made at 200 nm (Aβ peptide fragments), 254 nm (HAlks) and 260 nm (quinolone antibiotics). Capillaries were stored overnight filled with water. pH measurements were made with a Crison 2002 potentiometer and a Crison electrode 52-03 (Crison Instruments, Barcelona, Spain).

2.4. Determination of electrophoretic mobility and pK_a values

The m_e of the Aβ peptide fragments was measured by CE-UV as the difference between the apparent mobility of each peptide, m_{app}, and the mobility of the neutral marker, m_{EOF}:

$$m_e = m_{app} - m_{EOF} = \frac{L_T L_D}{V}\left(\frac{1}{t_{app}} - \frac{1}{t_{EOF}}\right) \quad (5)$$

where L_T is the capillary length, L_D is the distance from the injection point to the detector and t_{app} and t_{EOF} are the migration time of the peptide and the neutral marker, respectively. Individual solutions of each peptide were injected at each pH and m_e was obtained as the average of five replicates. BGEs indicated in Section 2.2 were run in sequence from low to high pH. In a previous study [10], accurate pK_a values of the studied Aβ peptide fragments were determined from these m_e–pH measurements, taking into account the number and type of ionizable groups in each case to establish appropriate equations relating m_e and pH of the BGE [10]. The CE-UV pK_a values of the studied Aβ peptide fragments are shown in Table 1.

2.5. Classical semiempirical models and calculation of $t'_{i,j}$ and T'

Details about the assumptions made to deduce the equations of the different classical semiempirical models that describe electrophoretic migration of peptides, and other ionizable compounds, can be found elsewhere [13,14]. The general form of the equation relating m_e, M_r and q is as follows:

$$m_e = B\frac{q}{M_r^{\alpha}} \quad (6)$$

where B is a constant and the parameter α takes different values depending on the semiempirical model (α = 1/2, 1/3 and 2/3 for the classical polymer model, the Stoke's law and the Offord's surface law, respectively). In a previous study [10], it was shown that migration behavior of Aβ peptide fragments in CE can be modelled using the classical polymer model (m_e vs. $q/M_r^{1/2}$). In order to obtain the $q/M_r^{1/2}$ values for the studied peptides, M_r was calculated from the amino acid sequences (Table 1) [23] and q was calculated at each separation pH using the pK_a values (Table 1) and Sillero and Ribeiro expression [24], which is based on the Henderson–Hasselbalch equation:

$$q = \sum_n \frac{P_n}{1 + 10^{pH - pK_a(P_n)}} - \sum_j \frac{N_j}{1 + 10^{pK_a(N_j) - pH}} \quad (7)$$

where P_n and N_n are the number of equivalent cationic (i.e. P_1 = terminal NH_2, P_2 = His (H), P_3 = Lys (K) and P_4 = Arg (R)) and anionic (i.e. N_1 = terminal COOH, N_2 = Asp (D), N_3 = Glu (E) and N_4 = Tyr (Y)) groups found in the considered peptides, while pK_a (P_n) and pK_a (N_n) are the pK_a values of these groups. The accuracy of the q calculated for the Aβ peptide fragments relies on the accuracy of the considered pK_a values. All the pK_a values required for calculations are gathered in Table 1. Values reported in the CE-UV column were determined previously by our group [10], while in the column beside are indicated the values reported by Rickard et al. [25]. From these latter values, only the data associated to the guanidine group in the R residue was used (pK_a = 12.5), because this pK_a value could not be obtained by CE-UV. Once $q/M_r^{1/2}$ were calculated for all the peptides at the different pH values, $t'_{i,j}$ or T' were calculated from equations (3) and (4), respectively, to predict the optimized conditions for the separation.

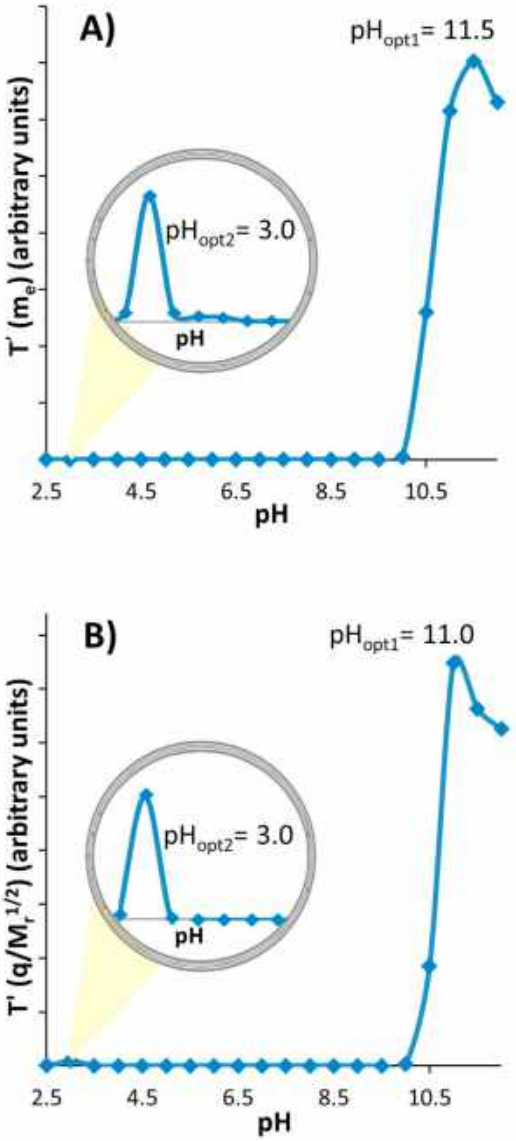

Fig. 1. Plot of T' vs. pH of the BGE for the separation of a mixture of five Aβ peptide fragments (Aβ (1–15), (10–20), (20–29), (25–35) and (33–42)). A) $T'(m_e)$ and B) $T'(q/M_r^{1/2})$.

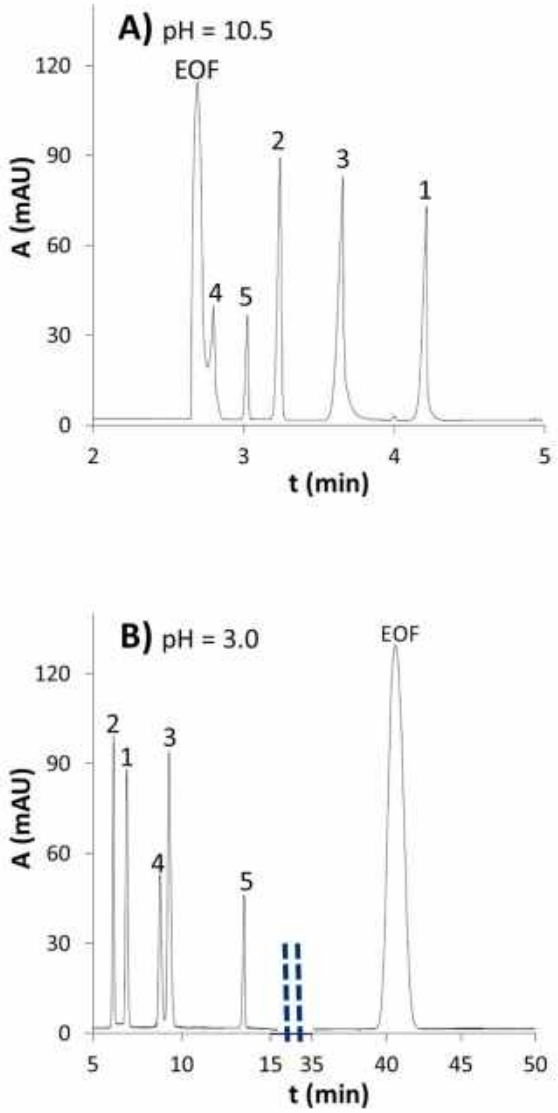

Fig. 2. Experimental electropherograms of a mixture of the five Aβ peptide fragments (Aβ (1–15) (1), Aβ (10–20) (2), Aβ (20–29) (3), Aβ (25–35) (4) and Aβ (33–42) (5)) at pH A) 10.5 and B) 3.0 (30 mM H_3BO_3 or H_3PO_4 adjusted with NaOH in both cases). Instrument: Agilent HP 3DCE. Bare fused silica capillary (57 cm (L_T) × 48.5 cm (L_D) x 75 μm (i.d.)), hydrodynamic injection: 3 s, 50 mbar, 25 °C, 25 kV and 195 nm.

3. Results and discussion

The m_e values of the studied Aβ peptide fragments as a function of pH of the BGE were measured in a previous study to model their migration behavior and determine their pK_a values by CE-UV (Table 1) [10]. The predicted m_e values were used now to calculate T′ and select the optimum pH value for the separation of the five peptides (Fig. 1-A). As can be observed, the best separations were supposed to be obtained in the pH range 10.5–12.0 where T′(m_e) values were higher (the absolute maximum was at pH 11.5). Furthermore, when the plot was carefully inspected zooming into shorter pH ranges, a relative maximum at pH 3.0 was also found (Fig. 1-B, see the zoomed area as an inset). For the rest of pH values the separations were poorer because of either the slight differences between the m_e of the peptides or their comigration with the EOF. Fig. 2-A and -B show the experimental electropherograms of the mixture at pH 10.5 and 3.0, respectively. In the basic pH range (Fig. 2-A), a pH value of 10.5 was selected to preserve the fused silica capillary, which is known to be less stable at extremely basic pH values [26]. At this pH value, the mixture of the five Aβ fragments was separated in less than 5 min, and only one of the peptides slightly comigrated with the EOF. At pH 3.0 (Fig. 2-B), separation between the different peptides was in some cases worse than at pH 10.5, but none of them partially comigrated with the EOF, which was detected at around 40 min. This suggested an acceptable performance of the proposed acidic conditions in terms of resolution, and the convenience of considering as potential pH value to obtain optimized separations, both the absolute and the relative maxima from the T′(m_e) vs pH plot. In this particular case, the total analysis time at pH 3.0 was higher than at pH 10.5 due to the reduced EOF, requiring almost 15 min to separate the mixture of five Aβ fragments. In any case, in peptide analysis by CE with fused silica capillaries very often acidic BGEs are preferred to minimize peptide adsorption in the inner capillary walls [27,28]. Furthermore, the higher availability of acidic volatile BGEs to obtain the best sensitivity in capillary electrophoresis-mass spectrometry (CE-MS) in positive electrospray ionization mode (ESI+) is another important factor [27–29].

It is widely known that the m_e of ionizable compounds can be modelled as a function of pH using appropriate equations that consider the type (i.e. acid or basic) and number of ionizable groups [10,11,16–19]. Although the number of experimental m_e-pH data pairs required for an accurate prediction of migration is small for monoprotic species (i.e. three data pairs), it dramatically increases with the number of ionizable groups. This fact was previously demonstrated for Aβ peptide fragments, apothioneins and peptides and glycopeptides from tryptic digests of glycoproteins [10,20,21]. As can be observed from the many pK_a values in Table 1, Aβ peptide fragments (1–15), (10–20) and (20–29) are a clear example of how complex the experimental modelling of polyprotic compounds m_e as a function of pH can be.

This drawback predicting mobilities can be solved calculating T′ from other variables related to mobility, which do not require experimental measurements. This is the case with ionizable compounds of the charge-to-mass ratios, which can be calculated if accurate pK_a values or good pK_a estimations are available in the literature [10,17,18,20–22]. We have recently shown that m_e of the studied Aβ peptide fragments can be modelled in the pH range 2–12 with the classical polymer model (m_e α $q/M_r^{1/2}$, R^2~0.98) [10]. Fig. 1-B shows variation of T′ as a function of pH if $q/M_r^{1/2}$ values of the studied peptides are used in the calculations instead of m_e (CE-UV pK_a values of Table 1 were used for charge calculations). As can be observed, again the best separations were expected to be obtained in the pH range 10.5–12.0, but T′($q/M_r^{1/2}$) maximum was now slightly shifted to pH 11.0. Furthermore, the relative maximum was also observed at pH 3.0. The concordance between plots of T′(m_e) and T′($q/M_r^{1/2}$) vs pH was very good, and similar conclusions could be drawn. Therefore, if accurate pK_a values are available to predict $q/M_r^{1/2}$, this novel approach results more practical than experimental approaches and streamlines the process of separation optimization.

In order to further validate the performance of the T′ parameters, it was investigated the optimization of pH for the separation of mixtures of HAlks and quinolone antibiotics. Fig. 3-A (i) and (ii) show the plots of T′(m_e) and T′($q/M_r^{1/2}$) vs pH for the mixture of HAlks, as well as the good performance of the polymer's law in the studied pH range (R^2~0.99) (see the inset in Fig. 3-A-ii). As can be observed in Fig. 3-A T′ parameters were in all cases maxima at around pH 7.5. For this compound mixture no relative maxima were observed in the studied pH

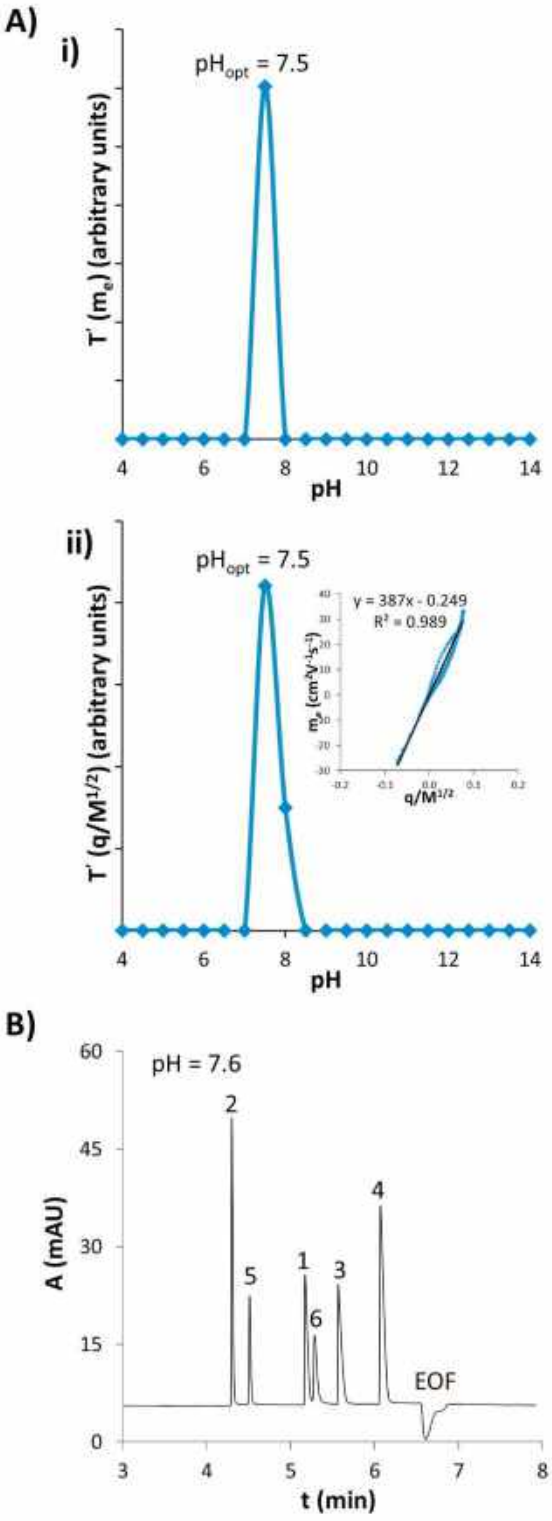

Fig. 3. A) Plot of T' vs. pH of the BGE for the separation of a mixture of six harmala alkaloids (HAlks) (i.e harmine (1), harmaline (2), harmane (3), norharmane (4), harmalol (5), harmol (6)). i) T'(m_e) and ii) T'($q/M_r^{1/2}$) (plot of m_e vs $q/M^{1/2}$ is shown as inset) (Charge-to-mass ratios were calculated using the CE-UV pK_a values given in reference [11]). B) Experimental electropherogram of the mixture at pH 7.6 (25 mM $(NH_4)_2HPO_4/NH_4H_2PO_4$ with 20% v/v of methanol). Instrument: Lumex Capel 105M CE. Bare fused silica capillary (60 cm (L_T) × 51 cm (L_D) x 75 μm (i.d.)), hydrodynamic injection: 3 s, 30 mbar, 25 °C, 20 kV and 254 nm. Organic solvent was added to further improve peak shape and increase separation efficiency [11].

range and Fig. 3-B shows the electropherogram under the optimized pH conditions [11]. Fig. 4-A (i) and (ii) show the plots of T'(m_e) and T'($q/M_r^{1/2}$) vs pH for the mixture of quinolones. In this case, an absolute maximum at pH 6.0 and a relative maximum at pH 8.0 were observed in the plot of T'(m_e) vs pH (Fig. 4-A-i). Both relative and absolute maxima were exchanged at the same values in the plot of T'($q/M_r^{1/2}$) vs pH (Fig. 4-A-ii). This was probably due to very small differences between the m_e or $q/M_r^{1/2}$ values considered at these pH values, as well as because of the accuracy of polymer's law for m_e prediction (R^2–0.99 [22]). These results reinforce the idea of considering absolute and relative maxima of T' vs pH plots as candidates for selection of an optimized pH value for the separation. Fig. 4-B shows the electropherograms for the mixture of quinolones at pH 6.0 and 8.2 conditions, and separations were globally quite similar in both cases [22]. From the results obtained for these three different families of ionizable compounds, the novel approach for optimization of the separation pH based on calculation of T' using charge-to-mass ratios would be perfectly valid for all kind of ionizable compounds.

4. Conclusions

In this study we have demonstrated that the multicriterium optimization function T', which is derived from the elementary criterion t', can be used for a rapid, simple and reliable selection of optimized pH conditions for the separation of complex mixtures of ionizable compounds, such as Aβ peptide fragments, HAlks and quinolone antibiotics. T' shows clear advantages for an accurate optimization, because it includes the separation between compounds, the separation from the EOF and changes in the migration orders. It has been shown that in addition to the m_e, the charge-to-mass ratios of the polyprotic compounds, which can be obtained if accurate pK_a values are available, can be used to calculate T' as a function of pH for a straightforward and experimental-free separation optimization. The optimized pH values for the separation are easily selected from inspection of the plot of T' vs pH, which must be screened to find absolute and relative maxima. The proposed approach has a great usability and an enormous potential to streamline the optimization of separation pH in CE analysis of polyprotic compounds. Once selected the pH, peak widths and shapes and total analysis time, which affect separation resolution, can be finely tuned experimentally by investigating the BGE composition (nature and concentration of the ionizable components, ionic strength, presence of organic solvents or other additives, etc.), the EOF magnitude or direction in bare or coated fused silica capillaries, the capillary diameter, the sample injection mode and volume or the separation voltage and temperature.

Declaration of competing interest

The authors have declared no conflict of interest.

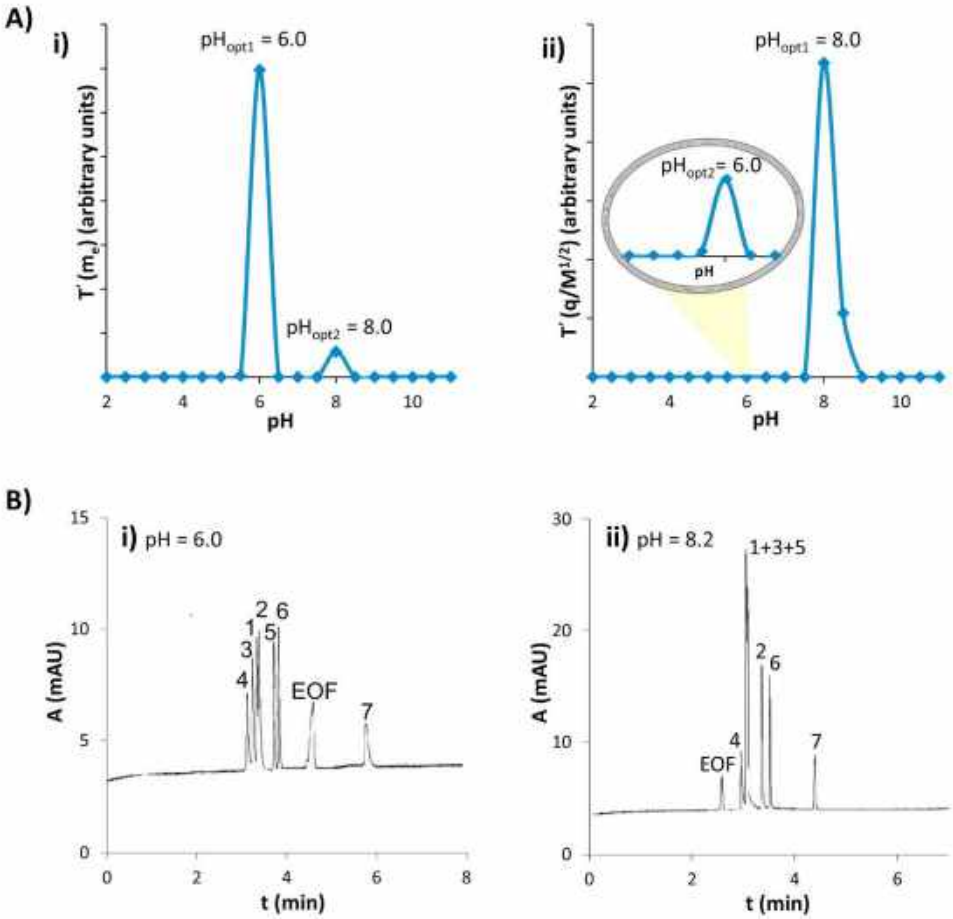

Fig. 4. A) Plot of T' vs. pH of the BGE for the separation of a mixture of seven quinolone antibiotics (i.e ciprofloxacin (1), enrofloxacin (2), norfloxacin (3), danofloxacin (4), sarafloxacin (5), difloxacin (6) and flumequine (7)). i) T'(m_e) and ii) T'($q/M_r^{1/2}$) (m_e vs $q/M^{1/2}$ and CE-UV pK_a values are reported in reference [22]). B) Experimental electropherogram of the mixture at pH i) 6.0 and ii) pH 8.2 (50 or 25 mM H_3PO_4 adjusted with NaOH in both cases). Instrument: Beckman Coulter P/ACE 5500. Bare fused silica capillary (47 cm (L_T) × 40 cm (L_D) x 75 μm (i.d.)), hydrodynamic injection: 3 s, 33.5 mbar, 25 °C, 20 kV and 260 nm [22].

Acknowledgements

This study was supported by grants from the Spanish Ministry of Economy and Competitiveness (RTI2018-097411-B-I00), the Cathedra UB Rector Francisco Buscarons Ubeda (Forensic Chemistry and Chemical Engineering), the Agencia Nacional de Promoción Científica y Técnica (ANPCyT PICT 2014 Nº3597 and PICT 2016 Nº0553) and the Universidad Nacional de La Plata (UNLP 11X/836 and 11N/790). Roger Pero-Gascon acknowledges the Spanish Ministry of Education, Culture and Sport for a FPU (Formación del Profesorado Universitario) fellowship.

References

[1] H.H. Lauer, G.P. Rozing (Eds.), High Performance Capillary Electrophoresis, second ed., Agilent Technologies, Waldbronn, Germany, 2014.

[2] V. Dolník, Selectivity, differential mobility and resolution as parameters to optimize capillary electrophoretic separation, J. Chromatogr., A 744 (1996) 115–121, https://doi.org/10.1016/0021-9673(96)00449-9.

[3] S. Orlandini, R. Gotti, S. Furlanetto, Multivariate optimization of capillary electrophoresis methods: a critical review, J. Pharm. Biomed. Anal. 87 (2014) 290–307, https://doi.org/10.1016/j.jpba.2013.04.014.

[4] P.J. Schoenmakers, Optimization of Chromatographic Selectivity. A Guide to Method Development, first ed., Elsevier Science, 1986.

[5] I. Molnar, Computerized design of separation strategies by reversed-phase liquid chromatography: development of DryLab software, J. Chromatogr., A 965 (2002) 175–194.

[6] M. Riesová, V. Hruška, B. Gaš, A nonlinear electrophoretic model for PeakMaster: II. Experimental verification, Electrophoresis 33 (2012) 931–937, https://doi.org/10.1002/elps.201100555.

[7] J.C. Giddings, Generation of variance,"theoretical plates", resolution, and peak capacity in electrophoresis and sedimentation, Separ. Sci. 4 (1969) 181–189, https://doi.org/10.1080/01496396908052249.

[8] J.W. Jorgenson, K.D. Lukacs, Zone electrophoresis in open-tubular glass capillaries, Anal. Chem. 53 (1981) 1298–1302, https://doi.org/10.1002/jhrc.1240040507.

[9] K.D. Lukacs, J.W. Jorgenson, Capillary zone electrophoresis: effect of physical parameters on separation efficiency and quantitation, J. High Resolut. Chromatogr. 8 (1985) 407–411, https://doi.org/10.1002/jhrc.1240080810.

[10] R. Peró-Gascón, F. Benavente, J. Barbosa, V. Sanz-Nebot, Determination of acidity constants and prediction of electrophoretic separation of amyloid beta peptides, J. Chromatogr., A 1508 (2017) 148–157, https://doi.org/10.1016/j.chroma.2017.05.069.

[11] M. Tascon, F. Benavente, C.B. Castells, L.G. Gagliardi, Quality criterion to optimize separations in capillary electrophoresis : application to the analysis of harmala alkaloids, J. Chromatogr., A 1460 (2016) 190–196, https://doi.org/10.1016/j.chroma.2016.07.032.

[12] C. Lancioni, S. Keunchkarian, C.B. Castells, L.G. Gagliardi, Enantiomeric separations by capillary electrophoresis: theoretical method to determine optimum chiral selector concentration, J. Chromatogr., A 1539 (2018) 71–77, https://doi.org/10.1016/j.chroma.2018.01.002.

[13] N.J. Adamson, E.C. Reynolds, Rules relating electrophoretic mobility, charge and molecular size of peptides and proteins, J. Chromatogr. B Biomed. Appl. 699 (1997)

133–147, https://doi.org/10.1016/S0378-4347(97)00202-8.
[14] A. Cifuentes, H. Poppe, Behavior of peptides in capillary electrophoresis: effect of peptide charge, mass and structure, Electrophoresis 18 (1997) 2362–2376, https://doi.org/10.1002/elps.1150181227.
[15] V. Solínová, V. Kasicka, D. Koval, J. Hlaváček, Separation and investigation of structure-mobility relationships of insect oostatic peptides by capillary zone electrophoresis, Electrophoresis 25 (2004) 2299–2308, https://doi.org/10.1002/elps.200405924.
[16] V. Solínová, V. Kasicka, P. Sázelová, T. Barth, I. Miksík, Separation and investigation of structure-mobility relationship of gonadotropin-releasing hormones by capillary zone electrophoresis in conventional and isoelectric acidic background electrolytes, J. Chromatogr., A 1155 (2007) 146–153, https://doi.org/10.1016/j.chroma.2007.01.019.
[17] F. Benavente, E. Balaguer, J. Barbosa, V. Sanz-Nebot, Modelling migration behavior of peptide hormones in capillary electrophoresis-electrospray mass spectrometry, J. Chromatogr., A 1117 (2006) 94–102, https://doi.org/10.1016/j.chroma.2006.03.049.
[18] V. Sanz-Nebot, F. Benavente, E. Hernández, J. Barbosa, Evaluation of the electrophoretic behaviour of opioid peptides. Separation by capillary electrophoresis-electrospray ionization mass spectrometry, Anal. Chim. Acta 577 (2006) 68–76, https://doi.org/10.1016/j.aca.2006.06.035.
[19] L. Sun, V. Spicer, O.V. Krokhin, N.J. Dovichi, G. Anderson, Predicting electrophoretic mobility of tryptic peptides for high-throughput CZE-MS analysis, Anal. Chem. 89 (2017) 2000–2008, https://doi.org/10.1021/acs.analchem.6b04544.
[20] F. Benavente, B. Andón, E. Giménez, J. Barbosa, V. Sanz-Nebot, Modeling the migration behavior of rabbit liver apothioneins in capillary electrophoresis, Electrophoresis 29 (2008) 2790–2800, https://doi.org/10.1002/elps.200700852.
[21] A. Barroso, E. Gimenez, F. Benavente, J. Barbosa, V. Sanz-Nebot, Modelling the electrophoretic migration behaviour of peptides and glycopeptides from glycoprotein digests in capillary electrophoresis-mass spectrometry, Anal. Chim. Acta 854 (2015) 169–177, https://doi.org/10.1016/j.aca.2014.10.038.
[22] F. Benavente, E. Giménez, D. Barrón, J. Barbosa, V. Sanz-Nebot, Modeling the electrophoretic behavior of quinolones in aqueous and hydroorganic media, Electrophoresis 31 (2010) 965–972, https://doi.org/10.1002/elps.200900344.
[23] M. Strohalm, M. Hassman, B. Kosata, M. Kodicek, mMass data miner: an open source alternative for mass spectrometric data analysis, Rapid Commun. Mass Spectrom. 22 (2008) 905–908, https://doi.org/10.1002/rcm.
[24] A. Sillero, J. Ribeiro, Isoelectric points of proteins: theoretical determination, Anal. Biochem. (1989) 319–325.
[25] E.C. Rickard, M.M. Strohl, R.G. Nielsen, Correlation of electrophoretic mobilities from capillary electrophoresis with physicochemical properties of proteins and peptides, Anal. Biochem. 197 (1991) 197–207, https://doi.org/10.1016/0003-2697(91)90379-8.
[26] F. Benavente, V. Sanz-Nebot, J. Barbosa, R. van der Heijden, J. van der Greef, T. Hankemeier, CE-ESI-MS of biological anions in plastic capillaries at high pH, Electrophoresis 28 (2007) 944–949, https://doi.org/10.1002/elps.200600461.
[27] S. Štěpánová, V. Kašička, Recent applications of capillary electromigration methods to separation and analysis of proteins, Anal. Chim. Acta 933 (2016) 23–42, https://doi.org/10.1016/j.aca.2016.06.006.
[28] V. Kašička, Recent developments in capillary and microchip electroseparations of peptides (2015–mid 2017), Electrophoresis 39 (2018) 209–234, https://doi.org/10.1002/elps.201700295.
[29] A. Stolz, K. Jooß, O. Höcker, J. Römer, J. Schlecht, C. Neusüß, Recent advances in capillary electrophoresis-mass spectrometry: instrumentation, methodology and applications, Electrophoresis (2018) 1–34, https://doi.org/10.1002/elps.201800331.

Chapter 3. Improving the sensitivity and the selectivity in capillary electrophoresis by unidirectional on-line solid-phase extraction capillary electrophoresis

A major limitation of CE is the relatively poor concentration sensitivity for most analytes due to the small sample volume that can be injected in the separation capillary. In this regard, in addition to the use of more selective and sensitive detectors, the concentration sensitivity of CE can be enhanced by on-line preconcentration approaches, which, in addition, minimize sample handling and increase analysis throughput. SPE-CE is a powerful approach for sample clean-up and LOD reduction. In SPE-CE, analytes from a large volume of sample (~25-200 μL) are retained on a sorbent contained in a microcartridge. In unidirectional SPE-CE, the most typical configuration, the microcartridge is mounted in series to the separation capillary, inserted near the capillary inlet. After sample loading, the microcartridge is washed to remove non-selectively retained molecules. Then, the retained analytes are desorbed in a small volume of eluent (~50-100 nL), resulting in sample clean-up and concentration enhancement before electrophoretic separation and detection.

The present chapter is focused on the development of unidirectional SPE-CE-MS methodologies using affinity sorbents for the analysis of protein biomarkers related to neurodegenerative diseases and miRNA biomarkers related to cancer in biological fluids.

On the one hand, SPE-CE-MS has been evaluated for the analysis of intact protein biomarkers. First, immunoaffinity-SPE-CE-MS has been investigated for the analysis of human serum transthyretin, an oligomeric protein related to familial amyloidotic polyneuropathy type-I. Second, aptamer affinity-SPE-CE-MS has been demonstrated for the first time and applied for the analysis of blood α-synuclein, which is a potential biomarker of Parkinson's disease.

On the other hand, in order to reduce the complexity of the protein digests generated in bottom-up proteomic studies, immobilized metal affinity-SPE-CE-MS with a Ni(II) sorbent has been investigated for the selective enrichment of histidine containing peptides.

Finally, SPE-CE-MS with a silicon carbide sorbent has been investigated for the analysis of miRNA biomarkers and their post-transcriptional modifications in serum of patients with B-cell chronic lymphocytic leukemia.

This chapter includes the following publications:

- **Publication 3.1.** L. Pont, R. Pero-Gascon, E. Giménez, V. Sanz-Nebot, F. Benavente, A critical retrospective and prospective review of designs and materials in in-line solid-phase extraction capillary electrophoresis, Anal. Chim. Acta. 1079 (2019) 1–19. https://doi.org/10.1016/j.aca.2019.05.022.

- **Publication 3.2**. R. Pero-Gascon, L. Pont, F. Benavente, J. Barbosa, V. Sanz-Nebot, Analysis of serum transthyretin by on-line immunoaffinity solid-phase extraction capillary electrophoresis mass spectrometry using magnetic beads, Electrophoresis. 37 (2016) 1220–1231. https://doi.org/10.1002/elps.201500495.

- **Publication 3.3.** R. Pero-Gascon, F. Benavente, Z. Minic, M. V. Berezovski, V. Sanz-Nebot, On-line aptamer affinity solid-phase extraction capillary electrophoresis-mass spectrometry for the analysis of blood α-synuclein, Anal. Chem. 92 (2020) 1525–1533. https://doi.org/10.1021/acs.analchem.9b04802.

- **Publication 3.4.** R. Pero-Gascon, E. Giménez, V. Sanz-Nebot, F. Benavente, Enrichment of histidine containing peptides by on-line immobilised metal affinity solid-phase extraction capillary electrophoresis-mass spectrometry, Microchem. J. 157 (2020) 105013. https://doi.org/10.1016/j.microc.2020.105013.

- **Publication 3.5.** R. Pero-Gascon, V. Sanz-Nebot, M. V Berezovski, F. Benavente, Analysis of circulating microRNAs and their post-transcriptional modifications in cancer serum by on-line solid-phase extraction−capillary electrophoresis−mass spectrometry, Anal. Chem. 90 (2018) 6618–6625. https://doi.org/10.1021/acs.analchem.8b00405.

Analytica Chimica Acta 1079 (2019) 1–19

Contents lists available at ScienceDirect

Analytica Chimica Acta

journal homepage: www.elsevier.com/locate/aca

Review

A critical retrospective and prospective review of designs and materials in in-line solid-phase extraction capillary electrophoresis

L. Pont, R. Pero-Gascon, E. Gimenez, V. Sanz-Nebot, F. Benavente*

Department of Chemical Engineering and Analytical Chemistry, Institute for Research on Nutrition and Food Safety (INSA-UB), University of Barcelona, Martí i Franquès 1-11, 3rd floor, 08028, Barcelona, Spain

HIGHLIGHTS

- Limited sensitivity is a major concern in microscale separation techniques.
- Limits of detection can be decreased by several strategies in CE.
- An excellent option is in-line SPE-CE.
- Different alternatives to prepare and apply in-line SPE microcartridges are reviewed.

GRAPHICAL ABSTRACT

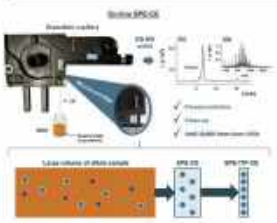

ARTICLE INFO

Article history:
Received 6 February 2019
Received in revised form
8 May 2019
Accepted 10 May 2019
Available online 15 May 2019

Keywords:
Capillary electrophoresis
Limit of detection
In-line solid-phase extraction /on-line solid-phase extraction
Preconcentration
Unidirectional

ABSTRACT

Several strategies have been developed to decrease the concentration limits of detection (LODs) in capillary electrophoresis (CE). Nowadays, chromatographic-based preconcentration using a microcartridge integrated in the separation capillary for in-line solid-phase extraction capillary electrophoresis (SPE-CE) is one of the best alternatives for high throughput and reproducible sample clean-up and analyte preconcentration. This review covers different designs (geometrical configurations, with frits or fritless, capillary types, compatibility with commercial instrumentation, etc.) and materials (sorbents, supports, affinity ligands, etc.) applied for almost 30 years to prepare in-line SPE-CE microcartridges (i.e. analyte concentrators), with emphasis on the conventional unidirectional configuration in capillary format. Advantages, disadvantages and future perspectives are analyzed in detail to provide the reader a wide overview about the great potential of this technique to enhance sensitivity and address trace analysis.

Contents

1. Introduction 2
2. SPE-CE designs and sorbents 2
2.1. Microcartridge configuration 2
2.2. Microcartridge with frits and fritless 3
2.2.1. Microcartridge with frits 4
2.2.2. Fritless microcartridges 6
2.3. SPE-CE sorbents 13

* Corresponding author.
E-mail address: fbenavente@ub.edu (F. Benavente).

https://doi.org/10.1016/j.aca.2019.05.022
0003-2670/

3. Conclusions and perspectives 15
Declarations of interest 16
Conflict of interest 16
Acknowledgements 16
References 16

1. Introduction

Over the years, different strategies have been described to decrease the limits of detection in capillary electrophoresis (CE) [1–6]. High selective and sensitive detectors (e.g mass spectrometry (MS) and fluorescence detectors [7,8]) or the traditional off-line sample clean-up and preconcentration techniques have been widely applied [9–12]. At the same time have been developed the on-line electrophoretic [1–3,13–15] and chromatographic approaches to minimize sample handling and increase analysis throughput [4–6].

Electrophoretic preconcentration based on stacking, focusing or isotachophoresis has been widely used to improve CE sensitivity, with preconcentration factors higher than 10,000 times in some cases [1–3,13–15]. However, the dependence of these techniques on the analyte and sample matrix physicochemical properties, especially the electrical charge, hinders their performance in many applications. Chromatographic preconcentration techniques, which can be broadly categorized as on-line solid-phase extraction capillary electrophoresis (SPE-CE), show a more general applicability and can be also very efficient yielding high preconcentration factors (typically between 100 and 10,000 times) [4–6,16–21]. In on-line SPE-CE, a microcartridge (or analyte concentrator) is inserted near the inlet of the separation capillary. As the microcartridge is connected to or it is part of the separation capillary and the extraction happens immediately before the separation, the coupling has been referred as "on-line" by many authors since the late 80s, including N.A. Guzman, one of the pioneers in the field [6,22–32]. This nomenclature coexists in the literature with the term "in-line" that was introduced in the late 90s by U. A. Th. Brinkman and co-workers [16]. The term in-line SPE-CE has been preferred in the last years by many authors because is more specific, as it allows differentiation from on-line devices using valves or more complex instrumental set-ups. In in-line SPE-CE the microcartridge is integrated in the separation capillary, the voltage is applied across to it and the system is operated without valves [4,5,17–21]. In either case, the microcartridge contains a sorbent to selectively retain the target analyte, hence enabling the hydrodynamic or electrokinetic introduction of a large volume of sample (~50–100 μL). After sample loading, the capillary is rinsed to eliminate non-retained molecules and filled with background electrolyte (BGE). Then, the analyte is eluted in a small volume of an appropriate solution (~25–50 nL), resulting in sample clean-up and concentration enhancement before the electrophoretic separation and detection [4]. The higher the loaded volume while the analyte is retained without exceeding the breakthrough volume, the higher the preconcentration factors are obtained for a certain elution volume [21].

Nowadays, the main disadvantage for SPE-CE applicability is that there are no commercially available capillary columns modified with microcartridges, which must be fabricated by the interested users. However, the description of a wide variety of microcartridge designs and construction procedures, as well as the availability of appropriate commercial sorbents or preparation protocols and high selective detectors, especially MS detectors, have continuously broadened the applicability of SPE-CE [4,5,17–21]. Furthermore, it has been also demonstrated that SPE-CE can be combined with on-line electrophoretic preconcentration techniques, such as with transient isotachophoresis (t-ITP), to further enhance the sensitivity [33–39]. The possibility of this combination, together with the low cost, simplicity, valve-free operation and robustness (with an appropriate specific training to reproducibly construct the microcartridges), makes SPE-CE highly advantageous versus similar approaches based on capillary or nano liquid chromatography-mass spectrometry and microfluidic separations.

The field of SPE-CE, using different detectors, has been comprehensively reviewed over the last 10 years, with a particular focus on the concept and applications [5,6,17–21,31,32]. In addition, we have recently published a detailed experimental protocol focused on the construction of a double-frit packed microcartridge, as well as on method development for the analysis of peptides by C18-SPE-CE-MS [4]. Many of the practical tips and tricks given in this protocol are applicable for other configurations, designs and sorbents. As a unique complement to this information, the present review will cover in detail different fundamental aspects related with the designs and materials applied for almost 30 years to prepare the different microcartridge variants to perform SPE-CE, with emphasis on the conventional unidirectional configuration in capillary format. Advantages and disadvantages will be analyzed in detail to provide the reader a wide and critical overview, as well as a clear guidance, about the different alternatives for construction of the extraction microcartridges in SPE-CE. Finally, some general conclusions and future perspectives will be given.

2. SPE-CE designs and sorbents

This section analyzes in detail the most important designs and materials that have been employed in several laboratories to prepare microcartridges for SPE-CE.

2.1. Microcartridge configuration

In the typical SPE-CE configuration, the microcartridge is mounted in series to the fused silica separation capillary, and sample loading is performed from the inlet to the outlet, in the same direction as later the separation (Fig. 1). This could be detrimental when analyzing complex samples, because some of the matrix components could be irreversibly adsorbed in the inner wall of the separation capillary. Another inconvenient of this unidirectional or one-dimensional configuration is that the time to load a certain sample volume by pressure, which is the typical introduction mode because it is more general than electrokinetic introduction, depends on the applied pressure (e.g. typically 930 mbar in Agilent Technologies CE instruments) and the capillary dimensions (total length (L_T) and internal diameter (i.d.)) [4]. In order to overcome these drawbacks, cruciform and staggered (i.e. zigzag or z-shaped) microcartridge configurations have been developed [6,27–29,31,32]. The operation in both cases is very similar, but in the staggered microcartridges the amount of sorbent, hence the

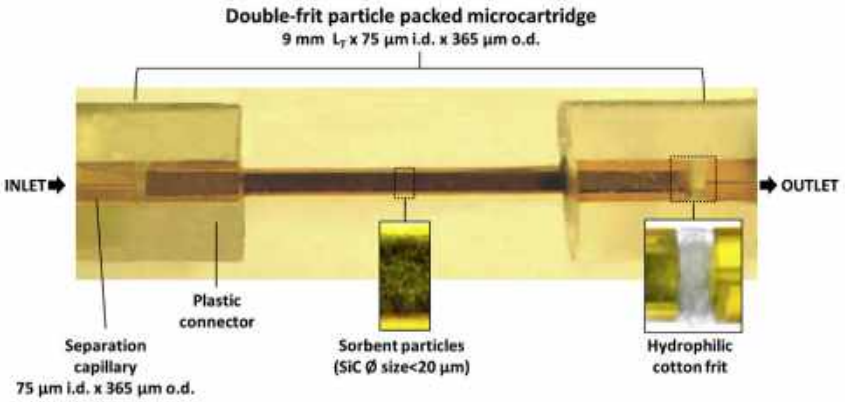

Fig. 1. Microphotograph of a double-frit silicon carbide (SiC) packed microcartridge mounted in series to the separation capillary (unidirectional or one-dimensional configuration). Hydrophilic cotton frits are placed inside the plastic connector between the microcartridge body and the separation capillary fragments. (For interpretation of the references to colour in this figure legend, the reader is referred to the Web version of this article.)

extraction capacity, is intended to be higher [31]. The sample is introduced through a transport tube or passage tube (usually made of a polymeric material such as PEEK tubing), which is orthogonal to the separation direction, whereas elution and separation are performed in the other direction, applying the voltage across to the microcartridge between the inlet and the outlet extremes of the separation capillary. In such configurations sample loading time by pressure is not determined by the separation capillary dimensions. Furthermore, they potentially allow no carry-over of substances into the separation capillary, extended lifetime of the capillaries and the possibility of multidimensional separations with several microcartridges mounted in series for high-throughput analyses [6,27–29,31,32]. However, these orthogonal microextraction devices are more difficult to construct than the typical microcartridges, as they require controlling the fluid flow with microvalves and moving from capillaries to microfluidics. This type of microfluidic set-ups have been described by different authors in articles [6,28,29,31,32] and patents [27,40,41], but, as other set-ups requiring specific instrumental multi-valve interfaces, they are out of the scope of this review, which will be focused on configurations for unidirectional SPE-CE with capillaries.

In addition to simplicity, another advantage of the conventional unidirectional configuration is that the capillaries modified with the microcartridges can be easily adapted to use the cartridge cassettes of the different commercial CE instruments (Fig. 2). These cartridge cassettes allow thermostatizing the capillary to compensate Joule heating during separation while the capillary is folded or coiled to minimize the space requirements. As can be observed in Fig. 2 a-c, the microcartridge is placed inside the cartridge cassette, as closest to the inlet as possible. Therefore, the microcartridge position from the capillary inlet differs between different instrument manufacturers. If the microcartridge is fabricated connecting with plastic tubing capillary fragments with different i.d. (Fig. 1), it is not recommended to install the microcartridge outside the cassette, closer to the inlet, due to the electrode configuration (in general, parallel (and coaxial or not) to the capillary), the mechanical operation during the analyses (vial lift movement, vial cap puncher, etc.) and the particularities of the injection (the inlet capillary end is submerged in the solutions, pressure application during hydrodynamic injection, etc.). In the typical situation, as the microcartridge is placed a few centimeters beyond the separation capillary inlet, several authors, after injection of the eluent and before applying the separation voltage, prefer to push by pressure the injected plug from the inlet until it flows through the microcartridge to ensure an appropriate elution [4]. However, this little adjustment is not completely necessary to achieve good results. Thus, for example, the eluent using fused silica capillaries in normal polarity (cathode in the outlet) migrates, after applying the voltage, towards the microcartridge with the velocity of the cathodic electroosmotic flow (EOF), which mainly depends on the BGE pH [4].

2.2. Microcartridge with frits and fritless

During the last almost 30 years, several microcartridge designs for SPE-CE have been described. In general, the microcartridges are mounted in 50–75 µm internal diameter (i.d.) x 365 µm outer diameter (o.d.) fused silica separation capillaries, using plastic tubing with an appropriate i.d. as zero death-volume connectors (e.g. Tygon® tube of 250 µm i.d.) (Fig. 1) [4]. In many cases, the microcartridge body consists in a small piece (total length (L_T) ~2–10 mm) of fused silica capillary with a wider i.d. than the separation capillary (the most typical i.d. are 150 or 250 µm) that is connected with two plastic connectors to the separation capillary (Fig. 1). Several authors have shown that extraction performance within this L_T range is good, but for the shortest microcartridges (L_T~2–4 mm) is better to introduce the microcartridge body completely inside a single plastic connector to reinforce the modified capillary [4,42]. With regard to the microcartridge i.d., we in general use microcartridges of 250 µm to ensure the maximum amount of sorbent inside [4]. Several authors have related the amount of different sorbents with an increase in sensitivity [43–45], but others have shown no effect [42] or worse results [46], because preconcentration factors depend on the compromise between the amount, porosity and packing of the sorbent for retention, and the volume necessary for an efficient elution and obtention of narrow electrophoretic peaks. Anyway, microcartridges of 250 µm i.d. guarantee with different sorbents a good compromise between extraction recoveries, effects on the EOF due to the chemical features of the sorbent, separation efficiency and backpressure due to flow restriction. Excessive backpressure especially affects the electroosmotic flow, separation efficiency, migration time and reproducibility, and in some cases prevents current circulation after applying the separation voltage. As an alternative to these microcartridges made on fused silica, several authors have proposed to introduce the sorbent inside the plastic tube used as connector, between both pieces of the separation capillary [47]. However, these SPE-CE capillaries are prone to poor

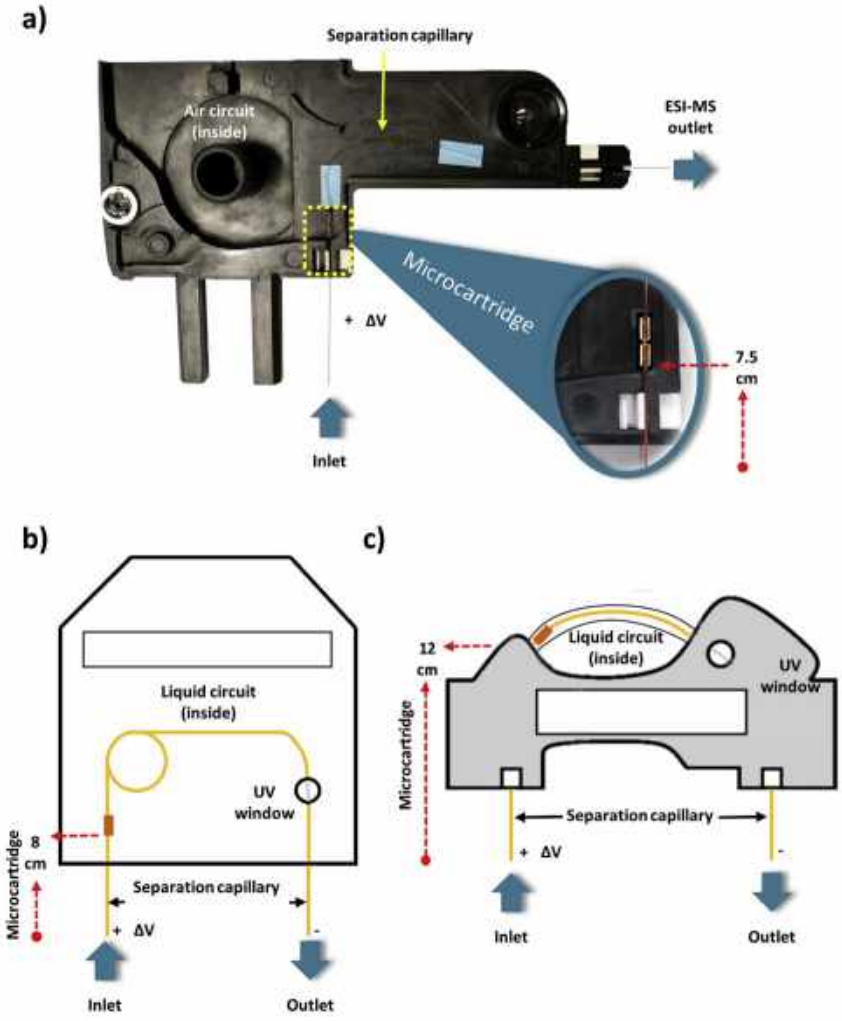

Fig. 2. Schematic representation of SPE-CE capillaries installed in the cartridge cassettes of different commercial CE instruments: a) CE-MS Agilent Technologies, b) CE-UV P/ACE 5500 Beckman Coulter and c) CE-UV MDQ Beckman Coulter.

electrical performance, worse separation and limited reproducibility. With regard to the separation capillary material, the use of coated capillaries to prevent the adsorption in the inner capillary wall of the analytes or some of the matrix components that could be detrimental for the method performance has been described, but to a lesser extent [48–50]. J. Cai et al. demonstrated for the first time the use of coated separation capillaries in SPE-CE-UV using capillaries coated with polyethylene glycol for the analysis of proteins with immobilized zinc affinity open-tubular microcartridges [48]. In this case, the permanently coated separation capillary is prepared before cutting and inserting the microcartridge to prevent sorbent degradation during the coating procedure, as we also demonstrated for the analysis of glycoproteins by SPE-CE-MS with immunoaffinity (IA) sorbents using capillaries coated with hexadimethrine bromide or an anionic derivative of polyacrylamide [49,50].

Once the microcartridge is assembled, if the plastic connectors provide a tight junction, no adhesive sealing is necessary and the microcartridge is completely replaceable (Figs. 1 and 3-a). In other cases, especially if microcartridge position or capillary installation inside the commercial cartridge cassette compromise microcartridge mechanical integrity, it is recommended to completely cover the microcartridge and the connectors with a thin layer of a two-component epoxy resin glue to reinforce the construction before installation. This is especially necessary when a liquid (Fig. 2-b and 2-c), instead of air (Fig. 2-a), circulates through the cartridge cassette in the capillary thermostatizing system, as in AB Sciex instruments (formerly Beckman Coulter instruments). We have recently shown that the internal thermostatizing system of the instrument or an external specific set-up designed for the microcartridge can be used to explore the influence of temperature in SPE-CE [51].

Fig. 3 a-h show the most important microcartridge designs for SPE-CE that can be divided into two main groups: with frits and fritless.

2.2.1. Microcartridge with frits

Microcartridges with frits are packed with sorbent particles and frits are used to avoid particle leaking during the analyses (Fig. 3 a-b). Microcartridges with frits can be tightly packed with smaller sorbent particles of a certain pore size, hence allowing a great active surface area for the extraction. However, extremely packed

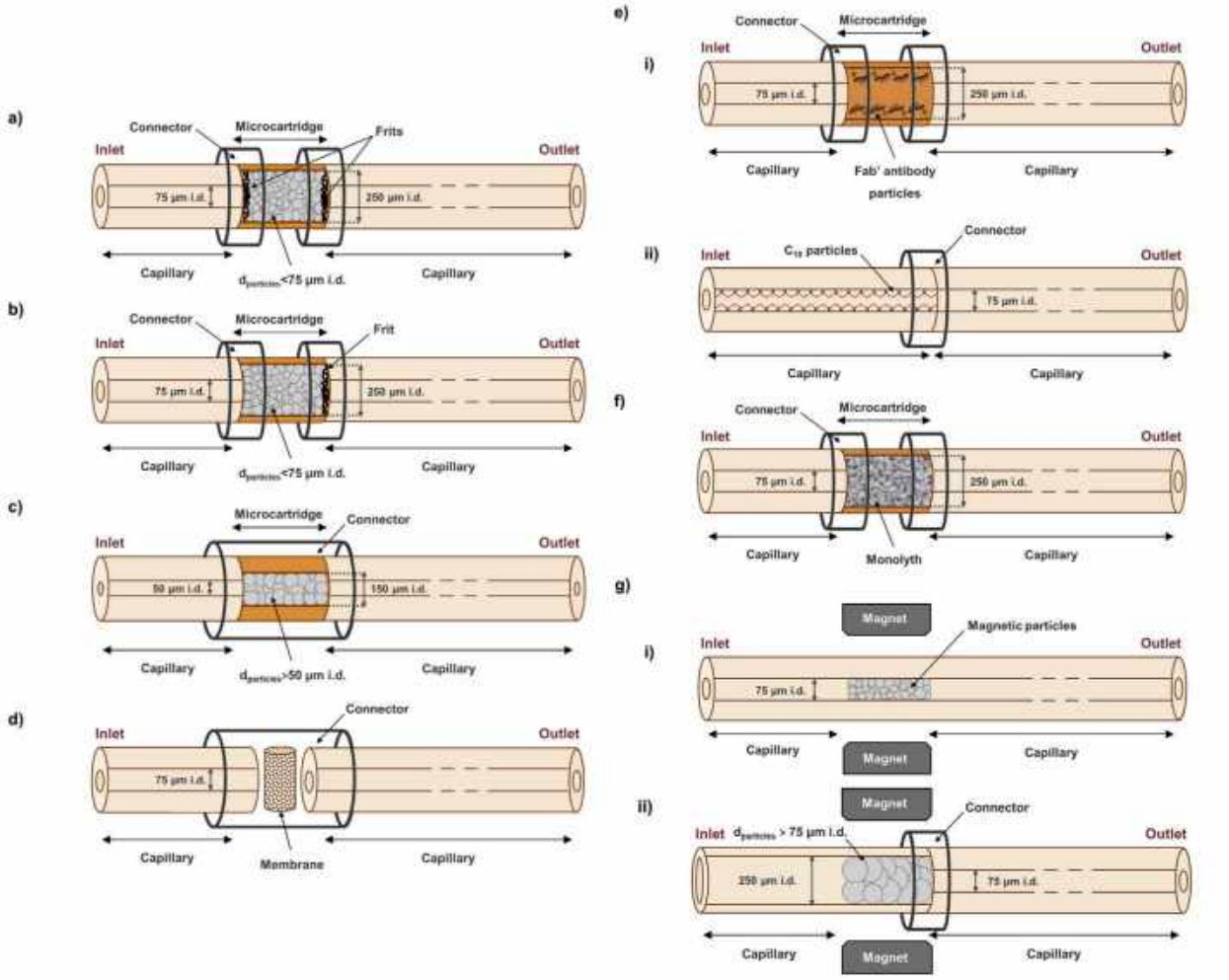

Fig. 3. Schematic representation of the most important microcartridge designs with frits and fritless for SPE-CE a) double-frit particle packed, b) single-frit particle packed, c) fritless packed with sorbent particles with a larger size than the inner diameter of the separation capillary, d) fritless with sorbent membranes, e) fritless open tubular (i-ii), f) fritless monolithic and g) fritless with magnetic particles (i-ii).

microcartridges, nonporous sorbents or too tighten frits promote flow restriction and excessive backpressure, hence EOF disturbance, bubble formation, current instability and power failures [4].

Frits form a porous wall or net structure (<100 μm thickness) that allow the passage of solution and analytes, without restricting the flow. For the same reasons as we suggested before for the location of the sorbent, we recommend placing the frits inside the microcartridge body (Fig. 3-a and -b) [4]. However, with very small sorbent particles (particle size<20 μm), it could be necessary to place the frits inside the plastic connector between the different capillary fragments (Fig. 1-a) [52,53]. Frits can be prepared inside the microcartridge body sintering porous glass beads after heating in an oven or with a fiber-optic fusion splicer, nichrome wire or microelectric arc device. In the first microcartridge for SPE-CE ever described in the literature, N.A. Guzman et al. used sintered porous borosilicate frits in a double-frit microcartridge (Fig. 3-a) containing sorbent particles with an antibody against methamphetamine covalently attached to irregularly shaped glass beads [22]. However, the high temperature needed for the fabrication could degrade and inactivate the sorbent and several alternatives have been described to these sintered frits. Metal frits, as those used in chromatographic columns, have been scarcely applied because of the poor performance and electrical issues [54]. Frits made on glass fiber or wool [43,55], polymeric membranes [56,57], sol-gel polymers [55] and hydrophilic cotton have been demonstrated [53]. These materials allow construction of tighten frits, which are especially needed with the smallest sorbent particles (diameter size<20 μm), but have to be prepared with care to ensure an appropriate performance of the system. Alternatively, we have widely applied microfrits prepared after cutting into small pieces (diameter size~100 μm) the original polyethylene filters of the commercial cartridges for off-line SPE [4]. These polyethylene microfrits allow a good electrical and flow performance with double-frit microcartridges packed with the typical sorbent microparticles that can be found in the commercial cartridges for off-line SPE [37,58,59] or with the microparticles that are commercialized as solid supports to prepare IA sorbents [49,50,60–62] (diameter size>30 μm, but typically between 50 and 100 μm, and pore size>100 Å). In general, double-frit microcartridges are preferred because sorbent leaking is totally prevented. However, packed microcartridges with a single frit in the outlet perform well when no sorbent leaking though the inlet or poor packing is

observed. Single-frit microcartridges can be necessary with certain sorbents and frit materials to avoid an excessive backpressure with two frits (Fig. 3-b) [53,63]. The feasibility of the single-frit design using a C4 sorbent (diameter size = 13 μm) and a sintered frit was first demonstrated by He et al. for the preconcentration and chiral separation by SPE-CE-UV of the enantiomeric drug verapamil in human plasma using C4 sorbent particles and a cyclodextrin containing background electrolyte (BGE) [63]. We have recently used a single-frit microcartridge with a silicon carbide (SiC) sorbent (diameter size<20 μm) and a hydrophilic cotton frit in the outlet end of the microcartridge for the analysis of circulating microRNAs in serum samples by SPE-CE-MS (single-frit version of the double-frit microcartridge presented in Fig. 1) [53].

Table 1-a shows a representative overview of some selected SPE-CE applications using microcartridges with frits that are of relevance to the field.

2.2.2. Fritless microcartridges

As an alternative to the microcartridge with frits, several authors have described the use of fritless microcartridges in SPE-CE. In some cases, the assembly of these fritless microcartridges can be much simpler, and certain designs can prevent some of the typical drawbacks of microcartridges with frits related with flow restriction. Fritless microcartridges have been fabricated using different designs (Fig. 3 c-h): packed with sorbent particles with a slightly larger size than the inner diameter of the separation capillary (Fig. 3-c) [42,46,47,64–71] or using sorbent membranes (Fig. 3-d) [25,33–36,46,72–75] and fibers [76–78], as well as coatings [79–86] or monoliths (Fig. 3-e and -f) [39,87–102] or retaining magnetic particles with a magnet (Fig. 3-g and -h) [44,45,103–110].

The most straightforward way to prepare a fritless particle-packed microcartridge is to pack sorbent particles with a slightly larger size than the inner diameter of the separation capillary (Fig. 3-c) [42,46,47,64–71]. If necessary, the sorbent particles can be sieved with an iron steel sieve of an appropriate size (sieve pore size > i.d. separation capillary) [42,68,69]. In general, 50 μm i.d. separation capillaries are preferred to avoid using extremely large sorbent particles that could generate loose packings. K. Jooβ et al. showed for the analysis of organic sulfonates and glycans by SPE-CE-MS that this can be prevented using fritless microcartridges with a bead string design (weak anionic-exchange sorbent particle size>90 μm, 4 mm L_T packing x 100 μm i.d. connected to a 50 μm i.d. separation capillary) [69]. In 1994, A.T. Tomlinson et al. described for the first time the fritless microcartridge design [47]. They used a fritless microcartridge packed with C18 particles inside a Teflon tube to analyze haloperidol and standard solutions of synthetic peptides. In the last years, the fritless particle-packed microcartridges made of fused silica have become very popular because of the widespread availability of sorbent microparticles, preparation simplicity and good performance, and different applications have been described using from conventional chromatographic sorbents (C18, hydrophilic-lipophilic balance (HLB), cationic exchange, etc.) [42,46,47,65–69], to molecular imprinted polymers (MIPs) [70,71] or IA [64] sorbents for the analysis of drugs, herbicides and biomarkers (e.g. Aminopirene trisulfonate (APTS)-labeled glycans, amino acid derivatives or peptides), in standard solutions, biological fluids and foodstuff with UV and MS detection (Table 1-b). Recently, we investigated the potential of sheathless SPE-CE-MS with this microcartridge design for the highly sensitive analysis of opioid peptides in aqueous solutions [111]. This high sensitivity porous sprayer (HSPS) sheathless CE-MS interface necessarily runs with a 30 μm i.d. x 150 μm o.d. capillary, ended with a porous-tip in the outlet, instead of the typical 50 or 75 μm i.d. x 365 μm o.d. capillaries. As an alternative to the double-frit C8 microcartridge (C8 particle size~5 μm, 1 mm L_T packing x 100 μm i.d. x 365 μm o.d.) proposed by Y. Wang et al. for these special capillaries, which needed special connectors (Fig. 4) [38], we proposed a novel fritless C18 microcartridge (C18 particle size>50 μm, 4 mm L_T packing x 150 μm i.d. x 365 μm o.d.), which was inserted in the separation capillary just employing the typical plastic tubing and an epoxy resin to seal the capillaries with different o.d (Fig. 5). [111]. In this case, LODs for the analyzed opioid peptides could be decreased down to the picomolar level, which represented an improvement of 5000-fold with respect to the LODs achieved by sheathless CE-MS without preconcentration, which was five times more sensitive than sheathflow CE-MS [37]. Nowadays, this HSPS sheathless SPE-CE-MS approach provides the most promising performance in terms of sensitivity of SPE-CE with on-line MS detection [38,111]. Other authors have also shown remarkable results in SPE-CE-MS with different types of microcartridges and sheathless interfaces [73,112]. P. Viberg et al. described a double-frit C18 microcartridge (C18 particle size~5 μm, 1–2 mm L_T packing x 200 μm i.d. x 300 μm o.d.) to analyze heterocyclic aromatic amines until concentrations of 22 nM with a sheathless interface made with a nanospray emitter. The microcartridge was connected and sealed with epoxy glue near the separation capillary without plastic connectors, taking advantage of the diameter differences with the separation capillary (30 μm i.d. x 190 μm o.d), which was gold-coated and etched in the outlet end [112]. G. M. Janini et al. tapered and etched 75 μm i.d. x 190 μm o.d fused silica capillaries in the outlet end to prepare 30 μm i.d spray tips for sheathless SPE-CE-MS. They were using fritless microcartridges containing a sorbent membrane (3 mm, C18) (Fig. 3-d), which will be discussed later in detail, to enhance sensitivity in the analysis of tryptic digests from diluted protein solutions (until 250 nM of digested protein) [73]. Despite all this progress, the increased reproducibility and robustness, as well as the lower cost of the instrumental set-up and materials required for sheathflow SPE-CE-MS, makes today very difficult a widespread use of sheathless SPE-CE-MS.

With regard to the performance of this particle-packed fritless microcartridge compared to microcartridges with frits, we have demonstrated that results with a certain sorbent sieved to select particles of certain diameters are not better than those that can be obtained with a double-frit microcartridge packed with the unsieved sorbent particles [42]. In that study we developed a C18-SPE-CE-MS method for the analysis of opioid peptides in cerebrospinal fluid [42]. A fritless microcartridge of 4 mm L_T x 150 μm i.d. was packed with a C18 sorbent (particle size>50 μm) and was connected near the inlet of the separation capillary (50 μm i.d.). Under the optimized conditions, the LODs for the studied peptides were 0.5–1.0 ng/mL, while they were detected at 0.1 ng/mL by C18-SPE-CE-MS using a double-frit microcartridge (7 mm L_T x 250 μm i.d. connected to a 75 μm i.d. separation capillary) that was packed without sieving the same C18 sorbent particles (20 μm < particle size<100 μm). This was mainly because the microcartridge with frits, which was longer and wider and was tightly packed with smaller unsieved sorbent particles, was connected to 75 μm i.d. separation capillaries that allowed to introduce in a shorter time a larger volume of sample.

Another way to prepare a fritless microcartridge is to insert a coated/impregnated sorbent membrane (1–3 mm) in the plastic tube connecting the two pieces of separation capillaries (Fig. 3-d) [25,33–35]. This design was firstly used [33], and later widely demonstrated [25,34,35], by A.J. Tomlinson et al. for the analysis of drugs and peptides by SPE-CE-MS using C18 or polymeric-impregnated membranes. Using these membranes, it was possible to minimize the sorbent bed volume at the inlet of the separation capillary and no flow restriction was reported. High retention capacity of the membranes permitted the analysis of the typical large sample volumes with double-frit or fritless packed

Table 1
Representative overview of some selected unidirectional SPE-CE applications using microcartridges a) with frits and b) without frits (fritless).

a) With frits

Analyte	Sample	Microcartridge design	Sorbent	Detection	LODs	Remarks*	[Ref.]
Methamphetamine	Urine	Double-frit microcartridge	mAb particles	UV	–	The first report of SPE-CE	[22,23]
Glycopeptides	Urine	Double-frit microcartridge	Lectin (ConA) particles	UV	–	The first report of lectin-SPE-CE	[25]
Gonadotropin-releasing hormone (GnRH)	Serum and urine	Double-frit microcartridge	Fab' polyclonal antibody (pAb) fragment particles	MS	1 ng/mL	The first report of IA-SPE-CE-MS	[123]
Peptides	Standards	Double-frit microcartridge	C18 particles	MS	Until 10 ng/mL	BGE was 20 mM N-[carbamoylmethyl]-2-aminoethanesulfonic acid (ACES) at pH 7.4	[30]
Opioid peptides	Human plasma	Double-frit microcartridge	C18 particles	MS	Until 1.1 ng/mL (with t-ITP)	Detailed experimental protocol Development and reoptimization of a double step plasma pretreatment (precipitation with acetonitrile followed by centrifugal filtration) Evaluation of different sorbents: C2, C8, C18, HLB, etc. Combination with t-ITP	[4] [9,58,59] [124] [37]
Peptides	Mixture of proteins and *pyrococcus furiosus* tryptic digests	Double-frit microcartridge	C8 particles	MS	–	Combination with t-ITP, separation capillary coated with poly-ethylenimine and HSPS sheathless CE-MS interface	[38]
Erythropoietin	Standards	Double-frit microcartridge	pAb particles	UV	–	Separation capillary coated with hexadimethrine bromide	[49]
Transferrin	Human plasma	Double-frit microcartridge	pAb particles	MS	–	Separation capillary coated with an anionic derivative of polyacrylamide	[50]
β-carboline alkaloids	Standards	Double-frit microcartridge	C18 particles	UV	–	Use of the internal thermostatizing system of the instrument or an external specific set-up to optimize T in SPE-CE	[51]
β-carboline alkaloids	Algae extracts	Double-frit microcartridge	C18 particles	MS	Until 2 pg/mL	*Undaria pinnatifida* (wakame) algae were extracted with methanol followed by centrifugal filtration	[131]
Amyloid peptide fragments	Human serum	Double-frit microcartridge	Ni (II) immobilized metal ion affinity (IMA) particles	MS	2.5 μg/mL	For one of the tested sorbents frits were placed inside the plastic connector, not in the microcartridge body	[52]
MicroRNAs	Human serum	Single-frit microcartridge	Silicon carbide (SiC) particles	MS	10 nM	A single hydrophilic cotton frit was placed inside the plastic connector of the outlet	[53]
Sulfonylurea drug	Standards	Double-frit microcartridge	C18 particles	UV	Until 5 ng/mL	Sorbent in the plastic connector between two glass fiber frits	[43]
Clorophenols	River water	Double-frit microcartridge	C18 particles	UV	Until 17 pg/mL	Sol-gel frit in the outlet and glass wool frit in the inlet. A hole is made after the microcartridge to speed-up sample loading and avoid sample flowing through the separation capillary	[55]
Metallothioneins	Sheep liver extracts	Double-frit microcartridge	C18 particles	UV	–	Nitrocellulose membrane frits	[56]
Peptides	Yeast proteins separated by two-dimensional gel electrophoresis (2D-PAGE) and digested with trypsin	Double-frit microcartridge	C18 particles	MS	33 amol/μL (MS) and 300 amol/μL (MS/MS)	Zytex teflon membrane frits	[57]
Opioid peptides	Human plasma	Double-frit microcartridge	pAb particles	MS	Until 100 ng/mL	Polyethylene microfrits	[60]
Opioid peptides	Human plasma	Double-frit microcartridge	Fab' pAb fragment particles	MS	Until 1 ng/mL	Polyethylene microfrits	[61]
Transthyretin	Human serum	Double-frit microcartridgee	Fab' pAb fragment particles	MS	0.5 μg/mL	Polyethylene microfrits	[62]
Verapamil enantiomers	Human plasma	Single-frit microcartridge	C4 particles	UV	5 nM	The first single-frit microcartridge for SPE-CE. A BGE with a cyclodextrin is applied to separate the enantiomers.	[63]
Heterocyclic aromatic amines	Human urine	Double-frit microcartridge	C18 particles	MS	Until 22 nM	Glass-fiber frits. Sheathless CE-MS interface	[112]

(continued on next page)

Table 1 (*continued*)

a) With frits

Analyte	Sample	Microcartridge design	Sorbent	Detection	LODs	Remarks*	[Ref.]
Ceftiofur	River water	Double-frit microcartridge	C18 particles	UV	until 10 ng/L	Polyethylene microfrits Comparison with Large volume sample stacking River water preconcentrated off-line by C18-SPE	[125]
Oxprenolol	Human urine	Double-frit microcartridge	C18 particles	UV	Until 0.5 ng/mL	Sintered C18 particles frits. Urine was pretreated by liquid-liquid extraction	[126]
Naproxen	Tap water	Double-frit microcartridge	C18 particles	UV	Until 10 ng/L	Polyethylene microfrits. Elution from the outlet without injection of elution plug. Comparison with different stacking techniques. Tap water preconcentrated off-line by C18-SPE	[127]
Ochratoxin A	River water	Double-frit microcartridge	C18 particles	UV	1 ng/L	Polyethylene microfrits Comparison between off-line SPE CE and in-line SPE-CE	[130]
Rare earth elements	Tap water	Double-frit microcartridge	C18 particles	UV	Until 20 pg/L	Gadolinium and lanthanum form 2-(5-bromo-2-pyridylazo)-5-diethylaminophenol complexes.	[132]
Metabolites	Mouse plasma	Double-frit microcartridge	C18 patricles	MS	–	Metabolomics of Huntington. Plasma pretreatment: precipitation with acetonitrile followed by centrifugal filtration.	[133]

b) Fritless

Analyte	Sample	Microcartridge design	Sorbent	Detection	LODs	Remarks*	[Ref.]
Opioid peptides	Human cerebrospinal fluid (CSF)	Separation capillary i.d.<sorbent particle size	C18 particles	MS	Until 0.5 ng/mL	Comparison between fritless and double-frit microcartridges	[42]
Haloperidol and synthetic analogs	Standards	Separation capillary i.d.<sorbent particle size	C18 particles	MS	–	The first report of SPE-CE with this fritless design	[47]
Peptides	Erythropoietin (EPO) and novel erythropoiesis stimulating protein (NESP) tryptic digests	Separation capillary i.d.<sorbent particle size	pAb particles	MS	Until 6 μg/mL	CNBr-Sepharose 4B solid support swells and 75 μm i.d. separation capillary can be used	[64]
3-nitrotyrosine	Rat urine	Separation capillary i.d.<sorbent particle size	Mixed-mode strong cation-exchange (MCX) particles	UV	Until 4.4 μM	Reversed phase and strong cationic exchange mixed mode sorbent	[65]
Quinolones	Meat	Separation capillary i.d.<sorbent particle size	MCX particles	MS	Until 17 ng/mL (MS/MS)	Reversed phase and strong cationic exchange mixed mode sorbent. Meat sample pretreatment: pressurized liquid extraction (PLE)	[66]
Pharmaceuticals	River water	Separation capillary i.d.<sorbent particle size	HLB particles	UV	Until 0.19 ng/mL	Reversed phase hydrophilic-lipophilic polymeric sorbent	[67]
Drugs	Human urine	Separation capillary i.d.<sorbent particle size	HLB particles	MS	0.013 ng/mL	Reversed phase hydrophilic-lipophilic polymeric sorbent	[68]
Organic sulfonates and APTS-labeled glycans	Standards	Separation capillary i.d.<sorbent particle size	Strata X/XL AW (weak anion-exchange mixed mode polymeric) particles	MS	Low nM range	Reversed phase and weak anion exchange mixed mode sorbent. Bead string microcartridge design. Separation capillary coated with polyvinyl alcohol (PVA)	[69]
Triazine herbicides	Human urine	Separation capillary i.d.<sorbent particle size	MIP particles	UV	Until 0.2 μg/mL	Cetyltrimethylammonium bromide (CTAB) in the BGE to reverse the EOF. Comparison with HLB sorbent particles (fritless microcartridges)	[70]
Quinolones	Bovine milk	Separation capillary i.d < sorbent particle size	MIP particles	MS	Until 1 μg/kg (MS/MS)	Milk sample pretreatment: protein precipitation with acetic acid and defatting	[71]

Sulfonamides	Tap, bottled mineral and river waters	Separation capillary i.d < sorbent particle size	HLB particles	UV	Until 0.3 μg/L	Comparison with Strata-X and MCX sorbents particles and SDB-XC membranes (fritless microcartridges)	[46]
Opioid peptides	Standards	Separation capillary i.d < sorbent particle size	C18 particles	MS	Until 2 pg/mL	HSPS sheathless CE-MS interface	[111]
Cathinone derivatives	Human hair	Separation capillary i.d < sorbent particle size	HLB particles	UV	Until 0.05 ng/mg	β-cyclodextrin in the BGE for chiral separation. Hair sample pretreatment: pressurized liquid extraction (PLE)	[128]
Cocaine and metabolites	Human hair	Separation capillary i.d < sorbent particle size	HLB particles	UV	Until 0.1 ng/mg	α-Cyclodextrin in the BGE for chiral separation Hair sample pretreatment: pressurized liquid extraction (PLE)	[129]
Peptides	Standards	Membrane	Styrene Divinylbenzene (SDB) membrane	MS	Until 1 pg/mL	The first report of membrane-SPE-CE and of combination of SPE-CE with t-ITP Different variants are reviewed in Refs. [25,34,35]	[33]
Peptides	Standards	Membrane	SDB-XC membrane	UV	1 ng/mL	Combination with t-ITP	[36]
Peptides and lipopolysaccharides	Standards and pathogenic strains of *Haemophilus influenza*	Membrane	SDB-XC membrane	MS	Until 0.23 nM (peptides)	Comparison with C18 sorbent particles (fritless microcartridges). Complex sample pretreatment of the cells	[72]
Peptides	Protein tryptic digests.	Membrane	C18 membrane	MS	–	Sheathless CE-MS interface	[73]
Peptides	Standards and bovine serum albumin (BSA) tryptic digests	Membrane	SDB-XC membrane	MS	–	Comparison with LC-nanoESI-MS	[74]
BSA	Standard	Membrane	Cellulose acetate membrane	UV	–	Membrane in the inlet and sample electrokinetic loading from the outlet	[75]
Proteins	Standards	Fiber	Hollow fiber	UV	100 ng/mL		[76]
Phenols	Standards	Fiber	Poly(acrylate) (PA)-coated silica fiber	UV	–	The fiber is connected after the off-line loading step	[77]
Proteins	Phycoerythrins in cultured cyanobacteria	Fiber	Derivatized hollow fiber	LIF	Until 3.5 pM	Capillary isoelectric focusing (CIEF) with laser-induced fluorescence (LIF) whole column imaging detection (WCID)	[78]
Triazine herbicides	Water	Open-tubular (single tube)	C18 coating	UV	0.1 μg/mL	The first single-tube open-tubular microcartridge for SPE-CE	[79]
Methamphetamine	Urine	Open tubular (capillary bundle)	Monoclonal antibody (mAb) coating	UV	–	The first report of SPE-CE	[22,23]
IgE	Human serum	Open tubular (capillary bundle or solid rod of glass with multiple through holes)	mAb coating	UV	–	–	[23,24]
Proteins	Standards	Open-tubular (single tube)	Zn(II) coating	UV	1 μg/mL	Separation capillary coated with polyethylene glycol	[48]
Atrazine	Standards	Open-tubular (single tube)	mAb coating	LIF	1 nM	Separation capillary coated with C8 and BSA. Combination with sample stacking	[80]
Cyclosporin A	Human tears	Open-tubular (single tube)	Fab' mAb fragment coating	UV	6.2 ng/mL	–	[81]
Cytokines	Plasma, serum, urine, and saliva samples	Open-tubular (single tube)	Fab' mAb fragment coating	LIF	Until 5 ng/μL	–	[82]
Cytokines	Single-cell cultures	Open-tubular (single tube)	Fab' mAb fragment coating	LIF	0.1 fg/mL	Special incubation chamber and microdialysis sampling of the lymphocyte cells to induce cytokine secretion by neuropeptides	[83]
Neurothrophins	Human serum	Open-tubular (single tube)	Fab' mAb fragment coating	LIF	0.1 fg/mL	–	[84]
Testosterone derivatives	Human urine	Open-tubular (single tube)	MIP coating	UV	<50 ng/mL	Novel light-emitting diode-induced technology for in-capillary polymerization. Silylated separation capillary.	[86]
Peptides	Plasma samples	Open-tubular (Monolithic. Single tube)	C18-silica monolithic coating	MS	Until 0.01 μg/mL	–	[87]
Peptides	BSA and *E. Coli* tryptic digests	Monolithic. (completely filled)		MS	Low pg/mL range		[39]

(continued on next page)

Table 1 (*continued*)

b) Fritless

Analyte	Sample	Microcartridge design	Sorbent	Detection	LODs	Remarks[a]	[Ref.]
			Sulfonate-silica hybrid strong cation-exchange (SCX) monolith			Combination with dynamic pH junction. Electrokinetically pumped nanospray CE-MS interface	
S-propranolol	Standards	Monolithic, (completely filled)	Methacrylate monolith	UV	Low nM range	Reverse elution (from the outlet) with the BGE using the EOF as a pump (reversed polarity)	[88]
Immunoglobulin G	Human serum	Monolithic, (completely filled)	Protein G glycidyl methacrylate (GMA) monolith	UV	1 nM	Separation capillary coated with dextran and hexadimethrine bromide. Serum samples were diluted 1:10 and heated at 95 °C	[89]
Histidine-containing peptides	Standards and synthetic peptide mixture	Monolithic, (completely filled)	Cu(II) iminodiacetic acid (IDA) di(ethylene glycol) dimethacrylate (DEGDMA) and glycidyl methacrylate (GMA) monolith	UV	<25 μg/mL	–	[90]
Inorganic anions	Open ocean water	Monolithic, (completely filled)	Sulfonated methacrylate monolith coated with anion exchange latex nanoparticles	UV	Until 75 pM	Separation capillary coated with poly(diallyldimethylammonium) chloride (PDDAC) or quaternary ammonium functionalized latex nanoparticles. Combination with t-ITP	[91]
Organic anions	Standards	Monolithic, (completely filled)	Sulfonated methacrylate monolith coated with anion exchange latex nanoparticles	UV	Until 1.5 nM	Separation capillary coated with PDDAC. Combination with t-ITP	[92]
Carbamate pesticides	Tap and river water	Monolithic, (completely filled)	Divinylbenzene monolith	UV	Until 0.01 ng/mL	The BGE contained high percentage of ACN and SDS	[94]
Methionine-enkephalin	Human CSF	Monolithic, (completely filled)	Sol-gel silica monolith	MS	<1 ng/mL	CSF sample was deproteinized	[95]
Neurotransmitters	Human urine	Monolithic, (completely filled)	Methacrylate weak cation-exchange monolith	UV	Until 2.9 ng/mL	Combination with focusing by a pH step gradient	[96]
Cationic compounds	Standards	Monolithic, (completely filled)	Methacrylate weak cation-exchange monolith	UV	Until 8 ng/mL	Combination with focusing by a pH step gradient	[97]
Neurotransmitters	Standards	Monolithic, (completely filled)	Methacrylate weak cation exchange monolith templated with silica nanoparticles	UV	Until 0.5 ng/mL	Combination with focusing by a pH step gradient. Caffeine in human urine, cola drink and wastewater were also analyzed	[98]
DNA fragments	*E. Coli* cell lysates	Monolithic, (completely filled)	Amino silica monolith	LIF	Until 65 pg/mL	Linear poly(N-isopropylacrylamide) was used as a sieving media in the BGE	[99]
Phenols	Tap, snow and river water	Monolithic, (completely filled)	Poly(4-vinylpridine-co-ethylene glycol dimethacrylate) (4-VP-coEGDMA) monolith	UV	Until 1.3 ng/mL	β-cyclodextrin (β-CD) was used in the BGE	[100]
Ochratoxin A	Beer and wine	Monolithic, (completely filled)	Aptamer vinyl silica monolith	LIF	Until 40 pg/mL	The first report of Aptamer-SPE-CE	[101]
Peptides	*E. Coli* tryptic digests	Monolithic, (completely filled)	Sulfonate-silica hybrid strong cation-exchange (SCX) monolith	MS	–	Combination with dynamic pH junction. Linear polyacrylamide coated capillary. Electrokinetically pumped nanospray CE-MS interface. Comparison with UPLC-MS. MS/MS measurements	[102]
Mouse mAB	Standards	Magnetic particles	pAb particles	UV	–	Poly(vinyl alcohol) (PVA) coated capillary. Combination with t-ITP	[103]
β-Lactoglobulin	Bovine milk	Magnetic particles	pAb particles	UV	<1 μg/mL	Hydroxypropylcellulose (HPC) coated capillary. Sorbent was washed from the outlet. Elution of β-LG and pAb (Protein A particles). Combination with t-ITP. Defatted milk and whey fraction separation	[104]

Anti-*Helicobacter pylori* IgG	Human serum	Magnetic particles	*Helicobacter pylori* antigen particles	LIF	0.06 U/mL	A second specific labeled antibody against human IgG is used for indirect detection	[44]
Parabens and nonsteroidal anti-inflammatory drugs	Standards	Magnetic particles	C18 iron oxide particles	UV	–	Sorbent particles are injected after the off-line sample loading	[105]
β-Lactoglobulin and α-Lactoalbumin	Bovine milk	Magnetic particles	pAb particles	UV and off-line MS	0.5 μg/mL (UV) 0.02 μg/mL (MALDI-MS)	Hydroxypropylcellulose (HPC) coated capillary. Combination with t-ITP. Off-line MALDI-MS. Defatted milk and whey fraction separation	[106]
Immunoglobulin E (IgE) and milk proteins	Human serum and milk protein fractions	Magnetic particles	pAb particles and crosslinked IgE-pAb particles	UV and off-line MS	0.24 ng/mL (IgE, UV)	Hydroxypropylcellulose (HPC) coated capillary. Combination with t-ITP. Off-line MALDI-MS. Total IgE quantification (serum + IgE pAb sorbent) followed by immunocomplex crosslinking (milk protein fraction + new crosslinked sorbent) for allergen identification	[107]
α-1-acid glycoprotein	Human serum	Magnetic particles	pAb particles	UV	<1 mg/mL	Reversed introduction of the BGE, which contained putrescine and urea. Protein precipitation of serum samples	[108]
Drugs of abuse Transthyretin	Human urine Human serum	Magnetic particles Magnetic particles (or Separation capillary i.d.<sorbent particle size)	C18 iron oxide particles pAb particles	UV MS	Until 0.5 ng/mL 1 μg/mL	Urine was pretreated by liquid-liquid extraction Two different microcartridge designs. Serum samples were precipitated with phenol	[45,109] [110]

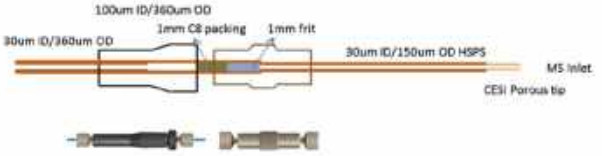

Fig. 4. Double-frit microcartrige (C8 particle size ~ 5 μm, 1 mm L_T packing x 100 μm i.d. x 360 μm o.d.) for the high sensitivity porous sprayer (HSPS) capillaries (30 μm i.d. x 150 μm o.d. capillary) needed for sheathless CE-MS in the interface commercialized by AB/Sciex. Reproduced with permission from Ref. [38].

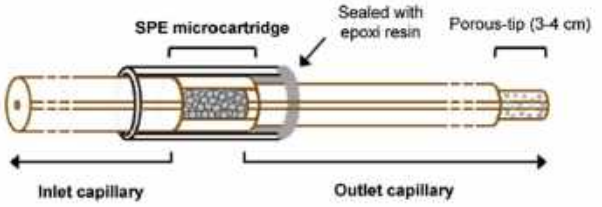

Fig. 5. Fritless microcartridge (C18 particle size > 50 μm, 4 mm L_T packing x 150 μm i.d. x 365 μm o.d.) for the high sensitivity porous sprayer (HSPS) capillaries (30 μm i.d. x 150 μm o.d. capillary) needed for sheathless CE-MS in the interface commercialized by AB/Sciex. Reproduced with permission from [111].

microcartridges (>100 μL) and high preconcentration factors, without compromising either analyte resolution or separation efficiency. Furthermore, the authors demonstrated for the first time the combination of SPE-CE-MS with t-ITP to further enhance the preconcentration factors for the analysis of peptide mixtures [33]. The methanol-water (80:20 v/v) plug with the eluted peptides (~60 nL) was sandwiched between two small volumes of leading electrolyte (LE) (~60 nL, 1% ammonium hydroxide) and BGE (~90 nL 2 mM ammonium acetate-1% acetic acid (pH 2.9), which acted also as terminating electrolyte (TE). After voltage application, when the steady state was reached, peptides were preconcentrated as discrete narrow bands with the same velocity because the LE and TE ions moved faster and slower, respectively. Despite all the benefits of using sorbent membranes, only very few authors have tested this design [36,46,72–75], probably because of issues related with fabrication reproducibility and availability of impregnated membranes with appropriate pore size, permeability and active surface area. Other similar approaches based on fibers have been described but also with very limited success [76–78].

Open tubular microcartridges for SPE-CE (Fig. 3-e) were first described by J. Cai et al. [79], in parallel to the developments on the on-line coupling of open tubular enzymatic microreactors to CE [113,114]. They connected to the inlet of the separation capillary as a microcartridge a 50 μm i.d. x 20 cm L_T piece of a fused silica capillary derivatized (i.e. coated) with C18 groups to analyze standard solutions of two herbicides (prometon and prometryne) by SPE-CE-UV [79]. After preparing a coated capillary of a certain length, the SPE-CE capillary column was very easy to assemble, as it was only necessary to cut a "plug-and-play" microcartridge to the desired length, connect and analyze. However, as the affinity surface area in these microcartridges is small, preconcentration factors are very limited (e.g. 10–35 times for prometon and prometryne [79]), and only a limited number of publications have been reported [80–87]. Most of the applications have been described with IA-SPE-CE immobilizing antibodies or antibody fragments in the open tubular microcartridge to analyze peptides in biological samples [80–84], especially with antibody fragments by T.M. Phillips and coworkers [81–84], before they moved to explore similar IA-SPE-CE approaches in microchips [115,116]. As an example of the

limitations of open tubular microcartridges but with other sorbents, H. Wang et al. presented a 100 cm L_T x 50 μm i.d. open tubular capillary coated with gold nanoparticles for off-line SPE of monohydroxy-polycyclic aromatic hydrocarbons in spiked urine samples before CE-UV and enrichment factors were lower than 100 times [85]. In order to extend the active surface area with IA open tubular microcartridges, N.A. Guzman proposed to use as a microcartridge body multiple channels bored through a single glass rod or a bundle of multiple capillaries (25 μm (i.d.)) [23–25], but this extremely complex multi-bore design has demonstrated a very limited applicability. A simpler alternative to improve extraction capacity of single-bore capillaries is to increase the thickness and porosity of the sorbent layer in the inner wall of the open tubular microcartridge. X. Zhang et al. directly prepared in the separation capillary, using a novel light-emitting diode (LED) induced polymerization technology, a 3 mm L_T x 75 μm i.d. open-tubular microcartridge coated with a MIP to preconcentrate until 200 times some testosterone derivatives in standards and spiked urine samples [86]. Similarly, we recently evaluated a 7 mm L_T x 250 μm i.d. open-tubular C18-silica monolithic microcartridge for the analysis of neuropeptides in human plasma [87]. In this case the monolith was not prepared in situ, but ex situ as a column of a certain length that was later cut to obtain several "plug-and-play" microcartridges. The LODs by SPE-CE-MS with the C18-silica monolithic microcartridge were 100 times lower than without preconcentration, but 100 times higher than with a C18 double-frit particle-packed microcartridge [58,59]. In order to maximize the microcartridge capacity and extraction recovery, it is recommended that the monolith fills completely the lumen of the microcartridge body (Fig. 3-f). The monolith length (typically from approximately 1 cm), structure and the number and type of active groups on the surface can be tailored to avoid flow restriction, as well as to maximize selectivity and extraction recoveries. Silica- and polymer-based monoliths have been described to prepare fully-filled microcartridges for SPE-CE [39,88–102]. However, polymer-based monoliths have been mainly preferred, because preparation by polymerization of monomers and cross-linkers is more simple and reproducible than the sol-gel procedure necessary to prepare silica-based monoliths [93]. It is well known that polymer-based monoliths can show a less uniform mesopore structure. However, polymer-based monoliths present improved stability, once selected appropriate solutions to prevent shrink or swell. Today, monoliths are probably the most promising way to prepare "plug-and-play" fritless microcartridges, but progress must be made improving extraction capacity and decreasing non-specific binding for the minute amount of sorbent used in SPE-CE. In this sense, P.R. Haddad and coworkers have been exploring the use of nanoparticles (i.e. functionalized quaternary ammonium latex [91,92] or silica [98] nanoparticles) to expand the extraction capacity of polymer-based monolithic microcartridges while tuning their selectivity to analyze by ion-exchange SPE-CE-UV anions [91,92] or weak bases [98]. Thus, they reported a sensitivity enhancement between 1500–1900 with regard to conventional CE for a mixture of three neurotransmitters (dopamine, norepinephrine and metanephrine) with a microcartridge (8 cm L_T x 75 μm i.d.) containing a polymeric monolith coated with silica nanoparticles (LODs were between 0.5 and 0.7 ng/mL) [98]. With regard to more selective monolithic microcartridges, recently A. Marechal et al. described for the first time the use of an aptamer-based monolithic sorbent in SPE-CE [101]. They applied an aptamer silica-based monolithic microcartridge (1.5 cm L_T x 75 μm i.d.) for the analysis by SPE-CE with laser-induced fluorescence (LIF) detection of ochratoxin A in standards, beer and wine at concentrations of a few ng/mL.

Nowadays, there are many commercially available magnetic particles (i.e. beads) with different surface chemistries ready for the immobilization of a wide variety of affinity ligands to develop bioanalytical applications [117,118]. The versatility and reasonable price of the commercial magnetic beads and the simplicity of operation are rapidly expanding their application in dispersive SPE [118]. As magnetic beads can be held in position by an external magnet or electromagnet, they have been used for preparation of fritless microcartridges (Fig. 3-g and -h), in particular for IA-SPE-CE. Since the pioneering work of Rashkovetsky et al. [103], several authors have described the use of IA magnetic particles in IA-SPE-CE with fluorescence [44,103–105], ultraviolet (UV) [45,108,109] and MALDI-MS [106,107] detection. Recently, we reported for the first time a IA-SPE-CE-MS method, with on-line electrospray ionization mass spectrometry (ESI-MS), using magnetic agarose microparticles (45 μm < particle size<165 μm) with an intact antibody against human serum transthyretin (TTR), which performed better than magnetic silica microparticles of smaller size (particle size~2.8 μm) [110]. In this case, two fritless microcartridge designs (9 mm L_T x 250 μm i.d.) were described. As agarose magnetic microparticles swell when suspended in aqueous solutions, one of the designs was taking advantage of their larger size than the inner diameter of the separation capillary (75 μm i.d., Fig. 3-c). In the other case, a magnet was used to hold a 9 mm length of magnetic particles in the outlet end of a capillary fragment (8.5 cm L_T x 250 μm i.d.) that was connected with a plastic tube to the separation capillary (75 μm i.d., Fig. 3-h). In all cases, the performance of both fritless microcartridges was similar. However, the "magnetic" design (Fig. 3-h) had several remarkable advantages, such as the presence of only one capillary connector and the simplicity to replace the sorbent through the inlet after certain number of analysis. Under the optimized conditions, LODs for TTR standard solutions were 25-fold lower than those obtained by CE-MS and the method could be applied for the analysis of serum samples [110]. With regard to non IA magnetic particles, Y. H. Tennico et al. reported for the first time the use of C18 silica-coated Fe_3O_4 magnetic nanoparticles (particle size~500 nm) for the SPE-CE-UV analysis of parabens and drugs in standards [105]. However, these authors proposed to mix the magnetic nanoparticles with the sample in a vial before injecting a small plug of the reacted nanoparticles (length~1 mm in a 50 μm i.d. fused silica separation capillary) for SPE-CE-UV analysis and LODs were around 1 μg/mL for standards of parabens. T. Baciu et al. proposed later a typical SPE-CE-UV procedure with C18 silica-coated Fe_3O_4 magnetic nanoparticles (particle size~75 nm) for the SPE-CE-UV analysis of drugs of abuse in urine samples at concentrations ranging from 20 to 50 ng/mL. In this case, the magnetic nanoparticles were retained first inside the short section (length~1.5 mm) of the inlet of a 50 μm i.d. fused silica separation capillary (Fig. 3-g) [45,109]. At the moment, the main limitations of using magnetic particles in SPE-CE is that many magnetic (micro or nano) particles commercialized for dispersive SPE are not porous, which could be a limitation for the active surface area when the amount of sorbent is small such as in SPE-CE. Another drawback affecting extraction capacity and reproducibility is particle aggregation [119]. In addition, the magnetic field holding the magnetic particles should be enough to avoid particle leaking during the washing and loading steps [44,45,104,108]. Magnetic particle leaking, especially with nanoparticles, could be a serious problem for the integrity of the mass spectrometer with on-line MS detection. Finally, little is known about the influence of the magnetic fields in immunoextraction in capillaries or microdevices [120,121].

Table 1-b shows a representative overview of some selected SPE-CE applications using fritless microcartridges reported to date in the literature.

2.3. SPE-CE sorbents

As noted above, many different sorbents have been described to analyze by SPE-CE a great variety of compounds, in a wide range of applications. Sorbents using particles as solid supports to immobilize the affinity ligands have been the most widely applied, from the low-selective conventional chromatographic sorbents (C8, C18, HLB, cationic or anionic exchange, etc.) until more selective sorbents with metals, molecular imprinted polymers, lectins, antibodies, antibody fragments, aptamers, etc. [4–6,17–21,31,32]. In SPE, recovery is mainly governed by the compromise between the eluotropic strength and the volume of the eluent and the sorbent capacity, which depends on the affinity strength and selectivity of the target analyte to the sorbent and the number of active sites available for the extraction that in particle sorbents are related to the particle size and porosity [122]. From the method development perspective in in-line SPE-CE, the only requirement of a good sorbent, in addition to reproducibility, is the compatibility between the extraction (high recovery, rapid elution and low non-specific retention), separation (high resolution, short analysis time) and detection (high selectivity and sensitivity). However, in some cases, this is difficult to accomplish, for example, if the retained analytes are eluted while filling the capillary with BGE before the separation, or with on-line MS detection, which is negatively affected by the presence of salts and requires the use of volatile solutions and BGEs. In other cases, it is the sorbent that is prone to degradation due to the presence of certain components in the solutions and BGE, such as when IA sorbents are exposed for a long time to BGEs with extreme pH values or organic solvents. These are the reasons why, for example, IA-SPE-CE was widely demonstrated with ultraviolet and fluorescence detection [22–26,80–82,103] before the first IA-SPE-CE-MS application was described in 2000 [123]. In that study, N.A. Guzman reported the analysis of gonadotropin-releasing hormone (GnRH) in serum and urine using a double-frit microcartridge with sorbent particles containing antigen-binding antibody fragments (Fab) against the peptide hormone. He was using a volatile BGE of ammonium bicarbonate pH 8.0 with 1% acetonitrile combined with a 0.3 M glycine-HCl buffer (pH 2.5) for the elution, which was not very compatible with on-line MS detection. Since then, our group have been very active in IA-SPE-CE-MS, describing applications for small peptides and proteins with intact antibodies or Fab antibody fragments using different microcartridge designs and neutral pH ammonium BGEs combined with eluents containing formic acid, acetic acid or ammonium hydroxide [50,60–62,64,110]. We recognize that making compatible and adapting the use of sorbents for in-line SPE-CE-MS is a challenge. In general, this challenge can be successfully faced with an appropriate method optimization. However first, as we mentioned before, the sorbent physical features (e. g. particle size, permeability and porosity) must allow operation without promoting flow restriction and backpressure, which may disturb the EOF and produce current instability or power failures.

In particle-packed microcartridges, the best compromise between active surface area, flow performance and durability is achieved using as a sorbent porous microparticles (e.g. pore size>100 Å and diameter size>50 μm), despite smaller microparticles [53,108], and even nanoparticles [45,109], have also been applied but to a lesser extent. Furthermore, if possible, our recommendation is to pack the microcartridge by vacuum using the dried sorbent particles instead of the slurry traditionally used to pack liquid chromatography columns [4]. With regard to continuous unitary sorbents, such as membranes and monoliths, there is very little information about the porosity of the membranes [25,33–35,46,74,75] or monoliths [39,87–102] used in microcartridges for SPE-CE, and probably this is one of the reasons of the limited amount of applications described. Our recommendation is preparing "completely full" monolithic microcartridges but avoiding extremely small pore sizes, as with particle sorbents, to ensure enough permeability and avoid excessive flow restriction. In either case, after preparing the SPE-CE capillaries with the microcartridge and before the analyses, it is highly recommended to flush water manually with a syringe through the system to check for abnormal flow restriction followed by a blank analysis to monitor current stability [4]. Not all the SPE-CE methods described have been fully validated and applied to complex real samples, but many good examples can be found in the literature with different sorbents [4–6,17–21,31,32]. In general, a microcartridge with an appropriate sorbent after method optimization can be reused between 10 and 30 times with standards and until 10 times with samples, depending on the sample matrix complexity [4]. For the analysis of complex biological samples, it is recommended to apply before SPE-CE a minimum sample pretreatment to prevent microcartridge saturation with matrix compounds and extend the microcartridge lifetime [4,9,52,53,60–62,110,124].

Nowadays, conventional chromatographic particle sorbents (C8, C18, HLB, cationic or anionic exchange, etc.) are the most commonly used for SPE-CE, as they fulfil most of the requirements for optimum performance. On the one hand, they provide a large active surface area, without interfering with the electrophoretic separation and detection. On the other hand, they are commercially available, have been optimized and widely used for the analysis of a great variety of compounds and the extraction methods are compatible with on-line MS detection (e.g. with C18 sorbents using formic and acetic acid BGEs and similar acidic hydroorganic mixtures with methanol for the elution). Especially reversed phase silica-based (e.g. C18) and polymeric sorbents (e.g. HLB) are widely recognized for their good recoveries, being the most common chromatographic sorbents used for SPE-CE-UV and -MS applications involving peptides (C18 [4,9,37,42,58,59,111,124]), antibiotics (C18 [125]), pharmaceuticals (C18 [126,127] and HLB [67]), drugs of abuse (HLB [68,128,129]), other bioactive compounds (e.g. ochratoxin A [130] or alkaloids [131] with C18), rare earth elements (C18 [132]) and metabolites (C18 [133]) in different environmental and biological samples (see Table 1a and b).

However, the major drawback of these chromatographic sorbents is their limited selectivity, which precludes the direct analysis of complex samples such as biological fluids. In such cases, a previous clean-up pretreatment, which can be more or less laborious, is required to purify and (optionally) enrich the target analytes in order to prevent microcartridge saturation. As an example, we have proposed a double-step sample pretreatment for the analysis of low molecular mass compounds in human plasma, which was optimized and validated for the analysis of neuropeptides by C18-SPE-CE-MS [4,9,59,124]. The method consisted of precipitation with acetonitrile followed by centrifugal filtration using 10,000 relative molecular mass cut-off filters. Using this double-step sample pretreatment, it was possible to obtain with preconcentration, LODs for these specific peptides in plasma samples between 100 and 1000 times lower than the LODs obtained using CE-MS. Fig. 6 shows detection at 1 ng/mL of three neuropeptides in a standard mixture and a plasma sample by C18-SPE-CE-MS with a double-frit particle-packed microcartridge after this sample pretreatment (LODs by CE-MS and C18-SPE-CE-MS for standards were 50 ng/mL and 0.1 ng/mL, respectively [4,37]). As can be observed in Fig. 6-b, different compounds from the plasma matrix still were detected after the sample pretreatment due to the limited selectivity of the C18 sorbent, and MS detection using an accurate mass and high resolution TOF mass spectrometer was necessary to reliably identify the different neuropeptides. This sample pretreatment has been also applied to analyze other low molecular mass

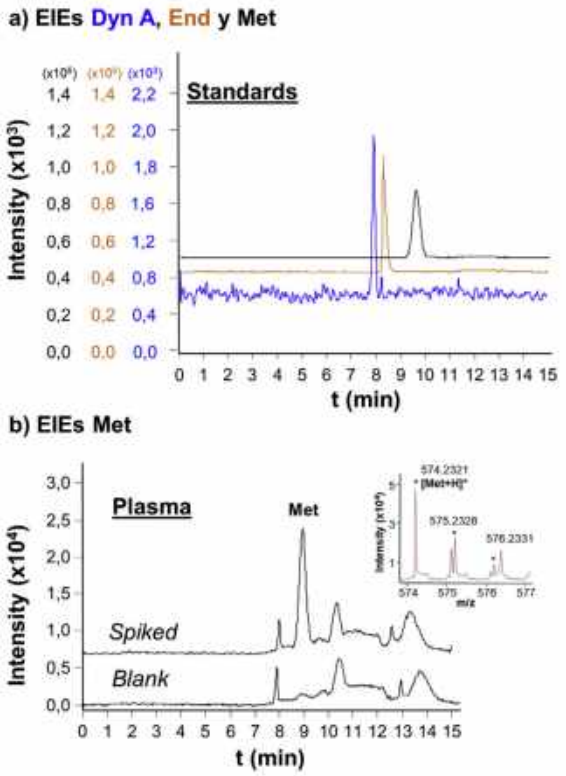

Fig. 6. a) Extracted Ion Electropherograms (EIEs) of three neuropeptides by C18-SPE-CE-MS using a double-frit particle packed microcartridge for a standard mixture containing 1 ng/mL of Dynorphin A (1–7) (DynA), Endomorphin 1 (End1) and Met-enkephalin (Met) and b) EIE and zoomed mass spectrum of Met for a plasma sample spiked with 1 ng/mL of each neuropeptide. Plasma samples were precipitated with acetonitrile followed by centrifugal filtration (10,000 M_r cut-off) before the analyses. For experimental methods see Refs. [4,37].

compounds as plasma metabolites in untargeted metabolomics studies by C18-SPE-CE-MS of samples from mice genetically modified to develop Huntington's disease (HD), an inherited neurodegenerative disorder [133].

In general, a certain type of sample pretreatment is even necessary when sorbents that present higher extraction selectivity are applied for the analysis of complex biological samples, such as when small molecules, peptides, proteins or microRNAs are analyzed in biological fluids using sorbents such as immobilized metals [52], SiC [53], antibodies [50,60,110] or antibody fragments [61,62]. Fig. 7 shows the extracted ion electropherograms (EIEs) and the total ion electropherograms (TIEs) obtained by IA-SPE-CE-MS and C18-SPE-CE-MS for two plasma samples containing two neuropeptides after the sample pretreatment explained above using a sorbent with a specific Fab antibody fragment and a double-frit particle-packed microcartridge. As can be observed in the EIEs of Fig. 7-a both neuropeptides were selectively detected, and no interferences were observed in the TIEs of Fig. 7-b ii. In contrast, many matrix compounds were still present, retained and detected by C18-SPE-CE-MS (Fig. 7-b i). Improving sorbent selectivity allows targeting specifically a certain compound and obtaining interference-free electropherograms, which are extremely helpful even with the most selective detectors (e.g. MS). However, there is always a remaining analyte-sample matrix interaction and non-specific retention to the affinity ligand or the solid support that, with the small amount of sorbent in the microcartridges, precludes in most cases direct or dilute-and-shoot analyses of the most complex biological fluids (e.g. serum or plasma, and in less extent urine or cerebrospinal fluid), complex environmental samples, beverages and foodstuff. Fig. 8 shows two examples of urine and beverage analysis with minimum sample pretreatment. As can be observed in the UV electropherograms of Fig. 8-a, F. J. Lara et al. were able to analyze by SPE-CE-UV triazine herbicides at 10 μg/mL in spiked urine samples using a fritless microcartridge packed with MIP particles. In this case, it was necessary to acidify urine until pH 1 with HCl, instead of the optimized pH 7 with the standards (75 μM H_3PO_4 adjusted to pH 7 with 1 M NaOH) [70]. In Fig. 8-b are shown the LIF electropherograms obtained by A. Marechal et al. who detected ochratoxin A at 0.5 ng/mL in white wine samples with an aptamer silica-based monolithic microcartridge, after diluting twice the sample with binding buffer (Tris 10 mM, NaCl 120 mM, $CaCl_2$ 20 mM, KCl 5 mM, pH 8.5) and readjusting pH to 9 [101]. As pointed out above for monoliths, improving extraction capacity and decreasing non-specific retention are again crucial to enhance the performance of these high selective sorbents in SPE-CE. Another difficulty of these sorbents, compared to the

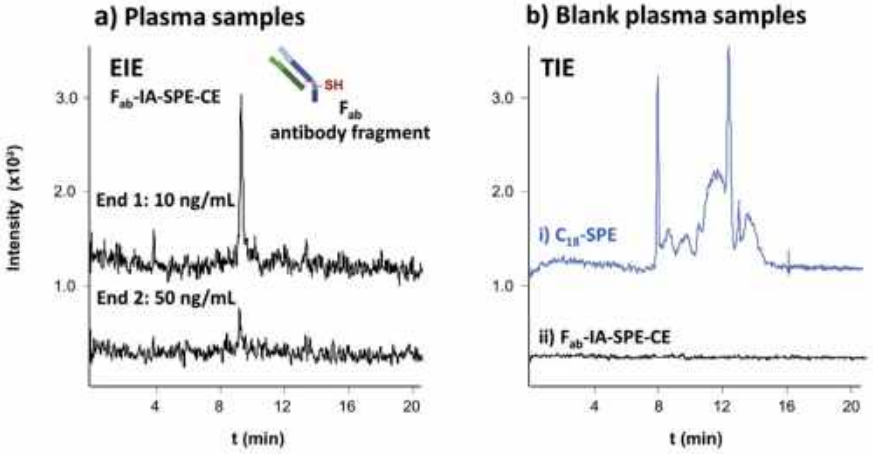

Fig. 7. a) Extracted ion electropherograms (EIEs) of two neuropeptides by Fab-IA-SPE-CE-MS using a double-frit particle packed microcartridge for a plasma sample spiked with 10 and 50 ng/mL of Endomorphin 1 (End1) and Endomorphin 2 (End2) and b) Total ion electropherograms (TIEs) for a blank plasma sample by i) C18-SPE-CE-MS and ii) F_{ab}-IA-SPE-CE-MS. Plasma samples were precipitated with acetonitrile followed by centrifugal filtration (10,000 M_r cut-off) before the analyses. For experimental methods see Refs. [4,61].

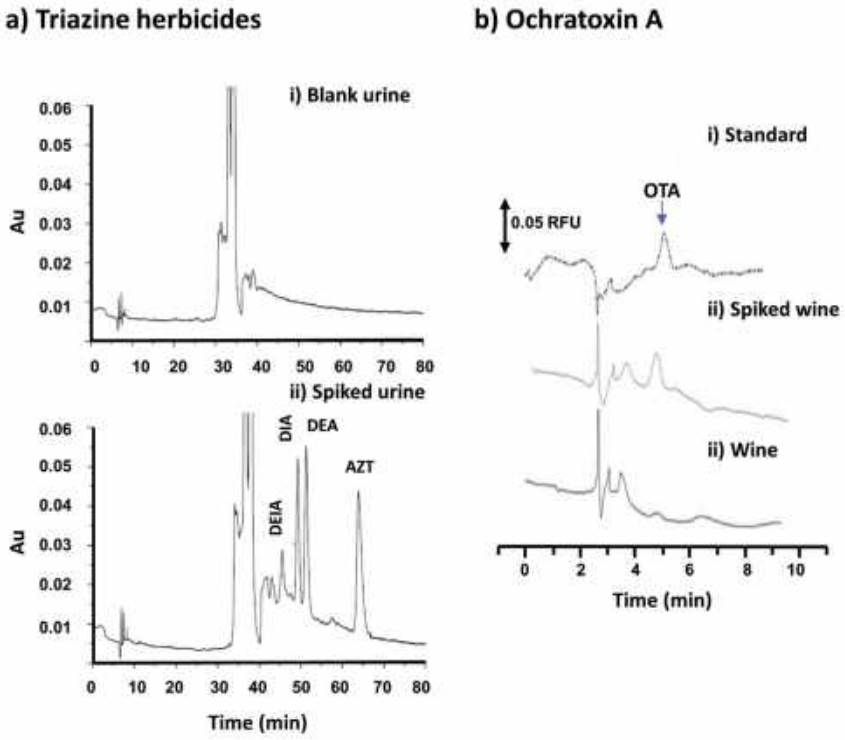

Fig. 8. a) UV electropherograms for the analysis of triazine herbizides (ATZ, atrazine; DEA, desethylatrazine; DIA, desisopropylatrazine; DEIA, desethyldesisopropylatrazine) by MIP-SPE-CE-UV using a fritless particle packed microcartridge. i) Blank urine sample and ii) urine sample spiked with 10 μg/mL of each compound. The pH of the urine samples was adjusted to 1 with HCl [70]. b) LIF electropherograms for the analysis of ochratoxin A (OTA) by aptamer-SPE-CE-LIF using an aptamer silica-based monolithic microcartridge. i) 0.5 ng/mL standard solution of OTA, ii) white wine sample spiked with 0.5 ng/mL of OTA and iii) blank white wine sample. The wine samples were diluted twice with binding buffer (Tris 10 mM, NaCl 120 mM, $CaCl_2$ 20 mM, KCl 5 mM, pH 8.5) and pH was readjusted to 9 [101]. Reproduced with permission.

conventional chromatographic sorbents, and despite the advancements made in the last years, is the limited commercial availability of activated supports or specific affinity ligands to prepare these sorbents. Therefore, nowadays, the number of applications described using high selective sorbents in SPE-CE is markedly lower than with conventional chromatographic sorbents, and the number decreases dramatically considering SPE-CE-MS. In the last case, this is because SPE-CE-MS faces the additional difficulty of making compatible the requirements of the extraction, separation and detection. Thus, for example, as we introduced before, there is only a publication demonstrating the use of an aptamer-based sorbent [101] and another showing a lectin-based sorbent [25] in SPE-CE-LIF and -UV or very few with IA [50,60–62,110,123], metal affinity [52] or MIP [71] in SPE-CE-MS. The use of high selective sorbents in SPE-CE-MS is one the most exciting fields to investigate and expand the applicability and impact of SPE-CE in the coming years.

3. Conclusions and perspectives

This review critically examines the different designs and materials applied to prepare in-line SPE-CE microcartridges since the pioneering studies of the early nineties. It is focused on unidimensional SPE-CE with capillaries because of simplicity, as no valves are required to control the fluid flow through the modified capillaries. This configuration is the best test bed at present for the future development of SPE-CE with microfluidic set-ups containing staggered microcartridges in series, which will allow routinely high-throughput multidimensional separations.

Nowadays, there are several well described microcartridge designs with frits and fritless for unidimensional SPE-CE with capillaries. Double-frit particle packed microcartridges have the potential to allow a greater active surface area for the extraction using tight packings of smaller porous sorbent particles. However, frit construction requires certain technical know-how to avoid flow restriction or sorbent degradation. The basic fritless microcartridge design which consists in packing sorbent particles with a slightly larger size than the inner diameter of the separation capillary smartly overcomes this issue and it is a straightforward way to construct the modified capillaries from commercially available sorbent particles. However, "plug-and-play" fritless microcartridges are probably the best allies to expand the applicability of SPE-CE. Specially (fully-filled) monolithic microcartridges are the best alternative to prepare such fritless microcartridges, but progress must be made improving extraction capacity and decreasing non-specific binding for the minute amount of monolithic sorbent used in SPE-CE. Keeping in mind this fact, the development of highly selective affinity sorbents, specially based on IA and aptamers, are another field to investigate in the coming years, with emphasis on using on-line MS detection and the combination of on-line electrophoretic preconcentration to further enhance detection sensitivity. SPE-CE-MS with highly selective affinity sorbents combines the specificity of the extraction, the resolving power and speed of the separation and the selectivity and sensitivity of the detection. Therefore, provides a promising tool to reliably and accurately address the analysis of trace components of complex samples, preventing false positives of currently applied analytical techniques that lack separation and molecular mass confirmation (e.g. ELISA).

Declarations of interest

None.

Conflict of interest

The authors have declared no conflict of interest.

Acknowledgements

This study was supported by grants from the Spanish Ministry of Economy and Competitiveness (CTQ2014-56777-R and RTI2018-097411) and the Cathedra UB Rector Francisco Buscarons Ubeda (Forensic Chemistry and Chemical Engineering).

References

[1] M.C. Breadmore, W. Grochocki, U. Kalsoom, M.N. Alves, S.C. Phung, M.T. Rokh, J.M. Cabot, A. Ghiasvand, F. Li, A.I. Shallan, A.S.A. Keyon, A.A. Alhusban, H.H. See, A. Wuethrich, M. Dawod, J.P. Quirino, Recent advances in enhancing the sensitivity of electrophoresis and electrochromatography in capillaries in microchips (2016–2018), Electrophoresis 40 (2019) 17–39, https://doi.org/10.1002/elps.201800384.

[2] A. Šlampová, Z. Malá, P. Gebauer, Recent progress of sample stacking in capillary electrophoresis (2016–2018), Electrophoresis 40 (2019) 40–54, https://doi.org/10.1002/elps.201800261.

[3] Z. Malá, P. Gebauer, Recent progress in analytical capillary isotachophoresis, Electrophoresis 40 (2019) 55–64, https://doi.org/10.1002/elps.201800239.

[4] F. Benavente, S. Medina-Casanellas, E. Giménez, V. Sanz-Nebot, On-line solid-phase extraction capillary electrophoresis mass spectrometry for preconcentration and clean-up of peptides and proteins, in: N.T. Tran, M. Taverna (Eds.), Capill. Electrophor. Proteins Pept. Methods Protoc. Methods Mol. Biol., Springer Science+Business Media, New York, NY, 2016, pp. 67–84, https://doi.org/10.1007/978-1-4939-4014-1_6.

[5] R. Ramautar, G.W. Somsen, G.J. de Jong, Developments in coupled solid-phase extraction-capillary electrophoresis 2013-2015, Electrophoresis 37 (2016) 35–44, https://doi.org/10.1002/elps.201500401.

[6] N.A. Guzman, D.E. Guzman, An emerging micro-scale immuno-analytical diagnostic tool to see the unseen. Holding promise for precision medicine and P4 medicine, J. Chromatogr. B Anal. Technol. Biomed. Life Sci. 1021 (2016) 14–29, https://doi.org/10.1016/j.jchromb.2015.11.026.

[7] A. Wuethrich, J.P. Quirino, Derivatisation for separation and detection in capillary electrophoresis (2015-2017), Electrophoresis 39 (2018) 82–96, https://doi.org/10.1002/elps.201700252.

[8] A. Stolz, K. Jooß, O. Höcker, J. Römer, J. Schlecht, C. Neusüß, Recent advances in capillary electrophoresis-mass spectrometry: instrumentation, methodology and applications, Electrophoresis (2018) 1–34, https://doi.org/10.1002/elps.201800331.

[9] L. Pont, F. Benavente, J. Barbosa, V. Sanz-Nebot, An update for human blood plasma pretreatment for optimized recovery of low-molecular-mass peptides prior to CE-MS and SPE-CE-MS, J. Sep. Sci. 36 (2013) 3896–3902, https://doi.org/10.1002/jssc.201300838.

[10] N. Drouin, S. Rudaz, J. Schappler, Sample preparation for polar metabolites in bioanalysis, Analyst 143 (2018) 16–20, https://doi.org/10.1039/c7an01333g.

[11] K.D. Clark, C. Zhang, J.L. Anderson, Sample preparation for bioanalytical and pharmaceutical analysis, Anal. Chem. 88 (2016) 11262–11270, https://doi.org/10.1021/acs.analchem.6b02935.

[12] V. Adam, M. Vaculovicova, Nanomaterials for sample pretreatment prior to capillary electrophoretic analysis, Analyst 142 (2017) 849–857, https://doi.org/10.1039/c6an02608g.

[13] Z. Malá, P. Gebauer, P. Boček, Analytical capillary isotachophoresis after 50 years of development: recent progress 2014-2016, Electrophoresis 38 (2017) 9–19, https://doi.org/10.1002/elps.201600289.

[14] V. Kašička, Z. Prusík, Isotachophoretic electrodesorption of proteins from an affinity adsorbent on a microscale, J. Chromatogr. B Biomed. Sci. Appl. 273 (1983) 117–128, https://doi.org/10.1016/S0378-4347(00)80928-7.

[15] M.C. Breadmore, A. Wuethrich, F. Li, S.C. Phung, U. Kalsoom, J.M. Cabot, T. Masoomeh, A.I. Shallan, A.S. Abdul Keyon, H.H. See, M. Dawod, J.P. Quirino, Recent advances in enhancing the sensitivity of electrophoresis and electrochromatography in capillaries and microchips (2014-2016), Electrophoresis 38 (2017) 33–59, https://doi.org/10.1002/elps.201600331.

[16] J. Veraart, H. Lingeman, U.A.T. Brinkman, Coupling of biological sample handling and capillary electrophoresis, J. Chromatogr., A 856 (1999) 483–514, https://doi.org/10.1016/S0021-9673(99)00588-9.

[17] P. Puig, F. Borrull, M. Calull, C. Aguilar, Recent advances in coupling solid-phase extraction and capillary electrophoresis (SPE-CE), TrAC Trends Anal. Chem. (Reference Ed.) 26 (2007) 664–678, https://doi.org/10.1016/j.trac.2007.05.010.

[18] R. Ramautar, G.W. Somsen, G.J. de Jong, Developments in coupled solid-phase extraction-capillary electrophoresis 2011-2013, Electrophoresis 35 (2014) 128–137, https://doi.org/10.1002/elps.201300335.

[19] R. Ramautar, G.W. Somsen, G.J. de Jong, Developments in coupled solid-phase extraction-capillary electrophoresis 2009-2011, Electrophoresis 33 (2012) 243–250, https://doi.org/10.1002/elps.201500401.

[20] R. Ramautar, G.W. Somsen, G.J. De Jong, Recent developments in coupled SPE-CE, Electrophoresis 31 (2010) 44–54, https://doi.org/10.1002/elps.200900510.

[21] F.W.A. Tempels, W.J.M. Underberg, G.W. Somsen, G.J. de Jong, Design and applications of coupled SPE-CE, Electrophoresis 29 (2008) 108–128, https://doi.org/10.1002/elps.200700149.

[22] N.A. Guzman, M.A. Trebilcock, J.P. Advis, The use of a concentration step to collect urinary components separated by capillary electrophoresis and further characterization of collected analytes by mass spectrometry, J. Liq. Chromatogr. 14 (1991) 997–1015.

[23] N.A. Guzman, Automated Capillary Electrophoresis Apparatus, 1993. US5202010.

[24] N.A. Guzman, Biomedical applications of on-line preconcentration-capillary electrophoresis using an analyte concentrator: investigation of design options, J. Liq. Chromatogr. 18 (1995) 3751–3768, https://doi.org/10.1080/10826079508014623.

[25] N.A. Guzman, S.S. Park, D. Schaufelberger, L. Hernandez, X. Paez, P. Rada, A.J. Tomlinson, S. Naylor, New approaches in clinical chemistry: on-line analyte concentration and microreaction capillary electrophoresis for the determination of drugs, metabolic intermediates, and biopolymers in biological fluids, J. Chromatogr. B Biomed. Appl. 697 (1997) 37–66, https://doi.org/10.1016/S0378-4347(97)00275-2.

[26] N.A. Guzman, R.J. Stubbs, The use of selective adsorbents in capillary electrophoresis-mass spectrometry for analyte preconcentration and microreactions: a powerful three-dimensional tool for multiple chemical and biological applications, Electrophoresis 22 (2001) 3602–3628, https://doi.org/10.1002/1522-2683(200109)22:17<3602::AID-ELPS3602>3.0.CO;2-X.

[27] N.A. Guzman, Multi-dimensional electrophoresis apparatus, U. S. Jpn. Outlook 6406604 (2002).

[28] N.A. Guzman, Improved solid-phase microextraction device for use in on-line immunoaffinity capillary electrophoresis, Electrophoresis 24 (2003) 3718–3727, https://doi.org/10.1002/elps.200305647.

[29] N.A. Guzman, T.M. Phillips, Immunoaffinity CE for proteomics studies, Anal. Chem. 77 (2005) 60A–67A, https://doi.org/10.1021/ac053325c.

[30] F. Benavente, M.C. Vescina, E. Hernández, V. Sanz-Nebot, J. Barbosa, N.A. Guzman, Lowering the concentration limits of detection by on-line solid-phase extraction-capillary electrophoresis-electrospray mass spectrometry, J. Chromatogr., A 1140 (2007) 205–212, https://doi.org/10.1016/j.chroma.2006.11.092.

[31] N.A. Guzman, T. Blanc, T.M. Phillips, Immunoaffinity capillary electrophoresis as a powerful strategy for the quantification of low-abundance biomarkers, drugs, and metabolites in biological matrices, Electrophoresis 29 (2008) 3259–3278, https://doi.org/10.1002/elps.200800058.

[32] N.A. Guzman, T.M. Phillips, Immunoaffinity capillary electrophoresis: a new versatile tool for determining protein biomarkers in inflammatory processes, Electrophoresis 32 (2011) 1565–1578, https://doi.org/10.1002/elps.201000700.

[33] A.J. Tomlinson, S. Naylor, Systematic development of on-line membrane preconcentration-capillary electrophoresis-mass spectrometry for the analysis of peptide mixtures, J. Capill. Electrophor. 2 (1995) 225–233.

[34] A.J. Tomlinson, L.M. Benson, N.A. Guzman, S. Naylor, Preconcentration and microreaction technology on-line with capillary electrophoresis, J. Chromatogr., A 744 (1996) 3–15, https://doi.org/10.1016/0021-9673(96)00332-9.

[35] Y. Qing, A.J. Tomlinson, S. Naylor, Membrane preconcentration CE, Anal. Chem. News Featur. 71 (1999) 183A–189A, https://doi.org/10.1021/ac990246q.

[36] J.C.M. Waterval, G. Hommels, J. Teeuwsen, A. Bult, H. Lingeman, W.J.M. Underberg, Quantitative analysis of pharmaceutically active peptides using on-capillary analyte preconcentration transient isotachophoresis, Electrophoresis 21 (2000) 2851–2858, https://doi.org/10.1002/1522-2683(20000801)21:14<2851::AID-ELPS2851>3.0.CO;2-Q.

[37] S. Medina-Casanellas, F. Benavente, J. Barbosa, V. Sanz-Nebot, Transient isotachophoresis in on-line solid phase extraction capillary electrophoresis time-of-flight-mass spectrometry for peptide analysis in human plasma, Electrophoresis 32 (2011) 1750–1759, https://doi.org/10.1002/elps.201100017.

[38] Y. Wang, B.R. Fonslow, C.C.L.L. Wong, A. Nakorchevsky, J.R. Yates, Improving the comprehensiveness and sensitivity of sheathless CE-MS/MS for proteomic analysis, Anal. Chem. 84 (2012) 8505–8513, https://doi.org/10.1021/ac301091m.

[39] Z. Zhang, L. Sun, G. Zhu, X. Yan, N.J. Dovichi, Integrated strong cation-exchange hybrid monolith coupled with capillary zone electrophoresis and simultaneous dynamic pH junction for large-volume proteomic analysis by mass spectrometry, Talanta 138 (2015) 117–122, https://doi.org/10.1016/j.talanta.2015.01.040.

[40] N.A. Guzman, Integrated Modular Unit Including an Analyte Concentrator Microreactor Device Connected to a Cartridge-Cassette, US2015/0093304A1, 2015.

[41] N.A. Guzman, Disease Detection System and Method, 2015. US9146234B2.

[42] S. Medina-Casanellas, Y.H. Tak, F. Benavente, V. Sanz-Nebot, J. Sastre Toraño, G.W. Somsen, G.J. de Jong, Evaluation of fritless solid-phase extraction

coupled on-line with capillary electrophoresis-mass spectrometry for the analysis of opioid peptides in cerebrospinal fluid, Electrophoresis 35 (2014) 2996–3002, https://doi.org/10.1002/elps.201400293.
[43] M.A. Strausbauch, S.J. Xu, J.E. Ferguson, M.E. Nunez, D. Machacek, G.M. Lawson, P.J. Wettstein, J.P. Landers, Concentration and separation of hypoglycemic drugs using solid-phase extraction-capillary electrophoresis, J. Chromatogr., A 717 (1995) 279–291, https://doi.org/10.1016/0021-9673(95)00743-6.
[44] P.W. Stege, J. Raba, G.A. Messina, Online immunoaffinity assay-CE using magnetic nanobeads for the determination of anti-Helicobacter pylori IgG in human serum, Electrophoresis 31 (2010) 3475–3481, https://doi.org/10.1002/elps.201000123.
[45] T. Baciu, F. Borrull, C. Neus, M. Calull, Capillary electrophoresis combined in-line with solid-phase extraction using magnetic particles as new adsorbents for the determination of drugs of abuse in human, Electrophoresis 37 (2016) 1232–1244, https://doi.org/10.1002/elps.201500515.
[46] F.J. Lara, A.M. García-Campaña, C. Neusüss, F. Alés-Barrero, Determination of sulfonamide residues in water samples by in-line solid-phase extraction-capillary electrophoresis, J. Chromatogr., A 1216 (2009) 3372–3379, https://doi.org/10.1016/j.chroma.2009.01.097.
[47] A.J. Tomlinson, L.M. Benson, W.D. Braddock, R.P. Oda, S. Naylor, On-line preconcentration-capillary electrophoresis-mass spectrometry (PC-CE-MS), J. High Resolut. Chromatogr. 17 (1994) 729–731, https://doi.org/10.1002/jhrc.1240171010.
[48] J. Cai, Z. El Rassi, Selective on-line preconcentration of proteins by tandem metal chelate capillaries-capillary zone electrophoresis, J. Liq. Chromatogr. 16 (1993) 2007–2024, https://doi.org/10.1080/10826079308019910.
[49] F. Benavente, E. Hernández, N.A. Guzman, V. Sanz-Nebot, J. Barbosa, Determination of human erythropoietin by on-line immunoaffinity capillary electrophoresis: a preliminary report, Anal. Bioanal. Chem. 387 (2007) 2633–2639, https://doi.org/10.1007/s00216-007-1119-0.
[50] S. Medina-Casanellas, F. Benavente, E. Giménez, J. Barbosa, V. Sanz-Nebot, On-line immunoaffinity solid-phase extraction capillary electrophoresis mass spectrometry for the analysis of large biomolecules: a preliminary report, Electrophoresis 35 (2014) 2130–2136, https://doi.org/10.1002/elps.201400119.
[51] M. Tascon, F. Benavente, V. Sanz-Nebot, L.G. Gagliardi, A high performance system to study the influence of temperature in on-line solid-phase extraction capillary electrophoresis, Anal. Chim. Acta 863 (2015) 78–85, https://doi.org/10.1016/j.aca.2014.12.053.
[52] L. Ortiz-Martin, F. Benavente, S. Medina-Casanellas, E. Giménez, V. Sanz-Nebot, Study of immobilized metal affinity chromatography sorbents for the analysis of peptides by on-line solid-phase extraction capillary electrophoresis-mass spectrometry, Electrophoresis 36 (2015) 962–970, https://doi.org/10.1002/elps.201400374.
[53] R. Pero-Gascon, V. Sanz-Nebot, M.V. Berezovski, F. Benavente, Analysis of circulating microRNAs and their post-transcriptional modifications in cancer serum by on-line solid-phase extraction-capillary electrophoresis-mass spectrometry, Anal. Chem. 90 (2018) 6618–6625, https://doi.org/10.1021/acs.analchem.8b00405.
[54] A.J.J. Debets, M. Mazereeuw, W.H. Voogt, D.J. van Iperen, H. Lingeman, K.P. Hupe, U.A.T. Brinkman, Switching valve with internal micro precolumn for on-line sample enrichment in capillary zone electrophoresis, J. Chromatogr., A 608 (1992) 151–158, https://doi.org/10.1016/0021-9673(92)87117-Q.
[55] L.H. Zhang, X.Z. Wu, Capillary electrophoresis with in-capillary solid-phase extraction sample cleanup, Anal. Chem. 79 (2007) 2562–2569, https://doi.org/10.1021/ac062159l.
[56] J.H. Beattie, R. Self, M.P. Richards, The use of solid phase concentrators for on-line preconcentration of metallothionein prior to isoform separation by capillary zone electrophoresis, Electrophoresis 16 (1995) 322–328, https://doi.org/10.1002/elps.1150160153.
[57] D. Figeys, A. Ducret, J.R. Yates III, R. Aebersold, Protein identification by solid phase microextraction—capillary zone electrophoresis—microelectrospray—tandem mass spectrometry, Nat. Biotechnol. 14 (1996) 1579–1583, https://doi.org/10.1038/nbt0898-773.
[58] E. Hernández, F. Benavente, V. Sanz-Nebot, J. Barbosa, Analysis of opioid peptides by on-line SPE-CE-ESI-MS, Electrophoresis 28 (2007) 3957–3965, https://doi.org/10.1002/elps.200700845.
[59] E. Hernández, F. Benavente, V. Sanz-Nebot, J. Barbosa, Evaluation of on-line solid phase extraction-capillary electrophoresis-electrospray-mass spectrometry for the analysis of neuropeptides in human plasma, Electrophoresis 29 (2008) 3366–3376, https://doi.org/10.1002/elps.200700872.
[60] S. Medina-Casanellas, F. Benavente, J. Barbosa, V. Sanz-Nebot, Preparation and evaluation of an immunoaffinity sorbent for the analysis of opioid peptides by on-line immunoaffinity solid-phase extraction capillary electrophoresis-mass spectrometry, Anal. Chim. Acta 717 (2012) 134–142.
[61] S. Medina-Casanellas, F. Benavente, J. Barbosa, V. Sanz-Nebot, Preparation and evaluation of an immunoaffinity sorbent with Fab' antibody fragments for the analysis of opioid peptides by on-line immunoaffinity solid-phase extraction capillary electrophoresis-mass spectrometry, Anal. Chim. Acta 789 (2013) 91–99.
[62] L. Pont, F. Benavente, J. Barbosa, V. Sanz-Nebot, On-line immunoaffinity solid-phase extraction capillary electrophoresis mass spectrometry using Fab'antibody fragments for the analysis of serum transthyretin, Talanta 170 (2017) 224–232, https://doi.org/10.1016/j.talanta.2017.03.104.
[63] J.Y. He, A. Shibukawa, M. Zeng, S. Amane, T. Sawada, T. Nakagawa, On-capillary sample preconcentration incorporated in chiral capillary electrophoresis, Anal. Sci. 12 (1996) 177–181, https://doi.org/10.2116/analsci.12.177.
[64] E. Giménez, F. Benavente, C. de Bolós, E. Nicolás, J. Barbosa, V. Sanz-Nebot, Analysis of recombinant human erythropoietin and novel erythropoiesis stimulating protein digests by immunoaffinity capillary electrophoresis-mass spectrometry, J. Chromatogr., A 1216 (2009) 2574–2582, https://doi.org/10.1016/j.chroma.2009.01.057.
[65] L. Saavedra, N. Maeso, A. Cifuentes, C. Barbas, Development of a frit-free SPE-based in-column preconcentration system for capillary electrophoresis, J. Pharm. Biomed. Anal. 44 (2007) 471–476, https://doi.org/10.1016/j.jpba.2006.12.031.
[66] F.J. Lara, A.M. García-Campaña, F. Alés-Barrero, J.M. Bosque-Sendra, In-line solid-phase extraction preconcentration in capillary electrophoresis-tandem mass spectrometry for the multiresidue detection of quinolones in meat by pressurized liquid extraction, Electrophoresis 29 (2008) 2117–2125, https://doi.org/10.1002/elps.200700666.
[67] I. Maijó, F. Borrull, M. Calull, C. Aguilar, An in-line SPE strategy to enhance sensitivity in CE for the determination of pharmaceutical compounds in river water samples, Electrophoresis 32 (2011) 2114–2122, https://doi.org/10.1002/elps.201100054.
[68] I. Botello, F. Borrull, M. Calull, C. Aguilar, G.W. Somsen, G.J. De Jong, In-line solid-phase extraction-capillary electrophoresis coupled with mass spectrometry for determination of drugs of abuse in human urine, Anal. Bioanal. Chem. 403 (2012) 777–784, https://doi.org/10.1007/s00216-012-5872-3.
[69] K. Jooß, J. Sommer, S.C. Bunz, C. Neusüß, In-line SPE-CE using a fritless bead string design-Application for the analysis of organic sulfonates including inline SPE-CE-MS for APTS-labeled glycans, Electrophoresis 35 (2014) 1236–1243, https://doi.org/10.1002/elps.201300388.
[70] F.J. Lara, F. Lynen, P. Sandra, A.M. García-Campaña, F. Alés-Barrero, Evaluation of a molecularly imprinted polymer as in-line concentrator in capillary electrophoresis, Electrophoresis 29 (2008) 3834–3841, https://doi.org/10.1002/elps.200700889.
[71] D. Moreno-González, F.J. Lara, L. Gámiz-Gracia, A.M. García-Campaña, Molecularly imprinted polymer as in-line concentrator in capillary electrophoresis coupled with mass spectrometry for the determination of quinolones in bovine milk samples, J. Chromatogr., A 1360 (2014) 1–8, https://doi.org/10.1016/j.chroma.2014.07.049.
[72] J. Li, P. Thibault, A. Martin, J.C. Richards, W.W. Wakarchuk, W. Van Der Wilp, Development of an on-line preconcentration method for the analysis of pathogenic lipopolysaccharides using capillary electrophoresis-electrospray mass spectrometry. Application to small colony isolates, J. Chromatogr., A 817 (1998) 325–336, https://doi.org/10.1016/S0021-9673(98)00341-0.
[73] G.M. Janini, M. Zhou, L.R. Yu, J. Blonder, M. Gignac, T.P. Conrads, H.J. Issaq, T.D. Veenstra, On-column sample enrichment for capillary electrophoresis sheathless electrospray ionization mass spectrometry: evaluation for peptide analysis and protein identification, Anal. Chem. 75 (2003) 5984–5993, https://doi.org/10.1021/ac0301548.
[74] M. Pelzing, C. Neusüß, Separation techniques hyphenated to electrospray-tandem mass spectrometry in proteomics: capillary electrophoresis versus nanoliquid chromatography, Electrophoresis 26 (2005) 2717–2728, https://doi.org/10.1002/elps.200410424.
[75] B. Yang, F. Zhang, H. Tian, Y. Guan, On-line preconcentration of protein in capillary electrophoresis with an end-column cellulose acetate-based porous membrane, J. Chromatogr., A 1117 (2006) 214–218, https://doi.org/10.1016/j.chroma.2006.03.105.
[76] X.Z. Wu, A. Hosaka, T. Hobo, An on-line electrophoretic concentration mmethod for capillary electrophoresis of proteins, Anal. Chem. 70 (1998) 2081–2084, https://doi.org/10.1021/ac9709110.
[77] C.W. Whang, J. Pawliszyn, Solid phase microextraction coupled to capillary electrophoresis, Anal. Commun. 35 (1998) 353–356, https://doi.org/10.1039/a806794e.
[78] Z. Liu, J. Pawliszyn, Coupling of solid-phase microextraction and capillary isoelectric focusing with laser-induced fluorescence whole column imaging detection for protein analysis, Anal. Chem. 77 (2005) 165–171, https://doi.org/10.1021/ac049229d.
[79] J. Cai, Z. El Rassi, On-line preconcentration of triazine herbicides with tandem octadecyl capillaries-capillary zone electrophoresis, J. Liq. Chromatogr. 15 (1992) 1179–1192, https://doi.org/10.1080/10826079208018857.
[80] K. Ensing, A. Paulus, Immobilization of antibodies as a versatile tool in hybridized capillary electrophoresis, J. Pharm. Biomed. Anal. 14 (1996) 305–315, https://doi.org/10.1016/0731-7085(95)01607-4.
[81] T.M. Phillips, J.J. Chmielinska, Immunoaffinity capillary electrophoretic analysis of cyclosporin in tears, Biomed. Chromatography 8 (1994) 242–246, https://doi.org/10.1002/bmc.1130080509.
[82] T.M. Phillips, B.F. Dickens, Analysis of recombinant cytokines in human body fluids by immunoaffinity capillary electrophoresis, Electrophoresis 19 (1998) 2991–2996, https://doi.org/10.1002/elps.1150191632.
[83] T.M. Phillips, Analysis of single-cell cultures by immunoaffinity capillary electrophoresis with laser-induced fluorescence detection, Luminescence 16 (2001) 145–152, https://doi.org/10.1002/bio.645.
[84] H. Kalish, T.M. Phillips, Analysis of neurotrophins in human serum by immunoaffinity capillary electrophoresis (ICE) following traumatic head

injury, J. Chromatogr. B Anal. Technol. Biomed. Life Sci. 878 (2010) 194–200, https://doi.org/10.1016/j.jchromb.2009.10.022.
[85] H. Wang, G. Knobel, W.B. Wilson, K. Calimag-Williams, A.D. Campiglia, Gold nanoparticles deposited capillaries for in-capillary microextraction capillary zone electrophoresis of monohydroxy-polycyclic aromatic hydrocarbons, Electrophoresis 32 (2011) 720–727, https://doi.org/10.1002/elps.201000516.
[86] X. Zhang, S. Xu, Y.I. Lee, S.A. Soper, LED-induced in-column molecular imprinting for solid phase extraction/capillary electrophoresis, Analyst 138 (2013) 2821–2824, https://doi.org/10.1039/c3an00257h.
[87] E. Ortiz-Villanueva, F. Benavente, E. Giménez, F. Yilmaz, V. Sanz-Nebot, Preparation and evaluation of open tubular C18-silica monolithic microcartridges for preconcentration of peptides by on-line solid phase extraction capillary electrophoresis, Anal. Chim. Acta 846 (2014) 51–59, https://doi.org/10.1016/j.aca.2014.06.046.
[88] N.E. Baryla, N.P. Toltl, On-line preconcentration in capillary electrophoresis using monolithic methacrylate polymers, Analyst 128 (2003) 1009–1012, https://doi.org/10.1039/b303701k.
[89] J.M. Armenta, B. Gu, P.H. Humble, C.D. Thulin, M.L. Lee, Design and evaluation of a coupled monolithic preconcentrator-capillary zone electrophoresis system for the extraction of immunoglobulin G from human serum, J. Chromatogr., A 1097 (2005) 171–178, https://doi.org/10.1016/j.chroma.2005.08.050.
[90] N.M. Vizioli, M.L. Rusell, M.L. Carbajal, C.N. Carducci, M. Grasselli, On-line affinity selection of histidine-containing peptides using a polymeric monolithic support for capillary electrophoresis, Electrophoresis 26 (2005) 2942–2948, https://doi.org/10.1002/elps.200410416.
[91] J.P. Hutchinson, P. Zakaria, A.R. Bowie, M. Macka, N. Avdalovic, P.R. Haddad, Latex-coated polymeric monolithic ion-exchange stationary phases. 1. Anion-exchange capillary electrochromatography and in-line sample preconcentration in capillary electrophoresis, Anal. Chem. 77 (2005) 407–416, https://doi.org/10.1021/ac048748d.
[92] J.P. Hutchinson, M. MacKa, N. Avdalovic, P.R. Haddad, On-line preconcentration of organic anions in capillary electrophoresis by solid-phase extraction using latex-coated monolithic stationary phases, J. Chromatogr., A 1106 (2006) 43–51, https://doi.org/10.1016/j.chroma.2005.08.032.
[93] F. Svec, Less common applications of monoliths: preconcentration and solid-phase extraction, J. Chromatogr. B Anal. Technol. Biomed. Life Sci. 841 (2006) 52–64, https://doi.org/10.1016/j.jchromb.2006.03.055.
[94] E. Rodríguez-Gonzalo, J. Domínguez-Álvarez, L. Ruano-Miguel, R. Carabias-Martínez, In-capillary preconcentration of pirimicarb and carbendazim with a monolithic polymeric sorbent prior to separation by CZE, Electrophoresis 29 (2008) 4066–4077, https://doi.org/10.1002/elps.200800277.
[95] R. Ramautar, C.K. Ratnayake, G.W. Somsen, G.J. de Jong, Capillary electrophoresis-mass spectrometry using an in-line sol-gel concentrator for the determination of methionine enkephalin in cerebrospinal fluid, Talanta 78 (2009) 638–642, https://doi.org/10.1016/j.talanta.2008.12.025.
[96] J.R.E. Thabano, M.C. Breadmore, J.P. Hutchinson, C. Johns, P.R. Haddad, Capillary electrophoresis of neurotransmitters using in-line solid-phase extraction and preconcentration using a methacrylate-based weak cation-exchange monolithic stationary phase and a pH step gradient, J. Chromatogr., A 1175 (2007) 117–126, https://doi.org/10.1016/j.chroma.2007.09.069.
[97] J.R.E. Thabano, M.C. Breadmore, J.P. Hutchinson, C. Johns, P.R. Haddad, Selective extraction and elution of weak bases by in-line solid-phase extraction capillary electrophoresis using a pH step gradient and a weak cation-exchange monolith, Analyst 133 (2008) 1380–1387, https://doi.org/10.1039/b804805c.
[98] J.R.E. Thabano, M.C. Breadmore, J.P. Hutchinson, C. Johns, P.R. Haddad, Silica nanoparticle-templated methacrylic acid monoliths for in-line solid-phase extraction-capillary electrophoresis of basic analytes, J. Chromatogr., A 1216 (2009) 4933–4940, https://doi.org/10.1016/j.chroma.2009.04.012.
[99] A. Feng, N.T. Tran, C. Chen, J. Hu, M. Taverna, P. Zhou, In-line coupling SPE and CE for DNA preconcentration and separation, Electrophoresis 32 (2011) 1623–1630, https://doi.org/10.1002/elps.201000484.
[100] Y. Wu, W. Zhang, Z. Chen, A poly (4-vinylpridine-co-ethylene glycol dimethacrylate) monolithic concentrator for in-line concentration-capillary electrophoresis analysis of phenols in water samples, Electrophoresis 33 (2012) 2911–2919, https://doi.org/10.1002/elps.201250004.
[101] A. Marechal, F. Jarrosson, J. Randon, V. Dugas, C. Demesmay, In-line coupling of an aptamer based miniaturized monolithic affinity preconcentration unit with capillary electrophoresis and laser induced fluorescence detection, J. Chromatogr., A 1406 (2015) 109–117, https://doi.org/10.1016/j.chroma.2015.05.073.
[102] Z. Zhang, X. Yan, L. Sun, G. Zhu, N.J. Dovichi, A detachable strong cation exchange monolith, integrated with capillary zone electrophoresis and coupled with pH gradient elution, produces improved sensitivity and numbers of peptide identifications during bottom-up analysis of complex proteomes, Anal. Chem. 87 (2015) 4572–4577, https://doi.org/10.1021/acs.analchem.5b00789.
[103] L.G. Rashkovetsky, Y.V. Lyubarskaya, F. Foret, D.E. Hughes, B.L. Karger, Automated microanalysis using magnetic beads with commercial capillary electrophoretic instrumentation, J. Chromatogr., A 781 (1997) 197–204, https://doi.org/10.1016/S0021-9673(97)00629-8.
[104] H.-X. Chen, J.-M. Busnel, A.-L. Gassner, G. Peltre, X.-X. Zhang, H.H. Girault, Capillary electrophoresis immunoassay using magnetic beads, Electrophoresis 29 (2008) 3414–3421, https://doi.org/10.1002/elps.200800106.
[105] Y.H. Tennico, V.T. Remcho, In-line extraction employing functionalized magnetic particles for capillary and microchip electrophoresis, Electrophoresis 31 (2010) 2548–2557, https://doi.org/10.1002/elps.201000256.
[106] N. Gasilova, A.-L. Gassner, H.H. Girault, Analysis of major milk whey proteins by immunoaffinity capillary electrophoresis coupled with MALDI-MS, Electrophoresis 33 (2012) 2390–2398, https://doi.org/10.1002/elps.201200079.
[107] N. Gasilova, H.H. Girault, Component-resolved diagnostic of cow's milk allergy by immunoaffinity capillary electrophoresis-matrix assisted laser desorption/ionization mass spectrometry, Anal. Chem. 86 (2014) 6337–6345, https://doi.org/10.1021/ac500525n.
[108] G. Morales-Cid, J.C. Diez-Masa, M. de Frutos, On-line immunoaffinity capillary electrophoresis based on magnetic beads for the determination of alpha-1 acid glycoprotein isoforms profile to facilitate its use as biomarker, Anal. Chim. Acta 773 (2013) 89–96, https://doi.org/10.1016/j.aca.2013.02.037.
[109] T. Baciu, F. Borrull, C. Aguilar, M. Calull, Sensitivity enhancement in capillary electrophoresis using magnetic particles as solid-phase extraction sorbents for the determination of drugs of abuse in urine, in: R.A. Musah (Ed.), Anal. Drugs Abus. Methods Mol. Biol., Springer Science+Business Media, New York, NY, 2018, pp. 89–96, https://doi.org/10.1007/978-1-4939-8579-1_8.
[110] R. Peró-Gascón, L. Pont, F. Benavente, J. Barbosa, V. Sanz-Nebot, Analysis of serum transthyretin by on-line immunoaffinity solid-phase extraction capillary electrophoresis mass spectrometry using magnetic beads, Electrophoresis 37 (2016) 1220–1231, https://doi.org/10.1002/elps.201500495.
[111] S. Medina-Casanellas, E. Domínguez-Vega, F. Benavente, V. Sanz-Nebot, G.W. Somsen, G.J. de Jong, Low-picomolar analysis of peptides by on-line coupling of fritless solid-phase extraction to sheathless capillary electrophoresis-mass spectrometry, J. Chromatogr., A 1328 (2014) 1–6, https://doi.org/10.1016/j.chroma.2013.12.080.
[112] P. Viberg, S. Nilsson, K. Skog, In-capillary micro solid-phase extraction and capillary electrophoresis separation of heterocyclic aromatic amines with nanospray mass spectrometric detection, Anal. Bioanal. Chem. 378 (2004) 1729–1734, https://doi.org/10.1007/s00216-003-2480-2.
[113] W. Nashabeh, Z. El Rassi, Enzymophoresis of nucleic acids by tandem capillary enzyme reactor-capillary zone electrophoresis, J. Chromatogr., A 596 (1992) 251–264, https://doi.org/10.1016/0021-9673(92)85014-K.
[114] L.N. Amankwa, W.G. Kuhr, Trypsin-modified fused-silica capillary microreactor for peptide mapping by capillary zone electrophoresis, Anal. Chem. 64 (1992) 1610–1613, https://doi.org/10.1021/ac00038a019.
[115] H. Kalish, T.M. Phillips, Assessment of chemokine profiles in human skin biopsies by an immunoaffinity capillary electrophoresis chip, Methods 56 (2012) 198–203, https://doi.org/10.1016/j.ymeth.2011.12.003.
[116] T.M. Phillips, E. Wellner, Detection of cerebral spinal fluid-associated chemokines in birth traumatized premature babies by chip-based immunoaffinity CE, Electrophoresis 34 (2013) 1530–1538, https://doi.org/10.1002/elps.201200634.
[117] Y.T. Chen, A.G. Kolhatkar, O. Zenasni, S. Xu, T.R. Lee, Biosensing using magnetic particle detection techniques, Sensors 17 (2017) 2300, https://doi.org/10.3390/s17102300.
[118] J. Kudr, Y. Haddad, L. Richtera, Z. Heger, M. Cernak, V. Adam, O. Zitka, Magnetic nanoparticles: from design and synthesis to real world applications, Nanomaterials 7 (2017) 243, https://doi.org/10.3390/nano7090243.
[119] L. Gutierrez, L. De la Cueva, M. Moros, E. Mazario, S. De Bernardo, J.M. De la Fuente, M.P. Morales, G. Salas, Aggregation effects on the magnetic properties of iron oxide colloids, Nanotechnology 30 (2019) 112001, https://doi.org/10.1088/1361-6528/aafbf.
[120] R.L. Henken, R. Chantiwas, S.D. Gilman, Influence of immobilized biomolecules on magnetic bead plug formation and retention in capillary electrophoresis, Electrophoresis 33 (2012) 827–833, https://doi.org/10.1002/elps.201100353.
[121] Y. Moliner-Martínez, H. Prima-Garcia, A. Ribera, E. Coronado, P. Campíns-Falcó, Magnetic in-tube solid phase microextraction, Anal. Chem. 84 (2012) 7233–7240, https://doi.org/10.1021/ac301660k.
[122] J. Pawliszyn, Sample preparation: quo vadis? Anal. Chem. 75 (2003) 2543–2558, https://doi.org/10.1021/ac034094h.
[123] N.A. Guzman, Determination of immunoreactive gonadotropin-releasing hormone in serum and urine by on-line immunoaffinity capillary electrophoresis coupled to mass spectrometry, J. Chromatogr. B Biomed. Sci. Appl. 749 (2000) 197–213, https://doi.org/10.1016/S0378-4347(00)00410-2.
[124] F. Benavente, S. Medina-Casanellas, J. Barbosa, V. Sanz-Nebot, Investigation of commercial sorbents for the analysis of opioid peptides in human plasma by on-line SPE-CE, J. Sep. Sci. 33 (2010) 1294–1304, https://doi.org/10.1002/jssc.200900669.
[125] P. Puig, F. Borrull, M. Calull, F. Benavente, V. Sanz-Nebot, J. Barbosa, C. Aguilar, Improving the sensitivity of the determination of ceftiofur by capillary electrophoresis in environmental water samples: in-line solid phase extraction and sample stacking techniques, Anal. Chim. Acta 587 (2007), https://doi.org/10.1016/j.aca.2007.01.043.
[126] A. De Rossi, C. Desiderio, High sensitivity analysis of oxprenolol in urine by capillary electrophoresis with C18 packed on-line preconcentrator, J. Chromatogr. B Anal. Technol. Biomed. Life Sci. 839 (2006) 6–11, https://doi.org/10.1016/j.jchromb.2005.11.046.
[127] A. Macià, F. Borrull, M. Calull, F. Benavente, E. Hernández, V. Sanz-Nebot, J. Barbosa, C. Aguilar, Sensitivity enhancement for the analysis of naproxen in tap water by solid-phase extraction coupled in-line to capillary electrophoresis, J. Sep. Sci. 31 (2008) 872–880, https://doi.org/10.1002/jssc.200700593.
[128] T. Baciu, F. Borrull, M. Calull, C. Aguilar, Enantioselective determination of

cathinone derivatives in human hair by capillary electrophoresis combined in-line with solid-phase extraction, Electrophoresis 37 (2016) 2352–2362, https://doi.org/10.1002/elps.201600149.
[129] T. Baciu, F. Borrull, C. Aguilar, M. Calull, Findings in the hair of drug abusers using pressurized liquid extraction and solid-phase extraction coupled in-line with capillary electrophoresis, J. Pharm. Biomed. Anal. 131 (2016) 420–428, https://doi.org/10.1016/j.jpba.2016.09.017.
[130] S. Almeda, L. Arce, F. Benavente, V. Sanz-Nebot, J. Barbosa, M. Valcárcel, Comparison of off- and in-line solid-phase extraction for enhancing sensitivity in capillary electrophoresis using ochratoxin as a model compound, Anal. Bioanal. Chem. 394 (2009), https://doi.org/10.1007/s00216-009-2696-x.
[131] M. Tascon, L.G. Gagliardi, F. Benavente, Parts-per-trillion detection of harmala alkaloids in Undaria pinnatifida algae by on-line solid phase extraction capillary electrophoresis mass spectrometry, Anal. Chim. Acta 954 (2017) 60–67, https://doi.org/10.1016/j.aca.2016.12.012.
[132] N. Vizioli, R. Gil, L.D. Martínez, M.F. Silva, On-line solid phase extraction CZE for the simultaneous determination of lanthanum and gadolinium at picogram per liter levels, Electrophoresis 30 (2009) 2681–2687, https://doi.org/10.1002/elps.200800819.
[133] L. Pont, F. Benavente, J. Jaumot, R. Tauler, J. Alberch, S. Ginés, J. Barbosa, V. Sanz-Nebot, Metabolic profiling for the identification of Huntington biomarkers by on-line solid-phase extraction capillary electrophoresis mass spectrometry combined with advanced data analysis tools, Electrophoresis 37 (2016) 795–808, https://doi.org/10.1002/elps.201500378.

Laura Pont Dr. Laura Pont received her M.Sc. in Chemistry and Ph.D. in Analytical Chemistry in 2013 and 2017 at the University of Barcelona (UB). She is currently an Assistant Professor at the Department of Chemical Engineering and Analytical Chemistry and member of the Nutrition and Food Safety Research Institute of the UB (INSA-UB). She has also done doctoral and postdoctoral research at the Leiden University Medical Center (2016, Leiden, The Netherlands) and the Innsbruck Medical University (2018, Innsbruck, Austria). Her research is mainly focused on the analysis of peptides, proteins and glycoproteins in biological fluids.

Roger Pero-Gascon Roger Pero-Gascon received his M.Sc. in Analytical Chemistry in 2015 at the University of Barcelona (UB). He is currently a PhD student with an FPU 2015 fellowship (Ayudas para la formación de profesorado universitario) of the Ministry of Education, Culture and Sport (Spain) in the Department of Chemical Engineering and Analytical Chemistry of the UB. His research focuses on bioanalytical chemistry and mass spectrometry, specifically, in the development of analytical methodologies for the purification, preconcentration, separation, quantitation and characterization of biomarkers of different diseases or biological processes by on-line solid-phase extraction capillary electrophoresis-mass spectrometry (SPE-CE-MS).

Estela Gimenez Dr. Estela Giménez received her B.Sc. in Chemistry from the University of Barcelona (UB) in 2003. After obtaining her Ph.D from the Department of Analytical Chemistry of the UB in 2008, she did several postdoctoral stays at the University of Vienna (Austria), Hospital del Mar Medical Research Institute and the Institute for Research in Biomedicine (IRB Barcelona). She is currently an Associate Professor in the Department of Chemical Engineering and Analytical Chemistry of the UB. Her research interests include glycoproteomics and analysis of protein biomarkers by mass spectrometry.

Victoria Sanz-Nebot Dr. Victoria Sanz Nebot is an Associate Professor in the Bioanalysis group of the Department of Chemical Engineering and Analytical Chemistry of the University of Barcelona (UB). She is also member of the Nutrition and Food Safety Research Institute of the University of Barcelona (INSA-UB). She received her Ph.D in Chemistry in 1992 and she was a postdoctoral researcher at the French National Council for Scientific Research (CNRS) in Lyon. Her main research interest is the development of LC-MS and CE-MS methods mainly focused on biomedicine, biopharmaceuticals and food analysis.

Fernando Benavente Dr. Fernando Benavente received his PhD in Analytical Chemistry in 2003 at the UB. He is currently an Associate Professor in the Bioanalysis group of the Department of Chemical Engineering and Analytical Chemistry of the UB and a member of the INSA-UB. He has also been a researcher at the RW Johnson Pharmaceutical Research Institute (2000 and 2007, Raritan, USA), the National University of Rosario (2004, Rosario, Argentina), the University of Leiden (2005, Leiden, The Netherlands) and the University of Ottawa (2016, Ottawa, Canada). His research is mainly focused on solving complex analytical problems related to biomedicine, biopharmaceuticals, food industry and forensic sciences through the combination of innovative sample pretreatments, high performance separation techniques coupled to mass spectrometry and chemometrics tools of multivariate data analysis.

1220 *Electrophoresis* 2016, *37*, 1220–1231

Roger Peró-Gascón
Laura Pont
Fernando Benavente
José Barbosa
Victoria Sanz-Nebot

Department of Analytical Chemistry, University of Barcelona, Barcelona, Spain

Received October 31, 2015
Revised January 12, 2016
Accepted January 21, 2016

Research Article

Analysis of serum transthyretin by on-line immunoaffinity solid-phase extraction capillary electrophoresis mass spectrometry using magnetic beads

In this paper, an on-line immunoaffinity solid-phase extraction capillary electrophoresis mass spectrometry (IA-SPE-CE-MS) method using magnetic beads (MBs) is described for the analysis of serum transthyretin (TTR), which is a protein related to different types of amyloidosis. First, purification of TTR from serum was investigated by off-line immunoprecipitation and CE-MS. The suitability of three Protein A (ProA) MBs (Protein A Ultrarapid Agarose™ (UAPA), Dynabeads® Protein A (DyPA) and SiMAG-Protein A (SiPA) and AffiAmino Ultrarapid Agarose™ (UAAF) MBs to prepare an IA sorbent with a polyclonal antibody (Ab) against TTR, was studied. In all cases, results were repeatable and it was possible the identification and the quantitation of the relative abundance of the six most abundant TTR proteoforms. Although recoveries were the best with UAPA MBs, UAAF MBs were preferred for on-line immunopurification because Ab was not eluted from the MBs. Under the optimized conditions with standards in IA-SPE-CE-MS, microcartridge lifetime (>20 analyses/day) and repeatability (2.9 and 4.3% RSD for migration times and peak areas) were good, the method was linear between 5 and 25 μg/mL and LOD was around 1 μg/mL (25 times lower than by CE-MS, ≈25 μg/mL). A simple off-line sample pretreatment based on precipitation of the most abundant proteins with 5% (v/v) of phenol was necessary to clean-up serum samples. The potential of the on-line method to screen for familial amyloidotic polyneuropathy type I (FAP-I), which is the most common hereditary systemic amyloidosis, was demonstrated analysing serum samples from healthy controls and FAP-I patients.

Keywords:
Capillary electrophoresis / Magnetic beads / Mass spectrometry / On-line immunopurification / Transthyretin
DOI 10.1002/elps.201500495

1 Introduction

Capillary electrophoresis mass spectrometry (CE-MS) is nowadays a mature technique with many interesting application areas, especially those that require the highly efficient separation and characterization of biomolecules, including peptides, protein isoforms, glycoforms, glycopeptides, protein–protein or drug–protein complexes [1–7]. However, the low concentration sensitivity for most analytes is very often a limitation that hinders a more widespread application [8–12]. The use of more selective and sensitive mass spectrometers is often not enough to decrease the LOD. Therefore, CE-MS has been often combined with different electrophoretic and chromatographic techniques for the on-line preconcentration of the target analytes after the injection of a large volume of sample, such as sample stacking, isotachophoresis or on-line solid phase extraction (SPE-CE) [10–14].

In SPE-CE, a microcartridge with an appropriate sorbent is inserted near the inlet of the separation capillary to preconcentrate and clean up the target analytes from a large volume of sample. As extraction occurs immediately before the electrophoretic separation without human handling, many pioneering authors in the field referred the coupling as "on-line" since the late 80s [8, 9, 15]. However, other authors have preferred the term "in-line" because the microcartridge is fully integrated with the separation capillary [10–12]. Both terms

Correspondence: Fernando Benavente, PhD, Department of Analytical Chemistry, University of Barcelona, Barcelona, Spain
E-mail: fbenavente@ub.edu
Fax: (+34) 934021233

Abbreviations: **Ab**, antibody; **Cys**, cysteine; **BS³**, bis(sulfosuccinimidyl)suberate; **EIE**, extracted ion electropherogram; **FAP-I**, familial amyloidotic polyneuropathy type I; **Glu**, glutamic acid; **Gly**, glycine; **HAc**, acetic acid; **HFor**, formic acid; **IA**, immunoaffinity; **MB**, magnetic bead; **MeOH**, methanol; **Met**, methionine; M_r, relative molecular mass; **MWCO**, molecular weight cut-off; **ProA**, protein A; **TIE**, total ion electropherogram; t_m, migration time; **TTR**, transthyretin; **UV**, ultraviolet spectrophotometry

are actually coexisting in the literature, something that has generated some controversy [16,17]. SPE-CE-MS has been extensively explored using the silica or polymeric sorbents typically used in off-line SPE (e.g. C18) [11–14, 16, 17], because of the versatility, the large active surface area, the compatibility with the on-line electrophoretic separation and detection and the commercial availability at a reasonable price. However, the limited selectivity of such sorbents hinders very often the analysis of complex samples, such as biological fluids, even with MS detection [14, 16, 17]. Immunoaffinity (IA) sorbents are an interesting alternative with improved selectivity, which may provide excellent extraction efficiency if the immunoreactivity and orientation of the antibody (Ab) and the active surface area are optimum and non-specific adsorption is minimized [8, 9, 18, 19]. However, in addition to the limited commercial availability of IA sorbents with the most appropriate features for immunoaffinity solid-phase extraction capillary electrophoresis mass spectrometry (IA-SPE-CE-MS), it is a challenge to make compatible IA sorbent stability, on-line immunoextraction and MS detection [18–22]. It is well-known that extreme ionic strength, high temperature and acidic or alkaline conditions may cause antibody denaturation. Furthermore, with on-line MS detection, solutions must be volatile to prevent salt build-up in the mass spectrometer. This is the reason why only a few authors have demonstrated IA-SPE-CE-MS with lab-made porous silica or agarose IA sorbents for the analysis of small peptides and proteins [18–22].

In the last decade, many different magnetic beads (MBs) have become commercially available with a wide range of surface chemistries to easily and reproducibly couple many types of microorganisms, cells or biological molecules, including Ab [23–25]. The robustness and versatility of the commercial MBs and the simplicity of operation are rapidly expanding the application areas, including IA-SPE-CE [26–33]. Since the pioneering work of Rashkovetsky et al. [26], several authors have described the use of IA-MBs in capillary or microchip format with ultraviolet (UV) [27, 31], fluorescence [26, 28–30] or MALDI-MS [32, 33] detection, but not yet with fully on-line ESI-MS detection. One of the great advantages of MBs in IA-SPE-CE is that facilitate the packing procedures and preparation of fritless microcartridges or microrreactors, because permanent magnets or electromagnets can be used to trap or move the particles. Between the disadvantages, it is worth mentioning that in general many commercial MBs are not porous, which is a limitation for the active surface area, especially when the amount of sorbent is small such as in capillaries and microchannels. Furthermore, little is known about the influence of the biological molecules on the formation and retention of MB plugs in a capillary or a microdevice [34] or about the influence of the external magnetic field in the extraction procedures [35].

In this paper is described, for the first time to the best of our knowledge, an IA-SPE-CE-MS method using MBs. The method is applied to the analysis of serum transthyretin (TTR). TTR is a homotetramer composed of four identical monomers (MO) (relative molecular mass (M_r)≈14 000) with different proteoforms (isoforms and PTMs) [36–41]. TTR is known to misfold and aggregate as stable insoluble fibrils due to mutations and conformational changes, causing different neurodegenerative diseases known as amyloidosis [42, 43]. Some of the 100 point mutations known in the TTR-gene are related to different types of hereditary TTR amyloidosis, such as familial amyloidotic polyneuropathy type I (FAP-I) [36, 37, 39, 44]. FAP-I is associated with a TTR variant that presents a single amino acid substitution of valine for methionine at position 30 (Met 30). First, analysis of TTR from serum was investigated by off-line immunoprecipitation and CE-MS with different MBs derivatized with a polyclonal Ab. Later, on-line IA-SPE-CE-MS was optimized and the potential to screen rapidly and reliably for FAP-I was demonstrated analysing serum samples from healthy controls and FAP-I patients.

2 Materials and methods

2.1 Chemicals and reagents

All the chemicals used in the preparation of background electrolytes (BGEs) and solutions were of analytical reagent grade or better. Propan-2-ol (≥99.9%), methanol (≥99.9%), formic acid (HFor) (99.0%), acetic acid (HAc) (glacial), ammonia (25%), hydrochloric acid (25%), sodium hydrogenphosphate (≥99.0%), sodium chloride (≥99.5%), sodium hydroxide (≥99.0%), phenol (≥99.5%), potassium dihydrogenphosphate (≥99.0%), potassium chloride (99.0%), glycine (Gly) (99.7%) and TTR (≥95.0%) were purchased from Merck (Darmstadt, Germany). Tris(hydroxymethyl)aminomethane (Tris) (≥99.5%) was purchased from Baker (Deventer, Holland). Water (LC-MS grade) and ACN (LC-MS grade) for sample pretratment and CE-MS experiments, and ammonium acetate (NH_4Ac) (≥99.9%) were supplied by Sigma (St. Louis, MO, USA). In the rest of experiments, water with a conductivity value lower than 0.05 μS/cm was obtained using a Milli-Q water purification system (Millipore, Molsheim, France).

Rabbit antihuman TTR polyclonal Ab was purchased from Dako (Glostrup, Denmark). The different MBs were provided by different manufacturers. Superparamagnetic agarose beads Protein A Ultrarapid Agarose™ (UAPA) and AffiAmino Ultrarapid Agarose™ (UAAF) of 45–165 μm diameter were supplied by Lab on a Bead (Uppsala, Sweden). Superparamagnetic silica beads Dynabeads® Protein A (DyPA) of 2.8 μm diameter were purchased from Life Technologies (Carlsbad, CA, USA). Superparamagnetic silica particles SiMAG-Protein A (SiPA) of 1 μm diameter were provided by Chemicell GmbH (Berlin, Germany). The crosslinker BS^3 (bis(sulfosuccinimidyl)suberate) was purchased from Pierce Biotechnology (Rockford, IL, EUA).

2.2 Electrolyte solutions, sheath liquid, protein standards and serum samples

The BGE for CE-MS separation contained 1.0 M HAc (pH 2.3) or 10 mM NH_4Ac, adjusted to pH 7.0 with ammonia,

for off-line immunoprecipitation or on-line IA-SPE-CE, respectively. Both BGEs were passed through a 0.22 μm nylon filter (MSI, Westboro, MA, USA). The sheath liquid solution consisted of a mixture of 60:40 (v/v) propan-2-ol:water with 0.05% or 0.25% (v/v) of HFor for the acidic or the neutral BGEs, respectively. With the neutral BGE, the percentage of HFor in the sheath liquid was higher for optimum detection sensitivity of TTR [45]. The sheath liquid and the BGEs were degassed for 10 min by sonication before use.

An aqueous standard solution (1000 μg/mL) of TTR was prepared and stored in a freezer at –20°C when not in use. Excipients of low M_r were removed from the sample by passage through 10 000 M_r cut-off (MWCO) cellulose acetate filters (Amicon Ultra-0.5, Millipore). The sample was centrifuged at 25°C for 10 min at 11 000 x g and the residue was washed three times for 10 min in the same way, with an appropriate volume of acidic BGE or phosphate buffered saline (PBS) (0.011 M sodium hydrogenphosphate, 0.0015 M potassium dihydrogenphospate, 0.14 M sodium chloride, 0.0027 M potassium chloride, pH 7.2) for off-line immunoprecipitation or IA-SPE-CE, respectively. The final residue was recovered by inverting the upper reservoir in a vial and spinning once more at a reduced centrifugal force (2 min at 300 x g). Sufficient acidic BGE or PBS was added to adjust the concentration of TTR to 1000 μg/mL.

Human blood samples from a healthy control and a symptomatic FAP-I patient were kindly supplied by the Hospital Universitari de Bellvitge (HUB, Hospitalet de Llobregat, Spain). The assay was approved by the Ethics Committee of the HUB and written informed consent was obtained from all participants in the study. Serum was prepared as described in our previous work [45]. Serum aliquots were stored in a freezer at –20°C when not in use.

2.3 Apparatus and procedures

pH measurements were made with a Crison 2002 potentiometer and a Crison electrode 52-03 (Crison Instruments, Barcelona, Spain). Centrifugal filtration was carried out in a cooled Rotanta 460 centrifuge (Hettich Zentrifugen, Tuttlingen, Germany) for centrifugation at controlled temperature (4 or 25°C). Agitation was performed with a Vortex Genius 3 (Ika®, Staufen, Germany). Neodymium block magnets (7×6×1.2 mm, N50) were supplied by Supermagnete (Gottmadingen, Germany). A neodymium cube magnet (12 mm, N48) was supplied by Lab on a Bead.

2.3.1 Off-line immunoprecipitation with MBs and CE-MS

Serum samples were immunopurified using the anti-TTR Ab coupled to the different MBs following the manufacturer's instructions. First, the solvent of the commercial Ab solution (2400 μg/mL) was changed to PBS by centrifugal filtration (as explained in Section 2.2 for the TTR standard). After that, 50 μL of MBs were vortexed and the supernatant was removed using a cube magnet to sediment the particles (magnetic separation). The MBs were washed with 100 μL of PBS twice and resuspended in 50 μL of PBS. 50 μL of Ab in PBS solution (2400 μg/mL) were then added to the MBs suspension. The mixture was moderately shaken for 40 min at room temperature. The supernatant was removed by magnetic separation and the MBs were subsequently washed three times with 100 μL of PBS. Only for crosslinking of UAPA MBs a 100 mM BS^3 in PBS stock solution was prepared immediately before use. A volume of 250 μL of a 30 mM BS^3 solution prepared from the stock solution was added to the MBs suspension in PBS. The mixture was moderately shaken for 30 min at room temperature. Then, 13 μL of a 1.0 M Tris (pH 7.5) solution were added and the mixture was shaken for 15 min. The crosslinked UAPA MBs were washed and stored in PBS as indicated before.

For off-line immunoprecipitation of TTR, 50 (DyPA) or 75 μL (UAPA, UAAF and SiPA) of serum sample were added to the MBs, depending on the binding capacity declared by the manufacturer (0.24, >3, >0.5 and 5 mg Ab/mL MB, respectively), and the mixture was incubated for 20 min at room temperature with gentle orbital shaking. Again, the supernatant was removed and the MBs were then washed three times with 200 μL of PBS. Finally, in order to elute TTR, 50 μL of 50 mM glycine (adjusted to pH 2.8 with HCl) were added and the mixture was incubated for 5 min at room temperature with orbital shaking. The supernatant containing the eluted TTR was collected and transferred into a clean microcentrifuge vial. Non-volatile components of low M_r were removed by centrifugal filtration (see Section 2.2) and solvent was changed to the acidic BGE for CE-MS. The protein samples were immediately analyzed.

Fused silica capillaries were supplied by Polymicro Technologies (Phoenix, AZ, EUA). All CE-MS experiments were performed in an HP^{3D} CE system coupled with an orthogonal G1603A sheath-flow interface to a 6220 oa-TOF LC/MS spectrometer (Agilent Technologies, Waldbronn, Germany). The sheath liquid was delivered at a flow rate of 3.3 μL/min by a KD Scientific 100 series infusion pump (Holliston, MA, USA). ChemStation and MassHunter softwares (Agilent Technologies) were used for CE and TOF mass spectrometer control, data acquisition, integration and m/z mass spectra deconvolution. The TOF mass spectrometer was operated under optimum conditions in positive mode using the following parameters: capillary voltage 4,000 V, drying gas temperature 300°C, drying gas flow rate 4 L/min, nebulizer gas 7 psig, fragmentor voltage 325 V, skimmer voltage 80 V, OCT 1 RF Vpp voltage 300 V. Data were collected in profile at 1 spectrum/s between 100 and 3200 m/z, with the mass range set to high resolution mode (4 GHz).

Separations were performed at 25°C in a 72 cm long (L_T) × 75 μm id × 365 μm od capillary. All capillary rinses were performed at high pressure (930 mbar). New capillaries were flushed with 1.0 M NaOH (15 min), water (15 min) and BGE (30 min). The system was finally equilibrated by applying

Electrophoresis 2016, *37*, 1220–1231

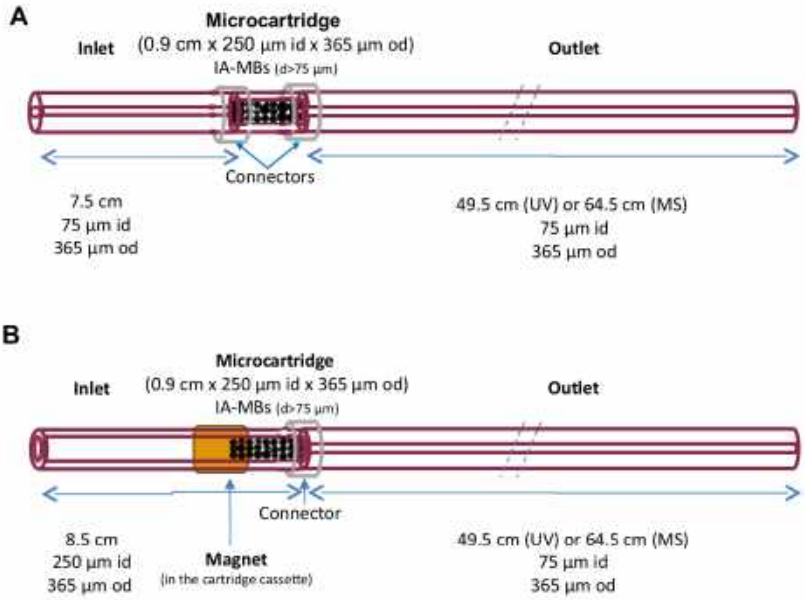

Figure 1. Representations of the microcartridge designs (A) UAPA or UAAF MBs are trapped in a microcartridge body of 250 µm id due to their particle size and (B) UAPA or UAAF MBs are retained in one of the ends of a piece of 250 µm id capillary and a magnet prevents the shift and loss of the MBs. (The first design could not be applied with SyPA and DyPA MBs because both are very small. Similarly, in the second case the magnet should cover the whole microcartridge body).

the 25 kV separation voltage (normal polarity, cathode in the outlet) for 15 min. Between workdays, the capillary was conditioned by rising successively with 0.1 M NaOH (5 min), water (10 min) and BGE (15 min). Both activation and conditioning procedures were performed off-line to avoid the unnecessary entrance of NaOH into the MS system. Samples were hydrodynamically injected at 50 mbar for 10 s. Between runs at 25 kV, capillary was conditioned flushing at 930 mbar for 2 min with BGE, 1 min with H_2O and 1 min with BGE.

2.3.2 On-line IA-SPE-CE-UV and IA-SPE-CE-MS

These experiments were performed only with UAPA and UAAF MBs, which were derivatized with the Ab as explained in Section 2.3.1. Each prepared IA-MB batch was stored in the fridge when not in use.

Construction of the IA microcartridge or analyte concentrator could be carried out as described elsewhere taking advantage of agarose MBs size [13,17] or their magnetic properties. In the first design, which is depicted in Fig. 1A, the microcartridge (0.9 cm L_T × 250 µm id × 365 µm od capillary) was inserted using two plastic sleeves at 7.5 cm from the inlet of a previously conditioned separation capillary (75 µm id × 365 µm od x L_T 57 or 72 cm, with UV and MS detection, respectively). It was filled before connection by vacuum, and the IA-MBs were retained mostly due to particle size (>75 µm id capillary) hence neither frits nor magnet were required [17]. In the second design, the 0.9 cm microcartridge was similarly constructed in one of the ends of an 8.5 cm L_T × 250 µm id × 365 µm capillary fragment (Fig. 1B). This capillary was connected with a plastic sleeve to the conditioned separation capillary (see dimensions above). A 12 mm cubic magnet helped during vacuum filling from the outlet end, since the particles were strongly retained and packed when they entered the strongly magnetized section in the end of the 250 µm id capillary. After this, the particles outside the 0.9 cm magnetized section were easily removed by applying vacuum in the opposite direction. The shift and loss of IA-MBs to the inlet vial during CE operation was prevented placing a smaller block magnet (7×6×1.2 mm) in the cartridge cassette to maintain the particles in the microcartridge. As can be observed in Fig. 1B, the magnet did not need to cover the whole microcartridge body.

In all these experiments, the neutral BGE was used to avoid extreme pH that would cause Ab denaturation and protein elution. Capillaries were first conditioned flushing at 930 mbar for 2 min with BGE. TTR standards in PBS and serum samples were hydrodynamically introduced at 930 mbar for 10 min (75 and 60 µL with UV and MS detection, respectively, using the Hagen-Poiseuille equation [46]). A final rinse with BGE (2 min, 930 mbar) eliminated non-retained molecules and equilibrated the capillary before the electrophoretic separation. Under optimized conditions, an eluent of 100 mM NH_4OH (pH 11.2) was injected at 50 mbar for 10 s (70 and 50 nL with UV and MS detection, respectively [46]). For a rapid and quantitative protein elution, a 25 mbar pressure was applied for 150 s (i.e. BGE was introduced) before beginning the separation in order to guarantee that the elution plug passed through the IA-MBs [14]. With MS detection, all these steps were performed by switching off the nebulizer gas and the ESI capillary voltage to prevent non-volatile and contaminants entrance into the MS. Then, both were switched on and separation was carried out at 25°C and +25 kV (normal polarity). Between runs, to avoid carry-over the capillary was rinsed with 100 mM NH_4Ac (pH 7.0) and water (2 min at 930 mbar both).

Table 1. Theoretical and deconvoluted average M_r and relative abundance for the detected TTR proteoforms of a healthy control serum sample by off-line immunoprecipitation with UAAF MBs and CE-MS. (BGE: 1.0 M HAc, pH 2.3)

N	Detected monomer TTR proteoforms	Theoretical average M_r	Off-line immunoprecipitation and CE-MS		
			Deconvoluted average M_r		%A[b] (%RSD)
			Experimental	E_r[a] (ppm)	
1.	TTR-Cys	13 880.4022	13 880.9073	36	100 (3.4)
2.	Free-TTR	13 761.2640	13 761.8857	45	64 (2.0)
3.	TTR-phosphorylated	13 841.2439	13 841.5820	24	40 (4.0)
	or TTR-sulfonated	13 841.3283		10	
4.	TTR-dehydroxylated or TTR-sulfinic	13 793.2628	13 794.0858	60	33 (5.7)
5.	(10) C-G	13 715.1713	13 715.4153	18	33 (4.8)
6.	TTR-glutathione	14 066.9600	14 067.8108	60	21 (4.7)

a) Relative error (E_r) was calculated in ppm as: $|M_r \text{ exp} - M_r \text{ theo}|/M_r \text{ theo} \times 10^6$ (exp = experimental and theo = theoretical).
b) The relative abundance (%A) was calculated normalizing to the area value of the most abundant form.

A simple off-line sample pretreatment was required to analyze TTR in serum samples to prevent microcartridge saturation and capillary inner surface damage due mostly to the presence of other high-abundance proteins, such as albumin. A method for the isolation of TTR from mouse serum and human cerebrospinal fluid was adapted [47,48]. At 2°C, 8 mg of NaCl were added to 100 μL of human serum and then dropwise 100 μL of 5% (v/v) phenol. Most of the proteins precipitated and TTR remained in solution, which lost the yellowish colour of the serum. Under the optimized conditions, the supernatant was collected after centrifugation for 10 min at 11 000 x g and then diluted 1:1 (v/v) with PBS before analysis.

2.3.3 Quality parameters

All quality parameters with MS detection were calculated from data obtained by measuring peak area and migration time (t_m) from the extracted ion electropherogram (EIE) of TTR proteoforms (considering the m/z of the most abundant molecular ions, i.e. ions with charges *+16, +15, +14, +13*). Repeatability was evaluated as the RSD (%RSD) of peak areas and t_m. Linearity range was established by analysing standard solutions of TTR at concentrations between 1 and 50 μg/mL. An estimation of the LODs was obtained by analysing low-concentration standard solutions of TTR (close to the LOD level, as determined from the approach based on S/N = 3). The lifetime of the microcartridges was evaluated by repeatedly analysing a standard solution of TTR at a concentration of 10 μg/mL and pretreated human serum samples.

3 Results and discussion

3.1 Off-line immunoprecipitation with MBs and CE-MS

The performance for TTR purification of all the MBs was investigated first by off-line immunoprecipitation and CE-MS with a 1.0 M HAc (pH 2.3) BGE. We selected three ProA MBs with different particle size and binding capacity from three manufacturers (UAPA, DyPA and SiPA) because Protein A strongly interacts with the Fc portion of the Ab (IgG) allowing an optimum Ab orientation. However, as there is no covalent bond between the Ab and the MBs, the elution conditions are typically harsh enough to elute the Ab together with the antigenic protein (e.g. 50 mM Gly-HCl (pH 2.8) in our case). As an alternative to the ProA MBs we also investigated UAAF MBs, which are functionalized with amino-reactive groups and covalently bound to the Ab without a preferred orientation. TTR was purified from serum samples by off-line immunoprecipitation and analyzed by CE-MS. The relative recoveries (referred to the highest one) and repeatabilities (as %RSD, $n = 6$) were calculated under the different conditions taking into account the peak area of the most abundant TTR proteoform (TTR-Cys, see Table 1). These values were 100% (2.3%), 80% (5.0%), 16% (4.3%) for UAPA, SiPA and DyPA, respectively, and 52% (4.6%) for UAAF. The best recoveries were obtained with UAPA and SiPA MBs which presented the highest binding capacity (>3 and 5 mg Ab/mL MB, respectively), but in both cases the Ab was eluted with TTR and could be detected by CE-MS (see the electropherogram and mass spectra for UAPA in Fig. 2A). In contrast, recoveries were slightly lower with UAAF MBs but the antibody was not detected (Fig. 2B). In all cases, results were repeatable and the same TTR proteoforms were detected with similar relative abundances. As an example, Fig. 2B shows the mass spectrum (ii) and the deconvoluted mass spectrum (iii), using UAAF MBs. Table 1 shows information about the detected proteoforms for monomeric (MO) TTR, the relative error (E_r) for experimental M_r, the relative abundance (%A) and its %RSD. Mass accuracy was good (E_r<60 ppm), as well as %A repeatability (%RSD<5.7%). The detected proteoforms agreed with those reported by other authors [36–41, 45]. Furthermore, the method allowed detecting TTR forms found at low concentration. This is the case, for example of TTR-Glutathione that presented a %A of 21% compared to TTR-Cys, which was the most abundant proteoform. However, it is

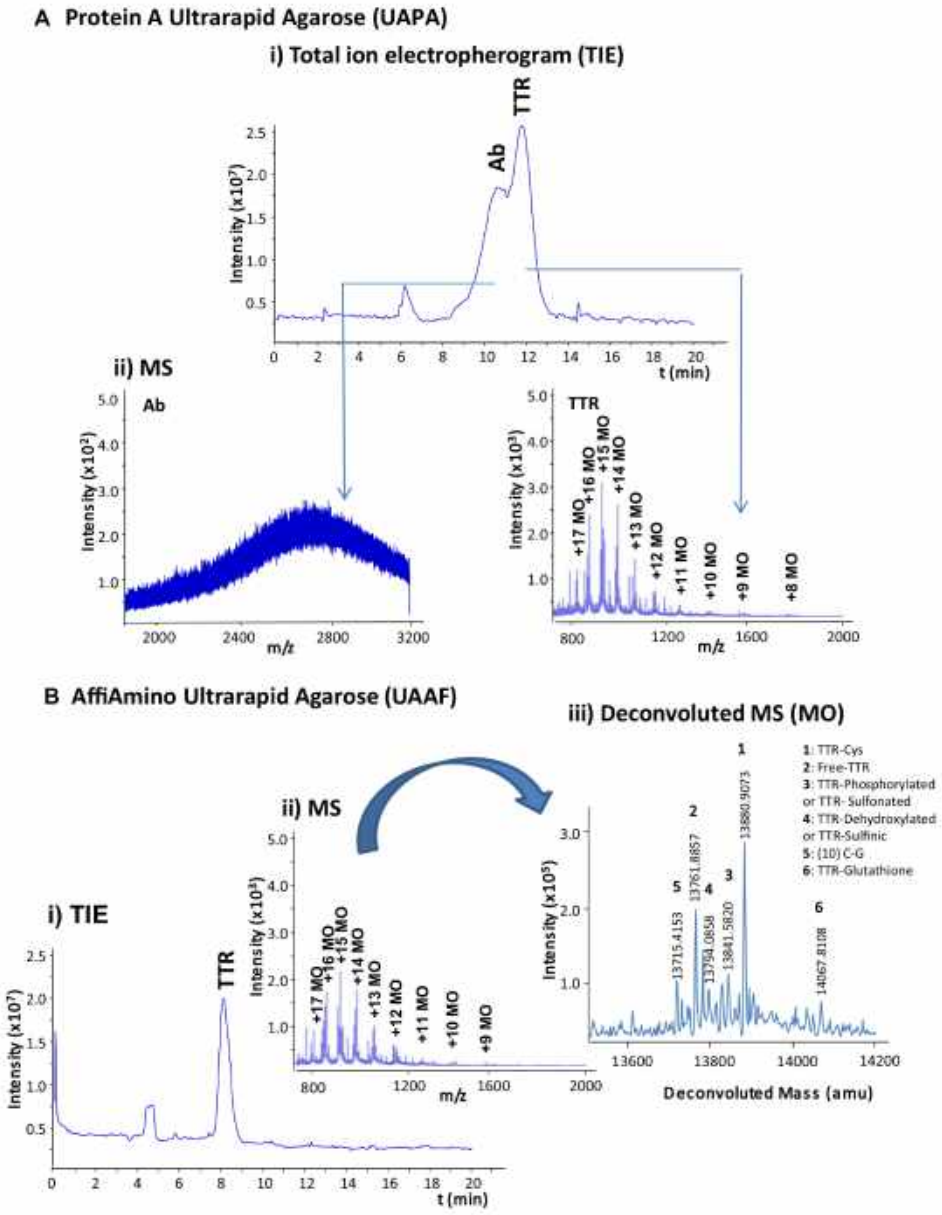

Figure 2. CE-MS using 1.0 M HAc as BGE after the off-line immunoprecipitation of a healthy control serum sample using (A) UAPA and (B) UAAF MBs. (i) Total ion electropherogram (TIE), (ii) mass spectrum and (iii) deconvoluted mass spectrum. (Ab: antibody; MO: monomer).

important to note that mass accuracy was not enough to differentiate between the TTR-Phosphorylated and TTR-Sulfonated (N = 3, Table 1) or between TTR-Dehydroxylated or TTR-Sulfinic (*N* = 4, Table 1) proteoforms, which were neither separated by electrophoresis. In these cases, reliability of the identification would improve running -MS and -MS/MS experiments using mass spectrometers with improved mass accuracy and resolution.

Although, reliable and repeatable results were obtained, the off-line method was time-consuming, it could not be automated and it was relatively expensive considering the amount of IA-MBs consumed in each analysis and that they were not reused. As an alternative to solve these issues, we investigated the on-line immunopurification.

3.2 On line IA-SPE-CE-UV and IA-SPE-CE-MS

As we mentioned before, in all these experiments a neutral BGE was used because the acidic BGE would cause Ab denaturation and protein elution during capillary conditioning [18–22]. In our previous work [45], we showed that this neutral BGE allowed detecting by CE-MS the same TTR proteoforms than the acidic BGE, but sensitivity was lower. For ease of comparison later with on-line IA-SPE-CE-MS, Fig. 3A shows the EIE, the mass spectrum and the deconvoluted mass spectrum for a 50 μg/mL TTR standard using the neutral BGE by CE-MS. As can be seen in the deconvoluted mass spectrum (Fig. 3A (iii)), only five of the six TTR proteoforms that were previously observed in serum with the acidic

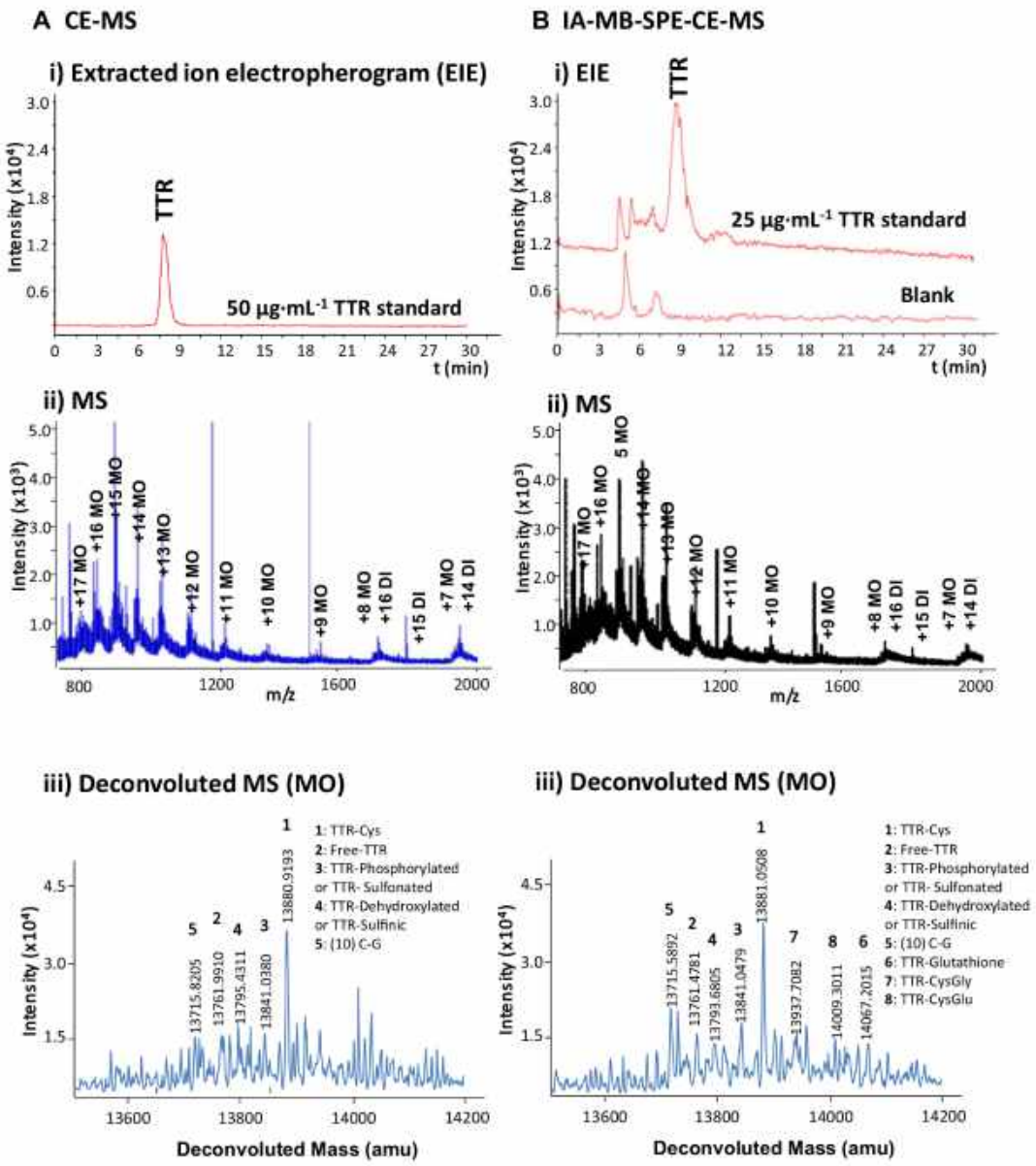

Figure 3. (A) CE-MS for a 50 µg/mL TTR standard using 10 mM NH_4Ac (pH 7.0) as BGE. (B) IA-SPE-CE-MS for a 25 µg/mL TTR standard using UAAF MBs. (i) Total ion electropherogram (TIE), (ii) mass spectrum and (iii) deconvoluted mass spectrum. (MO: monomer; DI: dimer).

BGE (Fig. 2B (iii)) were detected because this concentration was close to the LOD (≈25 µg/mL of TTR in standards).

3.2.1 IA-SPE-CE-UV

Some preliminary studies that were performed with UAPA and UAAF MBs and UV detection demonstrated that TTR standards needed to be dissolved in PBS, because TTR was not retained when dissolved in water or neutral BGE. PBS is a solution with a similar osmolarity and ion concentration to the human body fluids and probably benefited the interaction between TTR and the Ab. The performance of the two microcartridge designs depicted in Fig. 1A and B was similar. However, the second one (Fig. 1B) had several remarkable advantages, such as the presence of only one capillary connection and the simplicity to fill with MBs. These features increased the robustness and reusability of the system, because facilitated vacuum packing and particle replacement by removing the block magnet and applying pressure.

With regard to the volatile eluent, based on our experience, two acidic, 100 mM HAc (pH 2.9) and 50 mM:50 mM HAc:HFor (pH 2.3), and a basic eluent, 100 mM NH_4OH

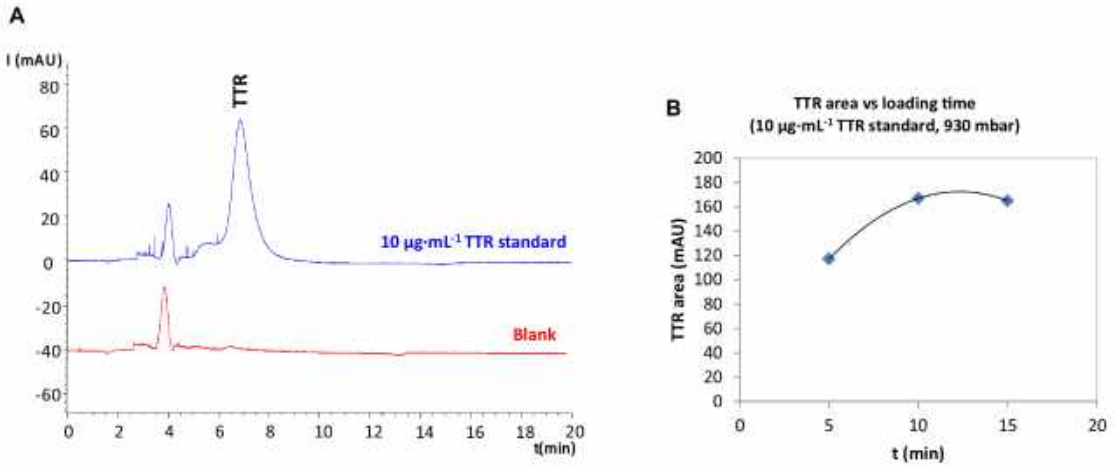

Figure 4. (A) IA-SPE-CE-UV for a 10 µg/mL TTR standard using UAAF MBs and 100 mM NH_4OH as eluent. (B) Study of sample loading time at 930 mbar on the peak area of the eluted TTR.

Table 2. Theoretical and deconvoluted average M_r and relative abundance for the detected proteoforms of a 1000 µg/mL TTR standard by CE-MS and 25 µg/mL TTR standard by IA-SPE-CE-MS with UAAF MBs. (BGE: 10 mM NH_4Ac, pH 7.0)

N	Detected MO TTR proteoforms	Theoretical Average M_r	A) CE-MS			B) IA-SPE-CE-MS		
			Deconvoluted Average M_r		%A[b] (%RSD)	Deconvoluted average M_r		%A[b] (%RSD)
			Experimental	E_r[a] (ppm)		Experimental	E_r[a] (ppm)	
1.	TTR-Cys	13 880.4022	13 880.9192	37	100 (1.6)	13 881.0508	47	100 (4.3)
2.	Free-TTR	13 761.2640	13 762.4781	53	41 (0.5)	13 761.7772	37	62 (0.9)
3.	TTR-phosphorylated or TTR-sulfonated	13 841.2439 13 841.3283	13 841.0308	15 21	35 (3.0)	13 841.0479	41 43	60 (2.6)
4.	TTR-dehydroxylated or TTR-sulfinic	13 793.2628	13 793.8311	41	37 (2.9)	13 793.6805	30	53 (1.9)
5.	(10) C-G	13 715.1713	13 715.8205	47	35 (5.9)	13 715.5892	30	62 (4.0)
6.	TTR-glutathione	14 066.9600	14 067.3258	26	20 (5.4)	14 067.2015	17	35 (1.7)
7.	TTR-CysGly	13 937.4541	13 938.2189	55	32 (4.9)	13 937.7082	18	48 (2.2)
8.	TTR-CysGlu	14 009.5177	Not detected	–	–	14 009.3011	15	27 (5.3)

a) Relative error (E_r) was calculated in ppm as: $|M_r$ exp – M_r theo$|/M_r$ theo × 10^6 (exp = experimental and theo = theoretical).
b) The relative abundance (%A) was calculated normalizing to the area value of the most abundant form.

(pH 11.2), were tested. When using UAPA MBs, TTR was eluted with all three eluents. However, repeatability was poor and TTR recovery diminished after several injections due to the gradual elution of the Ab. Crosslinking of UAPA MBs with BS^3 was studied in order to covalently bound the Ab to the ProA to avoid Ab elution. Nevertheless, crosslinked UAPA MBs did not allow detecting TTR by CE-MS, probably because antigen-binding site was modified and the Ab lost its function. The performance of the acidic eluents was also extremely poor with UAAF MBs because no TTR or Ab peaks were detected and the sorbent was irreversibly damaged for subsequent analyses with the basic eluent (repeatability was low, analysis time increased and TTR peak area decreased). When using UAAF MBs and the basic eluent, the Ab was not eluted and results for TTR were good. A higher amount than 100 mM of NH_4OH in the eluent was not tested to prevent Ab denaturation and expand the sorbent lifetime. The UV electropherograms of on-line preconcentration of TTR standards in PBS showed two peaks, the first related to the solvent and the second to TTR (Fig. 4A). In order to avoid carry-over, the postconditioning washing time with 100 mM NH_4Ac (pH 7.0) and water needed to be increased until 2 min.

Sample loading time was studied loading a 10 µg/mL TTR standard solution at 930 mbar for 5, 10 and 15 min. As can be seen in Fig. 4B, a loading time of 10 min was selected for the rest of experiments because peak area of the eluted TTR was maximum. At 15 min protein breakthrough during sample loading caused a decrease of peak area. Under the optimized conditions, consecutives analyses of TTR standards were repeatable in terms of t_m and peak area (%RSD ($n = 3$) 4.3 and 4.6%, respectively, for a 10 µg/mL TTR standard). LOD was around 2 µg/mL and the method was linear (r^2>0.99) between 5 and 25 µg/mL.

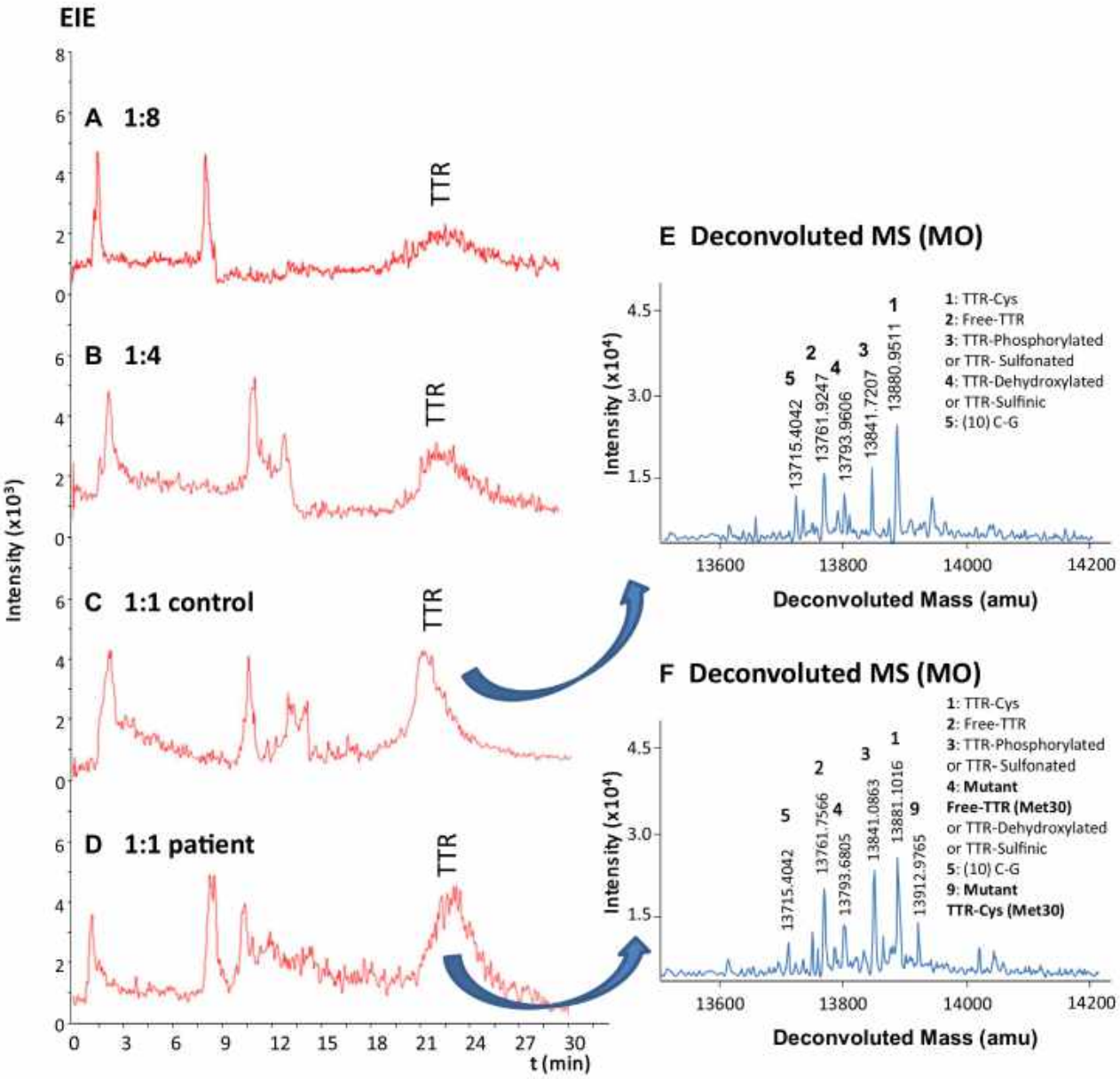

Figure 5. IA-SPE-CE-MS for serum samples pretreated with 5% (v/v) phenol solution. The supernatants of the healthy controls and the FAP-I patient samples were diluted with PBS (A) 1:8, (B) 1:4 (C) 1:1 and (D) 1:1 (v/v). In (C) and (D) are shown the TTR deconvoluted mass spectra.

3.2.2 IA-SPE-CE-MS

The optimized method with UV detection was evaluated with MS detection, but needed a small adjustment because TTR was sometimes eluted as a double peak. Several alternatives were explored to improve TTR elution. First, organic modifiers were added to the basic eluent, for example a 10% (v/v) of MeOH, but still two TTR peaks were detected. Next, a larger basic elution plug of 40 s at 50 mbar was tested but TTR peak broadened. Finally, the solution to reproducibly elute TTR as a single peak was to apply a 25 mbar pressure for 150 s after the elution plug injection and before beginning the separation in order to guarantee that the elution plug passed through the IA-MBs [14]. Figure 3B shows the EIE, the mass spectrum and the deconvoluted mass spectrum for a 25 μg/mL TTR standard, a concentration close to the LOD by CE-MS with the neutral BGE. Compared to the CE-MS electropherogram of a 50 μg/mL TTR standard shown in Fig. 3A preconcentration was significant. However, taking into account the volume of sample loaded on-line (60 μL) recoveries were much lower than previously with the off-line method, probably due to the limited amount of sorbent, smaller Ab-TTR ratio and the

Table 3. Theoretical and deconvoluted average M_r and relative abundance for the detected TTR proteoforms in serum samples pretreated with 5% (v/v) phenol solution (dilution 1:1 (v/v)) by IA-SPE-CE-MS. (BGE: 10 mM NH_4Ac, pH 7.0)

N	Detected MO TTR proteoforms	Theoretical Average M_r	A) Healthy control			B) FAP-I patient		
			Deconvoluted average M_r		%A[b] (%RSD)	Deconvoluted average M_r		%A[b] (%RSD)
			Experimental	E_r[a] (ppm)		Experimental	E_r[a] (ppm)	
1.	TTR-Cys	13 880.4022	13 880.9511	40	100 (3.2)	13 881.1016	50	100 (4.0)
2.	Free-TTR	13 761.2640	13 761.9247	48	64 (2.5)	13 761.7566	36	61 (3.2)
3.	TTR-phosphorylated	13 841.2439	13 841.7207	34	69 (1.3)	13 841.0863	22	67 (2.8)
	or TTR-sulfonated	13 841.3283		28			24	
4.	Mutant Free-TTR (Met30)	13 793.3301	Not detected	–	–	13 793.6805	25	64 (3.7)
	or TTR-dehydroxylated	13 793.2628	13 793.9606	51	51 (3.9)		30	
	or TTR-sulfinic							
5.	(10) C-G	13 715.1713	13 715.4042	17	53 (2.8)	13 715.4228	18	47 (4.8)
9.	Mutant TTR-Cys (Met30)	13 912.4683	Not detected	–	–	13 912.9765	37	44 (3.8)

a) Relative error (E_r) was calculated in ppm as: $|M_r \text{ exp} - M_r \text{ theo}|/M_r \text{ theo} \times 10^6$ (exp = experimental and theo = theoretical).
b) The relative abundance (%A) was calculated normalizing to the area value of the most abundant form.

shorter interaction time. Figure 3B shows that at 25 μg/mL with the on-line method three extra proteoforms were detected (TTR-glutathione, TTR-CysGly and TTR-CysGlu). As shown in Table 2, only at a concentration of 1000 μg/mL of TTR the number of detected proteoforms by CE-MS was similar than by IA-SPE-CE-MS, as well as the mass accuracy (E_r) and repeatability (%RSD %A). The increase of the %A for the different proteoforms in IA-SPE-CE-MS, which was referred to TTR-Cys, could be related to the lower recovery of TTR-Cys compared to the rest of proteoforms. Under the optimized conditions, results were repeatable in terms of t_m and peak area (TTR-Cys %RSD (n = 3) 2.9 and 4.3%, respectively), LOD was around 1 μg/mL (25 times lower than by CE-MS, ≈25 μg/mL) and the method was linear (r^2>0.99) between 5 and 25 μg/mL. The lifetime of the microcartridges was superior to 20 analyses during the same day. After that, peak areas decreased until no detecting TTR due to sorbent deterioration. Something similar happened, even after a smaller number of analyses, if capillaries were stored overnight in the fridge or at room temperature, even filled with PBS.

The on-line method optimized with standards was applied to the analysis of TTR in serum samples. Loading of serum samples without any pretreatment was not possible because of current instability and breakage. Several off-line sample pretreatments were studied in order to prevent microcartridge saturation and capillary inner surface damage due to the loading of salts and other high-abundance proteins, such as albumin. Serum filtration (0.22 μm pore) and dilution with water or PBS (1:1 or 1:10 (v/v)) or protein precipitation with ACN, were not useful. Finally we applied a very simple method of protein precipitation with 5% (v/v) of phenol that allowed excellent TTR recoveries (around 90% from comparison of CE-MS analysis of a serum sample pretreated and desalted with 10,000 MWCO filters and a 250 μg/mL TTR standard) [47,48]. Figures 5 A–C show the EIEs of the supernatant collected for a serum sample from a healthy control diluted 1:8, 1:4 and 1:1 (v/v) with PBS, respectively. As can be observed, TTR was detected at around 22 minutes and the largest peak was obtained in the less diluted sample. Furthermore, a small amount of albumin was still detected between 8 and 14 min in all cases. In this regard, the increase in t_m of TTR with serum samples compared to standards (Fig. 3B) was probably due to the modification of the inner wall of the separation capillary induced during loading by the remaining proteins that were not retained by the Ab. This modification was permanent, because TTR was also detected at this t_m when a standard was analyzed after a serum sample. Anyway, results were repeatable in terms of t_m and peak area (TTR-Cys %RSD (n = 3) were 4.7 and 3.2%, respectively, for a 1:1 (v/v) serum sample). In diluted 1:4 and 1:8 (v/v) samples only three of the main TTR proteoforms were detected (data not shown). In contrast, the five most abundant TTR proteoforms were detected in the 1:1 (v/v) sample (Fig. 5C), with similar figures of merit (Table 3A) compared to the TTR standard (Table 2B). For the 1:1 (v/v) dilution, the lifetime of the microcartridges was lower than for TTR standard solutions (>10 vs. >20 analyses during the same day) due to the higher sample matrix complexity. The on-line method was finally applied to the analysis of a serum sample from an FAP-I patient. Figure 5D shows the EIE and the deconvoluted mass spectrum of TTR in the FAP-I patient serum sample. Table 3B shows the information about the detected proteoforms, which are very similar to those obtained for the healthy control. As can be observed, all the main normal TTR proteoforms were detected as well as the main mutant proteoforms (TTR-Cys (Met30) and Free-TTR (Met30)). However, the mass spectrometer mass accuracy was not enough to differentiate between mutant free-TTR (Met30), TTR-Dehydroxylated or TTR-Sulfinic (N = 4, Table 3). Therefore, although the %A corresponding to these three proteoforms in the FAP-I patient was higher than the summed contribution of the two normal proteoforms in the healthy control (Table 3), only detection of the TTR-Cys

(Met30) proteoform would unambiguously confirm the TTR amyloidosis.

4 Concluding remarks

We have developed a method for purification, separation and characterization of TTR from serum samples by off-line immunoprecipitation with UAPA MBs and CE-MS with an acidic BGE. In order to minimize sample manipulation, increase analysis throughput and reduce consumption of IA-MBs, while maintaining the reproducibility and reliability of the method, we have also developed a novel on-line IA-SPE-CE-MS method. Although recoveries were the best with UAPA MBs in the off-line method, UAAF MBs were preferred for the on-line immunopurification because Ab was not eluted from the MBs. Under the optimized conditions with standards, migration times and peak areas were repeatable (%RSD <5%), microcartridge lifetime was good (>10 (serum samples) and >20 (standards) analyses/day), the method was linear between 5 and 25 μg/mL and LOD was 25 times lower (1 μg/mL) than in CE-MS (25 μg/mL). Finally, the potential of the on-line method to screen serum samples for FAP-I was confirmed after developing a simple off-line clean-up pretreatment based on protein precipitation with 5% (v/v) of phenol. In view of our experience and the results achieved, MBs offer a powerful alternative to expand the applicability of on-line IA-SPE-CE and an excellent opportunity to engage unskilled operators interested in IA or other type of sorbents. For example, we are currently exploring if the magnetic microcartridge design (Fig. 1B) can be applied to prepare frits with chemically inert MBs to pack non-magnetic sorbents (e.g. a conventional C18).

This study was supported by a grant from the Spanish Ministry of Economy and Competitiveness (CTQ2014-56777-R). We also thank Dr. C. Casasnovas and Dr. M. A. Alberti (Hospital Universitari de Bellvitge, HUB, Hospitalet de Llobregat, Spain) for providing the blood samples.

The authors have declared no conflict of interest.

5 References

[1] Klepárník, K., *Electrophoresis* 2015, *36*, 159–178.

[2] Štěpánová, S., Kašička, V., *J. Sep. Sci.* 2016, *39*, 198–211.

[3] Kašička, V., *Electrophoresis* 2014, *35*, 69–95.

[4] Heemskerk, A. A. M., Deelder, A. M., Mayboroda, O. A., *Mass Spectrom. Rev.* 2014, *35*, 1–13.

[5] Zhao, S. S., Chen, D. D. Y., *Electrophoresis* 2014, *35*, 96–108.

[6] Haselberg, R., de Jong, G. J., Somsen, G. W., *Electrophoresis* 2013, *34*, 99–112.

[7] Wenz, C., Barbas, C., López-Gonzálvez, Á., Garcia, A., Benavente, F., Sanz-Nebot, V., Blanc, T., Freckleton, G., Britz-McKibbin, P., Shanmuganathan, M., de l'Escaille, F., Far, J., Haselberg, R., Huang, S., Huhn, C., Pattky, M., Michels, D., Mou, S., Yang, F., Neususs, C., Tromsdorf, N., Baidoo, E. E. K., Keasling, J. D., Park, S. S., *J. Sep. Sci.* 2015, *38*, 3262–3270.

[8] Guzman, N. A., Blanc, T., Phillips, T. M., *Electrophoresis* 2008, *29*, 3259–3278.

[9] Guzman, N. A., Phillips, T. M., *Electrophoresis* 2011, *32*, 1565–1578.

[10] Breadmore, M. C., Tubaon, R. M., Shallan, A. I., Phung, S. C., Keyon, A. S. A., Gstoettenmayr, D., Prapatpong, P., Alhusban, A. A., Ranjbar, L., See, H. H., Dawod, M., Quirino, J. P., *Electrophoresis* 2015, *36*, 36–61.

[11] Ramautar, R., Somsen, G. W., de Jong, G. J., *Electrophoresis* 2014, *35*, 128–37.

[12] Ramautar, R., Somsen, G. W., de Jong, G. J., *Electrophoresis* 2016, *37*, 35–44.

[13] Benavente, F., Vescina, M. C., Hernández, E., Sanz-Nebot, V., Barbosa, J., Guzman, N. A., *J. Chromatogr. A* 2007, *1140*, 205–212.

[14] Medina-Casanellas, S., Benavente, F., Barbosa, J., Sanz-Nebot, V., *Electrophoresis* 2011, *32*, 1750–1759.

[15] Guzman, N. A., Trebilcock, M. A., Advis, J. P., *J. Liq. Chromatogr.* 1991, *14*, 997–1015.

[16] Hernández, E., Benavente, F., Sanz-Nebot, V., Barbosa, J., *Electrophoresis* 2008, *29*, 3366–3376.

[17] Medina-Casanellas, S., Tak, Y. H., Benavente, F., Sanz-Nebot, V., Sastre Toraño, J., Somsen, G. W., de Jong, G. J., *Electrophoresis* 2014, *35*, 2996–3002.

[18] Medina-Casanellas, S., Benavente, F., Barbosa, J., Sanz-Nebot, V., *Anal. Chim. Acta* 2012, *717*, 134–142.

[19] Medina-Casanellas, S., Benavente, F., Barbosa, J., Sanz-Nebot, V., *Anal. Chim. Acta* 2013, *789*, 91–99.

[20] Guzman, N. A., *J. Chromatogr. B. Biomed. Sci. Appl.* 2000, *749*, 197–213.

[21] Giménez, E., Benavente, F., de Bolós, C., Nicolás, E., Barbosa, J., Sanz-Nebot, V., *J. Chromatogr. A* 2009, *1216*, 2574–2582.

[22] Medina-Casanellas, S., Benavente, F., Giménez, E., Barbosa, J., Sanz-Nebot, V., *Electrophoresis* 2014, *35*, 2130–2136.

[23] Plouffe, B. D., Murthy, S. K., Lewis, L. H., *Rep. Prog. Phys.* 2014, *78*, 016601.

[24] Tekin, H. C., Gijs, M. A. M., *Lab Chip* 2013, *13*, 4711–4739.

[25] van Reenen, A., de Jong, A. M., den Toonder, J. M. J., Prins, M. W. J., *Lab Chip* 2014, *14*, 1966–1986.

[26] Rashkovetsky, L. G., Lyubarskaya, Y. V., Foret, F., Hughes, D. E., Karger, B. L., *J. Chromatogr. A* 1997, *781*, 197–204.

[27] Kaneta, T., Inoue, J., Koizumi, M., Imasaka, T., *Electrophoresis* 2006, *27*, 3218–3223.

[28] Chen, H.-X., Busnel, J.-M., Peltre, G., Zhang, X.-X., Girault, H. H., *Anal. Chem.* 2008, *80*, 9583–9588.

[29] Stege, P. W., Raba, J., Messina, G. A., *Electrophoresis* 2010, *31*, 3475–3481.

[30] Tennico, Y. H., Remcho, V. T., *Electrophoresis* 2010, *31*, 2548–2557.

[31] Morales-Cid, G., Diez-Masa, J. C., de Frutos, M., *Anal. Chim. Acta* 2013, *773*, 89–96.

[32] Gasilova, N., Gassner, A.-L., Girault, H. H., *Electrophoresis* 2012, *33*, 2390–2398.

[33] Gasilova, N., Girault, H. H., *Anal. Chem.* 2014, *86*, 6337–6345.

[34] Henken, R. L., Chantiwas, R., Gilman, S. D., *Electrophoresis* 2012, *33*, 827–833.

[35] Moliner-Martínez, Y., Prima-Garcia, H., Ribera, A., Coronado, E., Campíns-Falcó, P., *Anal. Chem.* 2012, *84*, 7233–7240.

[36] Ando, Y., Ueda, M., *Curr. Med. Chem.* 2012, *19*, 2312–2323.

[37] Poulsen, K., Bahl, J. M. C., Tanassi, J. T., Simonsen, A. H., Heegaard, N. H. H., *Methods* 2012, *56*, 284–292.

[38] Nakanishi, T., Sato, T., Sakoda, S., Yoshioka, M., Shimizu, A., *Biochim. Biophys. Acta* 2004, *1698*, 45–53.

[39] Terazaki, H., Ando, Y., Suhr, O., Ohlsson, P. I., Obayashi, K., Yamashita, T., Yoshimatsu, S., Suga, M., Uchino, M., Ando, M., *Biochem. Biophys. Res. Commun.* 1998, *249*, 26–30.

[40] Horvatovich, P., Franke, L., Bischoff, R., *J. Proteome Res.* 2014, *13*, 5–14.

[41] Gericke, B., Raila, J., Sehouli, J., Haebel, S., Könsgen, D., Mustea, A., Schweigert, F. J., *BMC Cancer* 2005, *5*, 133–141.

[42] Falk, R. H., Comenzo, R. L., Skinner, M., *N. Engl. J. Med.* 1997, *337*, 898–909.

[43] Johnson, S. M., Connelly, S., Fearns, C., Powers, E. T., Kelly, J. W., *J. Mol. Biol.* 2012, *421*, 185–203.

[44] Connors, L. H., Lim, A., Prokaeva, T., Roskens, V. A., Costello, C. E., *Amyloid J. Protein Fold. Disord.* 2003, *10*, 160–184.

[45] Pont, L., Benavente, F., Barbosa, J., Sanz-Nebot, V., *Electrophoresis* 2015, *36*, 1265–1273.

[46] Lauer, H. H., Rozing, G. P. (Eds.), *High Performance Capillary Electrophoresis*, Agilent Technologies, Germany 2014.

[47] Reuter, A. M., Hamoir, G., Marchand, R., Kennes, F., *Eur. J. Biochem.* 1968, *5*, 233–238.

[48] Bimanpalli, M. V, Ghaswala, P. S., *J. Biosci.* 1988, *13*, 159–169.

analytical chemistry

Article

Cite This: Anal. Chem. 2020, 92, 1525−1533

pubs.acs.org/ac

On-line Aptamer Affinity Solid-Phase Extraction Capillary Electrophoresis-Mass Spectrometry for the Analysis of Blood α-Synuclein

Roger Pero-Gascon,[†] Fernando Benavente,*[,†] Zoran Minic,[‡] Maxim V. Berezovski,[‡] and Victoria Sanz-Nebot[†]

[†]Department of Chemical Engineering and Analytical Chemistry, Institute for Research on Nutrition and Food Safety (INSA-UB), University of Barcelona, Barcelona 08028, Spain

[‡]Department of Chemistry and Biomolecular Sciences, University of Ottawa, Ottawa, Ontario K1N 6N5, Canada

Supporting Information

ABSTRACT: In this paper, an on-line aptamer affinity solid-phase extraction capillary electrophoresis-mass spectrometry method is described for the purification, preconcentration, separation, and characterization of α-synuclein (α-syn) in blood at the intact protein level. A single-stranded DNA aptamer is used to bind with high affinity and selectivity α-syn, which is a major component of Lewy bodies, the typical aggregated protein deposits found in Parkinson's disease (PD). Under the conditions optimized with recombinant α-syn, repeatability (2.1 and 5.4% percent relative standard deviation for migration times and peak areas, respectively) and microcartridge lifetime (around 20 analyses/microcartridge) were good, the method was linear between 0.5 and 10 $\mu g \cdot mL^{-1}$, and limit of detection was 0.2 $\mu g \cdot mL^{-1}$ (100 times lower than by CE-MS, 20 $\mu g \cdot mL^{-1}$). The method was subsequently applied to the analysis of endogenous α-syn from red blood cells lysate of healthy controls and PD patients.

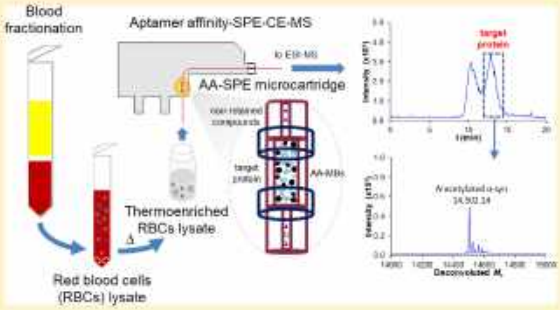

Capillary electrophoresis-mass spectrometry (CE-MS) is regarded nowadays as a powerful technique for the highly efficient separation and characterization of biomolecules, including peptides, protein isoforms, and post-translational modifications (PTMs) or protein complexes.[1−4] However, as in many other microscale separation techniques, the small sample volume injected for optimum separation (typically 1−2% of the capillary volume) compromises the concentration sensitivity for most analytes and is very often a limitation that hinders a more widespread application.[5−9] To improve the limits of detection (LODs), the use of more selective and sensitive mass spectrometers is in many cases not satisfactory enough. Therefore, for the on-line preconcentration of the target analytes after the injection of a large volume of sample, CE-MS has been often combined with different electrophoretic[5,6] and chromatographic[6−9] techniques. Within the chromatographic preconcentration techniques, on-line solid-phase extraction capillary electrophoresis (SPE-CE) is widely recognized as an excellent option to preconcentrate and clean up the target analytes, minimizing sample handling and increasing analysis throughput. In the most widely used SPE-CE configuration, a microcartridge with an appropriate sorbent to selectively retain the target analyte is integrated in-line near the entrance of the separation capillary, and no valves are necessary for the operation. After loading a large volume of sample (~50−100 μL), the capillary is rinsed to eliminate nonretained molecules and filled with background electrolyte (BGE). Then, the analyte is eluted and preconcentrated in a small volume of an appropriate solution (~25−50 nL) before the separation and the detection.[8,9]

Nowadays, the availability of a wide variety of commercial or lab-made sorbents has broadened the applicability of SPE-CE. SPE-CE has been explored using conventional chromatographic sorbents (e.g., C18 or HLB),[7−9] but there is an urgent need of high selective affinity sorbents to analyze complex samples such as biological fluids.[9−15] Immunoaffinity (IA) sorbents prepared by immobilization of antibodies or antibody fragments are for many authors the gold standard within the high selective sorbents and can provide excellent sample cleanup and extraction efficiency. However, the applicability of IA-SPE-CE-MS is limited by several constraints related to the conditions needed to guarantee the antibody stability. On-line MS detection is negatively affected by the presence of salts due to ionization suppression and requires the use of volatile solutions and BGEs to prevent salt buildup. The typically acidic BGEs used in CE-MS in positive electrospray ionization

Received: October 21, 2019
Accepted: December 11, 2019
Published: December 11, 2019

DOI: 10.1021/acs.analchem.9b04802
Anal. Chem. 2020, 92, 1525−1533

(ESI+) mode (e.g., from 0.1 to 1 M of acetic acid) may cause antibody denaturation, therefore, compromising IA sorbent stability. This issue is usually solved using neutral BGEs (e.g., 10 mM of ammonium acetate), but ionization efficiency is in general lower under these conditions. As an interesting alternative to antibodies, the use of aptamer-based sorbents has been proposed for sample preparation.[16] The most common aptamers are single-stranded oligonucleotides that are able to bind to a target molecule with high-affinity and selectivity. These features enable their application in diagnostics, imaging, therapeutics, targeted delivery, and biosensing.[17−20] In general, aptamers are isolated in vitro via systematic evolution of ligands by exponential enrichment (SELEX), an iterative cycle of selection and amplification steps that enriches high-affinity and selective aptamers from a large combinatorial library.[20,21] Aptamers have been generated for a wide variety of targets, ranging from simple inorganic molecules to proteins and whole cells.[20,21] Aptamers are chemically synthesized, which eliminates the requirement of animals or cells and the possible batch-to-batch variations associated with antibodies, and are significantly faster and cheaper to produce.[20] Other interesting advantages of aptamers are robustness, thermal stability, tolerance to wide ranges of pH, and salt concentration. Furthermore, they can be chemically modified at either 3′- or 5′-terminus to incorporate various functional groups and spacer arms to facilitate the covalent immobilization with an appropriate orientation and minimal steric hindrance on a solid support.[16,22]

The use of aptamer affinity (AA) sorbents has been previously described for off-line solid phase microextraction (SPME),[23] on-chip SPE,[24] and on-line SPE-nanoLC.[22] Recently, Marechal et al.[14] described an aptamer silica-based monolithic microcartridge for the analysis of ochratoxin A in standards, beer and wine by AA-SPE-CE with laser-induced fluorescence (LIF) detection. So far, to the best of our knowledge, no other applications of AA-SPE-CE have been described.

In this paper, AA-SPE-CE-MS is described for the first time, and a method for the analysis of α-synuclein (α-syn) in blood is developed. α-Syn is a 14 kDa protein, composed of 140 amino acids and numerous proteoforms, including PTMs as phosphorylation, ubiquitination, nitration, and acetylation.[25−27] It is present at high levels in the brain where it is mainly localized in presynaptic terminals of nerve cells,[25] but it can be also found in biological fluids such as cerebrospinal fluid (CSF), blood, and saliva.[28,29] The potential of certain α-syn proteoforms as biomarkers for early diagnosis and tracking progression of Parkinson's disease (PD), one of the most common neurodegenerative motor disorders, is continuously investigated. Phosphorylated α-syn at Ser-129 is a major component (90% of α-syn) in the aggregates of Lewy bodies (LB), which represent the morphological hallmark of PD.[25] In contrast, full-length *N*-terminal acetylated α-syn is the major proteoform in brain cytosol whereas phosphorylated α-syn involves only about 4% of normal α-syn.[25] α-Syn has been frequently analyzed in brain tissue or CSF.[26,30] However, more accessible biofluids, such as blood, are also being investigated,[30,31] where it is still necessary to broaden the knowledge about the different proteoforms using novel, sensitive, and selective analytical methods, as the one proposed in this study.

EXPERIMENTAL SECTION

Materials and Reagents. All the chemicals used in the preparation of background electrolytes (BGEs) and solutions were of analytical reagent grade or better. Acetic acid (HAc) (glacial), ammonium hydroxide (NH_4OH) (25%), formic acid (HFor) (99.0%), potassium chloride (99.0%), potassium dihydrogen phosphate (≥99.0%), sodium chloride (≥99.5%), and sodium hydrogen phosphate (≥99.0%), were purchased from Merck (Darmstadt, Germany). Acetonitrile (LC-MS) and ethanol (96%) were supplied by Panreac AppliChem (Barcelona, Spain). Ammonium acetate (NH_4Ac) (≥99.9%) and Tween 20 were supplied by Sigma-Aldrich (Steinheim, Germany). Propan-2-ol (LC-MS) was purchased from Scharlau (Barcelona, Spain). Water (LC-MS grade) was supplied by Fisher Scientific (Loughborough, UK).

The DNA aptamer MS-15[32] modified with a C6 spacer arm terminated by 5′amino (MS-15-5′, 66-mer, M_r = 20,690) and the masking DNA (T-SO508,[33] an off-target sequence single-stranded DNA that tested negative for α-syn by AA-SPE-CE-MS and was already available in the laboratory, 24-mer, M_r = 7708), both purified by HPLC, were purchased from Integrated DNA Technologies (Coralville, IA, USA).

Magnetic beads (MBs) LOABeads AffiAmino of 45−165 μm diameter were purchased from Lab on a Bead (Uppsala, Sweden).

Electrolyte Solutions, Sheath Liquid, Protein Standards, and Blood Samples. All the solutions were degassed for 10 min by sonication before use. The optimized BGE for the CE-MS and AA-SPE-CE-MS separation contained 100 mM HAc (pH 2.9). The BGE was passed through a 0.20 μm nylon filter (Macherey-Nagel, Düren, Germany). The sheath liquid solution consisted of a mixture of 60:40 (*v*/*v*) propan-2-ol/water with 0.05% (*v*/*v*) of HFor and was delivered at a flow rate of 3.3 $\mu L \cdot min^{-1}$ by a KD Scientific 100 series infusion pump (Holliston, MA, USA).

Recombinant human α-syn expressed in *Escherichia coli* was purchased from Analytik Jena (Jena, Germany). The solution provided by the manufacturer (5000 $\mu g \cdot mL^{-1}$ in phosphate buffered saline (PBS)) was aliquoted and stored in a freezer at −20 °C. Aliquots were thawed before use, and working standard solutions were prepared by dilution in water. These solutions were stored in the fridge at 5 °C when not in use.

Human blood samples from patients were provided by the Basque Biobank/Biodonostia Node (www.biobancovasco.org). Samples were processed following standard operation procedures with appropriate approval of the Ethical and Scientific Committees. Three healthy donor blood samples and three PD patient blood samples (one at stage III and two at stage IV of the disease) were analyzed. All the samples corresponded to males and females aged between 60 and 80 years.

Pretreatments of Red Blood Cells Lysates. Red blood cells (RBCs) lysates were prepared from blood as described in the Supporting Information.[34]

The RBCs lysates were precipitated with ethanol-chloroform to deplete hemoglobin as described elsewhere,[34] with some changes: 350 μL of cold ethanol and 200 μL of cold chloroform were added to 250 μL of RBCs lysate. The mixture was shaken for 5 min at 4 °C and centrifuged at 3000 *g* for 10 min at 4 °C. The supernatant was collected, and low M_r compounds were removed with 10,000 M_r cutoff (MWCO)

DOI: 10.1021/acs.analchem.9b04802
Anal. Chem. 2020, 92, 1525−1533

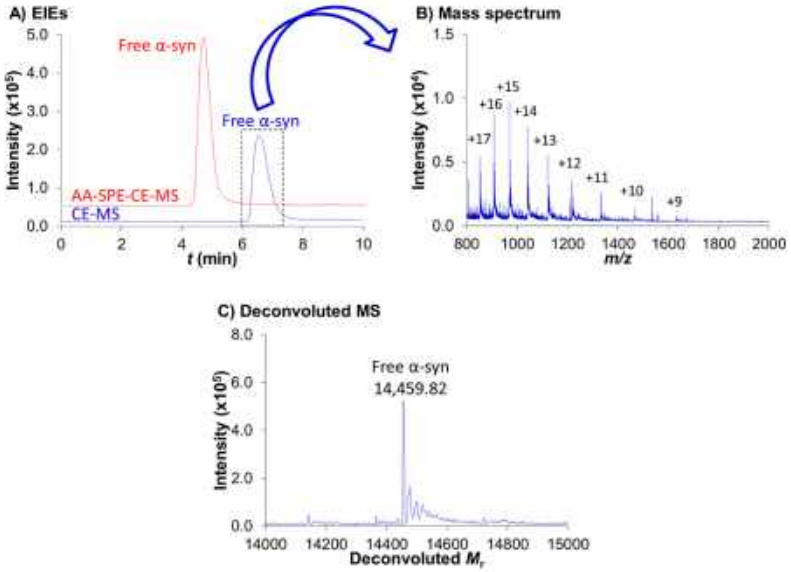

Figure 1. CE-MS and AA-SPE-CE-MS for a 100 and a 1 $\mu g \cdot mL^{-1}$ α-syn standard, respectively. (A) Extracted ion electropherograms (EIEs), (B) mass spectrum of the boxed time region (CE-MS), and (C) deconvoluted mass spectrum (CE-MS).

cellulose acetate centrifugal filters (Amicon Ultra-0.5, Millipore).

Thermoenrichment to deplete the nonthermostable proteins was performed on the RBCs lysates as follows:[31] 350 μL of RBCs lysate was heated at 90 °C for 10 min in a thermoshaker. The mixture was centrifuged at 12000 *g* for 5 min at 4 °C, and the supernatant (i.e., thermoenriched (TE) RBCs lysate) was filtered using a 0.22 μm polyvinylidene difluoride centrifugal filter (Ultrafree-MC, Millipore, Bedford, MA, USA) at 12000 *g* for 5 min.

Apparatus. pH measurements were made with a Crison 2002 potentiometer and a Crison electrode 52-03 (Crison Instruments, Barcelona, Spain). Agitation was performed with a Vortex Genius 3 (Ika, Staufen, Germany). Centrifugal filtration was carried out in a Mikro 220 centrifuge (Hettich Zentrifugen, Tuttlingen, Germany). Incubations were carried out in a TS-100 thermoshaker (Biosan, Riga, Latvian Republic). A neodymium cube magnet (12 mm, N48) was supplied by Lab on a Bead.

CE-MS. Fused silica capillaries were supplied by Polymicro Technologies (Phoenix, AZ, USA). All CE-MS experiments were performed in a 7100CE coupled with an orthogonal G1603A sheath-flow interface to a 6220 oa-TOF LC/MS spectrometer (Agilent Technologies, Waldbronn, Germany). ChemStation and MassHunter softwares (Agilent Technologies) were used for the CE and TOF mass spectrometer control, data acquisition, and processing. The TOF mass spectrometer was operated in ESI+ mode, and the optimized parameters are presented in the Supporting Information.

Separations were performed at 25 °C in a 72 cm long (L_T) × 75 μm i.d. × 365 μm o.d. capillary. All capillary rinses were performed flushing at 930 mbar. For new capillaries or between workdays, the capillaries were flushed off-line with 1 M NaOH (15 or 5 min, respectively), water (15 or 10 min), and BGE (30 or 15 min) to avoid the unnecessary contamination of the MS system. Samples were hydrodynamically injected at 50 mbar for 10 s (54 nL, i.e., 1.7% of the capillary, estimated using the Hagen−Poiseuille equation[35]), and a separation voltage of +25 kV (normal polarity, cathode in the outlet) was applied. The autosampler was kept at 10 °C using an external water bath (Minichiller 300, Peter Huber Kältemaschinenbau AG, Offenburg, Germany). Between runs, the capillary was conditioned flushing with water (2 min) and BGE (2 min).

AA-SPE-CE-MS. AA-MBs were prepared following the manufacturer recommendations. First, a 200 μL aliquot of MBs solution was vortexed, and the supernatant was removed after magnetic separation, using a cube magnet to sediment the particles (20 μL of sedimented MBs). The MBs were washed using 200 μL of PBS with 0.1% Tween 20 (PBS-T), the supernatant was removed by magnetic separation, and the MBs were resuspended with the same volume of PBS-T. Ten μL of activation buffer was added, and the MBs were moderately shaken for 15 min at room temperature. The supernatant was removed by magnetic separation, and the MBs were washed with 200 μL of PBS-T and resuspended with 150 μL of PBS-T. Fifty μL of the DNA aptamer M5-15-5′amino dissolved in PBS (100 $\mu mol \cdot L^{-1}$) was then added to the MBs suspension. The mixture was moderately shaken for 40 min at room temperature. The supernatant was removed, and the AA-MBs were subsequently washed three times with 200 μL of PBS and resuspended with the same volume of PBS. The remaining reactive groups on AA-MBs were blocked adding 20 μL of blocking buffer (50% (*v*/*v*) ethanolamine in PBS), and the mixture was moderately shaken for 45 min at room temperature. Finally, the supernatant was removed, and the AA-MBs were subsequently washed three times with 200 μL of PBS. The AA-MBs were stored in PBS with 20% (*v*/*v*) ethanol at 4 °C when not in use.

Construction of fritless particle-packed microcartridges for AA-SPE-CE-MS was carried out as described elsewhere, taking advantage of the average larger size of the sorbent particles compared to the inner diameter of the separation capillary.[9,13,36] The microcartridge (0.9 cm L_T × 250 μm i.d. × 365

DOI: 10.1021/acs.analchem.9b04802
Anal. Chem. 2020, 92, 1525−1533

μm o.d. capillary) was completely filled by vacuum with AA-MB sorbent and connected with plastic sleeves to two capillary fragments (7.5 cm L_T × 75 μm i.d. × 365 μm o.d. (inlet) and 64.5 cm L_T × 75 μm i.d. × 365 μm o.d. (outlet)), which were conditioned before beginning the construction.

Under the optimized conditions, AA-SPE-CE-MS capillaries were first conditioned flushing with BGE at 930 mbar for 2 min. Samples were introduced at 930 mbar for 5 min (30 μL[35]). A final flush with BGE for 2 min eliminated nonretained molecules and filled the capillary before the electrophoretic separation. All these steps were performed with the nebulizer gas and the ESI capillary voltage switched off to prevent the entrance of contaminants into the MS. Then, both were switched on, and a small volume of eluent with 100 mM NH_4OH (pH 11.2) was injected at 50 mbar for 20 s (100 nL[35]). For a rapid and repeatable protein elution, the small plug of eluent was pushed with BGE at 50 mbar for 100 s, before applying the separation voltage (+25 kV) and a small pressure (25 mbar) to compensate for the microcartridge counter-pressure. Between consecutive runs, to avoid carry-over, the capillary was flushed with water for 1 min, eluent was injected at 50 mbar for 40 s, and the capillary was flushed again with water for 1 min. All experiments were performed at 25 °C.

Quality Parameters. The details regarding the limit of detection (LOD), limit of quantification (LOQ), repeatability of migration time and peak area, linearity, and microcartridge lifetime in CE-MS and AA-SPE-CE-MS are given in the Supporting Information.

LC-Orbitrap-MS/MS. The details about TE RBCs lysate bottom-up proteomics workflow including LC-Orbitrap-MS/MS analysis are given in the Supporting Information.

■ RESULTS AND DISCUSSION

CE-MS. In general, the best results for the analysis of intact proteins by CE-MS in ESI+ are obtained using acidic volatile BGEs and sheath liquids because protein ionization is maximized and the best sensitivity is achieved. Different conditions were tested for the analysis of recombinant human α-syn (i.e., 50 mM HAc:50 mM HFor (pH 2.3); 100 mM HAc (pH 2.9) or 10 mM NH_4Ac (pH 7.0, 8.0, or 9.0) as BGEs combined with 60:40 (*v*/*v*) propan-2-ol/water with 0.05 or 0.25% (*v*/*v*) of HFor as sheath liquids). The best results for the analysis of α-syn were obtained with a BGE of 100 mM HAc (pH 2.9) and a sheath liquid of 60:40 (*v*/*v*) propan-2-ol/water with 0.05% (*v*/*v*) of HFor. As an example, Figure 1 shows the extracted ion electropherogram (EIE) (A), mass spectrum (B), and deconvoluted mass spectrum (C) for the CE-MS analysis of a 100 $\mu g \cdot mL^{-1}$ standard solution of recombinant human α-syn in the optimized conditions. The only detected proteoform was free α-syn because the recombinant human α-syn expressed in *E. coli* was not supposed to undergo post-translational modifications (PTMs) during bacterial synthesis (the minor peaks in the deconvoluted mass spectrum of Figure 1-C are mostly due to Na^+ and K+ adducts to the ion species of the mass spectrum of Figure 1-B). Table S-1 shows the theoretical average M_r of free α-syn and the relative error (E_r) for the experimental deconvoluted average M_r. Mass accuracy was good (E_r < 20 ppm). Under the optimized conditions, consecutive analyses of the α-syn standard were repeatable in terms of migration time and peak area (%*RSD* (n = 3) were 0.9 and 5.6% at 100 $\mu g \cdot mL^{-1}$). The LOD was 20 $\mu g \cdot mL^{-1}$, better than the 50 $\mu g \cdot mL^{-1}$LOD by CE-MS using a BGE of 10 mM NH_4Ac (pH 7.0) and a sheath liquid of 60:40 (*v*/*v*) propan-2-ol/water with 0.25% (*v*/*v*) of HFor. These latter conditions are typically required to analyze proteins by IA-SPE-CE-MS.[12,13]

AA-SPE-CE-MS Optimization. The DNA aptamer MS-15 was selected to prepare the aptamer affinity (AA) sorbent because it has been described to selectively bind with high affinity to α-syn monomer.[32] In contrast to our previous studies by IA-SPE-CE-MS,[12,13] it was observed that in AA-SPE-CE-MS the AA sorbent was stable even using acidic BGEs. Sensitivity and repeatability were investigated with different combinations of BGE and sheath liquid (see below), using a basic volatile eluent of 100 mM NH_4OH (pH 11.2).[12,13] Using a sheath liquid of 60:40 (*v*/*v*) propan-2-ol/water with 0.05% (*v*/*v*) of HFor, a BGE of 100 mM HAc (pH 2.9) allowed obtaining similar peak areas to a BGE of 50 mM HAc:50 mM HFor (pH 2.3). However, in the second case, a slight decrease of peak areas was detected after consecutive injections, probably because of AA sorbent deterioration due to the lower pH value. Using the basic eluent, the acidic BGEs provided higher sensitivity than the BGEs of 10 mM NH_4Ac at pH 7.0, 8.0, or 9.0, even with a sheath liquid of 60:40 (*v*/*v*) propan-2-ol/water with an increased amount of HFor (i.e., 0.25% (*v*/*v*) of HFor). To confirm that no analyte was eluted under acidic conditions, BGEs of 10 mM NH_4Ac and an eluent of 100 mM HAc (pH 2.9) were tested, and no α-syn was detected. Therefore, the BGE of 100 mM HAc (pH 2.9) was selected for the rest of the experiments.

The investigation of the volatile eluents was extended, testing different hydroorganic mixtures in the presence or absence of 100 mM NH_4OH. First, acetonitrile:water mixtures at 40% and 80% (*v*/*v*) were tested to disrupt analyte-aptamer interaction.[14,23] However, these acetonitrile:water eluents were rapidly discarded because electropherograms and mass spectra were extremely poor, probably due to sorbent deterioration during the elution. Results with 60% (*v*/*v*) MeOH in the presence or absence of 100 mM NH_4OH were neither satisfactory as shown in Figure 2A. The best sensitivity and repeatability of peak areas and migration times were obtained with the aqueous basic eluent of100 mM NH_4OH (pH 11.2). A higher concentration than 100 mM of NH_4OH in the aqueous eluent was not tested to prevent aptamer denaturation and expand the sorbent lifetime. The volume of the eluent plug was investigated injecting the eluent at 50 mbar for 10, 20, and 40 s (50, 100, and 200 nL[35]). A higher amount of α-syn was detected injecting the eluent 20 s instead of 10 s. However, for the 40 s eluent injection, the analyte peak broadened, and peak area decreased. Between consecutive runs of a 10 $\mu g \cdot mL^{-1}$ α-syn standard solution, a small amount of α-syn was detected as carry-over when only rinsing with water between injections. Therefore, to prevent carry-over, the capillary was rinsed with water, a small plug of eluent, and again water between injections.

With regard to the sample loading, the standard solutions were prepared in water because lower peak areas were observed when using PBS, probably due to the smaller binding efficiency in a salty environment. The sample loading time was studied introducing a 1 $\mu g \cdot mL^{-1}$ α-syn standard solution at 930 mbar from 3 to 15 min. As can be seen in Figure 2B, the maximum amount of α-syn was detected at around 5 min. When loading for a longer time, the sample breakthrough volume was exceeded, and the α-syn washed away was higher than the amount retained, causing a significant decrease of peak area. Therefore, to reduce the total analysis time and to

DOI: 10.1021/acs.analchem.9b04802
Anal. Chem. 2020, 92, 1525−1533

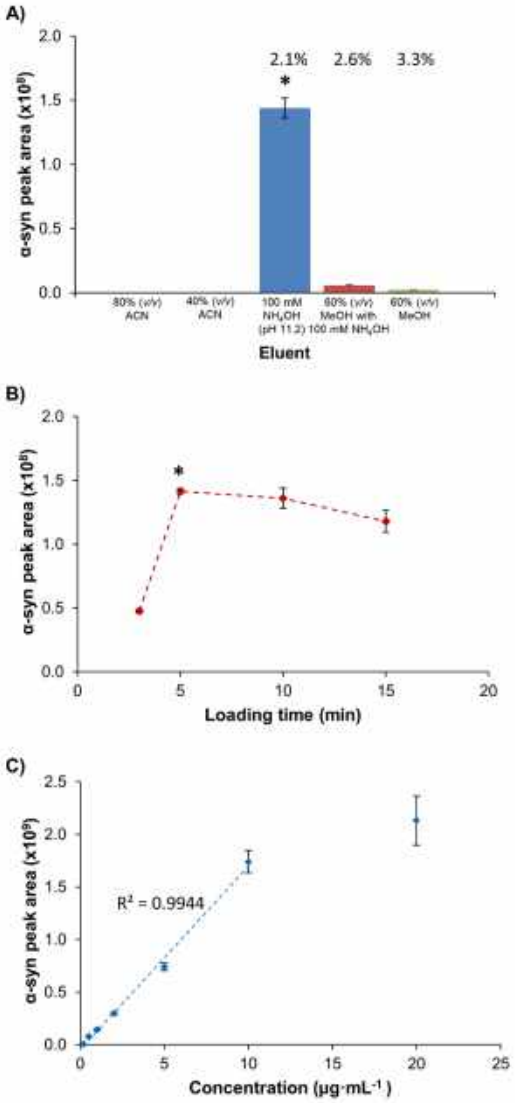

Figure 2. (A) Peak area of the detected α-syn for a 1 $\mu g \cdot mL^{-1}$ α-syn standard loaded for 5 min at 930 mbar in water by AA-SPE-CE-MS using different eluents and a BGE of 100 mM HAc (pH 2.9). (B) Plot of peak area of the detected α-syn vs loading time at 930 mbar (1 $\mu g \cdot mL^{-1}$ α-syn standard in water, using the optimized elution and separation conditions). (C) Plot of peak area of the detected α-syn vs concentration of the loaded standard solution, regression line, and R^2 value using the optimized loading, elution, and separation conditions. All measurements were performed in triplicate (standard deviation is given as error bars; %*RSD* for migration times is given in numbers). Optimized conditions are indicated in (A) and (B) with an asterisk.

obtain the highest recoveries, a sample loading time of 5 min was selected for the rest of the experiments.

Under the optimized conditions, consecutive analyses of the standard were repeatable in terms of migration time and peak area. At 1 $\mu g \cdot mL^{-1}$, the %*RSD*s (n = 3) were 2.1 and 5.4%, respectively, similar to the values in CE-MS. As can be seen in Figure 2C, the method was satisfactorily linear (R^2 > 0.994) between 0.5 and 10 $\mu g \cdot mL^{-1}$. The LOQ was 0.5 $\mu g \cdot mL^{-1}$, and the LOD was 0.2 $\mu g \cdot mL^{-1}$, which was an improvement of about 100 times compared to the CE-MS method. The lifetime of the microcartridges was around 20 analyses (at 1 $\mu g \cdot mL^{-1}$). As an example, Figure 1A shows the AA-SPE-CE-MS analysis of a 1 $\mu g \cdot mL^{-1}$ α-syn standard. Compared to CE-MS (Figures 1B, 1C and Table S-1), the mass spectrum and mass accuracy for experimental deconvoluted average M_r of free α-syn were similar (data not shown).

Analysis of α-Syn in Blood Samples. The AA-SPE-CE-MS method optimized with standards was applied to the analysis of blood. The concentration of α-syn has been shown to be higher in blood than in cerebrospinal fluid (CSF), and furthermore, drawing blood is less invasive than lumbar puncture to obtain CSF from patients.[29,30] More than 99% of the α-syn in human blood resides in the red blood cells (RBCs).[37] *N*-Terminal acetylation of proteins is a common occurrence, especially for those proteins initiated in Met residue, and this PTM of α-syn is the most abundant in blood and also in brain cytosol.[26]

A healthy control RBCs lysate was prepared, passed through a 0.20 μm nylon filter, and analyzed by CE-MS and AA-SPE-CE-MS. In both cases, was detected only hemoglobin (Hb) (Figure S-1 and Table S-2), which constitutes around 95% of the protein content in the RBCs.[38] Therefore, to analyze low abundant proteins (i.e., endogenous α-syn) it was necessary to study different pretreatments to remove the most abundant proteins from the RBCs lysate, reducing sample complexity and the dynamic concentration range of the proteins. Ethanol-chloroform extraction to deplete Hb from the RBCs lysate was tested as in our previous work to purify superoxide dismutase from RBCs lysates.[34] With this pretreatment, Hb quantitatively precipitated from the RBCs lysate because Hb was not detected in the analysis of both the organic and aqueous phases by CE-MS. However, both phases contained other high abundant proteins that interfered in α-syn detection. In the analysis by CE-MS and AA-SPE-CE-MS of both phases, ubiquitin and *N*-acetylated carbonic anhydrase 1 (CA-1) were detected but not α-syn (Figure S-2 and Table S-2). These results were consistent with the fact that ethanol-chloroform extraction has been also historically used to achieve quantitative removal of Hb in purification of carbonic anhydrases.[39] However, an alternative purification method was necessary for α-syn.

Taking into account that α-syn is a thermostable protein, and the solubility and the PTMs pattern of α-syn are not supposed to be altered upon heating,[27,31,40] the RBCs lysate was thermally treated to deplete nonthermostable proteins. With this pretreatment, both Hb and CA-1 were removed from the RBCs lysate, but endogenous α-syn was not detected by CE-MS. Only ubiquitin and apolipoprotein A-I, which were highly abundant in the RBCs,[38,41] were detected (Figure S-3 and Table S-2). With regard to the analysis of the TE RBCs lysate by AA-SPE-CE-MS (Figure 3), it was detected at around 14 min (Figure 3A) a protein with a deconvoluted M_r of 14,502.14 (Figure 3C), which is a highly consistent value with the expected average M_r for *N*-acetylated α-syn (M_r 14,502.06; Table S-1). In order to check if *N*-terminal acetylation of endogenous α-syn significantly affected the electrophoretic mobility of the protein and was causing the increase on migration time compared to the standard in water (~10 min increase), a TE RBCs lysate sample spiked with 0.3 $\mu g \cdot mL^{-1}$ of free α-syn standard was analyzed (recovery for free α-syn was 86%, by comparison of the AA-SPE-CE-MS analyses for the standard and the spiked sample at 0.3 $\mu g \cdot mL^{-1}$). As can be

DOI: 10.1021/acs.analchem.9b04802
Anal. Chem. 2020, 92, 1525−1533

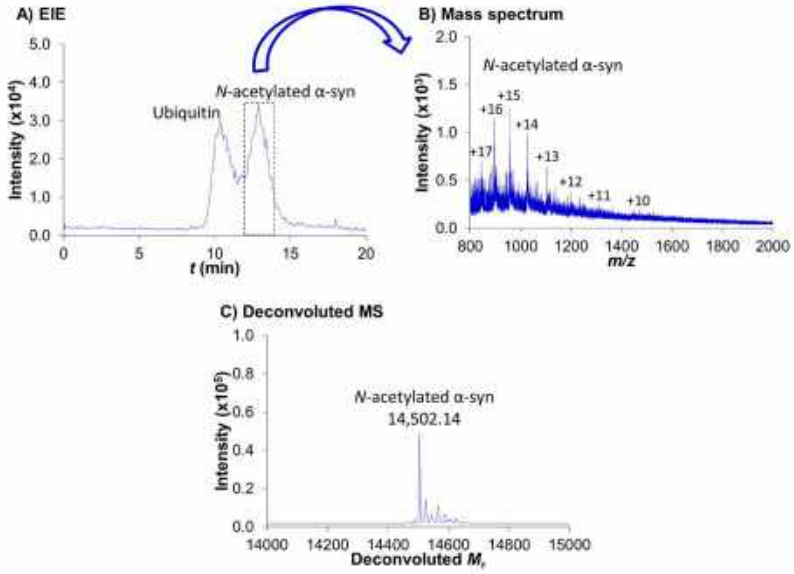

Figure 3. AA-SPE-CE-MS for a thermoenriched red blood cells (TE RBCs) lysate sample. (A) Extracted ion electropherogram (EIE), (B) mass spectrum of the boxed time region, and (C) deconvoluted mass spectrum. In addition to ubiquitin, very small amounts of apolipoprotein A-I were detected (see Figure S-4).

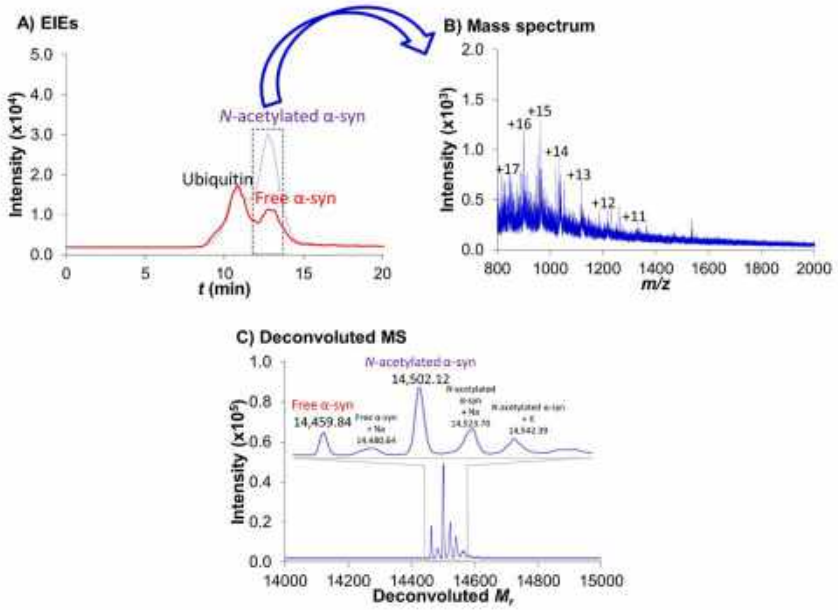

Figure 4. AA-SPE-CE-MS for a thermoenriched red blood cells (TE RBCs) lysate sample spiked with 0.3 $\mu g \cdot mL^{-1}$ of free α-syn standard. (A) Extracted ion electropherograms (EIEs) for *N*-acetylated α-syn (purple) and free α-syn (red), (B) mass spectrum of the boxed time region, and (C) deconvoluted mass spectrum (see the interpretation of the zoomed M_r region).

observed in Figure 4A, free α-syn and *N*-acetylated α-syn comigrated. However, the excellent mass accuracy and resolving power of the mass spectrometer allowed us to unambiguously identify both proteoforms in the deconvoluted mass spectrum of Figure 4C (ΔM_r = +42) and to obtain separate EIEs (Figure 4A). With regard to the migration time increase detected in TE RBCs lysates, it was probably due to the modification of the inner wall of the separation capillary induced during sample loading by the nonretained components of the complex sample matrix. This modification happened after the first analysis with a new microcartridge and was permanent, because repeatability was high (see the quality parameters below). Another proof of this permanent modification was that free α-syn was also detected at this increased migration time when a standard α-syn solution was analyzed after a TE RBCs lysate sample.

As can be also observed in Figures 3 and 4, *N*-acetylated α-syn slightly comigrated with ubiquitin, which was also retained

DOI: 10.1021/acs.analchem.9b04802
Anal. Chem. 2020, 92, 1525−1533

by the AA sorbent. In addition to ubiquitin, very small amounts of apolipoprotein A-I were detected (Figure S-4). Several experiments were made to investigate nonspecific adsorption on the AA sorbent. It is worth highlighting that compared to the typical aptamer- or antibody-based biosensors or bioassays, a great advantage of AA-SPE-CE-MS is that the electrophoretic separation and the selectivity of the MS detection prevent the possibility of a false positive or an erroneous quantification of the target protein in the presence of nonspecific adsorption. A microcartridge containing blank sorbent (i.e., activated and end-capped MBs, without aptamer) was tested by SPE-CE-MS. When loading a 1 $\mu g{\cdot}mL^{-1}$ α-syn standard solution a very small amount of α-syn was detected (6.4% compared to the AA sorbent). This suggested that nonspecific adsorption of α-syn was very limited because it was not efficiently retained by the end-capped sorbent without aptamer, hence also confirming that the aptamer was required for the binding of α-syn. In contrast, when the TE RBCs lysates were analyzed with the blank sorbent, only ubiquitin, in a similar amount to that observed by AA-SPE-CE-MS, was detected. To deplete ubiquitin from the TE RBCs lysate before the analysis by AA-SPE-CE-MS, the sample was incubated off-line with blank sorbent. However, no significant differences were observed. Results were also unsatisfactory in separate experiments, when a great concentration of off-target sequence single-stranded DNA (i.e., 200 nM) was added to the TE RBCs lysate for masking. Nonspecific adsorption of ubiquitin on the end-capped solid support was probably promoted by its high abundance in the TE RBCs lysate,[41] but a certain affinity to the α-syn aptamer could not be discarded. Once ruled out the possibility of reducing the amount of ubiquitin in the TE RBCs lysate, a 50 μm i.d. separation capillary was tested to improve the separation resolution between α-syn and ubiquitin. However, loading the TE RBCs lysate for AA-SPE-CE-MS promoted capillary blockage and current breakdowns during the separations, due to the complexity of the sample matrix and capillary narrowness. Therefore, the 75 μm i.d. separation capillary was necessary to analyze the TE RBCs. Under the optimized conditions, consecutive analyses of the TE RBCs lysate by AA-SPE-CE-MS were repeatable in terms of migration times and peak areas (%*RSDs* (n = 3) were 6.7 and 10.8%, respectively), and the lifetime of the microcartridges was halved (around 10 analyses) compared to standards due to the higher sample matrix complexity. The estimated concentration of the endogenous *N*-acetylated α-syn detected in the TE RBCs lysate was 0.6 $\mu g{\cdot}mL^{-1}$, calculated by comparison of the AA-SPE-CE-MS analyses for nonspiked and spiked samples with free α-syn standard at 0.3 $\mu g{\cdot}mL^{-1}$.

The developed AA-SPE-CE-MS method was applied to the analysis of TE RBCs lysate samples from blood of healthy controls and Parkinson's disease (PD) patients with stage III or IV of the disease. In both healthy controls and PD patients, ubiquitin and *N*-acetylated α-syn were detected but no other α-syn proteoforms, including PTMs or C-terminal truncated forms. To complement and validate the results at the intact protein level by AA-SPE-CE-MS and the limited information obtained about the most abundant proteins of the differently pretreated RBCs lysates by CE-MS without on-line AA-SPE (Table S-2), the TE RBCs lysate samples were digested with trypsin and analyzed by LC-Orbitrap-MS/MS. As can be seen in Table S-3, this bottom-up indirect approach provided more information, which resulted in the identification of 156 proteins in both groups of samples (no significant differences were found between PD patients and controls). The most relevant identified proteins in accordance to emPAI values were as follows: hemoglobin subunit alpha, *N*-acetylated α-syn, which was the only α-syn proteoform detected, apolipoprotein A-I, hemoglobin subunit beta, and apolipoprotein A-IV. Considering these results, the most probable form of the detected ubiquitin was ubiquitin-40S ribosomal protein S27a (P62979). Furthermore, it was confirmed the great complexity of the TE RBCs lysate, as well as that *N*-acetylated α-syn, was the main α-syn proteoform in RBCs. Therefore, the abundance of other minor proteoforms in RBCs from healthy controls and PD patients might be very low, in agreement with recent reports.[28,31] However, a larger set of samples must be analyzed to confirm this preliminary observation made from a small set of samples. At the moment, the presence of a high abundance of these typically very minor proteoforms has been only confirmed for phosphorylated α-syn at Ser-129 in LB deposited in the brain of patients with different synucleinopathies, including PD.[25,26]

CONCLUDING REMARKS

We have developed an on-line AA-SPE-CE-MS method for the purification, preconcentration, separation, and characterization of blood α-syn. Under the optimized conditions with standards, microcartridge lifetime (around 20 analyses/microcartridge) and repeatability (2.1 and 5.4%*RSD* for migration times and peak areas) were good, the method was linear between 0.5 and 10 $\mu g{\cdot}mL^{-1}$, and LOD was 0.2 $\mu g{\cdot}mL^{-1}$ (100 times lower than by CE-MS, 20 $\mu g{\cdot}mL^{-1}$). Regarding the analysis of blood samples, an off-line thermal pretreatment was necessary to remove the most abundant proteins in RBCs lysate. The AA-SPE-CE-MS method performed also reasonably well for the analysis of RBCs lysates despite the complexity of the sample matrix. However, repeatability was slightly smaller (%*RSDs* (n = 3) were 6.7 and 10.8% for migration times and peak areas, respectively), microcartridge lifetime was shorter (around 10 analyses/microcartridge), total analysis times increased 10 min, and nonspecific adsorption of mainly ubiquitin was observed. In view of the results achieved, because of the high affinity to bind to the target molecule and the improved tolerance to acidic and basic conditions, immobilized aptamers can be regarded as a powerful alternative to antibodies for SPE-CE-MS. With regard to the clinical implications of the case study, in the RBCs lysate *N*-acetylated α-syn was detected to be the main proteoform in healthy controls and stage III–IV PD patients, and no other minor proteoforms were detected. Therefore, no apparent alteration of blood α-syn proteoforms at the level of a few hundreds of $ng{\cdot}mL^{-1}$ seems to occur during PD. In the future, a larger set of blood samples could be analyzed to confirm this preliminary finding. Furthermore, the developed AA-SPE-CE-MS method could be applied to the analysis of α-syn from LBs isolated from the brain of patients with different synucleinopathies to screen for characteristic α-syn proteoforms.

ASSOCIATED CONTENT

Supporting Information

The Supporting Information is available free of charge at https://pubs.acs.org/doi/10.1021/acs.analchem.9b04802.

Preparation of RBCs lysates, optimized MS parameters, quality parameters, LC-Orbitrap-MS/MS analysis, M_r of detected proteins, AA-SPE-CE-MS for filtered RBCs

DOI: 10.1021/acs.analchem.9b04802
Anal. Chem. 2020, 92, 1525−1533

lysate and for ethanol-chloroform extracted RBCs lysate, CE-MS and AA-SPE-CE-MS for TE RBCs lysate (PDF)

Most relevant detected proteins in TE RBCs lysates after digestion with trypsin and LC-Orbitrap-MS/MS analysis (XLSX)

AUTHOR INFORMATION

Corresponding Author

*Phone: (+34) 934039116. Fax: (+34) 934021233. E-mail: fbenavente@ub.edu.

ORCID

Fernando Benavente: 0000-0002-1688-1477

Maxim V. Berezovski: 0000-0003-0514-599X

Notes

The authors declare no competing financial interest.

ACKNOWLEDGMENTS

This study was supported by a grant from the Spanish Ministry of Economy and Competitiveness (RTI2018-097411-B-I00) and the Cathedra UB Rector Francisco Buscarons Úbeda (Forensic Chemistry and Chemical Engineering). R.P.-G. acknowledges the Spanish Ministry of Education, Culture and Sport for a FPU (Formación del Profesorado Universitario) fellowship. M.V.B. thanks the NOVA DOMUS – CHEMEDPHO project funded by the Erasmus Mundus Action II of the European Commission and the Faculty of Chemistry of the UB for the travel grants. We thank Dr. Miguel Angel Vesga and Dr. Javier Ruiz Martínez from the node that the Basque Biobank has in Biodonostia for providing the blood samples from healthy controls and PD patients, respectively.

REFERENCES

(1) Faserl, K.; Sarg, B.; Gruber, P.; Lindner, H. H. *Electrophoresis* **2018**, *39*, 1208−1215.

(2) Qu, Y.; Sun, L.; Zhu, G.; Zhang, Z.; Peuchen, E. H.; Dovichi, N. J. *Talanta* **2018**, *179*, 22−27.

(3) Lubeckyj, R. A.; McCool, E. N.; Shen, X.; Kou, Q.; Liu, X.; Sun, L. *Anal. Chem.* **2017**, *89*, 12059−12067.

(4) Stolz, A.; Jooß, K.; Höcker, O.; Römer, J.; Schlecht, J.; Neusüß, C. *Electrophoresis* **2019**, *40*, 79−112.

(5) Šlampová, A.; Malá, Z.; Gebauer, P. *Electrophoresis* **2019**, *40*, 40−54.

(6) Breadmore, M. C.; Grochocki, W.; Kalsoom, U.; Alves, M. N.; Phung, S. C.; Rokh, M. T.; Cabot, J. M.; Ghiasvand, A.; Li, F.; Shallan, A. I.; et al. *Electrophoresis* **2019**, *40*, 17−39.

(7) Ramautar, R.; Somsen, G. W.; de Jong, G. J. *Electrophoresis* **2016**, *37*, 35−44.

(8) Benavente, F.; Medina-Casanellas, S.; Giménez, E.; Sanz-Nebot, V. In *Capillary Electrophoresis of Proteins and Peptides: Methods and Protocols*; Tran, N. T., Taverna, M., Eds.; Springer: New York, 2016; pp 67−84, DOI: 10.1007/978-1-4939-4014-1_6.

(9) Pont, L.; Pero-Gascon, R.; Gimenez, E.; Sanz-Nebot, V.; Benavente, F. *Anal. Chim. Acta* **2019**, *1079*, 1.

(10) Guzman, N. A.; Guzman, D. E. *J. Chromatogr. B: Anal. Technol. Biomed. Life Sci.* **2016**, *1021*, 14−29.

(11) Guzman, N. A.; Phillips, T. M. *Electrophoresis* **2011**, *32*, 1565−1578.

(12) Pont, L.; Benavente, F.; Barbosa, J.; Sanz-Nebot, V. *Talanta* **2017**, *170*, 224−232.

(13) Pero-Gascon, R.; Pont, L.; Benavente, F.; Barbosa, J.; Sanz-Nebot, V. *Electrophoresis* **2016**, *37*, 1220−1231.

(14) Marechal, A.; Jarrosson, F.; Randon, J.; Dugas, V.; Demesmay, C. *J. Chromatogr. A* **2015**, *1406*, 109−117.

(15) Gasilova, N.; Girault, H. H. *Anal. Chem.* **2014**, *86* (13), 6337−6345.

(16) Pichon, V.; Brothier, F.; Combès, A. *Anal. Bioanal. Chem.* **2015**, *407*, 681−698.

(17) Röthlisberger, P.; Gasse, C.; Hollenstein, M. *Int. J. Mol. Sci.* **2017**, *18*, 2430.

(18) Zamay, G. S.; Ivanchenko, T. I.; Zamay, T. N.; Grigorieva, V. L.; Glazyrin, Y. E.; Kolovskaya, O. S.; Garanzha, I. V.; Barinov, A. A.; Krat, A. V.; Mironov, G. G.; et al. *Mol. Ther.–Nucleic Acids* **2017**, *6*, 150−162.

(19) Zamay, G. S.; Zamay, T. N.; Kolovskii, V. A.; Shabanov, A. V.; Glazyrin, Y. E.; Veprintsev, D. V.; Krat, A. V.; Zamay, S. S.; Kolovskaya, O. S.; Gargaun, A.; et al. *Sci. Rep.* **2016**, *6*, 34350.

(20) Mairal, T.; Cengiz Özalp, V.; Lozano Sánchez, P.; Mir, M.; Katakis, I.; O'Sullivan, C. K. *Anal. Bioanal. Chem.* **2008**, *390* (4), 989−1007.

(21) Darmostuk, M.; Rimpelova, S.; Gbelcova, H.; Ruml, T. *Biotechnol. Adv.* **2015**, *33*, 1141−1161.

(22) Brothier, F.; Pichon, V. *Anal. Bioanal. Chem.* **2014**, *406*, 7875−7886.

(23) Du, F.; Alam, M. N.; Pawliszyn, J. *Anal. Chim. Acta* **2014**, *845*, 45−52.

(24) Perréard, C.; D'Orlyé, F.; Griveau, S.; Liu, B.; Bedioui, F.; Varenne, A. *Electrophoresis* **2017**, *38*, 2456−2461.

(25) Fujiwara, H.; Hasegawa, M.; Dohmae, N.; Kawashima, A.; Masliah, E.; Goldberg, M. S.; Shen, J.; Takio, K.; Iwatsubo, T. *Nat. Cell Biol.* **2002**, *4*, 160−164.

(26) Anderson, J. P.; Walker, D. E.; Goldstein, J. M.; De Laat, R.; Banducci, K.; Caccavello, R. J.; Barbour, R.; Huang, J.; Kling, K.; Lee, M.; et al. *J. Biol. Chem.* **2006**, *281*, 29739−29752.

(27) Miranda, H. V.; Xiang, W.; De Oliveira, R. M.; Simões, T.; Pimentel, J.; Klucken, J.; Penque, D.; Outeiro, T. F. *J. Neurochem.* **2013**, *126*, 673−684.

(28) Bergström, J.; Ingelsson, M. In *Immunotherapy and biomarkers in neurodegenerative disorders*; Ingelsson, M., Lannfelt, L., Eds.; Humana Press: New York, 2016; pp 215−234, DOI: 10.1007/978-1-4939-3560-4_14.

(29) Mollenhauer, B.; El-Agnaf, O. M.; Marcus, K.; Trenkwalder, C.; Schlossmacher, M. G. *Biomarkers Med.* **2010**, *4*, 683−699.

(30) Kasuga, K.; Nishizawa, M.; Ikeuchi, T. *Int. J. Alzheimer's Dis.* **2012**, *2012*, 437025.

(31) Miranda, H. V.; Cássio, R.; Correia-Guedes, L.; Gomes, M. A.; Chegão, A.; Miranda, E.; Soares, T.; Coelho, M.; Rosa, M. M.; Ferreira, J. J.; et al. *Sci. Rep.* **2017**, *7*, 13713.

(32) Tsukakoshi, K.; Harada, R.; Sode, K.; Ikebukuro, K. *Biotechnol. Lett.* **2010**, *32*, 643−648.

(33) Tsukakoshi, K.; Abe, K.; Sode, K.; Ikebukuro, K. *Anal. Chem.* **2012**, *84*, 5542−5547.

(34) Borges-Alvarez, M.; Benavente, F.; Barbosa, J.; Sanz-Nebot, V. *Electrophoresis* **2012**, *33*, 2561−2569.

(35) *High Performance Capillary Electrophoresis*, 2nd ed.; Lauer, H. H., Rozing, G. P., Eds.; Agilent Technologies: Waldbronn, Germany, 2014; pp 60−61.

(36) Pero-Gascon, R.; Pont, L.; Sanz-Nebot, V.; Benavente, F. In *Clinical Applications of Capillary Electrophoresis. Methods in Molecular Biology*; Phillips, T. M., Ed.; Humana Press: New York, NY, 2019; pp 57−76 DOI: 10.1007/978-1-4939-9213-3_5..

(37) Barbour, R.; Kling, K.; Anderson, J. P.; Banducci, K.; Cole, T.; Diep, L.; Fox, M.; Goldstein, J. M.; Soriano, F.; Seubert, P.; et al. *Neurodegener. Dis.* **2008**, *5*, 55−59.

(38) Ringrose, J. H.; Solinge Van, W. W.; Mohammed, S.; Flaherty, M. C. O.; Heck, A. J. R.; Slijper, M. *J. Proteome Res.* **2008**, *7*, 3060−3063.

(39) Chegwidden, W. R. In *The Carbonic Anhydrases*; Dodgson, S. J., Tashian, R. E., Gros, G., Carter, N. D., Eds.; Springer: Boston, 1991; pp 101−102, DOI: 10.1007/978-1-4899-0750-9_7.

(40) Park, S. M.; Jung, H. Y.; Chung, K. C.; Rhim, H.; Park, J. H.; Kim, J. *Biochemistry* **2002**, *41*, 4137−4146.

DOI: 10.1021/acs.analchem.9b04802
Anal. Chem. 2020, 92, 1525−1533

(41) Takada, K.; Nasu, H.; Hibi, N.; Tsukada, Y.; Shibasaki, T.; Fujise, K.; Fujimuro, M.; Sawada, H.; Yokosawa, H.; Ohkawa, K. *Clin. Chem.* **1997**, *43*, 1188−1195.

DOI: 10.1021/acs.analchem.9b04802
Anal. Chem. 2020, 92, 1525−1533

Supporting Information

Preparation of red blood cells (RBCs) lysates

Fresh blood was obtained by venipuncture and was collected into 4 mL BD Vacutainer® K_2EDTA Plus blood collection tubes (Plymouth, UK) to prevent coagulation. The plasma and the buffy coat were separated from the red blood cells (RBCs) by centrifugation at 500 g for 10 min at 4ºC. RBCs were aliquoted at 250 µL in Protein LoBind 1.5 mL Tubes (Eppendorf, Hamburg, Germany), and were washed three times with 250 µL of cold isotonic 0.1 M NaCl and centrifuged at 500 g for 5 min at 4ºC. Washed RBCs from healthy controls and PD patients were separately pooled, aliquoted and stored at -80ºC until further use. To obtain the RBCs lysate, 600 µL of ice-cold water was added to 200 µL of the washed RBCs. The mixture was shaken for 10 min, and centrifuged at 6000 g for 10 min at 4ºC. The supernatant (i.e. RBCs lysate) was collected and the membranes were discarded.

Optimized MS parameters

The TOF-MS parameters were optimized analyzing by CE-MS a 100 $\mu g \cdot mL^{-1}$ α-syn standard solution: capillary voltage 4000 V, drying gas temperature 300 ºC, drying gas flow rate 4 $L \cdot min^{-1}$, nebulizer gas 7 psig, fragmentor voltage 325 V, skimmer voltage 80 V, OCT 1 RF Vpp voltage 300 V. Data were collected in profile at 1 spectrum/s between 100 and 3200 *m/z*, with the mass range set to high resolution mode (4 GHz).

Quality parameters

All quality parameters were calculated from data obtained by measuring migration time (t_m) and peak area from the extracted ion electropherogram (EIE) of α-syn proteoforms (considering the *m/z* of the most abundant molecular ions, i.e. ions with charges *+16*, *+15*, *+14*, *+13*). Repeatability was evaluated as the percent relative standard deviation (%RSD) of t_m and peak areas. The LOD was obtained by analyzing low-concentration standard solution of α-syn (close to the LOD level, as determined from a S/N=3). LOQ was determined from a S/N=10. Linearity range was established by analyzing standard solutions of α-syn at concentrations between 0.2 and 20 $\mu g \cdot mL^{-1}$. The lifetimes of the microcartridges were investigated by repeatedly analyzing a 1 $\mu g \cdot mL^{-1}$ standard solution of α-syn and thermoenriched (TE) RBCs lysate samples. The microcartridge was discarded when the peak of α-syn in the EIE decreased more than 25% compared to the mean value of the first three analyses with the microcartridge under consideration.

LC-Orbitrap-MS/MS

One-hundred µL of TE RBCs lysate was evaporated to dryness using a Savant SPD-111 V SpeedVac concentrator (Thermo-Fisher Scientific, Waltham, MA, USA) and suspended in 100 µL of ice-cold extraction buffer (25 mM HEPES (pH 8.0), 1.5 M urea, 0.02% Triton X-100 and 5% (*v/v*) glycerol). The suspension was vortexed for 2 min and centrifuged for 30 s at 5000

g. Samples were reduced by addition of 3 mM tris(2-carboxyethyl)phosphine (TCEP) for 45 min at room temperature then alkylated with 15 mM iodoacetamide for 60 min in the dark at room temperature. Proteolytic digestion was performed by addition of 500 ng of Trypsin/Lis-C solution (Promega, Madison, Wisconsin, USA) and incubated under shaking at 500 rpm at ambient temperature overnight. The digestion was stopped by addition of formic acid (1% final concentration) and centrifuged at 15000 g for 2 minutes. The supernatant of digested proteins was desalted on disposable TopTip C-18 columns (Glygen, Columbia, MD, USA) and was evaporated to dryness.

All experiments were performed on an Orbitrap Fusion (Thermo Scientific) coupled to an Ultimate3000 nanoRLSC (Thermo Scientific). Protein digests were reconstituted in 10 µL of 70% acetonitrile (ACN)/ 0.1% formic acid and separated on an in-house packed column (15 cm x 75 µm i.d. x 365 µm o.d. fused silica capillary, Polymicro Technologies) packed with C18 particles (Luna C18(2), 3 µm, 100 Å, Phenomenex, Torrance, California, USA) using a water/ACN/0.1% formic acid linear gradient at a flow rate of 0.30 µL/min (0-7 min, 2-2% ACN; 7-77 min, 2-38% ACN; 77-86 min, 38-98% ACN; 86-96 min, 98-98% ACN; 96-99 min, 98-2% ACN; 99-109 min, 2-2% ACN). Two µL of sample were injected.

The Orbitrap-MS/MS parameters in ESI+ were as follows: ion source temperature 250 °C, ionspray voltage 2.1 kV, top speed mode, full-scan MS spectra (*m/z* 350–2000) acquired at a resolution of 60,000. Precursor ions were filtered according to monoisotopic precursor selection, charge state (*+2* to *+7*), and dynamic exclusion (30 s with a ± 10 ppm window). The automatic gain control settings were $4*10^5$ for full FTMS scans and $1*10^4$ for MS/MS scans. Fragmentation was performed with collision-induced dissociation (CID) in the linear ion trap. Precursors were isolated using a 2 *m/z* isolation window and fragmented with a normalized collision energy of 35%.

Proteome discoverer 2.1 (Thermo Scientific) was used for protein identification. The precursor mass tolerance was set at 20 ppm and 0.6 mass tolerance for fragment ions. Search engine: SEQUEST-HT implemented in Proteome Discovery was applied for all MS raw files. Search parameters were set to allow for dynamic modification of methionine oxidation, acetyl on N-terminus, phosphorylation on serine, threonine and tyrosine, nitration of tyrosine and cysteine carbamidomethylation. The search database consisted of a nonredundant human protein sequence FASTA file from the UniProt/SwissProt database. The false discovery rate (FDR) was set to 0.05 for both peptide and protein identifications.

Six digested TE RBCs lysate samples were analyzed with two replicates of each sample. Proteins identified with "low" or "medium" protein confidence values or detected in less than 9 of the 12 analyses were not reported.

Table S-1. Theoretical and deconvoluted average M_r for the detected α-syn proteoforms in recombinant human α-syn standard (CE-MS) and TE RBCs lysate (AA-SPE-CE-MS).

Sample	Detected α-syn proteoforms	Theoretical average M_r	Deconvoluted average M_r	
			Experimental	E_r[a] (ppm)
Recombinant human α-syn standard	Free α-syn	14,460.02	14,459.82	-14
TE RBCs lysate	*N*-acetylated α-syn	14,502.06	14,502.14	6

a) Relative error (E_r) was calculated in ppm as: (M_r exp – M_r theo)/M_r theo × 10^6 (exp = experimental and theo = theoretical). M_r exp was obtained as an average of three replicates.

Table S-2. Theoretical and deconvoluted average M_r for the detected proteins in pretreated RBCs lysates.

Abundant proteins detected	Uniprot accession number	Theoretical average M_r	Deconvoluted average M_r		Detected						
					CE-MS			AA-SPE-CE-MS			Blank SPE-CE-MS
			Experimental	E_r[a] (ppm)	Filtration	Ethanol-chloroform extraction	Thermo-enrichment	Filtration	Ethanol-chloroform extraction	Thermo-enrichment	Thermo-enrichment
Hemoglobin subunit alpha	P69905	15,126.20	15,126.29	6	X			X			
Hemoglobin subunit beta	P68871	15,867.05	15,866.67	-24	X			X			
Ubiquitin	P62979[b]	8564.76[c]	8564.91	17		X	X		X	X	X
N-acetylated carbonic anhydrase 1	P00915	28,780.75	28,780.78	1		X			X		
Apolipoprotein A-I	P02647	28,078.33	28,078.13	-7			X			X	
N-acetylated α-syn	P37840	14,502.06	14,502.14	6						X	

a) Relative error (E_r) was calculated in ppm as: $(M_r \text{ exp} - M_r \text{ theo})/M_r \text{ theo} \times 10^6$ (exp = experimental and theo = theoretical). M_r exp was obtained as an average of three replicates.

b) This Uniprot accession number corresponds to ubiquitin-40S ribosomal protein S27a and was assigned taking into account the results of the LC-Orbitrap-MS/MS analysis (see Table S-3).

c) This M_r value agrees with a fragment (1-76) of P62979 protein. This fragment is also found in Uniprot accession numbers P0CG47 (polyubiquitin-B), P0CG48 (polyubiquitin-C) and P62987 (ubiquitin-60S ribosomal protein L40).

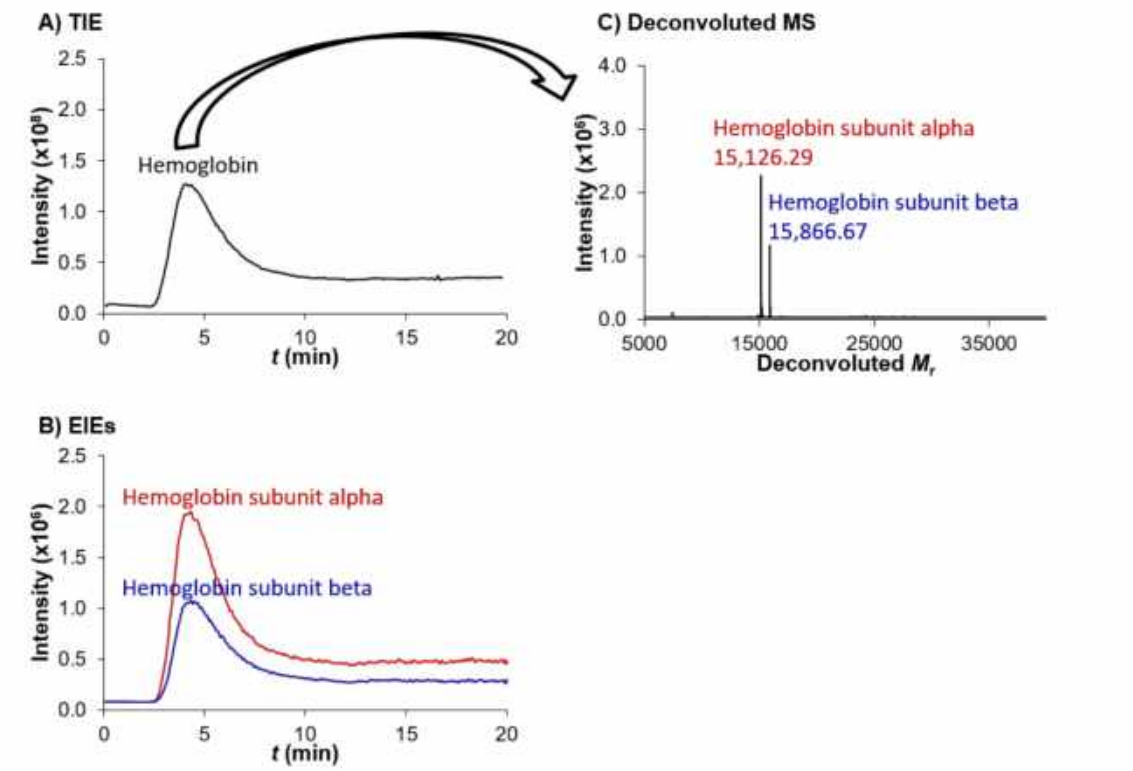

Figure S-1. AA-SPE-CE-MS for a filtered RBCs lysate. **(A)** Total ion electropherogram (TIE), **(B)** extracted ion electropherograms (EIEs), and **(C)** deconvoluted mass spectrum.

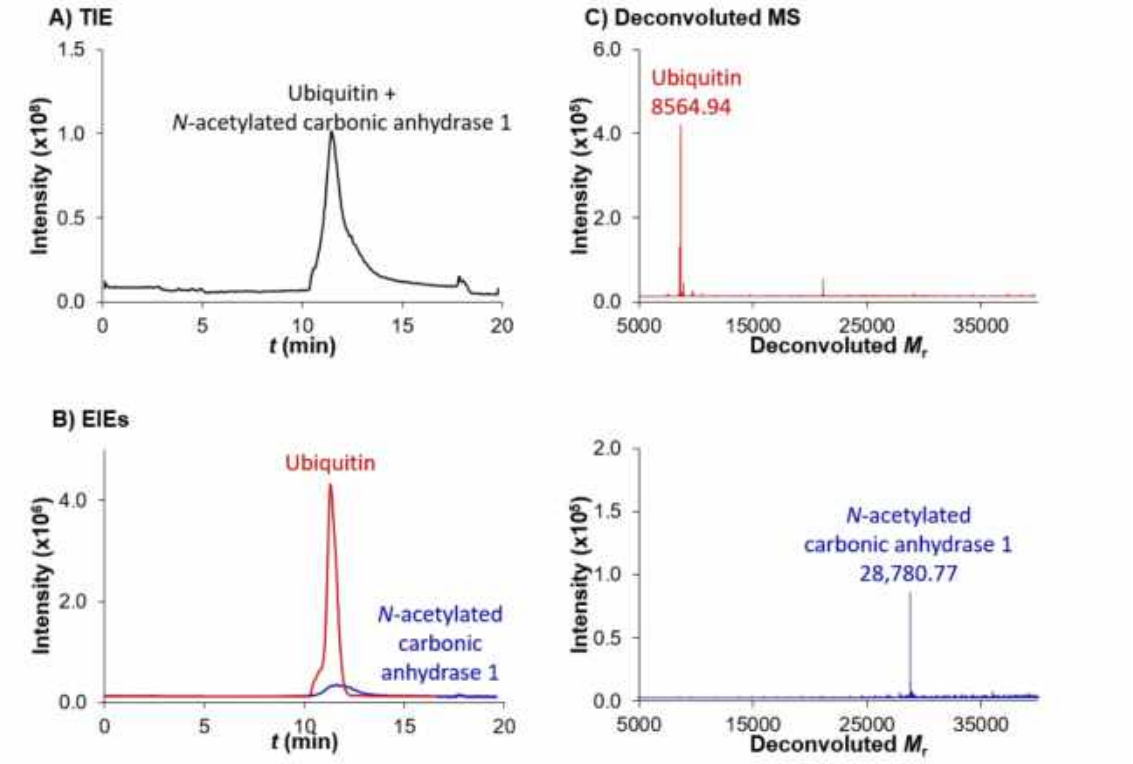

Figure S-2. AA-SPE-CE-MS for an ethanol-chloroform extracted RBCs lysate. **(A)** Total ion electropherogram (TIE), **(B)** extracted ion electropherograms (EIEs), and **(C)** deconvoluted mass spectra.

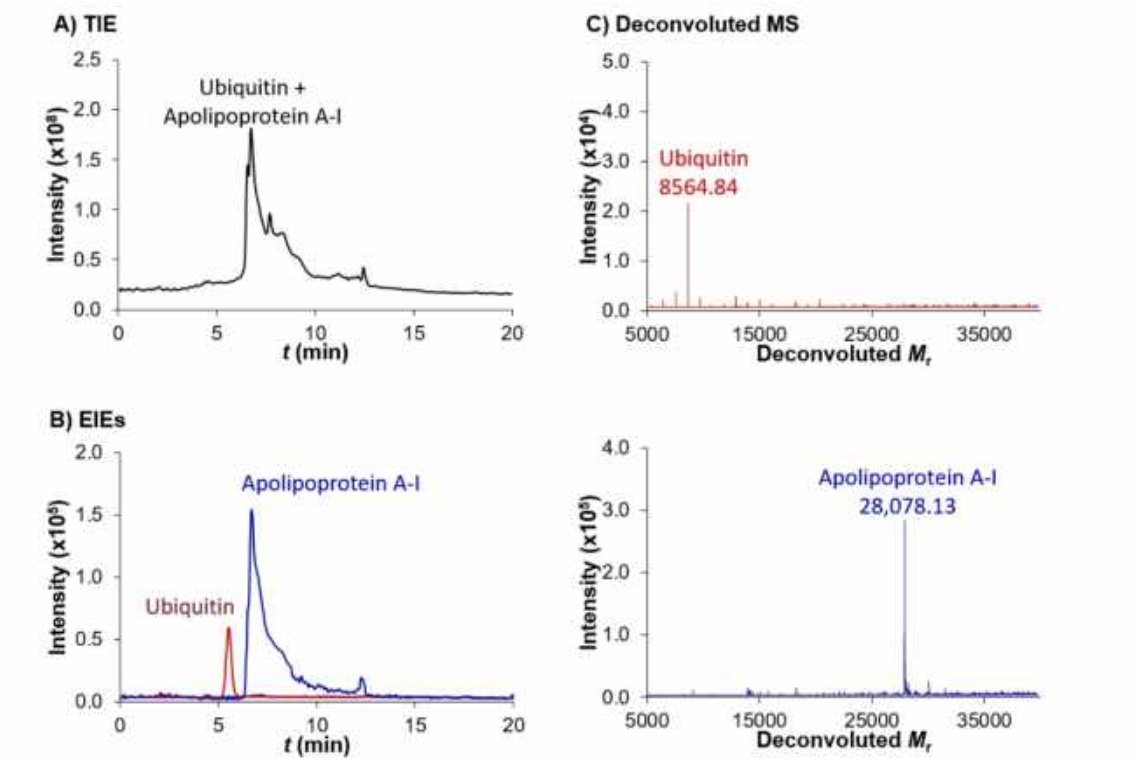

Figure S-3. CE-MS for a TE RBCs lysate. **(A)** Total ion electropherogram (TIE), **(B)** extracted ion electropherograms (EIEs), and **(C)** deconvoluted mass spectra.

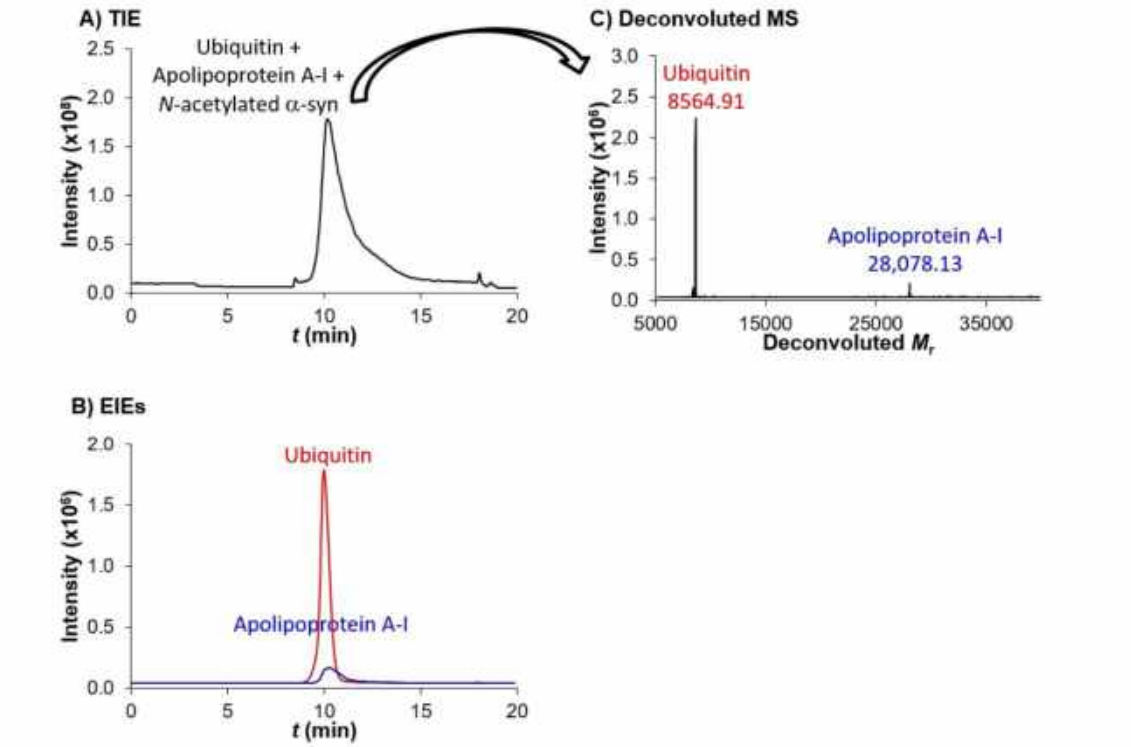

Figure S-4. AA-SPE-CE-MS for a TE RBCs lysate. **(A)** Total ion electropherogram (TIE), **(B)** extracted ion electropherograms (EIEs), and **(C)** deconvoluted mass spectrum. *N*-acetylated α-syn was also detected (see Figure 3).

Table S-3. Most relevant detected proteins in TE RBCs lysates after digestion with trypsin and LC-Orbitrap-MS/MS analysis.

Protein name	Uniprot accession number	PTMs	M, (x10^3)	Protein FDR Confidence	emPAI	Sum PEP Score	Coverage
Hemoglobin subunit alpha	P69905		15.2	High	3.16E+13	692.97	100.0
Alpha-synuclein	P37840	Acetyl [N-Term]	14.5	High	4.22E+09	429.92	100.0
Apolipoprotein A-I	P02647		30.8	High	1.25E+09	986.64	92.9
Hemoglobin subunit beta	P68871		16.0	High	2.85E+07	509.96	100.0
Apolipoprotein A-IV	P06727		45.4	High	2.28E+07	944.69	89.1
Haptoglobin	P00738		45.2	High	2.02E+07	882.80	78.8
Immunoglobulin kappa constant	P01834		11.8	High	3.98E+06	202.20	99.1
Apolipoprotein A-II	P02652		11.2	High	1.58E+06	138.46	74.0
Serum albumin	P02768		69.3	High	2.83E+05	1235.96	95.7
Superoxide dismutase [Cu-Zn]	P00441		15.9	High	1.21E+05	370.93	97.4
Alpha-1-antitrypsin	P01009		46.7	High	1.00E+05	686.32	72.0
Hemoglobin subunit delta	P02042		16.0	High	6.58E+04	268.94	100.0
Isoform 2 of Tropomyosin alpha-3 chain	P06753-2		29.0	High	4.64E+04	448.18	93.5
Immunoglobulin lambda constant 3	P0DOY3		11.3	High	1.00E+04	161.01	96.2
Immunoglobulin J chain	P01591		18.1	High	5.01E+03	189.28	76.1
Alpha-2-HS-glycoprotein	P02765		39.3	High	4.64E+03	397.49	58.9
Apolipoprotein C-II	P02655		11.3	High	3.98E+03	80.84	59.4
Alpha-1-acid glycoprotein 1	P02763		23.5	High	3.73E+03	270.64	69.7
Alpha-1-acid glycoprotein 2	P19652		23.6	High	3.73E+03	231.45	71.6
Tubulin-specific chaperone A	O75347		12.8	High	3.73E+03	121.54	80.6
Isoform 2 of Tropomyosin alpha-1 chain	P09493-2		26.7	High	3.38E+03	264.75	77.2
Isoform LMW of Kininogen-1	P01042-2		47.9	High	2.21E+03	526.90	78.7
Transthyretin	P02766		15.9	High	2.15E+03	180.90	73.5
Isoform 2 of Clusterin	P10909-2		57.8	High	1.82E+03	374.08	47.1
Alpha-1B-glycoprotein	P04217		54.2	High	1.73E+03	323.47	61.8
Ran-specific GTPase-activating protein	P43487		23.3	High	1.58E+03	146.71	72.6
SH3 domain-binding glutamic acid-rich-like protein 3	Q9H299		10.4	High	1.58E+03	62.26	94.6
Fibrinogen alpha chain	P02671		94.9	High	1.22E+03	738.95	43.3
Protein S100-A9	P06702		13.2	High	7.49E+02	97.80	91.2
Isoform 2 of Dematin	Q08495-2		43.1	High	6.57E+02	234.49	86.7
Zinc-alpha-2-glycoprotein	P25311		34.2	High	6.15E+02	263.33	64.8
Isoform 5 of Tropomyosin alpha-1 chain	P09493-5		28.4	High	5.92E+02	275.15	62.4
Apolipoprotein C-I	P02654		9.3	High	5.61E+02	35.74	32.5
Kininogen-1	P01042		71.9	High	5.53E+02	565.84	59.0
Platelet basic protein	P02775		13.9	High	5.17E+02	88.50	62.5
Peroxiredoxin-2	P32119		21.9	High	4.63E+02	154.05	90.4
Apolipoprotein C-III	P02656		10.8	High	4.63E+02	100.77	62.6
Ubiquitin-40S ribosomal protein S27a	P62979		18.0	High	4.32E+02	154.96	46.2
Tropomyosin alpha-3 chain	P06753		32.9	High	4.21E+02	292.64	60.4
Tropomyosin alpha-4 chain	P67936		28.5	High	3.72E+02	234.39	79.8
Calmodulin-3	P0DP25		16.8	High	1.99E+02	110.65	77.2

Thymosin beta-4	P62328		5.1	High	1.77E+02	43.50	54.5
26S proteasome non-ATPase regulatory subunit 9	O00233		24.7	High	1.51E+02	94.43	59.6
Immunoglobulin heavy constant alpha 1	P01876		37.6	High	1.46E+02	175.37	59.8
Apolipoprotein E	P02649		36.1	High	1.44E+02	241.43	79.5
Thioredoxin	P10599		11.7	High	1.38E+02	52.06	66.7
Isoform 2 of Cytochrome b5	P00167-2		11.3	High	1.32E+02	60.50	75.5
Lumican	P51884		38.4	High	1.14E+02	148.18	44.1
Leucine-rich alpha-2-glycoprotein	P02750		38.2	High	8.15E+01	220.77	57.9
Beta-2-glycoprotein 1	P02749		38.3	High	7.75E+01	156.39	63.2
Isoform 2 of Stathmin	P16949-2		19.8	High	7.40E+01	51.62	47.1
Histidine-rich glycoprotein	P04196		59.5	High	6.82E+01	184.59	44.6
Hemopexin	P02790		51.6	High	6.32E+01	190.28	50.2
Isoform Non-brain of Clathrin light chain A	P09496-2		23.6	High	6.21E+01	78.73	41.3
Carbonic anhydrase 1	P00915		28.9	High	5.31E+01	114.86	46.7
Immunoglobulin lambda-1 light chain	P0DOX8		22.8	High	4.54E+01	99.96	47.7
Hsc70-interacting protein	P50502	Acetyl [N-Term]	41.3	High	3.98E+01	106.95	40.7
Apolipoprotein D	P05090		21.3	High	3.06E+01	63.53	29.6
Programmed cell death protein 5	O14737		14.3	High	3.06E+01	59.05	60.8
Antithrombin-III	P01008		52.6	High	2.83E+01	170.51	55.0
Copper chaperone for superoxide dismutase	O14618		29.0	High	2.27E+01	94.88	58.0
Alpha-hemoglobin-stabilizing protein	Q9NZD4		11.8	High	2.05E+01	26.14	48.0
Isoform Non-brain of Clathrin light chain B	P09497-2		23.2	High	1.90E+01	49.93	33.2
Serum amyloid A-1 protein	P0DJI8		13.5	High	1.68E+01	50.25	75.4
Protein AMBP	P02760		39.0	High	1.57E+01	87.17	48.0
Complement factor I	P05156		65.7	High	1.48E+01	199.79	38.3
Uncharacterized protein C9orf40	Q8IXQ3		21.1	High	1.48E+01	60.65	56.7
Myosin light chain 4	P12829		21.6	High	1.09E+01	71.52	73.1
Fibrinogen gamma chain	P02679		51.5	High	1.07E+01	127.19	48.1
LIM and SH3 domain protein 1	Q14847		29.7	High	1.04E+01	78.12	45.2
Serotransferrin	P02787		77.0	High	9.53E+00	184.20	46.3
Complement factor H	P08603		139.0	High	9.34E+00	306.57	47.5
Protein S100-A4	P26447		11.7	High	9.00E+00	15.74	35.6
NSFL1 cofactor p47	Q9UNZ2		40.5	High	8.09E+00	97.24	46.8
Protein CDV3 homolog	Q9UKY7		27.3	High	7.48E+00	64.49	56.2
Hyaluronan-binding protein 2	Q14520		62.6	High	6.67E+00	98.22	21.1
SH3 domain-binding glutamic acid-rich-like protein	O75368		12.8	High	6.50E+00	38.94	37.7
Perilipin-3	O60664		47.0	High	6.36E+00	145.55	67.7
Isoform 2 of Nucleosome assembly protein 1-like 4	Q99733-2		44.1	High	6.20E+00	67.09	31.3
Protein/nucleic acid deglycase DJ-1	Q99497		19.9	High	6.02E+00	41.43	48.7
PEST proteolytic signal-containing nuclear protein	Q8WW12		18.9	High	5.81E+00	32.31	36.0
C4b-binding protein beta chain	P20851		28.3	High	5.49E+00	60.75	31.7
Isoform 2 of Eukaryotic translation initiation factor 5A-1	P63241-2		20.2	High	5.31E+00	37.69	27.7
Isoform 2 of Jupiter microtubule associated homolog 1	Q9UK76-2		19.9	High	5.31E+00	36.82	34.8

Charged multivesicular body protein 4b	Q9H444		24.9	High	5.11E+00	36.15	39.3
Fibrinogen beta chain	P02675		55.9	High	5.04E+00	108.11	43.4
Calcium-regulated heat-stable protein 1	Q9Y2V2		15.9	High	5.00E+00	18.51	44.2
Eukaryotic translation initiation factor 4B	P23588		69.1	High	4.82E+00	100.68	37.8
Carbonic anhydrase 2	P00918		29.2	High	4.82E+00	48.21	18.8
Isoform 2 of Charged multivesicular body protein 4a	Q9BY43-2		29.8	High	4.41E+00	44.39	23.0
Isoform 2 of Dynactin subunit 2	Q13561-2		44.8	High	4.38E+00	67.51	45.1
Protein 4.1	P11171		97.0	High	4.18E+00	153.43	25.6
Isoform 2 of L-selectin	P14151-2		43.6	High	3.87E+00	43.95	17.7
Prefoldin subunit 2	Q9UHV9		16.6	High	3.64E+00	30.91	52.6
Prefoldin subunit 6	O15212		14.6	High	3.64E+00	21.23	47.3
Vitronectin	P04004		54.3	High	3.49E+00	54.38	26.6
Myosin light polypeptide 6	P60660		16.9	High	3.33E+00	30.75	55.6
Eukaryotic translation initiation factor 4E-binding protein 1	Q13541		12.6	High	3.22E+00	17.13	62.7
Inter-alpha-trypsin inhibitor heavy chain H4	Q14624		103.3	High	3.17E+00	115.61	24.0
Heat shock protein beta-1	P04792		22.8	High	3.13E+00	28.25	49.3
Hepatoma-derived growth factor	P51858		26.8	High	2.88E+00	31.06	27.5
Catalase	P04040		59.7	High	2.77E+00	101.92	28.7
UV excision repair protein RAD23 homolog B	P54727		43.1	High	2.38E+00	39.51	22.7
Complement factor H-related protein 4	Q92496		65.3	High	2.36E+00	53.05	24.2
Triosephosphate isomerase	P60174		30.8	High	2.36E+00	38.37	48.6
Prothrombin	P00734		70.0	High	2.27E+00	102.34	30.1
Optineurin	Q96CV9		65.9	High	2.16E+00	73.46	31.4
Peptidyl-prolyl cis-trans isomerase A	P62937		18.0	High	2.16E+00	22.93	38.2
Low affinity immunoglobulin gamma Fc region receptor III-A	P08637		29.1	High	2.16E+00	21.32	16.9
Glutaredoxin-1	P35754		11.8	High	2.16E+00	9.30	18.9
Isoform 3 of Jupiter microtubule associated homolog 2	Q9H910-3	Acetyl [N-Term]	23.0	High	1.93E+00	24.93	43.6
Cadherin-5	P33151		87.5	High	1.87E+00	47.93	15.7
Isoform 4 of Extracellular matrix protein 1	Q16610-4		63.5	High	1.78E+00	57.28	39.9
DnaJ homolog subfamily B member 2	P25686		35.6	High	1.78E+00	39.90	32.1
Microtubule-associated protein RP/EB family member 1	Q15691		30.0	High	1.78E+00	32.47	23.1
Beta-adducin	P35612		80.8	High	1.70E+00	85.44	19.3
Hepatocyte growth factor activator	Q04756		70.6	High	1.66E+00	50.73	22.0
Y-box-binding protein 3	P16989		40.1	High	1.51E+00	34.11	37.1
Peptidase inhibitor 16	Q6UXB8		49.4	High	1.51E+00	28.03	12.5
Immunoglobulin kappa variable 2-40	A0A087WW87		13.3	High	1.51E+00	10.00	16.5
Vimentin	P08670		53.6	High	1.41E+00	46.70	28.3
Complement C1r subcomponent-like protein	Q9NZP8		53.5	High	1.35E+00	43.66	18.5
Plasma kallikrein	P03952		71.3	High	1.31E+00	55.85	20.2
Isoform 2 of Stress-induced-phosphoprotein 1	P31948-2		68.0	High	1.30E+00	73.76	26.4
Isoform 2 of Heterogeneous nuclear ribonucleoprotein K	P61978-2		51.0	High	1.15E+00	41.87	21.8
Tetranectin	P05452		22.5	High	1.15E+00	17.81	23.3
Afamin	P43652		69.0	High	1.04E+00	53.13	21.2

Complement C1r subcomponent	P00736		80.1	High	9.95E-01	44.80	13.2
Complement factor B	P00751		85.5	High	9.62E-01	43.21	13.9
Isoform 3 of Alpha-adducin	P35611-3		84.3	High	9.31E-01	29.07	10.5
Isoform 15 of Fibronectin	P02751-15		272.2	High	8.91E-01	114.09	13.2
Spectrin alpha chain, erythrocytic 1	P02549	Acetyl [N-Term]	279.8	High	8.48E-01	160.11	20.5
Actin, cytoplasmic 1	P60709		41.7	High	8.23E-01	19.41	10.4
Isoform Er3 of Ankyrin-1	P16157-5		203.3	High	8.08E-01	153.63	8.6
Apolipoprotein F	Q13790		35.4	High	7.78E-01	18.15	11.7
Isoform 3 of Vitamin D-binding protein	P02774-3		55.0	High	7.11E-01	31.54	17.4
Coagulation factor X	P00742		54.7	High	6.10E-01	17.47	6.8
Coiled-coil domain-containing protein 124	Q96CT7		25.8	High	5.85E-01	11.61	20.2
Alpha-2-macroglobulin	P01023		163.2	High	5.67E-01	67.20	9.0
Coagulation factor IX	P00740		51.7	High	5.62E-01	22.85	7.2
TSC22 domain family protein 4	Q9Y3Q8		41.0	High	5.20E-01	24.96	18.2
Complement C4-A	P0C0L4		192.7	High	5.03E-01	70.71	8.2
Serine/threonine-protein phosphatase 6 regulatory subunit 1	Q9UPN7		96.7	High	4.25E-01	26.93	13.6
Moesin	P26038		67.8	High	4.01E-01	18.15	11.6
Attractin	O75882		158.4	High	3.96E-01	51.79	10.2
Myosin-9	P35579		226.4	High	3.55E-01	70.35	11.4
(E3-independent) E2 ubiquitin-conjugating enzyme	Q9C0C9		141.2	High	3.16E-01	28.19	8.2
CD44 antigen	P16070		81.5	High	3.11E-01	18.65	4.7
Isoform 6 of Serine/threonine-protein kinase WNK1	Q9H4A3-7		299.5	High	2.92E-01	38.60	3.3
Isoform 2 of Immunoglobulin heavy constant mu	P01871-2		51.9	High	2.69E-01	9.11	7.4
Complement C3	P01024		187.0	High	2.62E-01	32.56	8.8
Protein FAM114A2	Q9NRY5		55.4	High	2.33E-01	8.72	7.7
Proteoglycan 4	Q92954		151.0	High	1.66E-01	25.66	5.8
Apolipoprotein(a)	P08519		501.0	High	1.39E-01	45.78	39.0
Isoform 2 of Spectrin beta chain, erythrocytic	P11277-2		267.7	High	1.09E-01	24.49	2.9
Tensin-1	Q9HBL0		185.6	High	1.00E-01	14.72	2.9

Microchemical Journal 157 (2020) 105013

Contents lists available at ScienceDirect

Microchemical Journal

journal homepage: www.elsevier.com/locate/microc

Enrichment of histidine containing peptides by on-line immobilised metal affinity solid-phase extraction capillary electrophoresis-mass spectrometry

Roger Pero-Gascon, Estela Giménez*, Victoria Sanz-Nebot, Fernando Benavente

Department of Chemical Engineering and Analytical Chemistry, Institute for Research on Nutrition and Food Safety (INSA·UB), University of Barcelona, Martí i Franquès 1-11, 08028 Barcelona, Spain

ARTICLE INFO

Keywords:
Capillary electrophoresis
Histidine
Immobilised metal affinity
Mass spectrometry
On-line solid-phase extraction
Peptides

ABSTRACT

The analysis and detection of targeted peptides has received due attention in many fields of proteomics research, such as discovery of biomarkers. In this regard, capillary electrophoresis-mass spectrometry (CE-MS) is widely used, however, direct analysis of low-abundance peptides such as histidine-containing peptides (His-peptides) in complex matrixes by CE-MS remains an analytical challenge. In the present study, an immobilised metal affinity solid-phase extraction containing Ni(II) coupled on-line to capillary electrophoresis-mass spectrometry (IMA-SPE-CE-MS) method has been developed to selectively enrich His-peptides from protein tryptic digests and enhance sensitivity. The method was optimised with α-casein and validated with other standard proteins (β-casein and κ-casein). Later, it was applied to an Escherichia Coli (*E. Coli*) whole cell lysate. IMA-SPE-CE-MS was very selective and allowed an enrichment factor up to 100-fold. The on-line enrichment and separation method coupled to MS detection is straightforward and advantageous over off-line pretreatment methods in terms of simplicity, cost-effectiveness and throughput.

1. Introduction

In proteomics, depletion of the most abundant proteins is recommended to reduce sample complexity and identify low-abundance proteins that usually provide more biologically and clinically relevant information. Among the proposed bottom-up strategies, the isolation of a subproteome based on the enrichment of peptides containing less abundant amino acids such as cysteine, histidine, methionine or tryptophan has always been of great interest [1,2]. In the case of histidine, it is present in the sequence of 85–95% of all the proteins in human and yeast proteomes, but only in 15–20% of the peptides that can be generated from these proteins after tryptic digestion [1,2]. Hence, the analysis of histidine containing peptides (His-peptides) from enzymatic digests enables to simplify the peptide mixture while keeping a significant coverage of the proteome accessible to quantification [3–6]. This could be an important complement to the comprehensive bottom-up proteomics studies supported by state-of-the-art high-end MS instruments, especially when specific parts of the protein structure need to be targeted.

Immobilised metal affinity (IMA) sorbents have been often used in off-line solid-phase extraction (SPE) for the selective enrichment of His-peptides before liquid chromatography-mass spectrometry (LC-MS) analysis [7,8]. In particular, pretreatment of enzymatic digests by IMA-SPE is regarded as an interesting approach to improve accuracy in quantitative proteomics because it is a simple and effective strategy to decrease sample complexity, hence reducing both interference and ion suppression effects in LC-MS analysis [5,6]. The choice of the metal ion immobilised on the support depends on the peptide to be purified. In the case of His-peptides, the most used are divalent cations such as Cu (II) and Ni(II) with iminodiacetic acid (IDA) as chelating ligand [4–11]. The on-line coupling of SPE to LC-MS allows minimising sample handling and increasing analysis throughput but require complex instrumental set-ups with valves, which are especially delicate when working in capillary or nano LC [12]. On-line solid-phase extraction capillary electrophoresis-mass spectrometry (SPE-CE-MS) can be regarded as an excellent alternative for automated sample clean-up and sensitive analyses [13–16]. In the typical SPE-CE-MS configuration, which is valve-free, a microcartridge filled with a sorbent that selectively retains the target analytes, is integrated in-line near the inlet of the separation capillary [15]. After loading a large sample volume (~50–100 μL), retained compounds are eluted into the separation capillary with a small volume of a suitable solution (~50 nL) before separation and detection by CE-MS. Reversed-phase sorbents (e.g., C18) have been preferentially used to analyse peptides by SPE-CE-MS [13–15]. Immobilised metal affinity solid-phase extraction capillary electrophoresis (IMA-SPE-CE) has been mostly demonstrated with UV

* Corresponding author.
E-mail address: estelagimenez@ub.edu (E. Giménez).

https://doi.org/10.1016/j.microc.2020.105013
Received 29 March 2020; Received in revised form 8 May 2020; Accepted 9 May 2020
Available online 12 May 2020
0026-265X/

detection [17–20]. IMA-SPE-CE-MS has been explored to a lesser extent [21–23]. So far, only Cao et al have demonstrated the analysis of phosphopeptides from complex protein digests by IMA-SPE-CE-MS with a Fe(III) sorbent [21,22]. More recently, we successfully established a IMA-SPE-CE-MS method with a Ni(II) sorbent for the analysis of β-amyloid peptides as model compounds with histidine residues in standards, plasma and serum samples [23].

In the present work, the potential of IMA-SPE-CE-MS with a Ni(II) sorbent is investigated to selectively enrich His-peptides from complex protein digests. The method was first optimised with tryptic digests of α-casein (α-CSN), and then its applicability was further validated with β-casein (β-CSN) and κ-casein (κ-CSN) digests and a digest of an Escherichia Coli (*E. Coli*) whole cell lysate containing a 6x-His tagged protein.

2. Materials and methods

2.1. Chemicals

All chemicals used in the preparation of buffers and solutions were of analytical reagent grade. Acetic acid (HAc, glacial), formic acid (HFor, 98–100%), sodium hydroxide, phosphoric acid (85%) and ammonium hydroxide (25%) were supplied by Merck (Darmstadt, Germany). DL-Dithiothreitol (DTT, ≥99%), iodoacetamide (IAA, ≥98%), imidazole (99.5%) and ammonium hydrogen carbonate (≥99.9%) were purchased from Sigma-Aldrich (St. Louis, MO, USA). Isopropanol was provided by Scharlab (Barcelona, Spain) while acetonitrile and water by Sigma-Aldrich (all of them of LC-MS quality grade). Trypsin (sequencing grade modified, 16,000 U·mg^{-1}) and chymotrypsin were purchased from Promega (Madison, WI, USA). ESI low concentration (ESI-L) tuning mix was supplied by Agilent Technologies (Waldbronn, Germany) for tuning and calibration of the mass spectrometer.

2.2. Protein samples

α-Casein (α-CSN, 70%), β-casein (β-CSN, 90%) and κ-casein (κ-CSN, ≥80%) were obtained from Sigma-Aldrich. Stock solutions of 1000 μg·mL^{-1} were prepared in water and aliquoted. Aliquots were evaporated to dryness using a Savant SPD-111V SpeedVac concentrator (Thermo-Fisher Scientific, Waltham, MA, USA) and stored at −20 °C until enzymatic digestion.

Escherichia Coli positive control whole cell lysate - expressing 6X His tag protein was obtained from Abcam (Cambridge, UK). The whole cell lysate of *E. Coli* contained 250 μg of total protein. The content of the vial was dissolved in water to obtain a 1000 μg·mL^{-1} protein solution. Excipients of low-molecular mass were removed by ultracentrifugation using Microcon YM-10 centrifugal filters from Millipore (Mr cut-off 10,000, Bedford, MA, USA) [24]. Centrifugations were carried out in a Mikro 20 centrifuge (Hettich, Tuttligen, Germany) at 25 °C. Finally, aliquots of 1000 μg·mL^{-1} of *E. Coli* whole cell lysate were evaporated to dryness by SpeedVac and stored at −20 °C until enzymatic digestion.

κ-Casein and *E. Coli* whole cell lysate were firstly reduced and alkylated to facilitate digestion. Briefly, an aliquot of 100 μg of dried protein was dissolved in 100 μL of 50 mM NH_4HCO_3 (pH 7.9) and 2.5 μL of 0.5 M DTT in the same buffer was added. The mixture was incubated in a TS-100 thermoshaker (Biosan, Riga, Latvian Republic) at 56 °C for 30 min and then alkylated by adding 7 μL of 0.73 M IAA (in the same buffer) and shaking for 30 min at room temperature in the dark. Excess of low-molecular mass reagents was removed with Microcon YM-10 centrifugal filters as described in [24]. The final protein residue was dissolved in 50 mM NH_4HCO_3 (pH 7.9) to obtain a final concentration of 1000 μg·mL^{-1}.

A 100 μL aliquot of 1000 μg·mL^{-1} protein solution in 50 mM NH_4HCO_3 (pH 7.9) was digested. Trypsin was added in an enzyme to protein ratio of 1:40 m/m. In the case of trypsin:chymotrypsin digestion, chymotrypsin was added simultaneously at 1:25 m/m. The mixture was vortexed and subsequently incubated at 37 °C for 18 h. Digestions were stopped by heating at 100 °C for 10 min, and the digest was evaporated to dryness by SpeedVac and stored at −20 °C until analysis. All digestions were performed in triplicate.

2.3. CE-MS

CE-MS experiments were performed in a 7100 CE system coupled to a 6220 oa-TOF LC/MS mass spectrometer with an orthogonal sheath-flow interface (Agilent Technologies). The sheath liquid was delivered at a flow rate of 3.3 μL·min^{-1} by a KD Scientific 100 series infusion pump (Holliston, MS, USA) and degassed for 10 min by sonication before use. CE control and separation data acquisition (e.g., voltage, temperature and current) were performed using Chemstation software (Agilent Technologies) that was running in combination with the MassHunter workstation software (Agilent Technologies) for control, data acquisition and processing of the mass spectrometer. The mass spectrometer was tuned and calibrated following the manufacturer's instructions. The operational conditions in positive electrospray ionization (ESI) mode were: capillary voltage 4000 V, drying gas (N_2) temperature 200 °C, drying gas flow rate 4 L·min^{-1}, nebuliser gas (N_2) 7 psig, fragmentor voltage 190 V, skimmer voltage 60 V and OCT 1 RF Vpp voltage 300 V. Data were collected in profile (continuum) at 1 spectrum·s^{-1} (approx. 10,000 transients·spectrum^{-1}) between m/z 100 and 3200 working in the highest resolution mode (4 GHz).

The extracted ion electropherogram of each peptide was obtained considering the theoretical m/z of the molecular ions and a mass tolerance window of 20 ppm. Mass spectra were checked manually to verify the isotopic distribution and accurate identification (mass error < 10 ppm).

A bare fused-silica capillary of 72 cm total length (L_T) × 75 μm internal diameter (i.d.) × 360 μm outer diameter (o.d.) (Polymicro Technologies, Phoenix, AZ, USA) was used in CE-MS. Activation and conditioning procedures were carried out off-line in order to avoid contamination with NaOH of the mass spectrometer. New capillaries were activated by flushing (930 mbar) sequentially for 30 min each with 1 M NaOH, water and background electrolyte (BGE). Samples were reconstituted in water and injected at 50 mbar for 15 s (approximately 80 nL, i.e., 2.5% of the capillary, estimated using the Hagen–Poiseuille equation [25]. This volume corresponds to 4 ng of protein for a 50 μg·mL^{-1} protein digest). Electrophoretic separations were performed at 25 °C and +15 kV (normal polarity: cathode in the outlet). Between runs, capillaries were flushed with water (1 min), 1 M HAc (3 min), water (1 min) and BGE (5 min). Before CE-MS, all solutions were passed through a 0.22-μm nylon filter (MSI, Westboro, MS, USA).

Two BGEs were used for the analysis of the protein digests: an acidic BGE of 50 mM HFor and 50 mM HAc (pH 2.2) with a sheath liquid of 60:40 (v/v) iPrOH:H_2O with 0.05% (v/v) of HFor, and a neutral BGE of 25 mM H_3PO_4 (adjusted to pH 7.5 with ammonium hydroxide) with a sheath liquid of 60:40 (v/v) iPrOH:H_2O with 0.5% (v/v) of HFor.

pH measurements were carried out with a Crison 2002 potentiometer and a Crison electrode 52–03 (Crison instruments, Barcelona, Spain).

2.4. SPE-CE-MS

A HisLink™ protein purification resin obtained from Promega (Madison, WI, USA) was used as immobilised metal affinity sorbent. It was made of 100 μm silica particles derivatised with nitrilotriacetic acid (NTA), which contained a high level of tetradentate-chelated Ni(II). Construction of the particle-packed microcartridge with frits for IMA-SPE-CE-MS was carried out as described elsewhere with little modifications [23]. Bare fused silica capillaries (Polymicro Technologies) were used for all the procedures. The microcartridge (0.7 cm L_T × 250 μm

i.d. × 365 μm o.d. capillary) was inserted at 7.5 cm from the inlet of the separation capillary (72 cm L_T × 75 μm i.d. × 365 μm o.d., activated as in CE-MS) using two plastic sleeves (Tygon® tube of 250 μm i.d., Thermo-Fisher Scientific). Previously the microcartridge was filled by vacuum with the IMA sorbent that was retained between two microfrits placed on each end of the microcartridge. These microfrits were obtained from the material of the original frits found in conventional C_{18} cartridges for SPE (Sep-Pack, Waters, Milford, MA, USA). As no glue was necessary to prevent microcartridge leaking, the microcartridge could be replaced to reuse the separation capillary.

The BGE for the IMA-SPE-CE-MS separation was the neutral BGE of 25 mM H_3PO_4 (adjusted to pH 7.5 with ammonium hydroxide) and the sheath liquid solution was the same as in CE-MS. Under the optimised conditions, the IMA-SPE-CE capillaries were first conditioned by applying pressure at 930 mbar (flush pressure) for 2 min with BGE. Afterwards, samples reconstituted in BGE and diluted to the desired concentration were loaded by flushing for 10 min (approximately 60 μL [25]). A final flush for 2 min with BGE was used for washing and removing non-specifically retained molecules. All these steps were performed with the nebuliser gas and the ESI capillary voltage switched off to prevent the introduction of contaminants into the MS. Then, both were switched on and a small volume of eluent (0.5% HAc) was injected at 50 mbar for 75 s (approximately 0.4 μL [25]). In order to prevent the eluent plug from traveling backwards due to the microcartridge back-pressure, BGE was also injected at 25 mbar for 150 s. Separation was conducted at + 15 kV for 40 min (cathode in the outlet). Post-conditioning to avoid carryover was performed by flushing for 1 min with 50 mM imidazole and 1 min of water. This postconditioning step was also performed switching off the nebulizer gas and the ESI capillary voltage. IMA-SPE-CE-MS columns were filled with water when they were stored overnight to avoid salt precipitation.

3. Results and discussion

A number of studies have taken advantage of the affinity selection of His-peptides with Cu(II)-IMA sorbents before LC-MS to reduce sample complexity and simplify identification of proteins in bottom-up proteomics, and virtually all these purification methods were off-line [3–6,9,10]. Very few studies have also explored the potential of off-line Ni(II)-IMA sorbents to preconcentrate His-peptides before LC-MS [11]. These Cu(II)- and Ni(II)-IMA sorbents typically contain IDA, which is a tridentate metal chelating agent. In general, it is well-known that chelating agents with a higher number of coordination sites prevent metal leaking because the sorbent become more stable at the expense of a weaker interaction with the target compounds [7,8]. In a previous study a Ni(II) sorbent with the tetradentate metal chelating agent NTA gave the best results in terms of reproducibility and sensitivity enhancement for the analysis by IMA-SPE-CE-MS of β-amyloid peptides, which contained histidine residues, in standards, plasma and serum samples [23]. In the present work, the potential of this Ni(II)-NTA sorbent was investigated to selectively enrich His-peptides from complex protein digests by IMA-SPE-CE-MS.

3.1. Analysis of His-peptides of α-CSN

With the aim of establishing a robust and reliable method to analyse His-peptides in complex protein digests, α-casein (α-CSN) was chosen as model protein because tryptic digestion yields a significant number of easily detected and well-characterised His-peptides. First, the coverage of peptides and, specifically His-peptides, in the tryptic digest of α-CSN was mapped by CE-MS using an acidic BGE (50 mM HFor and 50 mM HAc, pH 2.2) and a sheath liquid of iPrOH:H_2O (60:40, with 0.05% HFor). Based on the manufacturer information, α-CSN consists of two isoforms, i.e., α-CSN1 (23.7 kDa) and α-CSN2 (25.3 kDa), and α-CSN1 shows the highest abundance (80% *versus* 20% m/m, respectively in skim milk [26]). Table 1 shows the His-peptide sequences expected after trypsin digestion for α-CSN predicted by the PeptideMass tool from ExPASy (https://web.expasy.org/peptide_mass/). Additionally, Tables S1 and S2 show the peptide sequences expected after trypsin digestion of α-CSN, the theoretical m/z of the molecular ions and the peptides detected by CE-MS (and IMA-SPE-CE-MS). Fig. 1a shows the extracted ion electropherograms (EIEs) of the detected non-histidine containing peptides (non-His peptides; in black) and His-peptides (in colours) in the α-CSN digest using the acidic BGE. Under these conditions, at a protein concentration of 50 $\mu g \cdot mL^{-1}$, 17 non-His peptides from 35 (i.e., the total sum of α-CSN1 and α-CSN2 non-His peptides) were detected by CE-MS (48.6% of coverage). In the case of the His-peptides, 7 from 8 (i.e., the total sum of α-CSN1 and α-CSN2 His-peptides) were detected (87.5% of coverage): the 5 expected His-peptides for α-CSN1 and 2 out of 3 for α-CSN2. The α-CSN2 phosphorylated peptide [2–21] was the only His-peptide not detected, probably due to the lower ionization efficiency promoted by the presence of the phosphate groups and the relatively low-abundance of α-CSN2 in comparison to α-CSN1. Acidic BGEs with HAc or HFor are highly recommended for optimum detection sensitivity of peptides by CE-MS in positive ion mode [27]. However, acidic pH solutions promote metal ion leakage from the IMA sorbent in IMA-SPE-CE-MS. Hence, a neutral low ionic strength phosphate BGE (25 mM H_3PO_4, pH 7.5) was also evaluated by CE-MS, despite the lower volatility of phosphate solutions, as was the one which gave the best results for IMA-SPE-CE-MS in our previous study [23]. Fig. 1b shows the EIEs of the non-His peptides and His-peptides of α-CSN detected by CE-MS using this neutral BGE. As can be seen, peaks were slightly wider due to the longer migration times promoted by the lower global molecular charge that was not counterbalanced by the increase in the electroosmotic flow at pH 7.5. Furthermore, sensitivity was slightly lower and thus, the coverages of the non-His peptides and His-peptides decreased (37.1% and 75%, respectively, see also Tables S1 and S2).

Once analysed α-CSN digest by CE-MS, the coverage for the non-His peptides and for the His-peptides was evaluated by IMA-SPE-CE-MS. The eluent composition and volume were optimised in our previous study [23]. In order to ensure the elution of the His-peptides from the Ni(II)-NTA sorbent and to obtain an adequate repeatability, eluent injection at 50 mbar for 75 s was required. When decreasing the amount of HAc or the injection time (e.g., 0.1% HAc or 50 s, respectively), elution of the His-peptides was incomplete and repeatability decreased, as was previously observed with β-amyloid peptides [23]. Fig. 1c shows the EIEs of the non-His peptides and His-peptides detected by IMA-SPE-CE-MS in a 50 $\mu g \cdot mL^{-1}$ tryptic digest. As can be observed, only 2 non-His peptides (α-CSN1[1–3] and α-CSN2[189–197]) from a total of 35 were detected (5.7% of coverage). In contrast, 5 His-peptides from a total of 8 (62.5% of coverage) were detected (3 out of 5 and 2 out of 3 for α-CSN1 and α-CSN2, respectively), which demonstrated the selectivity of the methodology for the analysis of His-peptides (see Fig. 1c or Tables S1 and S2). With respect to the mass spectra of the His-peptides, the neutral BGE did not promote formation of peptide-phosphate adducts and protonated adducts were the most abundant as with the acidic BGE. To improve sensitivity and increase the His-peptide coverage, sample loading time was investigated loading the 50 $\mu g \cdot mL^{-1}$ α-CSN digest for 5, 10, 20 and 30 min at 930 mbar (Fig. 2a). For loading times up to 10 min, His-peptides peak area improved when the loading time increased, as expected due to the greater volume of sample loaded. However, longer loading times than 10 min did not favour detecting a larger number of His-peptides. In addition, the sample breakthrough volume was exceeded and peak areas decreased because the amounts of His-peptides washed away were higher than the amounts retained. Therefore, to obtain the best enrichment factors, a loading time of 10 min was selected for the rest of the experiments. The coverage and linearity of IMA-SPE-CE-MS was also studied analysing α-CSN tryptic digests at concentrations from 20 to 100 $\mu g \cdot mL^{-1}$. At 100 $\mu g \cdot mL^{-1}$ the coverage was the same as for 50 $\mu g \cdot mL^{-1}$. In contrast, at 20 $\mu g \cdot mL^{-1}$, only one His-peptide (α-CSN1[4–7]) was detected, with very low

Table 1
Sequence of the His-peptides expected after trypsin and trypsin:chymotrypsin digestion for α-CSN, β-CSN and κ-CSN predicted by the PeptideMass tool from ExPASy (https://web.expasy.org/peptide_mass/). His residues in His-peptides are marked in bold.

Protein		Trypsin		Trypsin:chymotrypsin
α-CSN1	[4–7]	**H**PIK	[4–7]	**H**PIK
	[8–22]	HQGLPQEVLNENLLR	[8–22]	HQGLPQEVLNENLLR
	[80–83]	**H**IQK	[80–83]	**H**IQK
	[120–124]	LHSMK	[120–124]	LHSMK
	[125–132]	EGI**H**AQQK	[125–132]	EGI**H**AQQK
α-CSN2	[2–21]	NTME**H**VSSSEESII**S**QETYK	[2–20]	NTME**H**VSSSEESII**S**QETY
	[77–80]	**H**YQK	[77–78]	**H**Y
	[182–188]	TVYQ**H**QK	[185–188]	Q**H**QK
β-CSN	[49–97]	I**H**PFAQTQSLVYPFPGPIPNSLPQNIPPLTQTPVVVPPFLQPEVMGVSK	[49–52]	I**H**PF
	[106–107]	**H**K	[106–107]	**H**K
	[114–169]	YPVEPFTESQSLTLTDVENL**H**LPLPLLQSWM**H**QP**H**QPLPPTVMFPPQSVLSLSQSK	[120–143]	TESQSLTLTDVENL**H**LPLPLLQSW
			[144–169]	M**H**QP**H**QPLPPTVMFPPQSVLSLSQSK
κ-CSN	[98–111]	**H**PH**P**H**L**SFMAIPPK	[98–105]	**H**PH**P**H**L**SF

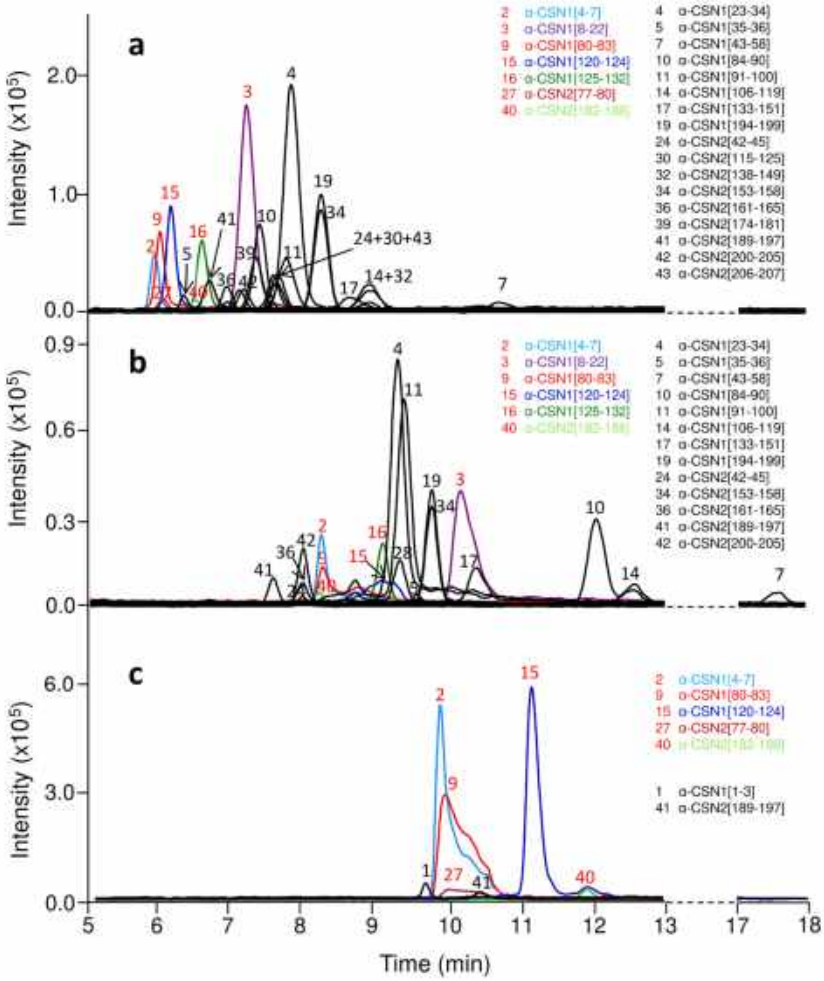

Fig. 1. Extracted ion electropherograms for the analysis of a 50 μg·mL^{-1} α-CSN tryptic digest by CE-MS using (A) an acidic BGE (50 mM HFor and 50 mM HAc (pH 2.2)) and (B) a neutral BGE (25 mM H_3PO_4 (adjusted to pH 7.5)), and (C) by IMA-SPE-CE-MS (BGE: 25 mM H_3PO_4 (adjusted to pH 7.5)).

intensity. Taking into account this His-peptide, the method was linear between 20 and 100 μg·mL^{-1} (R^2 > 0.98).

Consecutive analyses of the α-CSN digest were repeatable in terms of migration time and peak area (%*RSD* (n = 3) were < 3.0 and < 11% at 50 μg·mL^{-1}, respectively). The average lifetime of a microcartridge was 9 consecutive analyses (see supplementary Fig. S1). It was established by repeatedly analysing the 50 μg·mL^{-1} α-CSN tryptic digest until the peak areas for the His-peptides in the EIEs decreased more than 40% compared to the mean value of the first three analyses with the microcartridge under consideration.

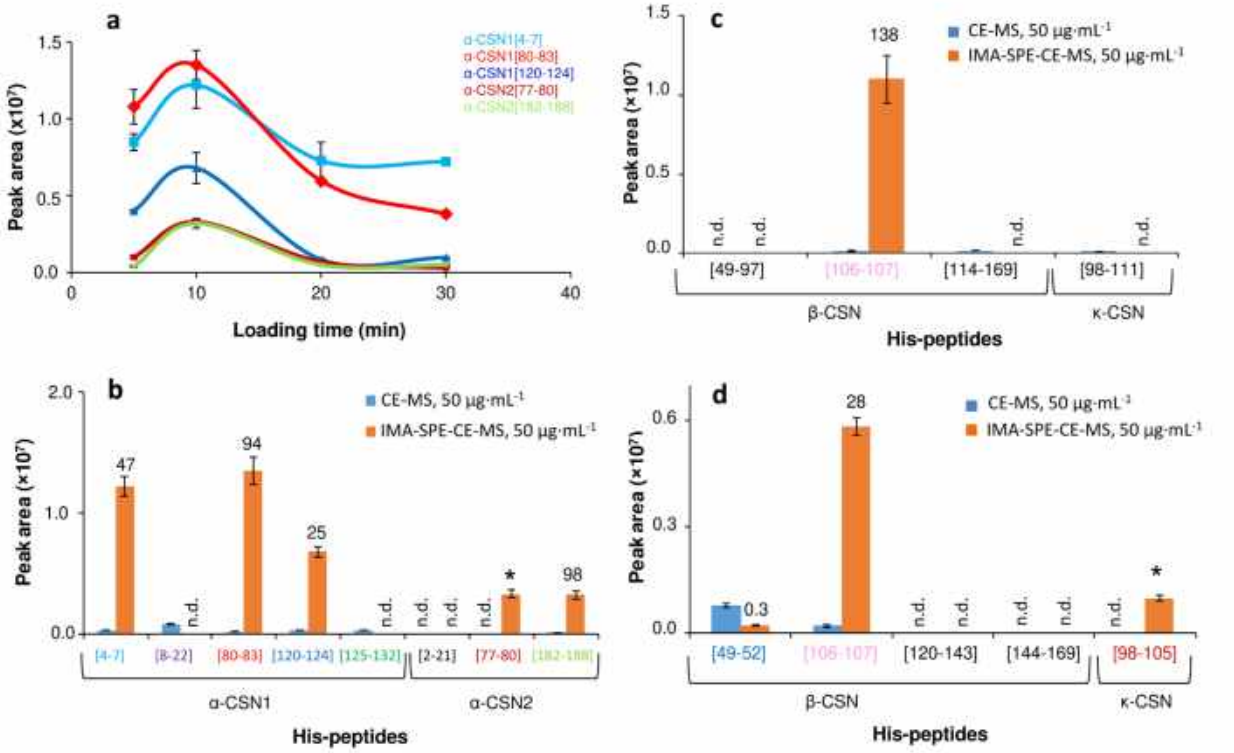

Fig. 2. Analysis of a 50 μg·mL^{-1} α-CSN tryptic digest. (A) Plot of His-peptides peak area vs loading time at 930 mbar for IMA-SPE-CE-MS. (B) Comparison of His-peptides peak areas for CE-MS and IMA-SPE-CE-MS (BGE: 25 mM H_3PO_4 (adjusted to pH 7.5) in both cases). Analysis of 50 μg·mL^{-1} β-CSN and κ-CSN tryptic digests. Comparison of His-peptides peak areas for CE-MS and IMA-SPE-CE-MS (BGE: 25 mM H_3PO_4 (adjusted to pH 7.5) in both cases). Digestion with (C) trypsin and (D) trypsin:chymotrypsin. Preconcentration factor is given in numbers. The asterisk indicates that the preconcentration factor was not calculated because the His-peptide was not detected (n.d.) by CE-MS. Standard deviation is given as error bars (n = 3).

The enrichment performance of IMA-SPE-CE-MS was examined with a 50 μg·mL^{-1} α-CSN digest. The graphic bar of Fig. 2b shows a comparison of the His-peptides peak area values obtained by CE-MS with the neutral BGE (Fig. 1b) and by IMA-SPE-CE-MS (Fig. 1c), and the corresponding preconcentration factors achieved. As can be observed, most His-peptides showed an increase in peak area by IMA-SPE-CE-MS, allowing detection of a short His-peptide (i.e., α-CSN2[77–80]), which was not detected by CE-MS. In contrast, His-peptides α-CSN1[8–22] and α-CSN1[125–132] were not detected by IMA-SPE-CE-MS probably due to its larger sequence and the position of the His residue (see the expected His-peptide sequences in Table 1). In addition to the sequence length, the number, accessibility and microenvironment of histidine residues may also be important in determining retention by the chelated metal [23,28]. Globally a lower coverage of His-peptides was achieved by IMA-SPE-CE-MS compared to CE-MS (5 His-peptides detected *versus* 6), but preconcentration factors from 25 to 98 were obtained for those detected, demonstrating the potential of the IMA sorbent to selectively target His-peptides, which are less abundant in the proteomes [1,2].

3.2. Analysis of His-peptides of other model proteins

To further validate the performance of the IMA-SPE-CE-MS method to selectively enrich His-peptides from protein digests, the method was also applied to the analysis of other standard proteins: β-casein (β-CSN) and κ-casein (κ-CSN) and it was compared to the analysis by CE-MS. Fig. 2c shows a graphic bar with the expected His-peptides and the peak area of those detected by CE-MS with the neutral BGE and IMA-SPE-CE-MS, when analysing tryptic digests of β-CSN and κ-CSN at 50 μg·mL^{-1}. In contrast to our previous results with α-CSN, after His-peptide enrichment, no non-His peptides were detected and the overall number of detected His-peptides was significantly reduced with regard to CE-MS. While 3 His-peptides from a total of 4 were detected by CE-MS, only the His-peptide [106–107] of β-CSN was detected by IMA-SPE-CE-MS. This was probably due to the length of the His-peptides that were, in general, larger in these tryptic digests than in the α-CSN digest (see Table 1). To study the influence of the peptide length in the retention of the IMA sorbent, β-CSN and κ-CSN were also digested with a mixture of trypsin and chymotrypsin. Table 1 shows the expected His-peptide sequences after trypsin and chymotrypsin digestion for β-CSN and κ-CSN. As can be observed in Fig. 2d, after digestion with trypsin:chymotrypsin, the number of His-peptides detected by IMA-SPE-CE-MS increased compared to CE-MS (60% *versus* 40% of the His-peptide coverage). Therefore, the reduction of the length of most of the His-peptides (see the sequences in Table 1) confirmed the selectivity of the IMA sorbent towards short His-peptides.

3.3. Analysis of E. Coli whole cell lysate

A whole cell lysate of *E. Coli* was analysed to explore the potential of the established methodology to selectively enrich His-peptides from complex and diluted biological samples. A whole cell lysate of *E. Coli* that expresses human α-lactalbumin with six additional histidine amino acids (6x-His) at its C-terminus was selected [29,30], which is typically used for quality control of purification of His-tagged proteins or as positive control for Western blots of 6x-His tagged protein samples. As in previous studies by LC-MS/MS [29] and CE-MS [30], 6x-His human α-lactalbumin, myoglobin C, cathepsin D, creatine kinase-MM and

Table 2
Detected peptides and identified proteins in the *E. Coli* whole cell lysate tryptic digest by CE-MS (1000 μg·mL^{-1}, BGE: 50 mM HFor:50 mM HAc, pH 2.2) and by IMA-SPE-CE-MS (50 μg·mL^{-1}, BGE: 25 mM H_3PO_4 (adjusted to pH 7.5)). His residues in His-peptides are marked in bold.

Identified protein*	CE-MS (1000 μg mL^{-1}, acidic BGE)		IMA-SPE-CE-MS (50 μg mL^{-1}, neutral BGE)	
6x-His tagged α-lactalbumin (M_r ~ 14 kDa)	[2–5] QFTK	[109–114] ALCTEK	[123–129] LH**HHHHH**	
Myoglobin C (M_r ~ 17 kDa)	[43–45] FDK	[48–50] H**L**K	[48–50] H**L**K	[97–98] H**K**
Creatine kinase-MM (M_r ~ 43 kDa)	[1–9] MPFGNTHNK	[149–151] GER	[26–32] HNNH**M**AK	
	[26–32] HNNH**M**AK	[173–177] YYPLK	[106–107] H**K**	
	[42–43] LR	[267–292] AGH**P**FMWNQHLGYVLTCPSNLGTGLR	[305–307] H**P**K	
	[44–45] DK	[315–316] LR		
	[131–132] VR	[317–319] LQK		
	[133–135] TGR	[359–365] LMVEMEK		
	[136–138] SIK	[367–369] LEK		
Cathepsin D (M_r ~ 38 kDa)	[110–112] VER	[278–281] LGGK		
	[113–120] QVFGEATK	[282–284] GYK		
	[131–141] FDGILGMAYPR	[285–293] LSPEDYTLK		
	[190–192] YYK	[294–299] VSQAGK		
	[246–249] ELQK	[340–347] VGFAEAAR		
Antithrombin III (M_r ~ 49 kDa)	[14–24] DIPMNPMCIYR	[223–226] GLWK		
	[48–53] VWELSK	[237–241] ELFYK		
	[54–57] ANSR	[263–275] VAEGTQVLELPFK		
	[140–145] LVSANR	[351–359] LPGIVAGR		
	[146–150] LFGDK	[394–399] SLNPNR		
	[177–183] ENAEQSR			
	[184–188] AAINK			

* Peptide and protein identification was based on the intact molecular ions of the detected peptides and on previous studies by LC-MS/MS [28] and CE-MS [29].

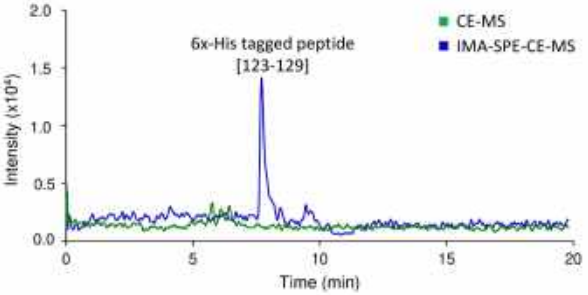

Fig. 3. Extracted ion electropherograms of the 6x-His tagged peptide of human α-lactalbumin ([123–129]) in the *E. Coli* whole cell lysate tryptic digest by CE-MS (1000 μg·mL^{-1}, BGE: 50 mM HFor and 50 mM HAc, pH 2.2) (green) and by IMA-SPE-CE-MS (50 μg·mL^{-1}, BGE: 25 mM H_3PO_4 (adjusted to pH 7.5)) (blue). (For interpretation of the references to colour in this figure legend, the reader is referred to the web version of this article.)

antithrombin III were identified by CE-MS and only the 6x-His tagged protein and those proteins producing short His-peptides were identified by IMA-SPE-CE-MS (i.e., 6x-His human α-lactalbumin, myoglobin and creatine kinase-MM). Table 2 shows the sequence of the peptides and His-peptides detected in the lysate tryptic digest (1000 μg·mL^{-1}) by CE-MS using the acidic BGE and by IMA-SPE-CE-MS using the neutral BGE (50 μg·mL^{-1}). The findings by IMA-SPE-CE-MS demonstrated the selectivity of the methodology towards short His-peptides, which could be useful to specifically map certain regions of the proteomes. Moreover, the detection of the 6x-His tagged peptide of α-lactalbumin ([123–129]) only by IMA-SPE-CE-MS (see Fig. 3) indicate a possible additional application in the on-line preconcentration of intact His-tagged proteins or other His-tagged compounds such lipids [31] or carbohydrates [32]. J. Partyka et al recently reported improved sensitivity in CE-MS for the analysis of oligosaccharides and N-linked glycans using multicharged labeling by 6x-His tags [32]. Better limits of detection could be further achieved analysing these labelled carbohydrates by IMA-SPE-CE-MS.

4. Conclusions

We have developed an on-line IMA-SPE-CE-MS method to selectively enrich His-peptides from protein tryptic digests using a Ni (II)-NTA IMA sorbent. The method was evaluated and validated with tryptic digests of α-CSN, β-CSN and κ-CSN. The selectivity of the IMA sorbent towards short His-peptides was confirmed when casein proteins were digested with a mixture of trypsin and chymotrypsin. Preconcentration factors for the detected His-peptides ranged between 25 and 100 times, and the IMA-SPE microcartridges could be used up to 9 analyses with good repeatability of migration times and peak areas (% *RSD* < 3.0 and < 11%, respectively). The good performance of the IMA-SPE-CE-MS method was also demonstrated with an *E. coli* cell lysate, which indicated the great potential of this approach to reduce sample complexity in proteomics compared to off-line sample pretreatment methods, ensuring simplicity, cost-effectiveness and throughput.

CRediT authorship contribution statement

Roger Pero-Gascon: Methodology, Investigation, Visualization, Writing - original draft. **Estela Giménez:** Conceptualization, Supervision, Visualization, Writing - original draft, Writing - review & editing. **Victoria Sanz-Nebot:** Writing - review & editing, Project administration, Funding acquisition. **Fernando Benavente:** Conceptualization, Supervision, Writing - review & editing, Project administration, Funding acquisition.

Acknowledgments

This study was supported by a grant from the Spanish Ministry of Economy and Competitiveness (RTI2018-097411-B-I00) and the Cathedra UB Rector Francisco Buscarons Ubeda (Forensic Chemistry and Chemical Engineering). Roger Pero-Gascon acknowledges the Spanish Ministry of Education, Culture and Sport for a FPU (Formación del Profesorado Universitario) fellowship.

Appendix A. Supplementary data

Supplementary data to this article can be found online at https://doi.org/10.1016/j.microc.2020.105013.

References

[1] H. Zhang, W. Yan, R. Aebersold, Chemical probes and tandem mass spectrometry: A strategy for the quantitative analysis of proteomes and subproteomes, Curr. Opin. Chem. Biol. 8 (2004) 66–75, https://doi.org/10.1016/j.cbpa.2003.12.001.

[2] F.E. Regnier, L. Riggs, R. Zhang, L. Xiong, P. Liu, A. Chakraborty, E. Seeley, C. Sioma, R.A. Thompson, Comparative proteomics based on stable isotope labeling and affinity selection, J. Mass Spectrom. 37 (2002) 133–145, https://doi.org/10.1002/jms.290.

[3] S. Wang, X. Zhang, F.E. Regnier, Quantitative proteomics strategy involving the selection of peptides containing both cysteine and histidine from tryptic digests of cell lysates, J. Chromatogr. A. 949 (2002) 153–162, https://doi.org/10.1016/S0021-9673(01)01509-6.

[4] R.R. Prasanna, S. Sidhik, A.S. Kamalanathan, K. Bhagavatula, M.A. Vijayalakshmi, Affinity selection of histidine-containing peptides using metal chelate methacrylate monolithic disk for targeted LC-MS/MS approach in high-throughput proteomics, J. Chromatogr. B Anal. Technol. Biomed, Life Sci. 955–956 (2014) 42–49, https://doi.org/10.1016/j.jchromb.2014.02.020.

[5] C. Mesmin, B. Domon, Improvement of the performance of targeted LC-MS assays through enrichment of histidine-containing peptides, J. Proteome Res. 13 (2014) 6160–6168, https://doi.org/10.1021/pr5008152.

[6] J. Yang, F. Tian, M. Zhang, Y. Zhao, X. Qian, Y. Cai, W. Ying, Targeted histidine-peptide enrichment improved the accuracy of isobaric-based quantitative proteomics, Anal. Methods. 8 (2016) 5255–5261, https://doi.org/10.1039/c6ay00332j.

[7] D. Todorova, M.A. Vijayalakshmi, Immobilized metal-ion affinity chromatography, in: D.S. Hage (Ed.), Handb. Affin. Chromatogr., 1, Taylor & Francis, Boca Raton, FL, 2006, pp. 257–280.

[8] R.C.F. Cheung, J.H. Wong, T.B. Ng, Immobilized metal ion affinity chromatography: a review on its applications, Appl. Microbiol. Biotechnol. 96 (2012) 1411–1420, https://doi.org/10.1007/s00253-012-4587-0.

[9] D. Ren, N.A. Penner, B.E. Slentz, H.D. Inerowicz, M. Rybalko, F.E. Regnier, Contributions of commercial sorbents to the selectivity in immobilized metal affinity chromatography with Cu(II), J. Chromatogr. A. 1031 (2004) 87–92, https://doi.org/10.1016/j.chroma.2003.10.041.

[10] D. Ren, N.A. Penner, B.E. Slentz, F.E. Regnier, Histidine-rich peptide selection and quantification in targeted proteomics, J. Proteome Res. 3 (2004) 37–45, https://doi.org/10.1021/pr034049q.

[11] Y. Wu, G. Chang, Y. Zhao, Y. Zhang, Preparation of hollow nickel silicate nanospheres for separation of His-tagged proteins, Dalt. Trans. 43 (2014) 779–783, https://doi.org/10.1039/c3dt52084f.

[12] J. Pan, C. Zhang, Z. Zhang, G. Li, Review of online coupling of sample preparation techniques with liquid chromatography, Anal. Chim. Acta. 815 (2014) 1–15, https://doi.org/10.1016/j.aca.2014.01.017.

[13] F. Benavente, S. Medina-Casanellas, E. Giménez, V. Sanz-Nebot, On-line solid-phase extraction capillary electrophoresis mass spectrometry for preconcentration and clean-up of peptides and proteins, in: N.T. Tran, M. Taverna (Eds.), Capill. Electrophor. Proteins Pept. Methods Protoc. Springer, New York, 2016, pp. 67–84, , https://doi.org/10.1007/978-1-4939-4014-1_6.

[14] R. Ramautar, G.W. Somsen, G.J. de Jong, Developments in coupled solid-phase extraction-capillary electrophoresis 2013–2015, Electrophoresis. 37 (2016) 35–44, https://doi.org/10.1002/elps.201500401.

[15] L. Pont, R. Pero-Gascon, E. Gimenez, V. Sanz-Nebot, F. Benavente, A critical retrospective and prospective review of designs and materials in in-line solid-phase extraction capillary electrophoresis, Anal. Chim. Acta. 1079 (2019) 1–19, https://doi.org/10.1016/j.aca.2019.05.022.

[16] M.C. Breadmore, W. Grochocki, U. Kalsoom, M.N. Alves, S.C. Phung, M.T. Rokh, J.M. Cabot, A. Ghiasvand, F. Li, A.I. Shallan, A.S.A. Keyon, A.A. Alhusban, H.H. See, A. Wuethrich, M. Dawod, J.P. Quirino, Recent advances in enhancing the sensitivity of electrophoresis and electrochromatography in capillaries and microchips (2016–2018), Electrophoresis. 40 (2019) 17–39, https://doi.org/10.1002/elps.201800384.

[17] J. Cai, Z. El Rassi, Selective on-line preconcentration of proteins by tandem metal chelate capillaries-capillary zone electrophoresis, J. Liq. Chromatogr. 16 (1993) 2007–2024, https://doi.org/10.1080/10826079308019910.

[18] N.M. Vizioli, M.L. Rusell, M.L. Carbajal, C.N. Carducci, M. Grasselli, On-line affinity selection of histidine-containing peptides using a polymeric monolithic support for capillary electrophoresis, Electrophoresis. 26 (2005) 2942–2948, https://doi.org/10.1002/elps.200410416.

[19] K. Tsukagoshi, Y. Shimadzu, T. Yamane, R. Nakajima, Preparation of an iminodiacetic acid-modified capillary and its performance in capillary liquid chromatography and immobilized metal chelate affinity capillary electrophoresis, J. Chromatogr. A. 1040 (2004) 151–154, https://doi.org/10.1016/j.chroma.2004.03.063.

[20] L. Zhang, L. Zhang, W. Zhang, Y. Zhang, On-line concentration of peptides and proteins with the hyphenation of polymer monolithic immobilized metal affinity chromatography and capillary electrophoresis, Electrophoresis. 26 (2005) 2172–2178, https://doi.org/10.1002/elps.200410377.

[21] P. Cao, J.T. Stults, Phosphopeptide analysis by on-line immobilized metal-ion affinity chromatography-capillary electrophoresis-electrospray ionization mass spectrometry, J. Chromatogr. A. 853 (1999) 225–235, https://doi.org/10.1016/s0021-9673(99)00481-1.

[22] P. Cao, J.T. Stults, Mapping the phosphorylation sites of proteins using on-line immobilized metal affinity chromatography/capillary electrophoresis/electrospray ionization multiple stage tandem mass spectrometry, Rapid Commun. Mass Spectrom. 14 (2000) 1600–1606, https://doi.org/10.1002/1097-0231(20000915)14:17<1600::AID-RCM68>3.0.CO;2-V.

[23] L. Ortiz-Martin, F. Benavente, S. Medina-Casanellas, E. Giménez, V. Sanz-Nebot, Study of immobilized metal affinity chromatography sorbents for the analysis of peptides by on-line solid-phase extraction capillary electrophoresis-mass spectrometry, Electrophoresis. 36 (2015) 962–970, https://doi.org/10.1002/elps.201400374.

[24] E. Giménez, R. Ramos-Hernan, F. Benavente, J. Barbosa, V. Sanz-Nebot, Analysis of recombinant human erythropoietin glycopeptides by capillary electrophoresis electrospray-time of flight-mass spectrometry, Anal. Chim. Acta. 709 (2012) 81–90, https://doi.org/10.1016/j.aca.2011.10.028.

[25] H.H. Lauer, G.P. Rozing, High performance capillary electrophoresis, second ed., Waldbronn, Germany, 2014, pp. 60–61.

[26] H.W. Modler, Functional properties of nonfat dairy ingredients - A review. Modification of products containing casein, J. Dairy Sci. 68 (1985) 2195–2205, https://doi.org/10.3168/jds.S0022-0302(85)81091-2.

[27] C. Wenz, C. Barbas, A. Lopez-Gonzalvez, A. Garcia, F. Benavente, V. Sanz-Nebot, T. Blanc, G. Freckleton, P. Britz-McKibbin, M. Shanmuganathan, F. De L'Escaille, J. Far, R. Haselberg, S. Huang, C. Huhn, M. Pattky, D. Michels, S. Mou, F. Yang, C. Neususs, N. Tromsdorf, E.E.K. Baidoo, J.D. Keasling, S.S. Park, Interlaboratory study to evaluate the robustness of capillary electrophoresis-mass spectrometry for peptide mapping, J. Sep. Sci. 38 (2015) 3262–3270, https://doi.org/10.1002/jssc.201500551.

[28] H. Block, B. Maertens, A. Spriestersbach, N. Brinker, J. Kubicek, R. Fabis, J. Labahn, F. Schäfer, Immobilized-metal affinity chromatography (IMAC): A review, in: R.R. Burgess, M.P. Deutscher (Eds.), Guid. to Protein Purif, 2nd ed., Academic Press, Miami, FL, USA, 2009, pp. 439–473, , https://doi.org/10.1016/S0076-6879(09)63027-5.

[29] J.C. Wright, M.O. Collins, L. Yu, L. Käll, M. Brosch, J.S. Choudhary, Enhanced peptide identification by electron transfer dissociation using an improved mascot percolator, Mol. Cell. Proteomics. 11 (2012) 478–491, https://doi.org/10.1074/mcp.O111.014522.

[30] L. Villegas, R. Pero-Gascon, F. Benavente, J. Barbosa, V. Sanz-Nebot, On-line protein digestion by immobilized enzyme microreactor capillary electrophoresis-mass spectrometry, Talanta. 199 (2019) 116–123, https://doi.org/10.1016/j.talanta.2019.02.039.

[31] T. Stora, Z. Dienes, H. Vogel, C. Duschl, Histidine-tagged amphiphiles for the reversible formation of lipid bilayer aggregates on chelator-functionalized gold surfaces, Langmuir 16 (2000) 5471–5478, https://doi.org/10.1021/la991711h.

[32] J. Partyka, J. Krenkova, R. Cmelik, F. Foret, Multi-charged labeling of oligosaccharides and N-linked glycans by hexahistidine-based tags for capillary electrophoresis-mass spectrometry analysis, J. Chromatogr. A. 1560 (2018) 91–96, https://doi.org/10.1016/j.chroma.2018.05.030.

Supporting Information

Table S1. Tryptic peptides of α-CSN1 detected by CE-MS and IMA-SPE-CE-MS analysing a 50 $\mu g \cdot mL^{-1}$ solution of α-CSN. His residues in His-peptides are marked in **bold** and phosphorylations in orange colour. Single amino acids were not taken into account.

	Peptide sequence[a]		[M+nH]$^{n+}$		Detected	
			m/z	n	CE-MS (acidic BGE)	CE-MS (neutral BGE)	IMA-SPE-CE-MS [b]
1	[1-3]	RPK	200.6370; 400.2667	2, 1	-	-	✓ (*)
2	**[4-7]**	**HPIK**	247.6579; 494.3085	2, 1	✓	✓	✓ (47)
3	**[8-22]**	**HQGLPQEVLNENLLR**	587.3198; 880.4761	3, 2	✓	✓	-
4	[23-34]	FFVAPFPEVFGK	462.2482; 692.8686	3, 2	✓	✓	-
5	[35-36]	EK	276.1534	1	✓	✓	-
6	[37-42]	VNELSK	385.1783; 769.3492	2, 1	-	-	-
7	[43-58]	DIGSESTEDQAMEDIK	643.2354; 964.3494	3, 2	✓	✓	-
8	[59-79]	QMEAESISSSEEIVPNSVEQK	-	-	-	-	-
9	**[80-83]**	**HIQK**	263.1609; 525.3144	2, 1	✓	✓	✓ (94)
10	[84-90]	EDVPSER	416.1958; 831.3843	2, 1	✓	✓	-
11	[91-100]	YLGYLEQLLR	423.2397; 634.3559	3, 2	✓	✓	-
12	[101-102]	LK	260.1969	1	-	-	-
13	[104-105]	YK	310.1761	1	-	-	-
14	[106-119]	VPQLEIVPNSAEER	554.2696; 830.9008	3, 2	✓	✓	-
15	**[120-124]**	**LHSMK**	308.1678; 615.3283	2, 1	✓	✓	✓ (25)
16	**[125-132]**	**EGIHAQQK**	304.1629; 455.7407	3, 2	✓	✓	-
17	[133-151]	EPMIGVNQELAYFYPELFR	772.7172; 1158.5721	3, 2	✓	✓	-
18	[152-193]	QEYQLDAYPSGAWYYVPLGTQYTDAPSFSDIPNPIGSENSEK	1180.2987; 573.3958	4, 3	-	-	-
19	[194-199]	TTMPLW	748.3698	1	✓	✓	-

[a] Peptide identification was based on the intact molecular ions of the detected non-His peptides and His-peptides.
[b] Preconcentration factors are indicated in parenthesis. The asterisk indicates that the preconcentration factor was not calculated because the His-peptide was not detected (-) by CE-MS (neutral BGE).

Table S2. Tryptic peptides of α-CSN2 detected by CE-MS and IMA-SPE-CE-MS analysing a 50 $\mu g \cdot mL^{-1}$ solution of α-CSN. His residues in His-peptides are marked in bold and phosphorylations in orange colour. Single amino acids were not taken into account.

Peptide sequence [a]			[M+nH]$^{n+}$		Detected		
			m/z	n	CE-MS (acidic BGE)	CE-MS (neutral BGE)	IMA-SPE-CE-MS [b]
20	**[2-21]**	NTME**H**VSSSEESIISQETYK	-	-	-	-	-
21	[22-24]	QEK	404.2140	1	-	-	-
22	[25-32]	NMAINPSK	477.7094; 954.4114	2, 1	-	-	-
23	[33-41]	ENLCSTFCK	522.7284	2, 1	-	-	-
24	[42-45]	EVVR	251.6528; 502.2984	2, 1	✓	✓	-
25	[46-70]	NANEEEYSIGSSSEESAEVATEEVK	-	-	-	-	-
26	[71-76]	ITVDDK	345.6871; 690.3668	2, 1	-	-	-
27	**[77-80]**	**H**YQK	288.1504; 575.2936	2, 1	✓	-	✓ (*)
28	[81-91]	ALNEINQFYQK	456.5700; 684.3513	3, 2	-	-	-
29	[92-113]	FPQYLQYLYQGPIVLNPWDQVK	903.8074; 1355.2074	3, 2	-	-	-
30	[115-125]	NAVPITPTLNR	598.3433; 1195.6793	2, 1	✓	-	-
31	[126-136]	EQLSTSEENSK	-	-	-	-	-
32	[138-149]	TVDMESTEVFTK	489.5422; 733.8097	3, 2	✓	-	-
33	[151-152], [198-199]	TK	248.1605	1	-	-	-
34	[153-158]	LTEEEK	748.3723	1	✓	✓	-
35	[159-160]	NR	-	-	-	-	-
36	[161-165]	LNFLK	317.6998; 634.3923	2, 1	✓	✓	-
37	[167-170]	ISQR	-	-	-	-	-
38	[171-173]	YQK	438.2347	1	-	-	-
39	[174-181]	FALPQYLK	490.2842; 979.5611	2, 1	✓	-	-
40	**[182-188]**	TVYQ**H**QK	301.8276; 452.2378	3, 2	✓	✓	✓ (98)
41	[189-197]	AMKPWIQPK	366.8762; 549.8103	3, 2	✓	✓	✓ (0.21)
42	[200-205]	VIPYVR	373.7316; 746.4559	2, 1	✓	✓	-
43	[206-207]	YL	295.1652	1	✓	-	-

[a] Peptide identification was based on the intact molecular ions of the detected non-His peptides and His-peptides.
[b] Preconcentration factors are indicated in parenthesis. The asterisk indicates that the preconcentration factor was not calculated because the His-peptide was not detected (-) by CE-MS (neutral BGE).

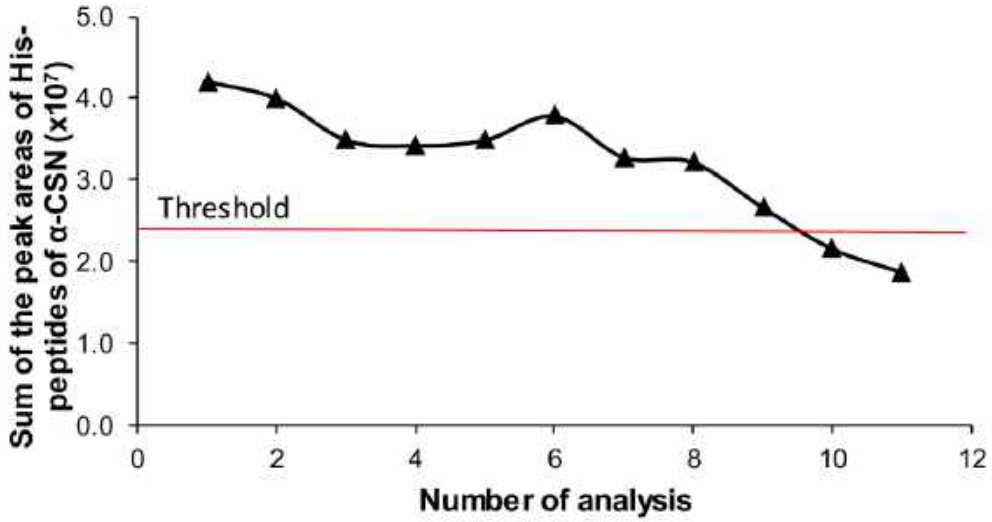

Figure S1. Evaluation of the lifetime of a microcartridge for consecutive analysis of a 50 $\mu g \cdot mL^{-1}$ α-CSN tryptic digest. The threshold was calculated as the 40% of decrease of the peak areas of His-peptides for the mean value of the first three analyses.

analytical chemistry

Article

Cite This: Anal. Chem. 2018, 90, 6618−6625

pubs.acs.org/ac

Analysis of Circulating microRNAs and Their Post-Transcriptional Modifications in Cancer Serum by On-Line Solid-Phase Extraction−Capillary Electrophoresis−Mass Spectrometry

Roger Pero-Gascon,[†] Victoria Sanz-Nebot,*[,†] Maxim V. Berezovski,[‡] and Fernando Benavente[†]

[†]Department of Chemical Engineering and Analytical Chemistry, Institute for Research on Nutrition and Food Safety (INSA-UB), University of Barcelona, Barcelona 08028, Spain

[‡]Department of Chemistry and Biomolecular Sciences, University of Ottawa, Ottawa, Ontario K1N 6N5, Canada

Supporting Information

ABSTRACT: In this paper, an on-line solid-phase extraction capillary electrophoresis−mass spectrometry (SPE-CE-MS) method is described for the purification, preconcentration, separation, and characterization of endogenous microRNA (miRNA) and their post-transcriptional modifications in serum. First, analysis by CE-MS was optimized using a standard mixture of hsa-miR-21-5p (miR-21-5p) and hsa-let-7g-5p (let-7g-5p). For SPE-CE-MS, a commercial silicon carbide (SiC) resin was used to prepare the microcartridges. Under the optimized conditions with standards, the microcartridge lifetime (>25 analyses) and repeatability (2.8% RSD for the migration times; 4.4 and 6.4% RSD for the miR-21-5p and let-7g-5p peak areas, respectively) were good, the method was linear between 25 and 100 nmol·L^{-1}, and the limit of detection (LOD) was around 10 nmol·L^{-1} (50 times lower than by CE-MS). In order to analyze human serum samples, an off-line sample pretreatment based on phenol/chloroform/isoamyl alcohol (PCA) extraction was necessary prior to SPE-CE-MS. The potential of the SPE-CE-MS method to screen for B-cell chronic lymphocytic leukemia (CLL) was demonstrated by an analysis of serum samples from healthy controls and patients. MicroRNAs, specifically miR-21-5p and a 23 nucleotide long 5′-phosphorylated miRNA with 3′-uridylation (iso-miR-16-5p), were only detected in the CLL patients.

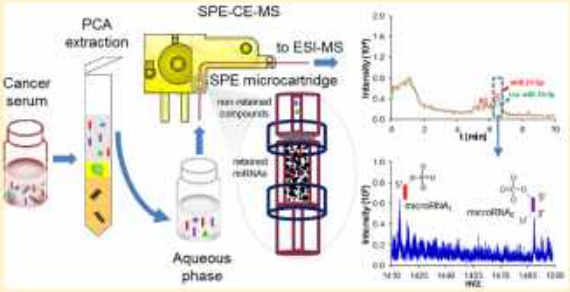

MicroRNAs (miRNAs) are a class of single-stranded, non-protein-coding RNAs that are 19−23 nucleotides long. The function of a miRNA is to control gene expression post-transcriptionally, regulating messenger RNA (mRNA) by binding to the 3′ untranslated region (3′ UTR) of the target mRNA.[1] miRNAs play a major role in a wide range of normal cellular processes, including cell proliferation, development, and apoptosis.[2] Circulating miRNAs have been found in the extracellular environment, including in various biological fluids, such as the blood, saliva, and urine of both diseased and healthy people. These extracellular miRNAs are packaged in extracellular vesicles[3] or associated with RNA-binding proteins,[4,5] leading to high stability and resistance to endogenous RNase activity, extreme temperature, and pH.[6]

Deregulation of miRNAs has been associated with different diseases, such as cardiovascular diseases, diabetes, aberrant immune function, and especially cancer.[7] In comparison with longer biomarker molecules, miRNAs present several advantages: they have relatively smaller numbers of candidate sequences and higher stability due to their smaller size, which leads to an improved robustness of detection. Furthermore, they are detectable in accessible biofluids, such as serum. For these reasons, miRNAs are great candidates as minimally invasive biomarkers for early disease diagnosis, prognosis, and treatment outcome for different diseases.[8] In this sense, miR-21-5p is one of the most frequently upregulated miRNAs in solid tumors, and its levels have been associated with relapse-free survival.[9,10]

Several analytical methods have been developed for the detection of miRNAs, and the most commonly used are Northern blotting,[11] microarrays,[12] and a two-step procedure of modified reverse transcription polymerase chain reaction followed by quantitative PCR (RT-qPCR).[13] The last method is very sensitive, but it is based on the indirect detection of complementary DNA. Furthermore, the above-mentioned methods are not capable of detecting the post-transcriptional modifications of miRNAs, such as 5′-end phosphorylation and dephosphorylation, or unexpected isoforms with differing ends due to trimming or nucleotide additions.[14] These modifications have been reported to affect the stability of miRNA and be a mechanism for the regulation of miRNA activity.[15] Thus, the development of direct analytical methods able to obtain information regarding post-transcriptional modifications of

Received: January 25, 2018
Accepted: May 6, 2018
Published: May 7, 2018

DOI: 10.1021/acs.analchem.8b00405
Anal. Chem. 2018, 90, 6618−6625

miRNA is of great interest. In this respect, capillary electrophoresis−mass spectrometry (CE-MS) is a highly efficient technique for the separation and characterization of biomolecules; it is generally applied in the field of proteomics and metabolomics and less in genomics because of the emergence of next-generation sequencing techniques (NGS).[16−20] CE-MS has rarely been used for the analysis of small RNAs, although it allows direct, label-free, multiplex analysis and precise mass identification of post-transcriptional modifications of miRNAs.[21] Small RNAs can be isolated from biological fluids using commercially available kits and then analyzed by CE-MS. However, the small injection volumes typical of CE compromise the concentration sensitivity. The use of highly selective and sensitive mass spectrometers is often not enough for robust detection; consequently, CE-MS has often been combined with different electrophoretic and chromatographic techniques for the on-line preconcentration of the target analytes, such as sample stacking, isotachophoresis, or on-line solid-phase extraction (SPE-CE).[22−27] In SPE-CE, a microcartridge with an appropriate sorbent is inserted near the inlet of the separation capillary to purify and preconcentrate the target analytes from a large volume of sample. SPE-CE-MS has been extensively applied for the analysis of small molecules (drugs, metabolites, etc.), peptides, and proteins using the silica or polymeric sorbents typically used in off-line SPE (e.g., C18)[28−30] because of the versatility of these sorbents and their commercial availability. The use of other sorbents for improved selectivity, such as immunoaffinity sorbents, has also been studied with good results, although the very specific conditions required for the extraction and compatibility with on-line MS detection.[31−33]

In recent years, different commercially available kits, based on SPE spin microcolumns used in combination with liquid−liquid extraction and precipitation, have been developed for miRNA isolation and purification from biological fluids. These multistep sample pretreatments are widely used prior to PCR-based analytical methods due to their excellent recoveries and simplicity of usage.[34−36] However, to the best of our knowledge, the on-line coupling of these SPE methods to a high-performance separation technique with MS detection has not yet been explored, although it may reduce manual handling and increase analysis throughput while obtaining valuable structural information.

In this paper, for the first time, an SPE-CE-MS method for the purification, preconcentration, separation, and untargeted multiplex analysis of miRNAs from serum samples is described. The SPE-CE-MS analysis of miRNA was optimized using standards, and the figures of merit were compared with those of a previously developed sample stacking CE-MS method.[21] Subsequently, the applicability of the developed SPE-CE-MS method was demonstrated by the analysis of serum samples from healthy controls and patients with chronic lymphocytic leukemia (CLL), the most common type of leukemia in adults.[37]

■ EXPERIMENTAL SECTION

Materials and Reagents. All the chemicals used in the preparation of background electrolytes (BGEs) and solutions were of analytical-reagent grade or better. Acetic acid (glacial), ammonium hydroxide (25%), guanidinium chloride (≥99.0%), ortho-phosphoric acid (85%), and sodium hydroxide (≥99.0%) were purchased from Merck (Darmstadt, Germany). Acetonitrile (LC-MS), 96% ethanol, and methanol (LC-MS) were supplied by Panreac AppliChem (Barcelona, Spain). Propan-2-ol (LC-MS) was purchased from Scharlau (Barcelona, Spain). Ammonium acetate (NH_4Ac, ≥99.999%), ammonium bicarbonate (for LC-MS), chloroform (≥99.0%), and the phenol/chloroform/isoamyl alcohol mixture (PCA, 25:24:1) were supplied by Sigma-Aldrich (Madrid, Spain). The TRIzol Reagent was purchased from Thermo Fisher Scientific (Barcelona, Spain). Synthetic miRNA hsa-miR-21-5p (miR-21-5p), hsa-let-7g-5p (let-7g-5p), and hsa-miR-16-5p with 3′-uridylation (iso-miR-16-5p) were purchased from IDT (Coralville, IA).

Electrolyte Solutions, Sheath Liquid, miRNA Standards, and Serum Samples. All the solutions were stored in plastic bottles to minimize cation-adduct formation due to glass-bottle Na^+ and K^+ leaching and were degassed for 10 min by sonication before use. The optimized BGE for the CE-MS and SPE-CE-MS separation contained 25 mM NH_4Ac and was adjusted to pH 8.0 with ammonium hydroxide. The BGE was passed through a 0.20 μm nylon filter (Macherey-Nagel, Düren, Germany). The sheath liquid solution consisted of a mixture of 80:20 (v/v) propan-2-ol/water with 2 mM NH_4Ac and was delivered at a flow rate of 3.3 $\mu L \cdot min^{-1}$ by a KD Scientific 100 series infusion pump (Holliston, MA).

Stock solutions (100 $\mu mol \cdot L^{-1}$) of each miRNA were stored in a freezer at −20 °C. The concentrations of these standard solutions were confirmed by measuring the absorbance at 260 nm (10 mm path length) using a Nanodrop spectrophotometer (Thermo Fisher Scientific, Rockford, IL). Working standard solutions were prepared from the stock solutions by dilution in water and were stored in the fridge at 5 °C when not in use.

Human serum samples and data from donors were provided by the INCLIVA BioBank (PT13/0010/0004, B.0000768 ISCIII), integrated in the Valencian Biobanking Network and the Spanish National Biobanks Network. They were processed following standard operating procedures with the appropriate approval of the Ethical and Scientific Committees. Three healthy donor serum samples and three CLL serum samples from patients with stage IV of the disease were analyzed. All the samples corresponded to males and females aged between 75 and 85 years. Serum aliquots were stored in a freezer at −80 °C. Healthy and CLL samples were thawed and separately pooled before the analysis.

Apparatus. pH measurements were made with a Crison 2002 potentiometer and 52-03 electrode (Crison Instruments, Barcelona, Spain).

Centrifugal filtration was carried out at 25 °C in a cooled Rotanta 460 centrifuge (Hettich Zentrifugen, Tuttlingen, Germany).

CE-MS. Fused silica capillaries were supplied by Polymicro Technologies (Phoenix, AZ). All CE-MS experiments were performed in a 7100 CE coupled with an orthogonal G1603A sheath-flow interface to a 6220 oa-TOF LC/MS spectrometer (Agilent Technologies, Waldbronn, Germany).

ChemStation and MassHunter softwares (Agilent Technologies) were used for the CE and TOF mass spectrometer control, data acquisition and integration, and mass spectrum deconvolution. The TOF mass spectrometer was operated in negative electrospray ionization mode (ESI−) and the optimized parameters are presented in the Supporting Information.

Separations were performed at 15 °C in a 72 cm long (L_T) × 75 μm i.d. × 365 μm o.d. capillary. All capillary rinses were performed at high pressure (930 mbar). For new ones and

DOI: 10.1021/acs.analchem.8b00405
Anal. Chem. 2018, 90, 6618−6625

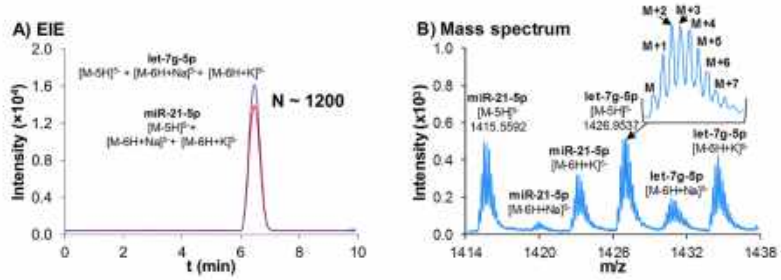

Figure 1. CE-MS for a 5000 nmol·L^{-1} miR-21-5p and let-7g-5p standard mixture. (A) Extracted ion electropherogram (EIE) and (B) mass spectrum. The number of theoretical plates (N) was calculated as $N = 5.54 \times (t_m/w_{1/2})^2$ where t_m is the migration time, and $w_{1/2}$ is the width at half the peak height.

between workdays, the capillaries were flushed with 1 M NaOH (15 or 5 min), water (15 or 10 min), and BGE (30 or 15 min) off-line to avoid the unnecessary contamination of the MS system. The samples were hydrodynamically injected at 50 mbar for 10 s, and a separation voltage of +20 kV (normal polarity, cathode in the outlet) was applied. The autosampler was kept at 10 °C using an external water bath (Minichiller 300, Peter Huber Kältemaschinenbau AG, Offenburg, Germany). Between consecutive runs, the capillary was conditioned by flushing with water (2 min) and BGE (2 min).

Sample Stacking CE-MS. An electrophoretic preconcentration CE-MS method for the analysis of miRNA, described elsewhere,[21] was adapted to our specific CE-MS setup. Separations were performed at 15 °C in a 158 cm long (L_T) × 50 μm i.d. × 365 μm o.d. capillary with a BGE of 25 mM NH_4Ac, adjusted to pH 6.0 with acetic acid. All capillary rinses were performed at high pressure (930 mbar). Before each injection, the capillary was rinsed with water (10 min) and BGE (3 min). Samples were injected at 930 mbar for 4 min (≈2.2 μL, according to the Hagen−Poiseuille equation),[38] and then the long plug of sample was pushed with BGE for 50 s (0.5 μL). Separation was performed at +20 kV.

SPE-CE-MS. The silicon carbide (SiC) resin was obtained from commercial microRNA purification kit spin columns (Norgen Biotek Corporation, Thorold, Canada).

Construction of the microcartridge or analyte concentrator was carried out as described elsewhere with little modifications.[31,39,40] The inlet end was prepared by connecting the microcartridge (0.7 cm L_T × 250 μm i.d. × 365 μm o.d. capillary) with a plastic sleeve to a previously conditioned inlet capillary (7.5 cm L_T × 75 μm i.d. × 365 μm o.d.). The microcartridge was completely filled by vacuum with the SiC particles. Another plastic sleeve was connected to the microcartridge, and a small piece of cotton (approximately 1 mm) was introduced in the plastic tube before connecting the separation capillary (64.5 cm L_T × 75 μm i.d. × 365 μm o.d.). This cotton frit prevented the SiC particles from leaking, which had promoted current instability or breakdown and poor reproducibility. Samples were hydrodynamically introduced at 930 mbar for 5 min (60 μL). A final flush for 40 s with BGE eliminated nonretained molecules and equilibrated the capillary before the electrophoretic separation. All these steps were performed by switching off the nebulizer gas and the ESI capillary voltage to prevent the entrance of contaminants into the MS. Then, both were switched on, a small volume of eluent with 60% (v/v) acetonitrile (ACN) was injected at 50 mbar for 10 s (50 nL); separation was conducted at +20 kV at 15 °C, and 25 mbar of pressure was applied to compensate for the microcartridge counter-pressure. Between consecutive runs, the capillary was rinsed for 4 min with water.

Before SPE-CE-MS, the serum samples were extracted with PCA or the TRIzol Reagent, both of which were followed by chloroform extraction. The detailed procedure is presented in the Supporting Information.

Quality Parameters. The details regarding the estimation of the limit of detection (LOD), limit of quantification (LOQ), repeatability of migration time and peak area, linearity, and microcartridge lifetime in CE-MS and SPE-CE-MS are given in the Supporting Information.

RESULTS AND DISCUSSION

CE-MS. CE-MS was optimized by analyzing standard solutions of the synthetic miR-21-5p and let-7g-5p miRNAs (Table S-1A).

Most MS studies on nucleic acids use ESI− because it yields a better signal for such acidic compounds.[21,41,42] However, because the phosphate groups of the miRNAs have cation-binding sites, clusters corresponding to Na^+ and K^+ adducts are typically detected in the mass spectrum, decreasing the signal of the expected $[M-nH]^{n-}$ molecular ions. In order to increase the sensitivity of the detection of miRNA in ESI− and to decrease cation-adduct formation, several BGE and sheath liquid compositions were tested. In general, an effective method to minimize alkali-adduct formation is the addition of organic bases or ammonium salts.[43] In our case, appropriate results were obtained with BGEs of ammonium acetate. Different BGE concentrations and acidities were tested at 10, 25, and 50 mM NH_4Ac and at pHs 6.0 and 8.0, adjusted with acetic acid and ammonium hydroxide, respectively. The lowest adduct formation and highest sensitivity were obtained with a BGE of 25 mM NH_4Ac at pH 8.0, in contrast to a previous study that reported a BGE of 25 mM NH_4Ac at pH 6.0 for the analysis of miRNA by sample stacking CE-MS.[21] This BGE was always freshly prepared in plastic tubes to minimize cation-adduct formation due to the leaching of Na^+ and K^+ from glass bottles.

Different hydroorganic mixtures were also tested as sheath liquids, such as propan-2-ol, methanol, and acetonitrile at 60 and 80% (v/v). The highest sensitivity for miRNA detection was obtained with 80% (v/v) propan-2-ol (Figure S-1A). NH_4OH (0.5%, v/v) was also added to this mixture to improve miRNA ionization, but the sensitivity was lower than with ammonium salts as additives. The optimized sheath liquid contained 80% (v/v) propan-2-ol and 2 mM NH_4Ac, as in the sample stacking CE-MS method indicated before,[21] which showed better results than those containing 1, 5, and 10 mM NH_4Ac.

DOI: 10.1021/acs.analchem.8b00405
Anal. Chem. 2018, 90, 6618−6625

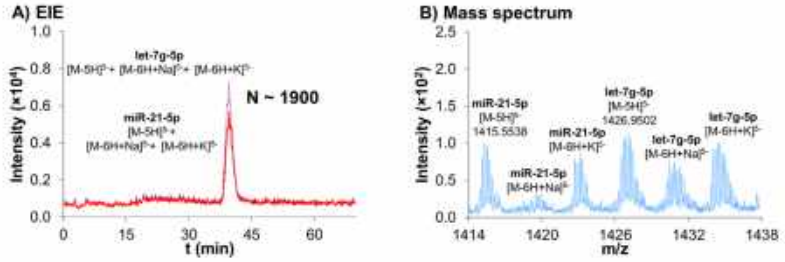

Figure 2. Sample stacking CE-MS for a 250 nmol·L^{-1} miR-21-5p and let-7g-5p standard mixture. (A) Extracted ion electropherogram (EIE) and (B) mass spectrum. The number of theoretical plates (N) was calculated as $N = 5.54 \times (t_m/w_{1/2})^2$ where t_m is the migration time, and $w_{1/2}$ is the width at half the peak height.

As an example, Figure 1 shows the extracted ion electropherogram (EIE) and mass spectrum of a 5000 nmol·L^{-1} standard mixture of miR-21-5p and let-7g-5p in the optimized conditions. Both miRNA comigrated but showed molecular ions with different m/z values because of the molecular-mass differences. The most abundant ion was the $[M-5H]^{5-}$, and some Na^+ and K^+ adducts were still detected ($[M-6H+Na]^{5-}$ and $[M-6H+K]^{5-}$). Under these conditions, the LOD of the CE-MS method was 500 nmol·L^{-1} for both miRNAs.

Sample Stacking CE-MS Adaptation. Before exploring SPE-CE-MS, we adapted the sample stacking CE-MS method previously described for the analysis of miRNAs to the specific instrumental setup used in this study.[21] Sample stacking preconcentration during CE-MS was achieved by dissolving the sample in water, which had a lower conductivity than the BGE. A large volume of sample was injected hydrodynamically into the capillary between two plugs of BGE. When the separation voltage was applied, focusing and preconcentration of the ions happened at the narrow zone of the interface between the sample solution and the BGE because of a change in electrophoretic velocity due to a difference in the conductivities and, hence, the electric field.

As an example, Figure 2 shows the analysis of a 250 nmol·L^{-1} standard mixture of miR-21-5p and let-7g-5p in the adapted conditions. As expected from the results of the previous study,[21] migration times were 5 times higher using sample stacking than by conventional CE-MS (Figure 2A), and the mass spectrum showed the same ion clusters as by CE-MS (compare Figures 2B and 1B). The LOD of the sample stacking CE-MS method adapted to our instrumental setup was 50 nmol·L^{-1}, 10 times lower than that by CE-MS, 500 nmol·L^{-1}. A slightly lower LOD (20 nmol·L^{-1}) was obtained by sample stacking CE-MS in the original study,[21] probably because of the better sensitivity of the mass spectrometer used in that case. Sample stacking allows a remarkable preconcentration factor, and in that study, it was demonstrated that it was possible to analyze miRNA from cancer serum samples.[21] As an alternative, in this study we investigated SPE-CE-MS to further enhance sensitivity, while reducing manual handling and increasing analysis throughput.

SPE-CE-MS Optimization. The SiC resin from the spin microcolumns of the Norgen microRNA-isolation kit was used to prepare the on-line SPE-CE microcartridges. The literature provided by the manufacturer cited better recoveries and linearities on miRNA purification than with silica-based or traditional phase-separation methods.[44] Another important aspect of the SiC resin was the small particle size, which facilitated packing the on-line microcartridges. The starting point for the optimization of the SPE-CE-MS methodology was the procedure recommended by the manufacturer, as well as on other procedures applied for the extraction of hydrophilic analytes, such as protein glycans, with graphitic carbon sorbents.[45,46]

In SPE-CE-MS, after sample loading, the microcartridge located at the capillary inlet needed to be washed to eliminate nonspecifically retained molecules and also filled with BGE before the elution, separation, and detection. In preliminary studies using the optimized BGE for CE-MS (25 mM NH_4Ac, pH = 8.0), some miRNA elution was detected during the washing and filling step with BGE (930 mbar, 2 min). This miRNA leakage was detrimental to achieving optimal sensitivity. Different strategies were explored, but it was found through those studies that changes in NH_4Ac concentration or pH and also ammonium phosphate and bicarbonate BGEs resulted in poorer performance.

Several modifications in the pressure and duration of the washing and filling step were, therefore, evaluated while the total volume of the flushed solution was minimized (4.0 μL, approximately 1.3 capillary volumes). This step was performed at low pressure (100 mbar, 360 s),[38] but lower sensitivities than those at high pressure (930 mbar, 40 s)[38] were obtained. Several other alternatives were explored, including the use of guanidinium chloride (<1 M) or alcohols, but the results were not better than those obtained with this fast and short washing and filling step. In the first case, the remaining guanidinium chloride caused later ion suppression during the analysis. In the second case, despite the manufacturer's recommendation of the use of alcohols to increase miRNA retention by the SiC sorbent, methanol, ethanol, and propan-2-ol at concentrations between 10% and 70% (v/v) in the miRNA standard solutions or in the washing step promoted lower repeatability. This was probably because of the difficulty in rehydrating the sorbent or miRNA precipitation. In general, protocols for off-line miRNA extraction using spin columns include a drying step after sample loading and washing to evaporate the organic solvents. In SPE-CE-MS, we attempted to dry the microcartridge with air after sample loading and washing, prior to filling it with BGE. However, this procedural modification was discarded because bubbles were generated within the microcartridge, and electrophoretic separation was compromised.

Regarding the elution, ACN and MeOH hydroorganic mixtures at 40, 60 and 80% (v/v) were tested. The best sensitivity and repeatability of peak areas and migration times were obtained with a 60% (v/v) ACN (Figure S-1B) and no carry-over was observed between consecutive analyses.

DOI: 10.1021/acs.analchem.8b00405
Anal. Chem. 2018, 90, 6618−6625

The sample loading time was studied by loading a 35 nmol·L^{-1} standard mixture of miR-21-5p and let-7g-5p at 930 mbar from 3 to 20 min. As can be seen in Figure 3, the maximum amount of miRNA was detected between 5 and 10 min. Between 15 and 20 min of sample loading, analyte breakthrough caused a significant decrease of peak area. Hence, to reduce the total analysis time and to obtain the highest recoveries, a sample loading time of 5 min was selected as the best compromise for the rest of the experiments.

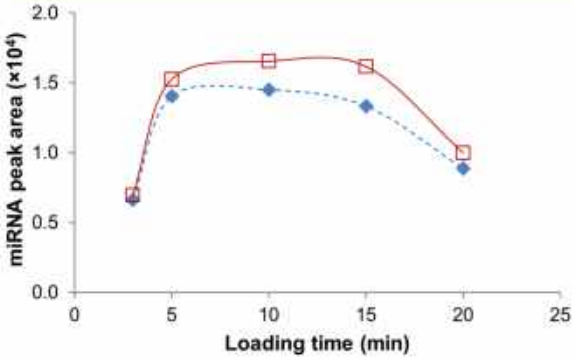

Figure 3. Plot of peak area of the eluted miR-21-5p (♦) and let-7g-5p (□) vs loading time at 930 mbar (35 nmol·L^{-1} standard mixture).

Under the optimized conditions, consecutive analyses of the standard mixture were repeatable in terms of migration times and peak areas: at 50 nmol·L^{-1}, the percent RSDs (n = 3) were 2.8 and 4.4% for miR-21-5p and 2.8 and 6.4% for let-7g-5p. As can be seen in Figure S-2, the method was satisfactorily linear (r^2 > 0.97) between 25 and 100 nmol·L^{-1} for both miRNAs. When loading a concentration of 150 mM, the sorbent was saturated, and there was not the expected increase in the peak areas. The LOD was 10 nmol·L^{-1}, which was an improvement of 50 and 5 times compared with those of the CE-MS and sample stacking CE-MS methods, respectively. The LOQ was 25 nmol·L^{-1}. The lifetimes of the microcartridges were around 25 analyses. As an example, Figure 4 shows the SPE-CE-MS analysis of a 50 nmol·L^{-1} miR-21-5p and let-7g-5p standard mixture in the optimized conditions. In comparison with CE-MS (Figure 1), the migration times were similar, the number of theoretical plates (N) was slightly higher, and the same ions were detected in the mass spectrum.

MicroRNA Detection in Cancer Serum. The SPE-CE-MS method optimized with standards was applied to the analysis of biological fluids. Considering that miRNA levels in serum and plasma samples are similar[6] and that serum samples are more abundant in many clinical-sample repositories, serum samples were selected for miRNA profiling. Extracellular circulating miRNAs are found in the sera of both diseased and healthy people but at differing levels of concentration. miRNAs are resistant to endogenous RNase activity as well as extreme pHs and temperatures[6,8] because they are contained within microvesicles or in protein and lipoprotein complexes.[9] For this reason, no miRNAs were detected when serum samples were loaded without any off-line pretreatment (e.g., addition of a lysis buffer or phenol solution). In addition, current instability and breakdown during the electrophoretic separation was observed because of saturation of the sorbent with the sample matrix components due to nonspecific retention. Therefore, an off-line sample pretreatment was required to inhibit RNase activity, dissociate the nucleocomplexes, precipitate proteins, and extract the miRNAs. Two extraction procedures based on TRIzol and PCA were tested and followed by chloroform extraction in both cases. In addition, it was necessary to desalt the extracts because the retention of the miRNAs was compromised as a result of the high abundance of salts. Drop dialysis was performed because it was a simple, rapid, and highly effective method to remove the salts from the small volume samples.[47,48]

The sample pretreatments were optimized with healthy control serum samples spiked with the standard miRNAs, miR-21-5p and let-7g-5p. The PCA-extraction procedure was selected because of the limited compatibility of the TRIzol Reagent with MS, due to the presence of high concentrations of chaotropic salts (i.e., guanidinium thiocyanate). In the optimized conditions, the sample pretreatment recoveries were high, approximately 85%, calculated by a comparison of the SPE-CE-MS analyses for a 50 nmol·L^{-1} standard solution and a healthy control serum sample spiked at the same concentration. Consecutive analyses were repeatable in terms of migration times and peak areas (the percent RSDs (n = 3) were 3.9 and 7.6% for miR-21-5p and 3.9 and 4.1% for let-7g-5p for the healthy control serum sample spiked at 50 nmol·L^{-1}). Furthermore, the lifetimes of the microcartridges and LOD were similar to those with the standards (around 20 analyses and 10 nmol·L^{-1}, respectively).

With the optimized sample pretreatment and SPE-CE-MS method, in concordance with the previous study using the sample stacking CE-MS method,[21] no endogenous miRNAs

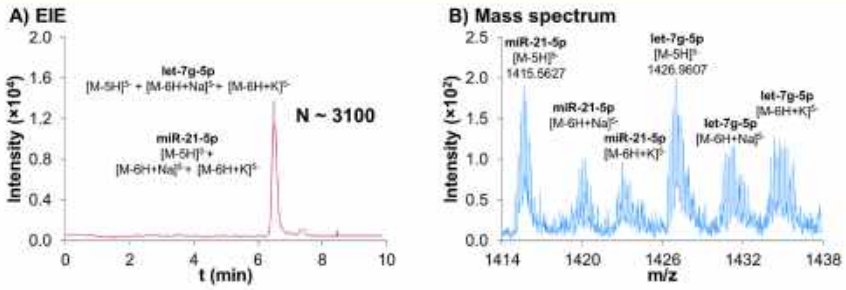

Figure 4. SPE-CE-MS for a 50 nmol·L^{-1} miR-21-5p and let-7g-5p standard mixture. (A) Extracted ion electropherogram (EIE) and (B) mass spectrum. The number of theoretical plates (N) was calculated as $N = 5.54 \times (t_m/w_{1/2})^2$ where t_m is the migration time, and $w_{1/2}$ is the width at half the peak height.

DOI: 10.1021/acs.analchem.8b00405
Anal. Chem. 2018, 90, 6618−6625

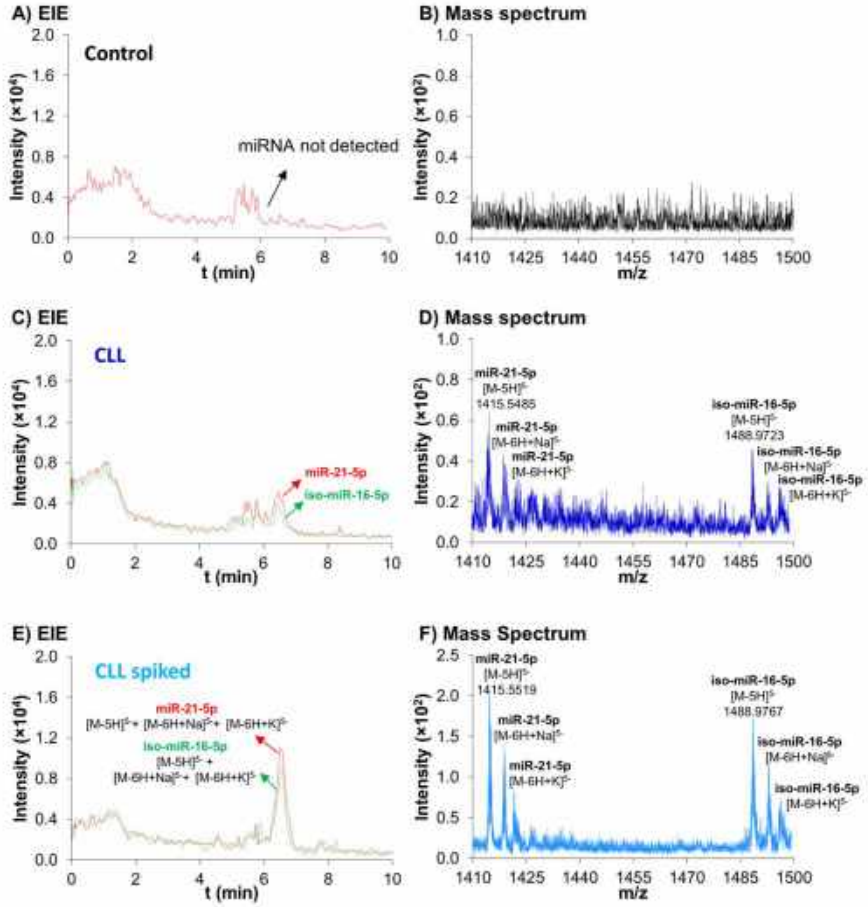

Figure 5. SPE-CE-MS for human serum samples. (A,C,E) Extracted ion electropherograms (EIEs) and (B,D,F) mass spectra of (A,B) a healthy control sample, (C,D) a CLL-patient sample, and (E,F) a CLL-patient sample spiked with 50 nM miR-21-5p and 50 nM iso-miR-16-5p. No endogenous miRNAs were detected in the control.

were detected in the (unspiked) healthy control serum samples (Figure 5A,B), because of the extremely low abundance of miRNA in this type of samples. It is well-known that some miRNAs are up-regulated in sera from patients with different types of cancer.[9,49−52] CLL is a cancer of B-lymphocytes and is the most common type of leukemia in adults.[37] CLL derives from a combination of genetic (chromosomal abnormalities and gene mutations) as well as epigenetic (altered microRNA expression and DNA methylation) modifications.[53] Specific miRNA profiles have been associated with CLL progression, prognosis, and drug resistance.[54] With SPE-CE-MS, in the analyzed CLL serum samples, two miRNAs were clearly detected at concentrations near the LODs (the EIEs and mass spectrum are shown in Figure 5C,D, respectively). The two miRNAs were tentatively identified using miRBase, which is a comprehensive database of miRNA sequences and expression (http://www.mirbase.org).[55] The current version (miRBase 21) indexes 28 645 miRNA entries and about 2000 sequences for humans. A screening of the most abundant miRNA species in CLL plasma and cell samples reported in the literature (Table S-2)[56−59] was performed, taking into account possible post-transcriptional modifications. The most likely possible candidates were miR-21-5p and miR-16-5p with 3′-uridylation (iso-miR-16-5p, Table S-1B). The analysis of a spiked CLL sample allowed the confirmation of the identities of the two miRNAs (Figure 5E,F). The detection of these two miRNA was in good agreement with the results reported for similar samples by sample stacking CE-MS and RT-qPCR.[21,60] miR-21-5p was the first serum miRNA biomarker discovered in the sera of CLL patients;[10] it is a representative oncogenic miRNA, and the overexpression of miR-21-5p as well as miR-16-5p in CLL has been previously reported.[21,60] In the future, the identities of the detected miRNAs could be unambiguously confirmed by high-resolution tandem-MS analysis with a hybrid mass spectrometer.

■ CONCLUDING REMARKS

We have developed an on-line SPE-CE-MS method for the purification, preconcentration, separation, and characterization of endogenous microRNAs and their post-transcriptional modifications in serum. Under the optimized conditions with standards, the microcartridge lifetime (around 25 analyses) and repeatability (2.8 and <6.4% RSD for migration times and peak areas) were good, the method was linear between 25 and 100 nmol·L^{-1}, and the LOD was 10 nmol·L^{-1} (i.e., 50 and 5 times lower than by CE-MS and sample stacking CE-MS, 500 and 50 nmol·L^{-1}, respectively). Regarding the analysis of the serum

DOI: 10.1021/acs.analchem.8b00405
Anal. Chem. 2018, 90, 6618−6625

samples, it was necessary to apply an off-line sample pretreatment based on PCA extraction, but the recoveries for the miRNAs were >85%, and the performance of the SPE-CE-MS method was similar to that when the standards were used. Under the optimized conditions, it was possible to distinguish the healthy controls and CLL patients, because two endogenous miRNAs were detected at very low concentrations only in the diseased group. The results achieved show that SPE-CE-MS can be regarded as a promising technique for direct, high-throughput, sensitive, multiplex analyses capable of the preconcentration, quantification, and characterization of miRNA. The method also provides the unique structural information necessary for understanding the post-transcriptional regulation of miRNA function and can be used in the discovery of new miRNA biomarkers for cancer and other diseases in noninvasive biological fluids, such as serum or plasma.

■ ASSOCIATED CONTENT

Supporting Information

The Supporting Information is available free of charge on the ACS Publications website at DOI: 10.1021/acs.analchem.8b00405.

Optimized MS parameters, serum-sample extraction, quality parameters, characteristics and molecular masses of the analyzed miRNAs, study of the sheath liquid in CE-MS and the eluent and linearity in SPE-CE-MS, and list of miRNAs used for the screening of the CLL serum sample (PDF)

■ AUTHOR INFORMATION

Corresponding Author

*E-mail: vsanz@ub.edu. Tel.: (+34) 934021283. Fax: (+34) 934021233.

ORCID

Maxim V. Berezovski: 0000-0003-0514-599X

Fernando Benavente: 0000-0002-1688-1477

Notes

The authors declare no competing financial interest.

■ ACKNOWLEDGMENTS

This study was supported by a grant from the Spanish Ministry of Economy and Competitiveness (CTQ2014-56777-R). R.P.-G. acknowledges the Spanish Ministry of Education, Culture and Sport for a Formación del Profesorado Universitario (FPU) fellowship. M.V.B. thanks the NOVA DOMUS–CHEMEDPHO project funded by the Erasmus Mundus Action II of the European Commission for a travel grant. We want to particularly acknowledge the patients and the INCLIVA BioBank (PT13/0010/0004, B.0000768 ISCIII) integrated in the Valencian Biobanking Network and the Spanish National Biobanks Network for providing the serum samples. The authors thank Ryan Girgrah and Emil Zaripov for English-grammar correction.

■ REFERENCES

(1) Krol, J.; Loedige, I.; Filipowicz, W. *Nat. Rev. Genet.* **2010**, *11* (9), 597–610.

(2) Ha, T.-Y. *Immune Netw.* **2011**, *11* (3), 135–154.

(3) Zhang, Y.; Liu, D.; Chen, X.; Li, J.; Li, L.; Bian, Z.; Sun, F.; Lu, J.; Yin, Y.; Cai, X.; Sun, Q.; Wang, K.; Ba, Y.; Wang, Q.; Wang, D.; Yang, J.; Liu, P.; Xu, T.; Yan, Q.; Zhang, J.; Zen, K.; Zhang, C. Y. *Mol. Cell* **2010**, *39* (1), 133–144.

(4) Wang, K.; Zhang, S.; Weber, J.; Baxter, D.; Galas, D. J. *Nucleic Acids Res.* **2010**, *38* (20), 7248–7259.

(5) Wagner, J.; Riwanto, M.; Besler, C.; Knau, A.; Fichtlscherer, S.; Röxe, T.; Zeiher, A. M.; Landmesser, U.; Dimmeler, S. *Arterioscler., Thromb., Vasc. Biol.* **2013**, *33* (6), 1392–1400.

(6) Mitchell, P. S.; Parkin, R. K.; Kroh, E. M.; Fritz, B. R.; Wyman, S. K.; Pogosova-Agadjanyan, E. L.; Peterson, A.; Noteboom, J.; O'Briant, K. C.; Allen, A.; Lin, D. W.; Urban, N.; Drescher, C. W.; Knudsen, B. S.; Stirewalt, D. L.; Gentleman, R.; Vessella, R. L.; Nelson, P. S.; Martin, D. B.; Tewari, M. *Proc. Natl. Acad. Sci. U. S. A.* **2008**, *105* (30), 10513–10518.

(7) Brase, J. C.; Wuttig, D.; Kuner, R.; Sültmann, H. *Mol. Cancer* **2010**, *9* (1), 306.

(8) Chen, X.; Ba, Y.; Ma, L.; Cai, X.; Yin, Y.; Wang, K.; Guo, J.; Zhang, Y.; Chen, J.; Guo, X.; Li, Q.; Li, X.; Wang, W.; Zhang, Y.; Wang, J.; Jiang, X.; Xiang, Y.; Xu, C.; Zheng, P.; Zhang, J.; Li, R.; Zhang, H.; Shang, X.; Gong, T.; Ning, G.; Wang, J.; Zen, K.; Zhang, J.; Zhang, C.-Y. *Cell Res.* **2008**, *18* (10), 997–1006.

(9) Schwarzenbach, H.; Nishida, N.; Calin, G. A.; Pantel, K. *Nat. Rev. Clin. Oncol.* **2014**, *11* (3), 145–156.

(10) Lawrie, C. H.; Gal, S.; Dunlop, H. M.; Pushkaran, B.; Liggins, A. P.; Pulford, K.; Banham, A. H.; Pezzella, F.; Boultwood, J.; Wainscoat, J. S.; Hatton, C. S. R.; Harris, A. L. *Br. J. Haematol.* **2008**, *141* (5), 672–675.

(11) Kim, S. W.; Li, Z.; Moore, P. S.; Monaghan, A. P.; Chang, Y.; Nichols, M.; John, B. *Nucleic Acids Res.* **2010**, *38* (7), e98.

(12) Love, C.; Dave, S. *Methods Mol. Biol.* **2013**, *999* (4), 285–296.

(13) *RT-PCR Protocols*, 2nd ed.; King, N., Ed.; Humana Press: New York, 2010.

(14) Roden, C.; Mastriano, S.; Wang, N.; Lu, J. microRNA Expression Profiling: Technologies, Insights, and Prospects. In *microRNA: Medical Evidence*; Santulli, G., Ed.; Springer: Cham, Switzerland, 2015; Vol. *888*, pp 409–421.

(15) Wyman, S. K.; Knouf, E. C.; Parkin, R. K.; Fritz, B. R.; Lin, D. W.; Dennis, L. M.; Krouse, M. A.; Webster, P. J.; Tewari, M. *Genome Res.* **2011**, *21* (9), 1450–1461.

(16) Týčová, A.; Ledvina, V.; Klepárník, K. *Electrophoresis* **2017**, *38* (1), 115–134.

(17) Zhang, Z.; Zhu, G.; Peuchen, E. H.; Dovichi, N. J. *Microchim. Acta* **2017**, *184* (3), 921–925.

(18) Štěpánová, S.; Kašička, V. *J. Sep. Sci.* **2016**, *39* (1), 198–211.

(19) Ramautar, R.; Somsen, G. W.; de Jong, G. J. *Electrophoresis* **2017**, *38* (1), 190–202.

(20) van Dijk, E. L.; Auger, H.; Jaszczyszyn, Y.; Thermes, C. *Trends Genet.* **2014**, *30* (9), 418–426.

(21) Khan, N.; Mironov, G.; Berezovski, M. V. *Anal. Bioanal. Chem.* **2016**, *408* (11), 2891–2899.

(22) Breadmore, M. C.; Wuethrich, A.; Li, F.; Phung, S. C.; Kalsoom, U.; Cabot, J. M.; Tehranirokh, M.; Shallan, A. I.; Abdul Keyon, A. S.; See, H. H.; Dawod, M.; Quirino, J. P. *Electrophoresis* **2017**, *38*, 33–59.

(23) Šlampová, A.; Malá, Z.; Gebauer, P.; Boček, P. *Electrophoresis* **2017**, *38* (1), 20–32.

(24) Malá, Z.; Gebauer, P.; Boček, P. *Electrophoresis* **2017**, *38* (1), 9–19.

(25) Ramautar, R.; Somsen, G. W.; de Jong, G. J. *Electrophoresis* **2016**, *37*, 35–44.

(26) Medina-Casanellas, S.; Benavente, F.; Barbosa, J.; Sanz-Nebot, V. *Electrophoresis* **2011**, *32* (13), 1750–1759.

(27) Benavente, F.; Medina-Casanellas, S.; Giménez, E.; Sanz-Nebot, V. On-Line Solid-Phase Extraction Capillary Electrophoresis Mass Spectrometry for Preconcentration and Clean-Up of Peptides and Proteins. In *Capillary Electrophoresis of Proteins and Peptides: Methods and Protocols*; Tran, N. T., Taverna, M., Eds.; Springer: New York, 2016; pp 67–84.

(28) Benavente, F.; Vescina, M. C.; Hernández, E.; Sanz-Nebot, V.; Barbosa, J.; Guzman, N. A. *J. Chromatogr. A* **2007**, *1140* (1–2), 205–212.

DOI: 10.1021/acs.analchem.8b00405
Anal. Chem. 2018, 90, 6618–6625

(29) Hernández, E.; Benavente, F.; Sanz-Nebot, V.; Barbosa, J. *Electrophoresis* **2008**, *29* (16), 3366−3376.
(30) Medina-Casanellas, S.; Tak, Y. H.; Benavente, F.; Sanz-Nebot, V.; Sastre Toraño, J.; Somsen, G. W.; de Jong, G. J. *Electrophoresis* **2014**, *35* (20), 2996−3002.
(31) Medina-Casanellas, S.; Benavente, F.; Giménez, E.; Barbosa, J.; Sanz-Nebot, V. *Electrophoresis* **2014**, *35* (15), 2130−2136.
(32) Peró-Gascón, R.; Pont, L.; Benavente, F.; Barbosa, J.; Sanz-Nebot, V. *Electrophoresis* **2016**, *37* (9), 1220−1231.
(33) Pont, L.; Benavente, F.; Barbosa, J.; Sanz-Nebot, V. *Talanta* **2017**, *170*, 224−232.
(34) El-Khoury, V.; Pierson, S.; Kaoma, T.; Bernardin, F.; Berchem, G. *Sci. Rep.* **2016**, *6*, 19529.
(35) McAlexander, M. A.; Phillips, M. J.; Witwer, K. W. *Front. Genet.* **2013**, *4*, 1−8.
(36) Eldh, M.; Lotvall, J.; Malmhall, C.; Ekstrom, K. *Mol. Immunol.* **2012**, *50* (4), 278−286.
(37) Rowswell-Turner, R. B.; Barr, P. M. *J. Geriatr. Oncol.* **2017**, *8* (5), 315−319.
(38) *High Performance Capillary Electrophoresis*, 2nd ed.; Lauer, H. H., Rozing, G. P., Eds.; Agilent Technologies: Waldbronn, Germany, 2014.
(39) Medina-Casanellas, S.; Benavente, F.; Barbosa, J.; Sanz-Nebot, V. *Anal. Chim. Acta* **2012**, *717*, 134−142.
(40) Medina-Casanellas, S.; Benavente, F.; Barbosa, J.; Sanz-Nebot, V. *Anal. Chim. Acta* **2013**, *789*, 91−99.
(41) Potier, N.; Van Dorsselaer, A.; Cordier, Y.; Roch, O.; Bischoff, R. *Nucleic Acids Res.* **1994**, *22* (19), 3895−3903.
(42) Kullolli, M.; Knouf, E.; Arampatzidou, M.; Tewari, M.; Pitteri, S. J. *J. Am. Soc. Mass Spectrom.* **2014**, *25* (1), 80−87.
(43) Birdsall, R. E.; Gilar, M.; Shion, H.; Yu, Y. Q.; Chen, W. *Rapid Commun. Mass Spectrom.* **2016**, *30*, 1667−1679.
(44) Lam, B.; Elmogy, M.; Geng, S.-S.; Roberts, P.; Rghei, N.; Haj-Ahmad, Y. *Silicon Carbide as a Novel RNA Affinity Medium with Improved Sensitivity and Size Diversity*. https://norgenbiotek.com/sites/default/files/resources/Poster-13-Silicon-Carbide-as-a-Novel-RNA-Affinity-Medium-with-Improved-Sensitivity-and-Size-Diversity.pdf (accessed May 2, 2018).
(45) Norgen Biotek Corporation. *microRNA Purification Kit*. https://norgenbiotek.com/sites/default/files/resources/MicroRNA-Purification-Kit-Insert-PI21300-22-M14_0.pdf (accessed May 2, 2018).
(46) Giménez, E.; Sanz-Nebot, V.; Rizzi, A. *Anal. Bioanal. Chem.* **2013**, *405* (23), 7307−7319.
(47) Marusyk, R.; Sergeant, A. *Anal. Biochem.* **1980**, *105* (2), 403−404.
(48) Saraswat, M.; Grand, R. S.; Patrick, W. M. *Biosci., Biotechnol., Biochem.* **2013**, *77* (2), 402−404.
(49) Liu, R.; Chen, X.; Du, Y.; Yao, W.; Shen, L.; Wang, C.; Hu, Z.; Zhuang, R.; Ning, G.; Zhang, C.; Yuan, Y.; Li, Z.; Zen, K.; Ba, Y.; Zhang, C. Y. *Clin. Chem.* **2012**, *58* (3), 610−618.
(50) Abue, M.; Yokoyama, M.; Shibuya, R.; Tamai, K.; Yamaguchi, K.; Sato, I.; Tanaka, N.; Hamada, S.; Shimosegawa, T.; Sugamura, K.; Satoh, K. *Int. J. Oncol.* **2015**, *46* (2), 539−547.
(51) Hu, G.-Y.; Tao, F.; Wang, W.; Ji, K.-W. *World J. Surg. Oncol.* **2016**, *14* (1), 82.
(52) Gao, Y.; Dai, M.; Liu, H.; He, W.; Lin, S.; Yuan, T.; Chen, H.; Dai, S. *Oncotarget* **2016**, *7* (42), 68894−68908.
(53) Schmittgen, T. *Blood* **2013**, *122* (11), 1843−1844.
(54) Ferracin, M.; Zagatti, B.; Rizzotto, L.; Cavazzini, F.; Veronese, A.; Ciccone, M.; Saccenti, E.; Lupini, L.; Grilli, A.; De Angeli, C.; Negrini, M.; Cuneo, A. *Mol. Cancer* **2010**, *9*, 123.
(55) Kozomara, A.; Griffiths-Jones, S. *Nucleic Acids Res.* **2011**, *39*, 152−157.
(56) Moussay, E.; Wang, K.; Cho, J.-H.; van Moer, K.; Pierson, S.; Paggetti, J.; Nazarov, P. V.; Palissot, V.; Hood, L. E.; Berchem, G.; Galas, D. J. *Proc. Natl. Acad. Sci. U. S. A.* **2011**, *108* (16), 6573−6578.
(57) Calin, G. A.; Ferracin, M.; Cimmino, A.; Di Leva, G.; Shimizu, M.; Wojcik, S. E.; Iorio, M. V.; Visone, R.; Sever, N. I.; Fabbri, M.; Iuliano, R.; Palumbo, T.; Pichiorri, F.; Roldo, C.; Garzon, R.; Sevignani, C.; Rassenti, L.; Alder, H.; Volinia, S.; Liu, C.; Kipps, T. J.; Negrini, M.; Croce, C. M. *N. Engl. J. Med.* **2005**, *353*, 1793−1801.
(58) Fulci, V.; Chiaretti, S.; Goldoni, M.; Azzalin, G.; Carucci, N.; Tavolaro, S.; Castellano, L.; Magrelli, A.; Citarella, F.; Messina, M.; Maggio, R.; Peragine, N.; Santangelo, S.; Mauro, F. R.; Landgraf, P.; Tuschl, T.; Weir, D. B.; Chien, M.; Russo, J. J.; Ju, J.; Sheridan, R.; Sander, C.; Zavolan, M.; Guarini, A.; Foà, R.; Macino, G. *Blood* **2007**, *109* (11), 4944−4951.
(59) Van Roosbroeck, K.; Calin, G. A. *Semin. Oncol.* **2016**, *43* (2), 209−214.
(60) Feng, Y.-H.; Tsao, C.-J. *Biomed. Rep.* **2016**, *5* (4), 395−402.

DOI: 10.1021/acs.analchem.8b00405
Anal. Chem. 2018, 90, 6618−6625

Supporting Information

Optimized MS parameters

The MS parameters, optimized by infusion experiments with a 5000 nmol·L^{-1} let-7g-5p standard solution, were the following: capillary voltage 3500 V, drying gas temperature 350ºC, drying gas flow rate 6 L·min^{-1}, nebulizer gas 7 psig, fragmentor voltage 225 V, skimmer voltage 70 V, OCT 1 RF Vpp voltage 300 V. Data were collected in profile at 1 spectrum/s between 100 and 3,200 *m/z*, with the mass range set to high resolution mode (4 GHz).

Serum samples extraction

According to the manufacturer's instructions, 0.3 mL of serum was mixed with 0.3 mL of PCA solution, centrifuged at 12,000 g and the aqueous phase (upper) was transferred to a new tube. To evaluate the extraction methodology, healthy control serum samples were spiked with 50 nmol·L^{-1} of the standard miRNAs, immediately after the first extraction to avoid degradation by endogenous serum RNases. Extraction with PCA was repeated twice more, until no protein was visible in the interface. Then, the aqueous phase was extracted with 0.2 mL chloroform to remove any residual phenol. Alternatively, for the extraction with the TRIzol Reagent, 0.3 mL serum was mixed with 3 mL of the TRIzol Reagent and 0.6 mL chloroform. In accordance to the manufacturer's instructions, the extraction was repeated only once. In both cases, drop dialysis of the obtained aqueous phases (upper) was performed with MF-Millipore membrane filters of mixed cellulose esters, with average pore size diameter of 25 nm and 25 mm of diameter (Millipore, Molsheim, France). The filter was floated with the glossy side up on a beaker with 50 mL of water. After 5 min for allowing the floating filter to wet completely, 100 µL of the sample extract was carefully placed on the center of the membrane and dialyzed for 1 hour at room temperature.

Quality parameters

All quality parameters were calculated from data obtained by measuring peak area and migration time (t_m) from the extracted ion electropherogram (EIE) considering the *m/z* of the most abundant miR-21-5p and let-7g-5p ions from the cluster resolved for the $[M-5H]^{5-}$, and the sodium and potassium adducts $[M-6H+Na]^{5-}$ and $[M-6H+K]^{5-}$.

An estimation of the LODs was obtained by analyzing low-concentration standard mixtures (close to the LOD level, as determined from the approach based on S/N=3). LOQ was determined from the approach based on S/N=10. Reproducibility in SPE-CE-MS was evaluated as the relative standard deviation (percent RSD) of peak areas and t_m. Linearity range was studied between 10 and 150 nmol·L^{-1}. The lifetimes of the microcartridges was investigated by iteratively analyzing a standard mixture of 50 nmol·L^{-1}.

Table S-1. Characteristics and molecular masses of the **(A)** standard miRNAs, **(B)** miRNA tentatively identified by SPE-CE-MS in a CLL-patient serum sample.

miRNA ID	Sequence	Modification	m/z $[M+2-5H]^{5-}$ [a]		Calculated M_r ([M+2]) [a]		
			Theoretical	Observed	Theoretical	Observed	Error (ppm)
(A) Standard miRNAs							
hsa-miR-21-5p (miR-21-5p)	UAGCUUAUCAGACUGAUGUUGA	5' phos	1415.5707	1415.5592	7082.89	7082.84	8
hsa-let-7g-5p (let-7g-5p)	UGAGGUAGUAGUUUGUACAGUU	5' phos	1426.9677	1427.9537	7139.88	7139.81	10
(B) miRNA tentatively identified in a CLL-patient serum sample							
hsa-miR-21-5p (miR-21-5p)	UAGCUUAUCAGACUGAUGUUGA	5' phos	1415.5707	1415.5485	7082.89	7082.78	15
hsa-iso-miR16-5p	UAGCAGCACGUAAAUAUUGGCGU	5' phos, 3'-U	1488.9890	1488.9723	7449.98	7449.90	11

[a] M+2 corresponds to the most abundant ion of the isotopic distribution cluster resolved for the -5 molecular ion.

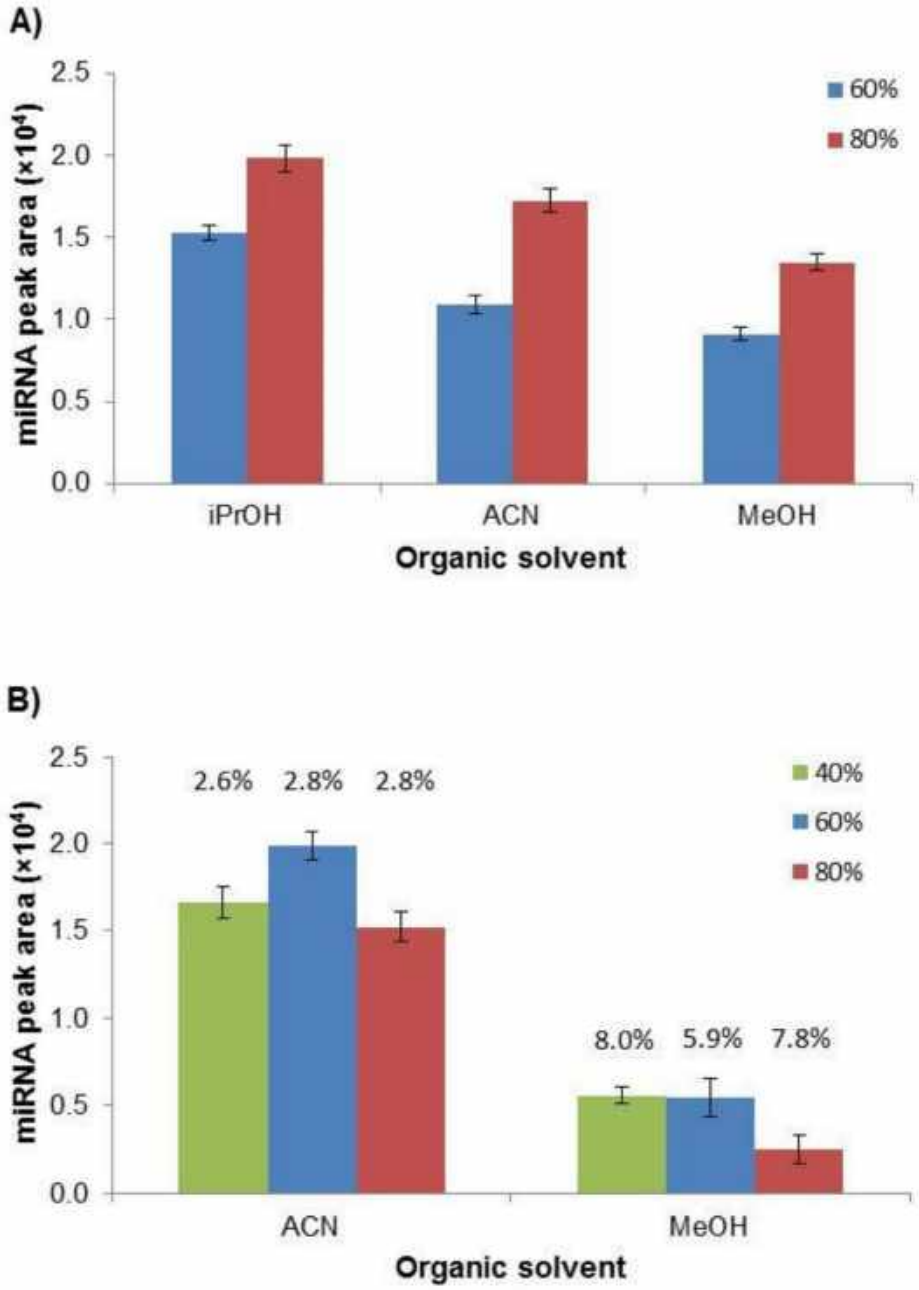

Figure S-1. Effect of the organic solvent **(A)** in the sheath liquid (CE-MS, 5,000 nmol·L^{-1} miR-21-5p standard) and **(B)** in the eluent (SPE-CE-MS, 50 nmol·L^{-1} miR-21-5p standard). Peak area of the injected (CE-MS) or eluted miRNA (SPE-CE-MS). All measurements were performed in triplicate (standard deviation is given as error bars, percentage RSD for migration times is given in numbers).

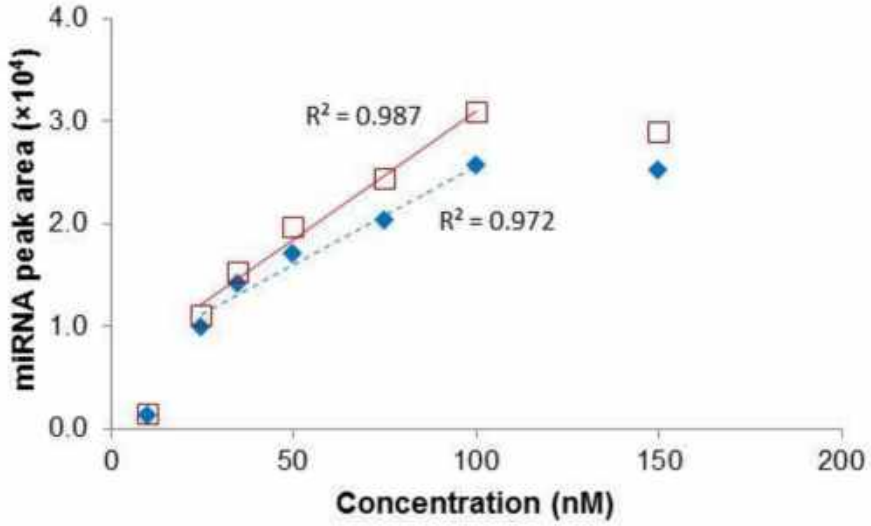

Figure S-2. Plot of peak area of the eluted miR-21-5p (♦) and let-7g-5p (□) vs concentration of the loaded standard mixture (930 mbar, 5 min). Regression line and R^2 value in the linearity range.

Table S-2. miRNAs reported in human B-cell chronic lymphocytic leukemia (CLL) plasma and cell samples used for the screening of endogenous miRNA in a CLL-patient serum sample by SPE-CE-MS (miRBase 21, http://www.mirbase.org [49]).

miRNA ID	Sequence	Length, nt
hsa-miR-15a-5p	UAGCAGCACAUAAUGGUUUGUG	22
hsa-miR-16-5p	UAGCAGCACGUAAAUAUUGGCG	22
hsa-miR-16-2-3p	CCAAUAUUACUGUGCUGCUUUA	22
hsa-miR-20a-5p	UAAAGUGCUUAUAGUGCAGGUAG	23
hsa-miR-21-5p	UAGCUUAUCAGACUGAUGUUGA	22
hsa-miR-23b-5p	UGGGUUCCUGGCAUGCUGAUUU	22
hsa-miR-24-3p	UGGCUCAGUUCAGCAGGAACAG	22
hsa-miR-29a-5p	ACUGAUUUCUUUUGGUGUUCAG	22
hsa-miR-93-5p	CAAAGUGCUGUUCGUGCAGGUAG	23
hsa-miR-101-5p	CAGUUAUCACAGUGCUGAUGCU	22
hsa-miR-106a-5p	AAAAGUGCUUACAGUGCAGGUAG	23
hsa-miR-146a-5p	UGAGAACUGAAUUCCAUGGGUU	22
hsa-miR-150-5p	UCUCCCAACCCUUGUACCAGUG	22
hsa-miR-155-5p	UUAAUGCUAAUCGUGAUAGGGGU	23
hsa-miR-195-5p	UAGCAGCACAGAAAUAUUGGC	21
hsa-miR-221-5p	ACCUGGCAUACAAUGUAGAUUU	22
hsa-miR-221-3p	AGCUACAUUGUCUGCUGGGUUUC	23
hsa-miR-222-5p	CUCAGUAGCCAGUGUAGAUCCU	22
hsa-miR-483-5p	AAGACGGGAGGAAAGAAGGGAG	22
hsa-miR-486-5p	UCCUGUACUGAGCUGCCCCGAG	22

Chapter 4. Improving the sensitivity and the selectivity in capillary electrophoresis by on-line solid-phase extraction capillary electrophoresis with a nanoliter valve

Unidirectional SPE-CE-MS, in which the microcartridge is mounted in series to the separation capillary, is straightforward to implement. However, this simple setup has some inherent limitations. On the one hand, the sample volumes introduced using pressure depend on the dimensions of the separation capillary. On the other hand, sample loading is conducted in the same direction as the subsequent separation. Therefore, some of the matrix components could be irreversibly adsorbed in the inner wall of the separation capillary. Furthermore, in many cases, the requirements of on-line preconcentration are incompatible with the BGE necessary for an efficient separation or sensitive MS detection. In order to overcome these drawbacks, some new configurations where the sample is introduced in an orthogonal direction to the separation have been proposed, requiring the use of valves.

In this chapter, we investigate nvSPE-CE-MS, a novel setup that uses an electrically isolated 4-port valve with an internal nanoliter loop. NvSPE-CE-MS is operated with a single CE instrument and two capillaries for independent and orthogonal SPE clean-up, preconcentration and electrophoretic separation. First, the analysis of a set of opioid peptides and Aβ peptide fragments by CE-MS has been evaluated. Then, a unidirectional SPE-CE-MS method with a C18 sorbent for the analysis of opioid peptides previously developed by our research group has been adapted to the new instrumentation. Finally, a nvSPE-CE-MS method has been developed and the advantages and disadvantages compared to the unidirectional SPE-CE-MS have been discussed.

This chapter includes the following publication:

- **Publication 4.1.** R. Pero-Gascon, F. Benavente, C. Neusüß, V. Sanz-Nebot, Evaluation of on-line solid-phase extraction capillary electrophoresis–mass spectrometry with a nanoliter valve for the analysis of peptide biomarkers, Anal. Chim. Acta. (2020) Submitted for publication.

Evaluation of on-line solid-phase extraction capillary electrophoresis–mass spectrometry with a nanoliter valve for the analysis of peptide biomarkers

Roger Pero-Gascon[1], Fernando Benavente[*1], Christian Neusüß[2], Victoria Sanz-Nebot[1]

[1] Department of Chemical Engineering and Analytical Chemistry, Institute for Research on Nutrition and Food Safety (INSA·UB), University of Barcelona, Barcelona 08028, Spain

[2] Faculty of Chemistry, Aalen University, Aalen 73430, Germany

[*]Corresponding author:

Fernando Benavente, PhD

fbenavente@ub.edu

Tel: (+34) 934039116, Fax: (+34) 934021233

KEYWORDS: capillary electrophoresis ; heart-cut ; mass spectrometry ; mechanical valve ; on-line solid-phase extraction ; peptides

ABSTRACT

On-line solid-phase extraction capillary electrophoresis-mass spectrometry (SPE-CE-MS) is a powerful technique for high throughput sample clean-up and analyte preconcentration, separation, detection, and characterization. The most typical design due to its simplicity and low cost is unidirectional SPE-CE-MS. However, in this configuration, the sample volumes introduced by pressure depend on the dimensions of the separation capillary and some matrix components could be irreversibly adsorbed in its inner walls. Furthermore, in many cases, the requirements of on-line preconcentration are incompatible with the background electrolyte necessary for an efficient separation and sensitive MS detection. Here, we present SPE-CE-MS with a nanoliter valve (nvSPE-CE-MS) to overcome these drawbacks while keeping the design simple. The nvSPE-CE-MS system is operated with a single CE instrument and two capillaries for independent and orthogonal SPE preconcentration and CE separation, which are interfaced through an external and electrically isolated valve with a 20 nL sample loop. The instrumental setup is proved for the analysis of opioid and amyloid beta peptide biomarkers in standards and plasma samples. NvSPE-CE-MS allowed decreasing the limits of detection (LODs) 200 times with regard to CE-MS. Compared to unidirectional SPE-CE-MS, peak efficiencies were better and repeatabilities similar, but total analysis times longer and LODs for standards slightly higher due to the heart-cut operation and the limited volume of the valve loop. This small difference on the LODs for standards was compensated for plasma samples by the improved tolerance of nvSPE-CE-MS to complex sample matrices. In view of these results, the presented setup can be regarded as a promising versatile alternative to avoid complicated matrix samples entering the separation capillary in SPE-CE-MS.

1. Introduction

The analysis of biomarkers of different diseases or physiological processes in biological samples is difficult, in general, due to their low concentration and the complexity of the sample matrix [1–3]. Capillary electrophoresis-mass spectrometry (CE-MS) is a proficient technique for the highly efficient separation and characterization of polar and charged biomarkers, including peptides and proteins [4–6]. However, as in many other microscale separation techniques, the limited concentration sensitivity of CE for most analytes, due to the reduced sample injection volumes needed for an appropriate separation (typically 1-2% of the capillary volume), very often hinders a more widespread application [7–9]. To lower the limit of detection (LOD), on-line solid-phase extraction capillary electrophoresis (SPE-CE) is recognized as an excellent alternative [8–10]. Unidirectional SPE-CE is the most typical design due to its simplicity and low cost [8,9]. In this configuration, an extraction microcartridge is inserted near the inlet of the separation capillary and contains an appropriate sorbent to retain the analytes from a large volume of sample (~50-100 µL). After sample loading, the capillary is rinsed to eliminate non-retained molecules and filled with background electrolyte (BGE). Then, the analytes are eluted in a small volume of an appropriate solution (~25-50 nL), resulting in sample clean-up and concentration enhancement before the electrophoretic separation and detection [11]. As can be noted from this method, the introduction of the sample and the washing of the microcartridge before the elution of the retained compounds are conducted in the same direction as the subsequent separation. This could be detrimental when loading complex samples, because some of the matrix components could be irreversibly adsorbed in the inner wall of the separation capillary, or when the requirements of on-line preconcentration are incompatible with the BGE necessary for an efficient separation and sensitive MS detection. In addition, the sample volumes introduced by pressure depend on the small internal diameter (id) and the total length (L_T) of the separation capillary. In order to overcome these drawbacks, other designs have been proposed, in which the sample is introduced in an orthogonal direction to the separation [3,8–10]. These orthogonal designs with microfluidic devices or capillaries require the use of valves and are more difficult to construct and operate than the typical unidirectional SPE-CE microcartridges.

In 1987, Tsuda et al. [12] devised a rotary-type valve suitable for sample injection in CE. This concept was considered by Debets et al. [13] to develop an on-line SPE-CE system that needed a liquid chromatography (LC) pump to load the sample in a SPE column contained in a rotary-type valve. After switching the valve position, the analytes were eluted and separated in the CE capillary. Later, Tempels et al. [14] demonstrated on-line SPE-CE-MS via a valve interface. However, the system implied certain complexity because a LC pump and three valves were required. In the following years, the contributions about SPE-CE using capillaries and valves were scarce, due to the complexity of the instrumental setups and poor performance of

the valves [8,15,16]. Recently, Kohl et al. [17] introduced a novel 4-port valve with an internal nanoliter loop for the direct coupling of two capillaries. This setup has shown high versatility for two-dimensional separation with on-line MS detection, having been successfully applied for two-dimensional capillary zone electrophoresis [18], capillary isoelectric focusing[19], imaged capillary isoelectric focusing [20], and capillary sieving electrophoresis with sodium dodecyl sulphate [21]. In these applications, the analytes are separated with high efficiency in the first dimension, using in most of the cases a BGE containing non-compatible components with on-line MS detection. Then, the peaks of interest are heart-cut, transferred, separated from the co-transferred MS interfering compounds and detected in the second dimension. Taking into account that capillaries used in both dimensions are independent, this setup for bidimensional CE separations could also be suitable for developing SPE-CE-MS with a nanoliter valve (nvSPE-CE-MS) methods for purification and preconcentration of biomarkers. The clean-up and preconcentration step will take place in the first-dimension capillary (loading capillary) and the separation and MS detection in the second-dimension (separation capillary).

In this study, we investigate for the first time the potential of nvSPE-CE-MS in comparison with unidirectional SPE-CE-MS for the analysis of peptide biomarkers in standards and plasma samples. Specifically, opioid peptides and amyloid beta (Aβ) peptide fragments were analyzed because of their importance in different neurological disorders, including chronic pain and Alzheimer's disease, respectively [22,23].

2. Materials and methods

2.1. Chemicals and reagents

Ultrapure water (18 MΩ*cm at 25 °C) from an SG UltraClear UV system (Siemens Water Technologies, Günzburg, Germany) was used to prepare all background electrolytes (BGEs), samples, and solutions. Acetic acid (HAc; ROTIPURAN, 100%, p.a.), acetonitrile (ACN; MS grade), ammonium hydroxide solution (ROTIPURAN, 30%, p.a.), formic acid (HFor; ROTIPURAN, ≥98%, p.a., ACS), methanol (MeOH; MS grade), propan-2-ol (MS grade), sodium formate (≥99% ACS), and sodium hydroxide (≥98%) were supplied by Carl Roth (Karlsruhe, Germany). Dynorphin A (1–7) (Dyn A), endomorphin 1 (End 1), methionine enkephalin (Met), and human plasma (P9523) were provided by Sigma-Aldrich (St. Louis, MO, USA). Aβ peptide fragments 1-15, 10-20, 20-29, and 25-35 were provided by Bachem (Bubendorf, Switzerland). Sep-Pak C18 cartridges (55–105 µm particle diameter, 125 Å pore size) were supplied by Waters (Milford, MA, USA). PEG (average M_r=8,000) was purchased from Fluka (Buchs, Switzerland).

2.2. Electrolyte solutions, sheath liquid, and standards

The method for the analysis of opioid peptides by unidirectional SPE-CE-MS was adapted from a previous work [11,24,25]. The separation BGE contained 50 mM HAc:50 mM HFor, pH 3.0 adjusted with ammonium hydroxide solution. The sheath liquid solution consisted of a hydroorganic mixture of 60:40 (v/v) propan-2-ol:water with 0.05% (v/v) of HFor and was delivered at a flow rate of 4.0 $\mu L \cdot min^{-1}$ by a syringe pump (Cole-Parmer, Vernon Hills, IL, USA). The eluent consisted of 60:40 (v/v) MeOH:water with 50 mM HAc:50 mM HFor. Elution conditions were reoptimized for nvSPE-CE-MS, and the optimized eluent consisted of 80:20 (v/v) ACN:water with 50 mM HAc:50 mM HFor.

An aqueous standard solution of each peptide at 2,500 $mg \cdot L^{-1}$ was prepared and stored in a freezer at -20ºC when not in use. Working standard solutions containing the three opioid peptides or the four Aβ peptide fragments were obtained by mixing and diluting with water. These mixtures were used to spike human plasma samples in order to obtain the fortified samples. Diluted solutions were discarded at the end of the day.

2.3. Apparatus, instrumentation and procedures

pH measurements were made with a pH-meter 691 (Metrohm, Herisau, Switzerland). Agitation was performed with a vortex mixer 7-2020 (NeoLab, Heidelberg, Germany). Centrifugations were performed in a Minispin plus (Eppendorf, Hamburg, Germany).

CE-MS experiments were performed on a PA 800 Plus pharmaceutical analysis system (Beckman Coulter, Brea, CA, USA) coupled to a micrOTOF-Q (Bruker Daltonics, Bremen, Germany) through a G1607A orthogonal sheath flow electrospray interface (Agilent Technologies, Waldbronn, Germany). CE control and data analysis were carried out using 32 Karat version 10.1 software (Beckman Coulter). MS control and data analysis were carried out using micrOTOF control version 2.3 software (Bruker Daltonics). The mass spectrometer was operated in ESI+ mode. MS parameters were optimized by infusion of the analytes at 0.7 psi through the capillary to the MS: end plate -500 V, capillary voltage 4500 V, nebulizer gas 0.5 bar, gas temperature 170 ºC, dry gas flow rate 2 $L \cdot min^{-1}$, transfer time 40 µs, prepuls storage 10 µs, scan range 100-1250 m/z.

Calibration was performed every day by infusing a 5 mM sodium formate solution in sheath liquid.

2.3.1. CE-MS

Separations were performed at 25°C in a 72 cm L_T × 50 µm id × 365 µm od bare fused-silica capillaries (Polymicro Technologies, Phoenix, AZ, USA). All capillary rinses were performed at 14 psi. For new capillaries or between workdays, the capillaries were activated flushing off-line to avoid the unnecessary contamination of the MS system, with 1 M NaOH (15

or 5 min, respectively), water (15 or 10 min), and BGE (30 or 15 min). Samples were hydrodynamically injected at 0.7 psi for 10 s (12 nL, estimated using the Hagen–Poiseuille equation [26]) and a separation voltage of +15 kV (normal polarity, cathode in the outlet) was applied. Between runs, the capillary was conditioned flushing with water (2 min) and BGE (2 min). The capillary was stored overnight filled with water.

2.3.2. CE-MS with a nanoliter valve (nvCE-MS)

The C4N-4354-.02D microinjector four-port valve, including rotors (internal sample loop of 20 nL) and stators both made from plastic material (PAEK and Valcon E, respectively), was obtained from VICI AG International (Schenkon, Switzerland). A detailed description of the general valve design can be found elsewhere [17]. Prior to assembling the valve, all channels and surfaces were carefully cleaned to avoid contamination and particles that may cause obstructions. The valve could be switched between two positions, loading position (Figure 1-A, with no SPE microcartridge installed for nvCE-MS) and separation position (Figure 1-B), using an actuator controlled via two buttons.

Capillaries were connected to the valve by 1/32″ fingertight fittings in combination with appropriate 1/32″ sleeves for the use of 365 µm od capillaries. The loading capillary (65 cm L_T × 75 µm id × 365 µm od) was cut into two fragments 1a and 1b (L_{cap1a} 50 cm and L_{cap1b} 15 cm) (Figure 1). Capillary 1a inlet was placed in the outlet of the CE instrument to apply pressure for washing, injecting and mobilizing the sample, while the outlet was connected to the valve port S. Capillary 1b was connected from port W to a waste vial. The separation capillary (100 cm L_T × 50 µm id × 365 µm od) was cut into two fragments 2a and 2b (L_{cap2a} 55 cm and L_{cap2b} 45 cm) (Figure 1). Capillary 2a inlet was placed in the inlet of the CE instrument, to apply voltage for the electrophoretic separation, and the outlet was connected to the valve port P. Capillary 2b was connected from port C to the MS interface.

Capillary 1a possessed a window at 8 cm before the valve (L_{eff} 42 cm). An external UV detector ECD2000 (ECOM spol, Chrastany u Prahy, Czech Republic) was used to monitor UV signal at 200 nm wavelength. Control and data processing were carried out by ECOMAC v0.281 software (ECOM spol).

The transfer of the sample from the loading to the separation capillary was made switching the valve when the sample reached the center of the valve sample loop (switching time, t_2). This time was calculated before each analysis taking into account the mobilization velocity (L_{eff} / t_1, where t_1 is the time measured when the sample plug was detected by UV) and the total distance covered by the sample plug up to the loop center (i.e., L_{cap1A} + 0.25 cm, if the 20 nL valve loop was assumed to be equivalent to a 0.5 cm L_T x 75 µm id capillary).

While in loading position, the nebulizer gas and the ESI capillary voltage were switched off to avoid bubble formation in the separation capillary during the sample transfer. First, the

separation capillary was equilibrated flushing with BGE at 14 psi for 2 min. After that, the loading capillary was flushed with water at 14 psi for 2 min. Then, the sample was hydrodynamically injected in the loading capillary at 0.7 psi for 30 s (190 nL [26]) and pushed at 1 psi with water. The mobilization was stopped at t_2 and the valve was switched to the separation position to transfer 20 nL of sample to the separation capillary. Separation was conducted applying a voltage of +15 kV (normal polarity). After the first 0.2 min of the separation, the nebulizer gas and the ESI capillary voltage were switched on. The capillaries were stored overnight filled with water.

It is worth highlighting that the setup for nvCE-MS using a PA 800 Plus pharmaceutical analysis system was straightforward because this CE instrument allows applying pressure up to 70 psi in both the inlet (separation capillary) and the outlet (loading capillary). Other CE instruments may require some modifications to work with a single instrument. For example, in a classical Agilent HP 3DCE instrument (Agilent Technologies) the low pressure (i.e., ≤50 mbar) used for sample injection and mobilization could be only applied in the inlet, hence the inlet and outlet tubings coming from the CE pump must be exchanged, and also the power and data cables of both lifts, to adapt the instrument for nvCE-MS.

2.3.3. Unidirectional SPE-CE-MS

The construction of the double-frit particle packed SPE microcartridge was monitored under a stereomicroscope and was carried out as described elsewhere [11,24,25] with some modifications due to the configuration of the cartridge cassette of the PA 800 Plus instrument. A capillary (72 cm L_T × 75 µm id × 365 µm od) was activated and, then, cut into two pieces of 30 and 42 cm to insert in between the microcartridge (0.7 cm L_T x 250 µm id x 365 µm od). Before, a polyethylene frit obtained from a small fragment of the original filters found in the C18 Sep-Pak cartridges was introduced in one of the ends of the microcartridge. This microcartridge end was coupled to the 30 cm capillary (inlet) using a 0.5 cm Tygon® tube of 250 µm id. Then, the microcartridge was vacuum-filled with C18 sorbent from the Sep-Pak cartridge until it was completely full. Finally, a second polyethylene frit was inserted in the end side and the microcartridge was connected to the 42 cm capillary (outlet) using another Tygon® tube.

The method for unidirectional SPE-CE-MS was adapted from our previous works [11,24,25]. SPE-CE-MS column was conditioned flushing at 14 psi consecutively with water (1 min), MeOH (1 min), water (1 min), and BGE (3 min). The sample was loaded by flushing at 14 psi for 10 min (approximately 60 µL). The non-retained molecules were eliminated and the capillary was equilibrated by rinsing with BGE for 2 min. Retained peptides were desorbed by injection of the eluent solution at 0.7 psi for 10 s (60 nL). Separation was conducted applying a voltage of +15 kV (normal polarity). Between runs, the capillary was rinsed with water (2 min)

and ACN (2 min) to avoid carry-over between consecutive analyses. The SPE-CE-MS capillary was stored overnight filled with ACN.

2.3.4. SPE-CE-MS with a nanoliter valve (nvSPE-CE-MS)

The microcartridge was prepared as described for unidirectional SPE-CE-MS (section 2.3.3) and inserted in the loading capillary 1a at 30 cm from the inlet (Figure 1).

While in loading position, as in nvCE-MS, the nebulizer gas and the ESI capillary voltage were switched off. First, the separation capillary was equilibrated flushing with BGE at 14 psi for 2 min. After that, the loading capillary was conditioned as in unidirectional SPE-CE-MS, flushing at 14 psi consecutively with water (1 min), MeOH (1 min), water (1 min), and BGE (3 min). The sample was loaded by flushing at 14 psi for 10 min (approximately 60 µL). After rinsing with water for 2 min, retained peptides were desorbed injecting the eluent solution at 1 psi for 30 s (280 nL). The eluent plug was pushed at 1 psi with water until stopping the mobilization at t_2. Then, the valve was switched to the separation position to transfer 20 nL of the eluent plug to the separation capillary. Three additional 20 nL heat-cuts were consecutively transferred repeating thrice the following two steps: first, the valve was switched back to the loading position (Figure 1-A) and another fraction of the elution plug from the loading capillary was pushed with water to the sample loop at 0.5 psi for 5 s (23 nL). Second, the valve was switched to the separation position (Figure 1-A) and the elution plug inside the sample loop was pushed to the separation capillary at 1 psi for 20 s (24 nL). Once the transfer of four heart-cuts was completed, separation was conducted applying a voltage of +15 kV (normal polarity). The nebulizer gas and the ESI capillary voltage were switched on after the first 0.2 min of separation. Between runs, the loading capillary was rinsed with water (2 min) and ACN (2 min), to avoid carry-over between consecutive analyses. The SPE-CE loading capillary was stored overnight filled with ACN. The separation capillary was stored overnight filled with water.

2.3.5. Plasma samples pretreatment

Lyophilized plasma was dissolved in 5 mL of water, aliquoted and frozen at -20 ºC. Aliquots of the frozen plasma were thawed at room temperature when required. In order to prepare spiked samples, an appropriate amount of the standard peptide mixture was added to each plasma aliquot at a ratio 99:1 (v/v) plasma:standard solution and was vortexed thoroughly. Precipitation with ACN was done as previously described [27] starting with 200 µL of spiked plasma. The pooled supernatant was evaporated using a Savant DNA 120 SpeedVac (Thermo Fisher Scientific, Massachusetts, USA) and was reconstituted with 100 µL of water. The solution was subjected to ultrafiltration using Amicon Ultra-0.5 10,000 M_r cut-off cellulose acetate filters (Millipore, Bedford, MA, USA) passivated with 5% (v/v) of PEG in water [27].

2.3.6. Quality parameters

All quality parameters with MS detection were calculated from data obtained by measuring peak area and migration time (t_m) from the extracted ion electropherogram (EIE) of each peptide. The m/z values of the molecular ions considered for each peptide are shown in Table 1. Repeatability was evaluated as percentage of the relative standard deviation (%RSD) of peak areas and t_m for triplicate analysis (n=3). The LOD (S/N=3) for each peptide was obtained analyzing low-concentration samples.

3. Results and discussion

3.1. CE-MS

In previous works, the acid-base properties of opioid peptides [28] and Aβ peptide fragments [29] were characterized by CE-UV to establish electrophoretic migration models and systematically optimize their separation. Accurate pK_a values were determined, which can be used to easily obtain charge-to-mass ratios (q/M_r) of the peptides and to calculate the multicriterium optimization function T^* for a simple, experiment-free and reliable selection of optimized separation conditions [30]. Figure 2A shows the plot of $T^*(q/M_r^{1/2})$ vs pH for the mixture of the three opioid peptides (Dyn A, End 1, and Met) where a maximum indicates that the best separation will be obtained at pH values ranging from 3.0 to 3.5. Figure 2B-i shows the EIEs for the analysis of standards at 10 $mg \cdot L^{-1}$ by CE-MS using 50 mM HAc:50 mM HFor, pH 3.0, as BGE demonstrating that the three opioid peptides were separated. At this concentration, %RSD values ranged from 8.7 to 10% for peak areas and 1.5 to 2.7% for t_m (Table S-1). The LOD for the analysis of the opioid peptides by CE-MS was 100 $\mu g \cdot L^{-1}$ (Table 1), similar to the value obtained in previous studies [24,31].

The same strategy was followed to select pH 3.0 for the separation of a mixture of the four Aβ peptide fragments (Aβ 1-15, 10-20, 20-29, and 25-35) [29]. Figure S-1A shows the EIEs for the analysis of standards at 10 $mg \cdot L^{-1}$ by CE-MS using 50 mM HAc:50 mM HFor, pH 3.0, as BGE and the four Aβ peptide fragments were separated. At this concentration, %RSD values ranged from 7.4 to 11% for peak areas and 0.92 to 1.3% for t_m (Table S-1). The LOD was slightly higher than for the opioid peptides, probably due to the larger M_r of the Aβ peptide fragments, and values ranged between 500 and 1,500 $\mu g \cdot L^{-1}$ (Table 1).

3.2. nvCE-MS

In order to evaluate the instrumental setup, nvCE-MS was tested, using the same separation conditions as in CE-MS. Sample was hydrodynamically injected in the loading capillary and transferred to the separation capillary through the valve. This transfer step is a crucial part of the nvCE-MS methodology because precise positioning of the sample in the loop is mandatory. A simple approach is to estimate the time required to mobilize the sample until it

reaches the center of the valve sample loop (t_2), as described in section 2.3.2. Mobilization of the sample through the loading capillary pushing with BGE was first tested, but UV detection of the sample plug was difficult due to the intense UV absorption of the HFor and HAc in the BGE. Therefore, it was decided to mobilize the sample by pushing with water. A pressure of 1 psi was selected because it resulted in a t_2 of around 7 min, which was a good compromise between the flow rate necessary for a precise peak cutting and total analysis time. Pressure was stopped at t_2 and the valve was switched from the loading to the separation position (Figure 1). Then, the analytes were electrophoretically separated, detected and characterized by CE-MS. Separation voltage was limited to +15 kV to prevent any current leakage due to the material properties of the valve and the close distance of the rotor channels [18]. Figure 2B-ii shows the analysis of the opioid peptides at 10 $mg \cdot L^{-1}$ by nvCE-MS. Compared to the analysis by CE-MS (Figure 2B-i), the total analysis time was shorter mainly due to the shorter separation distance (45 cm capillary 2b in nvCE-MS vs 72 cm capillary in CE-MS). The peak areas and repeatability were similar to those in CE-MS, %RSD values ranged from 5.9 to 8.3% for peak areas and 0.74 to 1.8% for t_m (Table S-1).

3.3. Unidirectional SPE-CE-MS

In order to lower the LODs of CE-MS, on-line preconcentration was used. First, the unidirectional SPE-CE-MS method developed in previous works for the analysis of opioid peptides [11,24,25] was adapted to the available CE-MS-instrumentation for a meaningful comparison with subsequent nvSPE-CE-MS. Figure 3A-i shows the analysis of the opioid peptides at 1 $\mu g \cdot L^{-1}$ by unidirectional SPE-CE-MS. Compared to CE-MS (Figure 2B-i), the peaks were slightly wider mainly due to the use of a wider capillary (75 vs 50 µm id), but the three peaks were still baseline separated. Repeatabilities were similar, with %RSD values from 6.9 to 12% for peak areas and 1.2 to 1.6% for t_m (Table S-1). The LOD was around 0.1 $\mu g \cdot L^{-1}$ (Table 1), an improvement of 1000 times compared to CE-MS.

For the analysis of plasma samples by unidirectional SPE-CE-MS, a double-step sample clean-up pretreatment consisting of precipitation with ACN followed by ultrafiltration through 10,000 M_r cut-off filters was necessary to prevent the microcartridge blockage due to saturation of the limited amount of C18 sorbent contained inside [27]. Figure 3B-i shows the analysis of a pretreated plasma sample spiked at 10 $\mu g \cdot L^{-1}$ by unidirectional SPE-CE-MS. Compared to the analysis of standards (Figure 3A-i), the separation resolution and repeatabilities for peak areas were similar, with %RSD values from 11 and 13% (Table S-1). %RSD values for t_m were slightly increased, ranging from 3.7 to 4.6%. The LODs were 1 $\mu g \cdot L^{-1}$ for End 1 and Met (Table 1), which supposed 10 times increase compared to standards due to the complexity of the sample matrix. Furthermore, Dyn A presented the highest LOD (10 $\mu g \cdot L^{-1}$) because its M_r was larger (Table 1) and recovery after the sample pretreatment was lower [27].

Unidirectional SPE-CE-MS is simple, low cost and valve-free operated and has been widely and successfully demonstrated [8,9]. However, it has several drawbacks due to performing both SPE preconcentration and electrophoretic separation in the same capillary. Consequently, capillary dimensions (i.e., L_T and id) must be selected as a compromise between sample loadability at a certain pressure and efficient electrophoretic separation. In addition, loaded sample matrix components could irreversible contaminate the separation capillary or the MS, if the ionization voltage or the nebulizer gas values are not set to zero. Finally, for an appropriate separation it is required to fill the loading capillary with an MS compatible BGE, which could promote undesired elution of the analytes in some applications. In order to overcome these disadvantages, we investigated nvSPE-CE-MS.

3.4. nvSPE-CE-MS

The starting point for the optimization of the nvSPE-CE-MS methodology was the optimized conditions for unidirectional SPE-CE-MS. The instrumental setup of nvSPE-CE-MS was the same as for nvCE-MS with the addition of a microcartridge in the loading capillary. The methodology was as follows: in loading position (Figure 1-A), the sample was loaded hydrodynamically in the loading capillary and the analytes were retained in the microcartridge. As loading and separation capillaries were independent, there was no contamination of the separation capillary or the MS due to the loaded sample matrix. Then, the loading capillary was washed to eliminate the non-retained compounds. The eluent was injected, mobilized by pressure pushing with water, and transferred to the separation capillary by switching the valve. In separation position (Figure 1-B), the voltage was applied and the eluted analytes were separated, detected, and characterized by CE-MS.

In nvSPE-CE-MS, the loading and separation capillaries were independent, hence their dimensions could be different. A loading capillary with wide id (i.e., 75 µm id) was selected for an adequate loadability (i.e., load a larger volume of sample for a given time or decrease the loading time for a certain sample volume) whereas a separation capillary with narrow id (i.e., 50 µm id) was used to obtain better peak efficiency. As the microcartridge was not inserted in the separation capillary, potential issues derived from current breakage due to backpressure were also avoided. In addition, the separation capillary could be always kept full with BGE while all the SPE pressure-based steps were done in the loading capillary.

Preliminary results by nvSPE-CE-MS showed that, of the three opioid peptides, only Dyn A was detected when the elution conditions of unidirectional SPE-CE-MS were applied (injection of 60:40 (v/v) MeOH:water with 50 mM HAc:50 mM HFor at 0.7 psi for 10 s). This poor elution was probably because the volume of eluent injected was lower than expected, due to the increased backpressure caused by the presence of the valve. Quantitative desorption of the analytes was achieved when the eluent was injected at 1 psi for 30 s. The eluent plug reached

the center of the valve after about 8 min of pushing with water at 1 psi, a slight increase compared to nvCE-MS (i.e., 7 min) due to the presence of the microcartridge.

The elution profile of the three opioid peptides using different hydroorganic eluents was investigated and characterized by the analysis of several consecutive heart-cuts of the elution plug, because of the limited volume of the valve sample loop (20 nL). Figure 4-A shows the elution profile using 60:40 (v/v) MeOH:water with 50 mM HAc:50 mM HFor as eluent. In the first two heart-cuts, mainly Dyn A was detected, indicating that Dyn A elution was faster than for End 1 and Met, coherently with the previous preliminary results. End 1 and Met were mainly detected in the third and fourth heart-cuts. Therefore, using an eluent of 60:40 (v/v) MeOH:water with 50 mM HAc:50 mM HFor at least four or more heart-cuts would be needed for a quantitative transfer of the eluted opioid peptides. To elute the analytes in a narrower zone, the eluotropic strength of the eluent was increased. Figure 4-B shows the elution profile using an eluent of 80:20 (v/v) ACN:water with 50 mM HAc:50 mM HFor. In this case, although Dyn A still eluted slightly faster, the elution profile of all the opioid peptides was coincident and more than 85% of the total sum of peak areas of the three opioid peptides was detected considering the second and third heart-cuts. However, it was decided to apply four consecutive heart-cuts (4x20 nL=80 nL) in order to ensure a complete and repeatable transfer of the eluted peptides. Figure 3A-ii shows the analysis of the three opioid peptides at 1 $\mu g \cdot L^{-1}$ by nvSPE-CE-MS in the optimized conditions. Compared to the analysis by unidirectional SPE-CE-MS (Figure 3A-i), the total analysis time was shorter, mainly due again to the shorter separation distance (45 cm capillary 2b in nvSPE-CE-MS vs 72 cm capillary in unidirectional SPE-CE-MS). In addition, the peak efficiency was better because a narrower separation capillary was used for the separation (50 vs 75 µm id in nvSPE-CE-MS and unidirectional SPE-CE-MS, respectively). The differences in the peak intensities may be due to the lower volume of sample loaded because of the extra backpressure promoted by the valve or because of partial loss of the elution plug in the multiple heart-cut transfer. For 1 $\mu g \cdot L^{-1}$, repeatability was similar compared to CE-MS and unidirectional SPE-CE-MS, with %RSD values from 9.0 to 11% for peak areas and 1.4 to 2.4% for t_m (Table S-1). The LOD for the analysis of the opioid peptides by nvSPE-CE-MS was 0.5 $\mu g \cdot L^{-1}$ (Table 1), 200 times lower than by CE-MS and 5 times higher than by unidirectional SPE-CE-MS.

The analysis of pretreated plasma samples was also evaluated by nvSPE-CE-MS. Figure 3B-ii shows the analysis of a pretreated plasma sample spiked at 10 $\mu g \cdot L^{-1}$. Similarly to the analysis of standards, the total analysis time was shorter and the peak intensities were lower in nvSPE-CE-MS than in unidirectional SPE-CE-MS (Figure 3B-i), and %RSD values were similar, ranging from 5.3 to 13% for peak areas and 4.2 to 5.9% for t_m (Table S-1). This similarity in the %RSD of peak areas and t_m suggested that the separation capillary was not apparently contaminated during the sample loading in unidirectional SPE-CE-MS. Otherwise

the higher %RSD values compared to standards would be related in both cases to the impurities from the complex sample matrix eluted with the peptides, which did not affect separation resolution. The LODs for the opioid peptides in plasma samples ranged from 1 to 10 $\mu g \cdot L^{-1}$ (Table 1), hence 2 to 20 times higher compared to standards. This increase of the LODs could be explained by the complex sample matrix and the recoveries of the sample pretreatment, as also indicated before for unidirectional SPE-CE-MS. Nevertheless, as the LODs of both methodologies for plasma samples were similar, this would indicate a lower sample matrix effect in nvSPE-CE-MS.

To further validate the nvSPE-CE-MS approach with a different set of peptide biomarkers, a mixture of Aβ peptides at 10 $\mu g \cdot L^{-1}$ was analyzed (Figure S-1B). Compared to CE-MS at 10 $mg \cdot L^{-1}$ (Figure S-1A), the relative peak area of Aβ 10-20 decreased probably due to the lower retention of this peptide in the C18 sorbent. Repeatability was similar to the obtained for the analysis of opioid peptides, with %RSD values from 5.3 to 12% for peak areas and 1.8 to 2.7% for t_m (Table S-1). The LOD for the analysis of Aβ peptides by nvSPE-CE-MS was 5 $\mu g \cdot L^{-1}$ (Table 1), around 200 times lower than by CE-MS.

Figure S-1C shows the analysis of a pretreated plasma sample spiked at 50 $\mu g \cdot L^{-1}$ by nvSPE-CE-MS. Compared to the analysis of standards (Figure S-1B), the separation resolution and the repeatability for peak areas were similar, with %RSD values from 5.1 to 13%, and the %RSD for t_m was again slightly higher, ranging from 2.7 to 4.0% (Table S-1). The LODs were 10 to 50 $\mu g \cdot L^{-1}$ (Table 1), 2 to 10 times higher than for standards.

In the current nvSPE-CE-MS setup, the small valve loop volume (20 nL) limited the volume transferred in each heart-cut. The slightly lower sensitivity enhancement compared to unidirectional SPE-CE-MS suggests that the transfer of the eluent plug in nvSPE-CE-MS should be further improved. In the future, a valve with a larger internal loop volume or a valve for the direct connection of the loading and separation capillaries is desirable to ensure a more efficient transfer of an appropriate eluent plug to the separation capillary. If this issue is addressed, the segregation of SPE preconcentration from CE separation by using a nanovalve shows potential for improving SPE-CE-MS applications with immunoaffinity [32–34], immobilized metal affinity [35,36], ion exchange [37] or hydrophilic interaction liquid chromatography sorbents. NvSPE-CE-MS will enable the use of the most appropriate loading conditions for optimum analyte retention and sorbent stability (e.g. salty and neutral pH conditions for immunoaffinity or immobilized metal affinity sorbent), in combination with the typical formic or acetic acid separation BGEs necessary to maximize ionization efficiency and sensitivity in positive ESI-MS mode. Moreover, nvSPE-CE-MS will enable a wider use of high hydroorganic content or non-aqueous BGEs, which is currently very limited, especially with the typical reversed-phase chromatographic sorbents (e.g. C18).

4. Concluding remarks

We have developed a nvSPE-CE-MS setup with a single CE instrument and demonstrated the applicability for purification, preconcentration, separation, detection, and characterization of opioid peptides and Aβ peptide fragments using a C18 sorbent. An improvement of the LODs of 200 times was obtained for standards compared to CE-MS. In the analysis of pretreated plasma samples, the LODs were slightly higher than for the standards. In comparison with unidirectional SPE-CE-MS, the LODs for standards were five times higher. However, they were similar for plasma samples, indicating an improved tolerance of nvSPE-CE-MS to complex sample matrices. The results with unidirectional SPE-CE-MS were very similar, but LODs were five times lower. Further optimization of parameters such as sorbent particle size, microcartridge dimensions or valve design can further improve the nvSPE-CE-MS method. In nvSPE-CE-MS, the loading and the separation capillaries, and, hence, SPE preconcentration and clean-up and CE separation, are independent. Therefore, it is possible to use a loading capillary with a wide id to maximize loadability of the sample and a separation capillary with a narrow id to obtain adequate peak efficiencies. There is no possibility of contamination of the separation capillary when loading a complex biological sample or during the washing step. In addition, the separation capillary can be filled with the optimized BGE for the separation and the detection without potential elution of the retained peptides, enabling additional modes of SPE-CE-MS. These advantages compared to unidirectional SPE-CE-MS have the cost of a more complex setup and methodology. The mobilization step transferring the eluted plug from the loading to the separation capillary adds to the total analysis time. In addition, an UV detector is required for method development. Furthermore, improved transfer volumes of the valve are desired in order to gain flexibility and ease-of-use of the nvSPE-CE-MS-setup. In summary, nvSPE-CE-MS is a promising technique for the analysis of low-concentration analytes in complex samples such as biological fluids that should be further investigated to exploit its full potential.

Acknowledgements

This study was supported by a grant from the Spanish Ministry of Science, Innovation and Universities (RTI2018-097411-B-I00) and the Cathedra UB Rector Francisco Buscarons Úbeda (Forensic Chemistry and Chemical Engineering). Roger Pero-Gascon acknowledges the Spanish Ministry of Education, Culture and Sport for a FPU (Formación del Profesorado Universitario) fellowship and for a "Ayuda complementaria de movilidad para estancias breves en centros extranjeros".

The authors have declared no conflict of interest.

References

[1] S.A. Byrnes, B.H. Weigl, Selecting analytical biomarkers for diagnostic applications: a first principles approach, Expert Rev. Mol. Diagn. 18 (2018) 19–26. https://doi.org/10.1080/14737159.2018.1412258.

[2] R. Schiess, B. Wollscheid, R. Aebersold, Targeted proteomic strategy for clinical biomarker discovery, Mol. Oncol. 3 (2009) 33–44. https://doi.org/10.1016/j.molonc.2008.12.001.

[3] N.A. Guzman, D.E. Guzman, An emerging micro-scale immuno-analytical diagnostic tool to see the unseen. Holding promise for precision medicine and P4 medicine, J. Chromatogr. B Anal. Technol. Biomed. Life Sci. 1021 (2016) 14–29. https://doi.org/10.1016/j.jchromb.2015.11.026.

[4] V. Kašička, Recent developments in capillary and microchip electroseparations of peptides (2015–mid 2017), Electrophoresis. 39 (2018) 209–234. https://doi.org/10.1002/elps.201700295.

[5] S. Štěpánová, V. Kašička, Recent developments and applications of capillary and microchip electrophoresis in proteomics and peptidomics (2015–mid 2018), J. Sep. Sci. 42 (2019) 398–414. https://doi.org/10.1002/jssc.201801090.

[6] A. Stolz, K. Jooß, O. Höcker, J. Römer, J. Schlecht, C. Neusüß, Recent advances in capillary electrophoresis-mass spectrometry: Instrumentation, methodology and applications, Electrophoresis. 40 (2019) 79–112. https://doi.org/10.1002/elps.201800331.

[7] M.C. Breadmore, W. Grochocki, U. Kalsoom, M.N. Alves, S.C. Phung, M.T. Rokh, J.M. Cabot, A. Ghiasvand, F. Li, A.I. Shallan, A.S.A. Keyon, A.A. Alhusban, H.H. See, A. Wuethrich, M. Dawod, J.P. Quirino, F. Li, S.C. Phung, U. Kalsoom, J.M. Cabot, M. Tehranirokh, A.I. Shallan, A.S. Abdul Keyon, H.H. See, M. Dawod, J.P. Quirino, Recent advances in enhancing the sensitivity of electrophoresis and electrochromatography in capillaries and microchips (2016–2018), Electrophoresis. 38 (2019) 17–39. https://doi.org/10.1002/elps.201800384.

[8] R. Ramautar, G.W. Somsen, G.J. de Jong, Developments in coupled solid-phase extraction–capillary electrophoresis 2013-2015, Electrophoresis. 37 (2016) 35–44. https://doi.org/10.1002/elps.201500401.

[9] L. Pont, R. Pero-Gascon, E. Gimenez, V. Sanz-Nebot, F. Benavente, A critical retrospective and prospective review of designs and materials in in-line solid-phase extraction capillary electrophoresis, Anal. Chim. Acta. 1079 (2019) 1–19. https://doi.org/10.1016/j.aca.2019.05.022.

[10] N.A. Guzman, T.M. Phillips, Immunoaffinity capillary electrophoresis: a new versatile tool for determining protein biomarkers in inflammatory processes, Electrophoresis. 32 (2011) 1565–1578. https://doi.org/10.1002/elps.201000700.

[11] F. Benavente, S. Medina-Casanellas, E. Giménez, V. Sanz-Nebot, On-line solid-phase extraction capillary electrophoresis mass spectrometry for preconcentration and clean-up of peptides and proteins, in: N.T. Tran, M. Taverna (Eds.), Capillary Electrophoresis of Proteins and Peptides. Methods and Protocols. Methods in Molecular Biology, Springer Science+Business Media, New York, NY, 2016: pp. 67–84. https://doi.org/10.1007/978-1-4939-4014-1_6.

[12] T. Tsuda, T. Mizuno, J. Akiyama, Rotary-type injector for capillary zone electrophoresis, Anal. Chem. 59 (1987) 799–800. https://doi.org/10.1021/ac00132a026.

[13] A.J.J. Debets, M. Mazereeuw, W.H. Voogt, D.J. van Iperen, H. Lingeman, K.P. Hupe, U.A.T. Brinkman, Switching valve with internal micro precolumn for on-line sample enrichment in capillary zone electrophoresis, J. Chromatogr. A. 608 (1992) 151–158. https://doi.org/10.1016/0021-9673(92)87117-Q.

[14] F.W.A. Tempels, W.J.M. Underberg, G.W. Somsen, G.J. de Jong, On-line coupling of SPE and CE-

MS for peptide analysis, Electrophoresis. 28 (2007) 1319–1326. https://doi.org/10.1002/elps.200600403.

[15] F.W.A. Tempels, W.J.M. Underberg, G.W. Somsen, G.J. de Jong, Design and applications of coupled SPE-CE, Electrophoresis. 29 (2008) 108–128. https://doi.org/10.1002/elps.200700149.

[16] R. Ramautar, G.W. Somsen, G.J. de Jong, Developments in coupled solid-phase extraction-capillary electrophoresis 2009-2011, Electrophoresis. 33 (2012) 243–250. https://doi.org/10.1002/elps.201100453.

[17] F.J. Kohl, C. Neusüß, CZE–CZE ESI–MS coupling with a fully isolated mechanical valve, in: Philippe Schmitt-Kopplin (Ed.), Capillary Electrophoresis: Methods and Protocols, Springer, New York, 2016: pp. 155–166. https://doi.org/10.1007/978-1-4939-6403-1.

[18] J. Schlecht, K. Jooß, C. Neusüß, Two-dimensional capillary electrophoresis-mass spectrometry (CE-CE-MS): coupling MS-interfering capillary electromigration methods with mass spectrometry, Anal. Bioanal. Chem. 410 (2018) 6353–6359. https://doi.org/10.1007/s00216-018-1157-9.

[19] J. Hühner, K. Jooß, C. Neusüß, Interference-free mass spectrometric detection of capillary isoelectric focused proteins, including charge variants of a model monoclonal antibody, Electrophoresis. 38 (2017) 914–921. https://doi.org/10.1002/elps.201600457.

[20] C. Montealegre, C. Neusüß, Coupling imaged capillary isoelectric focusing with mass spectrometry using a nanoliter valve, Electrophoresis. 39 (2018) 1151–1154. https://doi.org/10.1002/elps.201800013.

[21] J. Römer, C. Montealegre, J. Schlecht, S. Kiessig, B. Moritz, C. Neusüß, Online mass spectrometry of CE (SDS)-separated proteins by two-dimensional capillary electrophoresis, Anal. Bioanal. Chem. 411 (2019) 7197–7206. https://doi.org/10.1007/s00216-019-02102-8.

[22] P.J. McLaughlin, Proenkephalin-derived peptides, in: Handb. Biol. Act. Pept., 2nd ed., 2013: pp. 1602–1609. https://doi.org/10.1016/B978-0-12-385095-9.00219-0.

[23] E. Cabrera, P. Mathews, E. Mezhericher, T.G. Beach, J. Deng, T.A. Neubert, A. Rostagno, J. Ghiso, Aβ truncated species: Implications for brain clearance mechanisms and amyloid plaque deposition, Biochim. Biophys. Acta - Mol. Basis Dis. 1864 (2018) 208–225. https://doi.org/10.1016/j.bbadis.2017.07.005.

[24] E. Hernández, F. Benavente, V. Sanz-Nebot, J. Barbosa, Analysis of opioid peptides by on-line SPE-CE-ESI-MS, Electrophoresis. 28 (2007) 3957–3965. https://doi.org/10.1002/elps.200700845.

[25] E. Hernández, F. Benavente, V. Sanz-Nebot, J. Barbosa, Evaluation of on-line solid phase extraction-capillary electrophoresis-electrospray-mass spectrometry for the analysis of neuropeptides in human plasma, Electrophoresis. 29 (2008) 3366–3376. https://doi.org/10.1002/elps.200700872.

[26] H.H. Lauer, G.P. Rozing, eds., High performance capillary electrophoresis, 2nd ed., Agilent Technologies, Waldbronn, Germany, 2014. https://www.agilent.com/cs/library/primers/public/5990-3777EN.pdf (accessed March 30, 2020).

[27] L. Pont, F. Benavente, J. Barbosa, V. Sanz-Nebot, An update for human blood plasma pretreatment for optimized recovery of low-molecular-mass peptides prior to CE-MS and SPE-CE-MS, J. Sep. Sci. 36 (2013) 3896–3902. https://doi.org/10.1002/jssc.201300838.

[28] V. Sanz-Nebot, F. Benavente, E. Hernández, J. Barbosa, Evaluation of the electrophoretic behaviour of opioid peptides. Separation by capillary electrophoresis-electrospray ionization mass spectrometry, Anal. Chim. Acta. 577 (2006) 68–76. https://doi.org/10.1016/j.aca.2006.06.035.

[29] R. Pero-Gascon, F. Benavente, J. Barbosa, V. Sanz-Nebot, Determination of acidity constants and

prediction of electrophoretic separation of amyloid beta peptides, J. Chromatogr. A. 1508 (2017) 148–157. https://doi.org/10.1016/j.chroma.2017.05.069.

[30] R. Pero-Gascon, M. Tascon, V. Sanz-Nebot, L.G. Gagliardi, F. Benavente, Improving separation optimization in capillary electrophoresis by using a general quality criterion, Talanta. 208 (2020) 120399. https://doi.org/10.1016/j.talanta.2019.120399.

[31] S. Medina-Casanellas, F. Benavente, J. Barbosa, V. Sanz-Nebot, Transient isotachophoresis in on-line solid phase extraction capillary electrophoresis time-of-flight-mass spectrometry for peptide analysis in human plasma., Electrophoresis. 32 (2011) 1750–9. https://doi.org/10.1002/elps.201100017.

[32] L. Pont, F. Benavente, J. Barbosa, V. Sanz-Nebot, On-line immunoaffinity solid-phase extraction capillary electrophoresis mass spectrometry using Fab´antibody fragments for the analysis of serum transthyretin, Talanta. 170 (2017) 224–232. https://doi.org/10.1016/j.talanta.2017.03.104.

[33] R. Pero-Gascon, L. Pont, F. Benavente, J. Barbosa, V. Sanz-Nebot, Analysis of serum transthyretin by on-line immunoaffinity solid-phase extraction capillary electrophoresis mass spectrometry using magnetic beads, Electrophoresis. 37 (2016) 1220–1231. https://doi.org/10.1002/elps.201500495.

[34] S. Medina-Casanellas, F. Benavente, J. Barbosa, V. Sanz-Nebot, Preparation and evaluation of an immunoaffinity sorbent with Fab' antibody fragments for the analysis of opioid peptides by on-line immunoaffinity solid-phase extraction capillary electrophoresis-mass spectrometry., Anal. Chim. Acta. 789 (2013) 91–99. https://doi.org/10.1016/j.aca.2013.06.030.

[35] L. Ortiz-Martin, F. Benavente, S. Medina-Casanellas, E. Giménez, V. Sanz-Nebot, Study of immobilized metal affinity chromatography sorbents for the analysis of peptides by on-line solid-phase extraction capillary electrophoresis-mass spectrometry, Electrophoresis. 36 (2015) 962–970. https://doi.org/10.1002/elps.201400374.

[36] R. Pero-Gascon, E. Giménez, V. Sanz-Nebot, F. Benavente, Enrichment of histidine containing peptides by on-line immobilised metal affinity solid-phase extraction capillary electrophoresis-mass spectrometry, Microchem. J. 157 (2020) 105013. https://doi.org/10.1016/j.microc.2020.105013.

[37] J.R.E. Thabano, M.C. Breadmore, J.P. Hutchinson, C. Johns, P.R. Haddad, Selective extraction and elution of weak bases by in-line solid-phase extraction capillary electrophoresis using a pH step gradient and a weak cation-exchange monolith, Analyst. 133 (2008) 1380–1387. https://doi.org/10.1039/b804805c.

Table 1. Relative monoisotopic molecular mass (M_r) and mass-to-charge (m/z) ratios of the molecular ions for the opioid peptides and amyloid beta (Aβ) peptide fragments. Limit of detection (LOD) for the analysis of the peptides by CE-MS, unidirectional SPE-CE-MS, and nvSPE-CE-MS.

Peptide	M_r	$[M + n^*H]^{n+}$		LOD of standards ($\mu g \cdot L^{-1}$)			LOD in spiked plasma ($\mu g \cdot L^{-1}$)	
		m/z	n	CE	SPE-CE [a]	nvSPE-CE	SPE-CE [a]	nvSPE-CE
Dyn A	867.4715	434.7430	2	100	0.1	0.5	10	10
End 1	610.2904	611.2976	1	100	0.05	0.5	1	5
Met	573.2257	574.2330	1	100	0.1	0.5	1	1
Aβ 1-15	1825.7768	457.4515 609.5996	4 3	1500	-	5	-	10
Aβ 10-20	1445.7456	482.9225 723.8801	3 2	500	-	5	-	50
Aβ 20-29	1022.4669	512.2407	2	1000	-	5	-	10
Aβ 25-35	1059.5747	530.7946	2	500	-	5	-	10

[a] The analysis of Aβ peptide fragments by unidirectional SPE-CE-MS was not performed (-).

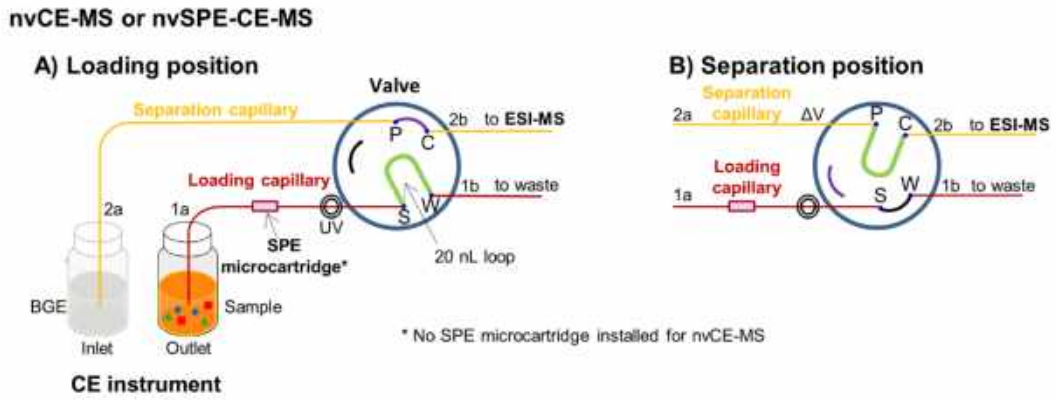

Figure 1. Setups for nvCE-MS or nvSPE-CE-MS. (A) Loading (no SPE microcartridge installed for nvCE-MS) and (B) separation positions.

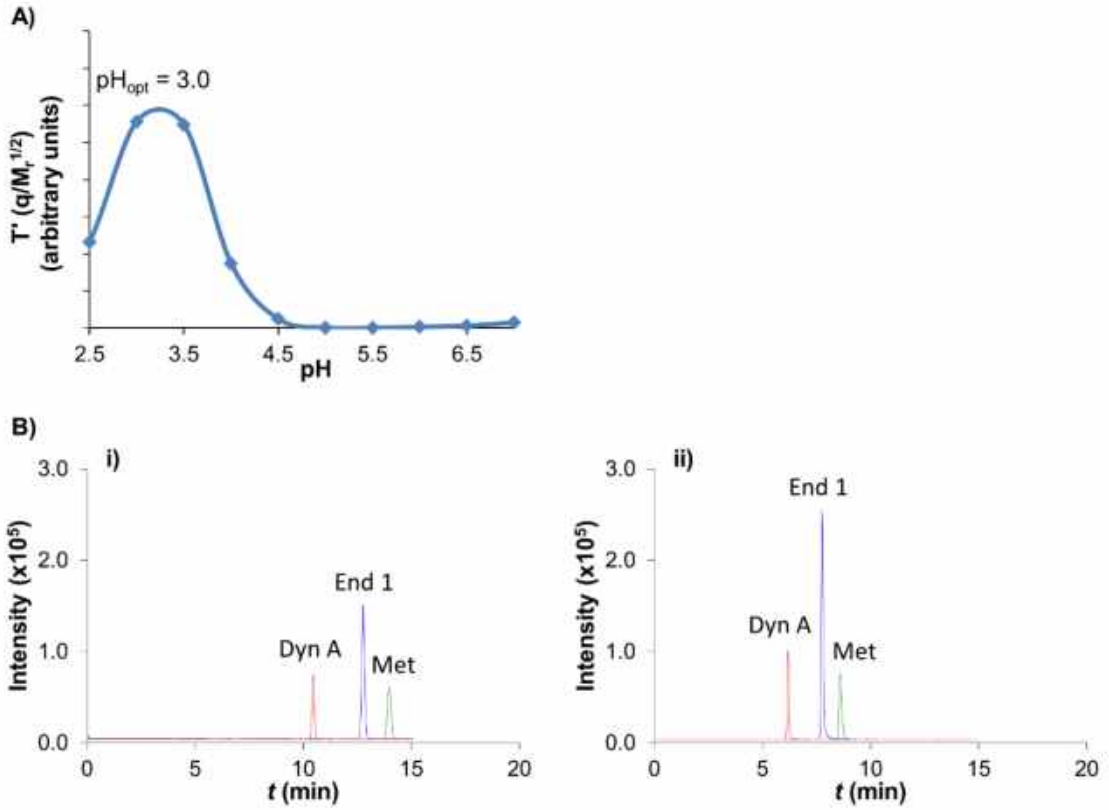

Figure 2. Separation of the opioid peptides. A) Plot of T' vs pH of the BGE (a BGE of 50 mM HAc:50 mM HFor, pH=3.0 was finally selected for the analyses). B) Extracted ion electropherograms in the optimized conditions for the analysis of standards at 10 $mg \cdot L^{-1}$ by (i) CE-MS, and (ii) nvCE-MS.

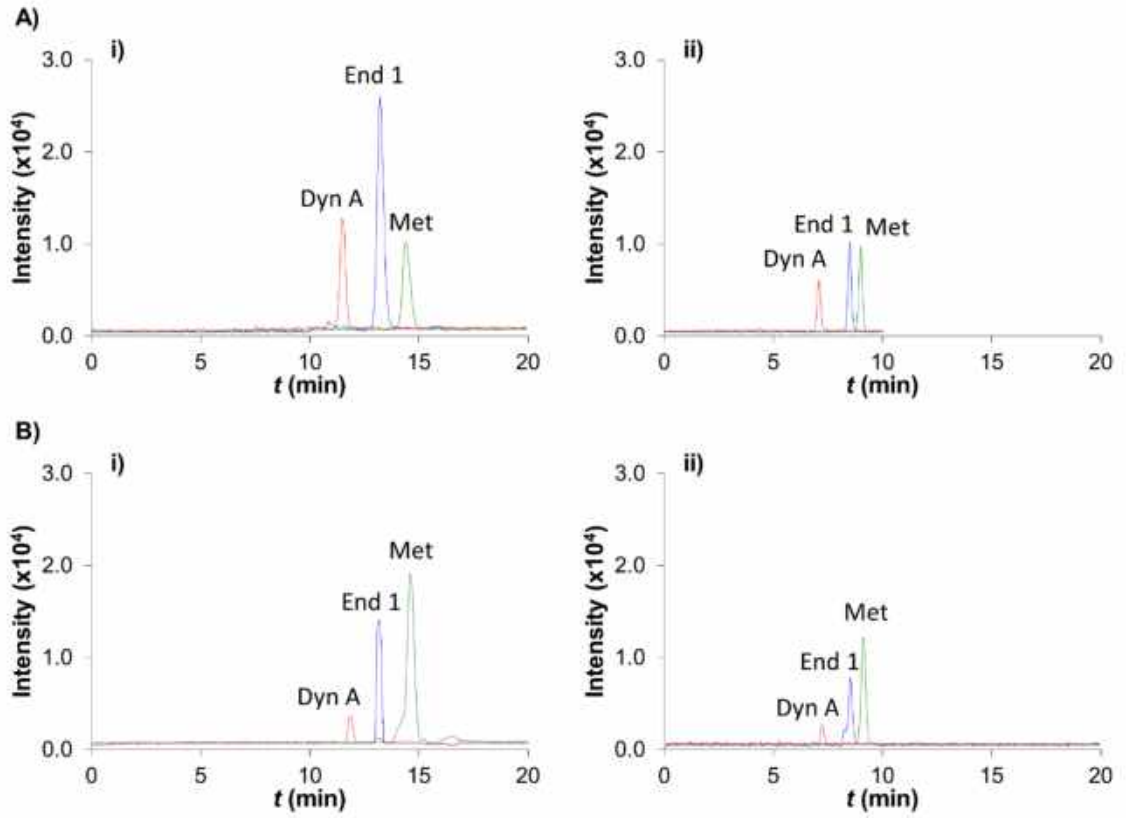

Figure 3. Extracted ion electropherograms of the opioid peptides in the optimized conditions for the analysis of A) a standard mixture at 1 $\mu g \cdot L^{-1}$ and B) a plasma sample spiked at 10 $\mu g \cdot L^{-1}$ by (i) unidirectional SPE-CE-MS, and (ii) nvSPE-CE-MS.

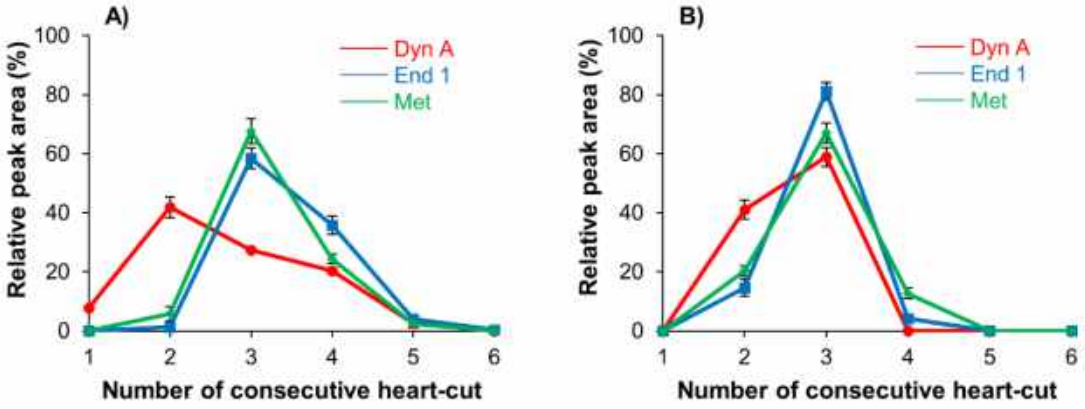

Figure 4. Characterization of the opioid peptide elution profile by analyzing several consecutive heart-cuts in nvSPE-CE-MS using different eluents containing 50 mM HAc:50 mM HFor and (A) 60% (v/v) MeOH and (B) 80% (v/v) ACN. Percent relative peak area was calculated normalizing to the sum of the peak areas of all the analyses for the peptide under consideration.

Supporting Information

Table S-1. Repeatability (n=3) for the analysis of the opioid peptides and amyloid beta (Aβ) peptide fragments by CE-MS, nvCE-MS, unidirectional SPE-CE-MS, and nvSPE-CE-MS.

	%RSD (n=3)											
	Peak area						Migration time					
	CE (standards) [a]	nvCE (standards) [a]	SPE-CE (standards) [b]	SPE-CE (plasma) [c]	nvSPE-CE (standards) [b]	nvSPE-CE (plasma) [c]	CE (standards) [a]	nvCE (standards) [a]	SPE-CE (standards) [b]	SPE-CE (plasma) [c]	nvSPE-CE (standards) [b]	nvSPE-CE (plasma) [c]
Opioid peptide												
Dyn A	8.7	8.0	11	11	11	13	2.7	1.8	1.2	4.0	1.4	5.9
End 1	10	5.9	6.9	13	11	5.3	1.7	0.74	1.6	3.7	2.4	4.2
Met	10	8.3	12	11	9.0	5.6	1.5	1.3	1.4	4.6	2.4	4.7
Aβ peptide fragment												
Aβ 1-15	11	-	-	-	12	5.1	1.0	-	-	-	1.8	2.7
Aβ 10-20	10	-	-	-	8.8	13	1.1	-	-	-	2.7	2.9
Aβ 20-29	7.4	-	-	-	5.3	8.3	0.92	-	-	-	2.4	4.0
Aβ 25-35	8.0	-	-	-	9.0	8.7	1.3	-	-	-	2.4	3.3

Analysis at
[a] 10 mg·L^{-1}
[b] 1 µg·L^{-1} for opioid peptides and 10 µg·L^{-1} for Aβ peptide fragments
[c] 10 µg·L^{-1} for opioid peptides and 50 µg·L^{-1} for Aβ peptide fragments

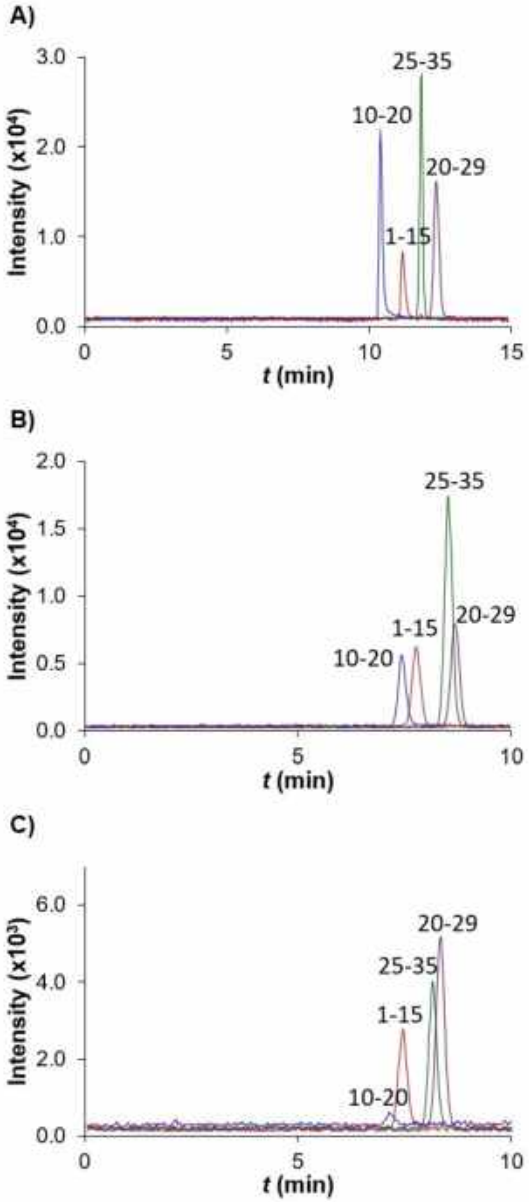

Figure S-1. Extracted ion electropherograms of the Aβ peptide fragments in the optimized conditions. A) A standard mixture at 10 $mg \cdot L^{-1}$ by CE-MS. B) A standard mixture at 10 $\mu g \cdot L^{-1}$ and C) a plasma sample spiked at 50 $\mu g \cdot L^{-1}$ by nvSPE-CE-MS.

Chapter 5. High-throughput bottom-up analysis of proteins. On-line immobilized enzyme microreactor capillary electrophoresis-mass spectrometry

CE-MS analysis at the intact protein level is a suitable strategy for the detection of a large number of proteins and the characterization of their different isoforms and post-translational modifications. However, the top-down strategy has some limitations mainly due to the difficulty in ionizing and measuring the mass of large molecules. Bottom-up proteomics, in which protein samples are enzymatically digested into peptides prior to the analysis, offers multiple advantages including increased separation efficiency and limited number of charges on each peptide, which are all beneficial for MS detection. Trypsin is the most typically used proteolytic enzyme due to its specificity, effectiveness and low price. Tryptic digestion has been traditionally conducted in solution and requires long digestion times. Immobilized enzymes have been alternatively explored to decrease the sample volume and the total digestion times, minimize the sample handling, improve the digestion yields, as well as to stabilize the enzyme, avoid its autoproteolysis and simplify its recovery making it reusable. In order to further reduce the sample handling and the required sample volumes and to increase the analysis throughput, IMER-CE-MS has been proposed.

In this chapter, we investigate the bottom-up analysis of proteins by IMER-CE-MS using microreactors packed with immobilized trypsin particles. First, the off-line digestion of β-lactoglobulin with trypsin in solution and with commercial immobilized trypsin particles has been evaluated. Then, the IMER-CE-MS methodology has been optimized with β-lactoglobulin and the developed method has been validated with α-casein, β-casein and κ-casein. Finally, the potential of the IMER-CE-MS methodology for the analysis of complex mixtures of proteins has been demonstrated by analyzing an *Escherichia coli* cell lysate.

This chapter includes the following publication:

- **Publication 5.1.** L. Villegas, R. Pero-Gascon, F. Benavente, J. Barbosa, V. Sanz-Nebot, On-line protein digestion by immobilized enzyme microreactor capillary electrophoresis-mass spectrometry, Talanta. 199 (2019) 116–123. https://doi.org/10.1016/j.talanta.2019.02.039.

Talanta 199 (2019) 116–123

Contents lists available at ScienceDirect

Talanta

journal homepage: www.elsevier.com/locate/talanta

On-line protein digestion by immobilized enzyme microreactor capillary electrophoresis-mass spectrometry

Lorena Villegas[1], Roger Pero-Gascon[1], Fernando Benavente*, José Barbosa, Victoria Sanz-Nebot

Department of Chemical Engineering and Analytical Chemistry, Institute for Research on Nutrition and Food Safety (INSA-UB), University of Barcelona, 1–11 Martí i Franques street, 3rd floor, Barcelona 08028, Spain

ARTICLE INFO

Keywords:
Bottom-up proteomics
Capillary electrophoresis
Immobilized enzyme
Mass spectrometry
Microreactor
On-line digestion

ABSTRACT

In this study, we present the use of microreactors packed with immobilized trypsin particles for the rapid and efficient bottom-up analysis of proteins by on-line immobilized enzyme microreactor capillary electrophoresis mass spectrometry (IMER-CE-MS). The results obtained digesting β-lactoglogulin (β-LG) off-line with free trypsin in solution and with immobilized trypsin particles were taken as a reference for the optimization of the on-line protein digestion. Under the optimized conditions, on-line digestion, separation and characterization of the protein digests were possible in less than 30 min. The limit of detection for complete sequence coverage was around 10 μg mL^{-1} (−500 μM) of β-LG, the repeatability was comparable to the off-line digestion methods and the microreactor could be reused until thirty times. The good performance of IMER-CE-MS was also demonstrated for several other proteins as α-casein (α-CSN), β-casein (β-CSN), and κ-casein (κ-CSN), as well as for a complex protein mixture (an *Escherichia coli* whole cell lysate).

1. Introduction

A huge number of studies have been developed to monitor the functions, interactions, location, and regulation of proteins due to their essential role in most biological processes and their relationship with many diseases [1]. In proteomics research, peptide mapping is essential for characterization of the different proteoforms of a certain protein, including their primary amino acid sequence and their co-translational and post-translational modifications [2,3]. The bottom-up analysis of proteins by mass spectrometry (MS) requires the enzymatic digestion of proteins into peptides. Trypsin is the most typically used proteolytic enzyme due to its specificity, effectiveness, and low price. This enzyme cleaves proteins at the C-terminal side of lysine and arginine residues, resulting in peptides of small relative molecular mass (M_r) usually between 500 and 3000 [3]. These peptides are in general detected in MS as singly, doubly or triply charged ions in positive electrospray ionization mode (ESI+) [4], which facilitates the most sensitive detection, the fragmentation by MS/MS and the interpretation of the mass spectra.

Traditionally, the enzymatic digestion with trypsin has been performed in a homogeneous solution after mixing the free enzyme and the protein solutions. The pH, the temperature, the enzyme-to-protein ratio and the reaction time can be optimized to obtain the maximum digestion yield. However, in general, very long times (e.g. 18 h) are recommended for an appropriate digestion, before separation and characterization by liquid chromatography mass spectrometry (LC-MS) or capillary electrophoresis mass spectrometry (CE-MS) [5]. Immobilized enzymes have been alternatively explored to decrease the sample volume and the total digestion times, minimize the sample handling, improve the digestion yields, as well as to stabilize the enzyme, avoid its autoproteolysis, simplify its recovery and make it reusable [6]. The possibility of using an immobilized enzyme microreactor (IMER) coupled on-line to LC-MS or CE-MS has interesting advantages such as further reducing the sample handling and the required sample volumes while increasing the analysis throughput [7–10]. Furthermore, IMER-CE-MS has the additional advantage over the on-line approaches based on LC-MS that does not require the use of complex instrumental set-ups with valves [9,10].

In the last 25 years, a limited number of scientific articles about the enzymatic digestion of proteins by IMER-CE have been published, probably due to the instrumental and methodological difficulties of the on-line coupling and the limited applicability of the methods without on-line MS detection [7]. Most of the applications were based on open tubular microreactors with immobilized trypsin on the inner capillary surface [11–19] and only a few were reported with monolithic [20,21], particle packed [8,22,23] or sol-gel [24,25] microreactors. Since the pioneering studies of Amankwa et al. [11–13], the use of open tubular

* Corresponding author.
E-mail address: fbenavente@ub.edu (F. Benavente).
[1] Both authors contributed equally to this study.

https://doi.org/10.1016/j.talanta.2019.02.039
Received 13 September 2018; Received in revised form 7 February 2019; Accepted 8 February 2019
Available online 10 February 2019
0039-9140/

microreactors has been proposed by other research groups [14–19]. However, now is widely accepted that digestion yields with these microreactors are in general low because of the scarce interaction between the protein and the immobilized trypsin within the very short time of the on-line digestion [7,8]. Monolithic, sol-gel and particle packed supports with immobilized trypsin were developed to increment the digestion yield due to the extended active surface areas and the reduced distances between the protein and the immobilized enzyme [8,20–25]. Nowadays, preparation of monoliths with immobilized trypsin requires rather challenging, specialized and long and tedious synthesis procedures to obtain reproducible results [7]. In contrast, a wide range of activated particle supports ready to immobilize trypsin or with immobilized trypsin are commercially available [8,22,23]. These immobilized trypsin particles can be simply and reproducibly packed in the on-line microreactors for IMER-CE-MS. Unfortunately, the number of studies describing completely on-line IMER-CE-MS are rather scarce, and all of them are using open tubular IMERs [14,17,18]. Recently, Liu et al. described a novel method with packed IMERs using commercial silica particles with immobilized trypsin for the on-line digestion of proteins by IMER-CE with UV and fluorescence detection, and fractions were collected to be analyzed by MS [8]. In this study, we use commercial cellulose resin particles with immobilized trypsin for the packed IMERs and we develop a completely on-line IMER-CE-MS method for the bottom-up analysis of standard proteins (e.g. β-lactoglobulin (β-LG), α-casein (α-CSN), β-casein (β-CSN) and κ-casein, (κ-CSN)) and complex protein mixtures (e.g. an *Escherichia coli* whole cell lysate). The performance of the on-line protein digestion is compared with the off-line digestion using free trypsin and immobilized trypsin to demonstrate the potential of the novel method, and expand the applicability of IMER-CE-MS.

2. Materials and methods

2.1. Chemicals and reagents

All the chemicals used in the preparation of the background electrolyte (BGE) and the rest of solutions were of analytical reagent grade or better. Water (LC-MS grade), ammonium acetate (NH_4Ac, ≥99.9%), ammonium bicarbonate (LC-MS grade), DL-dithiothreitol (DTT, ≥99.0%) and iodoacetamide (IAA, ≥98.0%) were purchased from Sigma-Aldrich (St. Louis, MO, USA). Acetic acid (HAc, glacial), formic acid (HFor, 99.0%), ammonia (25%) and sodium hydroxide (≥99.0%) were supplied by Merck (Darmstadt, Germany). Iodoacetamide (IAA, ≥98.0%) was provided by Fluka (Buchs, Switzerland). Acetonitrile (≥99.9%) was purchased from Panreac (Castellar del Vallès, Spain). 2-propanol (≥99.9%) was supplied by Scharlau (Sentmenat, Spain).

Free trypsin (*sequencing grade modified trypsin*) and particles with immobilized trypsin (*immobilized trypsin*) were provided by Promega (Madison, Wisconsin, USA). β-LG (~90%, PAGE), α-CSN (> 70%), β-CSN (> 90%) and κ-CSN (≥80%) were purchased from Sigma-Aldrich. An *Escherichia coli* cell lysate (*E. coli* positive control whole cell lysate – expressing 6X His tag protein) was supplied by Abcam (Cambridge, UK).

2.2. Electrolyte solutions, sheath liquid, protein standards and samples

The BGE for the CE-MS separation was a solution of 50 mM HAc: 50 mM HFor (pH 2.3) and was filtered through a 0.22 μm nylon filter (MSI, Westboro, MA, USA). The sheath liquid solution consisted of a mixture of 60:40 (v/v) 2-propanol: water with 0.05% (v/v) of HFor. The sheath liquid and the BGE were degassed for 10 min by sonication before use.

An aqueous standard solution (2000 μg mL^{-1}) of each model protein (β-LG, α-CSN, β-CSN and κ-CSN) was prepared and aliquoted into 50 μL portions. These aliquots (100 μg protein each) were dried at 37 °C and stored in a freezer at −20 °C when not in use.

The *E. coli* cell lysate was a lyophilized pellet that contained 250 μg of protein and was dissolved in 125 μL of 50 mM NH_4HCO_3 (2000 μg mL^{-1} of protein). Excipients of low M_r were removed by passage through a 10,000 M_r cut-off cellulose acetate centrifugal filters (Millipore Microcon Ultracel PL, Merck). The sample (25 μL) was centrifuged at 25 °C for 7 min at 11,300 × g and the residue was washed three times for 7 min in the same way, with 50 μL of digestion buffer. Under the optimized conditions, the digestion buffer was 50 mM NH_4HCO_3, pH = 7.9 for the off-line digestions and 10 mM NH_4HCO_3, pH = 7.9 for the on-line digestion. The final residue was recovered by placing the filter upside down in a new vial and centrifuging once more at a reduced centrifugal force (2 min at 700 × g). Sufficient digestion buffer was added to the vial to adjust the final volume to 50 μL (1000 μg mL^{-1}). Filtered samples were stored in the fridge at 4 °C when not in use.

2.3. Apparatus and procedures

pH measurements were made with a Crison 2002 potentiometer and a Crison electrode 52-03 (Crison Instruments, Barcelona, Spain). Protein stock aliquots were dried in a Savant™ SPD111V SpeedVac™ (Thermo Fisher Scientific, Waltham, MA, USA). Centrifugal filtration was carried out in a Mikro 20 centrifuge (Hettich Zentrifugen, Tuttlingen, Germany). Agitation was performed with a Vortex Genius 3 (Ika®, Staufen, Germany). Digestion mixtures were incubated in a Thermo-Shaker TS-100 (Biosan, Riga, Latvia) at controlled temperature.

All CE-MS experiments were performed in a 7100 CE system coupled with an orthogonal G1603 sheath-flow interface to a 6220 oa-TOF LC/MS spectrometer (Agilent Technologies, Waldbronn, Germany). The sheath liquid was delivered at a flow rate of 3.3 μL min^{-1} by a KD Scientific 100 series infusion pump (Holliston, MA, USA). The TOF mass spectrometer was operated under optimized conditions in positive mode using the following parameters: capillary voltage 4000 V, drying temperature 200 °C, drying gas flow rate 2.9 L min^{-1}, nebulizer gas 7 psig, fragmentor voltage 190 V, skimmer voltage 60 V, OCT 1 RF Vpp voltage 300 V. Chemstation and MassHunter softwares (Agilent Technologies) were used for CE and TOF mass spectrometer control, data acquisition and integration. Data were collected in profile at 1 spectrum/s between 100 and 3200 m/z, with the mass range set to high resolution mode (4 GHz).

2.4. Off-line digestion with free and immobilized trypsin and CE-MS

The off-line digestion with trypsin in solution was conducted following the procedures described elsewhere [5,26]. A dried stock aliquot of β-LG was reconstituted with 100 μL of digestion buffer (50 mM NH_4HCO_3 under the optimized conditions) and was reduced adding 2.5 μL of 0.5 M DTT in digestion buffer (1000 μg mL^{-1} of β-LG, i.e. ~50 μM). The mixture was incubated with agitation at 56 °C for 30 min and let it cool down to room temperature. Then, the reduced protein was alkylated adding 7 μL of a 0.73 M IAA solution in digestion buffer (30 min at room temperature with agitation in the dark). To remove the excess of DDT and IAA, the mixture was filtered using 10,000 M_r cut-off centrifugal filters at 25 °C. First, the filters were washed with 100 μL of the digestion buffer and centrifuged for 10 min at 11,300 × g. Then, the sample was added and centrifuged (10 min at 11,300 × g). Finally, the sample was washed three times with 100 μL of digestion buffer (10 min at 11,300 × g). The final residue was recovered by placing the filter upside down in a new vial and centrifuging at a reduced centrifugal force (2 min at 700 × g). Sufficient digestion buffer was added to the vial to adjust the final volume to 100 μL (1000 μg mL^{-1} of β-LG). Trypsin (2.5 μL at 1000 μg mL^{-1}) was added to the protein sample and the mixture was vortexed and incubated with agitation at 37 °C for 18 h. The reaction was stopped by heating the mixture for 10 min at 100 °C. The protein digests were dried at 37 °C and stored in a freezer at −20 °C

when not in use. Before the digestion, the *E. coli* cell lysate solution in digestion buffer (50 µL, 1000 µg mL^{-1} of protein) was reduced and alkylated as β-LG adding 1.25 µL of 0.5 M DTT in digestion buffer and 3.5 µL of IAA 0.73 M.

The off-line enzymatic digestion procedure with immobilized trypsin was performed following the manufacturer instructions [27]. β-LG (1000 µg mL^{-1}) was reduced and alkylated as explained above in digestion buffer (10 mM NH_4HCO_3 under the optimized conditions) and dried at 37 °C before use. First, 5 µL of digestion buffer were added to the dried reduced and alkylated protein. After that, 16 µL of acetonitrile and 19 µL of digestion buffer were added to prepare the final protein sample. A spin column was placed in a 1.5 mL centrifuge tube and 200 µL of the suspension with the immobilized trypsin resin were added. Then, the liquid was separated from the resin by centrifugation at 25 °C, and the resin was washed three times with 200 µL of the digestion buffer (5 s at 300 × g in all cases). The spin column was placed in a clean 1.5 mL tube, the protein sample was added, and it was incubated without agitation at room temperature for 30 min. Then, 100 µL of the digestion buffer were added to recover the peptides by centrifugation at 25 °C (5 s at 300 × g). This last step was repeated three times. The protein digests were dried at 37 °C and stored in a freezer at −20 °C when not in use. The dried protein digests were reconstituted with 100 µL of digestion buffer before the analysis (1000 µg mL^{-1} of β-LG). To study the reusability of the immobilized trypsin resin, the spin column was washed four times with 100 µL of the digestion buffer between digestions to prevent carry-over effects. Otherwise, the resin was discarded.

Fused silica capillaries (72 cm total length (L_T) × 75 µm internal diameter (id) × 365 µm outer diameter (od)) were supplied by Polymicro Technologies (Phoenix, AZ, USA) and were activated flushing at 930 mbar with water (5 min), 1 M NaOH (15 min), water (15 min) and BGE (50 mM HAc: 50 mM HFor, pH = 2.3, 10 min). Activation was performed off-line to avoid mass spectrometer contamination. Before CE-MS analysis, capillaries were conditioned flushing with water (1 min), 1 M HAc (3 min), water (1 min) and BGE (5 min). Samples were hydrodynamically injected at 50 mbar for 15 s (~80 nL with the Hagen-Poiseuille equation [28]) and the separation was carried out at 25 °C or 37 °C applying 25 kV during 30 min. The analyses were performed in triplicate.

2.5. On-line IMER-CE-MS

The on-line enzymatic digestion was performed in an IMER (0.7 cm L_T × 250 µm id × 365 µm od fused silica capillary) that was inserted at 7.5 cm of the beginning of an activated separation capillary (72 cm L_T × 75 µm id × 365 µm od fused silica capillary) [29]. The IMER preparation was very simple. First, a polymeric frit was placed at the beginning of the microreactor and this side was connected to a 7.5 cm separation capillary using a plastic sleeve. Second, the microreactor was filled with the immobilized enzyme resin applying vacuum during 10 s. The packing was checked under an optical microscope (100×) and the procedure was repeated until the microcartridge was completely packed. Then, another polymeric frit was introduced at the end of the microreactor that was finally connected to a 64.5 cm separation capillary using another plastic sleeve. The IMER-CE capillary was checked for abnormal flow restriction, flushing with water and BGE with a syringe, and applying the separation voltage for 15 min (25 kV).

Under the optimized conditions, IMER-CE capillaries were conditioned flushing with BGE (50 mM HAc: 50 mM HFor, pH = 2.3) for 2 min. Two plugs of digestion buffer (10 mM NH_4HCO_3 under the optimized conditions) were injected at 50 mbar for 8 s (−40 nL, i.e. −1 cm) before and after the protein sample, which was injected at 50 mbar for 15 s (~80 nL, i.e. ~2 cm). Then, the BGE was introduced at 5 mbar for 600 s (~325 nL, i.e. ~7 cm) to ensure that the sample plug passed through the microreactor giving enough time for the protein digestion. Finally, 25 kV were applied for the separation. Between the analyses, the capillary was flushed with BGE (5 min) and water (5 min). The analyses were performed in triplicate.

β-LG, α-CSN, β-CSN and κ-CSN (1000 µg mL^{-1} all; i.e. ~50, ~40, ~40 and ~50 µM, respectively) and the *E. coli* cell lysate (1000 µg mL^{-1} of protein) were analyzed by on-line IMER-CE-MS. Before the on-line digestion, β-LG, κ-CSN and the *E. coli* cell lysate were reduced and alkylated as explained in Section 2.4. α-CSN and β-CSN dried stock aliquots were reconstituted directly with the digestion buffer, because no disulfide bonds were present.

3. Results and discussion

3.1. Off-line digestion with trypsin in solution and CE-MS

Protein digestion with trypsin has been traditionally conducted in solution using free trypsin and long digestion times (≥18 h) at 37 °C and pH around 8 to ensure efficient and reproducible digestions [3,5,26]. The use of a digestion buffer of 50 mM NH_4HCO_3, at pH 7.9 has been widely described in the literature [5]. In this study, as an alternative, we also tested digestion buffers of 10 mM NH_4HCO_3 and 10 mM NH_4Ac at pH 7.9, because low ionic strength buffers are more recommendable for the analysis of protein digests by CE-MS and IMER-CE-MS. Furthermore, we also evaluated the influence on peptide sensitivity of the separation temperature in CE-MS and on the digestion yield of the digestion time, because later the on-line digestion and the separation by IMER-CE-MS were performed at the same temperature, and digestion was produced in a very short time.

Table 1 shows the sequence and the mass-to-charge (m/z) ratio of the molecular ions of the peptides detected by CE-MS for β-LG (1000 µg mL^{-1}). β-LG was chosen as a model protein due to its low M_r (~19,900) and structural simplicity, even though the presence of disulfide bonds that needed reduction and alkylation for an efficient digestion. At this protein concentration, all the expected peptides after tryptic digestion were detected by CE-MS (sequence coverage was 100%, calculated considering the number of amino acids detected from the peptide sequence). Table 1 also shows the relative peak area and the migration time values, as well as the percentages of relative standard deviation (%RSD, n = 3), for the CE-MS separation at 37 °C, with a 50 mM NH_4HCO_3 digestion buffer and 18 h of digestion time. As can be observed, repeatability was good, ranging between 0.1% and 8.0% and 1.6–1.8% for peak areas and migration times, respectively. These values agreed with the values obtained by CE-MS for peptide digests in previous studies [30]. To easily compare the results with the different digestion buffers, separation temperatures and digestion times, Fig. 1 shows two bar graphs with the total sum of the peak areas for the detected tryptic peptides in the different conditions. As can be observed in Fig. 1-A, at 18 h of digestion, sensitivity was higher when separation by CE-MS was conducted at 37 °C. At higher separation temperatures, the peaks were narrower and the migration times were shorter due the lower viscosity of the BGE, improving ionization efficiency and peak areas. In addition, peak areas were higher with NH_4HCO_3 digestion buffers, due to the higher digestion yields compared to the NH_4Ac digestion buffer. Figs. 1-C and 1-D show the total ion electropherogram (TIE) and extracted ion electropherograms (EIEs) for the CE-MS separation at 37 °C of the tryptic digest of β-LG with a 50 mM NH_4HCO_3 digestion buffer (1000 µg mL^{-1} of protein digested at 37 °C during 18 h), which allowed the highest digestion yield and detection sensitivity (Fig. 1-A). Under these optimized conditions, total separation times were shorter than 9 min (Fig. 1-D). Regarding the digestion time, Fig. 1-B shows that the peak areas significantly decreased when it was reduced to 30 min, which is the time recommended by the manufacturer for the off-line digestion with immobilized trypsin particles, as shown in the next section. The digestion yield decreased because the interaction time between the enzyme and the protein was shorter. However, it is worth mentioning that at this protein concentration, digestion yield with 30 min of digestion was enough to have total sequence coverage, as with 18 h of digestion.

Table 1
Digestion of β-LG (1000 μg mL^{-1}). Relative peak areas, migration times and percentage of relative standard deviations (%RSD) of the peptides detected by the off-line digestion with free and immobilized trypsin in solution and CE-MS and by the on-line digestion with immobilized trypsin in IMER-CE-MS. The analyses were performed in triplicate under the optimized conditions in all cases. Single amino acids were not taken into account.

Peptide sequence		[M + nH]$^{n+}$		Off-line digestion with trypsin in solution and CE-MS				Off-line digestion with immobilized trypsin and CE-MS				On-line digestion with immobilized trypsin by IMER-CE-MS			
				Relative peak area[a]		Migration time (min)		Relative peak area[a]		Migration time (min)		Relative peak area[a]		Migration time (min)	
		m/z	n	Mean	% RSD	Mean	% RSD	Mean	% RSD	Mean	% RSD	Mean	% RSD	Mean	%RSD
[1–8]	LIVTQTMK	467.2758	2	0.101	1.8	6.9	1.8	0.137	0.6	7.8	0.7	0.181	4.3	9.6	6.1
[9–14]	GLDIQK	337.1979	2	0.102	1.0	6.6	1.8	0.112	0.9	7.6	0.5	0.137	2.2	8.9	5.7
[15–40]	VAGTWYSLAMAASDISLLDAQSAPLR	903.1306	3	0.009	1.6	8.1	1.8	0.0003	14	8.9	0.7	0.018	10	13.3	7.5
[41–60]	VYVEELKPTPEGDLEILLQK	771.7582	3	0.135	0.6	7.1	1.8	0.140	1.8	8.1	0.7	0.106	8.5	10.3	6.3
[61–69]	WENGECAQK	561.2379	2	0.002	4.9	7.0	1.7	0.007	12	8.0	0.7	0.010	15	10.0	6.2
[71–75]	HAEK	287.1842	2	0.071	0.7	6.4	1.8	0.084	3.4	7.5	0.6	0.085	4.3	8.4	5.6
[76,77]	TK	248.1605	1	0.015	8.0	5.4	1.7	0.012	5.8	6.8	0.4	0.006	11	6.6	4.8
[78–83]	IPAVFK	337.7157	2	0.089	0.8	6.5	1.7	0.102	1.4	7.5	0.6	0.067	6.6	8.7	5.7
[84–91]	IDALNENK	458.7406	2	0.085	0.8	6.9	1.7	0.099	2.0	8.0	0.7	0.122	6.1	9.9	6.1
[92–100]	VLVLDTDYK	533.2953	2	0.115	0.9	7.1	1.8	0.088	1.6	8.1	0.7	0.028	4.2	10.3	6.3
[102–124]	YLLFCMENSAEPEQSLACQCLVR	940.0941	3	0.002	7.3	8.1	1.8	0.000	9.8	8.9	1.3	0.009	7.8	13.3	7.6
[125–135]	TPEVDDEALEK	623.2962	2	0.098	0.1	7.3	1.8	0.047	3.7	8.3	0.6	0.047	6.0	11.0	6.5
[136–138]	FDK	409.2082	1	0.016	6.5	6.1	1.8	0.006	4.3	7.2	0.6	0.005	9.9	7.7	5.2
[139–141]	ALK	331.2340	1	0.018	4.4	5.8	1.6	0.018	4.1	6.9	0.6	0.015	7.1	7.0	5.0
[142–148]	ALPMHIR	419.2421	2	0.043	4.2	5.8	1.8	0.038	4.9	6.9	0.6	0.048	10	7.0	5.0
[149–162]	LSFNPTQLEEQCHI	858.4068	2	0.100	2.7	7.4	1.7	0.108	5.5	8.4	0.8	0.116	3.6	11.2	6.7

[a] The relative peak areas were obtained dividing the raw peak area of the peptide by the total sum of raw peak areas of the detected peptides.

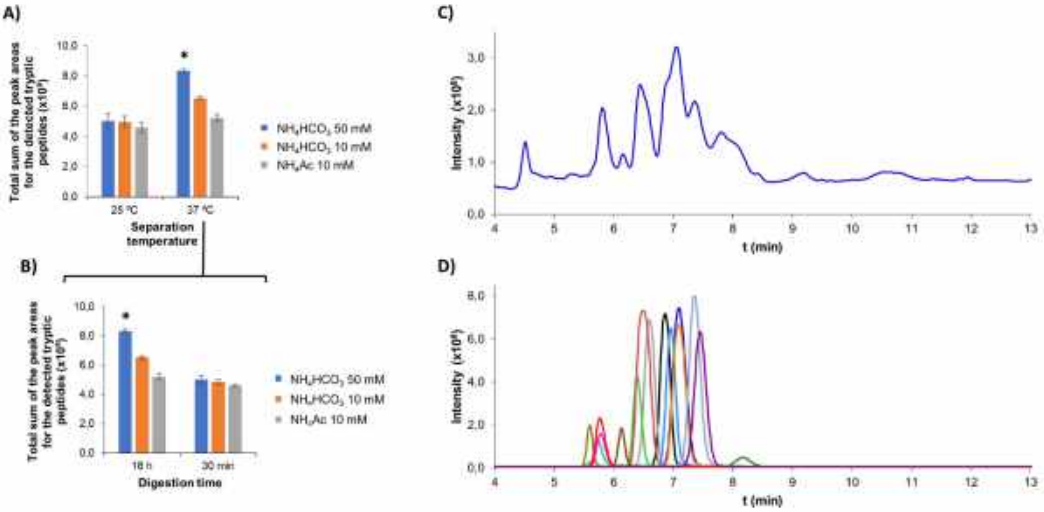

Fig. 1. Off-line protein digestion of β-LG (1000 μg mL^{-1}) with free trypsin at 37 °C and CE-MS analysis. Comparison of the total sum of peak areas for the detected tryptic peptides **(A)** with different separation temperatures and digestion buffers (18 h of digestion time) and **(B)** with different digestion times and digestion buffers (37 °C of separation temperature). **(C)** Total ion electropherogram (TIE) and **(D)** extracted ion electropherograms (EIEs) for 18 h of digestion time and CE-MS analysis at 37 °C using 50 mM NH_4HCO_3 as the digestion buffer. Optimized conditions are indicated in **(A)** and **(B)** with an asterisk.

3.2. Off-line digestion with immobilized trypsin and CE-MS

The off-line digestion with immobilized trypsin was first carried out using commercial particles and the digestion buffer, temperature and time recommended by the manufacturer (50 mM NH_4HCO_3 pH 7.9, 25 °C and 30 min) [27]. Under these digestion conditions, Table 1 shows that the sequence coverage was total as in the off-line digestion with trypsin in solution (1000 μg mL^{-1} of β-LG analyzed by CE-MS at 37 °C in both cases). In addition, the repeatability of peak areas and migration times was also similar, with %RSD ranging between 0.6% and 14% and 0.4–1.3%, respectively. Fig. 2-A shows a bar graph with the total sum of the peak areas for the detected tryptic peptides using the different digestion buffers and separation temperatures in CE-MS. Again, sensitivity was higher when CE-MS was conducted at 37 °C. However now, in contrast to the off-line digestion with trypsin in solution, peak areas were slightly higher with 10 mM NH_4HCO_3 or NH_4Ac digestion buffers. The reusability of the immobilized trypsin particles was also evaluated performing three consecutive digestions with the different digestion buffers. As can be observed in Fig. 2-B, the digestion yield was similar between consecutive digestions for the 10 and 50 mM NH_4HCO_3 digestion buffers, but significantly decreased for the 10 mM NH_4Ac after the first digestion, probably because of the enzyme degradation with the 10 mM NH_4Ac digestion buffer. Therefore, the use of NH_4HCO_3 digestion buffers allowed the highest digestion yields,

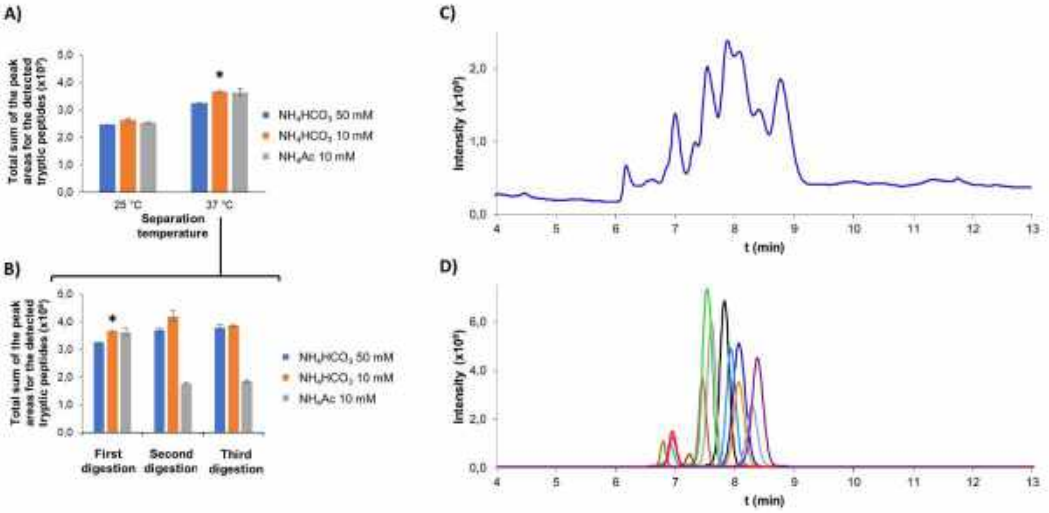

Fig. 2. Off-line protein digestion of β-LG (1000 μg mL^{-1}) with immobilized trypsin performed during 30 min at 25 °C and CE-MS analysis. Comparison of the total sum of peak areas for the detected tryptic peptides **(A)** with different separation temperatures and digestion buffers and **(B)** after consecutives enzymatic digestions with different digestion buffers (37 °C of separation temperature). **(C)** TIE and **(D)** EIEs for the CE-MS analysis at 37 °C using 10 mM NH_4HCO_3 as the digestion buffer. Optimized conditions are indicated in **(A)** and **(B)** with an asterisk.

detection sensitivities and made the enzyme reusable. Figs. 2-C and 2-D show the TIE and EIEs for the CE-MS separation of the tryptic digest of β-LG at 37 °C with a 10 mM NH_4HCO_3 digestion buffer (1000 μg mL^{-1} of protein digested at 25 °C during 30 min). Under these optimized conditions, total separation times were again shorter than 9 min (Fig. 2-C and D), but digestion yields with immobilized trypsin particles were lower than with free trypsin in solution (compare the total sum of the values of the peak areas for the detected tryptic peptides under the optimized conditions, which are labelled with an asterisk in Fig. 1 A-B and 2 A-B). Taking into account the information provided by the enzyme manufacturer, the main explanation could be that the quality of the immobilized trypsin was lower than the quality of the free trypsin, which was a *sequencing grade modified trypsin*. Nevertheless, the use of immobilized trypsin substantially reduced digestion times while allowing the enzyme reuse. This was an essential feature to develop the on-line IMER-CE-MS method, which allowed reducing the manual sample handling and increasing the analysis throughput.

3.3. On-line digestion by IMER-CE-MS

The typical digestion buffer of 50 mM NH_4HCO_3 pH 7.9 was rapidly discarded for IMER-CE-MS after some preliminary studies because of current instability and breakdowns during the electrophoretic runs. This was probably due to CO_2 bubble formation during the on-line mixing of the digestion buffer and the acidic BGE (50 mM HAc: 50 mM HFor, pH 2.3). This issue was not found with the 10 mM NH_4HCO_3 and 10 mM NH_4Ac digestion buffers. Fig. 3-A shows that the digestion yield and detection sensitivity for β-LG (1000 μg L^{-1}) at 25 °C were higher

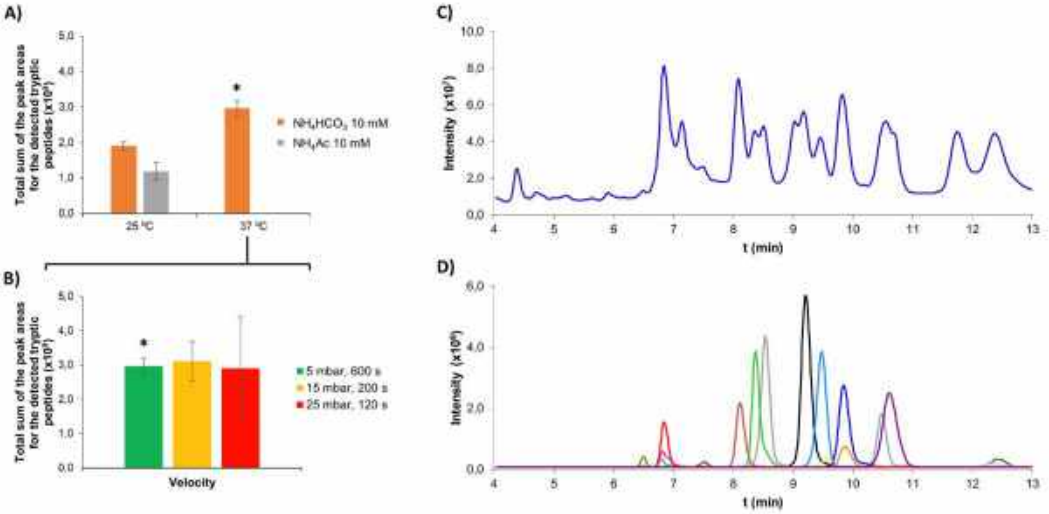

Fig. 3. On-line IMER-CE-MS protein digestion and analysis of β-LG (1000 μg mL^{-1}) with immobilized trypsin. Comparison of the total sum of peak areas for the detected tryptic peptides **(A)** with different digestion-separation temperatures and digestion buffers (with 5 mbar, 600 s of contact time) and **(B)** with different contact times between the protein and the enzyme of the microreactor (37 °C of digestion-separation temperatures). **(C)** TIE and **(D)** EIEs for the on-line IMER-CE-MS digestion-separation at 37 °C using 10 mM NH_4HCO_3 as the digestion buffer. Optimized conditions are indicated in **(A)** and **(B)** with an asterisk.

with the 10 mM NH_4HCO_3 digestion buffer than with the 10 mM NH_4Ac digestion buffer, and results were further improved at 37 °C. This temperature is well-known to be the optimum for trypsin digestion, despite the manufacturer of the immobilized trypsin particles recommended a digestion temperature of 25 °C as was indicated in the previous section. Furthermore, as we explained before, separations at 37 °C were faster and sensitivity was higher. Once selected these conditions, we evaluated the influence of the contact time between the β-LG and the immobilized trypsin. The protein solution (50 mbar, 15 s, −80 nL) was injected between two plugs of digestion buffer (50 mbar, 8 s, −40 nL) and the sandwich was pushed through the microreactor with BGE (~325 nL) at different velocities (5 mbar, 600 s; 15 mbar, 200 s and 25 mbar, 120 s). As can be observed in Fig. 3-B repeatability was higher when the protein solution passed through the microreactor at the smallest velocity (5 mbar, 600 s), probably because the contact time between the protein and the immobilized enzyme was longer. Figs. 3-C and 3-D show the TIE and EIEs for the analysis of β-LG (1000 μg mL^{-1}) by IMER-CE-MS at 37 °C with the 10 mM NH_4HCO_3 digestion buffer and the on-line digestion at the smallest velocity. Under these optimized conditions, separations were improved with regard to the off-line digestions because the total separation times were slightly longer (< 13 min) than by CE-MS (< 9 min, Fig. 1 C-D and 2C-D) probably because of the backpressure promoted by the presence of the microreactor. Furthermore, digestion yields were comparable, but slightly lower, than in the off-line digestion with immobilized trypsin (compare the total sum of the values of the peak areas for the detected tryptic peptides under the optimized conditions, which are labelled with an asterisk in Fig. 2 A-B and 3 A-B). This was probably due to the reduced contact time between the protein and the enzyme and the lower amount of protein. Digestion velocity could not be further reduced, because 5 mbar was the smallest pressure that can be applied by the CE instrument. With regard to the amount of protein, the injected volume of protein solution was increased, from 80 nL (50 mbar, 15 s) to 160 nL (50 mbar, 30 s) but results did not significantly improved. Under the optimized conditions, Table 1 shows that%RSD for peak areas and migration times ranged between 2.2 and 15 and 4.8–7.6%, respectively. Therefore, repeatabilities in peak areas and migration times were only slightly lower than for the off-line digestions (Table 1). With regard to the sequence coverage, it was found to be total until a concentration of around 10 μg mL^{-1} of β-LG, which was considered as the limit of detection (at 5 μg mL^{-1} of protein the coverage decreased to 80%). The reusability of a microreactor was tested studying the variation in peak area and migration time of the tryptic peptides through consecutive protein digestions and analysis of β-LG (1000 μg mL^{-1}). As can be observed in Fig. S-1A, the microreactor could be reused for more than 30 consecutive times without a significant decrease in the values and the repeatability of the total sum of peak areas of the detected tryptic peptides (average %RSD values for 5, 10, 20, and 30 consecutive digestions are inserted in the graphics of Fig. S-1). However, average migration times and their %RSD values increased through consecutive analyses because of gradual repacking of the immobilized trypsin particles (Fig. S-1B). Therefore, a maximum of ten analyses per microreactor would be a good compromise taking into account the overall performance of the system. No carry-over effect was observed when blank samples were analyzed between consecutive digestions.

To validate the IMER-CE-MS method, α-CSN (a mixture of α-CSN1 and α-CSN2), β-CSN and κ-CSN were also analyzed (1000 μg mL^{-1} of protein), and results in terms of repeatability and sequence coverage were similar as for β-LG (1000 μg mL^{-1} of protein). Supplementary Tables S-1, S-2, S-3 and S-4 show the %RSD (n = 3) for peak areas of the peptides detected by IMER-CE-MS for the different proteins. At this protein concentration, sequence coverages were 89%, 79%, 88% and 66% for α-CSN1, α-CSN2, β-CSN and κ-CSN, respectively. In α-CSN, the sequence coverage for α-CSN2 was lower because this proteoform was at lower abundance in the mixture. Among all the proteins, the sequence coverage was the lowest for κ-CSN because a high M_r peptide

Table 2
Sequence of detected peptides, sequence coverage and identified proteins for the off-line digestion with free trypsin and CE-MS analysis and for the on-line digestion and analysis by IMER-CE-MS of the *E. Coli* cell lysate (1000 μg mL^{-1}). Single amino acids were not taken into account.

Identified protein	Off-line digestion with free trypsin and CE-MS			On-line IMER-CE-MS digestion		
	Detected peptides		Coverage	Detected peptides		Coverage
α-lactalbumin M_r ~ 14,200	[2–5] QFTK	[109–114] ALCTEK	8%	[2–5] QFTK	[109–114] ALCTEK	8%
Myoglobin C M_r ~ 17,000	[43–45] FDK	[48–50] HLK	4%	[43–45] FDK	[48–50] HLK	4%
Cathepsin D M_r ~ 38,000	[110–112] VER	[278–281] LGGK	17%	[110–112] VER		7%
	[113–120] QVFGEATK	[282–284] GYK		[246–249] ELQK		
	[131–141] FDGILGMAYPR	[285–293] LSPEDYTLK		[282–284] GYK		
	[190–192] YYK	[294–299] VSQAGK		[285–293] LSPEDYTLK		
	[246–249] ELQK	[340–347] VGFAEAAR		[294–299] VSQAGK		
Creatine kinase-MM M_r ~ 43,000	[1–9] MPFGNTHNK	[149–151] GER	21%	[26–32] HNNHMAK	[267–292] AGHPFMWNQHLGYVLTCPSNLGTGLR	17%
	[26–32] HNNHMAK	[173–177] YYPLK		[42,43] LR	[315–316] LR	
	[42,43] LR	[267–292] AGHPFMWNQHLGYVLTCPSNLGTGLR		[44,45] DK	[317–319] LQK	
	[44,45] DK	[315–316] LR		[131–132] VR	[359–365] LMVEMEK	
	[131–132] VR	[317–319] LQK		[133–135] TGR	[367–369] LEK	
	[133–135] TGR	[359–365] LMVEMEK		[136–138] SIK		
	[136–138] SIK	[367–369] LEK		[149–151] GER		
Antithrombin III M_r ~ 49,200	[14–24] DIPMNPMCIYR	[184–188] AAINK	19%	[48–53] VWELSK		7%
	[48–53] VWELSK	[223–226] GLWK		[54–57] ANSR		
	[54–57] ANSR	[237–241] ELFYK		[140–145] LVSANR		
	[140–145] LVSANR	[263–275] VAEGTQVLELPFK		[146–150] LFGDK		
	[146–150] LFGDK	[351–359] LPGIVAGR		[223–226] GLWK		
	[177–183] ENAEQSR	[394–399] SLNPNR		[394–399] SLNPNR		

(53 amino acids long) was not detected. Supplementary Figures S-2 A, B and C show the TIE and EIEs for the IMER-CE-MS analysis of α-CSN1, β-CSN and κ-CSN, respectively, and total separation times were shorter than 15 min in all cases.

In order to demonstrate the feasibility of IMER-CE-MS for the analysis of complex real samples an *E. coli* cell lysate (1000 μg mL^{-1}) was analyzed under the optimized conditions by off-line digestion with free trypsin and CE-MS and by on-line IMER-CE-MS. Supplementary Figure S-2 D and E show the TIEs for the off-line and the on-line digestions, respectively. In both cases, a similar electrophoretic profile was obtained but it was difficult to appreciate electrophoretic peaks due to the tryptic peptides because of the low abundance of the different proteins in the cell lysate. The studied cell lysate was specifically prepared as a quality control for purification of His-tagged proteins, which contained an overexpressed protein with six additional His amino acids in the C-terminal position (6×-His, M, −14,200). Taking into account the western blot provided by the manufacturer and the LC-MS/MS bottom-up analysis study of Wright et al. [31], the 6 × -His protein was identified as 6 × -His human α-lactalbumin. As Wright et al. [31], it was also possible to identify other high abundant proteins in the cell lysate with the off-line and the on-line digestions. Table 2 shows the sequence of the detected peptides, the sequence coverage and the identified proteins in both cases. As can be observed, sequence coverages were only slightly lower with the on-line digestion, due to the shorter digestion times and the lower amount of protein, and in both cases 6 × -His human α-lactalbumin, myoglobin C, cathepsin D, creatine kinase-MM and antithrombin III were identified. The number of identified peptides and the sequence coverages were also very similar to those found by Wright et al. by LC-MS/MS [31], indicating the good performance of the on-line digestion by IMER-CE-MS compared to the traditional off-line digestion methods and the potential for the high-throughput bottom-up analysis of complex protein mixtures in proteomics research.

4. Conclusions

We have developed and validated an IMER-CE-MS method for the on-line enzymatic digestion, separation and characterization of proteins. Under the optimized conditions, using 10 mM NH_4HCO_3 pH 7.9 as the digestion buffer, a very low protein sample flow through the microreactor, a separation BGE of 50 mM HAc: 50 mM HFor, pH 2.3, and a temperature of digestion and separation of 37 °C, proteins were analyzed in less than 30 min (including all the steps). Furthermore, the sequence coverage for β-LG was complete until a concentration of 10 μg mL^{-1} of protein and the microreactor could be reused until 10 times with optimum performance, without decreasing repeatability or observing carry-over. Results were comparable to the off-line digestion with free or immobilized trypsin and CE-MS, despite a slightly smaller digestion yield was observed due to the shorter digestion times and the lower amount of protein. The good performance of the IMER-CE-MS method was also demonstrated for α-CSN1, α-CSN2, β-CSN and κ-CSN, as well as for an *E. coli* cell lysate, confirming the great potential of this approach to reduce the protein sample volume and the digestion times, while minimizing the sample handling and reusing the microreactors. These features are critical to perform rapid, reliable and high-throughput analysis of complex protein mixtures in proteomics research, with trypsin or any other proteolytic enzyme, in bottom-up or middle-down approaches using hybrid mass spectrometers.

Acknowledgements

This study was supported by a grant from the Spanish Ministry of Economy and Competitiveness (CTQ2014-56777-R) and the Cathedra UB Rector Francisco Buscarons Ubeda (Forensic Chemistry and Chemical Engineering). Roger Pero-Gascon acknowledges the Spanish Ministry of Education, Culture and Sport for a FPU (Formación del Profesorado Universitario) fellowship.

The authors declare no competing interests.

Appendix A. Supporting information

Supplementary data associated with this article can be found in the online version at doi:10.1016/j.talanta.2019.02.039.

References

[1] A.F.M. Altelaar, J. Munoz, A.J.R. Heck, Next-generation proteomics: towards an integrative view of proteome dynamics, Nat. Rev. Genet. 14 (2013) 35–48, https://doi.org/10.1038/nrg3356.
[2] L.M. Smith, N.L. Kelleher, Proteoform: a single term describing protein complexity, Nat. Methods 10 (2013) 186–187, https://doi.org/10.1038/nmeth.2369.
[3] L. Tsiatsiani, A.J.R. Heck, Proteomics beyond trypsin, FEBS J. 282 (2015) 2612–2626, https://doi.org/10.1111/febs.13287.
[4] A. Lapolla, D. Fedele, R. Reitano, N.C. Aricò, R. Seraglia, P. Traldi, E. Marotta, R. Tonani, Enzymatic digestion and mass spectrometry in the study of advanced glycation end products/peptides, J. Am. Soc. Mass Spectrom. 15 (2004) 496–509, https://doi.org/10.1016/j.jasms.2003.11.014.
[5] E. Giménez, R. Ramos-Hernan, F. Benavente, J. Barbosa, V. Sanz-Nebot, Analysis of recombinant human erythropoietin glycopeptides by capillary electrophoresis electrospray-time of flight-mass spectrometry, Anal. Chim. Acta 709 (2012) 81–90, https://doi.org/10.1016/j.aca.2011.10.028.
[6] A.A. Homaei, R. Sariri, F. Vianello, R. Stevanato, Enzyme immobilization: an update, J. Chem. Biol. 6 (2013) 185–205, https://doi.org/10.1007/s12154-013-0102-9.
[7] X. Liu, J. Yang, L. Yang, Capillary electrophoresis-integrated immobilized enzyme reactors, Rev. Anal. Chem. 35 (2016) 115–131, https://doi.org/10.1515/revac-2016-0003.
[8] L. Liu, B. Zhang, Q. Zhang, Y. Shi, L. Guo, L. Yang, Capillary electrophoresis-based immobilized enzyme reactor using particle-packing technique, J. Chromatogr. A 1352 (2014) 80–86, https://doi.org/10.1016/j.chroma.2014.05.058.
[9] S. Moore, S. Hess, J. Jorgenson, Characterization of an immobilized enzyme reactor for on-line protein digestion, J. Chromatogr. A 1476 (2016) 1–8, https://doi.org/10.1016/j.chroma.2016.11.021.
[10] G.A. Toth, Z. Kuklenyik, J.I. Jones, B.A. Parks, M.S. Gardner, D.M. Schieltz, J.C. Rees, M.L. Andrews, L.G. McWilliams, J.L. Pirkle, J.R. Barr, On-column trypsin digestion coupled with LC-MS/MS for quantification of apolipoproteins, J. Proteom. 150 (2017) 258–267, https://doi.org/10.1016/j.jprot.2016.09.011.
[11] L.N. Amankwa, W.G. Kuhr, Trypsin-modified fused-silica capillary microreactor for peptide mapping by capillary zone electrophoresis, Anal. Chem. 64 (1992) 1610–1613, https://doi.org/10.1021/ac00038a019.
[12] L.N. Amankwa, W.G. Kuhr, On-line peptide mapping by capillary zone electrophoresis, Anal. Chem. 65 (1993) 2693–2697, https://doi.org/10.1021/ac00067a025.
[13] L.N. Amankwa, K. Harder, F. Jirik, R. Aebersold, High-sensitivity determination of tyrosine-phosphorylated peptides by on-line enzyme reactor and electrospray ionization mass spectrometry, Protein Sci. 4 (1995) 113–125, https://doi.org/10.1002/pro.5560040114.
[14] L. Licklider, W.G. Kuhr, M.P. Lacey, T. Keough, M.P. Purdon, R. Takigiku, Online microreactors/capillary electrophoresis/mass spectrometry for the analysis of proteins and peptides, Anal. Chem. 67 (1995) 4170–4177, https://doi.org/10.1021/ac00118a021.
[15] L. Licklider, W.G. Kuhr, Optimization of on-line peptide mapping by capillary zone electrophoresis, Anal. Chem. 66 (1994) 4400–4407, https://doi.org/10.1021/ac00096a003.
[16] N.A. Guzman, Consecutive protein digestion and peptide derivatization employing an on-line analyte concentrator to map proteins using capillary electrophoresis, in: P.G. Righetti (Ed.), Capill. Electrophor. Anal. Biotechnol. CRC Press, Boca Raton, Fl., 1996, pp. 101–121.
[17] J. Gao, J. Xu, L.E. Locascio, C.S. Lee, Integrated microfluidic system enabling protein digestion, peptide separation, and protein identification, Anal. Chem. 73 (2001) 2648–2655, https://doi.org/10.1021/ac001126h.
[18] J. Křenková, K. Klepárník, F. Foret, Capillary electrophoresis mass spectrometry coupling with immobilized enzyme electrospray capillaries, J. Chromatogr. A 1159 (2007) 110–118, https://doi.org/10.1016/j.chroma.2007.02.095.
[19] Z. Yin, W. Zhao, M. Tian, Q. Zhang, L. Guo, L. Yang, A capillary electrophoresis-based immobilized enzyme reactor using graphene oxide as a support via layer by layer electrostatic assembly, Analyst 139 (2014) 1973–1979, https://doi.org/10.1039/c3an02241b.
[20] M. Ye, S. Hu, R.M. Schoenherr, N.J. Dovichi, On-line protein digestion and peptide mapping by capillary electrophoresis with post-column labeling for laser-induced flourescence detection, Electrophoresis 25 (2004) 1319–1326, https://doi.org/10.1002/elps.200305841.
[21] R.M. Schoenherr, M. Ye, M. Vannatta, N.J. Dovichi, CE-microreactor-CE-MS/MS for protein analysis, Anal. Chem. 79 (2007) 2230–2238, https://doi.org/10.1021/ac061638h.
[22] E. Bonneil, M. Mercier, K.C. Waldron, Reproducibility of a solid-phase trypsin microreactor for peptide mapping by capillary electrophoresis, Anal. Chim. Acta 404

(2000) 29–45, https://doi.org/10.1016/S0003-2670(99)00677-7.
[23] E. Bonneil, K.C. Waldron, On-line system for peptide mapping by capillary electrophoresis at sub-micromolar concentrations, Talanta 53 (2000) 687–699, https://doi.org/10.1016/S0039-9140(00)00554-3.
[24] K. Sakai-Kato, M. Kato, T. Toyo'oka, On-line trypsin-encapsulated enzyme reactor by the sol - gel method integrated into capillary electrophoresis, Anal. Chem. 74 (2002) 2943–2949, https://doi.org/10.1021/ac0200421.
[25] X. Xu, X. Wang, Y. Liu, B. Liu, H. Wu, P. Yang, Trypsin entrapped in poly(diallylmethylammoniumchloride) silica sol-gel microreactor coupled to matrix-assisted laser desorption/ionization time-of-flight mass spectrometry, Rapid Commun. Mass Spectrom. 22 (2008) 1257–1264, https://doi.org/10.1002/rcm.
[26] Promega, Sequencing grade modified trypsin. <https://www.promega.es/-/media/files/resources/protocols/product-information-sheets/n/sequencing-grade-modified-trypsin-protocol.pdf?la=es-es> (Accessed 5 May 2018), 2016.
[27] Promega, Immobilized trypsin. Instructions for use. <https://www.promega.es/-/media/files/resources/protocols/technical-manuals/0/immobilized-trypsin-protocol.pdf> (Accessed 5 May 2018), 2010.
[28] H.H. Lauer, G.P. Rozing (Eds.), High Performance Capillary Electrophoresis, 2nd ed., Agilent Technologies, Waldbronn, Germany, 2014, <https://www.agilent.com/cs/library/primers/Public/5990_3777EN.pdf> (Accessed 5 May 2018).
[29] F. Benavente, S. Medina-Casanellas, E. Giménez, V. Sanz-Nebot, On-line solid-phase extraction capillary electrophoresis mass spectrometry for preconcentration and clean-up of peptides and proteins, in: N.T. Tran, M. Taverna (Eds.), Capill. Electrophor. Proteins Pept. Methods Protoc. Springer, New York, 2016, pp. 67–84, , https://doi.org/10.1007/978-1-4939-4014-1_6.
[30] C. Wenz, C. Barbas, Á. López-Gonzálvez, A. Garcia, F. Benavente, V. Sanz-Nebot, T. Blanc, G. Freckleton, P. Britz-McKibbin, M. Shanmuganathan, F. De L'Escaille, J. Far, R. Haselberg, S. Huang, C. Huhn, M. Pattky, D. Michels, S. Mou, F. Yang, C. Neususs, N. Tromsdorf, E.E.K. Baidoo, J.D. Keasling, S.S. Park, Interlaboratory study to evaluate the robustness of capillary electrophoresis-mass spectrometry for peptide mapping, J. Sep. Sci. 38 (2015) 3262–3270, https://doi.org/10.1002/jssc.201500551.
[31] J.C. Wright, M.O. Collins, L. Yu, L. Käll, M. Brosch, J.S. Choudhary, Enhanced peptide identification by electron transfer dissociation using an improved mascot percolator, Mol. Cell Proteom. 11 (2012) 478–491, https://doi.org/10.1074/mcp.O111.014522.

Supporting Information

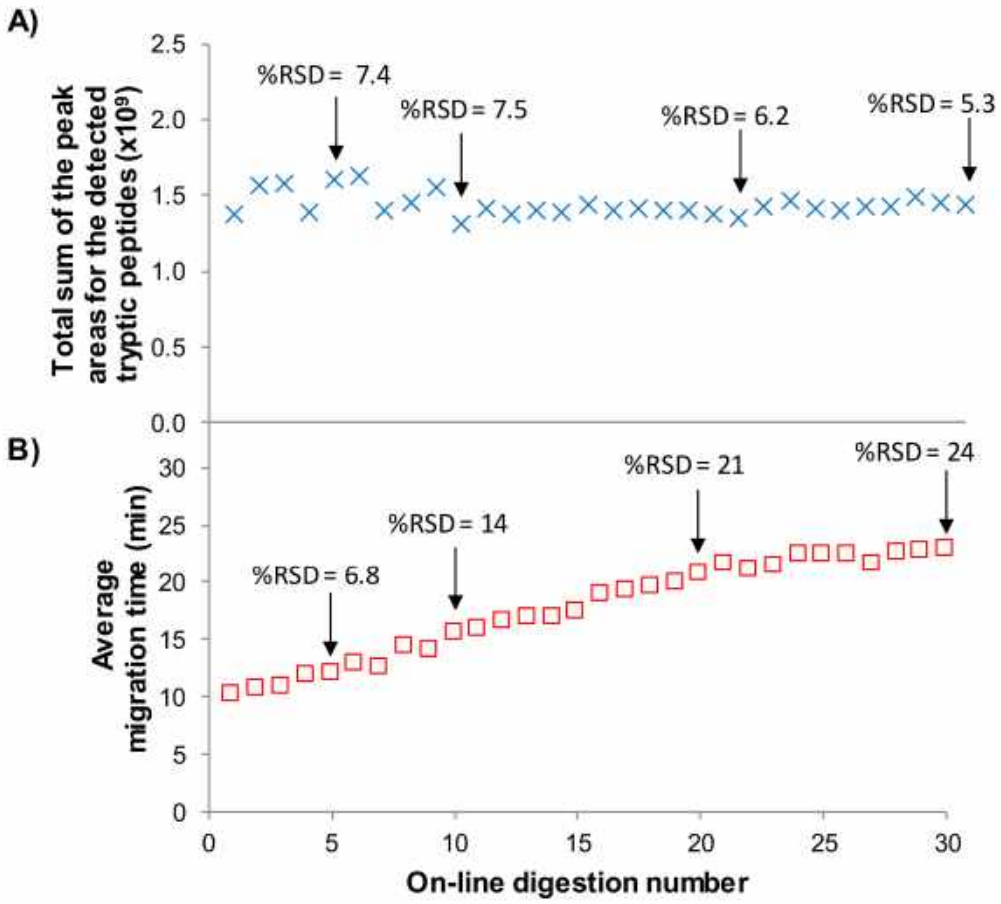

Figure S-1. Reusability of a microreactor for consecutive protein digestion and analysis of β-LG (1000 μg mL^{-1}) under the optimized conditions (37 ºC of digestion-separation temperatures and 5 mbar, 600 s of contact time**). (A)** Total sum of peak areas, and **(B)** average migration time for the detected tryptic peptides. Average %RSD values for the analysis n= 5, 10, 20 and 30 appear as insets.

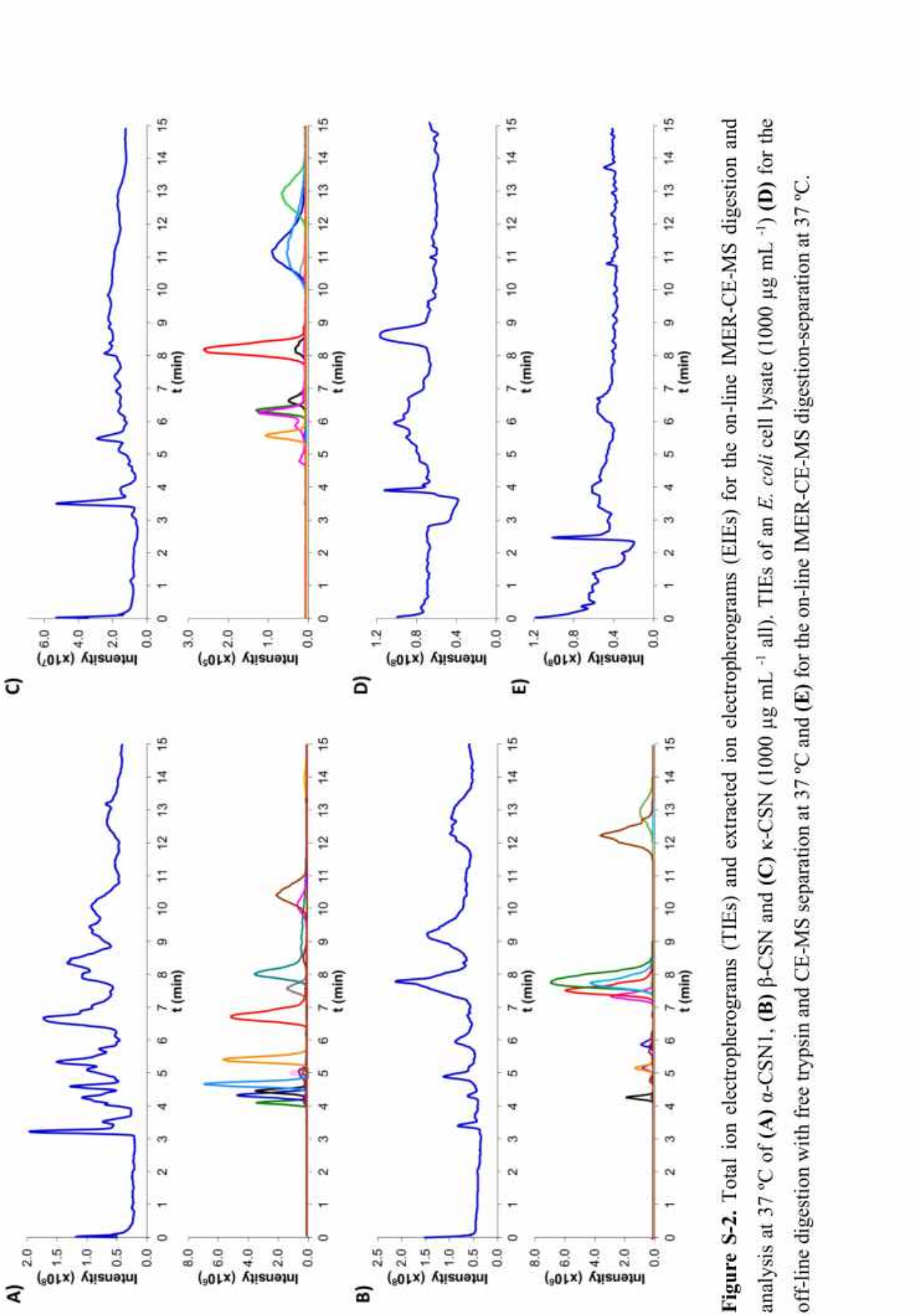

Figure S-2. Total ion electropherograms (TIEs) and extracted ion electropherograms (EIEs) for the on-line IMER-CE-MS digestion and analysis at 37 ºC of **(A)** α-CSN1, **(B)** β-CSN and **(C)** κ-CSN (1000 µg mL $^{-1}$ all). TIEs of an *E. coli* cell lysate (1000 µg mL $^{-1}$) **(D)** for the off-line digestion with free trypsin and CE-MS separation at 37 ºC and **(E)** for the on-line IMER-CE-MS digestion-separation at 37 ºC.

Table S-1. Relative peak areas and percentage of relative standard deviations (%RSD, n=3) of the peptides detected by the on-line IMER-CE-MS digestion and analysis at 37 °C of α-CSN1 (1000 μg mL^{-1} of α-CSN). Single amino acids were not taken into account.

Peptide sequence		$[M+nH]^{n+}$		Relative peak area [a]	
		m/z	n	Mean	% RSD
[1-3]	RPK	200.6373	2	0.029	9.9
[4-7]	HPIK	247.6582	2	0.093	5.4
[8-22]	HQGLPQEVLNENLLR	587.3202	3	0.203	1.7
[23-34]	FFVAPFPEVFGK	462.2486	3	0.013	4.4
[35-36]	EK	276.1554	1	0.014	1.2
[37-42]	VNELSK	385.1785	2	0.004	4.5
[43-58]	DIGSESTEDQAMEDIK	964.3497	2	0.017	3.5
[59-79]	QMEAESISSSEEIVPNSVEQK	-	-	-	-
[80-83]	HIQK	263.1611	2	0.093	5.9
[84-90]	EDVPSER	416.1961	2	0.076	2.6
[91-100]	YLGYLEQLLR	634.3562	2	0.148	5.0
[101-102]	LK	260.1969	1	0.004	4.3
[104-105]	YK	310.1761	1	0.013	4.1
[106-119]	VPQLEIVPNSAEER	830.9010	2	0.033	6.3
[120-124]	LHSMK	308.1681	2	0.093	4.5
[125-132]	EGIHAQQK	304.1633	3	0.069	2.7
[133-151]	EPMIGVNQELAYFYPELFR	772.7175	3	0.029	2.6
[152-193]	QFYQLDAYPSGAWYYVPLGTQYTDAPSFSDIPNPIGSENSEK	1572.7295	3	0.001	4.2
[194-199]	TTMPLW	748.3698	1	0.068	2.4

a)The relative peak areas were obtained dividing the raw peak area of the peptide by the total sum of raw peak areas of the detected peptides.

Table S-2. Relative peak areas and percentage of relative standard deviations (%RSD, n=3) of the peptides detected by the on-line IMER-CE-MS digestion and analysis at 37 ºC of α-CSN2 (1000 μg mL^{-1} of α-CSN). Single amino acids were not taken into account.

Peptide sequence		$[M+nH]^{n+}$		Relative peak area [a]	
		m/z	n	Mean	% RSD
[2-21]	NTMEHVSSSEESIISQETYK	873.6402	3	0.003	8.2
[22-24]	QEK	404.2140	1	0.004	9.9
[25-32]	NMAINPSK	477.7096	2	0.001	35
[33-41]	ENLCSTFCK	522.7284	2	0.002	2.7
[42-45]	EVVR	251.6531	2	0.028	5.3
[46-70]	NANEEEYSIGSSSEESAEVATEEVK	-	-	-	-
[71-76]	ITVDDK	345.6873	2	0.250	1.7
[77-80]	HYQK	288.1507	2	0.034	4.9
[81-91]	ALNEINQFYQK	684.3516	2	0.050	1.7
[92-113]	FPQYLQYLYQGPIVLNPWDQVK	903.8077	3	0.007	4.1
[115-125]	NAVPITPTLNR	598.3436	2	0.058	4.8
[126-136]	EQLSTSEENSK	-	-	-	-
[138-149]	VDMESTEVFTK	733.8100	2	0.028	5.4
[151-152]	TK	248.1605	1	0.023	2.0
[153-158]	LTEEEK	748.3723	1	0.165	0.6
[159-160]	NR	-	-	-	-
[161-165]	LNFLK	317.7001	2	0.077	4.0
[167-170]	ISQR	-	-	-	-
[171-173]	YQK	438.2347	1	0.007	5.2
[174-181]	FALPQYLK	490.2845	2	0.100	1.2
[182-188]	TVYQHQK	452.2381	2	0.019	6.4
[189-197]	AMKPWIQPK	366.8762	3	0.065	1.9
[198-199]	TK	248.1605	1	0.023	2.3
[200-205]	VIPYVR	373.7319	2	0.012	2.7
[206-207]	YL	295.1652	1	0.044	1.0

a) The relative peak areas were obtained dividing the raw peak area of the peptide by the total sum of raw peak areas of the detected peptides.

Table S-3. Relative peak areas and percentage of relative standard deviations (%RSD, n=3) of the peptides detected by the on-line IMER-CE-MS digestion and analysis at 37 ºC of β-CSN (1000 µg mL^{-1}). Single amino acids were not taken into account.

Peptide sequence		$[M+nH]^{n+}$		Relative peak area [a]	
		m/z	n	Mean	%RSD
[2-25]	ELEELNVPGEIVESLSSSEESITR	-	-	-	-
[26-28]	INK	187.6238	3	0.014	2.1
[30-32]	IEK	389.2395	2	0.004	3.9
[33-48]	FQSEEQQQTEDELQDK	687.9481	1	0.005	3.6
[49-97]	IHPFAQTQSLVYPFPGPIPNSLPQNIPPLTQTPVVVPPFLQPEVMGVSK	1772.9564	2	0.000	22
[98-99]	VK	246.1812	1	0.016	3.0
[100-105]	EAMAPK	323.6654	2	0.078	2.6
[106-107]	HK	284.1717	2	0.012	10
[108-113]	EMPFPK	374.6888	2	0.176	1.0
[114-169]	YPVEPFTESQSLTLTDVENLHLPLPLLQSWMHQPHQPLPPTVMFPPQSVLSLSQSK	2120.4239	1	0.000	30
[170-176]	VLPVPQK	390.7528	3	0.338	1.4
[177-183]	AVPYPQR	415.7299	2	0.146	0.3
[184-202]	DMPIQAFLLYQEPVLGPVR	729.3945	1	0.090	9.1
[203-209]	GPFPIIV	742.4498	1	0.121	2.8

a) The relative peak areas were obtained dividing the raw peak area of the peptide by the total sum of raw peak areas of the detected peptides.

Table S-4. Relative peak areas and percentage of relative standard deviation (%RSD, n=3) of the peptides detected by the on-line IMER-CE-MS digestion and analysis at 37 ºC of κ-CSN (1000 μg mL^{-1}). Single amino acids were not taken into account.

Peptide sequence		$[M+nH]^{n+}$		Relative peak area [a]	
		m/z	n	Mean	%RSD
[1-10]	QEQNQEQPIR	635.3130	2	0.007	66
[11-13]	CEK	436.1646	2	0.009	22
[14-16]	DER	419.1885	3	0.028	25
[17-21]	FFSDK	322.1582	3	0.293	19
[22-24]	IAK	331.2340	2	0.063	2.8
[25-34]	YIPIQYVLSR	626.3587	1	0.219	15
[35-68]	YPSYGLNYYQQKPVALINNQFLPYPYYAKPAAVR	1337.3599	2	0.002	69
[69-86]	SPAQILQWQVLSNTVPAK	660.7023	1	0.130	16
[87-97]	SCQAQPTTMAR	625.7740	2	0.191	6.9
[98-111]	HPHPHLSFMAIPPK	536.9542	2	0.058	6.6
[113-116]	NQDK	-	-	-	-
[117-169]	IPTINTIASGEPTSTPTTEAVESTVATLEDSPEVIESPPEINTVQVTSTAV	-	-	-	-

a)The relative peak areas were obtained dividing the raw peak area of the peptide by the total sum of raw peak areas of the detected peptides.

Capítulo 6. Resultados y discusión

6.1. Nuevos desarrollos para la predicción y optimización de las separaciones en CE

En las últimas décadas, la detección, caracterización y cuantificación de compuestos biomarcadores en fluidos biológicos se ha convertido en una herramienta esencial para el diagnóstico, seguimiento y pronóstico de diversas enfermedades. En este sentido, la espectrometría de masas (MS) es una técnica excelente para la identificación inequívoca de los analitos de interés debido a su selectividad y potencial respecto a la caracterización estructural detallada de compuestos desconocidos. Sin embargo, debido a la sensibilidad necesaria y a la complejidad de la mayoría de las muestras biológicas, es imprescindible su acoplamiento con las técnicas de separación de alta resolución. La separación previa de los compuestos permite la detección de los analitos como picos de elevada eficacia y evita la supresión de la ionización, lo que conduce a una mejora del límite de detección (LOD). Actualmente, la cromatografía de líquidos (LC) y la electroforesis capilar (CE) son las técnicas de separación más adecuadas para este propósito. En muchas aplicaciones están consideradas como técnicas complementarias y ortogonales debido a que sus mecanismos de separación son diferentes.

La CE es una técnica a escala micro cuyo mecanismo de separación en su modo más sencillo (electroforesis capilar de zona, CZE) se basa en la movilidad electroforética (m_e), que está relacionada con la relación carga iónica-radio de los solutos y, por consiguiente, es muy adecuada para la separación de biomoléculas cargadas. No obstante, para obtener separaciones rápidas, eficaces y de elevada resolución, los métodos de separación electroforéticos deben ser optimizados convenientemente.

Este capítulo se centra en el desarrollo de estrategias novedosas para la predicción y optimización de las separaciones en CE, concretamente en CZE. Para evaluar estas estrategias, se han estudiado los péptidos beta amiloides (Aβ) 1-40 y 1-42 y cinco de sus fragmentos (Aβ 1-15, 10-20, 20-29, 25-35 y 33-42) que cubren toda su secuencia aminoacídica. Los péptidos Aβ 1-40 y 1-42 son biomarcadores clínicos utilizados para el diagnóstico de la enfermedad de Alzheimer

y sus fragmentos también son investigados en relación con la patogénesis de la enfermedad [63,73,75,78,79]. Los métodos de inmunoensayo empleados habitualmente para el análisis de los péptidos Aβ 1-40 y 1-42 y sus fragmentos presentan una sensibilidad adecuada pero no son capaces de distinguirlos de forma fiable. Por lo tanto, existe la necesidad urgente de desarrollar métodos de análisis alternativos, siendo especialmente interesantes los que emplean técnicas de separación de alta resolución en microescala como la CE. En este desarrollo, una optimización rigurosa de las condiciones de separación resulta una pieza fundamental.

En este capítulo, se ha estudiado el comportamiento electroforético de los fragmentos de los péptidos Aβ en función del pH. Esto ha permitido la determinación de las constantes de acidez de sus grupos ionizables (K_a o pK_a, su logaritmo negativo) y, simultáneamente, la selección del pH óptimo para su separación. Dado que la determinación de los pK_as de compuestos polipróticos con muchos grupos ionizables es muy dificultosa, un enfoque interesante propuesto en este trabajo ha sido estimar los pK_as de los péptidos Aβ 1-40 y 1-42 a partir de los valores de pK_a determinados para sus fragmentos. Además, se ha predicho la migración electroforética de los péptidos Aβ mediante los modelos semiempíricos clásicos que relacionan su m_e con la estructura, específicamente con la relación carga-masa molecular ($q/M_r^{1/2}$, para el modelo clásico de los polímeros), que se puede calcular de forma directa y sin requerir de la obtención de más datos experimentales si se dispone de valores de pK_a adecuados (**Artículo 2.1**). Para seleccionar el pH de separación óptimo para la mezcla de péptidos Aβ, se han evaluado los criterios de calidad $S_{i,j}$ y T', demostrando que es posible utilizar como variable de optimización del pH tanto la m_e de los fragmentos de los péptidos Aβ como su $q/M_r^{1/2}$ (**Artículo 2.2**).

6.1.1. Determinación del comportamiento electroforético y las constantes de acidez de los fragmentos de los péptidos Aβ. Estimación de los valores de pK_a de los péptidos Aβ 1-40 y 1-42

El estudio del comportamiento electroforético de los cinco fragmentos de los péptidos Aβ en función del pH se utilizó para determinar sus pK_as mediante CE con detección ultravioleta

(CE-UV). El pK_a es un parámetro fundamental para la caracterización fisicoquímica de compuestos que presentan grupos ionizables, como es el caso de los péptidos [110,111]. La CE se ha utilizado ampliamente para la determinación de valores de pK_a y, además, en los últimos años se han propuesto diferentes alternativas para aumentar la reproducibilidad y la productividad en estos procedimientos, como la aplicación de instrumentación con múltiples capilares [270] y miniaturizada [271], los capilares recubiertos [272,273], la detección por espectrometría de masas [274,275] o métodos basados en el uso de un patrón interno [276].

En la **Tabla 6.1** se muestran la secuencia de aminoácidos, la M_r y los grupos ionizables ácidos y básicos de los fragmentos de los péptidos Aβ estudiados y de los péptidos Aβ 1-40 y 1-42. En el caso de estos últimos, ambos péptidos tienen el mismo número de grupos ionizables, 15 en total, de los cuales 8 son grupos ácidos y 7 son básicos. Este elevado número y, en algunos casos, la similitud de sus valores de pK_a, impiden su determinación por CE-UV. Por esta razón, se procedió a la determinación de los pK_as termodinámicos de los fragmentos de los péptidos Aβ mediante CE-UV y se utilizaron posteriormente para estimar los pK_as de los péptidos Aβ 1-40 y 1-42.

Para modelizar el comportamiento electroforético de los fragmentos peptídicos en función del pH, en algunos casos fue necesario considerar conjuntamente algunos de los grupos ionizables. Éstos presentarían valores de pK_a iguales o muy similares (menos de 0,5 unidades en los valores de pK_a para los aminoácidos descritos por Rickard et al, pK_a(R), en polipéptidos [277]) y no se podrían diferenciar mediante CE-UV. Así, por ejemplo, en el fragmento Aβ 1-15, que es el péptido de mayor tamaño y presenta once grupos ionizables, se consideraron conjuntamente, entre otros, los grupos ionizables ácidos del grupo carboxilo terminal de la glutamina (^{t}C-Q pK_a(R) 3,2) y el grupo carboxilo de los dos residuos de ácido aspártico (D pK_a(R) 3,5). En este fragmento concreto, es también necesario destacar que el equilibrio ácido-base para el grupo guanidina en el residuo arginina (R pK_a(R) 12,5) estaba fuera del intervalo de pH estudiado y no se pudo determinar por CE-UV.

Tabla 6.1. Secuencia de aminoácidos, M_r media y grupos ionizables de los péptidos Aβ 1-40 y 1-42 y los fragmentos estudiados.

Aβ secuencia de aminoácidos	M_r	Aminoácido ionizable [a]		Fórmula [b]	
		Ácido	Básico	$H_aABH_z^z$	H_nX^z
1-15 **DAEFRHDSGYEVHHQ**	1826,9	1 ^{t}C-Q [c1] 2 D [c1] 2 E [c2] 1 Y	1 ^{t}N-D 3 H [c3] 1 R [d]	$H_6ABH_5^{5+}$	$H_{11}X^{5+}$
10-20 **YEVHHQKLVFF**	1446,7	1 ^{t}C-F 1 E 1 Y [c2]	1 ^{t}N-Y 2 H [e1] 1 K [e2]	$H_3ABH_4^{4+}$	H_7X^{4+}
20-29 **FAEDVGSNKG**	1023,1	1 ^{t}C-G [f] 1 D [f] 1 E	1 ^{t}N-F 1 K	$H_3ABH_2^{2+}$	H_5X^{2+}
25-35 **GSNKGAIIGLM**	1060,3	1 ^{t}C-M	1 ^{t}N-G 1 K	$HABH_2^{2+}$	H_3X^{2+}
33-42 **GLMVGGVVIA**	915,2	1 tC-A	1 tN-G	$HABH^+$	H_2X^+
1-40 **DAEFRHDSGYEVHHQKLVFFAEDVGSNKGAIIGLMVGGVV**	4329,9	1 ^{t}C-V 3 D 3 E 1 Y	1 ^{t}N-D 3 H 2 K 1 R	$H_8ABH_7^{7+}$	$H_{15}X^{7+}$
1-42 **DAEFRHDSGYEVHHQK**LVFFA**ED**VGSN**K**GAIIGLMVGGVV**IA**	4514,1	1 ^{t}C-A 3 D 3 E 1 Y	1 ^{t}N-D 3 H 2 K 1 R	$H_8ABH_7^{7+}$	$H_{15}X^{7+}$

a) ^{t}C-: COOH terminal; ^{t}N-: NH_2 terminal.

b) Fórmula de la especie totalmente protonada (a = número de grupos ionizables ácidos; z = número de grupos ionizables básicos, que equivale a la carga neta positiva máxima; n = número total de grupos ionizables).

Los grupos ionizables de los siguientes aminoácidos fueron considerados conjuntamente para los cálculos porque se esperaba que los valores de pK_a fueran muy similares:

Aβ 1-15: c1) 1 ^{t}C-Q y 2 D; c2) 2 E; c3) 3 H.

Aβ 10-20: e1) 2 H; e2) 1 Y y 1 K.

Aβ 20-29: f) 1 ^{t}C-G y 1 D.

d) R no se consideró para los cálculos porque el pK_a esperado estaba fuera del intervalo de pH estudiado (2-12).

En la **Tabla 6.2** se muestran los modelos electroforéticos establecidos a partir de la **Ecuación 6**[3], considerando los grupos ionizables de cada fragmento de los péptidos Aβ estudiado. Paralelamente, se determinó experimentalmente la m_e de los cinco fragmentos mediante CE-UV en el intervalo de pH 2–12, utilizando disoluciones patrón y electrolitos de separación (BGEs) adecuados. En la **Figura 6.1** se muestran como símbolos las m_es experimentales de los cinco fragmentos de los péptidos Aβ en función del pH del BGE. Los pares de datos experimentales m_e-pH se ajustaron a las ecuaciones correspondientes de la **Tabla 6.2** utilizando análisis de regresión no lineal. Las correlaciones eran adecuadas (R^2 >0,995) y las m_es calculadas se muestran como líneas en la **Figura 6.1**. Estos resultados demostraron la validez de las aproximaciones realizadas para obtener las ecuaciones de los modelos electroforéticos de los Aβ 1-15, 10-20 y 20-29, es decir, considerar conjuntamente grupos ionizables con valores de pK_a iguales o muy similares. En cambio, cuando los modelos electroforéticos de dichos péptidos se modificaron para considerar todos los grupos ionizables por separado, el cálculo no convergía o los valores de pK_a obtenidos no tenían sentido químico.

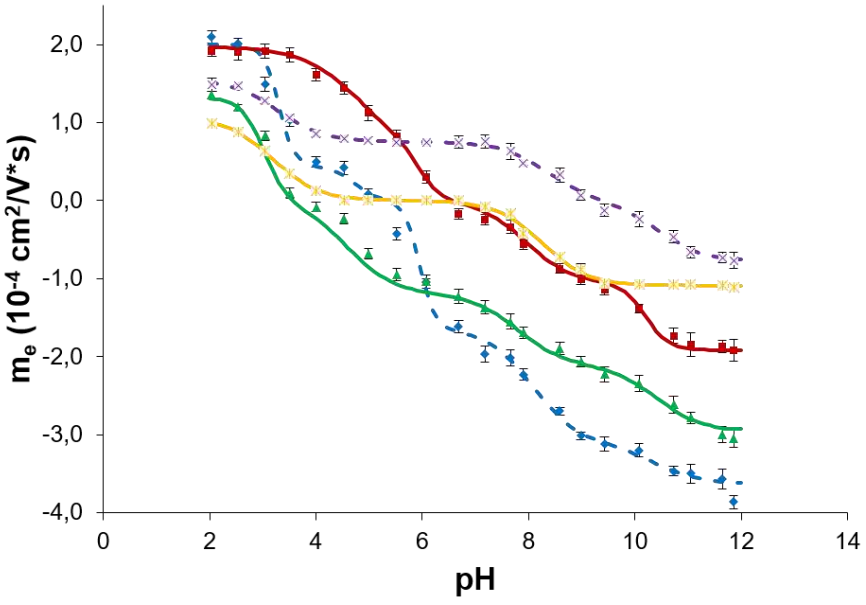

Figura 6.1. m_e experimental (símbolos) y calculada (líneas) en función del pH del BGE para los péptidos Aβ 1-15 (♦), 10-20 (■), 20-29 (▲), 25-35 (X) y 33-42 (ж). Las barras de error muestran la desviación estándar (número de replicados (n) = 5).

[3] Todas las ecuaciones empleadas en esta tesis doctoral se pueden encontrar en el **Apéndice**.

Tabla 6.2. Modelos electroforéticos para los fragmentos de los péptidos Aβ estudiados en el intervalo de pH 2-12.

Aβ	H_nX^z	Modelo electroforético
1-15 [a, b]	$H_{11}X^{5+}$	$m_e = \frac{10^{(3pK_1'+2pK_2'-5pH)}m_{H_{11}X^{5+}} + 10^{(2pK_2'-2pH)}m_{H_8X^{2+}} + 10^{(3pH-3pK_3')}m_{H_3X^{3-}} + 10^{(4pH-3pK_2'-pK_4')}m_{H_2X^{4-}} + 10^{(5pH-3pK_2'-pK_4'-pK_5')}m_{HX^{5-}}}{10^{(3pK_1'+2pK_2'-5pH)} + 10^{(2pK_2'-2pH)} + 1 + 10^{(3pH-3pK_3')} + 10^{(4pH-3pK_3'-pK_4')} + 10^{(5pH-3pK_3'-pK_4'-pK_5')}}$
10-20 [c]	H_7X^{4+}	$m_e = \frac{10^{(pK_1'+pK_2'+2pK_3'-4pH)}m_{H_7X^{4+}} + 10^{(pK_2'+2pK_3'-3pH)}m_{H_6X^{3+}} + 10^{(2pK_3'-2pH)}m_{H_5X^{2+}} + 10^{(pH-pK_4')}m_{H_2X^-} + 10^{(3pH-pK_4'-2pK_5')}m_{X^{3-}}}{10^{(pK_1'+pK_2'+2pK_3'-4pH)} + 10^{(pK_2'+2pK_3'-3pH)} + 10^{(2pK_3'-2pH)} + 1 + 10^{(pH-pK_4')} + 10^{(3pH-pK_4'-2pK_5')}}$
20-29 [d]	H_5X^{2+}	$m_e = \frac{10^{(2pK_1'-2pH)}m_{H_5X^{2+}} + 10^{(pH-pK_2')}m_{H_2X^-} + 10^{(2pH-pK_2'-pK_3')}m_{HX^{2-}} + 10^{(3pH-pK_2'-pK_3'-pK_4')}m_{X^{3-}}}{10^{(2pK_1'-2pH)} + 1 + 10^{(pH-pK_2')} + 10^{(2pH-pK_2'-pK_3')} + 10^{(3pH-pK_2'-pK_3'-pK_4')}}$
25-35	H_3X^{2+}	$m_e = \frac{10^{(pK_1'+pK_2'-2pH)}m_{H_3X^{2+}} + 10^{(pK_2'-pH)}m_{H_2X^-} + 10^{(pH-pK_3')}m_{X^-}}{10^{(pK_1'+pK_2'-2pH)} + 10^{(pK_2'-pH)} + 1 + 10^{(pH-pK_3')}}$
33-42	H_2X^+	$m_e = \frac{10^{(pK_1'-pH)}m_{H_2X^+} + 10^{(pH-pK_2')}m_{X^-}}{10^{(pK_1'-pH)} + 1 + 10^{(pH-pK_2')}}$

a) R no se consideró para los cálculos porque el pK_a esperado estaba fuera del intervalo de pH estudiado (2-12).

Los grupos ionizables de los siguientes aminoácidos fueron combinados para los cálculos porque se esperaba que los valores de pK_a fueran muy similares:

b) 1 C-Q y 2D (pK_1'), 2 E (pK_2'), 3 H (pK_3').

c) 2H (pK_3'), 1 Y y 1 K (pK_5').

d) 1 C-G y 1 D (pK_1').

Los pK_as aparentes (pK'_as) de los fragmentos de los péptidos Aβ se determinaron a partir de los parámetros de los ajustes y, considerando los coeficientes de actividad calculados a partir de la aproximación de Güntelberg de la ecuación de Debye-Hückel (**Ecuación 8**), se calcularon los pK_as termodinámicos. En la **Tabla 6.3** se muestran los valores de pK'_a y pK_a junto con los valores bibliográficos de pK_a(R) [277] y de los aminoácidos individuales (pK_a(A)) [278]. Se aprecia que, en general, los pK_as experimentales de los fragmentos de los péptidos Aβ determinados mediante CE-UV eran muy similares a los pK_a(R), especialmente en el caso de los Aβ 25-35 y 33-42, que presentan un menor número de grupos ionizables. En comparación con los pK_a(A), las diferencias más destacables se encontraban en los grupos ionizables ácido carboxílico y amino terminales, efecto que ya fue descrito por Rickard et al. [277]: la acidez del grupo carboxilo y la basicidad del grupo amino terminales disminuyen porque la formación del enlace peptídico induce un cambio electrostático en su carga. De acuerdo a los resultados obtenidos, es importante destacar, que si no se dispone de valores fiables de pK_as para los aminoácidos de péptidos y proteínas, ni de tiempo para determinarlos experimentalmente, los valores de pK_a(R) constituirían la mejor aproximación disponible en la bibliografía, tal y como ya ha sido descrito en anteriores trabajos de nuestro grupo de investigación [114,123,275,279].

En nuestro caso concreto, una vez conocidos los valores promedio de los pK_as termodinámicos de los fragmentos de los péptidos Aβ determinados mediante CE-UV, éstos se emplearon para estimar los pK_as de los péptidos Aβ 1-40 y 1-42, tal y como se muestra en la **Tabla 6.4**. Como se puede observar, la desviación estándar de los pK_as promedio calculados era inferior a 0,2, excepto en el residuo de tirosina, lo que demostraba la validez de la aproximación. Para el grupo guanidina en el residuo de arginina, se usó el valor de pK_a(R) porque este pK_a no se determinó por CE-UV.

Tabla 6.3. Fragmentos de los péptidos Aβ: pK_as aparentes (pK_a') y pK_as termodinámicos (pK_a) obtenidos mediante CE-UV, pK_as de Rickard et al. ($pK_a(R)$) y pK_as de los aminoácidos individuales ($pK_a(A)$).

Aβ	pK_a'	pK_i'	γ_i/γ_j	pK_a	$pK_a(R)$	$pK_a(A)$	Aminoácido [a]
1-15	3,5±0,3 [b]	1	γ_{5+}/γ_{4+}	**2,9**	3,2	2,2	**^{1}C-Q**
			γ_{4+}/γ_{3+}	**3,0**	3,5	3,7	**D**
			γ_{3+}/γ_{2+}	**3,1**	3,5	3,7	**D**
	4,7±0,7 [b]	2	γ_{2+}/γ_{+}	**4,5**	4,5	4,3	**E**
			γ_{+}/γ_{0}	**4,6**	4,5	4,3	**E**
	6,0±0,1 [b]	3	γ_{0}/γ_{-}	**6,0**	6,2	6,0	**H**
			γ_{-}/γ_{2-}	**6,2**	6,2	6,0	**H**
			γ_{2-}/γ_{3-}	**6,3**	6,2	6,0	**H**
	8,1±0,4	4	γ_{3-}/γ_{4-}	**8,6**	8,6	9,6	**^{1}N-D**
	10,4±0,7	5	γ_{4-}/γ_{5-}	**11,1**	10,3	10,1	**Y**
	- [c]	-	γ_{5-}/γ_{6-}	-	12,5	12,5	**R**
10-20	3,8±0,2	1	γ_{4+}/γ_{3+}	**3,3**	3,2	1,8	**^{1}C-F**
	4,9±0,6	2	γ_{3+}/γ_{2+}	**4,5**	4,5	4,3	**E**
	6,0±0,2 [b]	3	γ_{2+}/γ_{+}	**5,7**	6,2	6,0	**H**
			γ_{+}/γ_{0}	**5,9**	6,2	6,0	**H**
	8,0±0,1	4	γ_{0}/γ_{-}	**8,0**	7,7	9,1	**^{1}N-Y**
	10,2±0,1 [b]	5	γ_{-}/γ_{2-}	**10,4**	10,3	10,1	**Y**
			γ_{2-}/γ_{3-}	**10,6**	10,3	10,5	**K**
20-29	3,2±0,1 [b]	1	γ_{2+}/γ_{+}	**2,9**	3,2	2,3	**^{1}C-G**
			γ_{+}/γ_{0}	**3,1**	3,5	3,7	**D**
	4,6±0,1	2	γ_{0}/γ_{-}	**4,7**	4,5	4,3	**E**
	7,8±0,2	3	γ_{-}/γ_{2-}	**8,1**	7,7	9,1	**^{1}N-F**
	10,5±0,2	4	γ_{2-}/γ_{3-}	**10,8**	10,3	10,5	**K**
25-35	3,3±0,1	1	γ_{2+}/γ_{+}	**3,1**	3,2	2,3	**^{1}C-M**
	8,3±0,1	2	γ_{+}/γ_{0}	**8,2**	8,2	9,6	**^{1}N-G**
	10,5±0,1	3	γ_{0}/γ_{-}	**10,5**	10,3	10,5	**K**
33-42	3,2±0,1	1	γ_{+}/γ_{0}	**3,1**	3,2	2,3	**^{1}C-A**
	8,3±0,1	2	γ_{0}/γ_{-}	**8,3**	8,2	9,6	**^{1}N-G**

a) ^{1}C-: COOH terminal; ^{1}N-: NH_2 terminal.

b) Varios grupos ionizables se consideraron conjuntamente para los cálculos (ver **Tabla 6.1**).

c) R no se consideró para los cálculos porque el pK_a esperado estaba fuera del intervalo de pH estudiado (2-12).

Tabla 6.4. pK_as termodinámicos de los fragmentos de los péptidos Aβ determinados mediante CE-UV (ver **Tabla 6.3**) y pK_as estimados para los péptidos Aβ 1-40 y 1-42.

Aminoácido ionizable [a]	Aβ	pK_a [b]	pK_a promedio	Desviación estándar	Número de residuos en la secuencia de los péptidos Aβ	
					1-40	1-42
'C	1-15	2,9 (Q)	**3,1**	0,2	1 (V)	1 (A)
	10-20	3,3 (F)				
	20-29	2,9 (G)				
	25-35	3,1 (M)				
	33-42	3,1 (A)				
D	1-15	3,0 3,1	**3,1**	0,1	3	3
	10-20	3,1				
E	1-15	4,5 4,6 [c]	**4,6**	0,1	3	3
	10-20	4,5 [c]				
	20-29	4,7				
H	1-15	6,0 6,2 [c] 6,3 [c]	**6,0**	0,1	3	3
	10-20	5,7 [c] 5,9 [c]				
'N	1-15	8,6 (D)	**8,6**	-	1 (D)	1 (D)
K	10-20	10,6	**10,6**	0,2	2	2
	20-29	10,8 [c]				
	25-35	10,5 [c]				
Y	1-15	11,1	**10,8**	0,5	1	1
	10-20	10,4				
R	1-15	- [d]	**12,5** [e]	-	1	1

a) 'C: COOH terminal; 'N-: NH_2 terminal. Los aminoácidos terminales se indican entre paréntesis.

b) pK_as termodinámicos de los fragmentos de los péptidos Aβ determinados mediante CE-UV (ver **Tabla 6.3**).

c) La misma posición en la secuencia de aminoácidos se repite en ambos fragmentos de los péptidos Aβ.

d) El pK_a de R no se determinó por CE-UV porque el pK_a esperado estaba fuera del intervalo de pH estudiado (2-12).

e) pK_a de R de Rickard et al.

6.1.2. Predicción de la migración electroforética de los fragmentos de los péptidos Aβ mediante los modelos semiempíricos clásicos

La utilidad de las ecuaciones en la **Tabla 6.2** para la predicción del comportamiento electroforético de los péptidos estudiados en función del pH es limitada porque el número de pares de datos experimentales de m_e-pH necesarios para una predicción de la migración precisa es relativamente elevado y aumenta con el número de grupos ionizables. Si se dispone de valores de pK_a exactos o de una estimación adecuada, como, por ejemplo, los valores de pK_a(R), una opción más rápida y menos laboriosa para predecir el comportamiento electroforético de los compuestos es el uso de los modelos semiempíricos clásicos que relacionan la m_e y la q/M_r^{α} (donde α es una constante que depende del modelo). En trabajos anteriores de nuestro grupo de investigación, estos modelos dieron lugar a excelentes correlaciones para hormonas peptídicas [275], péptidos opioides [279], apotioneínas [114], péptidos y glicopéptidos de digestos trípticos de glicoproteínas [123] y quinolonas [115] al disponer de buenas estimaciones de los valores de pK_a para el cálculo de la carga, utilizando la ecuación de Sillero y Ribeiro (**Ecuación 10**).

Una vez determinados los valores de pK_a de los fragmentos de los péptidos Aβ mediante CE-UV (**Tabla 6.3**), se estudiaron los modelos semiempíricos clásicos para estos compuestos. En la **Figura 6.2** se muestra, para los fragmentos de los péptidos Aβ en el intervalo de pH 2-12, la gráfica de m_e vs q/M_r^{α} para el modelo clásico de los polímeros ($\alpha = 1/2$), la ley de Stoke ($\alpha = 1/3$) y la Ley de Offord ($\alpha = 2/3$). En los tres casos, se observaban buenas correlaciones lineales (R^2 >0,97), lo que confirmaba la validez de los modelos semiempíricos clásicos en el intervalo de pH considerado y la exactitud de los pK_as determinados mediante CE-UV, que se emplearon para el cálculo de la carga. El modelo clásico de los polímeros (m_e vs $q/M_r^{1/2}$), mostraba una correlación ligeramente mejor ($R^2 \geq 0,978$). Este modelo también fue el modelo preferido en trabajos previos de nuestro grupo de investigación para explicar el comportamiento de la migración de hormonas peptídicas [275], péptidos opioides [279], apotioneínas [114] y glicopéptidos de digestos trípticos de eritropoyetina humana recombinante [123]. De la validez de la relación entre m_e y $q/M_r^{1/2}$ se deriva que el comportamiento electroforético de los compuestos de interés se puede predecir

directamente y sin realizar experimentos a partir de los valores de $q/M_r^{1/2}$ calculados. En la **Figura 6.3** se muestra la gráfica de $q/M_r^{1/2}$ vs pH en el intervalo de pH 2-12 para los fragmentos de los péptidos Aβ.

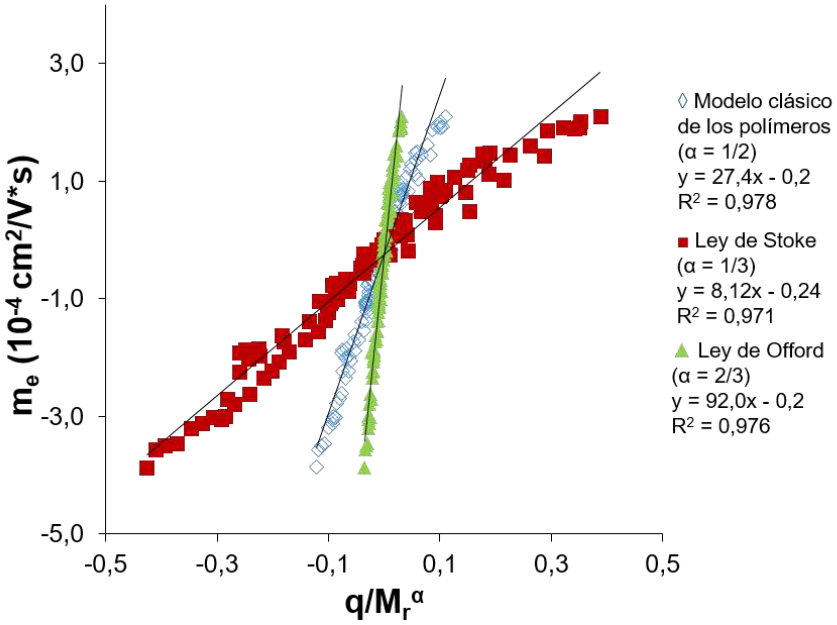

Figura 6.2. Correlación entre m_e y q/M_r^{α} para los fragmentos de los péptidos Aβ en el intervalo de pH 2-12. α = 1/2, 1/3 y 2/3 para el modelo clásico de los polímeros, la ley de Stoke y la ley de Offord, respectivamente. Los valores de q/M_r^{α} se calcularon a partir de los pK_as determinados por CE-UV, excepto para el grupo guanidino del residuo de arginina en el Aβ 1-15 (ver **Tabla 6.3**).

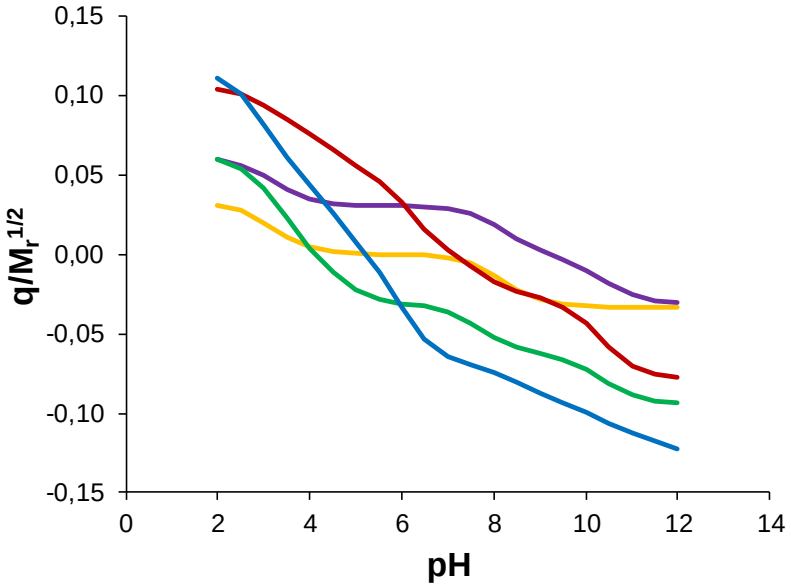

Figura 6.3. Valores de $q/M_r^{1/2}$ calculados a partir de los valores de pK_a determinados por CE-UV, en función del pH del BGE para los péptidos Aβ 1-15 (azul), 10-20 (rojo), 20-29 (verde), 25-35 (violeta) y 33-42 (naranja).

6.1.3. Optimización de la separación de los fragmentos de los péptidos Aβ

Una vez establecidos los modelos adecuados para explicar el comportamiento electroforético de los fragmentos de los péptidos Aβ, se evaluaron diferentes criterios de calidad para seleccionar el pH de separación óptimo de una mezcla de éstos. Los criterios de calidad para evaluar las separaciones en CE suelen emplear parámetros sencillos, basados en cocientes o diferencias entre los valores de m_e de los compuestos. La selectividad ($\alpha_{i,j}$) en CE se suele definir como el cociente de la m_e de dos compuestos que migran consecutivamente (**Ecuación 11**). Sin embargo, entre otras limitaciones, la $\alpha_{i,j}$ genera máximos sin sentido químico cuando el valor de m_e considerado en el denominador se aproxima a cero (carga neta cero, es decir, compuesto neutro o en el punto isoeléctrico). Este problema se soluciona considerando la diferencia de m_e entre los dos compuestos que migran consecutivamente, tal y como propusieron Jorgenson y Lukacs en su definición de selectividad ($S_{i,j}$), que además tiene en cuenta la influencia del flujo electrosmótico (EOF) (**Ecuación 12**) [101]. En el **Artículo 2.1**, se evaluó la separación de los fragmentos de los péptidos Aβ usando $S_{i,j}$. Considerando la m_e de cada compuesto a cada valor de pH ($m_e = 0$ para el EOF), se ordenaron los valores de m_e de forma decreciente y se calculó la diferencia entre cada par de compuestos que migraban consecutivamente, incluyendo el EOF, y la m_e promedio de cada par (m_{avg}). A partir de los valores de m_e ordenados, m_{avg} y una estimación de m_{EOF} para los capilares de sílice fundida [280], se calculó la $S_{i,j}(m_e)$ para cada par de picos consecutivos (los cinco fragmentos de los péptidos Aβ de la mezcla y el EOF). La selección del pH óptimo para la separación se llevó a cabo representando el valor mínimo de $S_{i,j}(m_e)$ ($S_{crítica}(m_e)$) en función del pH (**Figura 6.4**). A partir de esta representación fue fácil deducir que las mejores separaciones se obtenían a pH 3,0 en la región de pH ácido y a pH 10,5 en la región de pH básico. En la región de pH neutro se obtenían las peores separaciones ya que a esos valores de pH varios de los fragmentos de los péptidos Aβ no presentaban carga neta o tenía un valor muy pequeño, de manera que comigraban con el EOF.

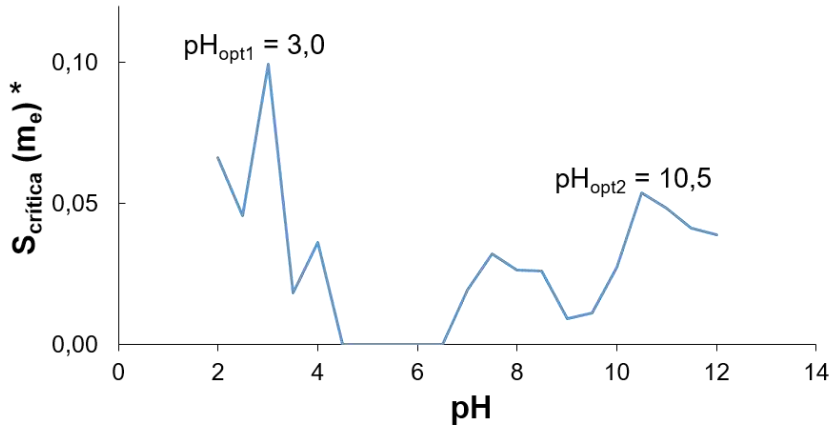

Figura 6.4. $S_{crítica}(m_e)$ obtenida a partir de los valores de m_e experimentales en función del pH del BGE para los picos que migran consecutivamente en una mezcla de los péptidos Aβ 1-15, 10-20, 20-29, 25-35 y 33-42 y considerando el EOF (m_e = 0). $* S_{i,j}(m_e) = \frac{m_{e,i} - m_{e,j}}{m_{avg} + m_{EOF}}$ ($m_{e,i} > m_{e,j}$; $S_{crítica} = S_{i,j}$ mínima)

De manera similar a como se ha explicado para la $S_{i,j}(m_e)$, se puede proceder para calcular la $S_{i,j}(q/M_r^{1/2})$, ya que ha quedado demostrada la relación entre m_e y $q/M_r^{1/2}$ (**Figura 6.2**):

$$S_{i,j}(q/M_r^{1/2}) = \frac{((q/M_r^{1/2})_i - (q/M_r^{1/2})_j)}{((q/M_r^{1/2})_{avg} + C*E)} \qquad ((q/M_r^{1/2})_i > (q/M_r^{1/2})_j) \qquad \textbf{Ec. 17}$$

En este caso, para el pico del EOF se consideró $q/M_r^{1/2} = 0$ y se reemplazó la m_{EOF} usada para calcular $S_{i,j}(m_e)$ por C*E, un parámetro con valores arbitrarios que considera la influencia del EOF sobre la separación a cada valor de pH. C toma valores entre 0 y 1 y tiene en cuenta el perfil relativo del EOF en capilares de sílice fundida en el intervalo de pH estudiado (**Figura 6.5-A**). C se calculó como la relación entre el valor de m_{EOF} al valor de pH considerado y el valor de m_{EOF} máximo, que corresponde a pH 12,0. Respecto a E, se trata de una constante utilizada para normalizar los valores de C, con el fin de evitar las diferencias de magnitud entre los valores de m_e y $q/M_r^{1/2}$. E se seleccionó arbitrariamente como 1,1 veces el valor más negativo de $q/M_r^{1/2}$ de todos los fragmentos de los péptidos Aβ considerados, de manera que el denominador de $S_{i,j}(q/M_r^{1/2})$ siempre presentaba un valor positivo, a fin de representar una separación electroforética donde todos los compuestos migraban hacia el detector. En la **Figura 6.5-B** se representa $S_{crítica}(q/M_r^{1/2})$ en función del pH. Como puede observarse, se llegaba a las mismas conclusiones que al considerar $S_{crítica}(m_e)$ (**Figura 6.4**) y las pequeñas diferencias en la forma de

los gráficos podían atribuirse a los pequeños desajustes entre m_e y $q/M_r^{1/2}$ o entre m_{EOF} y C*E. La gran ventaja que presentaba el uso de la $S_{crítica}(q/M_r^{1/2})$ es que se podía calcular sin requerir de datos experimentales si se disponía de valores de pK_a adecuados, teniendo en cuenta que C*E siempre se puede obtener a partir de los estudios de m_{EOF} en función del pH que se pueden encontrar en la bibliografía [280].

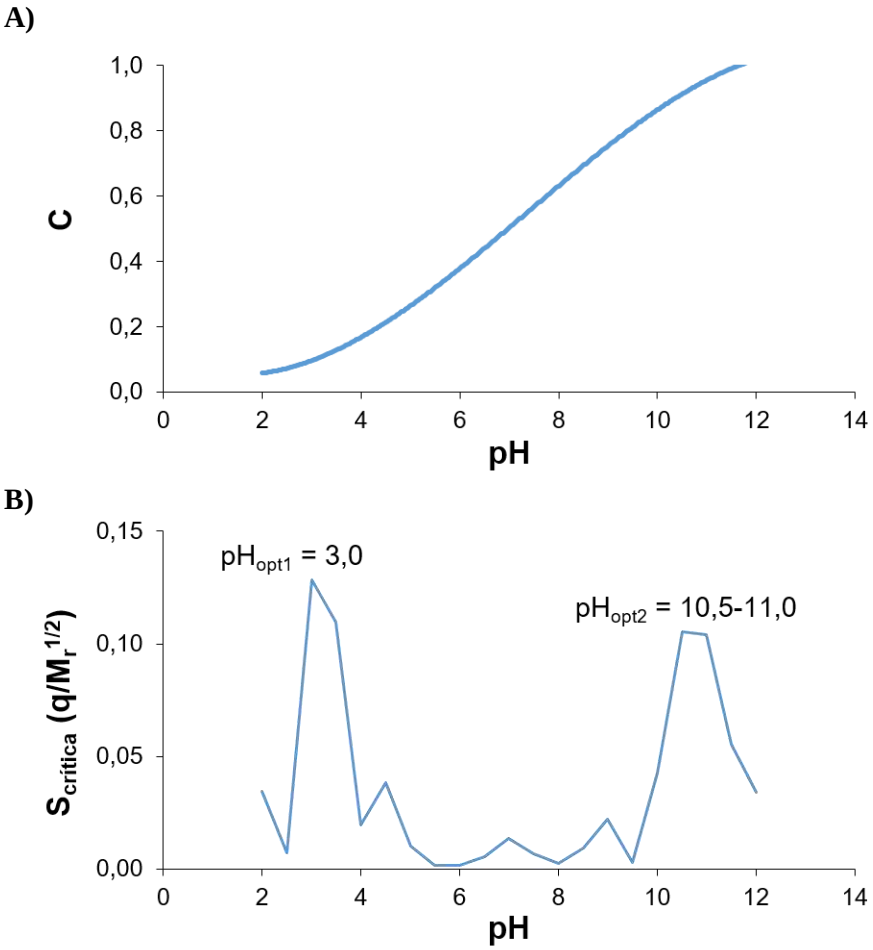

Figura 6.5. (A) Perfil relativo del EOF en función del pH para un capilar de sílice fundida. C se calculó como la relación entre el valor de m_{EOF} a cierto valor de pH y el valor de m_{EOF} máximo (pH 12,0). (B) $S_{crítica}(q/M_r^{1/2})$ obtenida a partir de los valores de $q/M_r^{1/2}$ calculados en función del pH del BGE para los picos que migran consecutivamente en una mezcla de los péptidos Aβ 1-15, 10-20, 20-29, 25-35 y 33-42 y considerando el EOF ($q/M_r^{1/2}$ = 0).

Una vez seleccionados los valores de pH del BGE para una separación óptima de los fragmentos de los péptidos Aβ, se simularon los electroferogramas de las separaciones a dichos valores de pH, tal y como se presenta en el **Artículo 2.1,** lo que permitió la evaluación rápida de

las separaciones sin hacer experimentos. Los electroferogramas se simularon de forma simple considerando, por un lado, que los valores de $q/M_r^{1/2}$ eran inversamente proporcionales al tiempo de migración (t_m). Por otro lado, que la separación disminuía a medida que aumentaba el EOF, que estaba relacionado con C*E, y que los compuestos cargados negativamente también migraban hacia el detector si la m_{EOF} era mayor que su m_e en valor absoluto. Para simplificar el procedimiento de simulación, se consideraron picos gaussianos y no se hicieron otras suposiciones con respecto a la forma del pico o la influencia de la composición del BGE en el t_m y la resolución. En la **Figura 6.6** se muestran los electroferogramas simulados y experimentales para la mezcla de fragmentos de los péptidos Aβ a los valores de pH de separación óptimos, 3,0 y 10,5. En ambos casos las simulaciones (**Figuras 6.6-A** y **-C**) fueron coherentes con los resultados experimentales (**Figuras 6.6-B** y **-D**). A pH 3,0 (**Figura 6.6-B**), todos los fragmentos de los péptidos Aβ estaban cargados positivamente y se separaban en menos de 15 minutos. Dado que a pH ácido la magnitud del EOF presenta un valor pequeño en capilares de sílice fundida, el EOF no se detectaba hasta los 40 minutos. A pH 10,5 (**Figura 6.6-D**), los cinco fragmentos de los péptidos Aβ estaban cargados negativamente, pero todos se detectaban en menos de 5 minutos a causa del efecto del EOF. Aún con estos tiempos de análisis tan cortos, la separación era adecuada y únicamente el péptido Aβ 25-35 comigraba ligeramente con el EOF.

La adecuada separación de los cinco fragmentos de los péptidos Aβ a los valores de pH del BGE seleccionados, confirmaba la aplicabilidad de $S_{i,j}(m_e)$ y $S_{i,j}(q/M_r^{1/2})$ para optimizar el pH de la separación. Sin embargo, en el procedimiento descrito en los párrafos anteriores se aprecia que la evaluación de las separaciones mediante el criterio de calidad $S_{i,j}$ era relativamente laboriosa. Además, únicamente se consideraba el par de picos que presentaba la peor separación a un determinado valor de pH, de manera que no se valoraba la separación de manera global. Por todas estas razones, se estudió como alternativa otro criterio de calidad, el parámetro $t'_{i,j}$ (**Artículo 2.2**). $t'_{i,j}$ ha sido propuesto recientemente como un criterio elemental perfeccionado para calificar y optimizar las separaciones en CE [126]. Este parámetro tiene en cuenta la separación relativa entre un par de compuestos, la separación de cada compuesto respecto al EOF y también los

cambios en el orden de migración (**Ecuación 13**). Además, se puede componer para mezclas complejas como una función global de optimización T' (**Ecuación 14**). Para simplificar la caracterización de la separación electroforética, en este caso no se considera el perfil del EOF. Hasta la fecha de la presente tesis, T' se había utilizado con éxito en unos pocos casos, como la optimización de la separación de mezclas complejas de alcaloides harmala en función del pH [126] y de mezclas racémicas de fármacos quirales en función de la concentración del selector quiral [281].

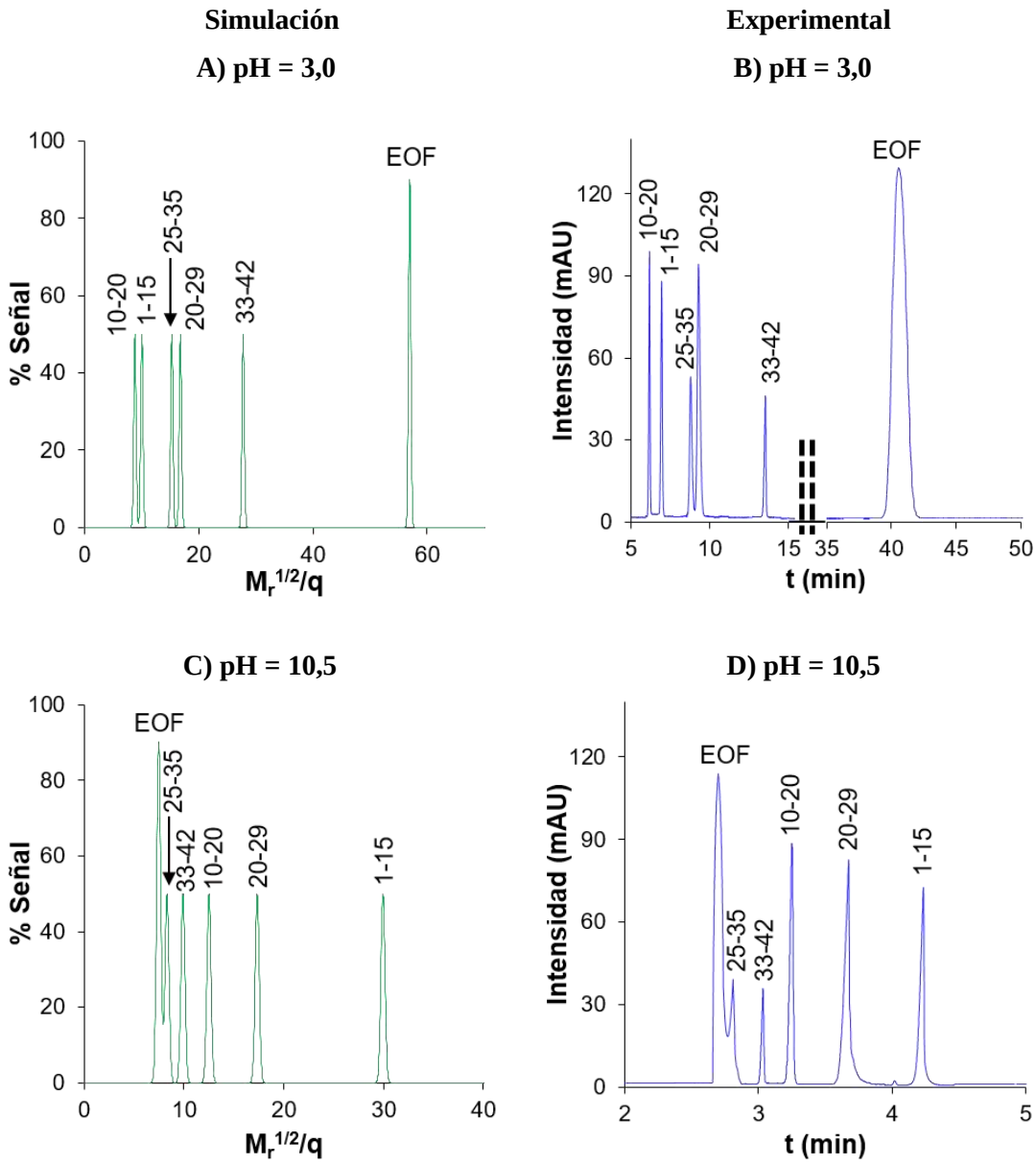

Figura 6.6. Electroferogramas simulados y experimentales para la separación de una mezcla de los péptidos Aβ 1-15, 10-20, 20-29, 25-35 y 33-42 mediante CE-UV a pH 3,0 (A y B) y 10,5 (C y D).

En el **Artículo 2.2**, se evaluó la separación de los fragmentos de los péptidos Aβ usando tanto T'(m_e) como T'($q/M_r^{1/2}$):

$$T'(q/M_r^{1/2}) = \left[\left(\prod_i^n \left(q/M_r^{1/2}\right)_i\right)\left(\prod_{(i,j)(j<i)}^{n,(n-1)} \Delta\left(q/M_r^{1/2}\right)_{(i,j)}\right)\right]^2 \qquad \textbf{Ec. 18}$$

En las **Figuras 6.7-A** y **-B** se representan T'(m_e) y T'($q/M_r^{1/2}$) en función del pH del BGE para la mezcla de los cinco fragmentos de los péptidos Aβ. Se obtenía un máximo a pH ácido (pH 3,0, en ambos casos) y otro a pH básico (pH 11,5 y 11,0, respectivamente). Estos valores de pH eran similares a los obtenidos empleando $S_{crítica}(m_e)$ y $S_{crítica}(q/M_r^{1/2})$ (**Figuras 6.4** y **6.5-B**), y las pequeñas diferencias en el valor de pH óptimo básico (11,5 y 11,0 vs 10,5) podían atribuirse a que T' considera la separación de todos los componentes de la mezcla entre sí y no únicamente la del par crítico. Respecto a la magnitud de los máximos, a diferencia de las representaciones $S_{crítica}$ vs pH, donde el máximo absoluto se encontraba en la región de pH ácido, en ambas representaciones de T' vs pH el máximo absoluto se encontraba en la región de pH básico. Para explicar esto, es necesario recordar que para que las predicciones sean más sencillas, T' no tiene en cuenta la influencia del EOF, que afecta negativamente a las separaciones, especialmente a pH básicos en capilares de sílice fundida. Por lo tanto, lo más recomendable al utilizar T' era considerar como posibles valores de pH óptimos para la separación tanto el máximo absoluto como los máximos relativos en el gráfico de T' vs pH. Tampoco debe olvidarse que, más allá de una separación electroforética óptima, no hay que subestimar otros factores experimentales importantes a considerar en la selección de las condiciones finales para los análisis. Por ejemplo, en el análisis de péptidos mediante CE usando capilares de sílice fundida, en general se suele preferir los BGEs ácidos para minimizar la adsorción de los péptidos en la pared interna del capilar [282,283]. Asimismo, para el análisis mediante CE-MS existe una mayor disponibilidad de BGEs volátiles ácidos, que son idóneos para obtener una sensibilidad adecuada en modo electrospray positivo (ESI+).

De los resultados obtenidos se desprendía la aplicabilidad de T' para la optimización del pH en la separación de la mezcla de fragmentos de los péptidos Aβ. Además de su simplicidad,

es importante destacar su versatilidad, pudiéndose usar como variable de cálculo la m_e u otras relacionadas, como la $q/M_r^{1/2}$. Como ya se ha indicado anteriormente, esta última es preferible ya que permite la optimización de la separación sin requerir de datos experimentales, si se dispone de valores de pK_a adecuados como, en este caso, los determinados por CE-UV para los fragmentos de los péptidos Aβ.

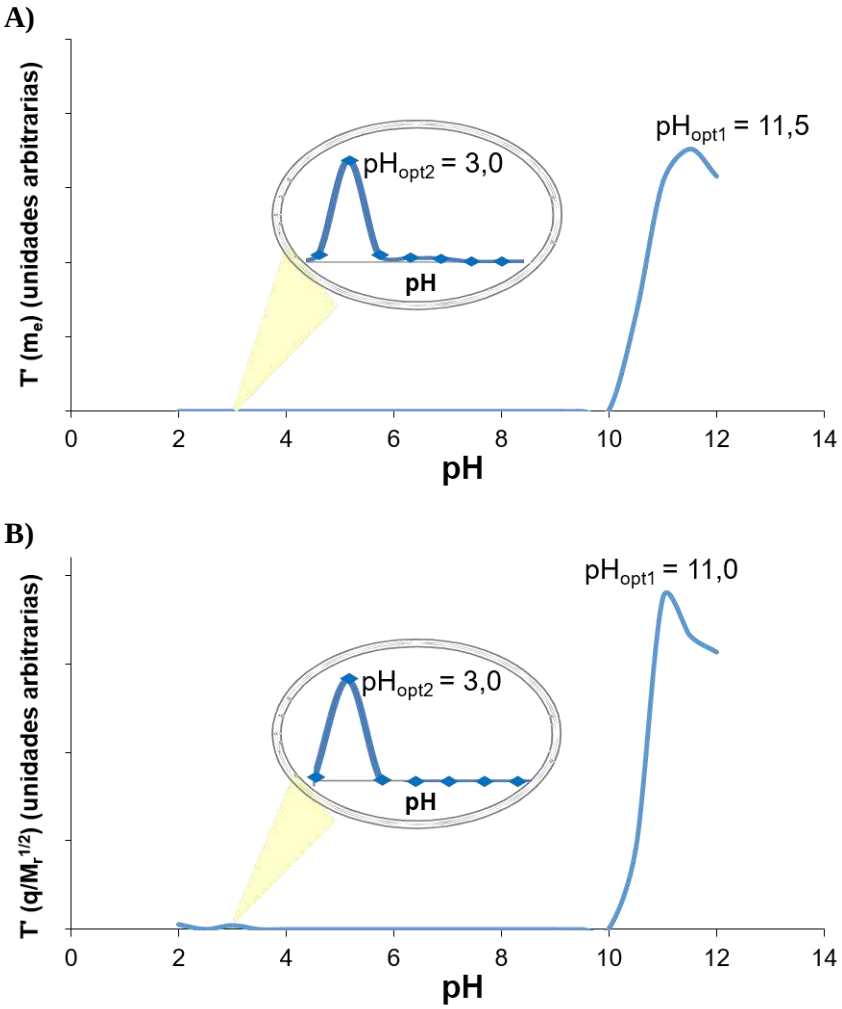

Figura 6.7. Representación de T' en función del pH del BGE para la separación de una mezcla de los péptidos Aβ 1-15, 10-20, 20-29, 25-35 y 33-42. T' calculada a partir de los valores de (A) m_e y (B) $q/M_r^{1/2}$.

6.1.4. Predicción de la migración electroforética de los péptidos Aβ y optimización de su separación

Los pK_as estimados de la **Tabla 6.4** se utilizaron para evaluar las separaciones de los péptidos Aβ 1-40 y 1-42. En la **Figura 6.8-A** se muestra el gráfico de $S_{crítica}(q/M_r^{1/2})$ vs pH para

la separación de los péptidos Aβ 1-40 y 1-42 en un capilar de sílice fundida (línea continua roja). Es importante destacar que en todo el intervalo de pH el valor de $S_{crítica}(q/M_r^{1/2})$ se correspondía con el de la separación de los dos péptidos, ya que ésta siempre era peor que la separación de ambos respecto al EOF.

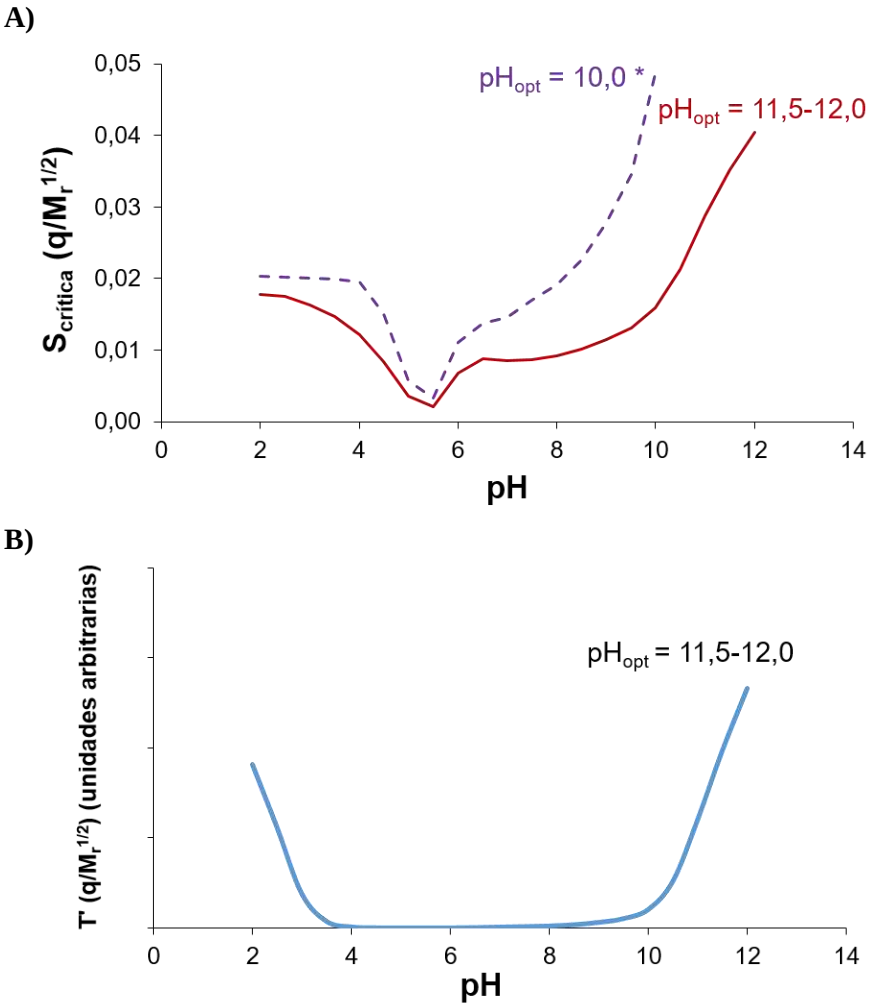

Figura 6.8. (A) $S_{crítica}(q/M_r^{1/2})$ y (B) $T'(q/M_r^{1/2})$ calculadas a partir de los valores de $q/M_r^{1/2}$ usando los pK_as estimados (**Tabla 6.4**) en función del pH del BGE para la separación de los péptidos Aβ 1-40 y 1-42 (capilar de sílice fundida, línea continua roja; capilar recubierto de alcohol de polivinilo, línea discontinua violeta). *Para preservar la estabilidad del recubrimiento no se consideraron valores de pH superiores a 10,0.

Si se comparaban los valores de $S_{crítica}(q/M_r^{1/2})$ para la separación de los péptidos Aβ 1-40 y 1-42 (escala del eje y) a los diferentes valores de pH con los del par con menor separación para la mezcla de fragmentos de los péptidos Aβ (**Figura 6.5-B**), se observaba que $S_{crítica}(q/M_r^{1/2})$ presentaba un valor mucho menor en el caso de los péptidos Aβ 1-40 y 1-42. Esto se debía a que

estos dos péptidos únicamente difieren en la presencia de dos aminoácidos que no contienen grupos ionizables en el péptido Aβ 1-42. Por lo tanto, ambos péptidos presentaban el mismo perfil de q vs pH y únicamente diferían ligeramente en el valor de M_r (**Tabla 6.4**). A partir del gráfico de la **Figura 6.8-A** era posible deducir que la mejor separación en el capilar de sílice fundida (línea continua roja) se obtenía a pH 11,5-12,0. La **Figura 6.8-B** muestra que se podía llegar a una conclusión similar a partir del gráfico de $T'(q/M_r^{1/2})$ vs pH, como ya se hizo en el caso de los fragmentos. En la **Figura 6.9-A** se muestra el electroferograma simulado para la separación de los péptidos Aβ 1-40 y 1-42 a pH 11,5 en un capilar de sílice fundida y en la **Figura 6.9-B** el electroferograma experimental. Los dos electroferogramas mostraban una gran concordancia, lo que indicaba que los valores de pK_a promedio (**Tabla 6.4**) eran una estimación adecuada para los pK_as de los péptidos Aβ 1-40 y 1-42. Como se esperaba a partir del gráfico de $S_{crítica}(q/M_r^{1/2})$ vs pH (**Figura 6.8-A**), la resolución entre ambos péptidos a este valor de pH era muy pequeña. Se intentó mejorar la separación mediante el uso de capilares de sílice fundida de diámetro interno (i.d.) más pequeño (50 µm y 30 µm i.d.), pero la resolución no mejoró. Como alternativa, se evaluó el uso de capilares recubiertos para disminuir el EOF, a la vez que se prevenían interacciones indeseadas analito-pared interna. Los recubrimientos no iónicos hidrófilos reducen significativamente el EOF, suprimen la adsorción de compuestos básicos en la pared capilar y, en algunos casos, pueden actuar como una fase pseudoestacionaria. Entre ellos, los capilares con recubrimientos permanentes de hidroxipropil celulosa (HPC) y alcohol de polivinilo (PVA) han demostrado tener buenas prestaciones en términos de estabilidad y reproducibilidad [284–287]. Para la separación de los péptidos Aβ 1-40 y 1-42 únicamente los capilares de PVA ofrecieron resultados destacables respecto a los capilares de sílice fundida. En la **Figura 6.8-A** se muestra como una línea discontinua violeta el valor de $S_{crítica}(q/M_r^{1/2})$ en función del pH para la separación de los péptidos Aβ 1-40 y 1-42 en un capilar de PVA. Para calcular $S_{crítica}(q/M_r^{1/2})$ se tuvo en cuenta la variación del EOF en el intervalo de pH estudiado en los capilares de PVA, que no es tan acusada como en los capilares de sílice fundida [288]. A diferencia de lo que se observa en la **Figura 6.8-A**, el efecto del recubrimiento en la separación no se refleja en el gráfico de $T'(q/M_r^{1/2})$ vs pH (**Figura 6.8-B)** porque T' no tiene en cuenta la influencia del EOF. En la **Figura 6.8-A** se

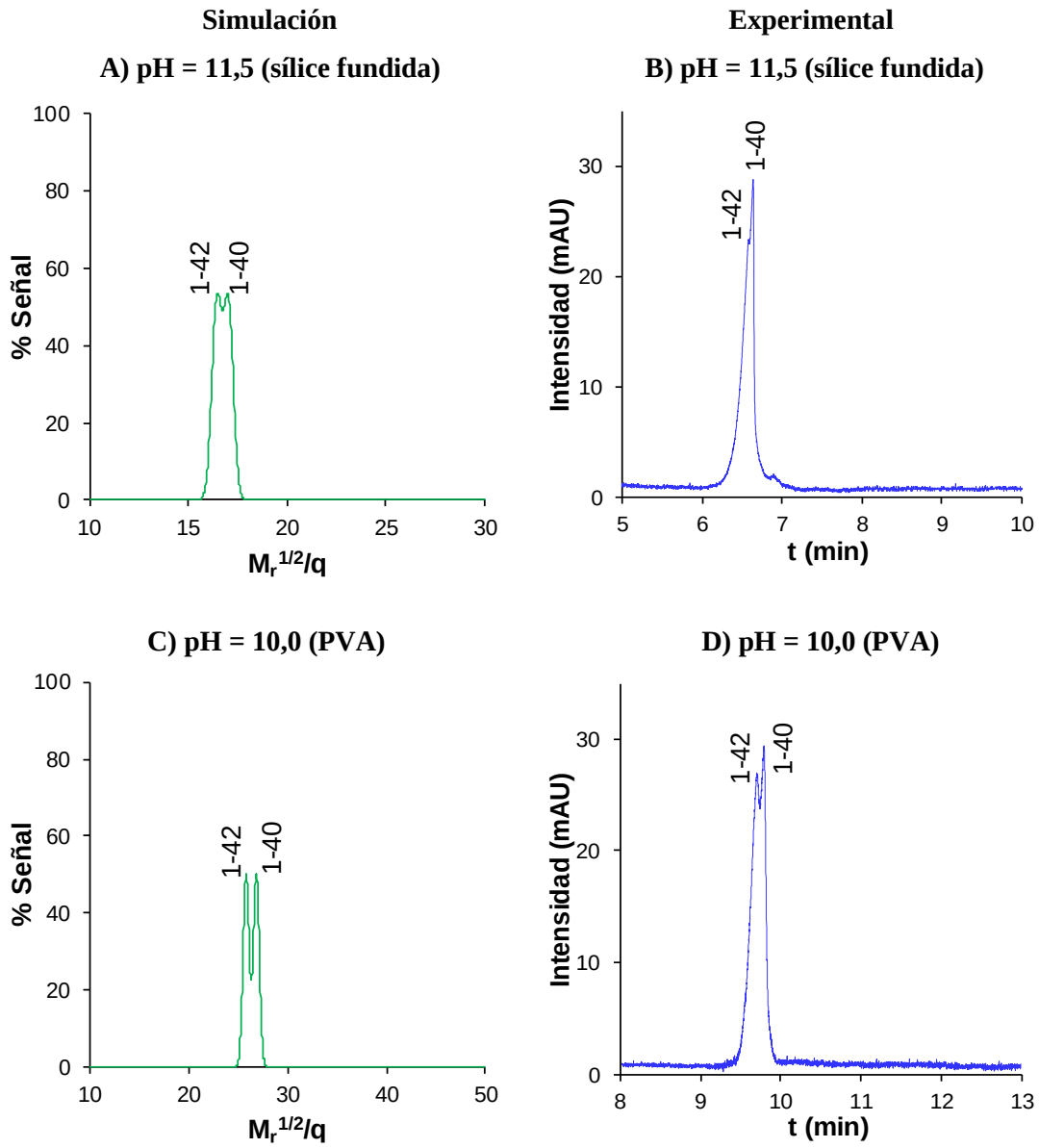

Figura 6.9. Electroferogramas simulados y experimentales de la separación de los péptidos Aβ 1-40 y 1-42 mediante CE-UV a pH 11,5 en un capilar de sílice fundida (A y B) y a pH 10,0 en un capilar recubierto de alcohol de polivinilo (C y D).

aprecia que la selectividad de la separación era ligeramente mayor en un capilar de PVA que en un capilar de sílice fundida, debido a la disminución del EOF en el capilar recubierto neutro. De nuevo el gráfico indicaba que la mejor separación se obtenía a valores de pH extremadamente básicos, pero se decidió llevar a cabo la separación a pH 10,0 para preservar la estabilidad del recubrimiento. Las **Figuras 6.9-C** y **–D** muestran de nuevo la gran concordancia entre los electroferogramas simulado y experimental, respectivamente, para la separación de los péptidos Aβ 1-40 y 1-42 a pH 10,0 en un capilar de PVA. Comparado con la separación en un capilar de

sílice fundida a pH 11,5 (**Figura 6.9-B**), el menor EOF en los capilares de PVA a pH 10,0 (una disminución de más del 40%) permitía una ligera mejora de la resolución a expensas de un ligero aumento en el tiempo de separación total. Para mejorar aún más estos resultados, sería necesario explorar mecanismos de separación complementarios basados en interacciones con una fase pseudoestacionaria o un agente complejante. La separación de compuestos con una elevada analogía estructural y M_r relativamente elevada como los péptidos Aβ 1-40 y 1-42, continúa siendo hoy en día uno de los grandes retos, no sólo de la CE, sino también de, en general, las técnicas de separación de alta resolución.

6.2. SPE-CE-MS unidireccional para la mejora de la sensibilidad y la selectividad

La CE-MS es una técnica muy adecuada para el análisis de biomoléculas cargadas. Sin embargo, al tratarse de una técnica de microescala, presenta como limitación importante su baja sensibilidad en términos de concentración para la mayoría de analitos a causa del pequeño volumen de inyección de muestra. La extracción en fase sólida en línea con la electroforesis capilar (SPE-CE) es una excelente estrategia para disminuir los LODs. En el **Artículo 3.1** se describen los diseños, configuraciones y materiales más relevantes que se han empleado en SPE-CE desde que fue descrita hace unos 30 años hasta nuestros días. En SPE-CE unidireccional, la configuración más habitual, se inserta cerca de la entrada del capilar de separación un preconcentrador o microcartucho de extracción, que contiene un sorbente adecuado para retener selectivamente los analitos de interés. De esta manera, es posible introducir grandes volúmenes de muestra y eluir los analitos retenidos en un volumen muy inferior de una solución adecuada, consiguiendo la purificación y preconcentración de los analitos de interés con una manipulación mínima. En muchos casos, se utilizan los sorbentes cromatográficos típicamente utilizados en SPE (por ejemplo, C8, C18, poliméricos con balance hidrofílico-lipofílico, etc.) cuyo principal inconveniente para el análisis de muestras complejas, como, por ejemplo, fluidos biológicos, puede ser su limitada selectividad. Este capítulo se centra en la investigación de sorbentes más selectivos, como los sorbentes de inmunoafinidad (IA), afinidad a aptámero (AA), afinidad a metal inmovilizado (IMA) y el carburo de silicio (SiC), para el análisis de proteínas intactas, péptidos y microARNs (miRNAs) mediante SPE-CE-MS unidireccional. De esta manera, se combina la selectividad del sorbente con la posibilidad de separar e identificar los analitos de forma fiable mediante CE-MS.

Los preconcentradores utilizados en esta tesis no se encuentran disponibles comercialmente, sino que se han preparado en el laboratorio. En función del tamaño de partícula del sorbente en comparación con el i.d. del capilar de separación (75 µm i.d., si no se indica lo contrario), se han construido preconcentradores sin fritas (*fritless*) o con fritas, que son estructuras

porosas que evitan la fuga de las partículas confinadas dentro del preconcentrador. En el **Artículo 3.2** (IA-SPE-CE-MS) y el **Artículo 3.3** (AA-SPE-CE-MS) se han preparado preconcentradores *fritless* con partículas magnéticas (MBs) de tamaño de partícula mayor que el i.d. del capilar de separación ($d_{partícula}$ > 75 µm). En el **Artículo 3.4** (IMA-SPE-CE-MS) se han empleado preconcentradores con dos fritas, una en cada extremo, empleando un sorbente con tamaño de partícula del orden de decenas de micrómetro (10 µm < $d_{partícula}$ < 75 µm). Finalmente, en el **Artículo 3.5** (SiC-SPE-CE-MS), debido al pequeño tamaño de partícula del sorbente de SiC, que es del orden de unidades de micrómetro (1 µm < $d_{partícula}$ < 10 µm), se han preparado preconcentradores con una sola frita de algodón en la salida del preconcentrador.

A modo de ejemplo, a continuación, se describe el procedimiento empleado en esta tesis para la construcción de preconcentradores con dos fritas (**Figura 6.10**). El cuerpo del preconcentrador consiste en un pequeño fragmento de capilar de sílice fundida (0,7 cm L_T x 250 µm i.d. x 365 µm o.d.). El i.d. del microcartucho es mayor que el del capilar de separación (72 cm L_T x 75 µm i.d. x 365 µm o.d.) para poder contener la mayor cantidad posible de sorbente. El proceso de construcción del microcartucho se supervisa a través de una lupa binocular:

- Se activa el capilar de separación (15 min de NaOH 1,0 M y 15 min de agua) donde se conectará en línea el microcartucho. De esta manera se evita la exposición del sorbente del microcartucho a las condiciones extremas de la disolución de NaOH.
- Se corta el capilar de separación en dos fragmentos: el fragmento del capilar de entrada mide 7,5 cm y el fragmento de salida 64,5 cm. El corte del capilar se realiza con un cortador de capilar específico para que sea lo más limpio posible y así minimizar los volúmenes muertos y pérdidas a través de las juntas.
- Se introduce una frita en el extremo de entrada del microcartucho (**Figura 6.10-A**).
- Se conecta el microcartucho al fragmento de entrada del capilar de separación con un tubo de Tygon™ de diámetro adecuado (**Figura 6.10-B**).
- Se aspiran las partículas de sorbente al interior del microcartucho mediante la aplicación de vacío (**Figura 6.10-B** y **-C**).

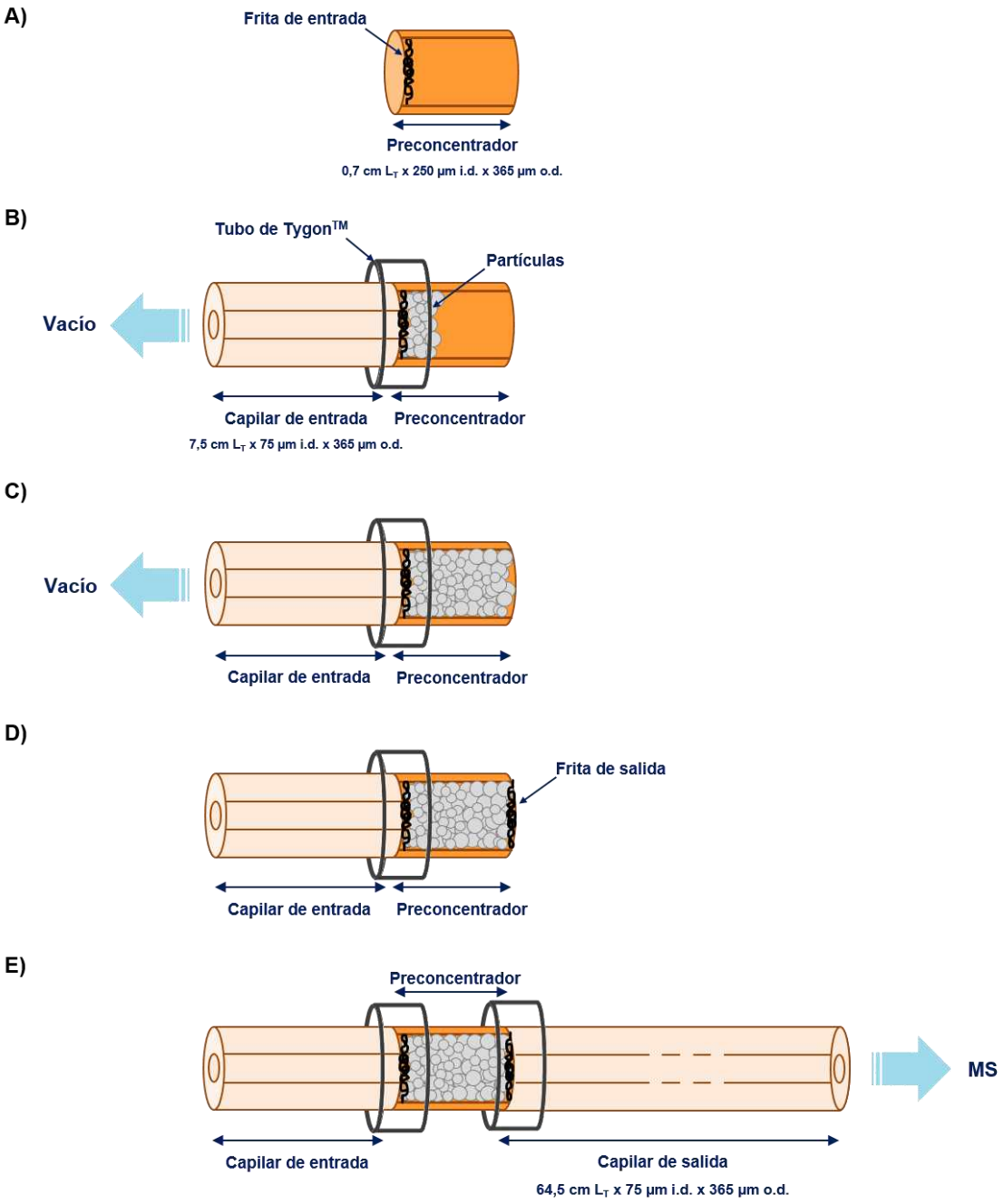

Figura 6.10. Proceso de construcción de un microcartucho con dos fritas para SPE-CE-MS unidireccional.

- Se introduce una frita en el extremo de salida del microcartucho (**Figura 6.10-D)**.
- Se conecta el microcartucho al fragmento de salida del capilar de separación mediante otro tubo de Tygon™ (**Figura 6.10-E**).
- Antes de comenzar los análisis se comprueba manualmente con una jeringa y agua que el microcartucho empaquetado no ofrece demasiada restricción al flujo. También se

comprueba mediante un experimento de CE que no existe inestabilidad en la corriente eléctrica.

El procedimiento de preparación de un preconcentrador *fritless* es similar, pero se omiten las operaciones que involucran a las fritas. Los preconcentradores con una sola frita en la salida del microcartucho se preparan insertando un pequeño trozo de algodón (aproximadamente 1 mm de longitud) en el tubo de Tygon™ que conecta el preconcentrador y el capilar de salida. En este caso, la frita se inserta dentro del conector a causa de la dificultad de introducir las fibras de algodón dentro del cuerpo del microcartucho. Dado que el algodón es hidrofílico, su presencia no causa inestabilidad en la corriente eléctrica durante las separaciones. Sin embargo, al generar una frita muy compacta sí que provoca bastante contrapresión, por eso es conveniente utilizar únicamente una frita en la salida del microcartucho.

A continuación, se discutirán las metodologías desarrolladas para mejorar la sensibilidad y la selectividad en el análisis de diferentes biomarcadores mediante SPE-CE-MS unidireccional. El desarrollo y optimización de estas metodologías analíticas constituye todo un desafío porque hay que compatibilizar los requerimientos de la extracción en línea, la separación electroforética y la detección por MS. Se han analizado proteínas intactas como la transtiretina (TTR) y la α-sinucleína (α-syn), digestos de proteínas y miRNAs.

6.2.1. Análisis dirigido de biomarcadores proteicos mediante IA-SPE-CE-MS. La transtiretina en la polineuropatía amiloidótica familiar tipo I

La IA-SPE-CE-MS cuenta con la gran selectividad de los sorbentes de inmunoafinidad como gran ventaja frente a otros modos de SPE-CE-MS [200–202,289]. Sin embargo, su utilización plantea también un gran reto debido a la dificultad para compatibilizar las condiciones necesarias para la immunoextracción, en relación con la estabilidad del sorbente y las recuperaciones del analito, y el uso de los BGEs necesarios para una separación eficaz por CE y una detección adecuada por MS. Por un lado, los BGEs con pH ácido o básico pueden provocar

la elución del anticuerpo (Ab) o su desnaturalización y, por otro lado, los BGEs deben tener el pH adecuado y ser lo suficientemente volátiles para conseguir la separación, maximizar la ionización de los analitos y evitar la acumulación de sales y la supresión de la ionización en la detección en línea con MS. Por estas razones, durante largo tiempo la IA-SPE-CE estuvo limitada a la detección UV y de fluorescencia [168,172,177,180,290,291] antes de que N.A. Guzman aplicara la IA-SPE-CE-MS al análisis de la hormona liberadora de gonadotropina (GnRH) en el año 2000 [181]. Desde entonces, nuestro grupo de investigación se ha mostrado muy activo en el desarrollo de métodos de IA-SPE-CE-MS, describiendo aplicaciones para péptidos y proteínas con Abs intactos o fragmentos de anticuerpo, usando diferentes diseños de microcartuchos y BGEs con sales de amonio volátiles y pH neutro combinados con eluyentes que contienen ácido fórmico (HFor), ácido acético (HAc) o hidróxido de amonio [201,202,289,292].

En los últimos años, ha aumentado la variedad de soportes disponibles que pueden ser adecuados para la preparación de sorbentes de inmunoafinidad para IA-SPE-CE-MS. En la actualidad, se comercializan muchos tipos de MBs, con diferentes grupos activos en la superficie que permiten inmovilizar una amplia diversidad de ligandos de afinidad [203,293]. La versatilidad, facilidad de uso y precio razonable de las MBs han provocado una rápida y amplia aplicación en SPE dispersiva, donde las MBs pueden sedimentarse y separarse fácilmente del sobrenadante mediante el uso de un imán o electroimán. Respecto a la SPE-CE, las MBs pueden utilizarse para preparar microcartuchos sin fritas. Rashkovetsky et al. [177] fueron los primeros en describir el uso de las MBs de inmunoafinidad (IA-MBs) para IA-SPE-CE. Posteriormente, diferentes investigadores han descrito metodologías de IA-SPE-CE usando IA-MBs y detección UV [178], de fluorescencia [294] y MALDI-MS [295]. Sin embargo, hasta la fecha de esta tesis, aún no se habían descrito metodologías de IA-SPE-CE-MS utilizando IA-MBs. Esto es probablemente debido, como ya se ha comentado, a la dificultad para compatibilizar las condiciones necesarias y a que, actualmente, muchas MBs comerciales no son porosas, lo que disminuye su área superficial activa y puede significar una limitación cuando la cantidad de sorbente es pequeña, como en IA-SPE-CE.

En el presente estudio (**Artículo 3.2**), se desarrolló un método de purificación de la TTR del suero basado en inmunoprecipitación (IP) *off-line* utilizando IA-MBs seguida por CE-MS para la detección e identificación de sus proteoformas, que están relacionadas con la polineuropatía amiloidótica familiar tipo I (FAP-I). Dado que este procedimiento *off-line* implicaba muchas etapas y tiempo, se evaluó como alternativa el análisis de la TTR sérica mediante IA-SPE-CE-MS.

6.2.1.1. Análisis de TTR en muestras de suero humano mediante inmunoprecipitación con partículas magnéticas y CE-MS

Los métodos tradicionalmente empleados para analizar las proteoformas de la TTR sérica requieren un pretratamiento *off-line* de la muestra antes de la separación e identificación por LC-MS [92,296–298]. En este estudio, se evaluó la IP *off-line* utilizando MBs con diferentes grupos funcionales y un Ab policlonal contra la TTR seguida de CE-MS para el análisis de las proteoformas de la TTR del suero, como alternativa a los métodos tradicionales. Se evaluaron MBs funcionalizadas con proteína A (Pro A) de tres proveedores diferentes. La Pro A (M_r~42000) es una proteína de superficie capaz de interaccionar con un Ab a través de su fragmento de región cristalizable (F_c) lo que permite una orientación óptima [205]. Sin embargo, como el Ab no está enlazado covalentemente a las MBs, las condiciones de elución en la IP *off-line* suelen ser lo suficientemente severas como para eluir el Ab junto con la proteína antigénica. Como alternativa a las ProA-MBs, también se investigaron MBs derivatizadas con grupos reactivos a grupos amino, lo que permite enlazar covalentemente el Ab, pero sin asegurar la orientación adecuada. La **Tabla 6.5** muestra las características de los cuatro tipos de MBs estudiadas, incluida la capacidad enlazante. Este parámetro está muy relacionado con el buen desempeño de las MBs. Para un mismo volumen de MBs, a mayor capacidad enlazante, mayor es la cantidad de Ab que retienen las MBs y, en consecuencia, mayor es la cantidad de antígeno que pueden purificar las IA-MBs.

Tabla 6.5. Características de las partículas magnéticas (MBs) estudiadas. Recuperaciones relativas en el análisis de la TTR del suero mediante IP *off-line* y CE-MS.

MBs	Enlace	Material del soporte	Tamaño de partícula (µm)	Capacidad enlazante (mg Ab/mL MB)	%R [a] (%RSD, n = 6)
Dynabeads® Protein A (DyPA)	No covalente (región F_c)	Sílice	2,8	0,24	16 (4,3)
Protein A Ultrarapid Agarose (UAPA)	No covalente (región F_c)	Agarosa	45-165	>3	100 (2,3)
SiMAG-Protein A (SiPA)	No covalente (región F_c)	Sílice	1	5	80 (5,0)
AffiAmino Ultrarapid Agarose (UAAF)	Covalente (grupos amino)	Agarosa	45-165	>0,5	52 (4,6)

a) La recuperación relativa (%R) se calculó considerando el valor del área del pico de la TTR-Cys (proteoforma más abundante) y comparando la MB en cuestión con las UAPA, que eran las que proporcionaban la mayor recuperación.

La TTR sérica se purificó mediante IP *off-line* usando un eluyente de glicina-HCl 50 mM (pH 2,8) y se analizó mediante CE-MS empleando un BGE de HAc 1,0 M (pH 2,3) y un líquido auxiliar coaxial (SL) de 60:40 (v/v) propan-2-ol:agua con 0,05% (v/v) de HFor para obtener una buena sensibilidad en ESI+. En la **Tabla 6.5** se muestran las recuperaciones relativas (%R) obtenidas con cada IA-MB respecto al valor más elevado, considerando el área del pico (A_p) de la proteoforma de la TTR más abundante (TTR-Cys). En todos los casos los resultados eran precisos (desviación estándar relativa porcentual (%RSD) (número de replicados (n) = 6) ≤5,0%). Las recuperaciones eran coherentes con los valores de capacidad enlazante especificados por los fabricantes. Los mejores valores de %R se obtenían con las UAPA (100%) y SiPA (80%), que presentaban la mayor capacidad enlazante (>3 y 5 mg Ab/mL MB, respectivamente). Las menores recuperaciones se obtenían con las DyPA (16%) y UAAF (52%), que presentaban la menor capacidad enlazante (0,24 y >0,5 mg Ab/mL MB, respectivamente). Por lo tanto, se concluyó que, como se preveía, el principal factor a considerar para obtener las mejores recuperaciones en IP *off-line* era la capacidad enlazante, que tiene en cuenta la densidad de los grupos funcionales para enlazar Ab en la superficie de las MBs. En la **Figura 6.11-A** se muestran el electroferograma de iones totales (TIE) (i) y los espectros de masas (ii) de la IP *off-line* usando las MBs UAPA y CE-MS. Como puede apreciarse, se detectaba el Ab juntamente con la TTR, lo que indicaba que el Ab se desorbía durante la elución en la IP *off-line*. Este fenómeno sucedía con todas las ProA-MBs lo que disminuía posteriormente su aplicabilidad en IA-SPE-CE-MS. En cambio, el Ab no se detectaba empleando las MBs UAAF, porque la unión con el Ab era de carácter covalente. En la **Figura 6.11-B** se muestran el TIE (i), el espectro de masas (ii) y el espectro de masas deconvolucionado (iii) tras el tratamiento de IP *off-line* usando las MBs UAAF y CE-MS. Como se aprecia en el TIE y los espectros de masas, únicamente se detectaba la TTR monomérica (MO) y las proteoformas en un suero control coincidían con las descritas por otros autores [92,297,299,300].

A) Protein A Ultrarapid Agarose (UAPA)

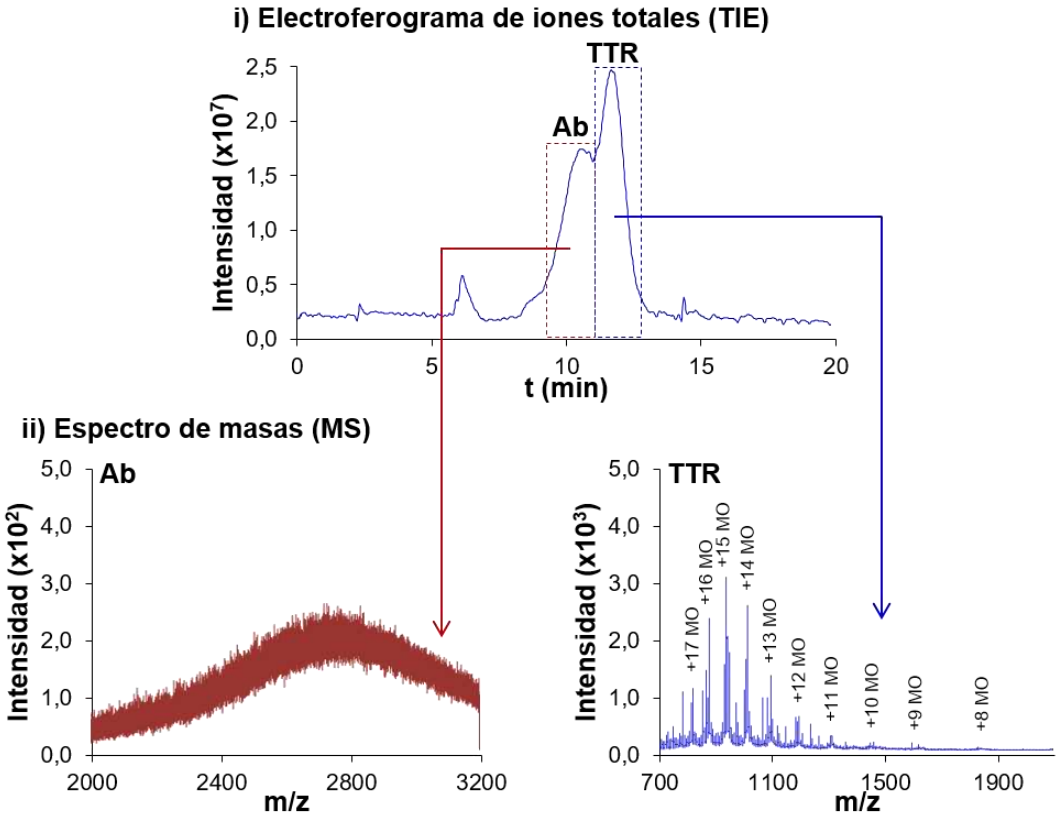

B) AffiAmino Ultrarapid Agarose (UAAF)

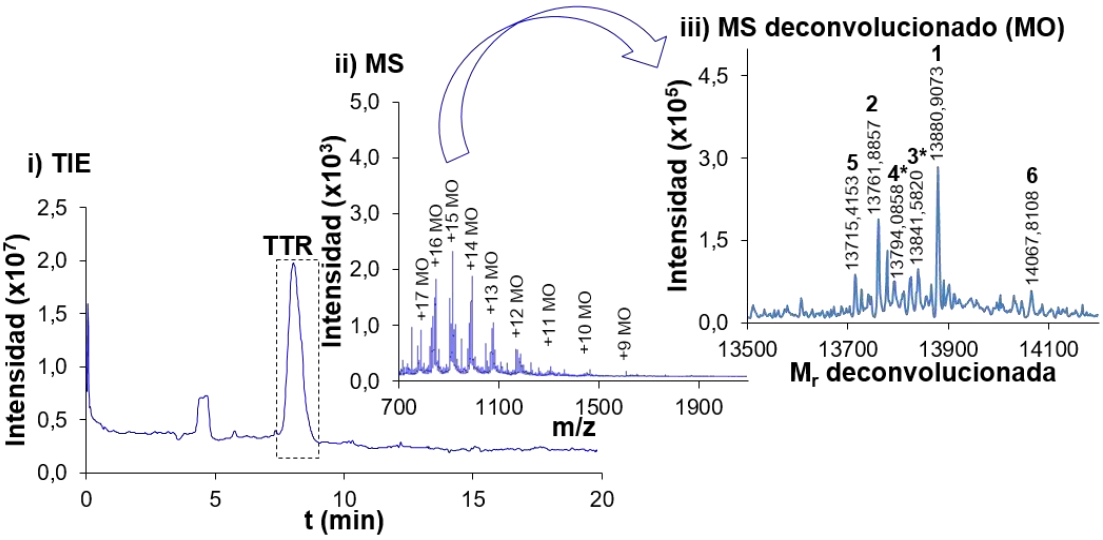

Figura 6.11. CE-MS (BGE 1,0 M HAc (pH 2,3) y SL 60:40 (v/v) propan-2-ol:agua 0,05% (v/v) de HFor) después de la IP *off-line* para una muestra de suero de control sano empleando las MBs (A) UAPA y (B) UAAF. (i) TIE, (ii) MS y (iii) MS deconvolucionado. Las proteoformas del MO corresponden a (1): TTR-Cys, (2): TTR-Libre, (3*): TTR-Fosforilada o TTR-Sulfonada, (4*): TTR-Dihidroxilada o TTR-Sulfínico, (5): (10) C-G, (6): TTR-Glutatión. *La exactitud de masa y la resolución del espectrómetro de masas no fueron suficientes para diferenciar entre estas proteoformas, que presentan la misma M_r o muy similar (ver la **Tabla 6.6**).

En la **Tabla 6.6** se muestran las proteoformas de la TTR MO detectadas con las MBs UAAF, su M_r y abundancia relativa (%A) respecto a la proteoforma más abundante, es decir, la TTR-Cys. Se detectaron hasta seis proteoformas de la TTR MO, en orden decreciente de %A: TTR-Cys, TTR-Libre, TTR-Fosforilada o TTR-Sulfonada, TTR-Dihidroxilada o TTR-Sulfínico, (10) C-G y TTR-Glutatión. La exactitud de masa no era suficiente para diferenciar entre las proteoformas que se indican emparejadas y tampoco se separaban por CE. Para diferenciarlas, sería necesario realizar experimentos de MS/MS utilizando espectrómetros de masas de elevada exactitud y resolución. Por otra parte, destacar que se consiguió detectar la TTR-Glutatión, una proteoforma que se encuentra a baja concentración, por debajo del LOD de otro método desarrollado previamente por nuestro grupo de investigación, basado en el uso de la IP *off-line* convencional (Ab en disolución) y CE-MS [300]. Para todas las proteoformas, la repetibilidad era adecuada (%RSD (n = 3) $\leq$5,7%), así como la exactitud de la masa (error relativo (E_r) <90 ppm).

Aunque se obtuvieron buenos resultados mediante la IP *off-line* empleando MBs seguida por CE-MS, este procedimiento resulta relativamente largo, laborioso, no se puede automatizar y su coste económico es elevado, considerando la cantidad de IA-MBs consumidas en cada análisis y que no se pueden reutilizar. Como alternativa para resolver estos problemas, se investigó la IA-SPE-CE-MS.

Tabla 6.6. M_r y abundancia relativa de las proteoformas de la TTR detectadas en muestras de suero de controles sanos mediante IP *off-line* con UAAF MBs y CE-MS (BGE 1,0 M HAc (pH 2,3) y SL 60:40 (v/v) propan-2-ol:agua 0,05% (v/v) de HFor).

N	Proteoformas monoméricas de la TTR detectadas	M_r teórica	M_r experimental	E_r [a] (ppm)	%A [b] (%RSD, n = 3)
1.	**TTR-Cys**	13880,4022	13880,9073	36	100 (3,4)
2.	**TTR-Libre**	13761,2640	13761,8857	45	64 (2,0)
3*.	**TTR-Fosforilada**	13841,2439	13841,5820	24	40 (4,0)
	o TTR-Sulfonada	13841,3283		18	
4*.	**TTR-Dihidroxilada o TTR-Sulfínico**	13793,2628	13794,0858	60	33 (5,7)
5.	**(10) C-G**	13715,1713	13715,4153	18	33 (4,8)
6.	**TTR-Glutatión**	14066,5732	14067,8108	88	21 (4,7)

a) El error relativo (E_r) se calculó en ppm como: $|M_r \text{ experimental} - M_r \text{ teórica}| / M_r \text{ teórica} * 10^6$.

b) La abundancia relativa (%A) se calculó normalizando el valor del área respecto a la proteoforma más abundante.

* La exactitud de masa y la resolución del espectrómetro de masas no fueron suficientes para diferenciar entre estas proteoformas, que presentan la misma M_r o muy similar.

6.2.1.2. Análisis de patrones de TTR por IA-SPE-CE-MS

El desarrollo de una metodología de IA-SPE-CE-MS no es sencillo, como ya se ha apuntado anteriormente, y, en este caso, lo primero que se tuvo que hacer fue prescindir del BGE ácido que se había utilizado en CE-MS tras la IP *off-line*. El BGE ácido provocaba la elución de la TTR durante los lavados del capilar y probablemente también la del Ab o su desnaturalización, ya que las IA-MBs perdían la capacidad de retener a la TTR. Por esta razón, se decidió utilizar un BGE de acetato de amonio (NH_4Ac) a pH neutro que había dado buenos resultados en anteriores estudios del grupo de investigación con otros biomarcadores proteicos por IA-SPE-CE-MS [200–202]. El uso de un BGE NH_4Ac 10 mM (pH 7,0) en combinación con un SL de 60:40 (v/v) propan-2-ol:agua con 0,25% (v/v) de HFor permitía detectar mediante CE-MS las mismas proteoformas de la TTR detectadas en el análisis de patrones con el BGE ácido, aunque los LODs eran ligeramente superiores (25 µg/mL vs 10 µg/mL para la TTR-Cys). En la **Figura 6.12** se muestran el electroferograma de iones extraídos (EIE) (i), el espectro de masas (ii) y el espectro de masas deconvolucionado (iii) para el análisis de un patrón de TTR de 1000 µg/mL mediante CE-MS empleando el BGE NH_4Ac 10 mM (pH 7,0). En estas condiciones, en el espectro de masas se detectó principalmente la TTR MO, pero, a diferencia del uso del BGE ácido, también se apreciaba a baja intensidad la TTR dimérica (DI). En el espectro de masas deconvolucionado se detectaron siete proteoformas de la TTR MO (**Tabla 6.7**).

Para el desarrollo de la metodología IA-SPE-CE-MS se evaluaron las MBs UAPA, que eran las que habían permitido las mayores recuperaciones de la TTR en el caso de la IP *off-line*, y las UAAF, en las que el Ab se enlaza covalentemente. El material de soporte de ambas MBs era agarosa y el tamaño de las micropartículas ($d_{partícula}$ >75 µm, **Tabla 6.5**) permitió la preparación de preconcentradores *fritless*. Durante el proceso de optimización, se observó que al introducir la TTR patrón disuelta en agua o en el BGE neutro, cuya fuerza iónica es limitada, no se detectaba la proteína durante los análisis. Se vio que para retener la TTR durante la etapa de carga, la proteína tenía que estar disuelta en tampón fosfato salino (PBS). El PBS es una disolución con una osmolaridad y concentración de iones similares a los fluidos corporales humanos y probablemente favorecía la interacción entre la TTR y el Ab.

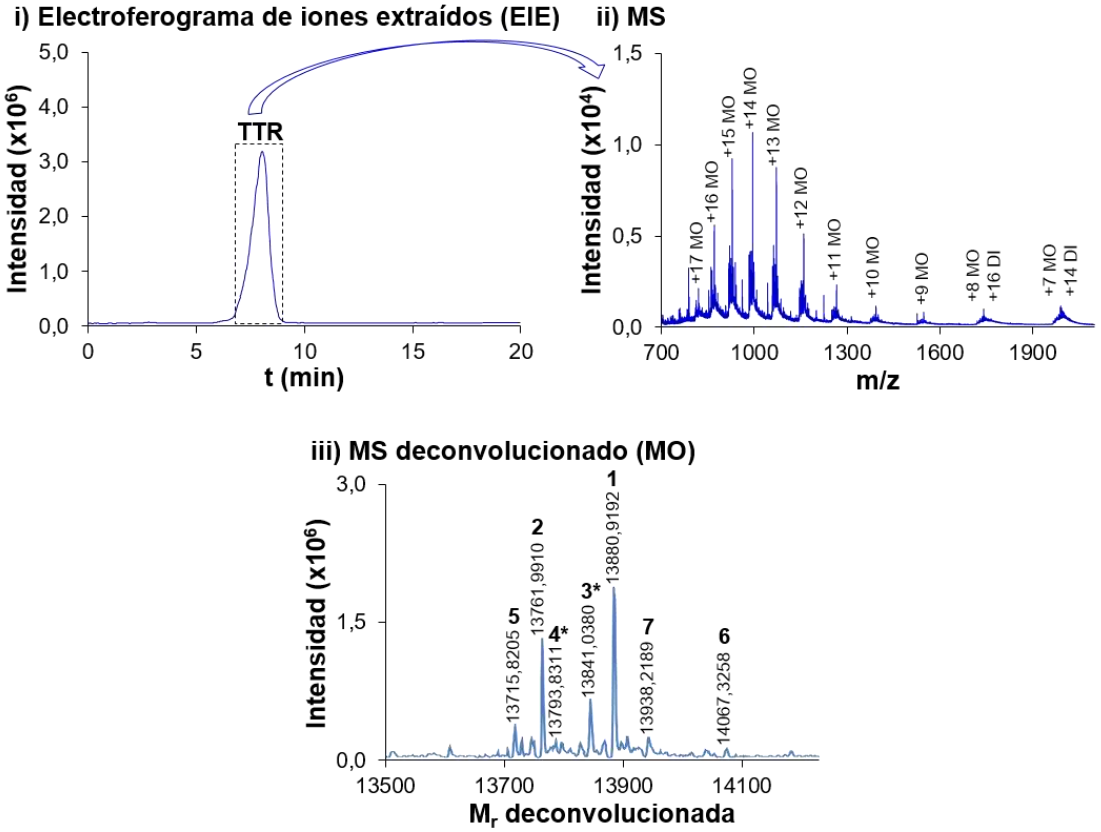

Figura 6.12. CE-MS (BGE NH_4Ac 10 mM (pH 7,0) y SL 60:40 (v/v) propan-2-ol:agua 0,25% (v/v) de HFor) para un patrón de TTR de 1000 µg/mL. (i) Electroferograma de iones extraídos (EIE), (ii) espectro de masas y (iii) espectro de masas deconvolucionado. Los números relativos a las proteoformas del monómero (MO) se describen en la **Tabla 6.7**. (DI: dímero).

Con respecto al sorbente empleado, las MBs UAPA se descartaron después de realizar varias pruebas con dos eluyentes ácidos (HAc 50 mM:HFor 50 mM (pH 2,3) y HAc 100 mM (pH 2,9)) y uno básico (NH_4OH 100 mM (pH 11,2)). En los tres casos, se detectó TTR, pero la repetibilidad era pobre y la cantidad de TTR detectada disminuía entre inyecciones consecutivas debido a la elución gradual del Ab. Se hizo un intento para estabilizar la unión del Ab con la Pro A (*crosslinking* con bisulfosuccinimidilsuberato, BS3). Sin embargo, no pudo detectarse la TTR empleando el sorbente modificado, probablemente porque este procedimiento inactivaba el Ab. Para las MBs UAAF, se obtuvieron resultados adecuados sólo con el eluyente básico, que permitía preconcentrar y detectar la TTR sin eluir el Ab y reutilizar el preconcentrador. En cambio, con los eluyentes ácidos no se detectó la TTR ni el Ab y el sorbente se dañaba irreversiblemente.

Tabla 6.7. M_r y abundancia relativa de las proteoformas detectadas en patrones de TTR de 1000 µg/mL por CE-MS y de 25 µg/mL por IA-SPE-CE-MS.

N	Proteoformas monoméricas de la TTR detectadas	M_r teórica	A) CE-MS			B) IA-SPE-CE-MS		
			M_r experimental	E_r [a] (ppm)	%A [b] (%RSD, n = 3)	M_r experimental	E_r [a] (ppm)	%A [b] (%RSD, n = 3)
1.	**TTR-Cys**	13880,4022	13880,9192	37	100 (1,6)	13881,0508	25	100 (4,3)
2.	**TTR-Libre**	13761,2640	13761,9910	53	41 (0,5)	13761,7772	37	62 (0,9)
3*.	**TTR-Fosforilada**	13841,2439	13841,0380	15	35 (3,0)	13841,0479	14	60 (2,6)
	o TTR-Sulfonada	13841,3283		21			20	
4*.	**TTR-Dihidroxilada o TTR-Sulfínico**	13793,2628	13793,8311	41	37 (2,9)	13793,6805	30	53 (1,9)
5.	**(10) C-G**	13715,1713	13715,8205	47	35 (5,9)	13715,5892	30	62 (4,0)
6.	**TTR-Glutatión**	14066,5732	14067,3258	54	20 (5,4)	14067,2015	45	35 (1,7)
7.	**TTR-CysGly**	13937,4541	13938,2189	55	32 (4,9)	13937,7082	18	48 (2,2)
8.	**TTR-CysGlu**	14009,5177	No detectada	-	-	14009,3011	15	27 (5,3)

a) El error relativo (E_r) se calculó en ppm como: $|M_r \text{ experimental} - M_r \text{ teórica}| / M_r \text{ teórica} * 10^6$.

b) La abundancia relativa (%A) se calculó normalizando el valor del área respecto a la proteoforma más abundante.

* La exactitud de masa y la resolución del espectrómetro de masas no fueron suficientes para diferenciar entre estas proteoformas, que presentan la misma M_r o muy similar.

Empleando el eluyente básico y las MBs UAAF, se evaluó el efecto del tiempo de introducción de muestra (5, 10 y 15 min) a 930 mbar con una disolución de TTR de 10 µg/mL (**Figura 6.13**). Como se puede observar, para tiempos de carga de hasta 10 minutos, la cantidad de proteína detectada aumentaba con el tiempo de carga al incrementarse el volumen de muestra cargada. Sin embargo, para un tiempo de carga mayor que 10 minutos, se excedía el volumen de ruptura y la cantidad de proteína detectada disminuía con el tiempo de carga. Por lo tanto, para reducir el tiempo total de análisis y obtener las mejores recuperaciones de la TTR, se seleccionó un tiempo de carga de 10 minutos.

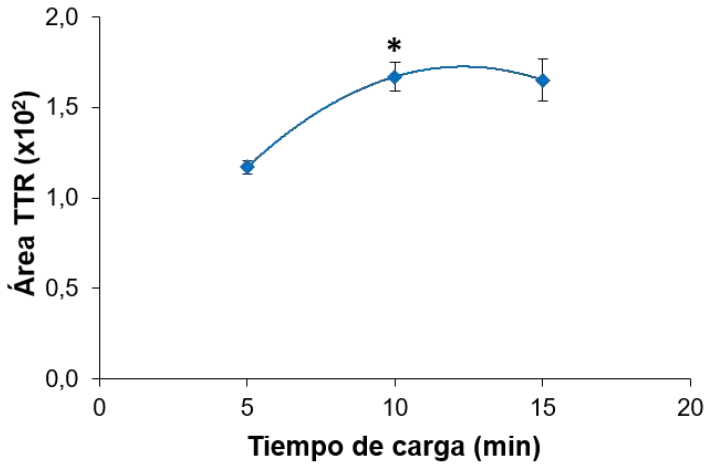

Figura 6.13. Estudio del efecto del tiempo de introducción de muestra (5, 10 y 15 min) a 930 mbar en IA-SPE-CE-MS (patrón de TTR de 10 µg/mL). Las barras de error indican la desviación estándar (n = 3). Las condiciones optimizadas se indican con un asterisco.

En la **Figura 6.14** se muestra el análisis de un patrón de TTR de 25 µg/mL por IA-SPE-CE-MS en las condiciones optimizadas y en la **Tabla 6.7-B** se indican las ocho proteoformas detectadas. Comparado con el análisis de un patrón de TTR de 1000 µg/mL por CE-MS (**Figura 6.12** y **Tabla 6.7-A**), el número de proteoformas detectadas, la exactitud de masa y la repetibilidad eran similares. En IA-SPE-CE-MS, el incremento en la proporción de las diferentes proteoformas de la TTR respecto a la TTR-Cys podría estar relacionado con una menor recuperación de la TTR-Cys en comparación con el resto de proteoformas.

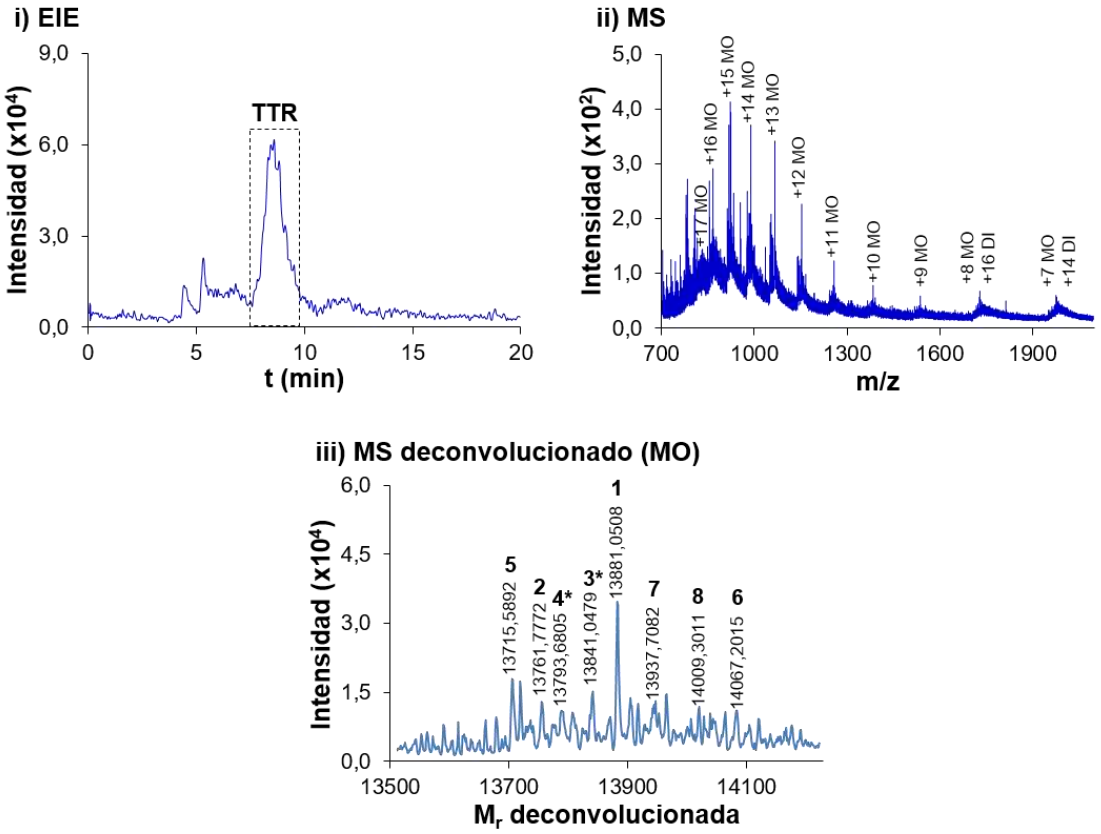

Figura 6.14. IA-SPE-CE-MS para un patrón de TTR de 25 µg/mL. (i) EIE, (ii) espectro de masas y (iii) espectro de masas deconvolucionado. Los números relativos a las proteoformas del MO se describen en la **Tabla 6.7**.

Para finalizar con el establecimiento del método de IA-SPE-CE-MS con los patrones, se calcularon sus parámetros de calidad. El método presentaba buena repetibilidad (%RSD (n = 3) en t_m y A_p de 2,9% y 4,3%, respectivamente, para la TTR-Cys con un patrón de TTR de 25 µg/mL), era lineal entre 5 y 25 µg/mL (R^2 >0,99) y los LODs eran de aproximadamente 1 µg/mL (25 veces menos que en CE-MS). Además, los microcartuchos podían emplearse durante más de 20 análisis a lo largo del mismo día hasta que se deterioraba el sorbente y era necesario sustituir el preconcentrador.

6.2.1.3. Análisis de TTR en muestras de suero humano por IA-SPE-CE-MS

Una vez optimizada y validada la metodología analítica con patrones, se procedió a analizar la TTR en muestras de suero de controles sanos y de un paciente sintomático de FAP-I. El análisis directo de las muestras de suero por IA-SPE-CE-MS no fue posible, principalmente debido a la saturación del sorbente por la retención no específica de otras proteínas mayoritarias del suero, como, por ejemplo, albúmina, y a su precipitación en el capilar de separación, lo que provocaba inestabilidad en la corriente y la obturación del capilar. Por este motivo se investigaron diferentes pretratamientos de las muestras de suero. No resultaron adecuados ni la filtración del suero con filtros de jeringa de tamaño de poro de 0,22 µm, ni la dilución entre 2 y 10 veces con agua o PBS. Tampoco funcionó la precipitación de las proteínas mayoritarias con acetonitrilo (ACN), pretratamiento que se había empleado en estudios anteriores del grupo de investigación para el análisis de péptidos en plasma por SPE-CE-MS e IA-SPE-CE-MS [201,202,301]. Finalmente, se adaptó un método sencillo basado en el uso de 5% (v/v) de fenol para precipitar proteínas mayoritarias del suero, descrito con anterioridad para purificar la TTR [302,303], y que proporcionó recuperaciones cercanas al 90%. En la **Figura 6.15** se muestran los EIEs (i) y espectros de masas deconvolucionados (ii) de las muestras de suero pretratadas y analizadas por IA-SPE-CE-MS. Como se puede observar en los EIEs, el t_m de la TTR en el análisis de muestras de suero se incrementó en comparación con los patrones (**Figura 6.14-i**). Este hecho se relacionó con la modificación de la pared interna del capilar de separación inducida durante la carga de la muestra que, aunque pretratada, seguía presentando una matriz compleja. Esta modificación resultó ser permanente ya que el t_m de la TTR se mantenía constante al analizar patrones tras el análisis de una muestra de suero. La repetibilidad de los análisis de las muestras de suero era adecuada (para la TTR-Cys, %RSD (n = 3) en t_m y A_p de 4,7% y 3,2%). No obstante, a causa de la complejidad de la matriz de la muestra, la durabilidad de los preconcentradores se reducía a unos 10 análisis.

En muestras de suero de controles sanos se detectaron cinco proteoformas de la TTR (**Figura 6.15-A** y **Tabla 6.8-A**), que coincidían con las cinco proteoformas más abundantes detectadas por IP *off-line* y CE-MS (**Figura 6.11** y **Tabla 6.6**). Estos resultados demuestran la

validez de la metodología de análisis de la TTR sérica mediante IA-SPE-CE-MS. En la muestra del paciente de FAP-I se detectaron estas mismas cinco proteoformas normales y, además, la proteoforma mutante más abundante, la TTR(Met30)-Cys (proteoforma 9, **Figura 6.15-B** y **Tabla 6.8-B**). Ésta era la única proteoforma mutante que podía detectarse inequívocamente y que permitía la confirmación de la FAP-I, ya que la exactitud de masa no era suficiente para diferenciar la TTR(Met30)-Libre de la TTR-Dihidroxilada o la TTR-Sulfínico (proteoforma 4*).

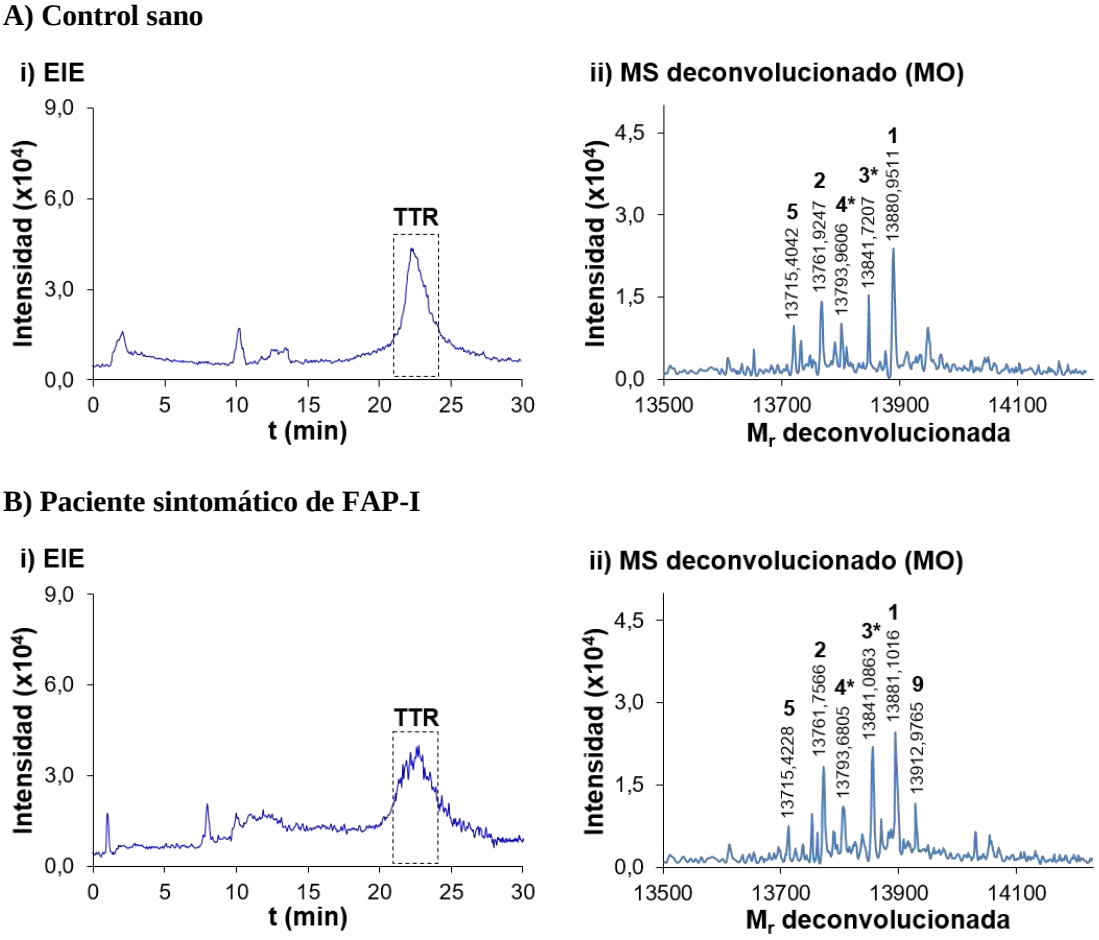

Figura 6.15. IA-SPE-CE-MS para muestras de suero humano pretratadas (A) control sano y (B) paciente sintomático de FAP-I. (i) EIE y (ii) espectro de masas deconvolucionado. Los números relativos a las proteoformas del MO se describen en la **Tabla 6.8**.

Tabla 6.8. M_r y abundancia relativa de las proteoformas de la TTR detectadas por IA-SPE-CE-MS en muestras de suero pretratado.

N	Proteoformas monoméricas de la TTR detectadas	M_r teórica	A) Control sano			B) Paciente sintomático de FAP-I		
			M_r experimental	E_r [a] (ppm)	%A [b] (%RSD, n = 3)	M_r experimental	E_r [a] (ppm)	%A [b] (%RSD, n = 3)
1.	**TTR-Cys**	13880,4022	13880,9511	40	100 (3,2)	13881,1016	50	100 (4,0)
2.	**TTR-Libre**	13761,2640	13762,9247	48	64 (2,5)	13761,7566	36	61 (3,2)
3*.	**TTR-Fosforilada**	13841,2439	13841,7207	34	69 (1,3)	13841,0863	11	67 (2,8)
	o TTR-Sulfonada	13841,3283		28			17	
4*.	**TTR(Met30)-Libre**	13793,3301	No detectada inequívocamente	-	-	13793,6805	25	64 (3,7)
	o TTR-Dihidroxilada o TTR-Sulfínico	13793,2628	13793,9606	51	51 (3,9)		30	
5.	**(10) C-G**	13715,1713	13715,4042	17	53 (2,8)	13715,4228	18	47 (4,8)
9.	**TTR(Met30)-Cys**	13912,4683	No detectada	-	-	13912,9765	37	44 (3,8)

a) El error relativo (E_r) se calculó en ppm como: $|M_r \text{ experimental} - M_r \text{ teórica}| / M_r \text{ teórica} * 10^6$.

b) La abundancia relativa (%A) se calculó normalizando el valor del área respecto a la proteoforma más abundante.

* La exactitud de masa y la resolución del espectrómetro de masas no fueron suficientes para diferenciar entre estas proteoformas, que presentan la misma M_r o muy similar.

6.2.2. Análisis dirigido de biomarcadores proteicos mediante AA-SPE-CE-MS. La α-sinucleína en la enfermedad de Parkinson

Los aptámeros son biomoléculas poliméricas que se pliegan en estructuras tridimensionales definidas y pueden interaccionar con la molécula diana con elevada selectividad y una afinidad similar a la de los Ab monoclonales [227,228]. Aunque se han descrito aptámeros peptídicos [304], son más frecuentes los aptámeros de ácidos nucleicos, típicamente oligonucleótidos monocatenarios con menos de 100 bases [206,207]. A diferencia de los Abs, los aptámeros, una vez seleccionados, se sintetizan químicamente, de manera que para producirlos no son necesarios animales o células, luego se pueden obtener de forma más reproducible, rápida y económica [212,213]. Otras ventajas interesantes de los aptámeros son su menor tamaño, elevada robustez, estabilidad térmica, tolerancia a amplios intervalos de pH y concentración de sales y posibilidad de modificarlos adecuadamente para inmovilizarlos en un soporte con la orientación adecuada [207,221].

Los aptámeros tienen muchas aplicaciones, y diversos autores han descrito el uso de sorbentes de AA en SPE [230,233,234]. Sin embargo, hasta la fecha, solamente Marechal et al. [174] han demostrado la posibilidad de realizar análisis mediante AA-SPE-CE. En dicho trabajo se utiliza un microcartucho monolítico con un aptámero contra la ocratoxina A para analizarla en patrones, cerveza y vino por AA-SPE-CE con detección de fluorescencia inducida por láser (LIF). En el presente trabajo (**Artículo 3.3**), se investiga por primera vez la AA-SPE-CE-MS, usando un aptámero de ADN monocatenario contra la proteína α-syn, que está relacionada con la enfermedad de Parkinson (PD).

6.2.2.1. Análisis de patrones de α-syn por CE-MS

En primer lugar, se investigó el análisis de un patrón comercial de α-syn recombinante expresada en *Escherichia coli* (*E. coli*) por CE-MS. Se evaluaron diferentes BGEs y SL que fueron adecuados en anteriores estudios del grupo de investigación para el análisis de péptidos y de proteínas intactas mediante CE-MS [201,300,301,305]. Se probaron dos BGEs ácidos, HAc

50 mM:HFor 50 mM (pH 2,3) y HAc 100 mM (pH 2,9), y tres de pH neutro, NH_4Ac 10 mM (pH 7,0, 8,0 o 9,0), en combinación con un SL 60:40 (v/v) propan-2-ol:agua con 0,05 o 0,25% (v/v) de HFor. La mejor sensibilidad y eficacia del pico para la α-syn se obtuvo con el BGE HAc 100 mM (pH 2,9) y el SL 60:40 (v/v) propan-2-ol:agua con 0,05% (v/v) de HFor. En la **Figura 6.16** se muestran el EIE (i), el espectro de masas (ii) y el espectro de masas deconvolucionado (iii) para el análisis de un patrón de α-syn de 100 µg/mL mediante CE-MS. Como se aprecia en el espectro de masas deconvolucionado (**Figura 6.16-iii)**, la única proteoforma detectada era la α-syn-Libre (M_r teórica = 14460,02) ya que la α-syn recombinante expresada en *E. coli* no presenta modificaciones postraduccionales (PTMs). La exactitud de la masa era adecuada (E_r <20 ppm). Los picos poco intensos que se detectan a valores de M_r deconvolucionada ligeramente más elevados que la M_r de la α-syn-Libre, se corresponden con aductos de la proteína con los cationes alcalinos Na^+ y K^+.

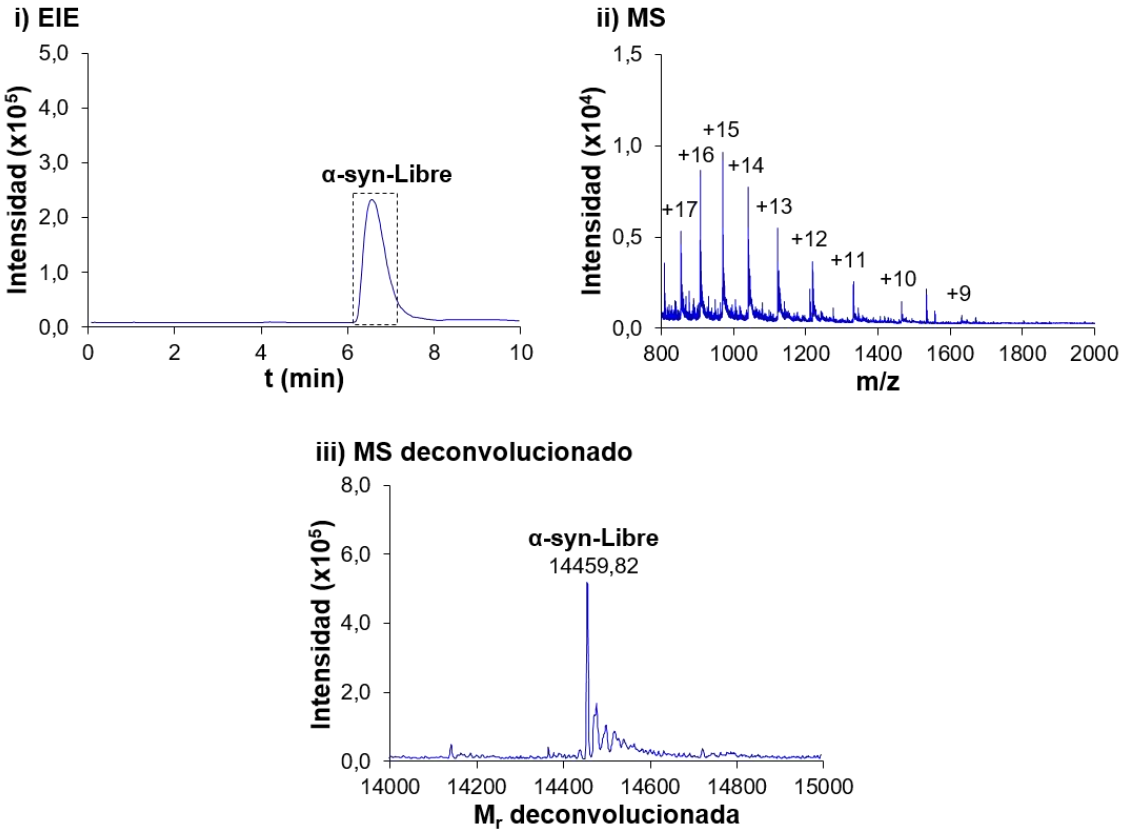

Figura 6.16. CE-MS (BGE HAc 100 mM (pH 2,9) y SL 60:40 (v/v) propan-2-ol:agua 0,05% (v/v) de HFor) para un patrón de α-syn de 100 µg/mL. (i) EIE, (ii) espectro de masas y (iii) espectro de masas deconvolucionado.

En las condiciones optimizadas, la repetibilidad de los análisis era adecuada (%RSD (n = 3) en t_m y A_p de 0,9% y 5,6% con un patrón de α-syn de 100 µg/mL) y el LOD era 20 µg/mL. Es importante destacar que, a diferencia de lo que ocurría en IA-SPE-CE-MS, que requiere utilizar BGEs neutros, los BGEs ácidos, que permiten una mejor sensibilidad en MS en ESI+, sí que son potencialmente compatibles con AA-SPE-CE-MS.

6.2.2.2. Análisis de patrones de α-syn por AA-SPE-CE-MS

Para preparar el sorbente de AA se inmovilizó un aptámero previamente descrito en la bibliografía [306] sobre las MBs UAAF, con las que se obtuvieron los mejores resultados en el análisis de TTR por IA-SPE-CE-MS (**Artículo 3.2**). Para poder inmovilizar covalentemente el aptámero con una orientación adecuada en las MBs UAAF, durante la síntesis del aptámero se incorporó un grupo funcional amino en el extremo 5'.

En estudios preliminares se observó que el sorbente de AA era estable utilizando BGEs relativamente ácidos. Se investigaron diferentes combinaciones de BGE y SL, usando el eluyente que había dado mejores resultados en IA-SPE-CE-MS (NH_4OH 100 mM (pH 11,2), **Artículo 3.2**). Empleando los BGEs HAc 50 mM:HFor 50 mM (pH 2,3) y HAc 100 mM (pH 2,9) en combinación con el SL 60:40 (v/v) propan-2-ol:agua con 0,05% (v/v) de HFor, se detectaban cantidades similares de α-syn. Sin embargo, usando el BGE más ácido (HAc 50 mM:HFor 50 mM (pH 2,3)) esta cantidad disminuía después de diversas inyecciones consecutivas, probablemente debido al deterioro gradual del sorbente de AA. Empleando BGEs de pH neutro o ligeramente básico (NH_4Ac 10 mM (pH 7,0, 8,0 o 9,0)) la sensibilidad era menor que con los BGEs ácidos, incluso usando un SL 60:40 (v/v) propan-2-ol:agua con 0,25% (v/v) de HFor. Por otra parte, se investigó la elución en condiciones ácidas, empleando el BGE NH_4Ac 10 mM (pH 7,0) y un eluyente de HAc 100 mM (pH 2,9). Sin embargo, en estas condiciones no se detectó la α-syn, confirmando que las disoluciones ácidas no permitían eluir la proteína. En vista de todos estos resultados, se seleccionó para el resto de experimentos el BGE HAc 100 mM (pH 2,9) y el SL 60:40 (v/v) propan-2-ol:agua con 0,05% (v/v) de HFor.

A continuación, se optimizó la composición y el volumen del eluyente volátil. Se evaluaron diferentes eluyentes volátiles acuosos y hidroorgánicos a pH neutro o añadiendo NH_4OH. En la bibliografía se ha descrito frecuentemente el uso mezclas de ACN:agua para romper las interacciones entre el aptámero y el analito [174,233]. Sin embargo, en la presente investigación se descartó rápidamente el uso de ACN ya que los eluyentes con un 40% o 80% (v/v) de ACN daban lugar a electroferogramas pobres y espectros de masas que presentaban clústeres de m/z equiespaciados que se atribuyeron a compuestos poliméricos que indicaban probablemente la degradación del sorbente durante la elución. El desempeño de eluyentes con 60% (v/v) de metanol (MeOH) en presencia o ausencia de NH_4OH 100 mM también fue pobre. Como se aprecia en la **Figura 6.17-A**, la mejor sensibilidad y repetibilidad se obtenía con el eluyente acuoso NH_4OH 100 mM (pH 11,2). No se empleó una mayor concentración de NH_4OH para prevenir la desnaturalización del aptámero y asegurar la durabilidad del sorbente. El volumen del eluyente se investigó con un patrón de α-syn de 1 µg/mL, inyectando el eluyente a 50 mbar durante 10, 20 y 40 s (50, 100 y 200 nL, respectivamente, [107]). El A_p de la α-syn era superior al inyectar el eluyente durante 20 s, en comparación con 10 s. En cambio, al inyectar el eluyente durante 40 s, el pico de la α-syn se ensanchaba y el A_p disminuía. Inyectando el eluyente durante 20 s, en el análisis de patrones de α-syn de mayor concentración, por ejemplo, 10 µg/mL, se detectó contaminación cruzada en análisis consecutivos. Para evitarla se lavó entre análisis con agua, eluyente y, otra vez, agua.

Con respecto a la introducción de la muestra se comprobó, que a diferencia de lo que pasaba en IA-SPE-CE-MS (**Artículo 3.2**), la cantidad de α-syn detectada disminuía al preparar los patrones en PBS, probablemente debido a una menor eficiencia de retención en condiciones salinas. Utilizando patrones en agua, la máxima cantidad de α-syn se detectaba cargando la muestra durante 5 minutos a 930 mbar (**Figura 6.17-B**). Para tiempos de carga superiores, se superaba el volumen de ruptura.

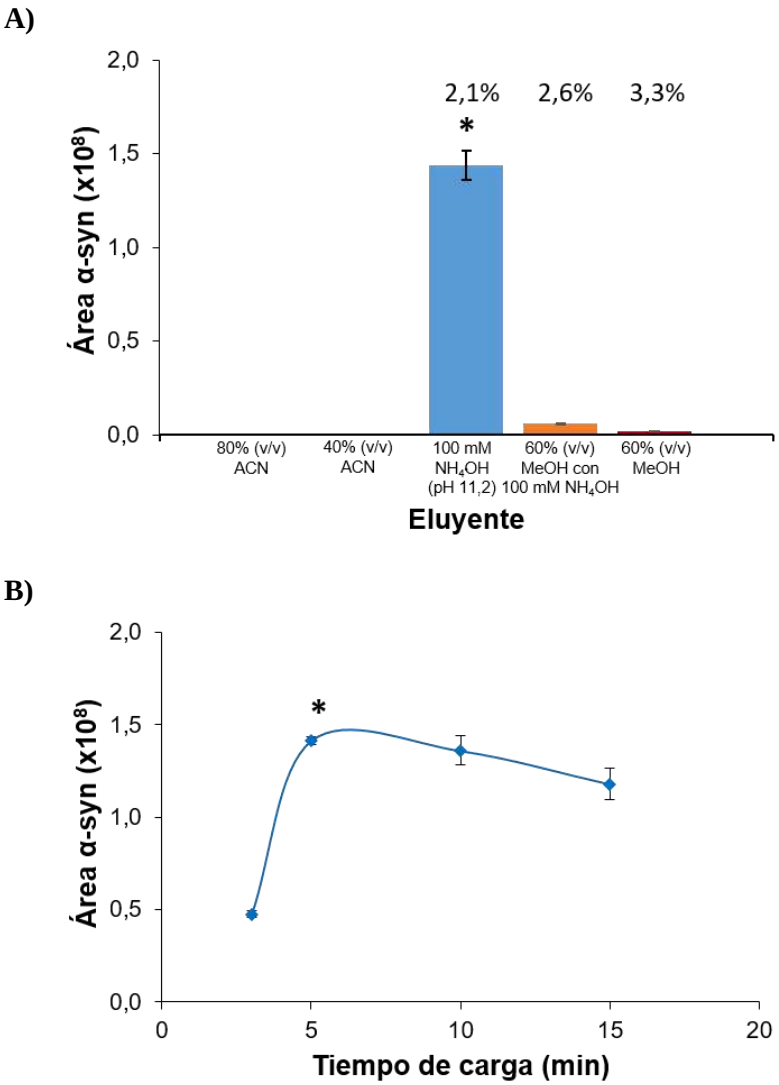

Figura 6.17. A_p de la α-syn para un patrón de 1 µg/mL analizado por AA-SPE-CE-MS (A) empleando diferentes eluyentes (introducción de muestra 5 min a 930 mbar) y (B) introduciendo la muestra durante diferentes valores de tiempo (3, 5, 10 y 15 min) a 930 mbar. Las barras de error indican la desviación estándar (n = 3). Las condiciones optimizadas se indican con un asterisco.

En la **Figura 6.18** se muestran el EIE (i) y el espectro de masas deconvolucionado (ii) para el análisis de un patrón de α-syn de 1 µg/mL por AA-SPE-CE-MS en las condiciones optimizadas. En estas condiciones, el método era preciso (%RSD (n = 3) en t_m y A_p de 2,1% y 5,4% con un patrón de α-syn de 1 µg/mL), lineal entre 0,5 y 10 µg/mL (R^2 >0,99) y los LODs eran de aproximadamente 0,2 µg/mL (100 veces menos que en CE-MS). Además, los microcartuchos podían emplearse alrededor de 20 análisis durante el mismo día, una durabilidad similar a la obtenida en IA-SPE-CE-MS (**Artículo 3.2)**.

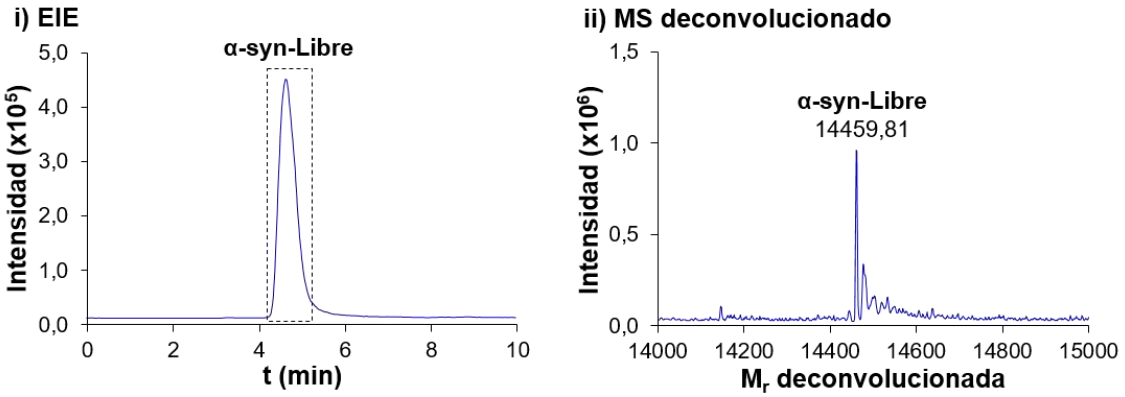

Figura 6.18. AA-SPE-CE-MS para un patrón de α-syn de 1 µg/mL. (i) EIE y (ii) espectro de masas deconvolucionado.

6.2.2.3. Análisis de α-syn en muestras de sangre por AA-SPE-CE-MS

Una vez optimizada con patrones, la metodología de AA-SPE-CE-MS se empleó para el análisis de la α-syn en sangre. Dado que más del 99% de la α-syn sanguínea se encuentra en los glóbulos rojos [307], se prepararon y analizaron lisados de éstos. Al analizar por CE-MS y AA-SPE-CE-MS un lisado de eritrocitos de un control sano filtrado con un filtro de jeringa de 0,20 µm de tamaño de poro, únicamente se detectó la hemoglobina (**Figura 6.19** y **Tabla 6.9**), que constituye aproximadamente el 95% del contenido proteico de los glóbulos rojos [308].

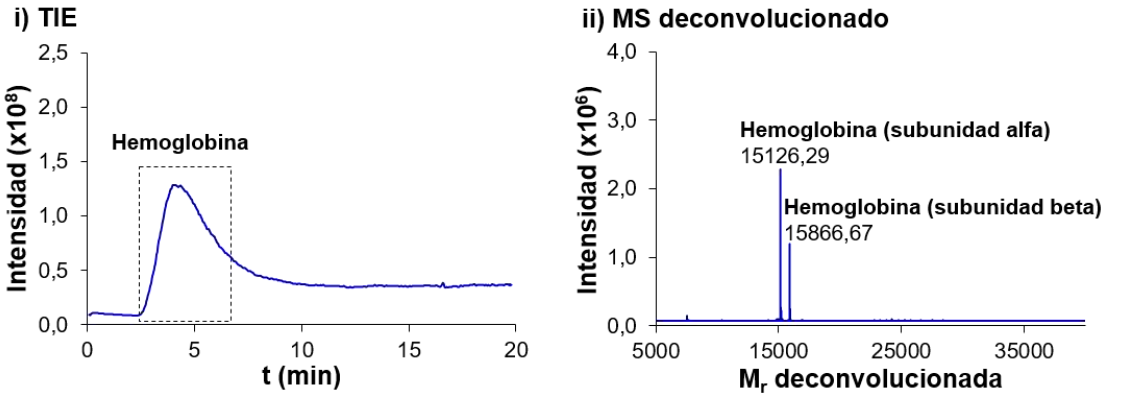

Figura 6.19. AA-SPE-CE-MS para un lisado de eritrocitos filtrado. (i) TIE y (ii) espectro de masas deconvolucionado.

Tabla 6.9. M_r teórica y deconvolucionada para las proteínas detectadas en lisados de eritrocitos pretratados.

Proteínas abundantes detectadas	Número de identificación de Uniprot	M_r teórica	M_r experimental	E_r [a] (ppm)	Detectada						
					CE-MS			AA-SPE-CE-MS			Blanco SPE-CE-MS
					Filtración	Extracción etanol-cloroformo	Tratamiento térmico	Filtración	Extracción etanol-cloroformo	Tratamiento térmico	Tratamiento térmico
Hemoglobina (subunidad alfa)	P69905	15126,20	15126,29	6	X			X			
Hemoglobina (subunidad beta)	P68871	15867,05	15866,67	24	X			X			
Ubiquitina	P62979 [b]	8564,76 [c]	8564,94	22		X	X		X	X	X
Anhidrasa carbónica N-acetilada	P00915	28780,75	28780,77	1		X			X		
Apolipo-proteína A-I	P02647	28078,33	28078,13	7			X			X	
α-syn N-acetilada	P37840	14502,06	14502,14	6						X	
α-syn-Libre (fortificada)	P37840	14460,02	14459,84	12						X	

a) El error relativo (E_r) se calculó en ppm como: $|M_r \text{ experimental} - M_r \text{ teórica}| / M_r \text{ teórica} * 10^6$.

b) El número de identificación de Uniprot indicado corresponde a la ubiquitina-40S ribosomal S27a y se asignó a partir de los resultados del análisis por LC-Orbitrap-MS/MS.

c) El valor de M_r indicado es coherente con el fragmento (1-76) de la proteína P2979. Este fragmento también se encuentra en las proteínas con número de identificación de Uniprot P0CG47 (poliubiquitina-B), P0CG48 (poliubiquitina-C) y P62987 (ubiquitina-60S ribosomal L40).

Por lo tanto, como ya ocurrió con la TTR, para analizar la α-syn endógena fue necesario estudiar diferentes pretratamientos de muestra que permitieran eliminar las proteínas más abundantes. En estudios anteriores del grupo de investigación se optimizó un pretratamiento basado en una extracción con etanol-cloroformo para purificar la superóxido dismutasa de lisados de eritrocitos [309], que permitía eliminar la hemoglobina durante el proceso. Con este pretratamiento, la hemoglobina precipitó cuantitativamente de los lisados ya que no se detectó por CE-MS ni en la fase orgánica de la extracción ni en la fase acuosa. Sin embargo, ambas fases contenían otras proteínas abundantes que interferían en la detección de la α-syn. Tanto por CE-MS como por AA-SPE-CE-MS, en ambas fases se detectaron la ubiquitina y la anhidrasa carbónica N-acetilada, pero no la α-syn (**Figura 6.20** y **Tabla 6.9**).

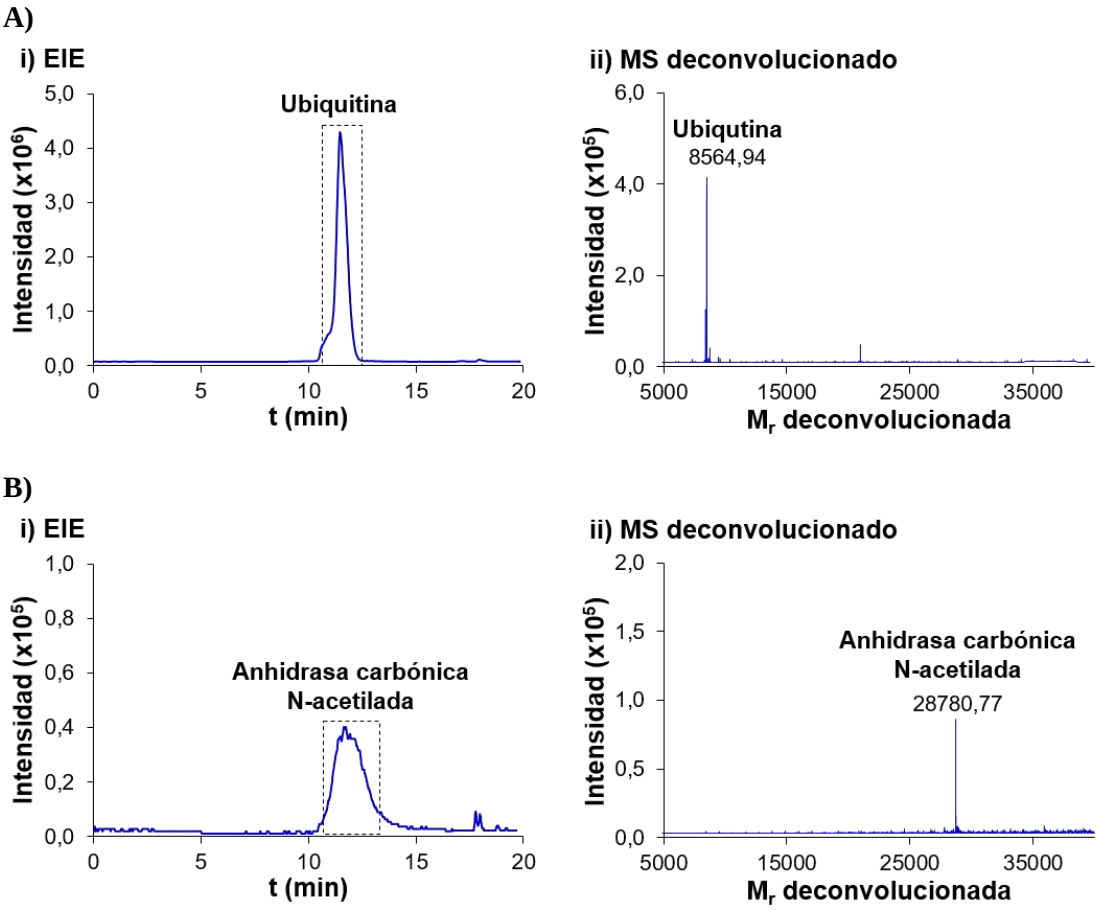

Figura 6.20. AA-SPE-CE-MS para un lisado de eritrocitos tratado mediante extracción etanol-cloroformo. (i) EIE y (ii) espectro de masas deconvolucionado para la (A) ubiquitina y (B) anhidrasa carbónica N-acetilada.

Como alternativa, teniendo en cuenta que la α-syn es una proteína termoestable y que su solubilidad y PTMs no se alteran con la temperatura [88,89,310], se realizó un tratamiento térmico para eliminar las proteínas termolábiles del lisado de eritrocitos. Con este pretratamiento, precipitaron cuantitativamente la hemoglobina y la anhidrasa carbónica N-acetilada. Por CE-MS únicamente se detectaron la ubiquitina y la apolipoproteína A-I (**Figura 6.21** y **Tabla 6.9**).

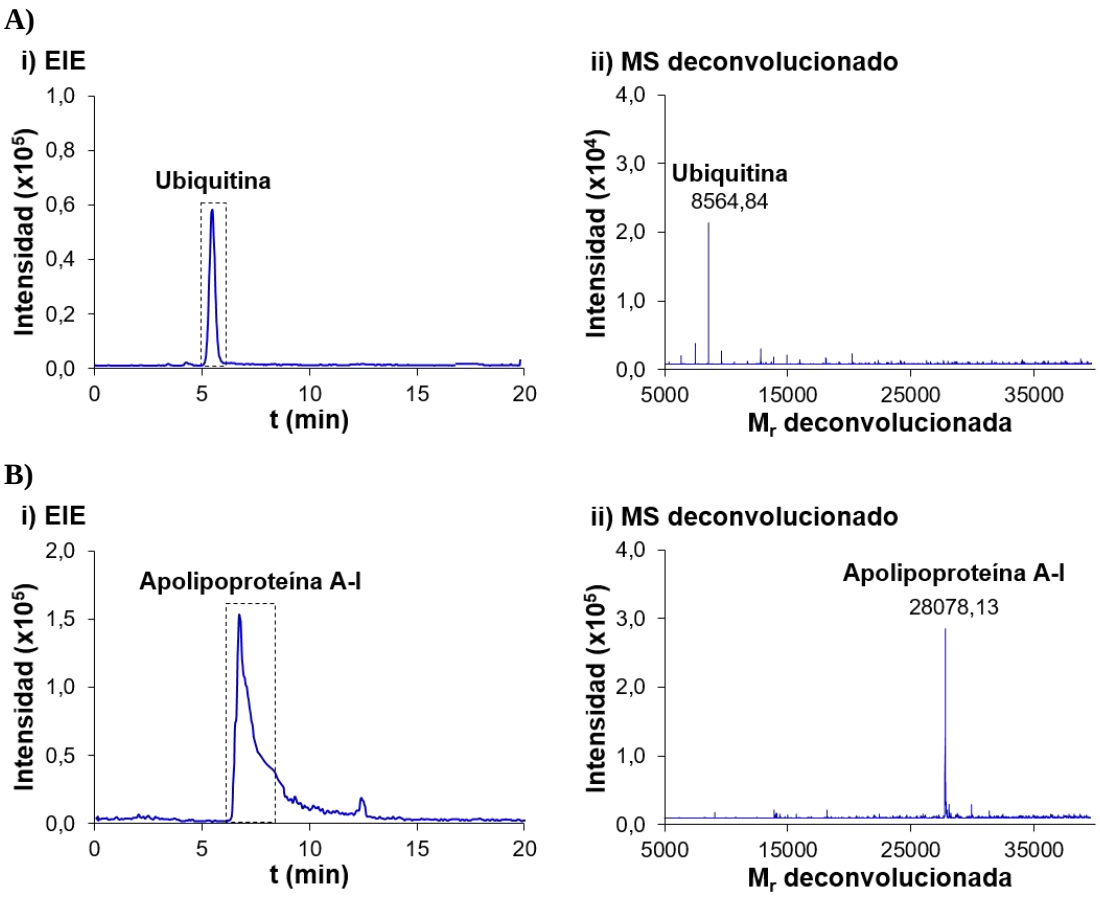

Figura 6.21. CE-MS para un lisado de eritrocitos tratado térmicamente. (i) EIE y (ii) espectro de masas deconvolucionado para la (A) ubiquitina y (B) apolipoproteína A-I.

En la **Figura 6.22-A** se muestran el EIE (i), el espectro de masas (ii) y el espectro de masas deconvolucionado (iii) para el análisis por AA-SPE-CE-MS del lisado de eritrocitos tratado térmicamente (TE). Como se puede observar en el espectro de masas deconvolucionado (**Figura 6.22-A(iii)**), se detectó una proteína con M_r 14502,14, que se corresponde con el valor esperado para la α-syn N-acetilada (**Tabla 6.9**). La acetilación N-terminal es muy frecuente en proteínas, especialmente cuando se conserva la metionina iniciadora como primer aminoácido de la

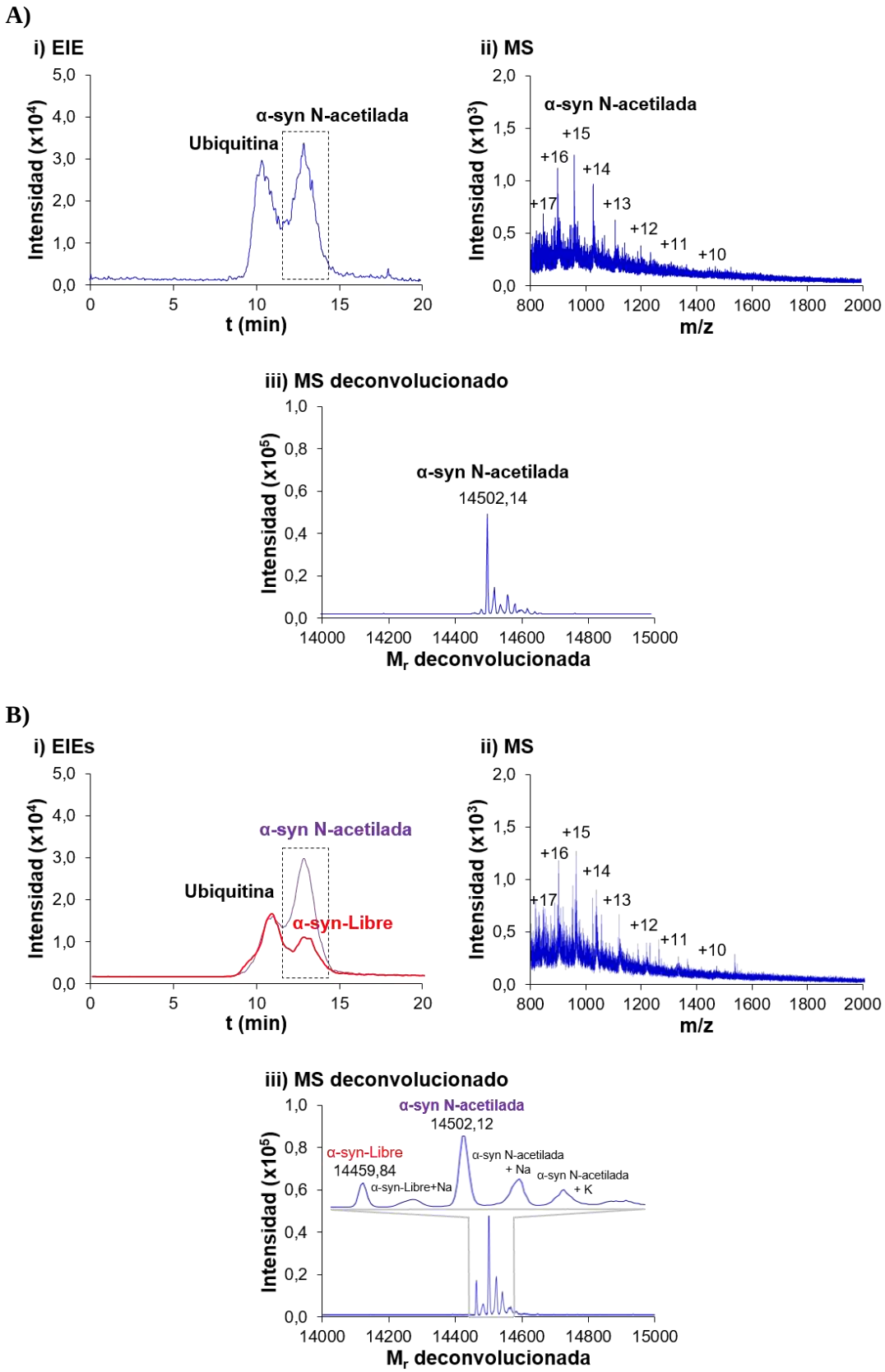

Figura 6.22. AA-SPE-CE-MS para un lisado de eritrocitos tratado térmicamente (TE) (A) sin fortificar y (B) fortificado con un patrón de α-syn de 0,3 µg/mL. (i) EIEs, (ii) espectro de masas y (iii) espectro de masas deconvolucionado.

secuencia peptídica [311]. La α-syn N-acetilada es la proteoforma más abundante de esta proteína en la sangre y también en el citosol cerebral [84]. Como se aprecia en el EIE (**Figura 6.22-A(i)**), el t_m de la α-syn N-acetilada en el análisis de lisados de eritrocitos TE se incrementó en comparación con el t_m del patrón de α-syn (**Figura 6.18-i**). Para confirmar si esto se debía a la acetilación N-terminal de la α-syn o a la modificación de la pared interna del capilar de separación inducida durante la carga de la muestra compleja, se fortificó el lisado de eritrocitos TE con un patrón de α-syn de 0,3 µg/mL y se analizó por AA-SPE-CE-MS (**Figura 6.22-B**). Como puede observarse, la α-syn N-acetilada y la α-syn-Libre comigraban pero la excelente exactitud de masa y el poder de resolución del espectrómetro de masas permitieron obtener EIEs separados (**Figura 6.22-B(i)**) e identificar inequívocamente las dos proteoformas en el espectro de masas deconvolucionado (**Figura 6.22-B(iii)**). Por lo tanto, el incremento en el t_m de la α-syn era debido a la modificación de la pared interna del capilar de separación inducida durante la carga de la muestra, que se comprobó que era permanente mediante sucesivos análisis del patrón de α-syn. Esto mismo ya ocurrió con la TTR en el análisis de muestras de suero por IA-SPE-CE-MS (**Artículo 3.2**).

Como se aprecia en los EIEs del análisis por AA-SPE-CE-MS de lisados de eritrocitos TE (**Figuras 6.22-A(i)** y **6.22-B(i)**), la α-syn comigraba ligeramente con la ubiquitina que también quedaba retenida en el sorbente de AA, al igual que la apolipoproteína A-I que no interfería en el EIE de la α-syn (**Tabla 6.9**). Se investigó la naturaleza de esta retención en el sorbente. En primer lugar, se preparó un microcartucho empleando un blanco del sorbente, es decir, MBs sin aptámero enlazado, con el objeto de investigar la posibilidad de retención no específica. Al analizar un lisado de eritrocitos TE por SPE-CE-MS empleando este preconcentrador, se detectó únicamente la ubiquitina y en cantidades similares a las detectadas por AA-SPE-CE-MS, confirmando la retención no específica de la ubiquitina. Se intentó minimizar esta retención incubando el lisado de eritrocitos TE con un blanco de sorbente antes de su análisis por AA-SPE-CE-MS. Sin embargo, no se apreció un incremento en el pico de la α-syn N-acetilada ni una disminución en el de la ubiquitina. Con el objetivo de enmascarar la ubiquitina, también se probó a añadir una

elevada concentración (200 nM) de una secuencia de ADN monocatenario que no interacciona con la α-syn, pero tampoco se obtuvieron resultados satisfactorios.

Una vez descartada la posibilidad de reducir la cantidad de ubiquitina presente en el lisado de eritrocitos TE, se intentó mejorar la separación de los picos de la α-syn y la ubiquitina. Los capilares de separación de 50 µm i.d. permitieron una mejora en la eficacia del pico de la α-syn en patrones. Sin embargo, en el caso de los lisados de eritrocitos TE, la complejidad de la muestra cargada provocaba la obturación del capilar de 50 µm i.d. y caídas en la corriente durante la separación electroforética. Por lo tanto, fue necesario continuar empleando capilares de separación de 75 µm i.d. para analizar las muestras de lisados de eritrocitos TE por AA-SPE-CE-MS. No obstante, es importante destacar que, en comparación con los biosensores o ensayos típicos empleando aptámeros o anticuerpos, una gran ventaja de la AA-SPE-CE-MS es que la separación electroforética y la selectividad de la detección por MS evita la posibilidad de falsos positivos o de una cuantificación errónea causada por la coextracción de interferencias.

En las condiciones optimizadas, la repetibilidad de los análisis de lisados de eritrocitos TE era adecuada (%RSD (n = 3) en t_m y A_p de 6,7% y 10,8%). No obstante, como ya ocurría con la TTR en el análisis de muestras de suero por IA-SPE-CE-MS (**Artículo 3.2**), a causa de la complejidad de la matriz de la muestra, la durabilidad de los preconcentradores se reducía a unos 10 análisis.

El método de AA-SPE-CE-MS desarrollado se aplicó al análisis de lisados de eritrocitos TE de controles sanos y pacientes de PD en estadios III-IV. Tanto en las muestras de controles sanos como en las de pacientes de PD, se detectaron la ubiquitina, la apolipoproteína A-I y la α-syn N-acetilada y no se detectó ninguna otra proteoforma de la α-syn, considerando tanto PTMs como fragmentos truncados en el carboxilo-terminal. Para complementar y validar estos resultados *top-down*, se empleó una estrategia *bottom-up*. Las proteínas del lisado de eritrocitos TE se digirieron con tripsina y se analizaron por LC-Orbitrap-MS/MS. Tampoco en este caso se detectaron diferencias entre las muestras de controles sanos y las de pacientes de PD, donde se identificaron 156 proteínas, confirmando la elevada complejidad de los lisados de eritrocitos TE. Además, las proteínas identificadas con mayor fiabilidad fueron coherentes con los resultados

obtenidos por CE-MS y AA-SPE-CE-MS mediante la estrategia *top-down*: la hemoglobina (subunidades alfa y beta), la apolipoproteína A-I, la ubiquitina-40S ribosomal S27a y la α-syn N-acetilada, que fue la única proteoforma de la α-syn detectada.

Los resultados obtenidos tanto por la estrategia *top-down* como la *bottom-up* indican que, a excepción de la α-syn N-acetilada, la abundancia de otras proteoformas de la α-syn debe ser muy baja en los eritrocitos de controles sanos y pacientes de PD, tal y como han descrito otros autores recientemente [89,312]. Sin embargo, deberían analizarse un mayor número de muestras de sangre para confirmar los resultados obtenidos y descartar la modificación sistémica de la α-syn, que podría ser de gran utilidad para el diagnóstico temprano de la PD. Por el momento, únicamente se ha confirmado la presencia de una gran abundancia de α-syn fosforilada en la Ser-129 en los cuerpos de Lewy depositados en el cerebro de pacientes de esta enfermedad [66,84].

6.2.3. Análisis de un subproteoma. Enriquecimiento de His-peptides mediante IMA-SPE-CE-MS

En proteómica, son de gran interés los tratamientos que permiten reducir la complejidad de la muestra e identificar proteínas que se encuentran a baja concentración, que generalmente brindan información biológica y clínicamente más relevante que las proteínas más abundantes. Para simplificar la muestra proteica, una opción muy adecuada son los pretratamientos que permiten precipitar las proteínas mayoritarias, como los empleados en esta tesis para el análisis *top-down* de la TTR del suero por IA-SPE-CE-MS (**Artículo 3.2**) y de la α-syn en eritrocitos por AA-SPE-CE-MS (**Artículo 3.3**). Una estrategia *bottom-up* interesante para eliminar la interferencia de las proteínas mayoritarias es el aislamiento de un subproteoma mediante el enriquecimiento de péptidos que contienen aminoácidos menos abundantes como la cisteína, la metionina, el triptófano o la histidina [313,314]. En particular, la histidina está presente en la secuencia aminoacídica del 85-95% de las proteínas humanas, pero solamente en el 15-20% de los péptidos que se generan a partir de su digestión tríptica [313,314]. Por lo tanto, el análisis de los péptidos que contienen histidina (His-peptides) de digestos enzimáticos permite simplificar la

mezcla de péptidos aun manteniendo una cobertura significativa del proteoma [315,316]. Además, en la síntesis de proteínas recombinantes es muy habitual añadir un marcador con seis o más residuos de histidina consecutivos (His-tag), que permite la purificación de la proteína sin afectar a su estructura o función [243].

Para purificar los His-peptides mediante SPE *off-line* se emplean habitualmente sorbentes de IMA que contienen cationes divalentes como el Cu(II) y el Ni(II) y el ácido iminodiacético (IDA) o el ácido nitrilotriacético (NTA) como agentes quelantes [239,245]. Estos sorbentes también se pueden emplear para preparar preconcentradores para el desarrollo de metodologías IMA-SPE-CE-MS, que permiten automatizar la purificación, separación e identificación de los His-peptides. En un trabajo previo, nuestro grupo de investigación desarrolló un método de IMA-SPE-CE-MS empleando un sorbente de Ni(II)-NTA y preconcentradores empaquetados con dos fritas, para el análisis de los fragmentos de péptidos Aβ 1-15 y 10-20 estudiados en el **Apartado 6.1** y que contienen histidinas (**Tabla 6.1**) [191]. En el presente estudio (**Artículo 3.4**), se investiga el potencial de esta metodología para enriquecer selectivamente los His-peptides presentes en los típicos digestos proteicos complejos generados en los estudios proteómicos *bottom-up*.

6.2.3.1. Análisis de la α-CSN

En primer lugar, se analizó mediante CE-MS un digesto tríptico de la α-caseína (α-CSN), una proteína que se encuentra bien caracterizada y que genera un número significativo de His-peptides fáciles de detectar. El patrón de α-CSN es una mezcla de dos proteínas, la α-S1-caseína (α-CSN1; 199 aminoácidos; M_r~23,700) y la α-S2-caseína (α-CSN2; 207 aminoácidos; M_r~25,300), que se obtienen por precipitación a partir de la leche bovina [317]. La α-CSN1 es aproximadamente 4 veces más abundante que la α-CSN2 [317]. En la **Tabla 6.10** se muestran los péptidos que se deberían generar en la digestión tríptica de la α-CSN1 y la α-CSN2 y los His-peptides, con los residuos de histidina marcados en negrita.

Tabla 6.10-A. Péptidos tripticos de la α-CSN1 detectados por CE-MS e IMA-SPE-CE-MS (patrón de 50 µg/mL). Los His-peptides y los residuos de histidina están marcados en negrita y las fosforilaciones en color rojo. Los aminoácidos individuales no se tienen en cuenta.

	Secuencia peptídica		$[M+nH]^{n+}$		Detectado		
			m/z	n	CE-MS (BGE ácido)	CE-MS (BGE neutro)	IMA-SPE-CE-MS
1	[1-3]	RPK	200,6370; 400,2667	2, 1	-	-	✓
2	**[4-7]**	**H**PIK	247,6579; 494,3085	2, 1	✓	✓	✓
3	**[8-22]**	**H**QGLPQEVLNENLLR	587,3198; 880,4761	3, 2	✓	✓	-
4	[23-34]	FFVAPFPEVFGK	462,2482; 692,8686	3, 2	✓	✓	-
5	[35-36]	EK	276,1554	1	✓	✓	-
6	[37-42]	VNELSK	385,1783; 769,3492	2, 1	-	-	-
7	[43-58]	DIGSESTEDQAMEDIK	643,2354; 964,3494	3, 2	✓	✓	-
8	[59-79]	QMEAESISSSEEIVPNSVEQK	-	-	-	-	-
9	**[80-83]**	**H**IQK	263,1609; 525,3144	2, 1	✓	✓	✓
10	[84-90]	EDVPSER	416,1958; 831,3843	2, 1	✓	✓	-
11	[91-100]	YLGYLEQLLR	423,2397; 634,3559	3, 2	✓	✓	-
12	[101-102]	LK	260,1969	1	-	-	-
13	[104-105]	YK	310,1761	1	-	-	-
14	[106-119]	VPQLEIVPNSAEER	554,2696; 830,9008	3, 2	✓	✓	-
15	**[120-124]**	**H**SMK	308,1678; 615,3283	2, 1	✓	✓	✓
16	**[125-132]**	EGI**H**AQQK	304,1629; 455,7407	3, 2	✓	✓	-
17	[133-151]	EPMIGVNQELAYFYPELFR	772,7172; 1158,5721	3, 2	✓	✓	-
18	[152-193]	QFYQLDAYPSGAWYYVPLGTQYTDAPSFSDIPNPIGSENSEK	944,0404; 1179,7987	5, 4	-	-	-
19	[194-199]	TTMPLW	748,3698	1	✓	✓	-

Los digestos tripticos se han simulado con el software PeptideMass de ExPASy (https://web.expasy.org/peptide_mass/).

Tabla 6.10-B. Péptidos trípticos de la α-CSN2 detectados por CE-MS e IMA-SPE-CE-MS (patrón de 50 µg/mL). Los His-peptides y los residuos de histidina están marcados en negrita y las fosforilaciones en color rojo. Los aminoácidos individuales no se tienen en cuenta.

Secuencia peptídica			[M+nH]$^{n+}$		Detectado		
			m/z	n	CE-MS (BGE ácido)	CE-MS (BGE neutro)	IMA-SPE-CE-MS
20	**[2-21]**	NTME**H**VSSSEESIISQETYK	-	-	-	-	-
21	[22-24]	QEK	404,2140	1	-	-	-
22	[25-32]	NMAINPSK	477,7094; 954,4114	2, 1	-	-	-
23	[33-41]	ENLCSTFCK	522,7284	2, 1	-	-	-
24	[42-45]	EVVR	251,6528; 502,2984	2, 1	✓	✓	-
25	[46-70]	NANEEEYSIGSSSEESAEVATEEVK	-	-	-	-	-
26	[71-76]	ITVDDK	345,6871; 690,3668	2, 1	-	-	-
27	**[77-80]**	**H**YQK	288,1504; 575,2936	2, 1	✓	-	✓
28	[81-91]	ALNEINQFYQK	456,5700; 684,3513	3, 2	-	-	-
29	[92-113]	FPQYLQYLYQGPIVLNPWDQVK	903,8074; 1355,2074	3, 2	-	-	-
30	[115-125]	NAVPITPTLNR	598,3433; 1195,6793	2, 1	✓	-	-
31	[126-136]	EQLSTSEENSK	-	-	-	-	-
32	[138-149]	TVDMESTEVFTK	489,5422; 733,8097	3, 2	✓	-	-
33	[151-152], [198-199]	TK	248,1605	1	-	-	-
34	[153-158]	LTEEEK	748,3723	1	✓	✓	-
35	[159-160]	NR	-	-	-	-	-
36	[161-165]	LNFLK	317,6998; 634,3923	2, 1	✓	✓	-
37	[167-170]	ISQR	-	-	-	-	-
38	[171-173]	YQK	438,2347	1	-	-	-
39	[174-181]	FALPQYLK	490,2842; 979,5611	2, 1	✓	-	-
40	**[182-188]**	TVYQ**H**QK	301,8276; 452,2378	3, 2	✓	✓	✓
41	[189-197]	AMKPWIQPK	366,8762; 549,8103	3, 2	✓	✓	✓
42	[200-205]	VIPYVR	373,7316; 746,4559	2, 1	✓	✓	-
43	[206-207]	YL	295,1652	1	✓	-	-

Los digestos trípticos se han simulado con el software PeptideMass de ExPASy (https://web.expasy.org/peptide_mass/).

Se analizó el digesto de α-CSN por CE-MS, empleando las condiciones típicas para el análisis de péptidos en ESI+, es decir, BGE ácido (HAc 50 mM:HFor 50 mM (pH 2,3)) y SL 60:40 (v/v) propan-2-ol:agua con 0,05% (v/v) de HFor [123,194,318]. En la **Figura 6.23-A** se muestran los EIEs de los péptidos detectados para un digesto de α-CSN de 50 µg/mL. Los His-peptides se muestran coloreados para diferenciarlos del resto de péptidos (non-His-peptides, en color negro). En estas condiciones, se detectaban 17 non-His-peptides de las α-CSN1 y α-CSN2 de los 35 posibles (**Tabla 6.10**). Esta relación corresponde a una cobertura peptídica de la secuencia total del 48,6%. En el caso de los His-peptides, se detectaban 7 de 8, es decir, una cobertura peptídica de la secuencia de His-peptides del 87,5%. Se detectaban los 5 His-peptides esperados para la α-CSN1 (**Tabla 6.10-A**) y 2 de 3 para la α-CSN2 (**Tabla 6.10-B**). El His-peptide fosforilado α-CSN2[2-21] era el único que no se detectaba, probablemente a causa de la peor ionización en ESI+ debida a la presencia de los grupos fosfato y a la menor abundancia de la α-CSN2 respecto a la α-CSN1.

A pesar de la idoneidad de los BGEs ácidos para una adecuada sensibilidad en CE-MS en modo ESI+, estos BGEs no son adecuados cuando se utiliza IMA-SPE-CE-MS ya que el pH ácido de la disolución provoca la eliminación de los cationes metálicos del sorbente. En el trabajo previo de nuestro grupo de investigación con este sorbente, se vio que el BGE más adecuado para IMA-SPE-CE-MS era un BGE de fosfato a pH neutro y de fuerza iónica limitada (H_3PO_4 25 mM (pH 7,5, ajustado con NH_4OH)) en combinación con un SL 60:40 (v/v) propan-2-ol:agua con 0,50% (v/v) de HFor [191]. En la **Figura 6.23-B** se muestran los EIEs de los péptidos detectados por CE-MS empleando el BGE neutro para un digesto tríptico de α-CSN de 50 µg/mL. En estas condiciones, la sensibilidad era menor que empleando el BGE ácido (**Figura 6.23-A**), siendo la cobertura peptídica del 37,1% y el 75% para los non-His-peptides y los His-peptides, respectivamente (**Tabla 6.10**).

Empleando estas nuevas condiciones, se analizó el digesto de α-CSN por IMA-SPE-CE-MS utilizando el mismo sorbente y las mismas condiciones de elución (0,5% (v/v) de HAc a 50 mbar durante 75 s) que en el trabajo previo del grupo de investigación [191]. Este volumen de elución (aproximadamente 400 nL) es relativamente elevado en comparación con los valores

típicos de elución en SPE-CE-MS empleando capilares de 75 µm i.d., que habitualmente se encuentran entre 50 y 100 nL. Sin embargo, al disminuir el volumen de eluyente o la cantidad de ácido, la elución de los His-peptides era incompleta y la repetibilidad disminuía. En la **Figura 6.23-C** se muestran los EIEs de los péptidos detectados por IMA-SPE-CE-MS para un digesto tríptico de α-CSN de 50 µg/mL. Como se puede observar, se detectaban únicamente 2 non-His-

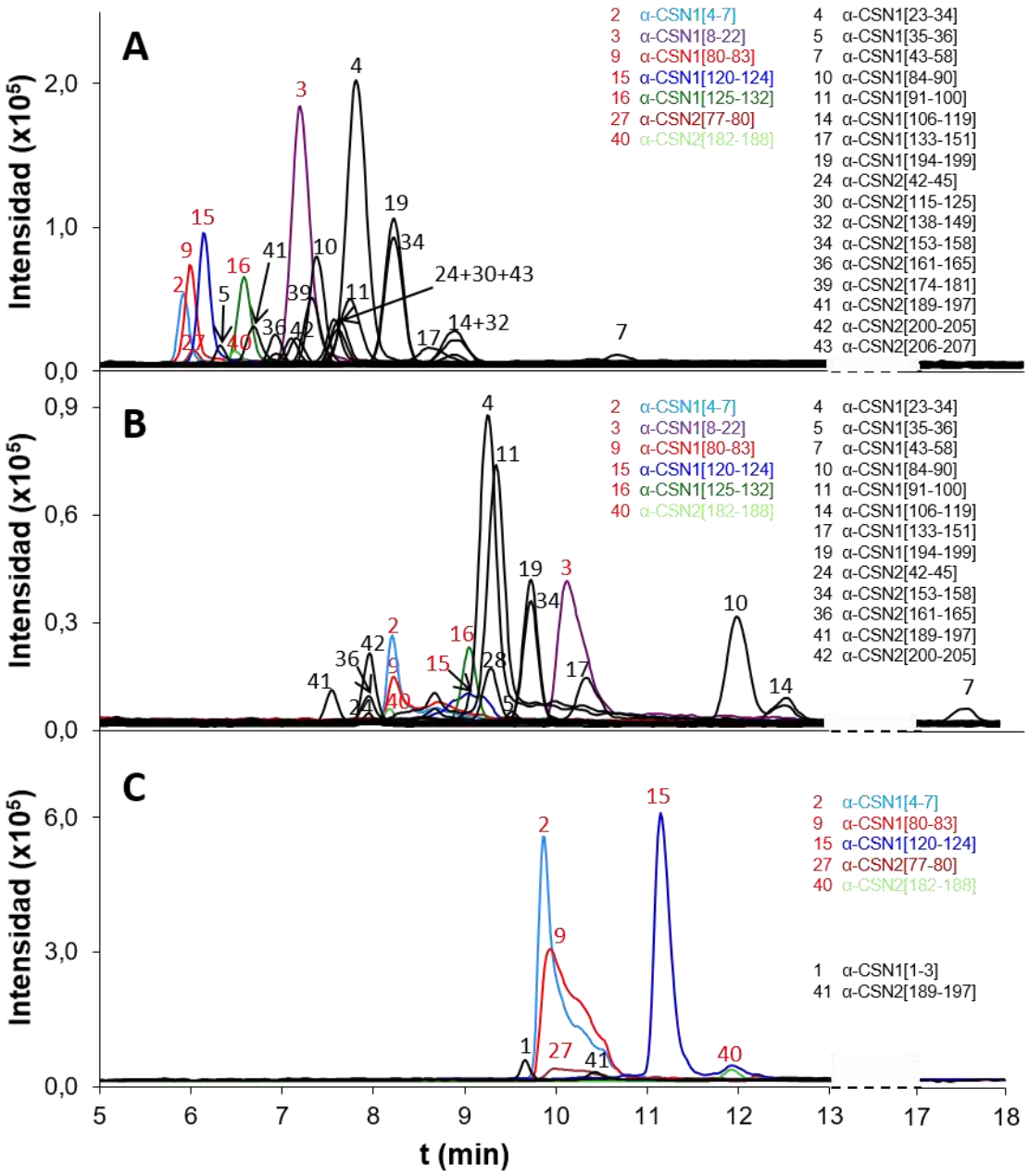

Figura 6.23. EIEs para el análisis de un digesto tríptico de α-CSN de 50 µg/mL por CE-MS empleando (A) BGE ácido (HAc 50 mM:HFor 50 mM (pH 2,3)) y (B) BGE neutro (H_3PO_4 25 mM (pH 7,5, ajustado con NH_4OH)) y (C) por IMA-SPE-CE-MS (BGE H_3PO_4 25 mM (pH 7,5, ajustado con NH_4OH)).

-peptides de un total de 35 (5,7% de cobertura peptídica). En cambio, se detectaban 5 His-peptides de un total de 8 (62,5% de cobertura peptídica): 3 de 5 para la α-CSN1 (**Tabla 6.10-A**) y 2 de 3 para la α-CSN2 (**Tabla 6.10-B**). El elevado valor de cobertura peptídica para los His-peptides en comparación con el de los non-His-peptides demuestra la selectividad de la metodología de IMA-SPE-CE-MS.

Para intentar mejorar aún más la sensibilidad y la cobertura peptídica de los His-peptides, se evaluó el efecto del tiempo de carga de la muestra (5, 10, 20 y 30 min) a 930 mbar con un digesto tríptico de α-CSN de 50 µg/mL (**Figura 6.24**). Como se puede observar, para tiempos de carga de hasta 10 minutos, la cantidad de His-peptides detectada aumentaba al incrementar el tiempo de introducción de la muestra en todos los casos. Sin embargo, a tiempos superiores se excedía el volumen de ruptura. Por lo tanto, se seleccionó un tiempo de carga de 10 min para el resto de experimentos. También se estudió la cobertura peptídica de los His-peptides a diferentes concentraciones de proteína y la linealidad del método analizando digestos de α-CSN a concentraciones entre 20 y 100 µg/mL. A 100 µg/mL, se obtenía el mismo valor de cobertura peptídica que a 50 µg/mL. En cambio, a 20 µg/mL, únicamente se detectaba el His-peptide α-CSN1[4-7]. Considerando únicamente este His-peptide, el método era lineal entre 20 y 100 µg/mL (R^2 >0,98).

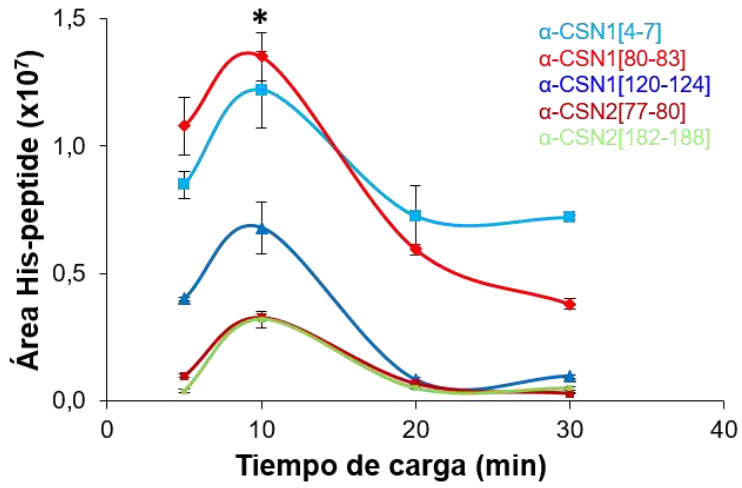

Figura 6.24. Estudio del efecto del tiempo de introducción de muestra (5, 10, 20 y 30 min) a 930 mbar en IMA-SPE-CE-MS (digesto tríptico de α-CSN de 50 µg/mL). Las barras de error indican la desviación estándar (n = 3). Las condiciones optimizadas se indican con un asterisco.

En las condiciones optimizadas, los análisis de α-CSN eran precisos (%RSD (n = 3) en t_m y A_p <3,0% y <11% con un digesto tríptico de α-CSN de 50 µg/mL) y los microcartuchos podían emplearse alrededor de 10 análisis. La **Figura 6.25** muestra la comparación del A_p de los His-peptides detectados por CE-MS empleando el BGE neutro y por IMA-SPE-CE-MS para un digesto de α-CSN de 50 µg/mL. Los correspondientes factores de preconcentración se indican en números, presentando valores de entre 25 y 98 para los His-peptides detectados. Es importante destacar que por IMA-SPE-CE-MS se detectaba el His-peptide de cadena corta α-CSN2[77-80], que no se detectaba por CE-MS empleando el BGE neutro. En cambio, los His-peptides α-CSN1[8-22] y α-CSN1[125-132] no se detectaban por IMA-SPE-CE-MS, probablemente a causa de su secuencia más larga.

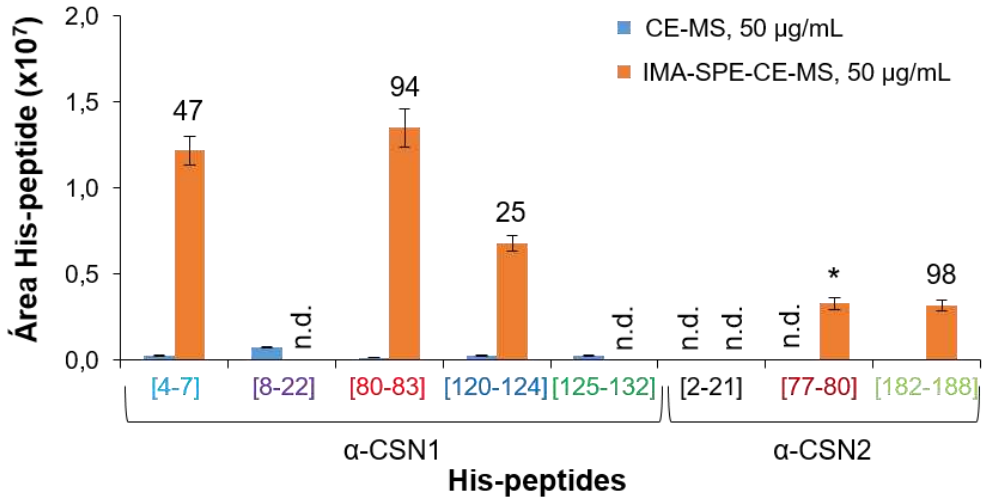

Figura 6.25. Comparativa del A_p de los His-peptides detectados por CE-MS e IMA-SPE-CE-MS (en ambos casos, BGE H_3PO_4 25 mM (pH 7,5, ajustado con NH_4OH) para un digesto tríptico de α-CSN de 50 µg/mL. Los factores de preconcentración se indican en números. El asterisco indica que no se calculó el factor de preconcentración porque el His-peptide no se detectó (n.d.) por CE-MS. Las barras de error indican la desviación estándar (n = 3).

6.2.3.2. Análisis de la β-CSN y la κ-CSN

Los estudios de IMA-SPE-CE-MS se ampliaron al análisis de otras proteínas modelo de la leche de vaca, concretamente la β-caseína (β-CSN) y la κ-caseína (κ-CSN). En la **Tabla 6.11-A** se muestran los His-peptides esperados en la digestión tríptica de la β-CSN y la κ-CSN. En la **Figura 6.26-A** se muestra la comparación del A_p de los His-peptides detectados en digestos trípticos de 50 μg/mL de β-CSN y κ-CSN analizados por CE-MS empleando el BGE neutro y por IMA-SPE-CE-MS. Por CE-MS, se detectaban 2 His-peptides de los 3 posibles para la β-CSN y el único His-peptide de la κ-CSN. En cambio, por IMA-SPE-CE-MS, aunque la selectividad era adecuada ya que no se detectaba ningún non-His-peptide, únicamente se detectaba el His-peptide corto β-CSN[106-107], con un factor de preconcentración de 138. Esto se atribuyó a la longitud de las secuencias peptídicas, ya que no se detectaban los His-peptides más largos. Para investigar la influencia de la longitud de la secuencia de los His-peptides en su retención en el sorbente de IMA, se llevó a cabo la digestión de la β-CSN y la κ-CSN con una mezcla de tripsina y quimotripsina. En la **Tabla 6.11-B** se muestran los His-peptides esperados para la digestión de la β-CSN y la κ-CSN con tripsina:quimotripsina, comprobándose que las secuencias son en general más cortas que en la digestión únicamente con tripsina (**Tabla 6.11-A**). En la **Figura 6.26-B** se puede apreciar que después de la digestión con tripsina:quimotripsina, el valor de la cobertura de los His-peptides detectados por IMA-SPE-CE-MS (60%) era superior al obtenido por CE-MS (40%), confirmándose que el sorbente de IMA empleado tiene preferencia por los His-peptides de secuencia corta.

Tabla 6.11. Secuencia de los His-peptides esperados para la digestión de β-CSN y κ-CSN con (A) tripsina y **(B)** tripsina:quimotripsina. Los residuos de histidina están marcados en negrita.

Proteína	A) Tripsina		B) Tripsina:quimotripsina	
β-CSN	[49-97]	IHPFAQTQSLVYPFPGPIPNSLPQNIPPLTQTPVVVPPFLQPEVMGVSK	[49-52]	I**H**PF
	[106-107]	**HK**	[106-107]	**HK**
	[114-169]	YPVEPFTESQSLTLTDVENL**H**LPLPLLQSWM**H**QP**H**QPLPPTVMFPPQSVLSLSQSK	[120-143]	TESQSLTLTDVENL**H**LPLPLLQSW
			[144-169]	M**H**QP**H**QPLPPTVMFPPQSVLSLSQSK
κ-CSN	[98-111]	**HPHPH**LSFMAIPPK	[98-105]	**HPHPH**LSF

Los digestos se han simulado con el software PeptideMass de ExPASy (https://web.expasy.org/peptide_mass/).

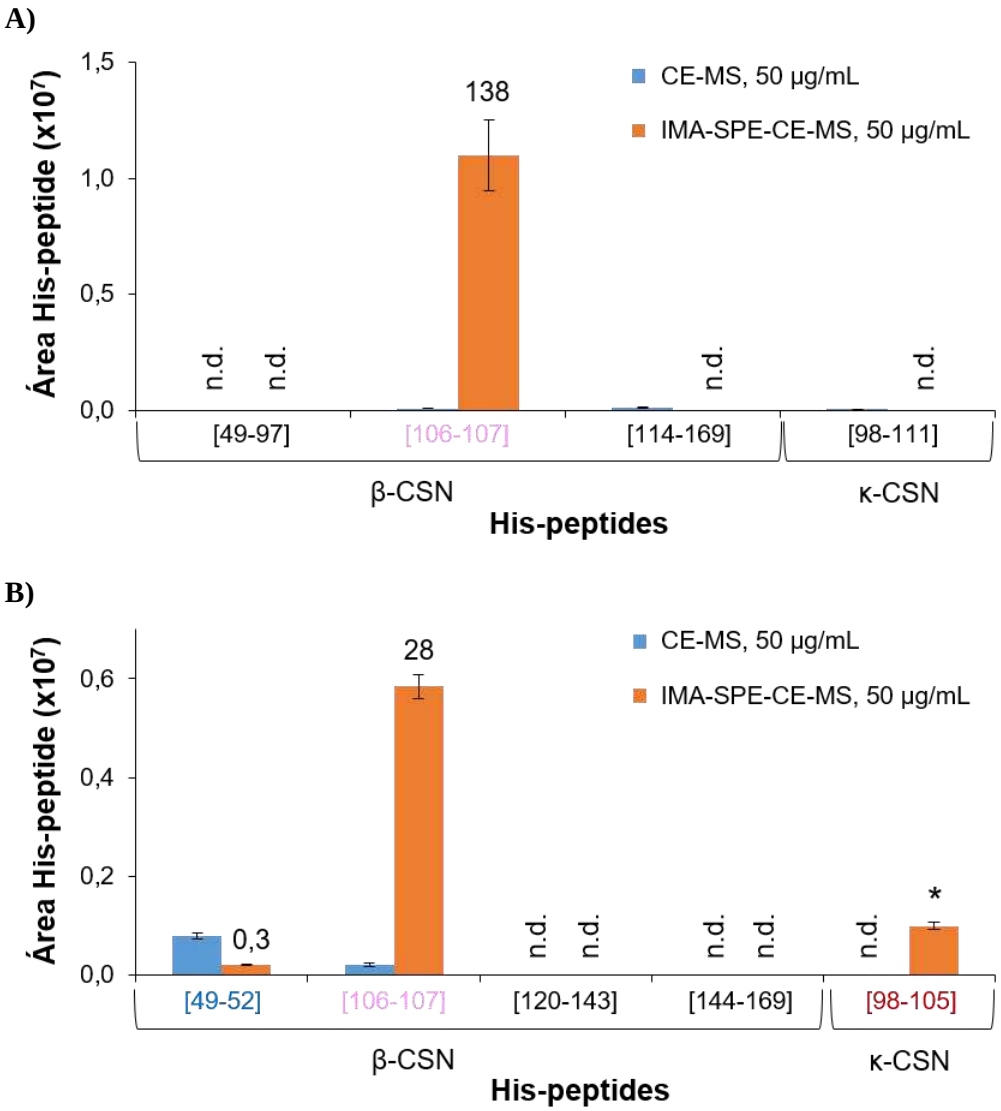

Figura 6.26. Comparativa del A_p de los His-peptides detectados por CE-MS e IMA-SPE-CE-MS (en ambos casos, BGE H_3PO_4 25 mM (pH 7,5, ajustado con NH_4OH) para un digesto de β-CSN y κ-CSN de 50 µg/mL. Digestión con (A) tripsina y (B) tripsina:quimotripsina. Los factores de preconcentración se indican en números. El asterisco indica que no se calculó el factor de preconcentración porque el His-peptide no se detectó (n.d.) por CE-MS. Las barras de error indican la desviación estándar (n = 3).

6.2.3.3. Análisis de un lisado celular de *E. coli*

Para investigar el potencial de la metodología de IMA-SPE-CE-MS para enriquecer selectivamente His-peptides en digestos proteicos complejos, se analizó un lisado celular de *E. coli* modificada para expresar la proteína α-lactalbúmina con un His-tag en el carboxilo-terminal [319]. Este lisado se emplea habitualmente para el control de calidad en la purificación de proteínas recombinantes con un His-tag o como control en el análisis de estas proteínas por

Western blot. Tomando como referencia análisis previos realizados por LC-MS/MS [319], se identificaron por CE-MS las proteínas α-lactalbúmina, mioglobina C, creatina quinasa-MM, catepsina D y antitrombina III. En la **Tabla 6.12-A** se muestran los péptidos detectados por CE-MS empleando el BGE ácido en un digesto del lisado celular de *E. coli* de 1000 µg/mL. En la **Tabla 6.12-B** se muestran los His-peptides detectados por IMA-SPE-CE-MS en un digesto del lisado celular de *E. coli* de 50 µg/mL. Como puede comprobarse, por IMA-SPE-CE-MS se detectaron los His-peptides cortos, principalmente de entre 2 y 4 aminoácidos, de la mioglobina C y la creatina quinasa-MM, algunos de los cuales no fueron detectados mediante CE-MS. No se detectó ningún His-peptide de la catepsina D ni de la antritrombina III porque tienen cadenas peptídicas más largas. Por lo tanto, estos resultados corroboraron la preferencia del sorbente IMA empleado por los His-peptides de cadena corta. Esta selectividad puede ser útil a la hora de investigar específicamente ciertas regiones de los proteomas. Asimismo, el péptido 6x-His α-lactalbúmina[123-129] únicamente se detectó mediante IMA-SPE-CE-MS. En la **Figura 6.27** se muestra el EIE obtenidos para dicho péptido por CE-MS e IMA-SPE-CE-MS. La gran capacidad de retención del sorbente de IMA para este péptido que contiene un His-tag sugiere la posibilidad de preconcentrar mediante IMA-SPE-CE-MS proteínas intactas u otros compuestos sintetizados o derivatizados añadiendo un His-tag, por ejemplo, lípidos [320] o carbohidratos [321].

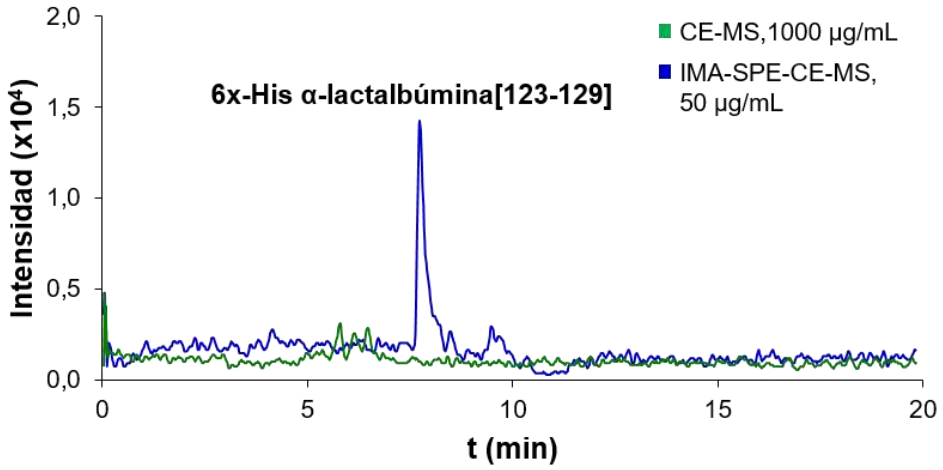

Figura 6.27. EIE para el péptido 6x-His α-lactalbúmina[123-129] en un digesto tríptico del lisado celular de *E. coli* analizado por CE-MS (1000 µg/mL, BGE HAc 50 mM:HFor 50 mM (pH 2,3)) (verde) y por IMA-SPE-CE-MS (50 µg/mL, BGE H_3PO_4 25 mM (pH 7,5, ajustado con NH_4OH)) (azul).

Tabla 6.12. Péptidos detectados y proteínas identificadas en un lisado celular de *E. coli* digerido con tripsina y analizado por CE-MS (1000 µg/mL, BGE HAc 50 mM:HFor 50 mM (pH 2,3)) y por IMA-SPE-CE-MS (50 µg/mL, BGE H_3PO_4 25 mM (pH 7,5, ajustado con NH_4OH)). Los His-peptides y los residuos de histidina están marcados en negrita. Los aminoácidos individuales no se tienen en cuenta.

Proteína identificada	Número de identificación de Uniprot	A) CE-MS (1000 µg/mL, BGE ácido)		B) IMA-SPE-CE-MS (50 µg/mL, BGE neutro)	
α-lactalbúmina 6x-His M_r ~14000	P00709	[2-5] QFTK	[109-114] ALCTEK	**[123-129]** L**HHHHHH**	
Mioglobina C M_r ~17000	P02144	[43-45] FDK	**[48-50]** H**L**K	**[48-50]** H**L**K	**[97-98]** H**K**
Creatina quinasa-MM M_r ~43000	P06732	**[1-9]** MPFGNT**H**NK **[26-32]** H**NNH**MAK [42-43] LR [44-45] DK [131-132] VR [133-135] TGR [136-138] SIK	[149-151] GER [173-177] YYPLK **[267-292]** AG**H**PFMWNQ**H**LGYVLTCPSNLGTGLR [315-316] LR [317-319] LQK [359-365] LMVEMEK [367-369] LEK	**[26-32]** HNN**H**MAK **[106-107]** H**K** **[305-307]** H**P**K	
Catepsina D M_r ~38000	P07339	[110-112] VER [113-120] QVFGEATK [131-141] FDGILGMAYPR [190-192] YYK [246-249] ELQK	[278-281] LGGK [282-284] GYK [285-293] LSPEDYTLK [294-299] VSQAGK [340-347] VGFAEAAR		
Antitrombina III M_r ~49000	P01008	[14-24] DIPMNPMCIYR [48-53] VWELSK [54-57] ANSR [140-145] LVSANR [146-150] LFGDK [177-183] ENAEQSR [184-188] AAINK	[223-226] GLWK [237-241] ELFYK [263-275] VAEGTQVLELPFK [351-359] LPGIVAGR [394-399] SLNPNR		

6.2.4. Análisis de biomarcadores miRNómicos. MicroRNAs en cáncer

La CE-MS es una técnica ampliamente utilizada en proteómica, tanto para análisis *top-down* (**Artículos 3.2** y **3.3**) como *bottom-up* (**Artículos 3.4** y **5.1**). En cambio, después del hito que representó la secuenciación del genoma humano, la CE ha sido superada ampliamente por otras técnicas para el análisis de oligonucleótidos, debido a que presentan ciertas ventajas. Así, las moléculas de ADN o ARN se pueden amplificar mediante la reacción en cadena de la polimerasa (PCR) para realizar posteriormente una detección altamente sensible [50]. Por otra parte, las técnicas de secuenciación de nueva generación (NGS) son capaces de secuenciar una enorme cantidad de nucleótidos simultáneamente en un corto período de tiempo [46]. No obstante, todas estas técnicas se basan en utilizar y amplificar una copia del ADN complementario a las moléculas diana originales. Por lo tanto, se trata de técnicas analíticas indirectas y de análisis dirigido, que además no son capaces de identificar las modificaciones postranscripcionales de los oligonucleótidos originales [322]. En cambio, la CE-MS permite el análisis directo y no dirigido de oligonucleótidos y la identificación fiable de su secuencia y modificaciones postranscripcionales [127]. En particular, el análisis de miRNAs y sus modificaciones postranscripcionales en fluidos biológicos es de un gran interés, ya que la alteración en las secuencias y concentraciones de los miRNAs está relacionada con diferentes procesos fisiológicos y enfermedades, especialmente el cáncer [30,31].

Sin embargo, el análisis de miRNAs en fluidos biológicos por CE-MS es muy complicado ya que estos biomarcadores se encuentran a concentraciones muy bajas en matrices muy complejas [127]. Así, incluso con las técnicas analíticas de rutina, es necesario el uso de diferentes pretratamientos de muestra para purificar y preconcentrar los miRNAs antes de su análisis. Entre estos pretratamientos de muestra destaca la SPE *off-line* empleando columnas de centrifugación que se comercializan en kits con diferentes sorbentes. Uno de los sorbentes empleados para la extracción de oligonucleótidos de cadena corta como los miRNAs es el carburo de silicio (SiC) [258]. En el **Artículo 3.5** de la presente tesis, se investiga el potencial de la SPE-CE-MS empleando un sorbente de SiC comercial para el análisis de miRNAs en suero humano.

6.2.4.1. Análisis de patrones de miRNAs por CE-MS y *sample stacking* CE-MS

Los miRNAs presentan grupos ionizables en las bases nitrogenadas y en los grupos fosfato esterificados, que están cargados negativamente en disolución acuosa tanto a pH neutro como básico [323]. Por esta razón, el modo de electrospray negativo (ESI-), en el que se generan iones moleculares del tipo $[M\text{-}nH]^{n-}$ debido a la pérdida de protones, permite obtener una mayor sensibilidad para su análisis mediante MS [127,324–326]. Además, también se suelen generar aductos con cationes metálicos debido a su elevada afinidad por los grupos fosfato, sobre todo con los cationes de los metales alcalinos sodio y potasio ($[M\text{-}(n+m)H+mNa/K]^{n-}$), cuya presencia es ubicua. La presencia de estos aductos es perjudicial para el análisis por MS ya que disminuyen la señal de los iones moleculares del tipo $[M\text{-}nH]^{n-}$, afectando a la sensibilidad y complicando la interpretación del espectro de masas. Por lo tanto, la pureza de la muestra de miRNAs y de los disolventes utilizados es esencial para una adecuada detección por MS. Algunos autores sugieren añadir a las disoluciones empleadas compuestos orgánicos fuertemente básicos como la trimetilamina, trietilamina o la piperidina para disminuir la formación de aductos con metales alcalinos mediante un mecanismo de desplazamiento. Sin embargo, estos compuestos orgánicos pueden provocar supresión de la señal en MS y es preferible el uso de NH_4Ac, que también es capaz de disminuir la formación de aductos alcalinos y es menos perjudicial para la detección de los analitos mediante MS [127].

En el presente estudio, primero se optimizó un método para el análisis de miRNAs por CE-MS empleando patrones sintéticos de los miRNAs hsa-miR-21-5p (miR-21) y hsa-let-7g-5p (let-7g), ambos biomarcadores relacionados con diferentes tipos de cáncer [39,40,327]. La secuencia de nucleótidos, las modificaciones postranscripcionales y la M_r de estos miRNAs se muestran en la **Tabla 6.13-A**.

Tabla 6.13. Características y M_r de los (A) patrones de miRNAs y (B) miRNAs identificados tentativamente por SiC-SPE-CE-MS en una muestra de suero de un paciente de leucemia linfocítica crónica (CLL).

miRNA	Secuencia	Modificaciones postranscripcionales	m/z $[M-5H]^{5-}$		M_r		
			Teórica	Experimental	Teórica	Experimental	E_r [a] (ppm)
A) miRNAs patrón							
hsa-miR-21-5p (miR-21)	UAGCUUAUCAGACUGAUGUUGA	Fosforilación en 5'	1415,5707	1415,5592	7082,89	7082,84	8
hsa-let-7g-5p (let-7g)	UGAGGUAGUAGUUUGUACAGUU	Fosforilación en 5'	1426,9677	1427,9537	7139,88	7139,81	10
B) miRNAs identificados tentativamente en una muestra de suero de un paciente de CLL							
miR-21	UAGCUUAUCAGACUGAUGUUGA	Fosforilación en 5'	1415,5707	1415,5485	7082,89	7082,78	15
hsa-iso-miR16-5p (iso-miR-16)	UAGCAGCACGUAAAUAUUGGCGU	Fosforilación en 5' Uridilación en 3'	1488,9890	1488,9723	7449,98	7449,90	11

a) El error relativo (E_r) se calculó en ppm como: $|M_r \text{ experimental} - M_r \text{ teórica}| / M_r \text{ teórica} * 10^6$.

Para conseguir una sensibilidad apropiada en ESI- a la vez que se minimizaba la formación de aductos de Na^+ y K^+, se seleccionaron diferentes BGEs de NH_4Ac a pH neutro o básico, algunos de los cuales ya habían dado buenos resultados en CE-MS e IA-SPE-CE-MS (**Artículo 3.2**). Se investigaron BGEs con diferentes concentraciones (NH_4Ac 10, 25 y 50 mM) y valores de pH (6,0 y 8,0, ajustados con HAc y NH_4OH, respectivamente), siempre preparados recientemente con agua de calidad MS en tubos de plástico para minimizar la posible lixiviación de cationes de metales alcalinos de las botellas de vidrio. La menor formación de aductos alcalinos y la mayor sensibilidad se obtenían con el BGE NH_4Ac 25 mM (pH 8,0).

También se evaluó la composición del SL, empleando mezclas hidroorgánicas con propan-2-ol, MeOH y ACN al 60% y 80% (v/v). En el gráfico de barras de la **Figura 6.28** se muestra que la mejor sensibilidad se obtenía con el SL 80% (v/v) de propan-2-ol. También se evaluó la adición de NH_4OH (0,5% (v/v)) y NH_4Ac (1, 2, 5 y 10 mM) a este SL. En las condiciones optimizadas, se empleó el SL 80% (v/v) de propan-2-ol con 2 mM de NH_4Ac, el mismo SL empleado en un estudio anterior por uno de los colaboradores de este trabajo para el análisis de miRNAs por *sample stacking* CE-MS [127]. En estas condiciones, el LOD era 500 nM para ambos miRNAs.

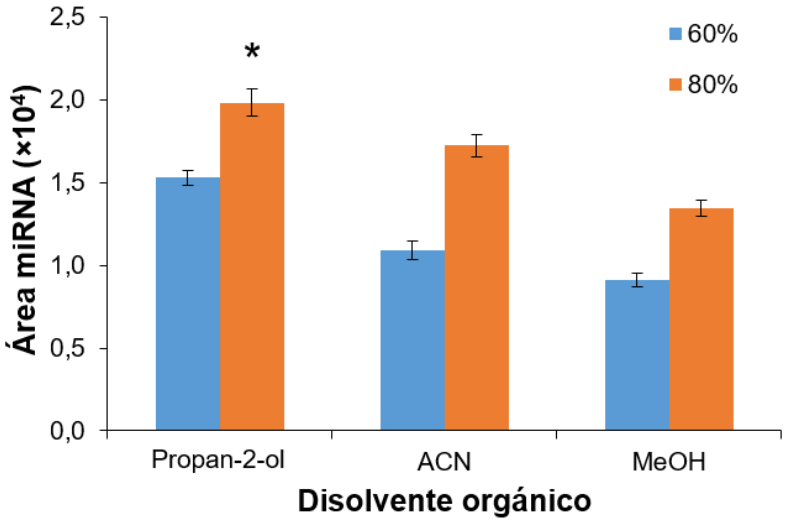

Figura 6.28. Efecto del disolvente orgánico en el líquido auxiliar coaxial en el análisis de un patrón de miR-21 de 5000 nM por CE-MS. Las barras de error indican la desviación estándar (n = 3). Las condiciones optimizadas se indican con un asterisco.

En la **Figura 6.29-A** se muestran los EIEs (i) y el espectro de masas (ii) para el análisis de un patrón 5000 nM de ambos miRNAs por CE-MS en las condiciones optimizadas. Los dos miRNAs comigraban, pero la excelente exactitud de masa (E_r <15 ppm, **Tabla 6.13-A**) y el poder de resolución del espectrómetro de masas permitieron obtener EIEs separados e identificar inequívocamente los miRNAs. En el espectro de masas, el ion más abundante era el $[M-5H]^{5-}$ en ambos casos, pero también se detectaban con cierta intensidad, a pesar de las precauciones tomadas, los aductos con Na^+ y K^+ ($[M-6H+Na]^{5-}$ y $[M-6H+K]^{5-}$).

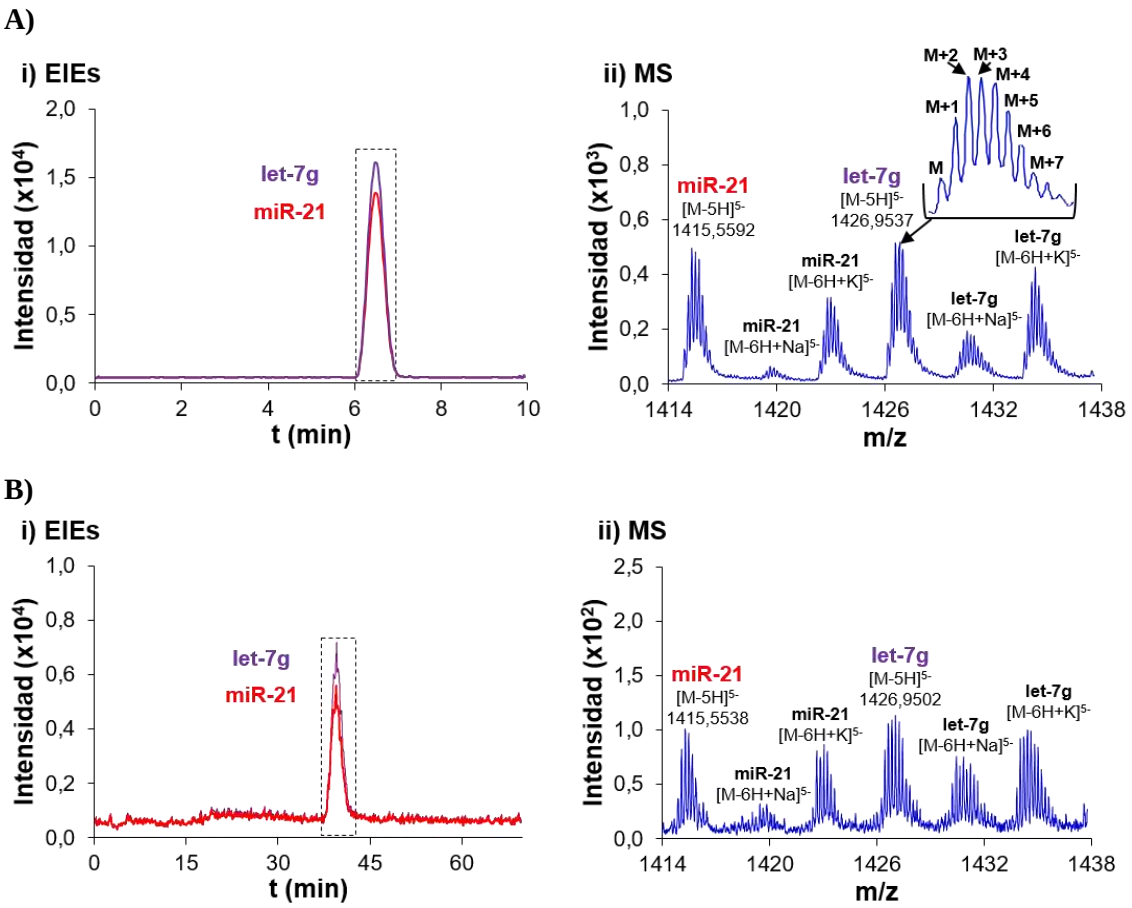

Figura 6.29. Análisis de un patrón de miR-21 y let-7g por (A) CE-MS (5000 nM) y (B) *sample stacking* CE-MS (250 nM). (i) EIEs y (ii) espectro de masas.

Antes de investigar el análisis de miRNAs mediante SiC-SPE-CE-MS, se adaptó a la instrumentación disponible en el laboratorio el método de *sample stacking* CE-MS indicado anteriormente [127]. Este método se basa en la diferencia de conductividad entre la muestra y el

BGE para conseguir una preconcentración electroforética en línea de los iones presentes en un gran volumen de muestra. Se usó un capilar de separación más largo que en CE-MS (158 cm L_T x 50 µm i.d. vs 72 cm L_T x 75 µm i.d.) y se inyectó un volumen mucho mayor (2200 nL vs 60 nL [107]) del patrón de miRNAs preparado en agua, entre dos volúmenes de BGE, de mayor conductividad. Al aplicar el voltaje de separación, la intensidad del campo eléctrico era mayor en la región de la muestra y, en consecuencia, los iones se enfocaban o apilaban durante la separación electroforética en la interfase entre la muestra y el BGE. Con este método de preconcentración electroforética se consiguió aumentar la eficacia e intensidad de los picos y, por lo tanto, mejorar el LOD. En la **Figura 6.29-B** se muestran los EIEs (i) y espectro de masas (ii) para el análisis por *sample stacking* CE-MS de un patrón de miR-21 y let-7g de 250 nM, una concentración que se encuentra por debajo del LOD del método de CE-MS. Como puede observarse, en *sample stacking* CE-MS, el t_m de los miRNAs era mucho mayor debido a la mayor longitud y menor i.d. del capilar de separación, lo que provoca una menor intensidad del campo eléctrico a lo largo del capilar, aplicando el mismo voltaje. Los miRNAs tampoco se pudieron separar por *sample stacking* CE-MS, hecho lógico teniendo en cuenta que la metodología se basa en el apilamiento de los iones de la muestra con el mismo tipo de carga. El LOD del método de *sample stacking* CE-MS era 50 nM, 10 veces menor que en CE-MS.

Como alternativa al método de *sample stacking* CE-MS, se investigó la SiC-SPE-CE-MS para el análisis de miRNAs.

6.2.4.2. Análisis de patrones de miRNAs por SiC-SPE-CE-MS

La construcción de los microcartuchos en este caso fue más complicada que en los casos descritos anteriormente. Esto se debía al pequeño tamaño de partícula del sorbente de SiC (1 µm < $d_{partícula}$ < 10 µm), que provocaba que las fritas convencionales empleadas en el **Artículo 3.4** no fueran adecuadas para evitar la fuga del sorbente empaquetado en el preconcentrador durante su uso. Para solucionar este problema y prevenir una contrapresión excesiva, fue necesario empaquetar preconcentradores con una sola frita de algodón en la salida.

En estudios preliminares se vio que el BGE optimizado para CE-MS, NH_4Ac 25 mM (pH 8,0), provocaba la elución parcial de los miRNAs retenidos en el sorbente de SiC durante la etapa de lavado y llenado del capilar. Por lo tanto, se evaluaron diferentes estrategias para minimizar la pérdida de los miRNAs retenidos en el sorbente de SiC, como cambios en la composición del BGE y en las disoluciones de lavado (adición de alcoholes o cloruro de guanidinio), pero ninguna de estas modificaciones ofreció buenos resultados. Por lo tanto, se decidió reducir el volumen de BGE utilizado para el lavado y llenado del capilar. Se evaluó el lavado con BGE a baja presión (100 mbar durante 3 min) y a elevada presión (930 mbar durante 40 s). La mejor sensibilidad se obtuvo con el lavado a elevada presión, que permitía minimizar la elución de los miRNAs y acortar la etapa de lavado y llenado del capilar.

También se optimizó la composición del eluyente. Se evaluaron mezclas hidroorgánicas con ACN o MeOH al 40%, 60% y 80% (v/v). Como se aprecia en la **Figura 6.30-A**, la mejor sensibilidad, así como la repetibilidad más adecuada, se obtenía con 60% (v/v) de ACN. En estas condiciones, no se detectó contaminación cruzada entre análisis.

Se investigó el tiempo de introducción de la muestra cargando a 930 mbar durante 3, 5, 10, 15 y 20 min un patrón de 35 nM de miR-21 y let-7g. Como se aprecia en la **Figura 6.30-B**, la mayor sensibilidad se obtenía cargando entre 5 y 15 min. Para tiempos de carga superiores a 15 min, se superaba el volumen de ruptura. Por lo tanto, para reducir el tiempo total de análisis y el consumo de la muestra, así como para obtener una sensibilidad adecuada, se seleccionó un tiempo de carga de 5 minutos.

En la **Figura 6.31** se muestran para un patrón de 50 nM de miR-21 y let-7g los EIEs (i) y el espectro de masas (ii) del análisis por SiC-SPE-CE-MS en las condiciones optimizadas. En comparación con el análisis por CE-MS (**Figura 6.29-A**), los t_m eran similares y la abundancia relativa de los aductos alcalinos también era parecida. A esta concentración, la repetibilidad era adecuada (%RSD (n = 3) en t_m y A_p de 2,8% y <6,5%), el método era lineal entre 25 y 100 nM (R^2 >0,97) y el LOD era 10 nM (50 veces menor que por CE-MS y 5 veces menor que por *sample stacking* CE-MS). Respecto a la durabilidad del microcartucho, también era muy adecuada y podían reutilizarse durante más de 25 análisis.

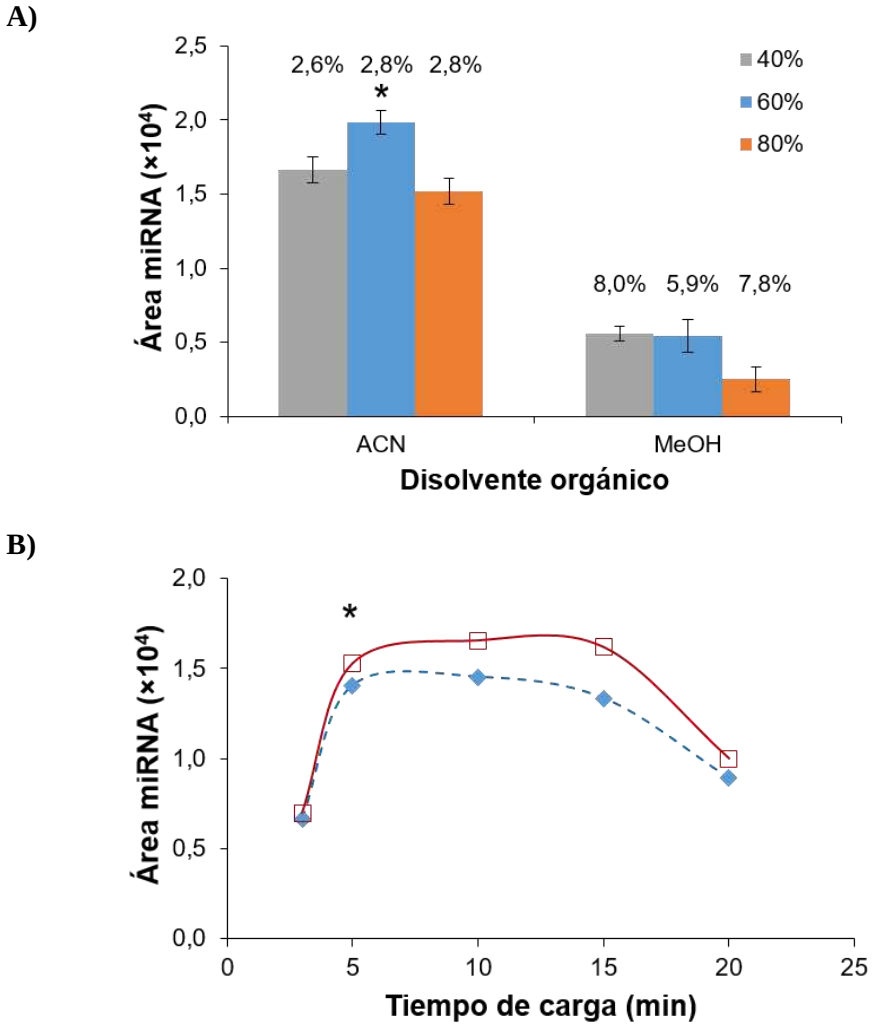

Figura 6.30. A_p de los miRNAs analizados por SiC-SPE-CE-MS (A) empleando diferentes eluyentes (patrón de 50 nM de miR-21, introducción de la muestra 5 min a 930 mbar) y (B) introduciendo la muestra durante diferentes valores de tiempo (3, 5, 10, 15 y 20 min) a 930 mbar (patrón de 35 nM de miR-21 (♦, azul) y let-7g (□, rojo)). Las barras de error indican la desviación estándar (n = 3) del A_p. Los números indican la %RSD del t_m. Las condiciones optimizadas se indican con un asterisco.

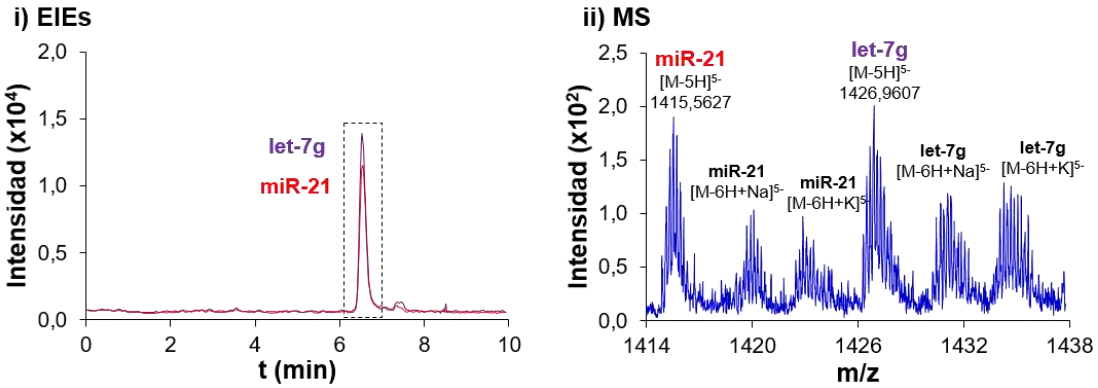

Figura 6.31. SiC-SPE-CE-MS para un patrón de 50 nM de miR-21 y let-7g. (i) EIEs y (ii) espectro de masas.

6.2.4.3. Análisis de miRNAs en suero humano por SiC-SPE-CE-MS

La metodología de SiC-SPE-CE-MS optimizada se empleó para el análisis de miRNAs en muestras de suero. Los miRNAs extracelulares que circulan en los fluidos biológicos son resistentes a la actividad de las RNasas, así como a las temperaturas y valores de pH extremos, porque se encuentran dentro de microvesículas o formando complejos con proteínas y lipoproteínas [41,51,328].

Para poder analizar los miRNAs del suero fue necesario aplicar pretratamientos a la muestra capaces de romper las membranas y complejos biológicos, inhibir la actividad de las RNasas y precipitar las proteínas [257]. Se evaluaron dos procedimientos ampliamente utilizados en la actualidad para purificar miRNAs de muestras biológicas, que están basados en el uso de las mezclas de tiocianato de guanidinio-fenol-cloroformo (Trizol^{TM}) [253,259] y fenol-cloroformo-alcohol isoamílico (PCA) [252,257]. Antes del análisis por SiC-SPE-CE-MS, fue necesario desalar los extractos ya que la gran abundancia de sales en la muestra comprometía el desempeño de la metodología. Para ello, se utilizaron membranas de microdiálisis que permitieron desalar los pequeños volúmenes de muestra disponibles de manera simple, rápida y efectiva [329]. A causa de la baja concentración de los miRNAs en el suero, el pretratamiento de muestra se optimizó fortificando muestras de suero de controles sanos con los patrones de miRNAs sintéticos. El método de extracción basado en el uso de Trizol^{TM} mostró una compatibilidad limitada con la SiC-SPE-CE-MS a causa de la elevada concentración de la sal caotrópica tiocianato de guanidinio en este reactivo. En cambio, el método de extracción basado en el uso de la mezcla PCA demostró mejores resultados. Las recuperaciones para los patrones de miRNAs eran elevadas, de aproximadamente 85%, comparando el análisis por SiC-SPE-CE-MS de un patrón de 50 nM y una muestra de suero de un control sano fortificada a la misma concentración. A esta concentración, la repetibilidad era adecuada (%RSD (n = 3) en t_m y A_p de 3,9% y ≤7,6%) y el LOD aproximadamente 10 nM, valor similar al obtenido en el análisis de patrones. Sin embargo, la durabilidad de los preconcentradores disminuía ligeramente, hasta los 20 análisis.

En la **Figura 6.32-A** se muestra el análisis por SiC-SPE-CE-MS de una muestra de suero de un control sano sin fortificar. Como puede comprobarse, no se detectaron miRNAs porque, en

general, la concentración de éstos es extremadamente baja en el suero de individuos sanos [127]. En cambio, se ha descrito la sobreexpresión de ciertos miRNAs en el suero de pacientes de diferentes tipos de cáncer [51], como por ejemplo, la leucemia linfocítica crónica (CLL) [97,330]. En la **Figura 6.32-B** se muestran los EIEs (i) y el espectro de masas (ii) del análisis por SiC-SPE-CE-MS de una muestra de suero de un paciente de CLL. Como puede observarse, en este caso, se detectaban dos miRNAs a una concentración cercana al LOD, que se identificaron como el miR-21 y el hsa-miR-16-5p con una uridilación en 3' (iso-miR-16) (E_r <20 ppm, **Tabla 6.13-B**). La presencia de estos dos miRNAs se confirmó analizando las muestras de suero fortificadas (**Figura 6.32-C**). Estos mismos miRNAs fueron también detectados en muestras de suero de pacientes de CLL mediante *sample stacking* CE-MS y confirmados por PCR cuantitativa con transcriptasa inversa (RT-qPCR), tal y como se recoge en la literatura [127].

Los resultados demuestran el gran potencial de la SiC-SPE-CE-MS para el análisis de miRNAs y sus modificaciones postranscripcionales en fluidos biológicos. Sin embargo, debido a la baja concentración de los miRNAs en los fluidos biológicos, es necesario investigar procedimientos que permitan disminuir aún más el LOD. Por ejemplo, sería necesario evaluar otros sorbentes que presenten una mayor capacidad de retención, aditivos que mejoren la señal de los miRNAs en ESI- o que permitan su separación electroforética y así evitar la supresión de la ionización y pretratamientos de la muestra para preconcentrar fracciones ricas en miRNAs, como las microvesículas.

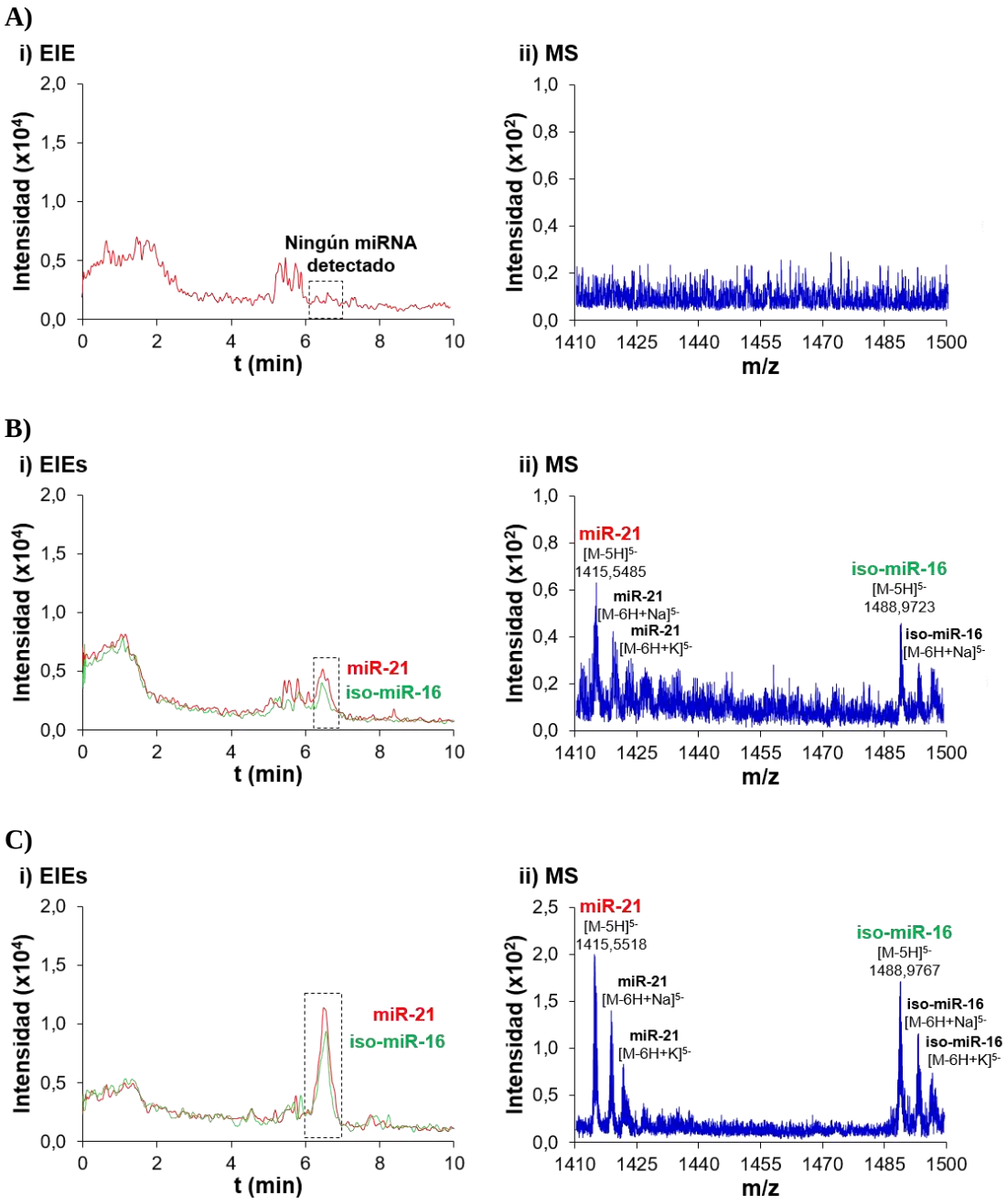

Figura 6.32. SiC-SPE-CE-MS para muestras de suero de un (A) control sano, (B) paciente de leucemia linfocítica crónica (CLL) y (C) paciente de CLL, fortificada con 50 nM del patrón de miR-21 y iso-miR-16. (i) EIEs y (ii) espectros de masas.

6.2.5. Comparativa de las metodologías de SPE-CE-MS unidireccional

A modo de resumen, en la **Tabla 6.14-A** se recogen, para las diferentes metodologías de SPE-CE-MS unidireccional desarrolladas en esta tesis, las condiciones optimizadas y los parámetros de calidad para el análisis de patrones. Para la detección de péptidos y proteínas en MS en ESI+, la mejor sensibilidad se obtuvo usando BGEs volátiles ácidos con HAc y/o HFor, como es el caso del BGE HAc 100 mM (pH 2,9) empleado en AA-SPE-CE-MS. Sin embargo, dado que los sorbentes de IA e IMA son lábiles si se exponen durante largos períodos de tiempo a condiciones ácidas, en IA-SPE-CE-MS e IMA-SPE-CE-MS se usaron BGEs de baja concentración y pH neutro volátiles (NH_4Ac 10 mM (pH 7,0)) o menos volátiles (H_3PO_4 25 mM (pH 7,5)). Para el análisis de miRNAs en ESI-, se empleó el BGE NH_4Ac 25 mM (pH 8,0), que resultó muy apropiado para una adecuada separación electroforética y detección por MS pero que, como ya se ha discutido anteriormente, provocaba una elución parcial de los miRNAs retenidos en el sorbente de SiC durante la etapa de lavado y llenado del capilar, por lo que se debió minimizar la duración de esta etapa. Estos resultados demuestran que la propia configuración unidireccional, aunque extremadamente sencilla de implementar, representa una dificultad a la hora de compatibilizar los requerimientos necesarios para conseguir una preconcentración en línea adecuada, una separación eficaz por CE y una detección sensible por MS.

En las cuatro metodologías, la muestra se introdujo a 930 mbar durante 5 o 10 minutos (30 y 60 µL [107], respectivamente), ya que para tiempos de carga superiores se excedía el volumen de ruptura. Este volumen depende de las propiedades del analito y del sorbente, pero también está condicionado por la limitada cantidad de sorbente en el preconcentrador. Como compromiso entre la capacidad de preconcentración y la contrapresión provocada por la presencia del microcartucho empaquetado en el capilar de separación en SPE-CE-MS unidireccional, en todos los casos se empleó un microcartucho de 250 µm i.d. y entre 0,7 y 0,9 cm de L_T, lo que equivale a un volumen inferior a 500 nL para alojar el sorbente, que en cada caso tenía un tamaño de partícula y porosidad diferente. En el futuro, debe incrementarse la superficie activa de los sorbentes para mejorar su

capacidad de retención, permitiendo cargar volúmenes de muestra más grandes sin exceder el volumen de ruptura y aumentar los factores de preconcentración conseguidos.

En tres de las metodologías, la elución de los analitos se basó en un cambio en el pH del eluyente respecto al BGE. En IA-SPE-CE-MS y AA-SPE-CE-MS se empleó el mismo eluyente básico (NH_4OH 100 mM (pH 11,2)) para eluir las proteínas intactas, pero en el segundo caso fue necesario inyectar un volumen mayor (50 vs 100 nL [107]), lo que podría indicar una mayor fuerza de las interacciones entre la α-syn y el aptámero que entre la TTR y el anticuerpo. En IMA-SPE-CE-MS fue necesario inyectar un volumen de eluyente ácido mucho mayor que éstos (400 nL [107] de 0,5% (v/v) de HAc) para desorber los His-peptides mediante la protonación de los grupos imidazol de los residuos de histidina. En un trabajo previo del grupo de investigación empleando el mismo sorbente [191], se vio que el eluyente imidazol 50 mM, que desorbe los His-peptides mediante un mecanismo de desplazamiento, presentaba una mayor fuerza de elución pero no era compatible con la detección por MS. En SiC-SPE-CE-MS se empleó un eluyente hidroorgánico (60% (v/v) de ACN) para desorber los miRNAs. Es el único caso en que el uso de disolventes orgánicos permitió mejorar significativamente la elución.

En todos los casos el intervalo de linealidad era relativamente estrecho (entre uno y dos órdenes de magnitud), hecho habitual en las metodologías de SPE-CE-MS unidireccional [173,191,201,202] debido a la limitada cantidad de sorbente en el preconcentrador. Los LODs eran del orden de µg/mL y los factores de preconcentración presentaban valores entre 25 y 100 respecto a CE-MS. En estudios anteriores del grupo de investigación [201,202], para el análisis de neuropéptidos por IA-SPE-CE-MS se obtuvieron factores de preconcentración de entre 100 y 200 respecto a CE-MS. Considerando que en las metodologías desarrolladas en esta tesis se han analizado biomarcadores mucho más complejos, es decir, proteínas intactas, digestos trípticos y oligonucleótidos de M_r relativamente elevada, los valores de LODs y factores de preconcentración obtenidos son muy apropiados. En cuanto a la durabilidad de los preconcentradores, era adecuada en la mayoría de casos (≥20 análisis). La menor durabilidad de los preconcentradores de IMA-SPE-CE-MS puede deberse a la pérdida de los cationes metálicos del sorbente, que no se encuentran enlazados covalentemente. Globalmente, son especialmente remarcables los

resultados obtenidos mediante AA-SPE-CE-MS para la α-syn, lo que augura un gran recorrido para los sorbentes de AA en SPE-CE-MS.

En la **Tabla 6.14-B** se resumen las condiciones del análisis de muestras biológicas. Por IMA-SPE-CE-MS se analizó un lisado celular de *E. coli*. El único pretratamiento necesario fue la reducción y alquilación de las proteínas para poder digerirlas eficazmente y no se apreciaron inconvenientes respecto al análisis de las proteínas patrón. En el resto de metodologías se analizaron muestras derivadas de la sangre y fue necesario aplicar pretratamientos sencillos para eliminar las proteínas mayoritarias como, por ejemplo, la hemoglobina, o para evitar la saturación del sorbente y la obturación del capilar de separación, debido a la complejidad de la matriz de la muestra. Los miRNAs del suero se extrajeron con la mezcla PCA. Dado que mediante este pretratamiento se conseguía una elevada purificación de los miRNAs y precipitaban cuantitativamente las proteínas del suero, el único inconveniente en el análisis de estas muestras respecto a los patrones fue una ligera disminución de la durabilidad del preconcentrador (20 vs ≥25 análisis). En cambio, en el análisis de la TTR en muestras de suero y de la α-syn en eritrocitos la disminución de la durabilidad del preconcentrador era más acentuada, reduciéndose hasta la mitad en comparación al análisis de patrones (10 vs 20 análisis). Además, incluso con los pretratamientos empleados para precipitar las proteínas mayoritarias de la muestra, al cargar la muestra la pared interna del capilar de separación se modificaba irreversiblemente a causa de la adsorción de los componentes de la matriz. Dado que en SPE-CE-MS unidireccional la introducción de la muestra y los lavados tienen lugar en la misma dirección que la posterior separación, para evitar esta modificación se deberían investigar pretratamientos de purificación de las proteínas de interés aún más selectivos o el uso de capilares recubiertos que prevengan la adsorción de los componentes de la matriz de la muestra en la pared interna del capilar de separación.

Tabla 6.14-A. Metodologías de SPE-CE-MS unidireccional desarrolladas en esta tesis. Condiciones optimizadas y parámetros de calidad en el análisis de patrones.

Metodología	Analito	Modo ESI	BGE	Carga de muestra (a 930 mbar)	Inyección eluyente	Linealidad (µg/mL)	LOD (µg/mL)	Factor de preconcentración	Durabilidad preconcentrador (análisis)
IA-SPE-CE-MS	TTR	+	NH_4Ac 10 mM (pH 7,0)	10 min (60 µL) [a]	50 mbar 10 s (50 nL) [a] NH_4OH 100 mM (pH 11,2)	5-25	1	25 [d]	20
AA-SPE-CE-MS	α-syn	+	HAc 100 mM (pH 2,9)	5 min (30 µL) [a]	50 mbar 20 s (100 nL) [a] NH_4OH 100 mM (pH 11,2)	0,5-10	0,2	100 [d]	20
IMA-SPE-CE-MS	His-peptides	+	H_3PO_4 25 mM (pH 7,5)	10 min (60 µL) [a]	50 mbar 75 s (400 nL) [a] 0,5% (v/v) HAc	20-100 [b]	20 [b]	25-100 [e]	10
SiC-SPE-CE-MS	miRNAs	-	NH_4Ac 25 mM (pH 8,0)	5 min (30 µL) [a]	50 mbar 10 s (50 nL) [a] 60% (v/v) ACN	25-100 [c]	10 [c]	50 [d]	25

a) Calculado empleando la ecuación de Hagen–Poiseuille [107].

b) Para el His-peptide α-CSN1[4-7] (concentración de proteína digerida).

c) nM (25-100 nM ~0,18-0,70 µg/mL; 10 nM ~0,07 µg/mL).

d) Calculado dividiendo el valor del LOD del análisis por CE-MS entre el de SPE-CE-MS, empleando el mismo BGE y SL.

e) Calculado para los His-peptides detectados en un digesto tríptico de α-CSN dividiendo el valor del A_p del análisis por CE-MS entre el A_p de SPE-CE-MS, empleando el mismo BGE, SL y concentración de proteína digerida.

Tabla 6.14-B. Metodologías de SPE-CE-MS unidireccional desarrolladas en esta tesis. Análisis de muestras biológicas.

Metodología	Analito	Muestra biológica	Sin pretratamiento	Pretratamiento	Modificación pared interna capilar de separación	Durabilidad preconcentrador (análisis)
IA-SPE-CE-MS	TTR	Suero humano	Saturación del sorbente y obturación del capilar	5% (v/v) de fenol	Permanente	10
AA-SPE-CE-MS	α-syn	Eritrocitos humanos	Únicamente se detectaba la hemoglobina	Tratamiento térmico	Permanente	10
IMA-SPE-CE-MS	His-peptides	Lisado celular de *E. coli*	No procede	Reducción, alquilación y digestión tríptica	No observada	10
SiC-SPE-CE-MS	miRNAs	Suero humano	Saturación del sorbente y obturación del capilar	PCA	No observada	20

6.3. SPE-CE-MS con una válvula para la mejora de la sensibilidad y la selectividad

La SPE-CE-MS unidireccional es una excelente estrategia para el análisis de moléculas biomarcadoras en fluidos biológicos, como se ha demostrado en el **Apartado 6.2** para la TTR y los miRNAs en suero (**Artículos 3.2** y **3.5**, respectivamente) y la α-syn en eritrocitos (**Artículo 3.3**). Sin embargo, esta sencilla configuración presenta algunas limitaciones intrínsecas. Por un lado, los volúmenes de muestra introducidos mediante presión dependen de las dimensiones del capilar de separación. Por otro lado, la introducción de la muestra, los lavados y el llenado del capilar con BGE antes de la elución de los compuestos retenidos tienen lugar en la misma dirección que la posterior separación. Por tanto, al cargar una muestra biológica compleja o durante la etapa de lavado posterior, los componentes de la matriz de la muestra pueden modificar irreversiblemente la pared interna del capilar, como se ha puesto de manifiesto en esta tesis en los análisis de muestras derivadas de la sangre (**Apartado 6.2**). Además, en muchos casos, los requisitos de la preconcentración en línea son incompatibles con el BGE necesario para una separación eficaz por CE y una detección sensible por MS.

Este capítulo se centra en investigar el potencial de la SPE-CE-MS con una nanoválvula (nvSPE-CE-MS) para solucionar estos inconvenientes. En este novedoso diseño se emplea un solo instrumento de CE y dos capilares acoplados mediante una válvula de 20 nL aislada eléctricamente, para realizar la preconcentración en línea y la separación electroforética de forma independiente y ortogonal (**Artículo 4.1)**. En primer lugar, se evaluó y optimizó el análisis de una serie de péptidos opioides y péptidos Aβ por CE-MS. A continuación, se adaptó a la nueva instrumentación un método de SPE-CE-MS unidireccional empleando un sorbente C18 [301]. Finalmente, se desarrolló un método de nvSPE-CE-MS y se compararon las ventajas e inconvenientes respecto a la SPE-CE-MS unidireccional.

6.3.1. Análisis de patrones de péptidos opioides y Aβ por CE-MS

En el **Apartado 6.1**, se ha demostrado que el criterio de calidad T' permite seleccionar el pH óptimo para la separación electroforética de una mezcla de analitos si se dispone de valores de pK_a apropiados. En un trabajo anterior del grupo de investigación [279], se determinaron por CE los valores de pK_a de los péptidos opioides. En la **Figura 6.33-A** se representa T'($q/M_r^{1/2}$) calculado empleando estos valores de pK_a en función del pH del BGE para la mezcla de los péptidos opioides dinorfina A (1-7) (Dyn A), endomorfina 1 (End 1) y Met-encefalina (Met).

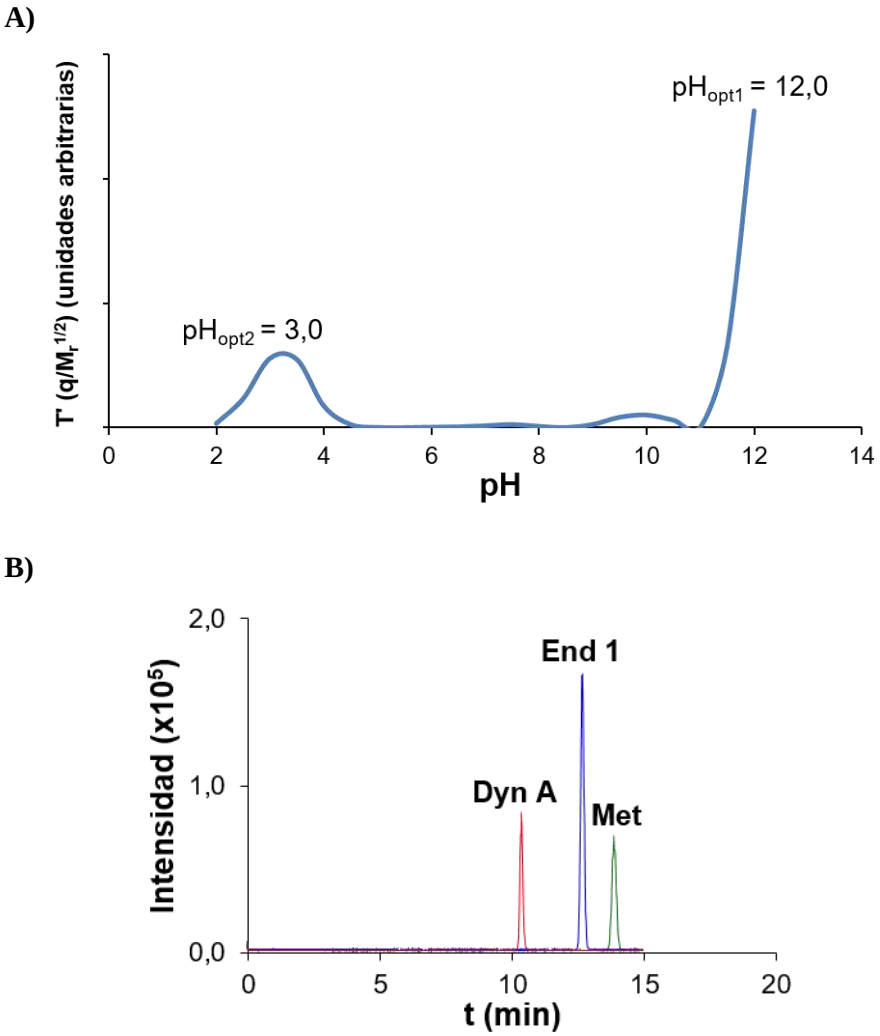

Figura 6.33. Separación de una mezcla de los péptidos opioides Dyn A, End 1 y Met. (A) Representación de T'($q/M_r^{1/2}$) calculado a partir de los valores de $q/M_r^{1/2}$ usando pK_as bibliográficos [279] en función del pH del BGE y (B) EIEs en las condiciones de CE-MS optimizadas para una mezcla de 10 µg/mL de los péptidos opioides (dimensiones del capilar de separación 72 cm L_T x 50 µm i.d., BGE HAc 50 mM:HFor 50 mM (pH 3,0, ajustado con NH_4OH)).

A partir de esta representación se dedujo que las mejores separaciones se obtenían a pH 3,0 en la región de pH ácido y a pH 12,0 en la región de pH básico. Como ya se ha indicado en el **Apartado 6.1**, T' no tiene en cuenta la influencia del EOF, que afecta negativamente a las separaciones, especialmente a pH básicos en capilares de sílice fundida. Dado que los BGEs volátiles ácidos suelen ser adecuados para minimizar la adsorción de los péptidos en la pared interna del capilar y obtener una sensibilidad adecuada en los análisis por CE-MS en ESI+, se seleccionó para el análisis por CE-MS de estos péptidos opioides el BGE HAc 50 mM:HFor 50 mM (pH 3,0, ajustado con NH_4OH) en combinación con un SL de 60:40 (v/v) propan-2-ol:agua con 0,05% (v/v) de HFor. En la **Tabla 6.15** se muestran los valores de m/z de los iones moleculares detectados en estas condiciones para los tres péptidos opioides y en la **Figura 6.33-B**, los EIEs para una mezcla de 10 µg/mL de los péptidos opioides en las condiciones de CE-MS optimizadas. En estas condiciones, se obtenía una buena separación de los analitos y la repetibilidad de los análisis era adecuada (%RSD (n = 3) en t_m y A_p de ≤2,7% y ≤10% (**Tabla 6.16**)). El LOD era de 100 pg/mL (**Tabla 6.15**), valor que era similar al obtenido en anteriores trabajos del grupo de investigación [301,331].

La optimización de la separación de los péptidos Aβ 1-15, 10-20, 20-29, 25-35 y 33-42 por CE se ha presentado en el **Apartado 6.1** de esta tesis doctoral. El pH de separación óptimo también era 3,0 (**Figuras 6.4** y **6.7**). En la **Figura 6.34** se muestran en las condiciones de CE-MS optimizadas los EIEs para una mezcla de 10 µg/mL de los fragmentos de los péptidos Aβ, excepto el Aβ 33-42, que no se usó en este nuevo estudio a causa de su limitada solubilidad en agua. A esta concentración, la repetibilidad de los análisis era similar a la obtenida para los péptidos opioides (%RSD (n = 3) en t_m y A_p de ≤1,3% y ≤11% (**Tabla 6.16**)). Sin embargo, el LOD (entre 500 y 1500 pg/mL) era ligeramente superior, probablemente a causa del mayor tamaño de los fragmentos de los péptidos Aβ (**Tabla 6.15**).

Tabla 6.15. M_r y m/z de los iones moleculares de los péptidos opioides y los fragmentos de péptidos Aβ. LODs por CE-MS, SPE-CE-MS unidireccional y nvSPE-CE-MS.

Péptido	M_r	$[M+nH]^{n+}$		LOD para los patrones (pg/mL)			LOD para las muestras de plasma fortificado (pg/mL)	
		m/z	n	CE	SPE-CE [a]	nvSPE-CE	SPE-CE [a]	nvSPE-CE
Dyn A	867,4715	434,7430	2	100	0,1	0,5	10	10
End 1	610,2904	611,2976	1	100	0,05	0,5	1	5
Met	573,2257	574,2330	1	100	0,1	0,5	1	1
Aβ 1-15	1825,7768	457,4515; 609,5996	4, 3	1500	-	5	-	10
Aβ 10-20	1445,7456	482,9225; 723,8801	3, 2	500	-	5	-	50
Aβ 20-29	1022,4669	512,2407	2	1000	-	5	-	10
Aβ 25-35	1059,5747	530,7946	2	500	-	5	-	10

a) Los fragmentos de péptidos Aβ no se analizaron por SPE-CE-MS unidireccional (-).

Tabla 6.16. Repetibilidad (%RSD (n = 3) en t_m y A_p) para el análisis de los péptidos opioides y los fragmentos de péptidos Aβ por CE-MS, SPE-CE-MS unidireccional y nvSPE-CE-MS.

Péptido	t_m					A_p				
	Patrones			Muestras de plasma fortificado		Patrones			Muestras de plasma fortificado	
	CE [a]	SPE-CE [b]	nvSPE-CE [b]	SPE-CE [c]	nvSPE-CE [c]	CE [a]	SPE-CE [b]	nvSPE-CE [b]	SPE-CE [c]	nvSPE-CE [c]
Dyn A	2,7	1,2	1,4	4,0	5,9	8,7	11	11	11	13
End 1	1,7	1,6	2,4	3,7	4,2	10	6,9	11	13	5,3
Met	1,5	1,4	2,4	4,6	4,7	10	12	9,0	11	5,6
Aβ 1-15	1,0	-	1,8	-	2,7	11	-	12	-	5,1
Aβ 10-20	1,1	-	2,7	-	2,9	10	-	8,8	-	13
Aβ 20-29	0,92	-	2,4	-	4,0	7,4	-	5,3	-	8,3
Aβ 25-35	1,3	-	2,4	-	3,3	8,0	-	9,0	-	8,7

Análisis a

a) 10 µg/mL.

b) 1 pg/mL para los péptidos opioides y 10 pg/mL para los fragmentos de péptidos Aβ (no se analizaron por SPE-CE-MS unidireccional (-)).

c) 10 pg/mL para los péptidos opioides y 50 pg/mL para los fragmentos de péptidos Aβ.

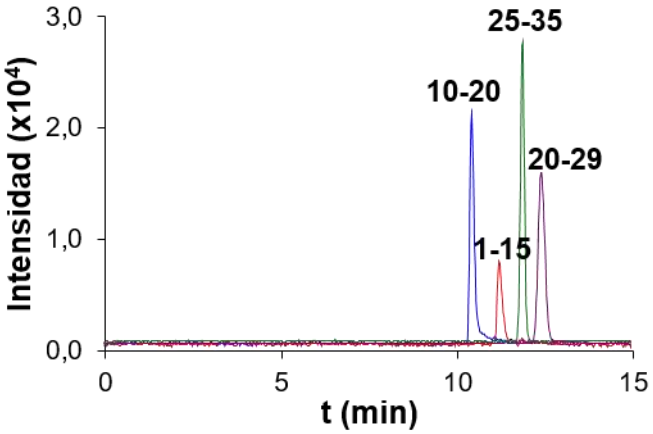

Figura 6.34. EIEs en las condiciones de CE-MS optimizadas para una mezcla de 10 µg/mL de los péptidos Aβ 1-15, 10-20, 20-29 y 25-35 (dimensiones del capilar de separación 72 cm L_T x 50 µm i.d., BGE HAc 50 mM:HFor 50 mM (pH 3,0, ajustado con NH_4OH)).

6.3.2. Análisis de péptidos opioides por SPE-CE-MS unidireccional

En trabajos previos de nuestro grupo de investigación se desarrolló un método para el análisis de los péptidos opioides por SPE-CE-MS unidireccional con un sorbente C18 [165,194,301]. En el presente trabajo, para posteriormente poder comparar adecuadamente la SPE-CE-MS unidireccional y la nvSPE-CE-MS, este método se evaluó empleando la nueva instrumentación disponible. En la **Figura 6.35-A** se muestran los EIEs para una mezcla de 1 pg/mL de los péptidos opioides por SPE-CE-MS unidireccional empleando como BGE HAc 50 mM:HFor 50 mM a (pH 3,0) y como eluyente 60:40 (v/v) MeOH:H_2O con HAc 50 mM:HFor 50 mM. Comparando con los EIEs de CE-MS (**Figura 6.33-B**), se obtuvieron picos ligeramente más anchos debido al uso de un capilar con mayor diámetro interno en SPE-CE-MS unidireccional (75 vs 50 µm id), pero los tres picos se separaban a línea de base y la repetibilidad era similar (%RSD (n = 3) en t_m y A_p de ≤1,6% y ≤12% (**Tabla 6.16**)). El LOD estaba en torno a 0,1 pg/mL (**Tabla 6.15**), una mejora de 1000 veces comparado con CE-MS.

Para el análisis de muestras de plasma se requirió un pretratamiento basado en una precipitación con ACN seguida de una ultrafiltración para evitar la obturación del capilar a causa de la saturación del sorbente C18 e inestabilidad en la corriente [167]. En la **Figura 6.35-B** se muestran los EIEs para una muestra de plasma fortificado a 10 pg/mL con los tres péptidos

opioides. Comparado con el análisis de patrones (**Figura 6.35-A**), la resolución de la separación y la repetibilidad en A_p eran similares (%RSD (n = 3) ≤13% (**Tabla 6.16**)), pero ligeramente menor en t_m (≤4,6%). El LOD era 1 pg/mL para la End 1 y la Met (**Tabla 6.15**), lo que suponía un incremento en torno a 10 veces debido a la complejidad de la matriz de la muestra. Este incremento era aún mayor para el LOD de la Dyn A (10 pg/mL) ya que era el péptido de mayor tamaño y la recuperación del pretratamiento de muestra era menor [167]. Las diferencias observadas para el análisis de plasma respecto al análisis de patrones estaban de acuerdo con los trabajos previos del grupo de investigación [165,194,301].

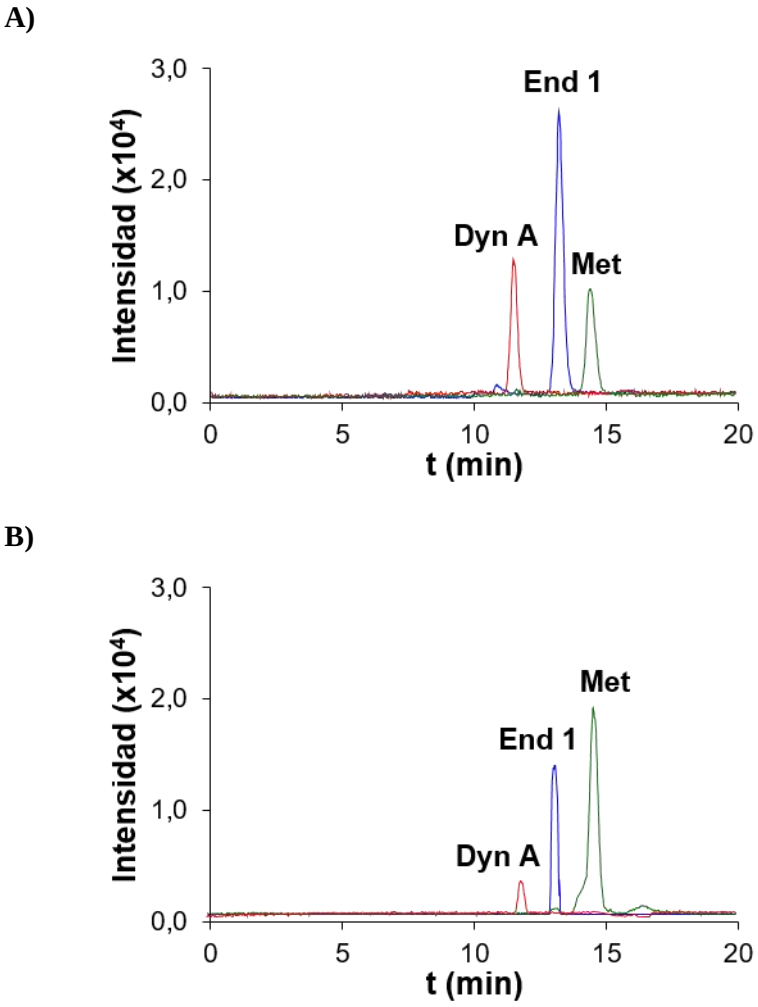

Figura 6.35. EIEs en las condiciones de SPE-CE-MS unidireccional optimizadas para una mezcla de péptidos opioides (dimensiones del capilar de separación 72 cm L_T x 75 µm i.d., BGE HAc 50 mM:HFor 50 mM (pH 3,0, ajustado con NH_4OH) y eluyente 60:40 (v/v) MeOH:H_2O con HAc 50 mM:HFor 50 mM) [301]. (A) Patrones de 1 pg/mL y (B) muestra de plasma fortificado a 10 pg/mL.

6.3.3. Análisis de péptidos opioides y Aβ por nvSPE-CE-MS

Los detalles del dispositivo instrumental necesario para nvSPE-CE-MS se describen detalladamente en la introducción de esta tesis doctoral. En la posición de carga (**Figura 1.15-i, página 51**) se llevan a cabo la introducción de la muestra en el capilar de carga que contiene el preconcentrador y, posteriormente, el lavado del capilar. A continuación, se inyecta el eluyente, que se moviliza mediante presión empujando con una disolución apropiada, y los analitos eluidos se transfieren al capilar de separación cambiando la posición de la válvula. En la posición de separación (**Figura 1.15-ii**), se aplica el voltaje y los analitos se separan y detectan mediante CE-MS.

Para optimizar la metodología de nvSPE-CE-MS se tomaron como punto de partida las condiciones optimizadas para el análisis de los péptidos opioides por SPE-CE-MS unidireccional. En estudios preliminares realizados por nvSPE-CE-MS se observó que para eluir los tres péptidos opioides era necesario inyectar eluyente a 70 mbar durante al menos 30 s, en lugar de a los 50 mbar y 10 s habituales en SPE-CE-MS unidireccional. Este hecho podría estar relacionado con un incremento de la contrapresión a causa del uso de la válvula.

En primer lugar, se investigó y caracterizó el perfil de elución de los péptidos analizando diversos *heart-cuts* (cortes o fracciones) consecutivos de 20 nL, correspondientes al volumen interno de la válvula. En la **Figura 6.36-A** se muestra el perfil de elución de los péptidos opioides por nvSPE-CE-MS empleando el eluyente optimizado para la SPE-CE-MS unidireccional (60:40 (v/v) MeOH:H_2O con HAc 50 mM:HFor 50 mM). Como se aprecia, en los dos primeros *heart-cuts* se detectaba mayoritariamente Dyn A, lo que indicaba que ésta se eluía más rápidamente que la End 1 y la Met. Estas dos se detectaban principalmente en los *heart-cuts* tercero y cuarto. Para eluir los péptidos opioides más rápidamente, se investigó una composición de eluyente con mayor fuerza eluotrópica. En la **Figura 6.36-B** se muestra el perfil de elución de los péptidos opioides por nvSPE-CE-MS empleando el eluyente 80:20 (v/v) ACN:H_2O con HAc 50 mM:HFor 50 mM. En este caso, los péptidos se eluían en una zona más estrecha y más del 85% de sus A_p se detectaban en los *heart-cuts* segundo y tercero. Sin embargo, a causa del limitado volumen del

bucle interno de la válvula, en ningún caso fue posible transferir cuantitativamente los analitos eluidos en un solo *heart-cut*, por lo que se seleccionó este último eluyente para el resto de los análisis.

A)

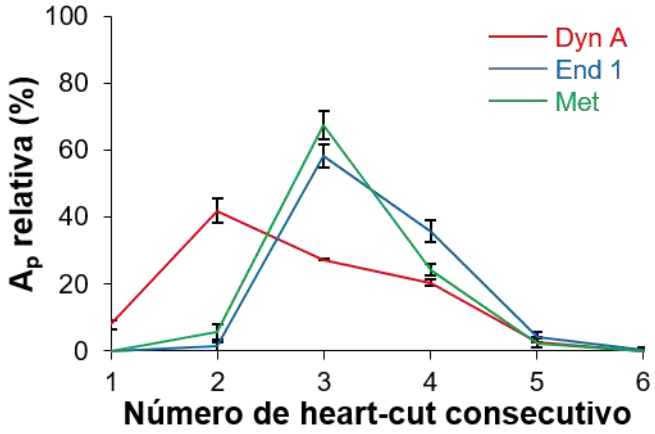

B)

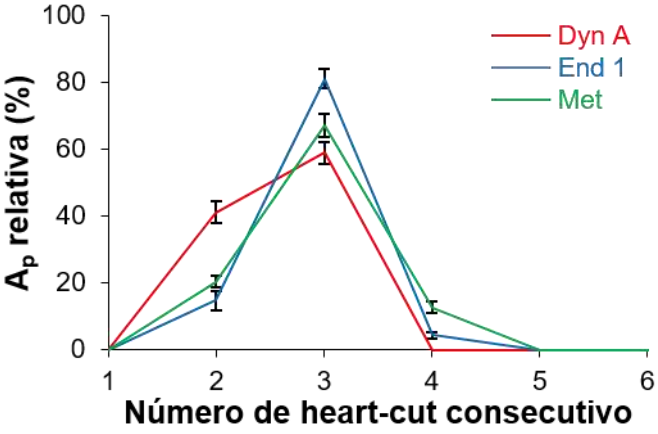

Figura 6.36. Caracterización del perfil de elución de los péptidos opioides mediante el análisis de varios *heart-cuts* consecutivos en nvSPE-CE-MS y usando diferentes eluyentes que contienen HAc 50 mM:HFor 50 mM y (A) 60% (v/v) MeOH y (B) 80% (v/v) ACN. El porcentaje de A_p relativa se calculó normalizando respecto al sumatorio de las A_p de todos los análisis para el péptido en consideración (n = 3).

En la **Figura 6.37-A** se muestran en las condiciones de elución optimizadas los EIEs para una mezcla de 1 pg/mL de los péptidos opioides. Comparado con la SPE-CE-MS unidireccional (**Figura 6.35-A**), el tiempo total de análisis era menor, principalmente a causa de la menor distancia de separación (L_D 45 cm (desde el puerto C de la válvula hasta ESI-MS, **Figura 1.15-i**)

vs 72 cm (**Figura 1.14, página 49**)) y los picos eran más estrechos a causa del menor i.d. del capilar (50 vs 75 µm i.d.). La repetibilidad era similar (%RSD (n = 3) en t_m y A_p de ≤2,4% y ≤11% (**Tabla 6.16**)) y el LOD (0,5 pg/mL, **Tabla 6.15**) 200 veces menor que por CE-MS, pero 5 veces mayor que por SPE-CE-MS unidireccional.

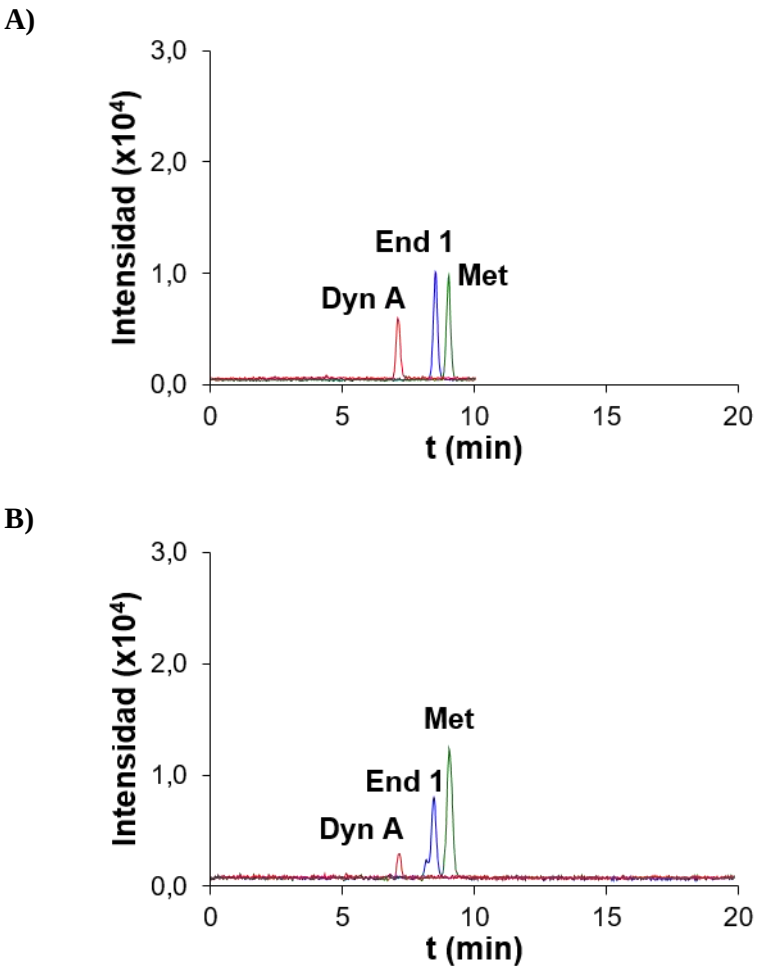

Figura 6.37. EIEs en las condiciones de nvSPE-CE-MS optimizadas para una mezcla de péptidos opioides (dimensiones del capilar de separación 100 cm L_T (45 cm L_D) x 50 µm i.d., BGE HAc 50 mM:HFor 50 mM (pH 3,0, ajustado con NH_4OH) y eluyente 80:20 (v/v) ACN:H_2O con HAc 50 mM:HFor 50 mM). (A) Patrones de 1 pg/mL y (B) muestra de plasma fortificado a 10 pg/mL.

El método establecido también se evaluó para el análisis de muestras de plasma pretratadas. En la **Figura 6.37-B** se muestran los EIEs por nvSPE-CE-MS para una muestra de plasma fortificado con los tres péptidos a 10 pg/mL. Comparado con el análisis de muestras de plasma por SPE-CE-MS unidireccional (**Figura 6.35-B**), se obtuvieron valores similares de repetibilidad

en t_m y A_p (%RSD (n = 3) ≤5,9% y ≤13% (**Tabla 6.16**)) y LOD (entre 1 y 10 pg/mL; **Tabla 6.15**). Como se puede observar en la **Tabla 6.15**, comparando el análisis de muestras de plasma y de patrones por nvSPE-CE-MS, el LOD se incrementaba menos que por SPE-CE-MS unidireccional (por ejemplo, 2 vs 10 veces para la Met). Así, los LODs de ambas metodologías para las muestras de plasma eran similares, lo que en conjunto podría indicar un menor efecto de la matriz de la muestra en el análisis por nvSPE-CE-MS, debido a la segregación de los capilares de carga y de separación.

Para incrementar la validez del método de nvSPE-CE-MS establecido para el análisis de péptidos opioides, se investigó el análisis de los fragmentos de los péptidos Aβ por nvSPE-CE-MS. En la **Figura 6.38-A** se muestran los EIEs para una mezcla de 10 pg/mL de los péptidos Aβ 1-15, 10-20, 20-29 y 25-35. Comparado con el análisis por CE-MS (**Figura 6.34**), el A_p relativa del péptido Aβ 10-20 era menor, probablemente a causa de una menor retención en el sorbente C18 que para el resto de fragmentos de los péptidos Aβ. La repetibilidad en t_m y A_p era similar (%RSD (n = 3) ≤2,7% y ≤12% (**Tabla 6.16**)) y el LOD era 5 pg/mL (**Tabla 6.15**), entre 100 y 300 veces menor que por CE-MS. Esto supone una mejora similar a la obtenida para los péptidos opioides.

En la **Figura 6.38-B** se muestran los EIEs para una muestra de plasma fortificado a 50 pg/mL con los fragmentos de los péptidos Aβ. Comparado con el análisis de patrones (**Figura 6.38-A**), como ya ocurría con los péptidos opioides, se mantenían la resolución de la separación y la repetibilidad en A_p (%RSD (n = 3) ≤13% (**Tabla 6.16**)), mientras que era ligeramente menor en t_m (≤4,0%). Por otro lado, como era de esperar para el análisis de muestras de plasma, los LOD (entre 10 y 50 pg/mL, **Tabla 6.15**) se incrementaron entre 2 y 10 veces respecto al análisis de patrones debido a la complejidad de la matriz de la muestra.

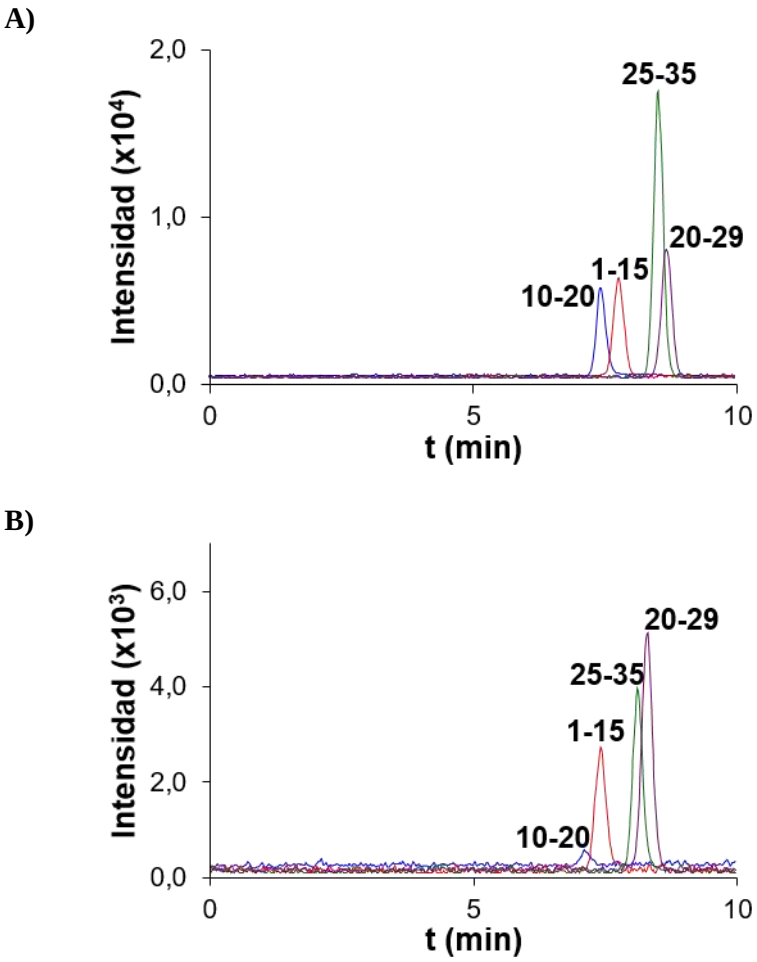

Figura 6.38. EIEs en las condiciones de nvSPE-CE-MS optimizadas para los péptidos Aβ 1-15, 10-20, 20-29 y 25-35 (dimensiones del capilar de separación 100 cm L_T (45 cm L_D) x 50 µm i.d., BGE HAc 50 mM:HFor 50 mM (pH 3,0, ajustado con NH_4OH) y eluyente 80:20 (v/v) ACN:H_2O con HAc 50 mM:HFor 50 mM). (A) Patrones de 10 pg/mL y (B) muestra de plasma fortificado a 50 pg/mL.

Comparada con la SPE-CE-MS unidireccional, la nvSPE-CE-MS es más compleja y laboriosa. Requiere la movilización de los analitos eluidos y su posicionamiento preciso en la válvula para llevar a cabo la transferencia al capilar de separación, lo que incrementa el tiempo total de los análisis. Además, en la configuración actual de nvSPE-CE-MS, los LODs para los patrones son aproximadamente 5 veces superiores que en SPE-CE-MS unidireccional, probablemente debido al menor volumen de muestra cargada a causa de la contrapresión producida por el uso de la válvula o a una transferencia no cuantitativa de los analitos desde el capilar de carga al de separación. En este caso, el volumen de 20 nL del bucle interno de la válvula limita el volumen transferido en un solo *heart-cut* y aunque, como se ha comprobado, es posible

transferir este volumen diversas veces consecutivamente, el proceso de transferencia es laborioso. Una posibilidad a investigar en el futuro sería emplear una válvula con un bucle interno de mayor volumen u otra cuya disposición permita la conexión directa entre el capilar de carga y de separación para llevar a cabo la transferencia.

Aún con estos inconvenientes, la nvSPE-CE-MS es una alternativa interesante a la SPE-CE-MS unidireccional dada su potencial gran versatilidad. En nvSPE-CE-MS, los capilares de carga y de separación, y, consecuentemente, la purificación y preconcentración mediante SPE y la separación y detección por CE-MS, son independientes. Por lo tanto, se ha podido emplear un capilar de carga de diámetro interno mayor para maximizar la capacidad de carga de la muestra y un capilar de separación más estrecho para obtener eficacias de separación adecuadas. Además, por un lado, no existe la posibilidad de contaminación del capilar de separación al cargar una muestra biológica compleja o durante la etapa de lavado posterior, lo que es beneficioso para el análisis de muestras con matrices complejas. En este sentido, es necesario remarcar que, a diferencia del análisis de los patrones, los LODs para las muestras de plasma por nvSPE-CE-MS fueron similares a los de SPE-CE-MS unidireccional. Por otro lado, el capilar de separación se puede llenar con el BGE acuoso, hidroorgánico o no-acuoso óptimo para la separación y detección por CE-MS, sin la potencial degradación del sorbente o la elución de los analitos retenidos en el preconcentrador, lo que permitiría mejorar las prestaciones de modos de SPE-CE-MS que emplean sorbentes especialmente lábiles, como los de inmunoafinidad, e investigar otros que no se han descrito hasta la fecha por su inherente limitada compatibilidad, como los sorbentes de cromatografía de líquidos de interacción hidrofílica.

6.4. Análisis *bottom-up* de proteínas por IMER-CE-MS

El análisis de proteínas intactas (*top-down*) por CE-MS es una estrategia adecuada para la detección de un gran número de proteínas y la caracterización de sus diferentes isoformas y PTMs, tal y como se ha demostrado en el **Apartado 6.2** para la TTR y la α-syn (**Artículos 3.2** y **3.3**, respectivamente). Sin embargo, esta estrategia presenta algunas limitaciones debidas, principalmente, a la dificultad en la ionización de las proteínas debido a su gran tamaño y en la interpretación de los espectros de masas. El análisis de los péptidos derivados de la digestión enzimática de una proteína intacta (*bottom-up*) permite simplificar estos problemas ya que los péptidos se ionizan más fácilmente y presentan un número limitado de cargas debido a su menor tamaño. Además, se pueden separar mejor, evitando la supresión iónica, y detectar como picos de elevada eficacia, lo que en conjunto permite mejorar los LODs [16].

En estas estrategias *bottom-up*, la tripsina es la enzima proteolítica más comúnmente utilizada [16,17]. La digestión se realiza habitualmente en disolución y suelen requerirse largos tiempos de digestión [17,123,260]. Como alternativa, se han propuesto las enzimas inmovilizadas en un soporte, que permiten disminuir el volumen de muestra, su manipulación y el tiempo total de análisis y mejorar la eficiencia de la digestión, así como estabilizar y reutilizar la enzima o evitar su autoproteólisis [261].

Habitualmente las partículas con tripsina inmovilizada se utilizan para realizar las digestiones *off-line*. Con el objetivo de incrementar la capacidad de procesar muestras y minimizar la manipulación, este capítulo se centra en el desarrollo de una metodología de análisis *bottom-up* empleando microrreactores empaquetados con partículas con tripsina inmovilizada en línea con la CE-MS (IMER-CE-MS) (**Artículo 5.1**). En primer lugar, se evaluaron y optimizaron las condiciones de la digestión *off-line* de la β-lactoglobulina (β-LG) con tripsina en disolución y con partículas con tripsina inmovilizada comerciales. A continuación, estas partículas se utilizaron para preparar microrreactores con dos fritas siguiendo el mismo procedimiento empleado para la construcción de preconcentradores de SPE-CE-MS (**Apartado 6.2**). La metodología de IMER-CE-MS se optimizó con patrones de β-LG y el método desarrollado se

validó con patrones de α-CSN, β-CSN y κ-CSN. A continuación, se demostró el potencial de la metodología para el análisis de mezclas complejas de proteínas analizando el mismo lisado de *E. coli* empleado en el desarrollo de la metodología IMA-SPE-CE-MS para enriquecer His-peptides (**Artículo 3.4**).

6.4.1. Análisis de β-LG por digestión *off-line* en disolución y CE-MS

La proteína β-LG es uno de los principales alérgenos de la leche de vaca [332] y se empleó como modelo para la optimización debido a su interés en materia de salud, facilidad de obtención, tamaño moderado (M_r~19,900) y estructura sencilla. En la **Tabla 6.17** se muestran los péptidos que se deberían generar en la digestión tríptica de la β-LG.

La digestión de proteínas con tripsina se realiza tradicionalmente en disolución mezclando las soluciones de enzima y proteínas. Las digestiones se realizan habitualmente a 37 ºC y a pH cercano a 8 (se suele utilizar como tampón de digestión NH_4HCO_3 50 mM (pH 7,9)) durante largos períodos de tiempo (8-24 h) para asegurar la eficacia y reproducibilidad del proceso [17,123,260]. Con el objetivo de optimizar la metodología de digestión *off-line* en disolución y posterior análisis por CE-MS, se investigaron varios tampones de digestión a pH 7,9 (NH_4HCO_3 50 mM y otros con menor fuerza iónica como NH_4HCO_3 10 mM y NH_4Ac 10 mM, más adecuados para CE-MS). También se investigó el efecto de la temperatura en la separación y la sensibilidad en CE-MS, ya que luego en la metodología IMER-CE-MS la digestión y la separación tenían lugar a la misma temperatura. En la **Figura 6.39-A** se muestra el sumatorio de las A_p de los péptidos detectados por CE-MS (empleando el BGE HAc 50 mM:HFor 50 mM (pH 2,3) y llevando a cabo la separación a 25 y 37 ºC) para un patrón de β-LG de 1000 µg/mL digerido *off-line* durante 18 h a 37 ºC con tripsina en disolución usando los diferentes tampones de digestión. Como se puede apreciar, el rendimiento de la digestión era mayor con los tampones de NH_4HCO_3 que con el de NH_4Ac. La mejor sensibilidad se obtenía digiriendo a 37 ºC en NH_4HCO_3 50 mM (pH 7,9) que, como ya se ha dicho anteriormente, es el tampón de digestión más habitual, y llevando a cabo la separación electroforética a 37 ºC.

Tabla 6.17. Péptidos tripticos de la β-LG detectados (patrón de 1000 µg/mL) por (A) digestión *off-line* con tripsina en disolución y CE-MS, (B) digestión *off-line* con tripsina inmovilizada y CE-MS y (C) IMER-CE-MS (n = 3). Los aminoácidos individuales no se tienen en cuenta.

Secuencia peptídica			$[M+nH]^{n+}$		A) Digestión *off-line* con tripsina en disolución y CE-MS		B) Digestión *off-line* con tripsina inmovilizada y CE-MS		C) IMER-CE-MS	
			m/z	n	A_p relativa [a]	%RSD	A_p relativa [a]	%RSD	A_p relativa [a]	%RSD
1	[1-8]	LIVTQTMK	467,2758	2	0,101	1,8	0,137	0,6	0,181	4,3
2	[9-14]	GLDIQK	337,1979	2	0,102	1,0	0,112	0,9	0,137	2,2
3	[15-40]	VAGTWYSLAMAASDISLLDAQSAPLR	903,1306	3	0,009	1,6	0,0003	14	0,018	10
4	[41-60]	VYVEELKPTPEGDLEILLQK	771,7582	3	0,135	0,6	0,140	1,8	0,106	8,5
5	[61-69]	WENGECAQK	561,2379	2	0,002	4,9	0,007	12	0,010	15
6	[71-75]	IIAEK	287,1842	2	0,071	0,7	0,084	3,4	0,085	4,3
7	[76-77]	TK	248,1605	1	0,015	8,0	0,012	5,8	0,006	11
8	[78-83]	IPAVFK	337,7157	2	0,089	0,8	0,102	1,4	0,067	6,6
9	[84-91]	IDALNENK	458,7406	2	0,085	0,8	0,099	2,0	0,122	6,1
10	[92-100]	VLVLDTDYK	533,2953	2	0,115	0,9	0,088	1,6	0,028	4,2
11	[102-124]	YLLFCMENSAEPEQSLACQCLVR	940,0941	3	0,002	7,3	0,0001	9,8	0,009	7,8
12	[125-135]	TPEVDDEALEK	623,2962	2	0,098	0,1	0,047	3,7	0,047	6,0
13	[136-138]	FDK	409,2082	1	0,016	6,5	0,006	4,3	0,005	9,9
14	[139-141]	ALK	331,2340	1	0,018	4,4	0,018	4,1	0,015	7,1
15	[142-148]	ALPMHIR	419,2421	2	0,043	4,2	0,038	4,9	0,048	10
16	[149-162]	LSFNPTQLEEQCHI	858,4068	2	0,100	2,7	0,108	5,5	0,116	3,6

a) El A_p relativa se calculó dividiendo el A_p del péptido entre el sumatorio del A_p de todos los péptidos detectados.

Los digestos tripticos se han simulado con el software PeptideMass de ExPASy (https://web.expasy.org/peptide_mass/).

Al emplear esta temperatura de separación, los t_m eran menores y los picos más estrechos debido a la menor viscosidad del BGE y mejoraba la eficiencia de la ionización, lo que en conjunto incrementaba el A_p. En cuanto al tiempo de digestión, se evaluaron los rendimientos de digestión a 18 h y a 30 minutos, para comparar posteriormente con la tripsina inmovilizada, cuyo fabricante recomienda tiempos de digestión de 30 minutos. La **Figura 6.39-B** muestra que el rendimiento de la digestión disminuía significativamente al digerir durante únicamente 30 min.

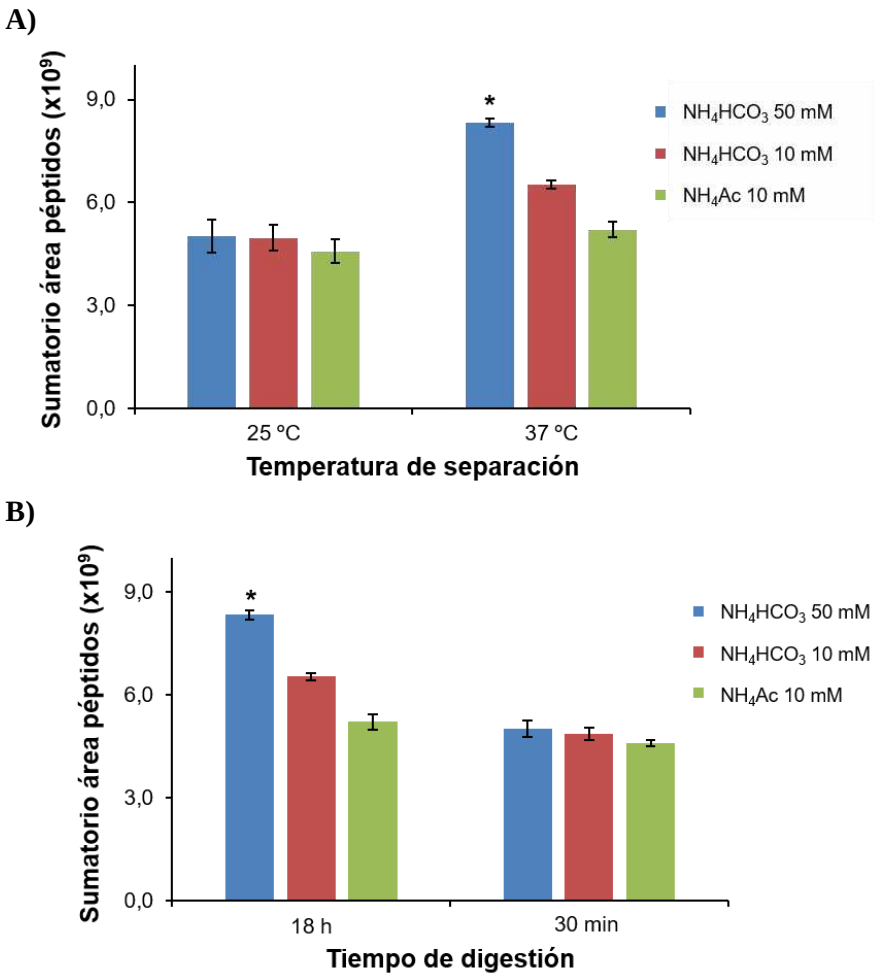

Figura 6.39. Comparativa del A_p de los péptidos detectados por CE-MS para un patrón de β-LG de 1000 µg/mL digerido *off-line* a 37 ºC con tripsina en disolución. (A) A diferentes temperaturas de separación y tampones de digestión (18 h de digestión) y (B) a diferentes tiempos de digestión y tampones de digestión (37 ºC de temperatura de separación). Las barras de error indican la desviación estándar (n = 3). Las condiciones optimizadas se indican con un asterisco.

En la **Figura 6.40** se muestran los EIEs de los péptidos detectados por CE-MS para un digesto de β-LG de 1000 µg/mL en las condiciones optimizadas, es decir, digiriendo durante 18 h a 37 ºC en NH_4HCO_3 50 mM (pH 7,9) y separando por CE-MS a 37 ºC. En la **Tabla 6.17-A** se

muestran los valores de m/z de los iones moleculares de los péptidos trípticos detectados en estas condiciones. A esta concentración, se detectaron todos los péptidos trípticos esperados (cobertura peptídica del 100%). En la **Tabla 6.17-A** también se muestran los valores del A_p relativa de los péptidos trípticos. La repetibilidad era adecuada (%RSD (n = 3) en t_m ≤1,8% y en A_p ≤8,0%) y similar a la descrita por otros autores en el análisis de digestos proteicos por CE-MS [143].

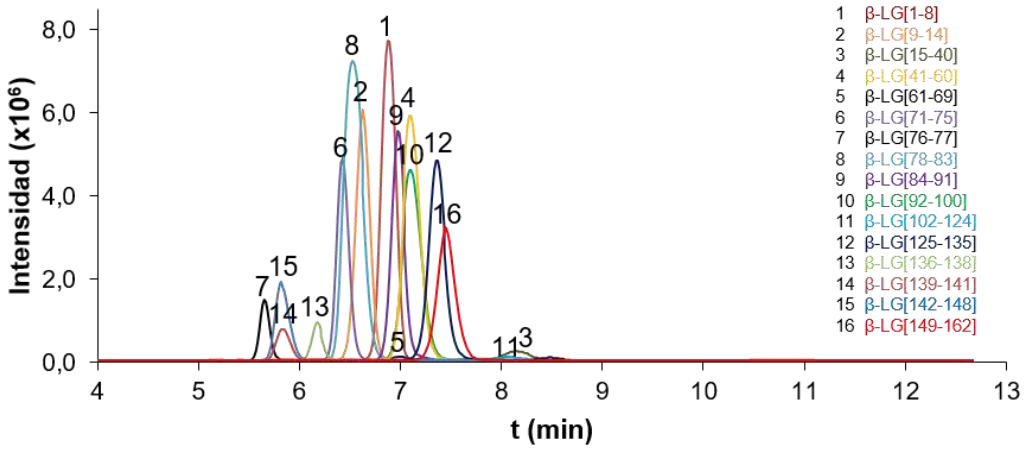

Figura 6.40. EIEs de los péptidos detectados por CE-MS (37 ºC de temperatura de separación) para un digesto de β-LG de 1000 µg/mL digerido *off-line* con tripsina en disolución en NH_4HCO_3 50 mM (pH 7,9) durante 18 h a 37 ºC.

6.4.2. Análisis de β-LG por digestión *off-line* con tripsina inmovilizada y CE-MS

Para que la comparación posterior fuera adecuada, también se optimizó el análisis de β-LG por digestión *off-line* con partículas con tripsina inmovilizada comerciales y CE-MS. Se investigaron los tres tampones de digestión a pH 7,9 evaluados en el apartado anterior y el efecto de la temperatura en la separación y la sensibilidad en CE-MS. La **Figura 6.41-A** muestra el sumatorio del A_p de los péptidos trípticos detectados por CE-MS, usando los diferentes tampones de digestión y llevando a cabo la separación a 25 y 37 ºC, para un patrón de β-LG de 1000 µg/mL digerido *off-line* con tripsina inmovilizada durante 30 min a 25 ºC, que eran las condiciones recomendadas para la digestión por el fabricante. Como puede observarse, al igual que en la digestión *off-line* con tripsina en disolución, la mejor sensibilidad por CE-MS se obtenía separando a 37 ºC. En cambio, a diferencia de las condiciones optimizadas con tripsina en

disolución, el sumatorio del A_p era inferior empleando el tampón de digestión NH_4HCO_3 50 mM (pH 7,9).

Una gran ventaja de la digestión con tripsina inmovilizada es la posibilidad de reutilizar la enzima. En la **Figura 6.41-B** se muestran los resultados obtenidos en digestiones consecutivas usando los diferentes tampones de digestión. Como puede observarse, el mejor rendimiento en todas las digestiones se obtenía con el tampón de digestión NH_4HCO_3 10 mM (pH 7,9). Asimismo, se observa una disminución significativa después de la primera digestión al emplear NH_4Ac 10 mM (pH 7,9), probablemente a causa de la degradación de la enzima inmovilizada al estar en contacto con este tampón durante 30 min.

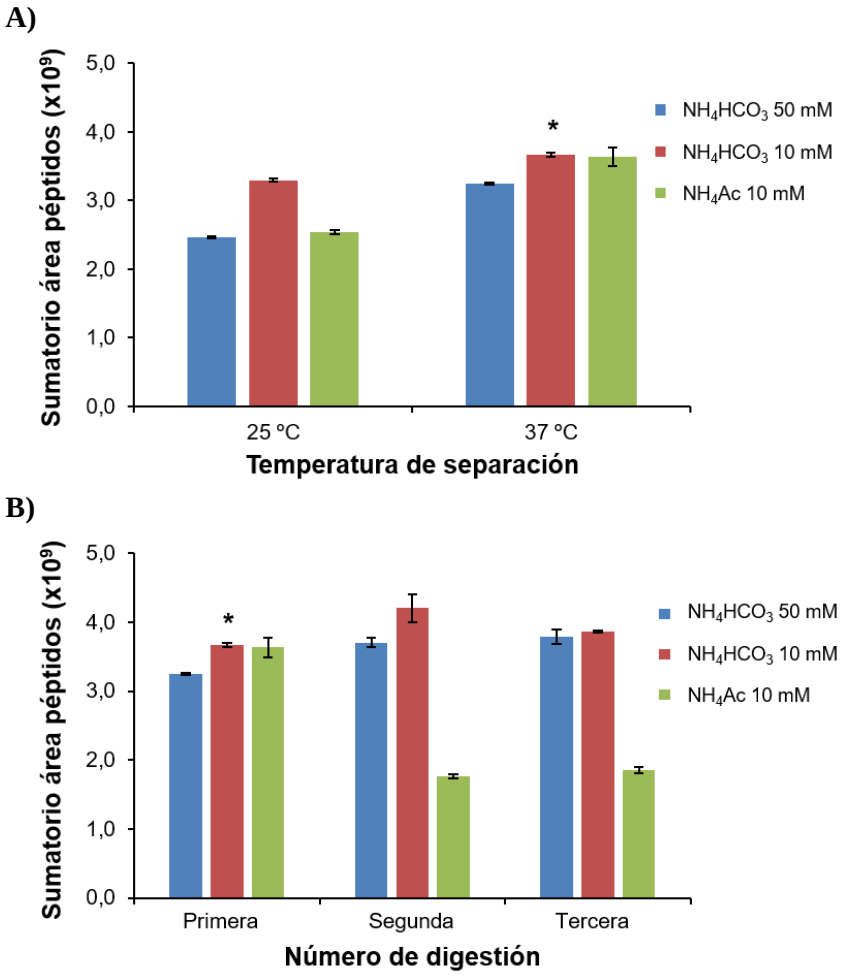

Figura 6.41. Comparativa del A_p de los péptidos detectados por CE-MS para un patrón de β-LG de 1000 µg/mL digerido *off-line* con tripsina inmovilizada durante 30 min a 25 ºC. (A) A diferentes temperaturas de separación y tampones de digestión y (B) en digestiones consecutivas con los diferentes tampones de digestión (37 ºC de temperatura de separación). Las barras de error indican la desviación estándar (n = 3). Las condiciones optimizadas se indican con un asterisco.

En la **Figura 6.42** se muestran los EIEs de los péptidos detectados por CE-MS separando a 37 ºC para un patrón de 1000 µg/mL de β-LG digerido en NH_4HCO_3 10 mM (pH 7,9) durante 30 min a 25 ºC. Al igual que con tripsina en disolución, la cobertura peptídica era del 100% (**Tabla 6.17-B**). La repetibilidad en t_m también era similar (%RSD (n = 3) ≤1,3%) y en A_p era ligeramente inferior (≤14%). Aunque el rendimiento de la digestión era menor (comparar el sumatorio del A_p de los péptidos trípticos detectados por CE-MS en las condiciones optimizadas, indicadas con un asterisco en las **Figuras 6.39-B** y **6.41-A**), la digestión con tripsina inmovilizada permitía reutilizar la enzima empleando tiempos de digestión de solamente 30 min con la misma cobertura del 100%.

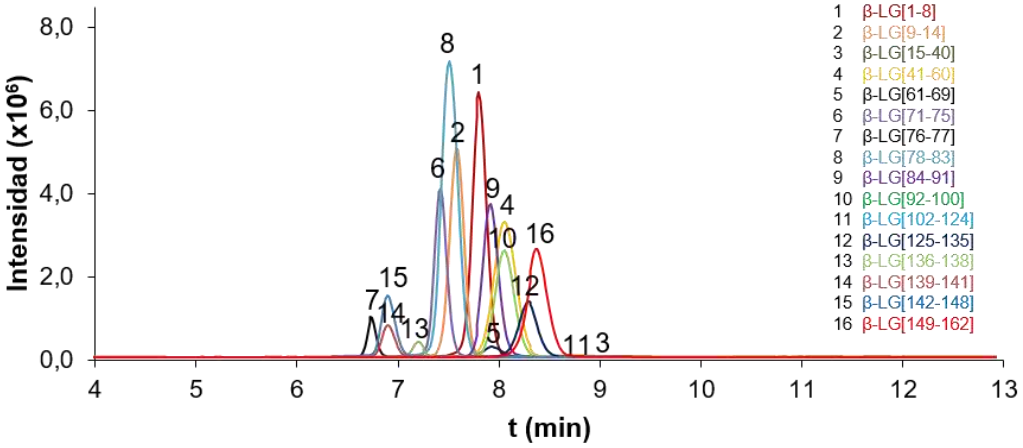

Figura 6.42. EIEs de los péptidos detectados por CE-MS (37 ºC de temperatura de separación) para un digesto de β-LG de 1000 µg/mL digerido *off-line* con tripsina inmovilizada en NH_4HCO_3 10 mM (pH 7,9) durante 30 min a 25 ºC.

6.4.3. Análisis de β-LG por IMER-CE-MS

La optimización del método de IMER-CE-MS comenzó con unos estudios preliminares donde se vio que el tampón de digestión optimizado para la digestión *off-line* con tripsina en disolución (NH_4HCO_3 50 mM (pH 7,9)) no era adecuado, ya que provocaba inestabilidad y caídas de corriente, probablemente a causa de la formación de burbujas de CO_2 al mezclarse dentro del capilar con el BGE ácido. En la **Figura 6.43-A** se ve que, para el análisis de un patrón de β-LG de 1000 µg/mL por IMER-CE-MS digiriendo y separando a 25 ºC, se obtenía una mejor

sensibilidad y repetibilidad usando el tampón de digestión NH_4HCO_3 10 mM (pH 7,9) que el NH_4Ac 10 mM (pH 7,9), en concordancia con los resultados obtenidos en los estudios off-line con tripsina inmovilizada. También se aprecia que la sensibilidad aumentaba digiriendo y separando a 37 ºC.

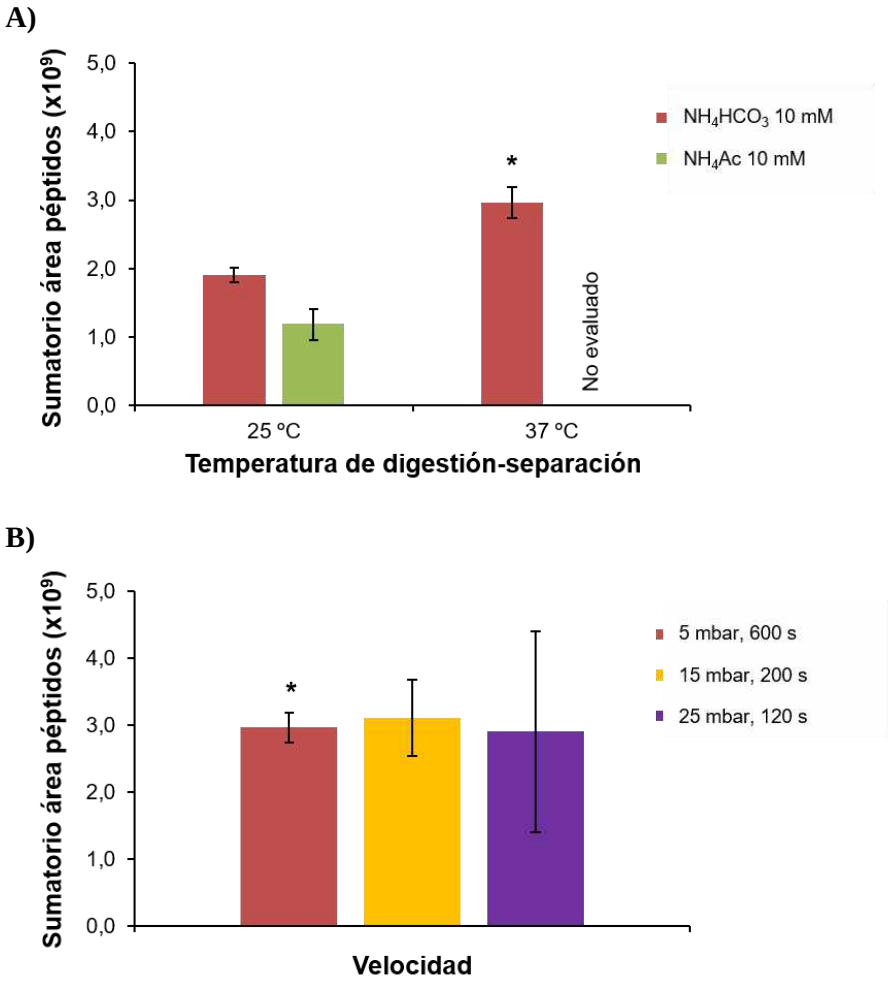

Figura 6.43. Comparativa del A_p de los péptidos detectados por IMER-CE-MS para un patrón de β-LG de 1000 µg/mL. (A) A diferentes temperaturas de digestión-separación y tampones de digestión (movilización de la muestra a 5 mbar durante 600 s) y (B) a diferentes velocidades de movilización de la muestra (37 ºC de temperatura de digestión-separación). Las barras de error indican la desviación estándar (n = 3). Las condiciones optimizadas se indican con un asterisco.

En estas condiciones, se evaluó la influencia del tiempo de contacto entre la β-LG y la tripsina inmovilizada. Se inyectó la β-LG entre dos pequeños volúmenes de NH_4HCO_3 10 mM (pH 7,9) y se empujó hacia el microrreactor a diferentes velocidades (5 mbar durante 600 s, 15 mbar y 200 s y 25 mbar y 120 s). Como se observa en la **Figura 6.43-B**, la mejor repetibilidad se

obtenía empleando la menor velocidad, de manera que el tiempo de contacto entre la β-LG y la tripsina inmovilizada era el mayor.

En la **Figura 6.44** se muestran los EIEs de los péptidos detectados por IMER-CE-MS en las condiciones optimizadas para 1000 µg/mL de β-LG. En comparación con las digestiones *off-line* con tripsina en disolución e inmovilizada y CE-MS (**Figuras 6.40** y **6.42**), la resolución de la separación mejoraba y el tiempo total del análisis se incrementaba ligeramente, probablemente a causa de la contrapresión provocada por la presencia del microrreactor. La repetibilidad era ligeramente peor en t_m (%RSD (n = 3) ≤7,6%) y similar en A_p (≤15%) (**Tabla 6.17-C**). La sensibilidad era comparable a la digestión *off-line* con tripsina inmovilizada y CE-MS, aunque ligeramente menor a causa del pequeño volumen de muestra inyectado y el menor tiempo de contacto entre la proteína y la enzima. La cobertura peptídica era del 100% a concentraciones ≥10 µg/mL de β-LG. La durabilidad de los microrreactores era muy adecuada y superior a 30 análisis.

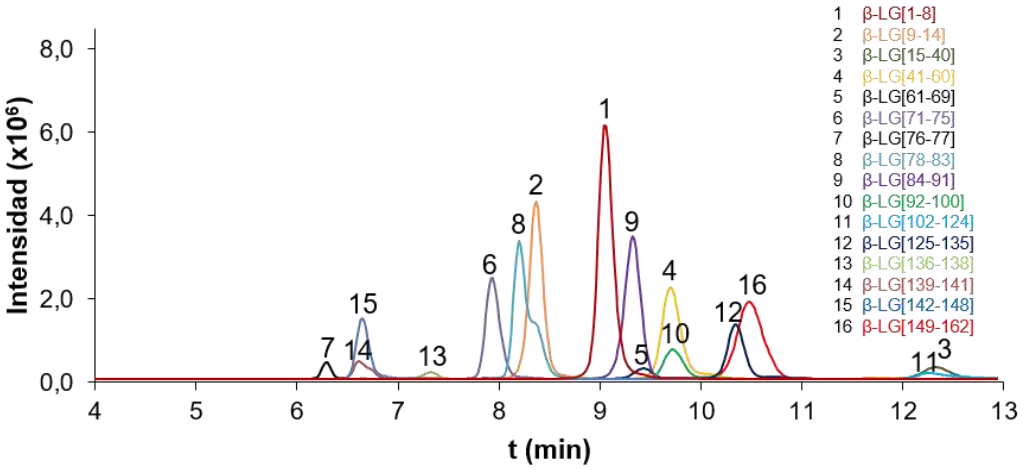

Figura 6.44. EIEs de los péptidos detectados por IMER-CE-MS para 1000 µg/mL de β-LG, empleando el tampón de digestión NH_4HCO_3 10 mM (pH 7,9) y digiriendo-separando a 37 ºC (movilización de la muestra a 5 mbar durante 600 s).

6.4.4. Análisis de α-CSN, β-CSN y κ-CSN por IMER-CE-MS

Los estudios de IMER-CE-MS se ampliaron al análisis de otras proteínas modelo, concretamente la α-CSN (mezcla de α-CSN1 y α-CSN2), β-CSN y κ-CSN, también empleadas para optimizar la metodología *bottom-up* de IMA-SPE-CE-MS (**Artículo 3.4**). En las **Tablas**

6.18, **6.19** y **6.20** se muestran los péptidos que se deberían generar en la digestión tríptica de la α-CSN, β-CSN y κ-CSN, respectivamente. En la **Figura 6.45** se muestran los EIEs de los péptidos detectados por IMER-CE-MS para 1000 µg/mL de α-CSN. Como puede observarse en la **Tabla 6.18-A** y la **Figura 6.45-A**, se detectaban 18 péptidos de la α-CSN1 de 19 posibles (94,7% de cobertura peptídica). La cobertura peptídica para la α-CSN2 era ligeramente menor (82,6%; ver **Tabla 6.18-B** y **Figura 6.45-B**, 19 péptidos de 23 posibles) a causa de su menor abundancia en la mezcla, como ya se comentó en IMA-SPE-CE-MS**.** La repetibilidad en el A_p era similar a la obtenida para la β-LG (%RSD (n = 3) <10% (**Tabla 6.18**)) si exceptuamos el péptido α-CSN2[25-32], cuyo pico era difícil de cuantificar a causa de su baja intensidad.

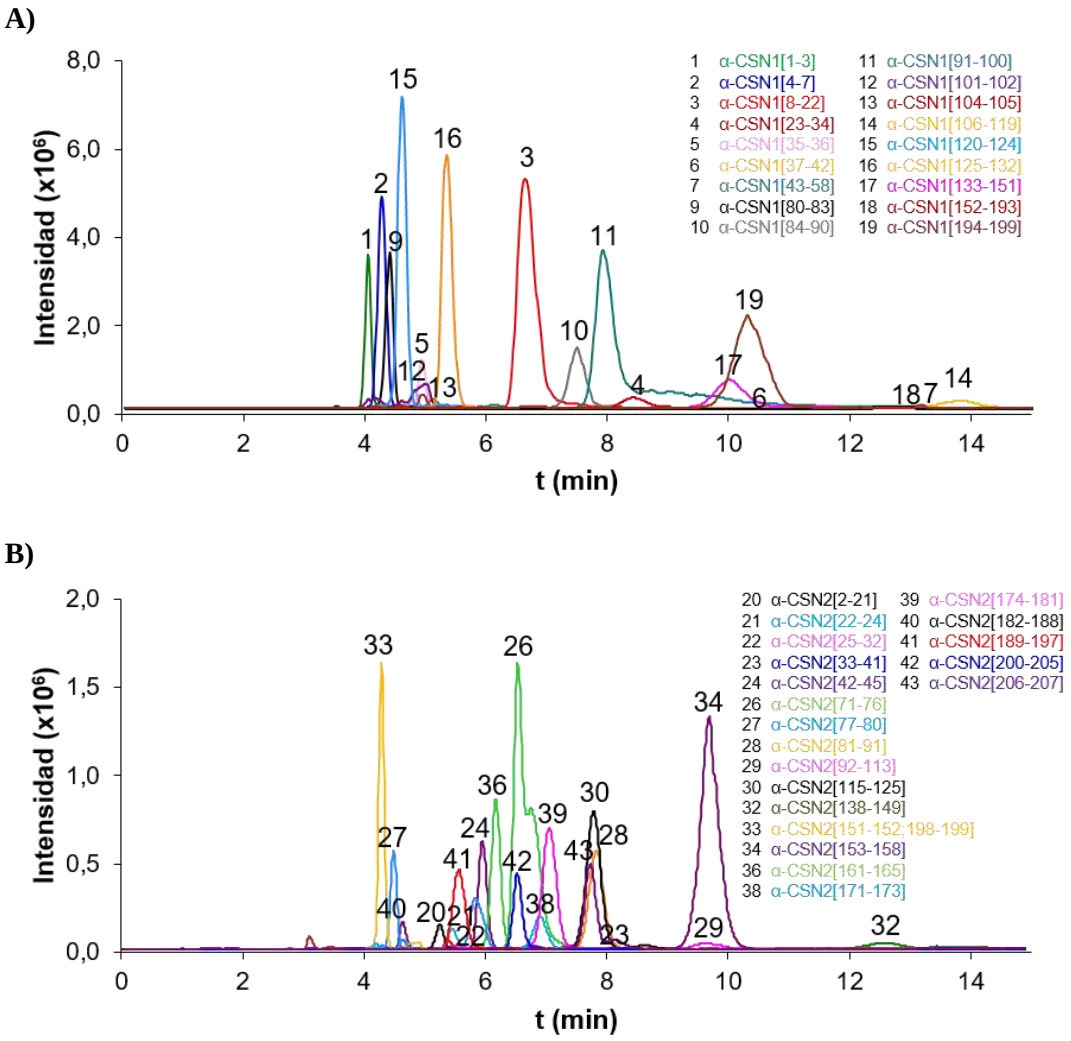

Figura 6.45. EIEs de los péptidos detectados por IMER-CE-MS para 1000 µg/mL de α-CSN. (A) α-CSN1 y (B) α-CSN2.

Tabla 6.18-A. Péptidos tripticos de la α-CSN1 detectados por IMER-CE-MS (patrón de 1000 µg/mL de α-CSN). Los aminoácidos individuales no se tienen en cuenta.

Secuencia peptídica			$[M+nH]^{n+}$		A_p relativa [a]	
			m/z	n	Promedio (n = 3)	%RSD
1	[1-3]	RPK	200,6370	2	0,029	9,9
2	[4-7]	HPIK	247,6579	2	0,093	5,4
3	[8-22]	HQGLPQEVLNENLLR	587,3198	3	0,203	1,7
4	[23-34]	FFVAPFPEVFGK	462,2482	3	0,013	4,4
5	[35-36]	EK	276,1554	1	0,014	1,2
6	[37-42]	VNELSK	385,1783	2	0,004	4,5
7	[43-58]	DIGSESTEDQAMEDIK	964,3494	2	0,017	3,5
8	[59-79]	QMEAESISSSEEIVPNSVEQK	-	-	-	-
9	[80-83]	HIQK	263,1609	2	0,093	5,9
10	[84-90]	EDVPSER	416,1958	2	0,076	2,6
11	[91-100]	YLGYLEQLLR	634,3559	2	0,148	5,0
12	[101-102]	LK	260,1969	1	0,004	4,3
13	[104-105]	YK	310,1761	1	0,013	4,1
14	[106-119]	VPQLEIVPNSAEER	830,9008	2	0,033	6,3
15	[120-124]	LHSMK	308,1678	2	0,093	4,5
16	[125-132]	EGIHAQQK	304,1629	3	0,069	2,7
17	[133-151]	EPMIGVNQELAYFYPELFR	772,7172	3	0,029	2,6
18	[152-193]	QFYQLDAYPSGAWYYVPLGTQYTDAPSFSDIPNPIGSENSEK	1179,7987	4	0,001	4,2
19	[194-199]	TTMPLW	748,3698	1	0,068	2,4

a) El A_p relativa se calculó dividiendo el A_p del péptido entre el sumatorio del A_p de todos los péptidos detectados.

Los digestos tripticos se han simulado con el software PeptideMass de ExPASy (https://web.expasy.org/peptide_mass/).

Tabla 6.18-B. Péptidos tripticos de la α-CSN2 detectados por IMER-CE-MS (patrón de 1000 μg/mL de α-CSN). Los aminoácidos individuales no se tienen en cuenta.

Secuencia peptídica			[M+nH]$^{n+}$		A_p relativa [a]	
			m/z	n	Promedio (n = 3)	%RSD
20	[2-21]	NTMEHVSSSEESIISQETYK	873,6402	3	0,003	8,2
21	[22-24]	QEK	404,2140	1	0,004	9,9
22	[25-32]	NMAINPSK	477,7094	2	0,001	35
23	[33-41]	ENLCSTFCK	522,7284	2	0,002	2,7
24	[42-45]	EVVR	251,6528	2	0,028	5,3
25	[46-70]	NANEEEYSIGSSSEESAEVATEEVK	-	-	-	-
26	[71-76]	ITVDDK	345,6871	2	0,250	1,7
27	[77-80]	HYQK	288,1504	2	0,034	4,9
28	[81-91]	ALNEINQFYQK	684,3513	2	0,050	1,7
29	[92-113]	FPQYLQYLYQGPIVLNPWDQVK	903,8074	3	0,007	4,1
30	[115-125]	NAVPITPTLNR	598,3433	2	0,058	4,8
31	[126-136]	EQLSTSEENSK	-	-	-	-
32	[138-149]	TVDMESTEVFTK	733,8097	2	0,028	5,4
33	[151-152], [198-199]	TK	248,1605	1	0,023	2,0
34	[153-158]	LTEEEK	748,3723	1	0,165	0,6
35	[159-160]	NR	-	-	-	-
36	[161-165]	LNFLK	317,6998	2	0,077	4,0
37	[167-170]	ISQR	-	-	-	-
38	[171-173]	YQK	438,2347	1	0,007	5,2
39	[174-181]	FALPQYLK	490,2842	2	0,100	1,2
40	[182-188]	TVYQHQK	452,2378	2	0,019	6,4
41	[189-197]	AMKPWIQPK	366,8762	3	0,065	1,9
42	[200-205]	VIPYVR	373,7316	1	0,023	2,3
43	[206-207]	YL	295,1652	2	0,012	2,7

a) El A_p relativa se calculó dividiendo el A_p del péptido entre el sumatorio del A_p de todos los péptidos detectados.

Los digestos tripticos se han simulado con el software PeptideMass de ExPASy (https://web.expasy.org/peptide_mass/).

Tabla 6.19. Péptidos tripticos de la β-CSN detectados por IMER-CE-MS (patrón de 1000 µg/mL). Los aminoácidos individuales no se tienen en cuenta.

Secuencia peptídica			$[M+nH]^{n+}$		A_p relativa[a]	
			m/z	n	Promedio (n = 3)	%RSD
1	[2-25]	ELEELNVPGEIVESLSSSEESITR	-	-	-	-
2	[26-28]	INK	187,6238	3	0,014	2,1
3	[30-32]	IEK	389,2395	2	0,004	3,9
4	[33-48]	FQSEEQQQTEDELQDK	687,9481	1	0,005	3,6
5	[49-97]	IHPFAQTQSLVYPFPGPIPNSLPQNIPPLTQTPVVVPPFLQPEVMGVSK	1772,9564	2	0,0001	22
6	[98-99]	VK	246,1812	1	0,016	3,0
7	[100-105]	EAMAPK	323,6654	2	0,078	2,6
8	[106-107]	HK	284,1717	2	0,012	10
9	[108-113]	EMPFPK	374,6888	2	0,176	1,0
10	[114-169]	YPVEPFTESQSLTLTDVENLHLPLPLLQSWMHQPHQPLPPTVMFPPQSVLSLSQSK	2120,4239	1	0,0001	30
11	[170-176]	VLPVPQK	390,7528	3	0,338	1,4
12	[177-183]	AVPYPQR	415,7299	2	0,146	0,3
13	[184-202]	DMPIQAFLLYQEPVLGPVR	729,3945	1	0,090	9,1
14	[203-209]	GPFPIIV	742,4498	1	0,121	2,8

a) El A_p relativa se calculó dividiendo el A_p del péptido entre el sumatorio del A_p de todos los péptidos detectados.

Los digestos tripticos se han simulado con el software PeptideMass de ExPASy (https://web.expasy.org/peptide_mass/).

Tabla 6.20. Péptidos tripticos de la κ-CSN detectados por IMER-CE-MS (patrón de 1000 µg/mL). Los aminoácidos individuales no se tienen en cuenta.

Secuencia peptídica			$[M+nH]^{n+}$		A_p relativa [a]	
			m/z	n	Promedio (n = 3)	%RSD
1	[1-10]	QEQNQEQPIR	635,3130	2	0,007	66
2	[11-13]	CEK	436,1646	2	0,009	22
3	[14-16]	DER	419,1885	3	0,028	25
4	[17-21]	FFSDK	322,1582	3	0,293	19
5	[22-24]	IAK	331,2340	2	0,063	2,8
6	[25-34]	YIPIQYVLSR	626,3587	1	0,219	15
7	[35-68]	YPSYGLNYYQQKPVALINNQFLPYPYYAKPAAVR	1003,2714	3	0,002	69
8	[69-86]	SPAQILQWQVLSNTVPAK	660,7023	1	0,130	16
9	[87-97]	SCQAQPTTMAR	625,7740	2	0,191	6,9
10	[98-111]	HPHPHLSFMAIPPK	536,9542	2	0,058	6,6
11	[113-116]	NQDK	-	-	-	-
12	[117-169]	IPTINTIASGEPTSTPTTEAVESTVATLEDSPEVIESPPEINTVQVTSTAV	-	-	-	-

a) El A_p relativa se calculó dividiendo el A_p del péptido entre el sumatorio del A_p de todos los péptidos detectados.

Los digestos tripticos se han simulado con el software PeptideMass de ExPASy (https://web.expasy.org/peptide_mass/).

En la **Figura 6.46** se muestran los EIEs de los péptidos detectados para 1000 µg/mL de β-CSN. Se detectaban 13 péptidos de un total de 14 (92,9% de cobertura peptídica) y la repetibilidad en el A_p también era adecuada (%RSD (n = 3) ≤10% (**Tabla 6.19**)), si exceptuamos los dos péptidos de mayor tamaño, β-CSN[49-97] y β-CSN[114-169], cuyo pico era muy poco intenso.

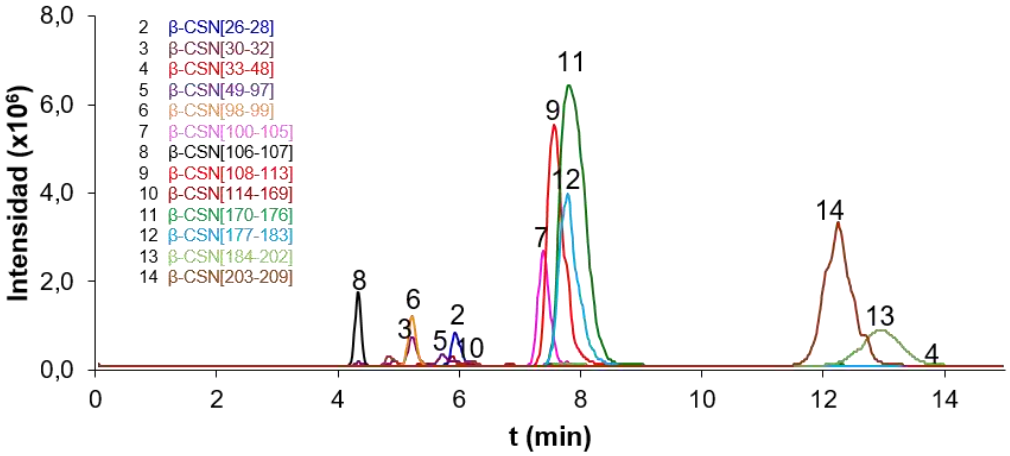

Figura 6.46. EIEs de los péptidos detectados por IMER-CE-MS para 1000 µg/mL de β-CSN.

En la **Figura 6.47** se muestran los EIEs de los péptidos detectados para 1000 µg/mL de κ-CSN. La cobertura peptídica también era adecuada (83,3%; 10 péptidos detectados de un total de 12). Sin embargo, la repetibilidad en A_p era peor que para el resto de proteínas (%RSD (n = 3) >15% para 7 de los péptidos detectados (**Tabla 6.20**)) debido a la menor intensidad de los picos (compárese los valores de intensidad en el eje y de las **Figuras 6.44, 6.45-A** y **6.46** (β-LG, α-CSN1 y β-CSN) respecto a la **Figura 6.47** (κ-CSN)), lo que indicaba una menor eficiencia de

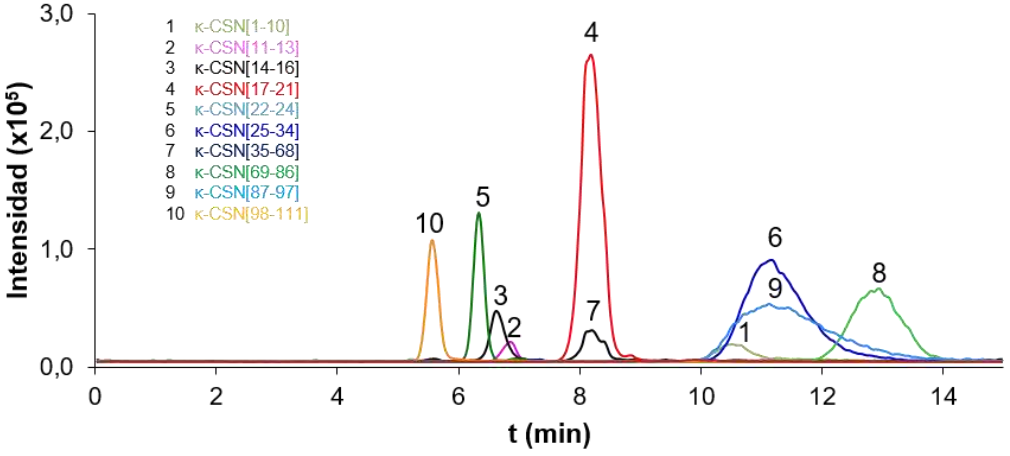

Figura 6.47. EIEs de los péptidos detectados por IMER-CE-MS para 1000 µg/mL de κ-CSN.

digestión en el caso de la κ-CSN. Este hecho se confirmó digiriendo *off-line* con tripsina en disolución 1000 μg/mL de las proteínas y analizándolas por CE-MS. La peor repetibilidad también correspondía en este caso a la κ-CSN (%RSD (n = 3) en A_p ≤23% para κ-CSN, respecto a ≤8,0% para β-LG (**Apartado 6.4.1**) y ≤8,3% y ≤7,7% para α-CSN y β-CSN).

6.4.5. Análisis de un lisado de *E. coli*

Para investigar el potencial de la metodología de IMER-CE-MS para el análisis de mezclas complejas de proteínas, se analizó un lisado de *E. coli*. Los péptidos detectados por CE-MS en la digestión *off-line* con tripsina en disolución de 1000 μg/mL del lisado de *E. coli* se indican en el estudio de IMA-SPE-CE-MS (**Tabla 6.12-A; Apartado 6.2.3.3**). En la **Tabla 6.21-A** solamente se ha incluido la cobertura peptídica en estas condiciones y se aprecia que para las proteínas identificadas estaba entre el 10 y el 36%. En la **Tabla 6.21-B** se muestran los péptidos detectados por IMER-CE-MS. Se identificaron las mismas cinco proteínas que en la digestión *off-line* con tripsina en disolución y la cobertura peptídica era similar (entre el 10 y el 28%), aunque ligeramente menor a causa del pequeño volumen de muestra inyectado y el menor tiempo de contacto entre las proteínas y la enzima.

Dado que los resultados obtenidos por IMER-CE-MS son comparables con los de los métodos tradicionales, la metodología en línea desarrollada muestra un gran potencial para el análisis *bottom-up* de proteínas, permitiendo reutilizar los microrreactores, reducir el volumen de muestra necesario, su manipulación y los tiempos de digestión. Además, en un futuro cercano, el acoplamiento en línea de los métodos de SPE-CE-MS unidireccional (**Apartado 6.2**) desarrollados en esta tesis con la metodología IMER-CE-MS podría suponer un hito en el análisis *bottom-up* de proteínas por CE-MS. En SPE-IMER-CE-MS, los biomarcadores proteicos se preconcentrarían primero empleando un microcartucho con un sorbente adecuado para, inmediatamente después de la elución, ser digeridos en el microrreactor con tripsina inmovilizada, generando los péptidos a separar e identificar por CE-MS. Esta combinación supone un gran reto, debido a la dificultad para compatibilizar las condiciones necesarias para conseguir una elevada

preconcentración, una digestión eficiente, una separación eficaz por CE y una detección adecuada por MS. En este sentido, el empleo de una nanoválvula, como la que se ha empleado para desarrollar la metodología de nvSPE-CE-MS (**Apartado 6.3**), permitiría segregar la SPE-CE y la IMER-CE entre ellas o éstas respecto a la CE-MS, para poder emplear las condiciones adecuadas para cada etapa y habilitar metodologías que de otra manera no serían posibles.

Tabla 6.21. Péptidos detectados, proteínas identificadas y cobertura peptídica para 1000 µg/mL del lisado de *E. coli*. (A) Digestión *off-line* con tripsina en disolución y CE-MS (los péptidos detectados se indican en la **Tabla 6.12-A; Apartado 6.2.3.3**) y (B) IMER-CE-MS. Los aminoácidos individuales no se tienen en cuenta.

Proteína identificada	A) Digestión *off-line* con tripsina en disolución y CE-MS	B) IMER-CE-MS	
	Cobertura peptídica (%)	Péptidos detectados	Cobertura peptídica (%)
α-lactalbúmina 6x-His M_r ~14000	16,7	[2-5] QFTK [109-114] ALCTEK	16,7
Mioglobina C M_r ~17000	11,1	[43-45] FDK [48-50] HLK	11,1
Creatina quinasa-MM M_r ~43000	31,8	[26-32] HNNHMAK [42-43] LR [44-45] DK [131-132] VR [133-135] TGR [136-138] SIK [149-151] GER [267-292] AGHPFMWNQHLGYVLTCPSNLGTGLR [315-316] LR [317-319] LQK [359-365] LMVEMEK [367-369] LEK	27,3
Catepsina D M_r ~38000	35,7	[110-112] VER [246-249] ELQK [282-284] GYK [285-293] LSPEDYTLK [340-347] VGFAEAAR	17,9
Antitrombina III M_r ~49000	24,5	[48-53] VWELSK [54-57] ANSR [140-145] LVSANR [146-150] LFGDK [223-226] GLWK [394-399] SLNPNR	12,2

Conclusions

- Novel strategies to estimate the pK_as of complex polyprotic peptides and to predict and optimize their separation in CE were evaluated:
  - The electrophoretic behavior and the pK_a values of Aβ peptide fragments Aβ 1-15, 10-20, 20-29, 25-35 and 33-42 were determined by CE-UV. The pK_as of Aβ 1-40 and 1-42 were successfully estimated from the pK_a values determined for their building peptide fragments.
  - The electrophoretic migration of Aβ peptides was predicted with the classical semiempirical models (m_e vs q/M_r^{α}). The best correlation was obtained with the classical polymer model ($q/M_r^{1/2}$).
  - The quality criteria $S_{i,j}$ and T' were used for a rapid, simple and reliable selection of optimized pH conditions for the separation of the mixture of Aβ peptide fragments. It was demonstrated that it was possible to use as a pH optimization variable both the m_e of the Aβ peptide fragments or their $q/M_r^{1/2}$.
  - The separation of Aβ 1-40 and 1-42 was evaluated with $S_{i,j}(q/M_r^{1/2})$ and $T'(q/M_r^{1/2})$. However, separation resolution of their mixtures was poor over the whole pH range due to their very similar structure. PVA coated capillaries allowed reducing the EOF and slightly improving the resolution.

- An IA-SPE-CE-MS method was developed for the analysis of TTR in standards and serum samples, improving the throughput with regard to off-line immunoprecipitation with IA-MBs and CE-MS:
  - UAAF MBs were preferred for IA-SPE-CE-MS because the antibody was not eluted from the MBs. A BGE of 10 mM NH_4Ac was used because acidic BGEs caused antibody denaturation. TTR was eluted with 100 mM NH_4OH (pH 11.2).
  - For TTR standards, repeatability for t_m and A_p was acceptable (%RSD (n = 3) was 2.9 and 4.3%, respectively, for TTR-Cys), microcartridge lifetime was good (>20 analyses in the same day), the method was linear between 5 and 25 µg/mL and LOD was around 1 µg/mL (25 times lower than by CE-MS, 25 µg/mL).

- For the analysis of serum samples, a simple off-line sample pretreatment based on precipitation of the most abundant proteins with 5% (v/v) of phenol was necessary to clean-up the samples. t_m increased compared to the analysis of TTR standards due to irreversible adsorption of matrix components in the inner wall of the separation capillary. Nevertheless, results were repeatable in terms of t_m and A_p (%RSD (n = 3) was 4.7 and 3.2%, for TTR-Cys) and microcartridge lifetime was >10 analyses during the same day.
- In serum samples from healthy controls, the five most abundant proteoforms of normal TTR were detected. In FAP-I patients samples, the main mutant TTR(Met30) proteoform (TTR(Met30)-Cys) was unequivocally detected, demonstrating the potential of the IA-SPE-CE-MS method to screen serum samples for FAP-I.

- An AA-SPE-CE-MS method was developed for the analysis of α-syn in standards and blood samples:
  - In contrast to IA-SPE-CE-MS, the AA sorbent was stable even using acidic BGEs (e.g. 100 mM HAc (pH 2.9)). Similar to TTR analysis by IA-SPE-CE-MS, α-syn was eluted with 100 mM NH_4OH (pH 11.2).
  - For α-syn standards the only detected proteoform was free α-syn. Repeatability for t_m and A_p was acceptable (%RSD (n = 3) was 2.1 and 5.4%, respectively), microcartridge lifetime was good (around 20 analyses in the same day), the method was linear between 0.5 and 10 µg/mL and LOD was 0.2 µg/mL (100 times lower than by CE-MS, 20 µg/mL).
  - For the analysis of erythrocyte lysate samples, an off-line thermal pretreatment was necessary to remove the most abundant proteins. Similar to the analysis of serum samples by IA-SPE-CE-MS, the inner wall of the separation capillary was modified due to irreversible adsorption of sample matrix components. Compared to the analysis of α-syn standards, repeatability was slightly poorer (%RSD (n = 3) was 6.7 and 10.8% for t_m and A_p, respectively) and microcartridge lifetime was shorter (around 10 analyses in the same day). Non-specific adsorption in the AA sorbent of mainly ubiquitin was observed.

- N-acetylated α-syn was detected to be the main proteoform in healthy controls and stage III-IV Parkinson's disease patient samples, and no other minor proteoforms were detected. Therefore, no apparent alteration of blood α-syn proteoforms at the level of a few hundreds of ng/mL seems to occur during Parkinson's disease.

- IMA-SPE-CE-MS with a Ni(II) sorbent was investigated for the selective enrichment of His-peptides:
  - Fifty µg/mL of α-CSN tryptic digests were analyzed by CE-MS using the neutral BGE 25 mM H_3PO_4 (pH 7.5). The coverages of the non-His peptides and His-peptides were 37.1 and 75%, respectively.
  - The IMA-SPE-CE-MS method was optimized and validated with α-CSN tryptic digests using the neutral BGE 25 mM H_3PO_4 (pH 7.5). His-peptides were eluted injecting 0.5% (v/v) of HAc. Under the optimized conditions, the coverages of the non-His peptides and His-peptides were 5.7 and 62.5% for 50 µg/mL of α-CSN tryptic digests, indicating the high selectivity of the IMA sorbent towards the His-peptides. Repeatability for t_m and A_p was good (%RSD (n = 3) were <3.0 and <11%) but microcartridge lifetime was short (10 analyses). Preconcentration factors for the detected His-peptides ranged from 25 to 98.
  - The IMA sorbent showed selectivity towards short His-peptides, which was confirmed analyzing β-CSN and κ-CSN after digestion with trypsin and trypsin:chymotrypsin mixture.
  - To explore the potential of the IMA-SPE-CE-MS method for the analysis of complex protein digests, a tryptic digest of a cell lysate of *E. Coli* that expresses human α-lactalbumin with a His-tag was analyzed. Short His-peptides, mainly between 2 and 4 amino acids long, were identified for myoglobin C and creatine kinase-MM, indicating the potential of the methodology to specifically map certain regions of the proteomes. The α-lactalbumin His-tagged peptide was also detected, suggesting a possible additional application for the on-line preconcentration of intact His-tagged proteins or other His-tagged compounds (e.g. lipids, carbohydrates).

- A SiC-SPE-CE-MS method was developed for the analysis of microRNAs and their post-transcriptional modifications in standards and serum samples:
    - The method was optimized with miR-21 and let-7g standards. The lowest alkali adduct formation and highest sensitivity were obtained with a BGE of 25 mM NH_4Ac (pH 8.0) and 60% (v/v) of ACN as eluent. Repeatability for the t_m and A_p (%RSD (n = 3) was 2.8 and <6.5%) and the microcartridge lifetime (>25 analyses) were good. The method was linear between 25 and 100 nM and LOD was around 10 nM (50 times lower than by CE-MS, 500 nM).
    - To analyze serum samples, an off-line sample pretreatment based on phenol-chloroform-isoamyl alcohol extraction was necessary prior to SiC-SPE-CE-MS.
    - The potential of the method to screen for CLL was demonstrated by the analysis of serum samples from healthy controls and patients. MiRNAs, specifically miR-21 and a 23 nucleotide long 5'-phosphorylated miRNA with 3'-uridylation (iso-miR-16), were only detected in the CLL patient samples.

- NvSPE-CE-MS using a C18 sorbent was investigated and compared to unidirectional SPE-CE-MS for the analysis of opioid peptides and Aβ peptide fragments in standards and plasma samples:
    - NvSPE-CE-MS allowed orthogonal SPE preconcentration and clean-up and CE separation with a single CE instrument. Therefore, it was possible to use different capillary dimensions for loading and separation, without flushing the sample through the separation capillary.
    - NvSPE-CE-MS allowed decreasing the LODs 200 times with regard to CE-MS.
    - Compared to unidirectional SPE-CE-MS, peak efficiencies were better and repeatabilities similar, but total analysis times were longer and LODs were 5 times higher for opioid peptides standards due to the heart-cut operation and the limited volume of the valve loop (20 nL). Nevertheless, the LODs of both methodologies for the analysis plasma samples

were similar, indicating a lower effect of the plasma sample matrix in the analysis by nvSPE-CE-MS.

- NvSPE-CE-MS setup can be regarded as a promising versatile alternative to avoid complicated matrix samples entering the separation capillary in SPE-CE-MS. The separation capillary can be filled with the optimized BGE for the separation and the detection without potential elution of the analytes, enabling additional modes of SPE-CE-MS.

- An IMER-CE-MS method was developed for high-throughput bottom-up analysis of proteins:

  - First, the off-line digestion of β-LG with trypsin in solution and immobilized trypsin, both followed by CE-MS analysis, were optimized. Best digestion efficiency, repeatability and analysis sensitivity were obtained digesting the protein in 50 mM NH_4HCO_3 (pH 7.9) digestion buffer with trypsin in solution at 37 ºC during 18 h, followed by CE-MS separation at 37 ºC.
  - The IMER-CE-MS methodology was also optimized with β-LG. The best sensitivity and repeatability were obtained using 10 mM NH_4HCO_3 (pH 7.9) as the digestion buffer, a very low protein sample flow through the microreactor, a separation BGE of 50 mM HAc:50 mM HFor (pH 2.3) and a temperature of digestion and separation of 37 ºC. Under these optimized conditions, the LOD for complete sequence coverage of β-LG was around 10 μg/mL, the repeatability was comparable to the off-line digestion methods (%RSD (n = 3) was ≤7.6% for t_m and ≤15% for A_p) and the microreactor could be reused until 30 times.
  - The good performance of IMER-CE-MS was also demonstrated for α-CSN, β-CSN and κ-CSN.
  - To explore the potential of the IMER-CE-MS method for the analysis of complex protein samples, an *E. Coli* cell lysate was analyzed. Five proteins (α-lactalbumin, myoglobin C, creatine kinase-MM, cathepsin D and antithrombin III) were identified by IMER-CE-MS and sequence coverages were comparable to the off-line digestion method with trypsin in

solution, confirming the great potential of IMER-CE-MS for the high-throughput bottom-up analysis of complex protein mixtures.

In conclusion, all the methods presented in this thesis for the analysis of peptide, intact protein, protein digests and miRNA biomarkers based on CE-MS approaches, represented a great progress in the field and demonstrated the suitability and potential of this technique for the rapid, sensitive and reliable separation and characterization of the studied biomarkers in biological fluids.

References

[1] R.P. Horgan, L.C. Kenny, 'Omic' technologies: genomics, transcriptomics, proteomics and metabolomics, Obstet. Gynaecol. 13 (2011) 189–195. https://doi.org/10.1576/toag.13.3.189.27672.

[2] S.T. O'Donnell, R.P. Ross, C. Stanton, The progress of multi-omics technologies: Determining function in lactic acid bacteria using a systems level approach, Front. Microbiol. 10 (2020) 3084. https://doi.org/10.3389/fmicb.2019.03084.

[3] K. Yang, X. Han, Lipidomics: Techniques, applications, and outcomes related to biomedical sciences, Trends Biochem. Sci. 41 (2016) 954–969. https://doi.org/10.1016/j.tibs.2016.08.010.

[4] P. Rudd, N.G. Karlsson, K.-H. Khoo, N.H. Packer, Glycomics and glycoproteomics, in: Varki A, Cummings RD, Esko JD, et al. (Eds.), Essentials of Glycobiology, 3rd ed., Cold Spring Harbor Laboratory Press, Cold Spring Harbor, NY, USA, 2017. https://doi.org/10.1101/glycobiology.3e.051.

[5] A.M. Yazbeck, K.R. Tout, P.F. Stadler, J. Hertel, Towards a consistent, quantitative evaluation of microRNA evolution, J. Integr. Bioinform. 14 (2017) 1–9. https://doi.org/10.1515/jib-2016-0013.

[6] B.E. Slatko, A.F. Gardner, F.M. Ausubel, Overview of next-generation sequencing technologies, Curr. Protoc. Mol. Biol. 122 (2018) e59. https://doi.org/10.1002/cpmb.59.

[7] C. Vogel, E.M. Marcotte, Insights into the regulation of protein abundance from proteomic and transcriptomic analyses, Nat. Rev. Genet. 13 (2012) 227–232. https://doi.org/10.1038/nrg3185.

[8] M. Smith, P.L. Flodman, Expanded insights into mechanisms of gene expression and disease related disruptions, Front. Mol. Biosci. 5 (2018) 101. https://doi.org/10.3389/fmolb.2018.00101.

[9] L.M. Smith, N.L. Kelleher, Proteoform: a single term describing protein complexity, Nat. Methods. 10 (2013) 186–187. https://doi.org/10.1038/nmeth.2369.

[10] T.K. Toby, L. Fornelli, N.L. Kelleher, Progress in top-down proteomics and the analysis of proteoforms, Annu. Rev. Anal. Chem. 9 (2016) 499–519. https://doi.org/10.1146/annurev-anchem-071015-041550.

[11] O. Pagel, S. Loroch, A. Sickmann, R.P. Zahedi, Current strategies and findings in clinically relevant post-translational modification-specific proteomics, Expert Rev. Proteomics. 12 (2015) 235–253. https://doi.org/10.1586/14789450.2015.1042867.

[12] R. Aebersold, M. Mann, Mass-spectrometric exploration of proteome structure and

function, Nature. 537 (2016) 347–355. https://doi.org/10.1038/nature19949.

[13] N. Nagaraj, J.R. Wisniewski, T. Geiger, J. Cox, M. Kircher, J. Kelso, S. Pääbo, M. Mann, Deep proteome and transcriptome mapping of a human cancer cell line, Mol. Syst. Biol. 7 (2011) 1–8. https://doi.org/10.1038/msb.2011.81.

[14] R.A. Lubeckyj, E.N. McCool, X. Shen, Q. Kou, X. Liu, L. Sun, Single-shot top-down proteomics with capillary zone electrophoresis-electrospray ionization-tandem mass spectrometry for identification of nearly 600 Escherichia coli proteoforms, Anal. Chem. 89 (2017) 12059–12067. https://doi.org/10.1021/acs.analchem.7b02532.

[15] R. Schiess, B. Wollscheid, R. Aebersold, Targeted proteomic strategy for clinical biomarker discovery, Mol. Oncol. 3 (2009) 33–44. https://doi.org/10.1016/j.molonc.2008.12.001.

[16] Y. Zhang, B.R. Fonslow, B. Shan, M.C. Baek, J.R. Yates, Protein analysis by shotgun/bottom-up proteomics, Chem. Rev. 113 (2013) 2343–2394. https://doi.org/10.1021/cr3003533.

[17] J.M. Burkhart, C. Schumbrutzki, S. Wortelkamp, A. Sickmann, R.P. Zahedi, Systematic and quantitative comparison of digest efficiency and specificity reveals the impact of trypsin quality on MS-based proteomics, J. Proteomics. 75 (2012) 1454–1462. https://doi.org/10.1016/j.jprot.2011.11.016.

[18] A.D. Catherman, O.S. Skinner, N.L. Kelleher, Top Down proteomics: Facts and perspectives, Biochem. Biophys. Res. Commun. 445 (2014) 683–693. https://doi.org/10.1016/j.bbrc.2014.02.041.

[19] Y. Shen, N. Tolić, P.D. Piehowski, A.K. Shukla, S. Kim, R. Zhao, Y. Qu, E. Robinson, R.D. Smith, L. Paša-Tolić, High-resolution ultrahigh-pressure long column reversed-phase liquid chromatography for top-down proteomics, J. Chromatogr. A. 1498 (2017) 99–110. https://doi.org/10.1016/j.chroma.2017.01.008.

[20] E.N. McCool, R.A. Lubeckyj, X. Shen, D. Chen, Q. Kou, X. Liu, L. Sun, Deep top-down proteomics using capillary zone electrophoresis-tandem mass spectrometry: Identification of 5700 proteoforms from the Escherichia coli proteome, Anal. Chem. 90 (2018) 5529–5533. https://doi.org/10.1021/acs.analchem.8b00693.

[21] C. Wu, J.C. Tran, L. Zamdborg, K.R. Durbin, M. Li, D.R. Ahlf, B.P. Early, P.M. Thomas, J. V Sweedler, N.L. Kelleher, A protease for "middle-down" proteomics, Nat. Methods. 9 (2012) 822–824. https://doi.org/10.1038/nmeth.2074.

[22] A.M. Belov, L. Zang, R. Sebastiano, M.R. Santos, D.R. Bush, B.L. Karger, A.R. Ivanov, Complementary middle-down and intact monoclonal antibody proteoform

characterization by capillary zone electrophoresis - mass spectrometry, Electrophoresis. 39 (2018) 2069–2082. https://doi.org/10.1002/elps.201800067.

[23] C.A. Sobsey, S. Ibrahim, V.R. Richard, V. Gaspar, G. Mitsa, V. Lacasse, R.P. Zahedi, G. Batist, C.H. Borchers, Targeted and untargeted proteomics approaches in biomarker development, Proteomics. 20 (2020) 1900029. https://doi.org/10.1002/pmic.201900029.

[24] N.P. Manes, A. Nita-Lazar, Application of targeted mass spectrometry in bottom-up proteomics for systems biology research, J. Proteomics. 189 (2018) 75–90. https://doi.org/10.1016/j.jprot.2018.02.008.

[25] J. Muntel, Y. Xuan, S.T. Berger, L. Reiter, R. Bachur, A. Kentsis, H. Steen, Advancing urinary protein biomarker discovery by data-independent acquisition on a quadrupole-orbitrap mass spectrometer, J. Proteome Res. 14 (2015) 4752–4762. https://doi.org/10.1021/acs.jproteome.5b00826.

[26] J.G. Meyer, B. Schilling, Clinical applications of quantitative proteomics using targeted and untargeted data-independent acquisition techniques, Expert Rev. Proteomics. 14 (2017) 419–429. https://doi.org/10.1080/14789450.2017.1322904.

[27] R.C. Lee, R.L. Feinbaum, V. Ambros, The C. elegans heterochronic gene lin-4 encodes small RNAs with antisense complementarity to lin-14, Cell. 75 (1993) 843–854. https://doi.org/10.1016/0092-8674(93)90529-Y.

[28] B. Wightman, I. Ha, G. Ruvkun, Posttranscriptional regulation of the heterochronic gene lin-14 by lin-4 mediates temporal pattern formation in C. elegans, Cell. 75 (1993) 855–862. https://doi.org/10.1016/0092-8674(93)90530-4.

[29] A. Kozomara, M. Birgaoanu, S. Griffiths-Jones, MiRBase: From microRNA sequences to function, Nucleic Acids Res. 47 (2019) D155–D162. https://doi.org/10.1093/nar/gky1141.

[30] M. Esteller, Non-coding RNAs in human disease, Nat. Rev. Genet. 12 (2011) 861–874. https://doi.org/10.1038/nrg3074.

[31] G. Romano, D. Veneziano, M. Acunzo, C.M. Croce, Small non-coding RNA and cancer, Carcinogenesis. 38 (2017) 485–491. https://doi.org/10.1093/carcin/bgx026.

[32] C. Roden, S. Mastriano, N. Wang, J. Lu, MicroRNA expression profiling: Technologies, insights, and prospects, in: G. Santulli (Ed.), MicroRNA: Medical Evidence. Advances in Experimental Medicine and Biology, Vol 888, 1st ed., Springer, Cham, Switzerland, 2015: pp. 409–421. https://doi.org/10.1007/978-3-319-22671-2_21.

[33] M. Konno, J. Koseki, A. Asai, A. Yamagata, T. Shimamura, D. Motooka, D. Okuzaki, K. Kawamoto, T. Mizushima, H. Eguchi, S. Takiguchi, T. Satoh, K. Mimori, T. Ochiya, Y.

Doki, K. Ofusa, M. Mori, H. Ishii, Distinct methylation levels of mature microRNAs in gastrointestinal cancers, Nat. Commun. 10 (2019) 3888. https://doi.org/10.1038/s41467-019-11826-1.

[34] T. Katoh, Y. Sakaguchi, K. Miyauchi, T. Suzuki, T. Suzuki, S.I. Kashiwabara, T. Baba, Selective stabilization of mammalian microRNAs by 3' adenylation mediated by the cytoplasmic poly(A) polymerase GLD-2, Genes Dev. 23 (2009) 433–438. https://doi.org/10.1101/gad.1761509.

[35] M.R. Jones, L.J. Quinton, M.T. Blahna, J.R. Neilson, A.R. Ivanov, D.A. Wolf, J.P. Mizgerd, Zcchc11-dependent uridylation of microRNA directs cytokine expression, Nat Cell Biol. 11 (2009) 1157–1163. https://doi.org/10.1038/ncb1931.

[36] S. Ikeda, S.W. Kong, J. Lu, E. Bisping, H. Zhang, P.D. Allen, T.R. Golub, B. Pieske, W.T. Pu, Altered microRNA expression in human heart disease, Physiol. Genomics. 31 (2007) 367–373. https://doi.org/10.1152/physiolgenomics.00144.2007.

[37] J. Feng, W. Xing, L. Xie, Regulatory roles of microRNAs in diabetes, Int. J. Mol. Sci. 17 (2016) 1–12. https://doi.org/10.3390/ijms17101729.

[38] J. Lu, G. Getz, E.A. Miska, E. Alvarez-Saavedra, J. Lamb, D. Peck, A. Sweet-Cordero, B.L. Ebert, R.H. Mak, A.A. Ferrando, J.R. Downing, T. Jacks, H.R. Horvitz, T.R. Golub, MicroRNA expression profiles classify human cancers, Nature. 435 (2005) 834–838. https://doi.org/10.1038/nature03702.

[39] S. Volinia, G.A. Calin, C.G. Liu, S. Ambs, A. Cimmino, F. Petrocca, R. Visone, M. Iorio, C. Roldo, M. Ferracin, R.L. Prueitt, N. Yanaihara, G. Lanza, A. Scarpa, A. Vecchione, M. Negrini, C.C. Harris, C.M. Croce, A microRNA expression signature of human solid tumors defines cancer gene targets, Proc. Natl. Acad. Sci. USA. 103 (2006) 2257–2261. https://doi.org/10.1073/pnas.0510565103.

[40] C.H. Lawrie, S. Gal, H.M. Dunlop, B. Pushkaran, A.P. Liggins, K. Pulford, A.H. Banham, F. Pezzella, J. Boultwood, J.S. Wainscoat, C.S.R. Hatton, A.L. Harris, Detection of elevated levels of tumour-associated microRNAs in serum of patients with diffuse large B-cell lymphoma, Br. J. Haematol. 141 (2008) 672–675. https://doi.org/10.1111/j.1365-2141.2008.07077.x.

[41] P.S. Mitchell, R.K. Parkin, E.M. Kroh, B.R. Fritz, S.K. Wyman, E.L. Pogosova-Agadjanyan, A. Peterson, J. Noteboom, K.C. O'Briant, A. Allen, D.W. Lin, N. Urban, C.W. Drescher, B.S. Knudsen, D.L. Stirewalt, R. Gentleman, R.L. Vessella, P.S. Nelson, D.B. Martin, M. Tewari, Circulating microRNAs as stable blood-based markers for cancer detection, Proc. Natl. Acad. Sci. U.S.A. 105 (2008) 10513–10518.

https://doi.org/10.1073/pnas.0804549105.

[42] A. Michael, S.D. Bajracharya, P.S.T. Yuen, H. Zhou, R.A. Star, G.G. Illei, I. Alevizos, Exosomes from human saliva as a source of microRNA biomarkers, Oral Dis. 16 (2010) 34–38. https://doi.org/10.1111/j.1601-0825.2009.01604.x.

[43] M. Hanke, K. Hoefig, H. Merz, A.C. Feller, I. Kausch, D. Jocham, J.M. Warnecke, G. Sczakiel, A robust methodology to study urine microRNA as tumor marker: MicroRNA-126 and microRNA-182 are related to urinary bladder cancer, Urol. Oncol. Semin. Orig. Investig. 28 (2010) 655–661. https://doi.org/10.1016/j.urolonc.2009.01.027.

[44] A. Gallo, M. Tandon, I. Alevizos, G.G. Illei, The majority of microRNAs detectable in serum and saliva is concentrated in exosomes, PLoS One. 7 (2012) 1–5. https://doi.org/10.1371/journal.pone.0030679.

[45] R.A. Boon, K.C. Vickers, Intercellular transport of microRNAs, Arterioscler. Thromb. Vasc. Biol. 33 (2013) 186–192. https://doi.org/10.1161/ATVBAHA.112.300139.

[46] E.L. van Dijk, H. Auger, Y. Jaszczyszyn, C. Thermes, Ten years of next-generation sequencing technology, Trends Genet. 30 (2014) 418–426. https://doi.org/10.1016/j.tig.2014.07.001.

[47] R.T. Fuchs, Z. Sun, F. Zhuang, G.B. Robb, Bias in ligation-based small RNA sequencing library construction is determined by adaptor and RNA structure, PLoS One. 10 (2015) 1–24. https://doi.org/10.1371/journal.pone.0126049.

[48] S.W. Kim, Z. Li, P.S. Moore, A.P. Monaghan, Y. Chang, M. Nichols, B. John, A sensitive non-radioactive northern blot method to detect small RNAs, Nucleic Acids Res. 38 (2010) e98. https://doi.org/10.1093/nar/gkp1235.

[49] W. Li, K. Ruan, MicroRNA detection by microarray, Anal. Bioanal. Chem. 394 (2009) 1117–1124. https://doi.org/10.1007/s00216-008-2570-2.

[50] C. Chen, D.A. Ridzon, A.J. Broomer, Z. Zhou, D.H. Lee, J.T. Nguyen, M. Barbisin, N.L. Xu, V.R. Mahuvakar, M.R. Andersen, K.Q. Lao, K.J. Livak, K.J. Guegler, Real-time quantification of microRNAs by stem-loop RT-PCR, Nucleic Acids Res. 33 (2005) 1–9. https://doi.org/10.1093/nar/gni178.

[51] H. Schwarzenbach, N. Nishida, G.A. Calin, K. Pantel, Clinical relevance of circulating cell-free microRNAs in cancer, Nat. Rev. Clin. Oncol. 11 (2014) 145–56. https://doi.org/10.1038/nrclinonc.2014.5.

[52] T. Tian, J. Wang, X. Zhou, A review: MicroRNA detection methods, Org. Biomol. Chem. 13 (2015) 2226–2238. https://doi.org/10.1039/c4ob02104e.

[53] R. Jaksik, M. Iwanaszko, J. Rzeszowska-Wolny, M. Kimmel, Microarray experiments and factors which affect their reliability, Biol. Direct. 10 (2015) 1–14. https://doi.org/10.1186/s13062-015-0077-2.

[54] FDA-NIH biomarker working group, BEST (Biomarkers, EndpointS, and other Tools) Resource, (2016). www.ncbi.nlm.nih.gov/books/NBK326791/ (accessed September 11, 2020).

[55] P. Davidsson, M. Sjögren, The use of proteomics in biomarker discovery in neurodegenerative diseases, Dis. Markers. 21 (2005) 81–92. https://doi.org/10.1155/2005/848676.

[56] A. Nayak, G. Salt, S.K. Verma, U. Kishore, Proteomics approach to identify biomarkers in neurodegenerative diseases, Int. Rev. Neurobiol. 121 (2015) 59–86. https://doi.org/10.1016/bs.irn.2015.05.003.

[57] H. Lan, H. Lu, X. Wang, H. Jin, MicroRNAs as potential biomarkers in cancer: Opportunities and challenges, Biomed Res. Int. 2015 (2015) 125094. https://doi.org/10.1155/2015/125094.

[58] S. Filipów, Ł. Łaczmański, Blood circulating miRNAs as cancer biomarkers for diagnosis and surgical treatment response, Front. Neurosci. 13 (2019) 1–7. https://doi.org/10.3389/fgene.2019.00169.

[59] G.G. Kovacs, H. Adle-Biassette, I. Milenkovic, S. Cipriani, J. van Scheppingen, E. Aronica, Linking pathways in the developing and aging brain with neurodegeneration, Neuroscience. 269 (2014) 152–172. https://doi.org/10.1016/j.neuroscience.2014.03.045.

[60] C. Soto, S. Pritzkow, Protein misfolding, aggregation, and conformational strains in neurodegenerative diseases, Nat. Neurosci. 21 (2018) 1332–1340. https://doi.org/10.1038/s41593-018-0235-9.

[61] L.C. Walker, Prion-like mechanisms in Alzheimer disease, in: M. Pocchiari, J. Manson (Eds.), Human Prion Diseases. Handbook of Clinical Neurology, Vol 153, 1st ed., Elsevier, Amsterdam, Netherlands, 2018: pp. 303–319. https://doi.org/10.1016/B978-0-444-63945-5.00016-7.

[62] G. Meisl, L. Rajah, S.A.I. Cohen, M. Pfammatter, A. Šarić, E. Hellstrand, A.K. Buell, A. Aguzzi, S. Linse, M. Vendruscolo, C.M. Dobson, T.P.J. Knowles, Scaling behaviour and rate-determining steps in filamentous self-assembly, Chem. Sci. 8 (2017) 7087–7097. https://doi.org/10.1039/c7sc01965c.

[63] M. Vinicius, C. De Mello, L. Vieira, L. Cruz de Souza, K. Gomes, M. Carvalho, Alzheimer's disease: risk factors and potentially protective measures, J. Biomed. Sci. 26

(2019) 1–11. https://doi.org/10.1186/s12929-019-0524-y.

[64] J.A. Kamp, L.G. Moursel, J. Haan, G.M. Terwindt, S.A.M.J. Lesnik Oberstein, S.G. Van Duinen, W.M.C. Van Roon-Mom, Amyloid β in hereditary cerebral hemorrhage with amyloidosis-Dutch type, Rev. Neurosci. 25 (2014) 641–651. https://doi.org/10.1515/revneuro-2014-0008.

[65] B. Falcon, W. Zhang, A.G. Murzin, G. Murshudov, H.J. Garringer, R. Vidal, R.A. Crowther, B. Ghetti, S.H.W. Scheres, M. Goedert, Structures of filaments from Pick's disease reveal a novel tau protein fold, Nature. 561 (2018) 137–140. https://doi.org/10.1038/s41586-018-0454-y.

[66] H. Fujiwara, M. Hasegawa, N. Dohmae, A. Kawashima, E. Masliah, M.S. Goldberg, J. Shen, K. Takio, T. Iwatsubo, α-Synuclein is phosphorylated in synucleinopathy lesions, Nat. Cell Biol. 4 (2002) 160–164. https://doi.org/10.1038/ncb748.

[67] A.L. Olsen, M.B. Feany, Glial α-synuclein promotes neurodegeneration characterized by a distinct transcriptional program in vivo, Glia. 67 (2019) 1933–1957. https://doi.org/10.1002/glia.23671.

[68] P. Gambetti, Q. Kong, W. Zou, P. Parchi, S.G. Chen, Sporadic and familial CJD: classification and characterisation, Br. Med. Bull. 66 (2003) 213–239. https://doi.org/10.1093/bmb/66.1.213.

[69] O. Hardiman, A. Al-Chalabi, A. Chio, E.M. Corr, G. Logroscino, W. Robberecht, P.J. Shaw, Z. Simmons, L.H. van den Berg, Amyotrophic lateral sclerosis, Nat. Rev. Dis. Prim. 3 (2017) 17071. https://doi.org/10.1038/nrdp.2017.71.

[70] G.P. Bates, R. Dorsey, J.F. Gusella, M.R. Hayden, C. Kay, B.R. Leavitt, M. Nance, C.A. Ross, R.I. Scahill, R. Wetzel, E.J. Wild, S.J. Tabrizi, Huntington disease, Nat. Rev. Dis. Prim. 1 (2015) 1–21. https://doi.org/10.1038/nrdp.2015.5.

[71] Y. Ando, M. Ueda, Diagnosis and therapeutic approaches to transthyretin amyloidosis, Curr. Med. Chem. 19 (2012) 2312–2323. https://doi.org/10.2174/092986712800269317.

[72] R.A. Stelzmann, H. Norman Schnitzlein, F. Reed Murtagh, An english translation of Alzheimer's 1907 paper, "Über eine eigenartige erkankung der hirnrinde," Clin. Anat. 8 (1995) 429–431. https://doi.org/10.1002/ca.980080612.

[73] Alzheimer's Association, 2019 Alzheimer's disease facts and figures, 2019. https://doi.org/10.1016/j.jalz.2019.01.010.

[74] M. Goedert, M.G. Spillantini, A century of Alzheimer's Disease, Science. 314 (2006) 777–781. https://doi.org/10.1126/science.1132814.

[75] K. Blennow, H. Hampel, M. Weiner, H. Zetterberg, Cerebrospinal fluid and plasma biomarkers in Alzheimer disease, Nat. Rev. Neurol. 6 (2010) 131–144. https://doi.org/10.1038/nrneurol.2010.4.

[76] J.T. Jarrett, E.P. Berger, P.T. Lansbury, The carboxy terminus of the β amyloid protein is critical for the seeding of amyloid formation: Implications for the pathogenesis of Alzheimer's Disease, Biochemistry. 32 (1993) 4693–4697. https://doi.org/10.1021/bi00069a001.

[77] I.W. Hamley, The amyloid beta peptide: A chemist's perspective. Role in Alzheimer's and fibrillization, Chem. Rev. 112 (2012) 5147–5192. https://doi.org/10.1021/cr3000994.

[78] O. Hansson, H. Zetterberg, P. Buchhave, U. Andreasson, E. Londos, L. Minthon, K. Blennow, Prediction of Alzheimer's disease using the CSF Aβ42/Aβ40 ratio in patients with mild cognitive impairment, Dement. Geriatr. Cogn. Disord. 23 (2007) 316–320. https://doi.org/10.1159/000100926.

[79] N. Fandos, V. Pérez-Grijalba, P. Pesini, S. Olmos, M. Bossa, V.L. Villemagne, J. Doecke, C. Fowler, C.L. Masters, M. Sarasa, Plasma amyloid β 42/40 ratios as biomarkers for amyloid β cerebral deposition in cognitively normal individuals, Alzheimer's Dement. Diagnosis, Assess. Dis. Monit. 8 (2017) 179–187. https://doi.org/10.1016/j.dadm.2017.07.004.

[80] E. Cabrera, P. Mathews, E. Mezhericher, T.G. Beach, J. Deng, T.A. Neubert, A. Rostagno, J. Ghiso, Aβ truncated species: Implications for brain clearance mechanisms and amyloid plaque deposition, Biochim. Biophys. Acta - Mol. Basis Dis. 1864 (2018) 208–225. https://doi.org/10.1016/j.bbadis.2017.07.005.

[81] O. Wirths, S. Zampar, Emerging roles of N- and C-terminally truncated Aβ species in Alzheimer's disease, Expert Opin. Ther. Targets. 23 (2019) 991–1004. https://doi.org/10.1080/14728222.2019.1702972.

[82] K. Kasuga, M. Nishizawa, T. Ikeuchi, α-synuclein as CSF and blood biomarker of dementia with Lewy Bodies, Int. J. Alzheimers. Dis. 2012 (2012) 437025. https://doi.org/10.1155/2012/437025.

[83] G.T. Corbett, J.H. Kordower, The native form of α-synuclein: Monomer, tetramer, or a combination in equilibrium, Mov. Disord. 30 (2015) 1870. https://doi.org/10.1002/mds.26361.

[84] J.P. Anderson, D.E. Walker, J.M. Goldstein, R. De Laat, K. Banducci, R.J. Caccavello, R. Barbour, J. Huang, K. Kling, M. Lee, L. Diep, P.S. Keim, X. Shen, T. Chataway, M.G. Schlossmacher, P. Seubert, D. Schenk, S. Sinha, W.P. Gai, T.J. Chilcote, Phosphorylation

of Ser-129 is the dominant pathological modification of α-synuclein in familial and sporadic lewy body disease, J. Biol. Chem. 281 (2006) 29739–29752. https://doi.org/10.1074/jbc.M600933200.

[85] J. Parkinson, An essay on the shaking palsy. 1817, J. Neuropsychiatry Clin. Neurosci. 14 (2002) 223–236. https://doi.org/10.1176/jnp.14.2.223.

[86] T. Pringsheim, N. Jette, A. Frolkis, T.D.L. Steeves, The prevalence of Parkinson's disease: A systematic review and meta-analysis, Mov. Disord. 29 (2014) 1583–1590. https://doi.org/10.1002/mds.25945.

[87] I.G. McKeith, Clinical Lewy Body syndromes, Ann. N. Y. Acad. Sci. 920 (2000) 1–8. https://doi.org/10.1111/j.1749-6632.2000.tb06898.x.

[88] H.V. Miranda, W. Xiang, R.M. De Oliveira, T. Simões, J. Pimentel, J. Klucken, D. Penque, T.F. Outeiro, Heat-mediated enrichment of α-synuclein from cells and tissue for assessing post-translational modifications, J. Neurochem. 126 (2013) 673–684. https://doi.org/10.1111/jnc.12251.

[89] H.V. Miranda, R. Cássio, L. Correia-Guedes, M.A. Gomes, A. Chegão, E. Miranda, T. Soares, M. Coelho, M.M. Rosa, J.J. Ferreira, T.F. Outeiro, Posttranslational modifications of blood-derived alpha-synuclein as biochemical markers for Parkinson's disease, Sci. Rep. 7 (2017) 13713. https://doi.org/10.1038/s41598-017-14175-5.

[90] R.F. Ritchie, J.T. Whicher, Serum proteins, Encycl. Anal. Chem. (2006). https://doi.org/10.1002/9780470027318.a0542.

[91] C. Andrade, A peculiar form of peripheral neuropathy: Familiar atypical generalized amyloidosis with special involvement of the peripheral nerves, Brain. 75 (1952) 408–427. https://doi.org/10.1093/brain/75.3.408.

[92] K. Poulsen, J.M.C. Bahl, J.T. Tanassi, A.H. Simonsen, N.H.H. Heegaard, Characterization and stability of transthyretin isoforms in cerebrospinal fluid examined by immunoprecipitation and high-resolution mass spectrometry of intact protein, Methods. 56 (2012) 284–292. https://doi.org/10.1016/j.ymeth.2011.12.009.

[93] I. Vaxman, A. Dispenzieri, E. Muchtar, M. Gertz, New developments in diagnosis, risk assessment and management in systemic amyloidosis, Blood Rev. 40 (2020) 100636. https://doi.org/10.1016/j.blre.2019.100636.

[94] American Cancer Society, Cancer facts and figures 2020, (2020). https://www.cancer.org/content/dam/cancer-org/research/cancer-facts-and-statistics/annual-cancer-facts-and-figures/2020/cancer-facts-and-figures-2020.pdf (accessed September 11, 2020).

[95] D. Hanahan, R.A. Weinberg, Hallmarks of cancer: The next generation, Cell. 144 (2011) 646–674. https://doi.org/10.1016/j.cell.2011.02.013.

[96] F. Bray, J. Ferlay, I. Soerjomataram, R.L. Siegel, L.A. Torre, A. Jemal, Global cancer statistics 2018: GLOBOCAN estimates of incidence and mortality worldwide for 36 cancers in 185 countries, CA. Cancer J. Clin. 68 (2018) 394–424. https://doi.org/10.3322/caac.21492.

[97] K. Van Roosbroeck, G.A. Calin, MicroRNAs in chronic lymphocytic leukemia: MiRacle or miRage for prognosis and targeted therapies?, Semin. Oncol. 43 (2016) 209–214. https://doi.org/10.1053/j.seminoncol.2016.02.015.

[98] G.A. Calin, C.D. Dumitru, M. Shimizu, R. Bichi, S. Zupo, E. Noch, H. Aldler, S. Rattan, M. Keating, K. Rai, L. Rassenti, T. Kipps, M. Negrini, F. Bullrich, C.M. Croce, Frequent deletions and down-regulation of micro-RNA genes miR15 and miR16 at 13q14 in chronic lymphocytic leukemia, Proc. Natl. Acad. Sci. USA. 99 (2002) 15524–15529. https://doi.org/10.1073/pnas.242606799.

[99] S. Štěpánová, V. Kašička, Recent developments and applications of capillary and microchip electrophoresis in proteomics and peptidomics (2015–mid 2018), J. Sep. Sci. 42 (2019) 398–414. https://doi.org/10.1002/jssc.201801090.

[100] L. Yi, P.D. Piehowski, T. Shi, R.D. Smith, W.-J. Qian, Advances in microscale separations towards nanoproteomics applications, J. Chromatogr. A. 1523 (2017) 40–48. https://doi.org/10.1016/j.chroma.2017.07.055.

[101] J.W. Jorgenson, K.D. Lukacs, Zone electrophoresis in open-tubular glass capillaries, Anal. Chem. 53 (1981) 1298–1302. https://doi.org/10.1002/jhrc.1240040507.

[102] R.K. Harstad, A.C. Johnson, M.M. Weisenberger, M.T. Bowser, Capillary electrophoresis, Anal. Chem. 88 (2016) 299–319. https://doi.org/10.1021/acs.analchem.5b04125.

[103] R.L.C. Voeten, I.K. Ventouri, R. Haselberg, G.W. Somsen, Capillary electrophoresis: Trends and recent advances, Anal. Chem. 90 (2018) 1464–1481. https://doi.org/10.1021/acs.analchem.8b00015.

[104] J. Sastre Toraño, R. Ramautar, G. de Jong, Advances in capillary electrophoresis for the life sciences, J. Chromatogr. B. 1118–1119 (2019) 116–136. https://doi.org/10.1016/j.jchromb.2019.04.020.

[105] A. Lechner, J. Giorgetti, R. Gahoual, A. Beck, E. Leize-Wagner, Y.N. François, Insights from capillary electrophoresis approaches for characterization of monoclonal antibodies and antibody drug conjugates in the period 2016–2018, J. Chromatogr. B Anal. Technol.

Biomed. Life Sci. 1122–1123 (2019) 1–17. https://doi.org/10.1016/j.jchromb.2019.05.014.

[106] S. Bernardo-Bermejo, E. Sánchez-López, M. Castro-Puyana, M.L. Marina, Chiral capillary electrophoresis, Trends Anal. Chem. 124 (2020) 115807. https://doi.org/10.1016/j.trac.2020.115807.

[107] H.H. Lauer, G.P. Rozing, eds., High performance capillary electrophoresis, 2nd ed., Agilent Technologies, Waldbronn, Germany, 2014. https://www.agilent.com/cs/library/primers/public/5990-3777EN.pdf (accessed September 11, 2020).

[108] A. Tiselius, The moving boundary method of studying the electrophoresis of proteins, Nov. Acta Regiae Soc. Sci. Ups. 7 (1930) 1–107.

[109] S. Hjerten, Free zone electrophoresis, Chromatogr. Rev. 9 (1967) 122–219.

[110] S.K. Poole, S. Patel, K. Dehring, H. Workman, C.F. Poole, Determination of acid dissociation constants by capillary electrophoresis, J. Chromatogr. A. 1037 (2004) 445–454. https://doi.org/10.1016/j.chroma.2004.02.087.

[111] P. Nowak, M. Wozniakiewicz, P. Koscielniak, Application of capillary electrophoresis in determination of acid dissociation constant values, J. Chromatogr. A. 1377 (2015) 1–12. https://doi.org/10.1016/j.chroma.2014.12.032.

[112] V. Sanz-Nebot, F. Benavente, I. Toro, J. Barbosa, Migration behavior of therapeutic peptide hormones: prediction of optimal separation by capillary electrophoresis, Electrophoresis. 22 (2001) 4333–40. https://doi.org/10.1002/1522-2683(200112)22:20<4333::AID-ELPS4333>3.0.CO;2-8.

[113] S. Babić, A.J.M. Horvat, D. Mutavdžić Pavlović, M. Kaštelan-Macan, Determination of pKa values of active pharmaceutical ingredients, TrAC - Trends Anal. Chem. 26 (2007) 1043–1061. https://doi.org/10.1016/j.trac.2007.09.004.

[114] F. Benavente, B. Andón, E. Giménez, J. Barbosa, V. Sanz-Nebot, Modeling the migration behavior of rabbit liver apothioneins in capillary electrophoresis, Electrophoresis. 29 (2008) 2790–2800. https://doi.org/10.1002/elps.200700852.

[115] F. Benavente, E. Giménez, D. Barrón, J. Barbosa, V. Sanz-Nebot, Modeling the electrophoretic behavior of quinolones in aqueous and hydroorganic media, Electrophoresis. 31 (2010) 965–972. https://doi.org/10.1002/elps.200900344.

[116] Z. Qiang, C. Adams, Potentiometric determination of acid dissociation constants (pKa) for human and veterinary antibiotics, Water Res. 38 (2004) 2874–2890.

https://doi.org/10.1016/j.watres.2004.03.017.

[117] R.I. Allen, K.J. Box, J.E.A. Comer, C. Peake, K.Y. Tam, Multiwavelength spectrophotometric determination of acid dissociation constants of ionizable drugs, J. Pharm. Biomed. Anal. 17 (1998) 699–712. https://doi.org/10.1016/S0731-7085(98)00010-7.

[118] J. Bezençon, M.B. Wittwer, B. Cutting, M. Smieško, B. Wagner, M. Kansy, B. Ernst, pKa determination by 1H NMR spectroscopy - An old methodology revisited, J. Pharm. Biomed. Anal. 93 (2014) 147–155. https://doi.org/10.1016/j.jpba.2013.12.014.

[119] R. Konášová, J.J. Dytrtová, V. Kašička, Determination of acid dissociation constants of triazole fungicides by pressure assisted capillary electrophoresis, J. Chromatogr. A. 1408 (2015) 243–249. https://doi.org/10.1016/j.chroma.2015.07.005.

[120] N.J. Adamson, E.C. Reynolds, Rules relating electrophoretic mobility, charge and molecular size of peptides and proteins, J. Chromatogr. B Biomed. Appl. 699 (1997) 133–147. https://doi.org/10.1016/S0378-4347(97)00202-8.

[121] A. Cifuentes, H. Poppe, Behavior of peptides in capillary electrophoresis: effect of peptide charge, mass and structure, Electrophoresis. 18 (1997) 2362–2376. https://doi.org/10.1002/elps.1150181227.

[122] A. Sillero, J.M. Ribeiro, Isoelectric points of proteins: theoretical determination, Anal. Biochem. 179 (1989) 319–325. https://doi.org/10.1016/0003-2697(89)90136-X.

[123] A. Barroso, E. Gimenez, F. Benavente, J. Barbosa, V. Sanz-Nebot, Modelling the electrophoretic migration behaviour of peptides and glycopeptides from glycoprotein digests in capillary electrophoresis-mass spectrometry, Anal. Chim. Acta. 854 (2015) 169–177. https://doi.org/10.1016/j.aca.2014.10.038.

[124] V. Dolník, Selectivity, differential mobility and resolution as parameters to optimize capillary electrophoretic separation, J. Chromatogr. A. 744 (1996) 115–121. https://doi.org/10.1016/0021-9673(96)00449-9.

[125] L.S. Ettre, Nomenclature for chromatography (IUPAC recommendations 1993), Pure Appl. Chem. 65 (1993) 819–872. https://doi.org/10.1351/pac199365040819.

[126] M. Tascon, F. Benavente, C.B. Castells, L.G. Gagliardi, Quality criterion to optimize separations in capillary electrophoresis : application to the analysis of harmala alkaloids, J. Chromatogr. A. 1460 (2016) 190–196. https://doi.org/10.1016/j.chroma.2016.07.032.

[127] N. Khan, G. Mironov, M. V. Berezovski, Direct detection of endogenous microRNAs and their post-transcriptional modifications in cancer serum by capillary electrophoresis-mass

spectrometry, Anal. Bioanal. Chem. 408 (2016) 2891–2899. https://doi.org/10.1007/s00216-015-9277-y.

[128] I.A. Brewis, P. Brennan, Proteomics technologies for the global identification and quantification of proteins, in: R. Donev (Ed.), Advances in Protein Chemistry and Structural Biology, Vol 80, 1st ed., Academic Press, Oxford, UK, 2010: pp. 1–44. https://doi.org/10.1016/B978-0-12-381264-3.00001-1.

[129] W.M.A. Niessen, MS–MS and MSn, in: J.C. Lindon, G.E. Tranter, D.W. Koppenaal (Eds.), Encyclopedia of Spectroscopy and Spectrometry, 3rd ed., Academic Press, Oxford, UK, 2017: pp. 936–941. https://doi.org/10.1016/B978-0-12-409547-2.05219-7.

[130] A. El-Aneed, A. Cohen, J. Banoub, Mass spectrometry, review of the basics: Electrospray, MALDI, and commonly used mass analyzers, Appl. Spectrosc. Rev. 44 (2009) 210–230. https://doi.org/10.1080/05704920902717872.

[131] M. Dole, L.L. Mack, R.L. Hines, R.C. Mobley, L.D. Ferguson, M.B. Alice, Molecular beams of macroions, J. Chem. Phys. 49 (1968) 2240–2249. https://doi.org/10.1063/1.1670391.

[132] J.B. Fenn, M. Mann, C.K. Meng, S.F. Wong, C.M. Whitehouse, Electrospray ionization for mass spectrometry of large biomolecules, Science. 246 (1989) 64–71. https://doi.org/10.1126/science.2675315.

[133] E. Domínguez-Vega, R. Haselberg, G.W. Somsen, Capillary zone electrophoresis–mass spectrometry of intact proteins, in: N.T. Tran, M. Taverna (Eds.), Capillary Electrophoresis of Proteins and Peptides. Methods in Molecular Biology, Vol 1466, 1st ed., Humana Press, New York, NY, USA, 2016: pp. 25–41. https://doi.org/10.1007/978-1-4939-4014-1_3.

[134] E.J. Maxwell, D.D.Y. Chen, Twenty years of interface development for capillary electrophoresis-electrospray ionization-mass spectrometry, Anal. Chim. Acta. 627 (2008) 25–33. https://doi.org/10.1016/j.aca.2008.06.034.

[135] P.W. Lindenburg, R. Haselberg, G. Rozing, R. Ramautar, Developments in interfacing designs for CE–MS: Towards enabling tools for proteomics and metabolomics, Chromatographia. 78 (2014) 367–377. https://doi.org/10.1007/s10337-014-2795-5.

[136] A. Stolz, K. Jooß, O. Höcker, J. Römer, J. Schlecht, C. Neusüß, Recent advances in capillary electrophoresis-mass spectrometry: Instrumentation, methodology and applications, Electrophoresis. 40 (2019) 79–112. https://doi.org/10.1002/elps.201800331.

[137] R.D. Smith, J.A. Olivares, N.T. Nguyen, H.R. Udseth, Capillary zone electrophoresis-mass spectrometry using an electrospray ionization interface, Anal. Chem. 60 (1988) 436–

441. https://doi.org/10.1021/ac00156a013.

[138] G. Bonvin, J. Schappler, S. Rudaz, Capillary electrophoresis-electrospray ionization-mass spectrometry interfaces: fundamental concepts and technical developments, J. Chromatogr. A. 1267 (2012) 17–31. https://doi.org/10.1016/j.chroma.2012.07.019.

[139] Z. Kele, G. Ferenc, É. Klement, G.K. Tóth, T. Janáky, Design and performance of a sheathless capillary electrophoresis/mass spectrometry interface by combining fused-silica capillaries with gold-coated nanoelectrospray tips, Rapid Commun. Mass Spectrom. 19 (2005) 881–885. https://doi.org/10.1002/rcm.1866.

[140] Y. Ishihama, H. Katayama, N. Asakawa, Y. Oda, Highly robust stainless steel tips as microelectrospray emitters, Rapid Commun. Mass Spectrom. 16 (2002) 913–918. https://doi.org/10.1002/rcm.647.

[141] L. Fang, R. Zhang, E.R. Williams, R.N. Zare, On-line time-of-flight mass spectrometric analysis of peptides separated by capillary electrophoresis, Anal. Chem. 66 (1994) 3696–3701. https://doi.org/10.1021/ac00093a025.

[142] M. Moini, Simplifying CE-MS operation. 2. Interfacing low-flow separation techniques to mass spectrometry using a porous tip, Anal. Chem. 79 (2007) 4241–4246. https://doi.org/10.1021/ac0704560.

[143] C. Wenz, C. Barbas, Á. López-Gonzálvez, A. Garcia, F. Benavente, V. Sanz-Nebot, T. Blanc, G. Freckleton, P. Britz-McKibbin, M. Shanmuganathan, F. de l'Escaille, J. Far, R. Haselberg, S. Huang, C. Huhn, M. Pattky, D. Michels, S. Mou, F. Yang, C. Neusuess, N. Tromsdorf, E.E.K. Baidoo, J.D. Keasling, S.S. Park, Interlaboratory study to evaluate the robustness of capillary electrophoresis-mass spectrometry for peptide mapping, J. Sep. Sci. 38 (2015) 3262–3270. https://doi.org/10.1002/jssc.201500551.

[144] J. Schappler, V. González-Ruiz, S. Rudaz, CE-MS in drug analysis and bioanalysis, in: G. de Jong (Ed.), Capillary Electrophoresis–Mass Spectrometry: Principles and Applications, 1st ed., Wiley-VCH, Weinheim, Germany, 2016: pp. 129–157. https://doi.org/10.1002/9783527693801.ch6.

[145] A. Taichrib, M. Pelzing, C. Pellegrino, M. Rossi, C. Neusüß, High resolution TOF MS coupled to CE for the analysis of isotopically resolved intact proteins, J. Proteomics. 74 (2011) 958–966. https://doi.org/10.1016/j.jprot.2011.01.006.

[146] R. Haselberg, G. Somsen, CE-MS for the analysis of intact proteins, in: G. de Jong (Ed.), Capillary Electrophoresis–Mass Spectrometry: Principles and Applications, 1st ed., Wiley-VCH, Weinheim, Germany, 2016: pp. 159–192. https://doi.org/10.1002/9783527693801.ch7.

[147] R. Ramautar, P. Britz-McKibbin, CE-MS for clinical proteomics and metabolomics: Strategies and applications, in: G. de Jong (Ed.), Capillary Electrophoresis–Mass Spectrometry: Principles and Applications, 1st ed., Wiley-VCH, Weinheim, Germany, 2016: pp. 315–343. https://doi.org/10.1002/9783527693801.ch11.

[148] A.G. Marshall, C.L. Hendrickson, High-resolution mass spectrometers, Annu. Rev. Anal. Chem. 1 (2008) 579–599. https://doi.org/10.1146/annurev.anchem.1.031207.112945.

[149] R.J. Cotter, Time-of-flight mass spectrometry for the structural analysis of biological molecules, Anal. Chem. 64 (1992) 1027–1039. https://doi.org/10.1021/ac00045a002.

[150] M. Guilhaus, D. Selby, V. Mlynski, Orthogonal acceleration time-of-flight mass spectrometry, Mass Spectrom. Rev. 19 (2000) 65–107. https://doi.org/10.1002/(SICI)1098-2787(2000)19:2<65::AID-MAS1>3.0.CO;2-E.

[151] K.D. Clark, C. Zhang, J.L. Anderson, Sample preparation for bioanalytical and pharmaceutical analysis, Anal. Chem. 88 (2016) 11262–11270. https://doi.org/10.1021/acs.analchem.6b02935.

[152] N. Drouin, S. Rudaz, J. Schappler, Sample preparation for polar metabolites in bioanalysis, Analyst. 143 (2018) 16–20. https://doi.org/10.1039/c7an01333g.

[153] M.C. Breadmore, R.M. Tubaon, A.I. Shallan, S.C. Phung, A.S.A. Keyon, D. Gstoettenmayr, P. Prapatpong, A.A. Alhusban, L. Ranjbar, H.H. See, M. Dawod, J.P. Quirino, Recent advances in enhancing the sensitivity of electrophoresis and electrochromatography in capillaries and microchips (2012-2014), Electrophoresis. 36 (2015) 36–61. https://doi.org/0.1002/elps.201400420.

[154] M.C. Breadmore, A. Wuethrich, F. Li, S.C. Phung, U. Kalsoom, J.M. Cabot, T. Masoomeh, A.I. Shallan, A.S. Abdul Keyon, H.H. See, M. Dawod, J.P. Quirino, Recent advances in enhancing the sensitivity of electrophoresis and electrochromatography in capillaries and microchips (2014-2016), Electrophoresis. 38 (2017) 33–59. https://doi.org/10.1002/elps.201600331.

[155] M.C. Breadmore, W. Grochocki, U. Kalsoom, M.N. Alves, S.C. Phung, M.T. Rokh, J.M. Cabot, A. Ghiasvand, F. Li, A.I. Shallan, A.S.A. Keyon, A.A. Alhusban, H.H. See, A. Wuethrich, M. Dawod, J.P. Quirino, Recent advances in enhancing the sensitivity of electrophoresis and electrochromatography in capillaries in microchips (2016–2018), Electrophoresis. 40 (2019) 17–39. https://doi.org/10.1002/elps.201800384.

[156] P. Puig, F. Borrull, M. Calull, C. Aguilar, Sorbent preconcentration procedures coupled to capillary electrophoresis for environmental and biological applications, Anal. Chim. Acta. 616 (2008) 1–18. https://doi.org/10.1016/j.aca.2008.03.062.

[157] F.W.A. Tempels, W.J.M. Underberg, G.W. Somsen, G.J. de Jong, Design and applications of coupled SPE-CE, Electrophoresis. 29 (2008) 108–128. https://doi.org/10.1002/elps.200700149.

[158] R. Ramautar, G.W. Somsen, G.J. de Jong, Developments in coupled solid-phase extraction-capillary electrophoresis 2009-2011, Electrophoresis. 33 (2012) 243–250. https://doi.org/10.1002/elps.201100453.

[159] R. Ramautar, G.W. Somsen, G.J. de Jong, Developments in coupled solid-phase extraction-capillary electrophoresis 2011-2013, Electrophoresis. 35 (2014) 128–37. https://doi.org/10.1002/elps.201300335.

[160] R. Ramautar, G.W. Somsen, G.J. de Jong, Developments in coupled solid-phase extraction–capillary electrophoresis 2013-2015, Electrophoresis. 37 (2016) 35–44. https://doi.org/10.1002/elps.201500401.

[161] A. Šlampová, Z. Malá, P. Gebauer, Recent progress of sample stacking in capillary electrophoresis (2016–2018), Electrophoresis. 40 (2019) 40–54. https://doi.org/10.1002/elps.201800261.

[162] Z. Malá, P. Gebauer, Recent progress in analytical capillary isotachophoresis, Electrophoresis. 40 (2019) 55–64. https://doi.org/10.1002/elps.201800239.

[163] A.A. Kazarian, E.F. Hilder, M.C. Breadmore, Online sample pre-concentration via dynamic pH junction in capillary and microchip electrophoresis, J. Sep. Sci. 34 (2011) 2800–2821. https://doi.org/10.1002/jssc.201100414.

[164] U. Pyell, A.H. Rageh, M. El-Awady, The concept of stationary and moving boundaries modelled as accelerating or decelerating planes in the understanding of sweeping processes employed for online focusing in capillary zone electrophoresis and electrokinetic chromatography, Chromatographia. 80 (2017) 359–382. https://doi.org/10.1007/s10337-017-3261-y.

[165] F. Benavente, S. Medina-Casanellas, E. Giménez, V. Sanz-Nebot, On-line solid-phase extraction capillary electrophoresis mass spectrometry for preconcentration and clean-up of peptides and proteins, in: N.T. Tran, M. Taverna (Eds.), Capillary Electrophoresis of Proteins and Peptides. Methods in Molecular Biology, Vol 1466, 1st ed., Humana Press, New York, NY, USA, 2016: pp. 67–84. https://doi.org/10.1007/978-1-4939-4014-1_6.

[166] K. Bielicka-Daszkiewicz, A. Voelkel, Theoretical and experimental methods of determination of the breakthrough volume of SPE sorbents, Talanta. 80 (2009) 614–621. https://doi.org/10.1016/j.talanta.2009.07.037.

[167] L. Pont, F. Benavente, J. Barbosa, V. Sanz-Nebot, An update for human blood plasma

pretreatment for optimized recovery of low-molecular-mass peptides prior to CE-MS and SPE-CE-MS, J. Sep. Sci. 36 (2013) 3896–3902. https://doi.org/10.1002/jssc.201300838.

[168] N.A. Guzman, M.A. Trebilcock, J.P. Advis, The use of a concentration step to collect urinary components separated by capillary electrophoresis and further characterization of collected analytes by mass spectrometry, J. Liq. Chromatogr. 14 (1991) 997–1015. https://doi.org/10.1080/01483919108049300.

[169] J.Y. He, A. Shibukawa, M. Zeng, S. Amane, T. Sawada, T. Nakagawa, On-capillary sample preconcentration incorporated in chiral capillary electrophoresis, Anal. Sci. 12 (1996) 177–181. https://doi.org/10.2116/analsci.12.177.

[170] S. Medina-Casanellas, Y.H. Tak, F. Benavente, V. Sanz-Nebot, J. Sastre Toraño, G.W. Somsen, G.J. de Jong, Evaluation of fritless solid-phase extraction coupled on-line with capillary electrophoresis-mass spectrometry for the analysis of opioid peptides in cerebrospinal fluid, Electrophoresis. 35 (2014) 2996–3002. https://doi.org/10.1002/elps.201400293.

[171] J. Cai, Z. El Rassi, On-line preconcentration of triazine herbicides with tandem octadecyl capillaries-capillary zone electrophoresis, J. Liq. Chromatogr. 15 (1992) 1179–1192. https://doi.org/10.1080/10826079208018857.

[172] T.M. Phillips, J.J. Chmielinska, Immunoaffinity capillary electrophoretic analysis of cyclosporin in tears, Biomed. Chromatogr. 8 (1994) 242–246. https://doi.org/10.1002/bmc.1130080509.

[173] E. Ortiz-Villanueva, F. Benavente, E. Giménez, F. Yilmaz, V. Sanz-Nebot, Preparation and evaluation of open tubular C18-silica monolithic microcartridges for preconcentration of peptides by on-line solid phase extraction capillary electrophoresis, Anal. Chim. Acta. 846 (2014) 51–59. https://doi.org/10.1016/j.aca.2014.06.046.

[174] A. Marechal, F. Jarrosson, J. Randon, V. Dugas, C. Demesmay, In-line coupling of an aptamer based miniaturized monolithic affinity preconcentration unit with capillary electrophoresis and laser induced fluorescence detection, J. Chromatogr. A. 1406 (2015) 109–117. https://doi.org/10.1016/j.chroma.2015.05.073.

[175] C.W. Whang, J. Pawliszyn, Solid phase microextraction coupled to capillary electrophoresis, Anal. Commun. 35 (1998) 353–356. https://doi.org/10.1039/a806794e.

[176] A.J. Tomlinson, S. Naylor, Systematic development of on-line membrane preconcentration-capillary electrophoresis-mass spectrometry for the analysis of peptide mixtures, J. Capillary Electrophor. 2 (1995) 225–233.

[177] L.G. Rashkovetsky, Y. V. Lyubarskaya, F. Foret, D.E. Hughes, B.L. Karger, Automated

microanalysis using magnetic beads with commercial capillary electrophoretic instrumentation, J. Chromatogr. A. 781 (1997) 197–204. https://doi.org/10.1016/S0021-9673(97)00629-8.

[178] G. Morales-Cid, J.C. Diez-Masa, M. de Frutos, On-line immunoaffinity capillary electrophoresis based on magnetic beads for the determination of alpha-1 acid glycoprotein isoforms profile to facilitate its use as biomarker, Anal. Chim. Acta. 773 (2013) 89–96. https://doi.org/10.1016/j.aca.2013.02.037.

[179] A.J. Tomlinson, N.A. Guzman, S. Naylor, Enhancement of concentration limits of detection in CE and CE-MS: a review of on-line sample extraction, cleanup, analyte preconcentration, and microreactor technology, J. Capillary Electrophor. 2 (1995) 247–266.

[180] N.A. Guzman, S.S. Park, D. Schaufelberger, L. Hernandez, X. Paez, P. Rada, A.J. Tomlinson, S. Naylor, New approaches in clinical chemistry: On-line analyte concentration and microreaction capillary electrophoresis for the determination of drugs, metabolic intermediates, and biopolymers in biological fluids, J. Chromatogr. B Biomed. Appl. 697 (1997) 37–66. https://doi.org/10.1016/S0378-4347(97)00275-2.

[181] N.A. Guzman, Determination of immunoreactive gonadotropin-releasing hormone in serum and urine by on-line immunoaffinity capillary electrophoresis coupled to mass spectrometry, J. Chromatogr. B. Biomed. Sci. Appl. 749 (2000) 197–213. https://doi.org/10.1016/S0378-4347(00)00410-2.

[182] N.A. Guzman, T.M. Phillips, Immunoaffinity capillary electrophoresis: a new versatile tool for determining protein biomarkers in inflammatory processes, Electrophoresis. 32 (2011) 1565–1578. https://doi.org/10.1002/elps.201000700.

[183] J.R. Veraart, H. Lingeman, U.A.T. Brinkman, Coupling of biological sample handling and capillary electrophoresis, J. Chromatogr. A. 856 (1999) 483–514. https://doi.org/10.1016/S0021-9673(99)00588-9.

[184] A.J.J. Debets, M. Mazereeuw, W.H. Voogt, D.J. van Iperen, H. Lingeman, K.P. Hupe, U.A.T. Brinkman, Switching valve with internal micro precolumn for on-line sample enrichment in capillary zone electrophoresis, J. Chromatogr. A. 608 (1992) 151–158. https://doi.org/10.1016/0021-9673(92)87117-Q.

[185] F.W.A. Tempels, W.J.M. Underberg, G.W. Somsen, G.J. de Jong, On-line coupling of SPE and CE-MS for peptide analysis, Electrophoresis. 28 (2007) 1319–1326. https://doi.org/10.1002/elps.200600403.

[186] N.A. Guzman, T. Blanc, T.M. Phillips, Immunoaffinity capillary electrophoresis as a

powerful strategy for the quantification of low-abundance biomarkers, drugs, and metabolites in biological matrices, Electrophoresis. 29 (2008) 3259–3278. https://doi.org/10.1002/elps.200800058.

[187] N.A. Guzman, D.E. Guzman, An emerging micro-scale immuno-analytical diagnostic tool to see the unseen. Holding promise for precision medicine and P4 medicine, J. Chromatogr. B Anal. Technol. Biomed. Life Sci. 1021 (2016) 14–29. https://doi.org/10.1016/j.jchromb.2015.11.026.

[188] F.J. Kohl, C. Neusüß, CZE–CZE ESI–MS coupling with a fully isolated mechanical valve, in: Philippe Schmitt-Kopplin (Ed.), Capillary Electrophoresis. Methods in Molecular Biology, Vol 1483, 1st ed., Humana Press, New York, NY, USA, 2016: pp. 155–166. https://doi.org/10.1007/978-1-4939-6403-1_9.

[189] J. Pawliszyn, Sample preparation: quo vadis?, Anal. Chem. 75 (2003) 2543–2558. https://doi.org/10.1021/ac034094h.

[190] F. Benavente, S. Medina-Casanellas, J. Barbosa, V. Sanz-Nebot, Investigation of commercial sorbents for the analysis of opioid peptides in human plasma by on-line SPE-CE, J. Sep. Sci. 33 (2010) 1294–1304. https://doi.org/10.1002/jssc.200900669.

[191] L. Ortiz-Martin, F. Benavente, S. Medina-Casanellas, E. Giménez, V. Sanz-Nebot, Study of immobilized metal affinity chromatography sorbents for the analysis of peptides by on-line solid-phase extraction capillary electrophoresis-mass spectrometry, Electrophoresis. 36 (2015) 962–970. https://doi.org/10.1002/elps.201400374.

[192] D. Moreno-González, F.J. Lara, L. Gámiz-Gracia, A.M. García-Campaña, Molecularly imprinted polymer as in-line concentrator in capillary electrophoresis coupled with mass spectrometry for the determination of quinolones in bovine milk samples, J. Chromatogr. A. 1360 (2014) 1–8. https://doi.org/10.1016/j.chroma.2014.07.049.

[193] S. Yamamoto, S. Suzuki, S. Suzuki, Microchip electrophoresis of oligosaccharides using lectin-immobilized preconcentrator gels fabricated by in situ photopolymerization, Analyst. 137 (2012) 2211–2217. https://doi.org/10.1039/c2an16015c.

[194] E. Hernández, F. Benavente, V. Sanz-Nebot, J. Barbosa, Evaluation of on-line solid phase extraction-capillary electrophoresis-electrospray-mass spectrometry for the analysis of neuropeptides in human plasma, Electrophoresis. 29 (2008) 3366–3376. https://doi.org/10.1002/elps.200700872.

[195] C.A. Janeway Jr, P. Travers, M. Walport, M.J. Shlomchik, Immunobiology: The immune system in health and disease, 5th ed., Garland Science, New York, NY, USA, 2001.

[196] J.K.H. Liu, The history of monoclonal antibody development - Progress, remaining

challenges and future innovations, Ann. Med. Surg. 3 (2014) 113–116. https://doi.org/10.1016/j.amsu.2014.09.001.

[197] N.S. Lipman, L.R. Jackson, L.J. Trudel, F. Weis-Garcia, Monoclonal versus polyclonal antibodies: Distinguishing characteristics, applications, and information resources, ILAR J. 46 (2005) 258–268. https://doi.org/10.1093/ilar.46.3.258.

[198] D.S. Hage, Handbook of Affinity Chromatography, 2nd ed., Taylor & Francis, Boca Raton, FL, USA, 2006. https://doi.org/10.1201/9780824751982.

[199] A. Singh, S. Chaudhary, A. Agarwal, A.S. Verma, Antibodies: Monoclonal and polyclonal, in: A.S. Verma, A. Singh (Eds.), Animal Biotechnology: Models in Discovery and Translation, 1st ed., Academic Press, London, UK, 2014: pp. 265–287. https://doi.org/10.1016/B978-0-12-416002-6.00015-8.

[200] E. Giménez, F. Benavente, C. de Bolós, E. Nicolás, J. Barbosa, V. Sanz-Nebot, Analysis of recombinant human erythropoietin and novel erythropoiesis stimulating protein digests by immunoaffinity capillary electrophoresis-mass spectrometry, J. Chromatogr. A. 1216 (2009) 2574–82. https://doi.org/10.1016/j.chroma.2009.01.057.

[201] S. Medina-Casanellas, F. Benavente, J. Barbosa, V. Sanz-Nebot, Preparation and evaluation of an immunoaffinity sorbent for the analysis of opioid peptides by on-line immunoaffinity solid-phase extraction capillary electrophoresis-mass spectrometry, Anal. Chim. Acta. 717 (2012) 134–142. https://doi.org/10.1016/j.aca.2011.11.057.

[202] S. Medina-Casanellas, F. Benavente, J. Barbosa, V. Sanz-Nebot, Preparation and evaluation of an immunoaffinity sorbent with Fab' antibody fragments for the analysis of opioid peptides by on-line immunoaffinity solid-phase extraction capillary electrophoresis-mass spectrometry, Anal. Chim. Acta. 789 (2013) 91–99. https://doi.org/10.1016/j.aca.2013.06.030.

[203] J. Kudr, Y. Haddad, L. Richtera, Z. Heger, M. Cernak, V. Adam, O. Zitka, Magnetic nanoparticles: From design and synthesis to real world applications, Nanomaterials. 7 (2017) 243. https://doi.org/10.3390/nano7090243.

[204] Z. Farka, T. Juřík, D. Kovář, L. Trnková, P. Skládal, Nanoparticle-based immunochemical biosensors and assays: Recent advances and challenges, Chem. Rev. 117 (2017) 9973–10042. https://doi.org/10.1021/acs.chemrev.7b00037.

[205] G.T. Hermanson, Immobilization of ligands on chromatography supports, in: G.T. Hermanson (Ed.), Bioconjugate Techniques, 3rd ed., Academic Press, Boston, MA, USA, 2013: pp. 589–740. https://doi.org/10.1016/B978-0-12-382239-0.00015-7.

[206] K. Sefah, D. Shangguan, X. Xiong, M.B. O'Donoghue, W. Tan, Development of DNA

aptamers using Cell-SELEX, Nat. Protoc. 5 (2010) 1169–1185. https://doi.org/10.1038/nprot.2010.66.

[207] J. Banerjee, M. Nilsen-Hamilton, Aptamers: Multifunctional molecules for biomedical research, J. Mol. Med. 91 (2013) 1333–1342. https://doi.org/10.1007/s00109-013-1085-2.

[208] A. Blanco, G. Blanco, Regulation of gene expression, in: A. Blanco, G. Blanco (Eds.), Medical Biochemistry, 1st ed., Academic Press, London, UK, 2017: pp. 525–533. https://doi.org/10.1016/B978-0-12-803550-4.00023-9.

[209] C. Tuerk, L. Gold, Systematic evolution of ligands by exponential enrichment: RNA ligands to bacteriophage T4 DNA polymerase, Science. 249 (1990) 505–510. https://doi.org/10.1126/science.2200121.

[210] A.D. Ellington, J.W. Szostak, In vitro selection of RNA molecules that bind specific ligands, Nature. 346 (1990) 818–822. https://doi.org/10.1038/346818a0.

[211] D.L. Robertson, G.F. Joyce, Selection in vitro of an RNA enzyme that specifically cleaves single-stranded DNA, Nature. 344 (1990) 467–468. https://doi.org/10.1038/344467a0.

[212] T. Mairal, V. Cengiz Özalp, P. Lozano Sánchez, M. Mir, I. Katakis, C.K. O'Sullivan, Aptamers: Molecular tools for analytical applications, Anal. Bioanal. Chem. 390 (2008) 989–1007. https://doi.org/10.1007/s00216-007-1346-4.

[213] M. Darmostuk, S. Rimpelova, H. Gbelcova, T. Ruml, Current approaches in SELEX : An update to aptamer selection technology, Biotechnol. Adv. 33 (2015) 1141–1161. https://doi.org/10.1016/j.biotechadv.2015.02.008.

[214] A. Ruscito, M.C. DeRosa, Small-molecule binding aptamers: Selection strategies, characterization, and applications, Front. Chem. 4 (2016) 1–14. https://doi.org/10.3389/fchem.2016.00014.

[215] M. Takahashi, Aptamers targeting cell surface proteins, Biochimie. 145 (2018) 63–72. https://doi.org/10.1016/j.biochi.2017.11.019.

[216] M. Chen, Y. Yu, F. Jiang, J. Zhou, Y. Li, C. Liang, L. Dang, A. Lu, G. Zhang, Development of cell-SELEX technology and its application in cancer diagnosis and therapy, Int. J. Mol. Sci. 17 (2016) 1–14. https://doi.org/10.3390/ijms17122079.

[217] E.W.M. Ng, D.T. Shima, P. Calias, E.T. Cunningham, D.R. Guyer, A.P. Adamis, Pegaptanib, a targeted anti-VEGF aptamer for ocular vascular disease, Nat. Rev. Drug Discov. 5 (2006) 123–132. https://doi.org/10.1038/nrd1955.

[218] A.T. Ponce, K.L. Hong, A mini-review: Clinical development and potential of aptamers for thrombotic events treatment and monitoring, Biomedicines. 7 (2019) 55.

https://doi.org/10.3390/biomedicines7030055.

[219] J. Zhou, J. Rossi, Aptamers as targeted therapeutics: Current potential and challenges, Nat. Rev. Drug Discov. 16 (2017) 181–202. https://doi.org/10.1038/nrd.2016.199.

[220] J.W.D. Foy, K. Rittenhouse, M. Modi, M. Patel, Local tolerance and systemic safety of pegaptanib sodium in the dog and rabbit, J. Ocul. Pharmacol. Ther. 23 (2007) 452–466. https://doi.org/10.1089/jop.2006.0149.

[221] A.D. Keefe, S. Pai, A. Ellington, Aptamers as therapeutics, Nat. Rev. Drug Discov. 9 (2010) 537–550. https://doi.org/10.1038/nrd3141.

[222] L. Zhang, A.F. Radovic-Moreno, F. Alexis, F.X. Gu, P.A. Basto, V. Bagalkot, S. Jon, R.S. Langer, O.C. Farokhzad, Co-delivery of hydrophobic and hydrophilic drugs from nanoparticle–aptamer bioconjugates, ChemMedChem. 2 (2007) 1268–1271. https://doi.org/10.1002/cmdc.200700121.

[223] U. Wullner, I. Neef, A. Eller, M. Kleines, M.K. Tur, S. Barth, Cell-specific induction of apoptosis by rationally designed bivalent aptamer-siRNA transcripts silencing eukaryotic elongation factor 2, Curr. Cancer Drug Targets. 8 (2008) 554–565. https://doi.org/10.2174/156800908786241078.

[224] P. Röthlisberger, C. Gasse, M. Hollenstein, Nucleic acid aptamers: Emerging applications in medical imaging, nanotechnology, neurosciences, and drug delivery, Int. J. Mol. Sci. 18 (2017) 2430. https://doi.org/10.3390/ijms18112430.

[225] G.S. Zamay, T.I. Ivanchenko, T.N. Zamay, V.L. Grigorieva, Y.E. Glazyrin, O.S. Kolovskaya, I. V. Garanzha, A.A. Barinov, A. V. Krat, G.G. Mironov, A. Gargaun, D. V. Veprintsev, S.S. Bekuzarov, A.K. Kirichenko, R.A. Zukov, M.M. Petrova, A.A. Modestov, M. V. Berezovski, A.S. Zamay, DNA aptamers for the characterization of histological structure of lung adenocarcinoma, Mol. Ther. - Nucleic Acids. 6 (2017) 150–162. https://doi.org/10.1016/j.omtn.2016.12.004.

[226] G.S. Zamay, T.N. Zamay, V.A. Kolovskii, A. V. Shabanov, Y.E. Glazyrin, D. V. Veprintsev, A. V. Krat, S.S. Zamay, O.S. Kolovskaya, A. Gargaun, A.E. Sokolov, A.A. Modestov, I.P. Artyukhov, N. V. Chesnokov, M.M. Petrova, M. V. Berezovski, A.S. Zamay, Electrochemical aptasensor for lung cancer-related protein detection in crude blood plasma samples, Sci. Rep. 6 (2016) 34350. https://doi.org/10.1038/srep34350.

[227] M.N. Win, J.S. Klein, C.D. Smolke, Codeine-binding RNA aptamers and rapid determination of their binding constants using a direct coupling surface plasmon resonance assay, Nucleic Acids Res. 34 (2006) 5670–5682. https://doi.org/10.1093/nar/gkl718.

[228] I.A. Ferreira-Bravo, C. Cozens, P. Holliger, J.J. DeStefano, Selection of 2′-deoxy-2′-

fluoroarabinonucleotide (FANA) aptamers that bind HIV-1 reverse transcriptase with picomolar affinity, Nucleic Acids Res. 43 (2015) 9587–9599. https://doi.org/10.1093/nar/gkv1057.

[229] J.G. Bruno, A.M. Richarte, M.P. Carrillo, A. Edge, An aptamer beacon responsive to botulinum toxins, Biosens. Bioelectron. 31 (2012) 240–243. https://doi.org/10.1016/j.bios.2011.10.024.

[230] F. Brothier, V. Pichon, Miniaturized DNA aptamer-based monolithic sorbent for selective extraction of a target analyte coupled on-line to nanoLC, Anal. Bioanal. Chem. 406 (2014) 7875–7886. https://doi.org/10.1007/s00216-014-8256-z.

[231] V. Pichon, F. Brothier, A. Combès, Aptamer-based-sorbents for sample treatment - A review, Anal. Bioanal. Chem. 407 (2015) 681–698. https://doi.org/10.1007/s00216-014-8129-5.

[232] B. Madru, F. Chapuis-Hugon, E. Peyrin, V. Pichon, Determination of cocaine in human plasma by selective solid-phase extraction using an aptamer-based sorbent, Anal. Chem. 81 (2009) 7081–7086. https://doi.org/10.1021/ac9006667.

[233] F. Du, M.N. Alam, J. Pawliszyn, Aptamer-functionalized solid phase microextraction-liquid chromatography/tandem mass spectrometry for selective enrichment and determination of thrombin, Anal. Chim. Acta. 845 (2014) 45–52. https://doi.org/10.1016/j.aca.2014.08.018.

[234] C. Perréard, F. D'Orlyé, S. Griveau, B. Liu, F. Bedioui, A. Varenne, Aptamer entrapment in microfluidic channel using one-step sol-gel process, in view of the integration of a new selective extraction phase for lab-on-a-chip, Electrophoresis. 38 (2017) 2456–2461. https://doi.org/10.1002/elps.201600575.

[235] Aptagen LLC, Apta-Index, (2019). https://www.aptagen.com/apta-index/ (accessed September 11, 2020).

[236] F.R.N. Gurd, P.E. Wilcox, Complex formation between metallic cations and proteins, peptides, and amino acids, in: M.L. Anson, K. Bailey, J.T. Edsall (Eds.), Advances in Protein Chemistry, 1st ed., Academic Press, Oxford, UK, 1956: pp. 311–427. https://doi.org/10.1016/S0065-3233(08)60424-6.

[237] G. Goldstein, Ligand-exchange chromatography of nucleotides, nucleosides, and nucleic acid bases, Anal. Biochem. 20 (1967) 477–483. https://doi.org/10.1016/0003-2697(67)90292-8.

[238] J. Porath, J. Carlsson, I. Olsson, G. Belfrage, Metal chelate affinity chromatography, a new approach to protein fractionation, Nature. 258 (1975) 598–599.

https://doi.org/10.1038/258598a0.

[239] D. Todorova, M.A. Vijayalakshmi, Immobilized metal-ion affinity chromatography, in: D.S. Hage (Ed.), Handbook of Affinity Chromatography, 2nd ed., Taylor & Francis, Boca Raton, FL, USA, 2006: pp. 257–280. https://doi.org/10.1201/9780824751982.

[240] E. Hochuli, W. Bannwarth, H. Döbeli, R. Gentz, D. Stüber, Genetic approach to facilitate purification of recombinant proteins with a novel metal chelate adsorbent, Bio/Technology. 6 (1988) 1321–1325. https://doi.org/10.1038/nbt1188-1321.

[241] H. Block, B. Maertens, A. Spriestersbach, N. Brinker, J. Kubicek, R. Fabis, J. Labahn, F. Schäfer, Immobilized-metal affinity chromatography (IMAC): A review, in: R.R. Burgess, M.P. Deutscher (Eds.), Guide to Protein Purification. Methods in Enzymology, Vol 463, 2nd ed., Academic Press, Oxford, UK, 2009: pp. 439–473. https://doi.org/10.1016/S0076-6879(09)63027-5.

[242] E. Sulkowski, The saga of IMAC and MIT, BioEssays. 10 (1989) 170–175. https://doi.org/10.1002/bies.950100508.

[243] A. Spriestersbach, J. Kubicek, F. Schäfer, H. Block, B. Maertens, Purification of His-tagged proteins, Methods Enzymol. 559 (2015) 1–15. https://doi.org/10.1016/bs.mie.2014.11.003.

[244] D. Ren, N.A. Penner, B.E. Slentz, F.E. Regnier, Histidine-rich peptide selection and quantification in targeted proteomics, J. Proteome Res. 3 (2004) 37–45. https://doi.org/10.1021/pr034049q.

[245] R.C.F. Cheung, J.H. Wong, T.B. Ng, Immobilized metal ion affinity chromatography: a review on its applications, Appl. Microbiol. Biotechnol. 96 (2012) 1411–1420. https://doi.org/10.1007/s00253-012-4507-0.

[246] K. Haupt, F. Roy, M.A. Vijayalakshmi, Immobilized metal ion affinity capillary electrophoresis of proteins - A model for affinity capillary electrophoresis using soluble polymer-supported ligands, Anal. Biochem. 234 (1996) 149–154. https://doi.org/10.1006/abio.1996.0066.

[247] K.-Y. Jiang, O. Pitiot, M. Anissimova, H. Adenier, M.A. Vijayalakshmi, Structure-function relationship in glycosylated α-chymotrypsin as probed by IMAC and IMACE, Biochim. Biophys. Acta - Protein Struct. Mol. Enzymol. 1433 (1999) 198–209. https://doi.org/10.1016/S1388-1981(99)00087-6.

[248] J. Cai, Z. El Rassi, Selective on-line preconcentration of proteins by tandem metal chelate capillaries-capillary zone electrophoresis, J. Liq. Chromatogr. 16 (1993) 2007–2024. https://doi.org/10.1080/10826079308019910.

[249] N.M. Vizioli, M.L. Rusell, M.L. Carbajal, C.N. Carducci, M. Grasselli, On-line affinity selection of histidine-containing peptides using a polymeric monolithic support for capillary electrophoresis, Electrophoresis. 26 (2005) 2942–2948. https://doi.org/10.1002/elps.200410416.

[250] L. Zhang, L. Zhang, W. Zhang, Y. Zhang, On-line concentration of peptides and proteins with the hyphenation of polymer monolithic immobilized metal affinity chromatography and capillary electrophoresis, Electrophoresis. 26 (2005) 2172–2178. https://doi.org/10.1002/elps.200410377.

[251] P. Cao, J.T. Stults, Phosphopeptide analysis by on-line immobilized metal-ion affinity chromatography-capillary electrophoresis-electrospray ionization mass spectrometry, J. Chromatogr. A. 853 (1999) 225–235. https://doi.org/10.1016/s0021-9673(99)00481-1.

[252] J. Sambrook, E.F. Fritsch, T. Maniatis, Molecular cloning: A laboratory manual, 2nd ed., Cold Spring Harbor Laboratory Press, Cold Spring Harbor, NY, USA, 1989. https://doi.org/10.1016/0167-7799(91)90068-S.

[253] P. Chomczynski, N. Sacchi, The single-step method of RNA isolation by acid guanidinium thiocyanate–phenol–chloroform extraction: twenty-something years on, Nat. Protoc. 1 (2006) 581–585. https://doi.org/10.1038/nprot.2006.83.

[254] I.A. Zaporozhchenko, E.S. Morozkin, T.E. Skvortsova, O.E. Bryzgunova, A.A. Bondar, E.M. Loseva, V. V. Vlassov, P.P. Laktionov, A phenol-free method for isolation of microRNA from biological fluids, Anal. Biochem. 479 (2015) 43–47. https://doi.org/10.1016/j.ab.2015.03.028.

[255] B. Lam, M. Elmogy, S.-S. Geng, P. Roberts, N. Rghei, Y. Haj-Ahmad, Silicon carbide as a novel RNA affinity medium with improved sensitivity and size diversity, (2008). https://norgenbiotek.com/sites/default/files/resources/Poster-13-Silicon-Carbide-as-a-Novel-RNA-Affinity-Medium-with-Improved-Sensitivity-and-Size-Diversity.pdf (accessed September 11, 2020).

[256] S.C. Tan, B.C. Yiap, DNA, RNA, and protein extraction: The past and the present, J. Biomed. Biotechnol. 2009 (2009) 574398. https://doi.org/10.1155/2009/574398.

[257] R.E. Farrell, RNA isolation strategies, in: R.E. Farrell (Ed.), RNA Methodologies: A Laboratory Guide for Isolation and Characterization, 4th ed., Academic Press, Oxford, UK, 2010: pp. 45–80. https://doi.org/10.1016/B978-0-12-374727-3.00002-4.

[258] Y. Haj-Ahmad, Methods and columns for nucleic acid purification, US9845463, 2017.

[259] M. Mraz, K. Malinova, J. Mayer, S. Pospisilova, MicroRNA isolation and stability in stored RNA samples, Biochem. Biophys. Res. Commun. 390 (2009) 1–4.

https://doi.org/10.1016/j.bbrc.2009.09.061.

[260] E. Giménez, R. Ramos-Hernan, F. Benavente, J. Barbosa, V. Sanz-Nebot, Analysis of recombinant human erythropoietin glycopeptides by capillary electrophoresis electrospray-time of flight-mass spectrometry, Anal. Chim. Acta. 709 (2012) 81–90. https://doi.org/10.1016/j.aca.2011.10.028.

[261] A.A. Homaei, R. Sariri, F. Vianello, R. Stevanato, Enzyme immobilization: An update, J. Chem. Biol. 6 (2013) 185–205. https://doi.org/10.1007/s12154-013-0102-9.

[262] L. Liu, B. Zhang, Q. Zhang, Y. Shi, L. Guo, L. Yang, Capillary electrophoresis-based immobilized enzyme reactor using particle-packing technique, J. Chromatogr. A. 1352 (2014) 80–86. https://doi.org/10.1016/j.chroma.2014.05.058.

[263] X. Liu, J. Yang, L. Yang, Capillary electrophoresis-integrated immobilized enzyme reactors, Rev. Anal. Chem. 35 (2016) 115–131. https://doi.org/10.1515/revac-2016-0003.

[264] L.N. Amankwa, W.G. Kuhr, Trypsin-modified fused-silica capillary microreactor for peptide mapping by capillary zone electrophoresis, Anal. Chem. 64 (1992) 1610–1613. https://doi.org/10.1021/ac00038a019.

[265] L. Licklider, W.G. Kuhr, M.P. Lacey, T. Keough, M.P. Purdon, R. Takigiku, Online microreactors/capillary electrophoresis/mass spectrometry for the analysis of proteins and peptides, Anal. Chem. 67 (1995) 4170–4177. https://doi.org/10.1021/ac00118a021.

[266] J. Křenková, K. Klepárník, F. Foret, Capillary electrophoresis mass spectrometry coupling with immobilized enzyme electrospray capillaries, J. Chromatogr. A. 1159 (2007) 110–118. https://doi.org/10.1016/j.chroma.2007.02.095.

[267] Z. Yin, W. Zhao, M. Tian, Q. Zhang, L. Guo, L. Yang, A capillary electrophoresis-based immobilized enzyme reactor using graphene oxide as a support via layer by layer electrostatic assembly, Analyst. 139 (2014) 1973–1979. https://doi.org/10.1039/c3an02241b.

[268] R.M. Schoenherr, M. Ye, M. Vannatta, N.J. Dovichi, CE-Microreactor-CE-MS/MS for protein analysis, Anal. Chem. 79 (2007) 2230–2238. https://doi.org/10.1021/ac061638h.

[269] K. Sakai-Kato, M. Kato, T. Toyo'oka, On-line trypsin-encapsulated enzyme reactor by the sol - gel method integrated into capillary electrophoresis, Anal. Chem. 74 (2002) 2943–2949. https://doi.org/10.1021/ac0200421.

[270] M. Shalaeva, J. Kenseth, F. Lombardo, A. Bastin, Measurement of dissociation constants (pKa values) of organic compounds by multiplexed capillary electrophoresis using aqueous and cosolvent buffers, J. Pharm. Sci. 97 (2008) 2581–2606.

https://doi.org/10.1002/jps.21287.

[271] C.A. Currie, W.R. Heineman, H.B. Halsall, C.J. Seliskar, P.A. Limbach, F. Arias, K.R. Wehmeyer, Estimation of pKa values using microchip capillary electrophoresis and indirect fluorescence detection, J. Chromatogr. B Anal. Technol. Biomed. Life Sci. 824 (2005) 201–205. https://doi.org/10.1016/j.jchromb.2005.07.035.

[272] X. Fu, Y. Liu, W. Li, Y. Bai, Y. Liao, H. Liu, Determination of dissociation constants of aristolochic acid I and II by capillary electrophoresis with carboxymethyl chitosan-coated capillary, Talanta. 85 (2011) 813–815. https://doi.org/10.1016/j.talanta.2011.03.088.

[273] G. Aptisa, F. Benavente, V. Sanz-Nebot, E. Chirila, J. Barbosa, Evaluation of migration behaviour of therapeutic peptide hormones in capillary electrophoresis using polybrene-coated capillaries, Anal. Bioanal. Chem. 396 (2010) 1571–1579. https://doi.org/10.1007/s00216-009-3344-1.

[274] H. Wan, A.G. Holmén, Y. Wang, W. Lindberg, M. Englund, M.B. Någård, R.A. Thompson, High-throughput screening of pKa values of pharmaceuticals by pressure-assisted capillary electrophoresis and mass spectrometry, Rapid Commun. Mass Spectrom. 17 (2003) 2639–2648. https://doi.org/10.1002/rcm.1229.

[275] F. Benavente, E. Balaguer, J. Barbosa, V. Sanz-Nebot, Modelling migration behavior of peptide hormones in capillary electrophoresis-electrospray mass spectrometry, J. Chromatogr. A. 1117 (2006) 94–102. https://doi.org/10.1016/j.chroma.2006.03.049.

[276] J.M. Cabot, E. Fuguet, M. Rosés, P. Smejkal, M.C. Breadmore, Novel instrument for automated pKa determination by internal standard capillary electrophoresis, Anal. Chem. 87 (2015) 6165–6172. https://doi.org/10.1021/acs.analchem.5b00845.

[277] E.C. Rickard, M.M. Strohl, R.G. Nielsen, Correlation of electrophoretic mobilities from capillary electrophoresis with physicochemical properties of proteins and peptides, Anal. Biochem. 197 (1991) 197–207. https://doi.org/10.1016/0003-2697(91)90379-8.

[278] D.L. Nelson, M.M. Cox, Lehninger Principles of Biochemistry, 5th ed., W. H. Freeman, New York, NY, USA, 2008.

[279] V. Sanz-Nebot, F. Benavente, E. Hernández, J. Barbosa, Evaluation of the electrophoretic behaviour of opioid peptides. Separation by capillary electrophoresis-electrospray ionization mass spectrometry, Anal. Chim. Acta. 577 (2006) 68–76. https://doi.org/10.1016/j.aca.2006.06.035.

[280] K.D. Lukacs, J.W. Jorgenson, Capillary zone electrophoresis: effect of physical parameters on separation efficiency and quantitation, J. High Resol. Chromatogr. 8 (1985) 407–411. https://doi.org/10.1002/jhrc.1240080810.

[281] C. Lancioni, S. Keunchkarian, C.B. Castells, L.G. Gagliardi, Enantiomeric separations by capillary electrophoresis: Theoretical method to determine optimum chiral selector concentration, J. Chromatogr. A. 1539 (2018) 71–77. https://doi.org/10.1016/j.chroma.2018.01.002.

[282] V. Kašička, Recent developments in capillary and microchip electroseparations of peptides (2015–mid 2017), Electrophoresis. 39 (2018) 209–234. https://doi.org/10.1002/elps.201700295.

[283] S. Štěpánová, V. Kašička, Recent applications of capillary electromigration methods to separation and analysis of proteins, Anal. Chim. Acta. 933 (2016) 23–42. https://doi.org/10.1016/j.aca.2016.06.006.

[284] M. Gilges, M.H. Kleemiss, G. Schomburg, Capillary zone electrophoresis separations of basic and acidic proteins using poly(vinyl alcohol) coatings in fused silica capillaries, Anal. Chem. 66 (1994) 2038–2046. https://doi.org/10.1021/ac00085a019.

[285] Y. Shen, R.D. Smith, High-resolution capillary isoelectric focusing of proteins using highly hydrophilic-substituted cellulose-coated capillaries, J. Microcolumn Sep. 12 (2000) 135–141. https://doi.org/10.1002/(SICI)1520-667X(2000)12:3<135::AID-MCS2>3.0.CO;2-5.

[286] D. Belder, A. Deege, H. Husmann, F. Kohler, M. Ludwig, Cross-linked poly(vinyl alcohol) as permanent hydrophilic column coating for capillary electrophoresis, Electrophoresis. 22 (2001) 3813–3818. https://doi.org/10.1002/1522-2683(200109)22:17<3813::AID-ELPS3813>3.0.CO;2-D.

[287] G.G. Wolken, E.A. Arriaga, Simultaneous measurement of individual mitochondrial membrane potential and electrophoretic mobility by capillary electrophoresis, Anal. Chem. 86 (2014) 4217–4226. https://doi.org/10.1021/ac403849x.

[288] M. Poitevin, A. Morin, J.M. Busnel, S. Descroix, M.C. Hennion, G. Peltre, Comparison of different capillary isoelectric focusing methods-use of “narrow pH cuts” of carrier ampholytes as original tools to improve resolution, J. Chromatogr. A. 1155 (2007) 230–236. https://doi.org/10.1016/j.chroma.2007.02.013.

[289] L. Pont, F. Benavente, J. Barbosa, V. Sanz-Nebot, On-line immunoaffinity solid-phase extraction capillary electrophoresis mass spectrometry using Fab´antibody fragments for the analysis of serum transthyretin, Talanta. 170 (2017) 224–232. https://doi.org/10.1016/j.talanta.2017.03.104.

[290] K. Ensing, A. Paulus, Immobilization of antibodies as a versatile tool in hybridized capillary electrophoresis, J. Pharm. Biomed. Anal. 14 (1996) 305–315.

https://doi.org/10.1016/0731-7085(95)01607-4.

[291] T.M. Phillips, B.F. Dickens, Analysis of recombinant cytokines in human body fluids by immunoaffinity capillary electrophoresis, Electrophoresis. 19 (1998) 2991–2996. https://doi.org/10.1002/elps.1150191632.

[292] S. Medina-Casanellas, F. Benavente, E. Giménez, J. Barbosa, V. Sanz-Nebot, On-line immunoaffinity solid-phase extraction capillary electrophoresis mass spectrometry for the analysis of large biomolecules: A preliminary report, Electrophoresis. 35 (2014) 2130–2136. https://doi.org/10.1002/elps.201400119.

[293] Y.T. Chen, A.G. Kolhatkar, O. Zenasni, S. Xu, T.R. Lee, Biosensing using magnetic particle detection techniques, Sensors. 17 (2017) 2300. https://doi.org/10.3390/s17102300.

[294] P.W. Stege, J. Raba, G.A. Messina, Online immunoaffinity assay-CE using magnetic nanobeads for the determination of anti-Helicobacter pylori IgG in human serum, Electrophoresis. 31 (2010) 3475–3481. https://doi.org/10.1002/elps.201000123.

[295] N. Gasilova, H.H. Girault, Component-resolved diagnostic of cow's milk allergy by immunoaffinity capillary electrophoresis-matrix assisted laser desorption/ionization mass spectrometry, Anal. Chem. 86 (2014) 6337–6345. https://doi.org/10.1021/ac500525n.

[296] R. Théberge, L. Connors, M. Skinner, J. Skare, C.E. Costello, Characterization of transthyretin mutants from serum using immunoprecipitation, HPLC/electrospray ionization and matrix-assisted laser desorption/ionization mass spectrometry, Anal. Chem. 71 (1999) 452–459. https://doi.org/10.1021/ac980531u.

[297] T. Nakanishi, T. Sato, S. Sakoda, M. Yoshioka, A. Shimizu, Modification of cysteine residue in transthyretin and a synthetic peptide: analyses by electrospray ionization mass spectrometry, Biochim. Biophys. Acta. 1698 (2004) 45–53. https://doi.org/10.1016/j.bbapap.2003.10.005.

[298] L. Pont, K. Poturcu, F. Benavente, J. Barbosa, V. Sanz-Nebot, Comparison of capillary electrophoresis and capillary liquid chromatography coupled to mass spectrometry for the analysis of transthyretin in human serum, J. Chromatogr. A. 1444 (2016) 145–153. https://doi.org/10.1016/j.chroma.2016.03.052.

[299] H. Terazaki, Y. Ando, O. Suhr, P.I. Ohlsson, K. Obayashi, T. Yamashita, S. Yoshimatsu, M. Suga, M. Uchino, M. Ando, Post-translational modification of transthyretin in plasma, Biochem. Biophys. Res. Commun. 249 (1998) 26–30. https://doi.org/10.1006/bbrc.1998.9097.

[300] L. Pont, F. Benavente, J. Barbosa, V. Sanz-Nebot, Analysis of transthyretin in human

serum by capillary zone electrophoresis electrospray ionization time-of-flight mass spectrometry. Application to familial amyloidotic polyneuropathy type I, Electrophoresis. 36 (2015) 1265–1273. https://doi.org/10.1002/elps.201400590.

[301] E. Hernández, F. Benavente, V. Sanz-Nebot, J. Barbosa, Analysis of opioid peptides by on-line SPE-CE-ESI-MS, Electrophoresis. 28 (2007) 3957–3965. https://doi.org/10.1002/elps.200700845.

[302] A.M. Reuter, G. Hamoir, R. Marchand, F. Kennes, Isolation and properties of a mouse serum prealbumin excreted in urine, Eur. J. Biochem. 5 (1968) 233–238. https://doi.org/10.1111/j.1432-1033.1968.tb00362.x.

[303] M. V Bimanpalli, P.S. Ghaswala, Isolation, purification and partial characterisation of prealbumin from cerebrospinal fluid, J. Biosci. 13 (1988) 159–169. https://doi.org/10.1007/BF02903098.

[304] S. Reverdatto, D. Burz, A. Shekhtman, Peptide aptamers: Development and applications, Curr. Top. Med. Chem. 15 (2015) 1082–1101. https://doi.org/10.2174/1568026615666150413153143.

[305] R. Pero-Gascon, L. Pont, F. Benavente, J. Barbosa, V. Sanz-Nebot, Analysis of serum transthyretin by on-line immunoaffinity solid-phase extraction capillary electrophoresis mass spectrometry using magnetic beads, Electrophoresis. 37 (2016) 1220–1231. https://doi.org/10.1002/elps.201500495.

[306] K. Tsukakoshi, R. Harada, K. Sode, K. Ikebukuro, Screening of DNA aptamer which binds to α-synuclein, Biotechnol. Lett. 32 (2010) 643–648. https://doi.org/10.1007/s10529-010-0200-5.

[307] R. Barbour, K. Kling, J.P. Anderson, K. Banducci, T. Cole, L. Diep, M. Fox, J.M. Goldstein, F. Soriano, P. Seubert, T.J. Chilcote, Red blood cells are the major source of alpha-synuclein in blood, Neurodegener. Dis. 5 (2008) 55–59. https://doi.org/10.1159/000112832.

[308] J.H. Ringrose, W.W. Van Solinge, S. Mohammed, M.C.O. Flaherty, A.J.R. Heck, M. Slijper, Highly efficient depletion strategy improves erythrocyte proteome coverage dramatically, J. Proteome Res. 7 (2008) 3060–3063. https://doi.org/10.1021/pr8001029.

[309] M. Borges-Alvarez, F. Benavente, J. Barbosa, V. Sanz-Nebot, Separation and characterization of superoxide dismutase 1 (SOD-1) from human erythrocytes by capillary electrophoresis time-of-flight mass spectrometry, Electrophoresis. 33 (2012) 2561–2569. https://doi.org/10.1002/elps.201100672.

[310] S.M. Park, H.Y. Jung, K.C. Chung, H. Rhim, J.H. Park, J. Kim, Stress-induced

aggregation profiles of GST-α-synuclein fusion proteins: role of the C-terminal acidic tail of α-synuclein in protein thermosolubility and stability, Biochemistry. 41 (2002) 4137–4146. https://doi.org/10.1021/bi015961k.

[311] R.A. Bradshaw, Protein translocation and turnover in eukaryotic cells, Trends Biochem. Sci. 14 (1989) 276–279. https://doi.org/10.1016/0968-0004(89)90063-7.

[312] J. Bergström, M. Ingelsson, Alpha-synuclein as a diagnostic biomarker for Parkinson's disease, in: M. Ingelsson, L. Lannfelt (Eds.), Immunotherapy and Biomarkers in Neurodegenerative Disorders. Methods in Pharmacology and Toxicology, Humana Press, New York, NY, USA, 2016: pp. 215–234. https://doi.org/10.1007/978-1-4939-3560-4_14.

[313] H. Zhang, W. Yan, R. Aebersold, Chemical probes and tandem mass spectrometry: A strategy for the quantitative analysis of proteomes and subproteomes, Curr. Opin. Chem. Biol. 8 (2004) 66–75. https://doi.org/10.1016/j.cbpa.2003.12.001.

[314] F.E. Regnier, L. Riggs, R. Zhang, L. Xiong, P. Liu, A. Chakraborty, E. Seeley, C. Sioma, R.A. Thompson, Comparative proteomics based on stable isotope labeling and affinity selection, J. Mass Spectrom. 37 (2002) 133–145. https://doi.org/10.1002/jms.290.

[315] R.R. Prasanna, S. Sidhik, A.S. Kamalanathan, K. Bhagavatula, M.A. Vijayalakshmi, Affinity selection of histidine-containing peptides using metal chelate methacrylate monolithic disk for targeted LC-MS/MS approach in high-throughput proteomics, J. Chromatogr. B Anal. Technol. Biomed. Life Sci. 955–956 (2014) 42–49. https://doi.org/10.1016/j.jchromb.2014.02.020.

[316] C. Mesmin, B. Domon, Improvement of the performance of targeted LC-MS assays through enrichment of histidine-containing peptides, J. Proteome Res. 13 (2014) 6160–6168. https://doi.org/10.1021/pr5008152.

[317] N.A.M. Eskin, H.D. Goff, Milk, in: Biochemistry of Foods, 3rd ed., Academic Press, Oxford, UK, 2013: pp. 187–214. https://doi.org/10.1016/B978-0-08-091809-9.00004-2.

[318] L. Pont, F. Benavente, J. Jaumot, R. Tauler, J. Alberch, S. Ginés, J. Barbosa, V. Sanz-Nebot, Metabolic profiling for the identification of Huntington biomarkers by on-line solid-phase extraction capillary electrophoresis mass spectrometry combined with advanced data analysis tools, Electrophoresis. 37 (2016) 795–808. https://doi.org/10.1002/elps.201500378.

[319] J.C. Wright, M.O. Collins, L. Yu, L. Käll, M. Brosch, J.S. Choudhary, Enhanced peptide identification by electron transfer dissociation using an improved mascot percolator, Mol. Cell. Proteomics. 11 (2012) 478–491. https://doi.org/10.1074/mcp.O111.014522.

[320] T. Stora, Z. Dienes, H. Vogel, C. Duschl, Histidine-tagged amphiphiles for the reversible formation of lipid bilayer aggregates on chelator-functionalized gold surfaces, Langmuir. 16 (2000) 5471–5478. https://doi.org/10.1021/la991711h.

[321] J. Partyka, J. Krenkova, R. Cmelik, F. Foret, Multi-charged labeling of oligosaccharides and N-linked glycans by hexahistidine-based tags for capillary electrophoresis-mass spectrometry analysis, J. Chromatogr. A. 1560 (2018) 91–96. https://doi.org/10.1016/j.chroma.2018.05.030.

[322] A.M.B. Giessing, F. Kirpekar, Mass spectrometry in the biology of RNA and its modifications, J. Proteomics. 75 (2012) 3434–3449. https://doi.org/10.1016/j.jprot.2012.01.032.

[323] P. Thaplyal, P.C. Bevilacqua, Experimental approaches for measuring pKa's in RNA and DNA, in: D.H. Burke-Aguero (Ed.), Riboswitch Discovery, Structure and Function. Methods in Enzymology, Vol 549, 1st ed., Academic Press, Oxford, UK, 2014: pp. 189–219. https://doi.org/10.1016/B978-0-12-801122-5.00009-X.

[324] M. Kullolli, E. Knouf, M. Arampatzidou, M. Tewari, S.J. Pitteri, Intact microRNA analysis using high resolution mass spectrometry, J. Am. Soc. Mass Spectrom. 25 (2014) 80–87. https://doi.org/10.1007/s13361-013-0759-x.

[325] B. Thomas, A. V. Akoulitchev, Mass spectrometry of RNA, Trends Biochem. Sci. 31 (2006) 173–181. https://doi.org/10.1016/j.tibs.2006.01.004.

[326] A. Apffel, J.A. Chakel, S. Fischer, K. Lichtenwalter, W.S. Hancock, Analysis of oligonucleotides by HPLC-electrospray ionization mass spectrometry, Anal. Chem. 69 (1997) 1320–1325. https://doi.org/10.1021/ac960916h.

[327] F. Biamonte, G. Santamaria, A. Sacco, F.M. Perrone, A. Di Cello, A.M. Battaglia, A. Salatino, A. Di Vito, I. Aversa, R. Venturella, F. Zullo, F. Costanzo, MicroRNA let-7g acts as tumor suppressor and predictive biomarker for chemoresistance in human epithelial ovarian cancer, Sci. Rep. 9 (2019) 5668. https://doi.org/10.1038/s41598-019-42221-x.

[328] X. Chen, Y. Ba, L. Ma, X. Cai, Y. Yin, K. Wang, J. Guo, Y. Zhang, J. Chen, X. Guo, Q. Li, X. Li, W. Wang, Y. Zhang, J. Wang, X. Jiang, Y. Xiang, C. Xu, P. Zheng, J. Zhang, R. Li, H. Zhang, X. Shang, T. Gong, G. Ning, J. Wang, K. Zen, J. Zhang, C.-Y. Zhang, Characterization of microRNAs in serum: a novel class of biomarkers for diagnosis of cancer and other diseases, Cell Res. 18 (2008) 997–1006. https://doi.org/10.1038/cr.2008.282.

[329] M. Saraswat, R.S. Grand, W.M. Patrick, Desalting DNA by drop dialysis increases library size upon transformation, Biosci. Biotechnol. Biochem. 77 (2013) 402–404.

https://doi.org/10.1271/bbb.120767.

[330] M. Ferracin, B. Zagatti, L. Rizzotto, F. Cavazzini, A. Veronese, M. Ciccone, E. Saccenti, L. Lupini, A. Grilli, C. De Angeli, M. Negrini, A. Cuneo, MicroRNAs involvement in fludarabine refractory chronic lymphocytic leukemia, Mol. Cancer. 9 (2010) 123. https://doi.org/10.1186/1476-4598-9-123.

[331] S. Medina-Casanellas, F. Benavente, J. Barbosa, V. Sanz-Nebot, Transient isotachophoresis in on-line solid phase extraction capillary electrophoresis time-of-flight-mass spectrometry for peptide analysis in human plasma, Electrophoresis. 32 (2011) 1750–1759. https://doi.org/10.1002/elps.201100017.

[332] C. Solinas, M. Corpino, R. Maccioni, U. Pelosi, Cow's milk protein allergy, J. Matern. Neonatal Med. 23 (2010) 76–79. https://doi.org/10.3109/14767058.2010.512103.

Appendix

Appendix. Equations used in this doctoral thesis in order of appearance.

Equation	Number	Page
$m_e = \frac{q}{6\pi\eta r}$	**1**	**29**
$m_e = m_{app} - m_{EOF} = \frac{L_T L_D}{V}\left(\frac{1}{t_m} - \frac{1}{t_{EOF}}\right)$	**2**	**31**
$H_{n-(i-1)}X^{z-(i-1)} \leftrightarrow H_{n-i}X^{z-i} + H^+ \qquad K_i = \frac{[H_{n-i}X^{z-i}]\gamma^{z-i}a_{H^+}}{[H_{n-(i-1)}X^{z-(i-1)}]\gamma^{z-(i-1)}}$	**3**	**32**
$K_i' = \frac{\gamma^{z-(i-1)}}{\gamma^{z-i}} \cdot K_i$	**4**	**32**
$m_e = \sum_{i=0}^{n} \chi_{H_{n-i}X^{z-i}} m_{H_{n-i}X^{z-i}}$	**5**	**32**
$m_e = \frac{\sum_{i=0}^{r-1} 10\left[-(r-i)pH + \sum_{j=i+1}^{r} pK_j'\right] m_{H_{n-i}X^{z-i}} + m_{H_{n-r}X^{z-r}} + \sum_{i=r+1}^{n} 10\left[(i-r)pH - \sum_{j=r+1}^{i} pK_j'\right] m_{H_{n-i}X^{z-i}}}{\sum_{i=0}^{r-1} 10\left[-(r-i)pH + \sum_{j=i+1}^{r} pK_j'\right] + 1 + \sum_{i=r+1}^{n} 10\left[(i-r)pH - \sum_{j=r+1}^{i} pK_j'\right]}$	**6**	**32**
$pK_i = pK_i' + log\frac{\gamma^{z-(i-1)}}{\gamma^{z-i}}$	**7**	**33**
$\log\gamma = \frac{-z^2 A\sqrt{I}}{1+\sqrt{I}}$	**8**	**33**
$m_e = B\frac{q}{M_r^{\alpha}}$	**9**	**34**
$q = \sum_{n=1-4} \frac{P_n}{1+10^{pH-pK(P_n)}} - \sum_{n=1-5} \frac{N_n}{1+10^{pK(N_n)-pH}}$	**10**	**34**
$\alpha_{i,j} = \frac{m_{e,i}}{m_{e,j}} \qquad (m_{e,i} > m_{e,j})$	**11**	**35**
$S_{i,j}(m_e) = \frac{m_{e,i} - m_{e,j}}{m_{avg} + m_{EOF}} \qquad (m_{e,i} > m_{e,j})$	**12**	**35**
$t'_{i,j}(m_e) = \left[m_{e,i}m_{e,j}\left(m_{e,i} - m_{e,j}\right)\right]^2$	**13**	**35**

$T'(m_e)=\left[\left(\prod_{i}^{n} m_{e,i}\right)\left(\prod_{(i,j)(j<i)}^{n,(n-1)} \Delta m_{e(i,j)}\right)\right]^2$	**14**	**36**
$m/z = \frac{2V_i}{L_F^2} t_F^2$	**15**	**42**
$V_{inj} = \frac{\Delta P\ t_{inj}\ id^4\ \pi}{128\ \eta\ L_T}$	**16**	**45**
$S_{i,j}(q/M_r^{1/2}) = \frac{((q/M_r^{1/2})_i - (q/M_r^{1/2})_j)}{((q/M_r^{1/2})_{avg} + C*E)}$ $((q/M_r^{1/2})_i > (q/M_r^{1/2})_j)$	**17**	**223**
$T'(q/M_r^{1/2})=\left[\left(\prod_{i}^{n}(q/M_r^{1/2})_i\right)\left(\prod_{(i,j)(j<i)}^{n,(n-1)} \Delta(q/M_r^{1/2})_{(i,j)}\right)\right]^2$	**18**	**227**